Synthesis of sequence defined brush glycooligomers and glycopolymers targeting Langerin

Inaugural-Dissertation

for the attainment of the title of doctor

in the Faculty of Mathematics and Natural Sciences

at the Heinrich-Heine University Düsseldorf

presented by

Serap Üclü

Düsseldorf, Juni 2023

from the Institute of Organic Chemistry and Macromolecular Chemistry

at the Heinrich-Heine University Düsseldorf

Statutory declaration

"I, Serap Üclü, declare under oath that I have compiled my dissertation independently and without any undue assistance by third parties under consideration of the `Principles for the Safeguarding of Good Scientific Practice at Heinrich-Heine-University Düsseldorf".

Eidesstattliche Erklärung

"Ich, Serap Üclü, versichere an Eides Staat, dass die Dissertation von mir selbstständig und ohne unzulässige fremde Hilfe unter Beachtung der „Grundsätze zur Sicherung guter wissenschaftlicher Praxis an der Heinrich-Heine-Universität Düsseldorf" erstellt worden ist."

Düsseldorf, Juni 2023

_____

Serap Üclü

Table of Content

Abstract

Oligo- and polysaccharides act as signaling, recognition and adhesion molecules in biological systems and play a crucial role in important biological signal transduction processes such as growth and cell-cell recognition, but also host-pathogen interactions. Since the binding of single carbohydrate moieties is usually weak, Nature utilizes multivalency, the simultaneous presentation and interaction of multiple carbohydrate motifs and their respective receptors, to enhance the binding strength. This concept has been successfully adapted for the development of glycomimetics, where multiple carbohydrate units are presented on a synthetic scaffold, e.g., a polymer or a nanoparticle. Such glycomimetics are especially relevant as model systems to better understand the biological function of carbohydrates but have also already found application in biomedicine e.g., in diagnosing and treating cancer or the fight against pathogen infections.

In this work, special focus is devoted to the development of glycomimetics targeting Langerin and DC-SIGN. Langerin and DC-SIGN are C-Typ lectin receptors expressed on dendritic cells and the Langerhans cell subset, respectively, and interface between the innate and adaptive immune systems by regulating the immune response. Although both lectins share many similarities, such as overlapping specificity for carbohydrates and similar roles in the immune response, Langerin and DC-SIGN play distinct roles in HIV infection. While DC-SIGN promotes HIV transmission, Langerin ensures HIV degradation through the formation of Birbeck granules. To better understand this mechanism, the development of multivalent ligands with high affinity and selectivity for Langerin is particularly important, as monovalent carbohydrate ligands have low affinity for Langerin.

In this work, brush glycooligomers and glycopolymers were synthesized for this purpose and examined for their binding to Langerin. (see Figure 1) The trimeric arrangement of carbohydrate-recognizing domains was used here as a template for a novel building block, termed a TT linker, to create umbrella-like glycooligomers to which three carbohydrate motifs can be attached in close proximity, similar to the natural representation in, for example, branched oligosaccharides. These umbrella-like glycooligomers were tested with other trivalent branched ligands in a binding study to Langerin. For this purpose, an inhibition-competitions assay was established using surface plasmon resonance (SPR). The comparison

between the branched glycooligomer and umbrella like glycooligomer showed a 7-fold increase of binding strength towards Langerin. The addition of an umbrella handle and further binding mannose units to these umbrella structures led to a further increase in affinity, which can be attributed to a clustering effect.
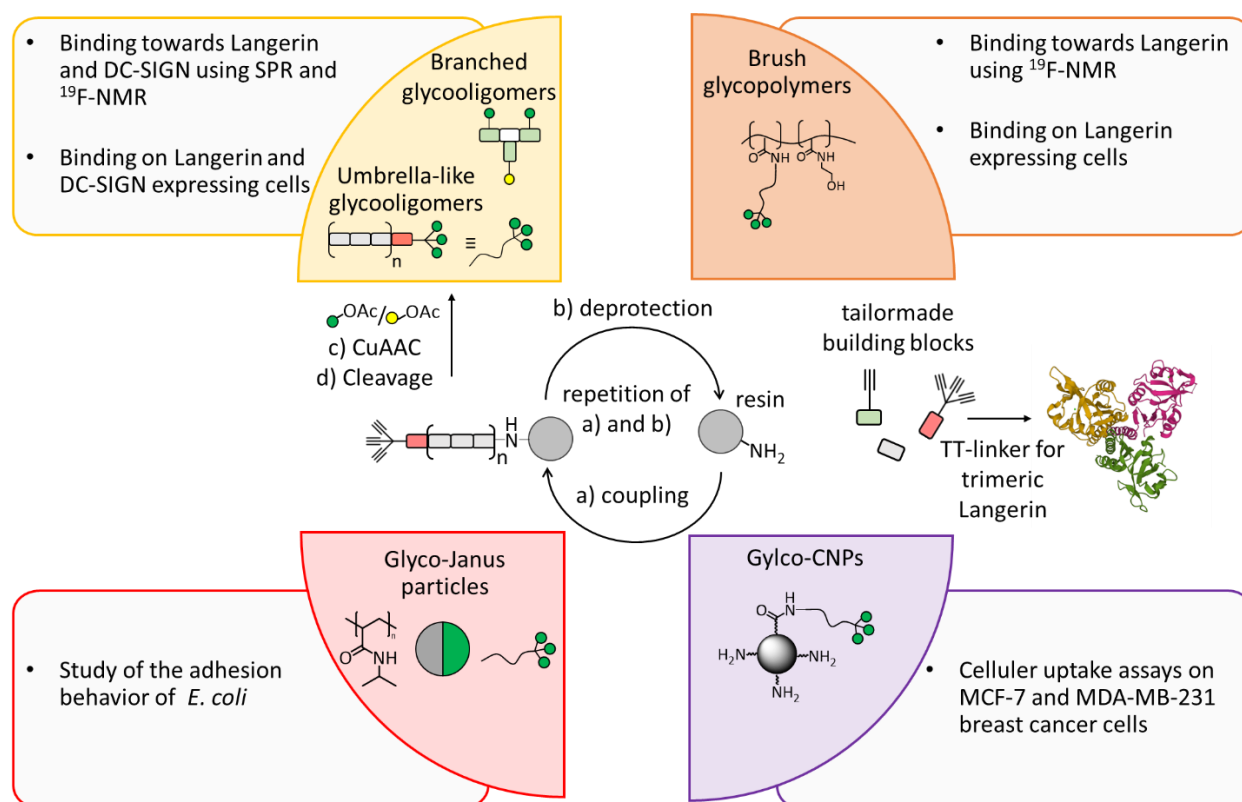

Figure 1: Overview of the topics of this thesis whereas the centre is the solid phase polymer synthesis using the novel building block TT-Linker. The inner circle shows the synthesis of various glycomimetics with different sizes, architectures and valences: branched glycooligomers and umbrella-like glycooligomers (yellow), brush glycopolymers (orange), glyco CNPs (purple) and glyco-Janus particles (red), as were established in this thesis. The outer circle shows the biological investigations of these different glycomimetics towards Langerin, DC-SiGN, *E. coli* and breast cancer cells.

The umbrella glycooligomers were then conjugated to polymeric scaffolds forming brush glycopolymers. This allows multiple receptors to be accessed simultaneously, resulting in clustering, which is important for targeting Langerin presented cell surface. A set of fluorescently labelled brush glycopolymers with increasing length of the side chain were

prepared varying the accessibility of the trivalent mannose head groups and investigated towards Langerin-expressing cells. Flow cytometric analysis showed a correlation between side chain length and cellular binding, with the glycopolymer with the longest side chain length showing the highest binding.

As alternative scaffold and for in situ fluorescent labelling, carbon-based nanoparticles were also functionalized with monosaccharides as well as brush glycooligomers and tested for their interaction with various breast cancer cell lines known to overexpress carbohydrate-recognizing lectin receptors. Similar intercellular distribution of nonfunctionalized and glyco-CNPs was observed. Microscopic examination showed that CNPs are preferentially stored in the endolysosomal pathway regardless of their functionalization. In general, this work highlights the difficulties in attempting to accomplish receptor-mediated uptake of glyco-CNPs via carbohydrate-recognizing cell surface receptors while also supporting the possible use of glyco-CNPs in biomedical applications.

As another particle system, carbohydrate-decorated Janus particles were used in this work to study the carbohydrate-mediated adhesion behavior of *E. coli* bacteria. For this purpose, Janus particles were functionalized with umbrella glycooligomer on the one side and thermoresponsive poly(N-isopropylacrylamide) (PNIPAM) on the opposite side. This is the first time that glyco-functionalized Janus particles have been reported and tested as inhibitors of *E. coli.* Microscopic studies showed that while glyco-Janus particles exhibited a halo-like arrangement on the surface of *E. coli* and led to the isolation of individual bacteria, the glyco-functionalized particles formed large clusters with the bacteria due to their uniform glyco-functionalization. Furthermore, temperature-dependent experiments with glycofunctionalized Janus particles and non-glycofunctionalized Janus particles showed particle aggregation above the LCST of PNIPAM.

Overall, this thesis demonstrates a bottom-up approach for the preparation of glycomimetics of various designs and sizes, starting from the smallest building block TT-linker specifically designed for Langerin and combining it with various polymeric and particle scaffolds. Use of the different glycomimetics in various biotechnological and biomedical applications was demonstrated, e.g. for targeted drug delivery, in immunotherapy or as markers for tumor cells. In the future, further glycomimetics can be designed by this bottom-up approach

targeting also other carbohydrate-mediated interactions e.g., by using the TT-linker for the close-proximity presentation of multiple sialic acids, fucose or sulphated carbohydrate and targeting viral entry receptors to derive inhibitors of viral infections.

List of Publications and Authorships

<u>Publications in preparation:</u>

One, two, three – heteromultivalent ligands with controlled variation of Mannose ligands targeting Langerin
Serap Üclü, Yunzhan Ning, Iris Bermejo, Nowras Rahhal, Jannis Langer, Christoph Rademacher, Laura Hartmann

Own Contribution:
Collaborative project design. Synthesis and purification of building blocks for solid phase polymer synthesis and of heteromultivalent and galactose-containing glycooligomers. Measurement and evaluation of all LC-MS experiments and evaluation of all NMR and UHR spectra. Design and performance of Inhibition-Competition Assay via SPR as well as evaluation and interpretation of the IC50 values. Writing of the first publication draft.

Homo- and heteromultivalent umbrella glycooligomers targeting Langerin and DC-SIGN
Serap Üclü, Iris Bermejo, Nowras Rahhal, Felicitas Drees, Christoph Rademacher, Laura Hartmann

Own Contribution:
Collaborative project design. Synthesis and purification of building blocks for solid phase polymer synthesis and synthesis of umbrella glycooligomers. Measurement and evaluation of all LC-MS experiments of the glycooligomers and evaluation of all NMR and UHR spectra of glycooligomers. Design and performance of Inhibition-Competition Assay via SPR as well as evaluation and interpretation of the IC_{50} values. Writing of the first publication draft.

Brush glycopolymer targeting Langerin on cells

Serap Üclü, Stig Hill Christiansen, Maxime Denis, Christoph Rademacher, Steffen Thiel, Laura Hartmann

Own Contribution:

Collaborative project design. Synthesis and purification of building blocks for solid phase polymer synthesis, glycooligomers and brush glycopolymers. Measurement and evaluation of all LC-MS experiments of the glycooligomers and evaluation of all NMR and UHR spectra of glycooligomers and brush glycopolymers. Collaborative planning and performance of the cell uptake experiments using Flow Cytometry. Collaborative writing of the first publication draft.

Sweet Janus Particles: glyco-functionalized janus particles for the binding and inhibition of E. coli

Serap Üclü, Claudia Marschelke, Markus Geisler, Dimitri Wilms, Thorben Koehler, Miriam Bäumers, Stephan Schmidt, Alla Synytska and Laura Hartmann

Own Contribution:

Collaborative project design. Synthesis and purification of building block for solid phase polymer synthesis. Measurement and evaluation of all LC-MS experiments of the glycooligomer and evaluation of all NMR and UHR spectra of glycooligomer. Conjugation of the glycooligomer to the particles and performance and evaluation of the phenol-sulfuric acid assay as well as the DLS assay regarding the carbohydrate loading. Design and performance of Inhibition-Competition Assay of the glycooligomer towards ConA via SPR as well as evaluation and interpretation of the K_D value. Collaborative performance of binding and inhibition studies of glycofunctionalized particles towards ConA and *E. coli*. Collaborative writing of the first publication draft.

Sweet carbon dots: synthesis of carbohydrate-functionalized carbon nanoparticles and their cellular uptake

Serap Üclü, Christian Wimmenauer, Cathrin Nollmann, Andrea Liu, Stephen A. Hill, Nicole L. Snyder, Thomas Heinzel and Laura Hartmann

Own Contribution:

Collaborative project design. Synthesis and purification of building blocks for solid phase polymer synthesis and glycooligomers. Measurement and evaluation of all LC-MS experiments and evaluation of all NMR and UHR spectra. Conjugation of the glycooligomer to the carbon nanoparticles and evaluation of the NMR analysis regarding the carbohydrate loading. Collaborative writing of the publication draft.

<u>Other publication that are not part of this work</u>

PEGylated sequence-controlled macromolecules using supramolecular binding to target the Taspase1/Importin α interaction

P. Pasch, A. Höing, S. Ueclue, M. Killa, J. Voskuhl, S. K. Knauer, L. Hartmann

Chem. Commun., 2021, *57*, 3091-3094.

<u>Presentation at a scientific conference:</u>

Branched precision glycomacromolecules targeting Langerin

Kira Neuhaus, <u>Serap Üclü</u>, Eike-Christian Wamhoff, Christoph Rademacher, Laura Hartmann

5. International Symposium of the SFB 765 "Multivalency in Chemistry and Biology", 30.09.2019 - 02.10.2019, Berlin.

1. Introduction

1.1 Carbohydrate - Lectin Interactions

Each mammalian cell is decorated with a layer of carbohydrates which is referred to as the glycocalyx, a term introduced in 1962 by H. Stanley Bennett. [1] This term describes the extracellular, carbohydrate-rich surface layer of cells and is characteristic of their appearance, type, and developmental stage of the cell. The glycocalyx forms the outer surface of the cellular plasma membrane and contains a multicomponent system of binding proteins, enzymes, hormone receptor sites, antigens, and glycoconjugates composed of glycolipids and glycoproteins (see Figure 2). [2] The carbohydrate structures are present on the outer cell surface as mono-, oligo-, and polysaccharides and act as specific mediators between cells and play an important role in numerous cellular processes such as cell growth and recognition, adhesion, cancer metastasis, bacterial and viral infections, and inflammation. Unlike other natural macromolecules/biomacromolecules such as nucleic acids and proteins, carbohydrates exhibit high structural diversity. [3] While nucleic acids and proteins are composed of bifunctional monomers, carbohydrates have monosaccharides that combine to form linear and branched oligo- and polysaccharides. This results in a wide variety of possible linkage types and thus a high potential for structural variability. [4] This unlimited structural diversity is at the same time the reason for the low level of knowledge about carbohydrates, but also for the increasing interest in their function. Thus, it has been found that storage and transport of biological information through cell-cell and host-cell interactions are among the most important functions of carbohydrates. [5]

In this context, information transfer is passed on through the formation of non-covalent complexes between carbohydrate ligands and protein receptors. The outer carbohydrate residues in the glycocalyx serve as docking sites for other cells or pathogens and are responsible for the uptake and processing of information. [6] [7] Thus, the glycocalyx is involved in the transfer of information between cells or within the cell, which plays a role, for example, in signal transduction, immune responses [8] and anti-inflammatory processes. [9] [10] To decode this information, specific mechanisms and signaling cascades need to be activated. Here, specific carbohydrate-recognizing proteins, also known as lectins, play an essential role in activation. [11]
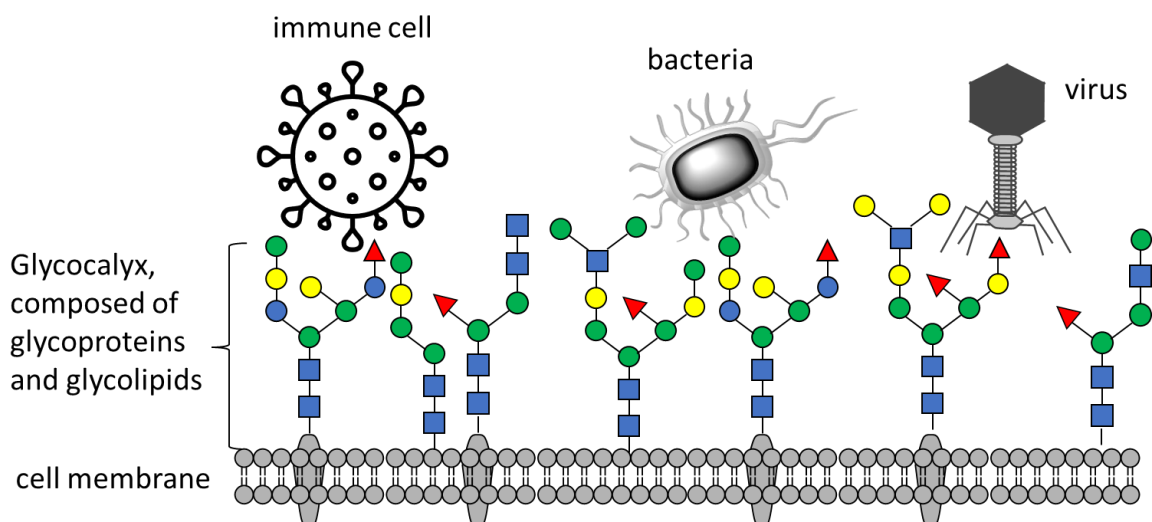
Figure 2: Schematic representation of the glycocalyx consisting of cell membrane, glycoproteins and glycolipids and the interaction with immune cells, bacteria and viruses. Figure adapted from [3].

The term lectins is derived from the Latin word "legere" (english: to select) and was introduced by Shapleigh and Boyd. [12] Lectins are found in all living organisms, fungi, bacteria, and viruses and are often used as tools to analyze fundamental processes in carbohydrate-mediated binding cell biology and have no enzymatic activity toward the bound sugars themselves. [13] [14] The interaction between a lectin and a monosaccharide is typically weak, in the mM range. [15] To circumvent this weak affinity, nature makes use of multivalency, in which multiple carbohydrates are simultaneously involved in the binding, increasing the affinity as well as selectivity. [16] Natural or non-natural multivalent ligands such as oligosaccharides on surface of the cells or glycomimetics by presenting carbohydrate on a polymeric scaffold can possess different types of multivalent binding modes and profit from a variety of multivalent effects to increase binding strength, such as receptor clustering, chelating effect, statistical rebinding and steric shielding. [17] (see Figure 3)

The chelate effect results from intramolecular bonding between a multivalent ligand and multiply carbohydrate recognition domains (CRDs) of a lectin. This binding mode can be related to an entropy effect that favors the binding of another ligand from the same system, thus allowing the increase of binding avidity. [18]
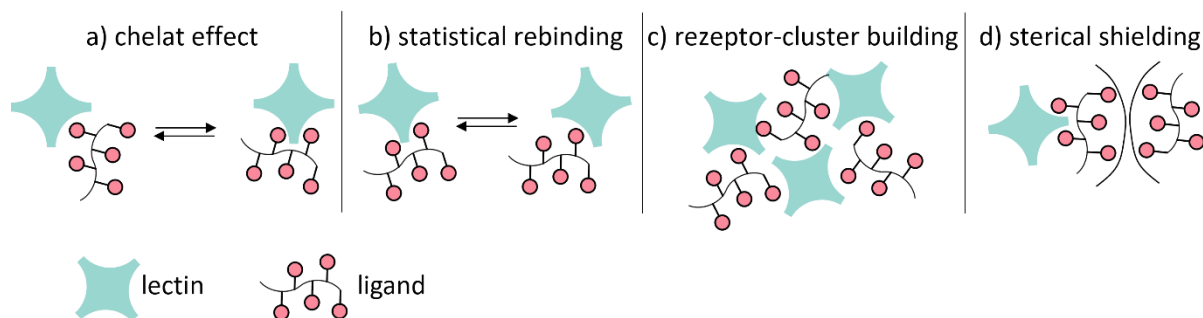
Figure 3: Multivalent interactions between multivalent lectin and multivalent ligands: a) chelate effect, b) statistical rebinding, c) receptor-cluster building, d) sterical shielding. Figure adapted from [17].

In contrast to the chelating effect, statistical rebinding is caused by the intramolecular reversible binding resulting of rapid association and dissociation rates of a ligand to a receptor and is based on the high local concentration of carbohydrate ligands. [19] The interactions between carbohydrate and lectin are usually very weak, so that individual carbohydrates are not tightly bound. When a ligand dissociates from the binding pocket, the spatial proximity of another ligand of the multivalent system can cause it to rebind to the receptor, resulting in increased affinity. [20]

When multivalent ligands are simultaneously linked to multiple receptors, this is referred to as the cluster glycoside effect. [21] The interactions between multiple multivalent carbohydrate ligands and multiple receptors of lectins can lead to a type of cross-linking that increases the overall avidity. This effect especially plays a role at the cell surface. This allows proteins to be brought into close proximity and intracellular processes to be triggered. [22]

Sterical shielding occurs when non-bound portions of a partially bound multivalent glycomimetic can shield the previously formed carbohydrate-lectin complex from competing ligands, thereby maintaining and stabilizing the original state. [23] The non-bound components or competing ligands may be nonbinding carbohydrate components, various scaffolds such as proteins or lipids, or binding sugars that are temporarily not involved in a binding event: Although they do not interact directly with the CRD of the lectin, they have a significant impact on the stability of the carbohydrate-lectin complex by serving as a steric shield and protecting the complex from competing ligands that might also bind to the CRD of the lectin. [24]

1.2 Innate and adaptive Immunity

In order to trigger the host defense mechanism, the immune system is composed of several cells and molecule types that particularly interact with each other. [25] So far, several studies have shown that interaction between carbohydrates and lectins play a crucial role in triggering an immune response. [26] In order to understand the importance of this interaction in more detail, the following chapter will discuss the basic mechanisms and the most important cells of the immune system.

The immune system can first be classified into two subgroups: innate immunity and adaptive immunity. [27] (see Figure 4) The non-specific innate immune system is our body's first defense against invaders, whether it is just a dust particle or a pathogen. [28] Therefore, the great goal of the innate immune system is to prevent any invasion of the body without distinguishing between different pathogens. The first and most important barrier of defense is the skin, since any invasion into our body is first prevented by the skin, and the mucous membrane, which intercepts the pathogen through the viscous fluid layer. These two components form the physical barrier and protect our body from external threats. [29] In addition, the body is protected by the chemical barrier, such as the stomach acid or the lysozymes in the tear fluid. [30]
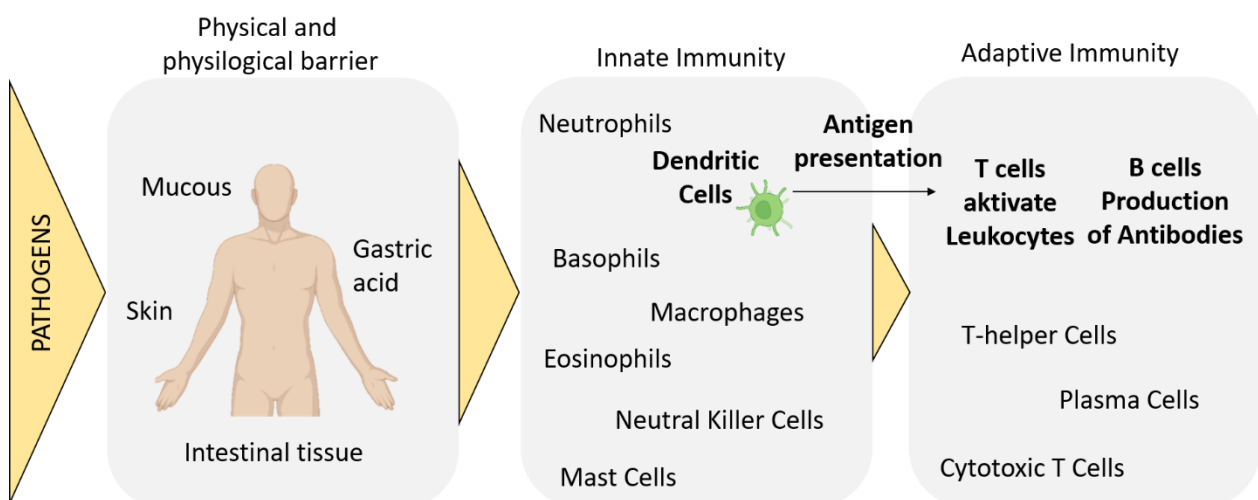

Figure 4: Overview of adaptive and innate immunity including the three stages of immune defense whereby the dendritic cells interact between the innate and adaptive immune system by presenting antigen to T and B cells.

Inflammatory reactions initiated by mast cells form the second stage of the defense system. [31] [32] When mast cells encounter a foreign surface, they release histamine, which triggers an inflammatory response resulting in increased blood flow to the affected area and consecutive increased number of leukocytes. [33] Phagocytes, neutrophils and macrophages that destroy pathogens and cancer cells, natural killer cells (NK cells) and dendritic cells (DCs) make up the various subtypes of leukocytes and belong to the family of innate immune system. NK cells are able to recognize and eliminate infected cells. [34] [35] Healthy cells produce the so-called major histocompatibility complex class I (MHC-I), which is recognized by NK cells. When cells are infected, MHC-I production stops, causing NK cells to recognize and bind to infected cells and kill the cell by releasing certain chemicals. [36]

DCs are localized in the skin and mucosa and interact between the innate and adaptive immunity. They also recognize and digest pathogens and transmit this information in the form of pathogen specific antigens to the cells of the adaptive immune system. [37] T lymphocytes and B lymphocytes, the cells of the adaptive immune system, can recognize and fight against the pathogens based on the antigens they display on their surface. As a result, the adaptive immune system is more efficient and can discriminate between pathogens. [38] After the immune response has initiated and the infection has already been triggered, T lymphocytes initiate a response, recruiting cytotoxic cells (killer cells) to eliminate the infected cells. [39] B lymphocytes form the humoral immune response and are used when the pathogens are already present but have not yet initiated infection. [40] B cells produce antibodies that match antigens on the surface of the pathogens, forming a protective shield for the pathogens. This sends a signal to macrophages that eliminates the pathogen. In addition, B and T cells form so-called memory cells that store all past infections, thus enhancing the immune response to the infection that has already been overcome. [41]

Hence, DCs play a crucial role as mediators at the interface between innate and adaptive immunity. The main functions in the innate immune system are a) antigen uptake and processing, b) presentation of antigens to cells of the adaptive immune system, and c) mediation of their polarization to effector cells. [42] DCs are divided into two subtypes: plasmacytoid DCs (pDCs) and myeloid DCs (mDCs). mDCs are specialized in recognizing subtypes of pathogen-associated molecular patterns (PAMPs) due to their unique distribution of pathogen recognition receptors (PRRs) such as toll-like receptors (TLRs), C-type lectins

(CTLs) and intercellular nucleic acid sensors. [43] [44] [45] In previous studies, many different C-type lectins of DCs have been reported including DC-SIGN (dendritic cell-specific ICAM-3 seizing non-integrin), the Langerhans cell specific lectin Langerin, the mannose receptors, Dendritic cell-specific ICAM-3-grabbing nonintegrin (DC-SIGN), Dectin-1 and asialoglycoprotein receptors (ASGPR), which function as antigen receptors and are involved in various infections and diseases. [46]
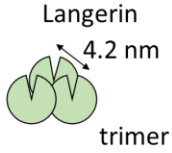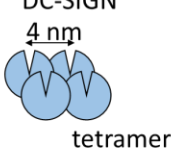
1.3 Lectins of innate immunity – Langerin and DC-SIGN

Langerin and DC-SIGN belong to the C-type lectin family and are among the important lectins of the immune system. Their function as cell surface receptors with N-terminal domain and a single extracellular domain (ECD) and are crucial for cell-cell interactions as adhesion receptors. [47] [48] The C-type lectins (CTLs) form a family of calcium-dependent carbohydrate-binding proteins. CTLs are expressed by dendritic cells and can recognize pathogens and subsequently activate adaptive and innate immune responses. [49] Although both lectins have many overlapping properties, they have different functionalities with respect to the immune response.

Langerin is a trimeric transmembrane protein and categorized as a type II CTL, which is expressed exclusively on Langerhans cells, which are found in the epidermis and initiate an immune response upon encountering pathogens. [50] This lectin composed of a cytoplasmic domain, a transmembrane region and ECD, which consists of an α-helical neck domain and a carbohydrate recognition domain (CRD) containing a calcium ion. Due to the interactions between the CRDs and the neck domains, the ECD forms a rigid trimer with the three symmetrically arranged carbohydrate binding pockets spaced 4.2 nm apart [51] (see Table 1). DC-SIGN is expressed on subepithelial DCs and macrophages and enables dendritic cells to interact with T cells by binding to intercellular adhesion molecule 3 (ICAM-3). [52] The ECD of DC-SIGN consists of 4 CRDs formed into a tetramer with a distance between 4 and 9,5 nm apart. (see Table 1). [53] [54] Both lectins have overlapping carbohydrate specificities, for mannose (Man), fucose (Fuc) and acetyl-glucosamine (GlcNAc) monosaccharides. [55] [56] [57] DC-SIGN and Langerin are pattern recognition receptors (PRRs) that are important for a variety of viruses such as HIV-1 (human immunodeficiency virus type 1) [58], HCV (hepatitis C virus) [59]

and bacteria, e.g. Mycobacterium tuberculosis. [60] Similar to other Toll-like receptors, DC-SIGN and Langerin are involved in antigen formation and antigen uptake, leading to migration of DCs to the lymph nodes, followed by presentation of the antigen in the context of the MHC. This activates T cells, triggering the adaptive immune response. However, these CTL receptors are misused by some pathogens and tumor cells to evade the immune response. [61] [62] For instance, there is a significant variance in HIV-1. Langerin has a protective effect by internalizing the virus and then destroying it through the production of Birbeck granules, whereas DC-SIGN promotes survival, infection of additional cells, and thus the spread of HIV- 1. [63] [64] [65] Birbeck granules, which are unique to LCs, are a part of the endosomal recycling mechanism. [66] On the other hand, Langerin also serves as an entry receptor for influenza A virus (IAV), despite the fact as LC does not contain sialic acid on its cell surface, which is necessary for IAV attachment. [67]

Table 1: Overview and comparison of the C-type lectins Langerin and DC-SIGN including localization, carbohydrate recognition and characteristics.

	Localization	Carbohydrate recognition	Characteristics
Langerin 4.2 nm trimer	Langerhans Cells (LCs), subtyp of DC, located in the epidermis and mucosa	mannose, fucose, GlcNAc, sulfated glycans	• Induces Birbeck granule formation • promotes the internalization and presentation of antigens
DC-SIGN 4 nm tetramer	Dendritic Cells (DCs) located in the epidermis, sub-epithelium, rectal mucosa and lymph nodeosa	mannose, fucose, GlcNAc	• Adhesion receptor • Regulates the immune function and antigen presentation

Due to these ambivalences, Langerin is a challenging target for therapeutic development, as Langerin can increase infectivity in some situations, while acting as a protective mechanism and promoting BG formation in others. Considering these facts, the development of highly specific drugs to differentiate DC-SIGN from Langerin has arisen as a leading priority without affecting the innate immune function of Langerin. In contrast to Langerin, DC-SIGN interacts with complex multiantennary glycans in nature. [68] Moreover, certain differences in Lewis-type antigen recognition are supported. Despite DC-SIGN, Langerin is unable to bind to the

LeX and LeA antigens, but it still recognizes the LeY and LeB antigens as well as the blood group antigens A and B. [69] These findings suggest to a restricted capacity to detect only terminal 1- 2-linked Fuc residues, pointing to a possible protective function for natural LeX-containing antigens as DC-SIGN elective binders. [70] One opportunity to address this issue is that the targeted multivalent presentation of carbohydrate ligands can influence an increase in selectivity to lectin. For example, the binding pockets of a lectin can be used as a template and the multivalent ligands can be arranged in such a way that they geometrically fit into only one binding pocket of a lectin and not into the other, thus achieving selective binding and inhibition of the lectin.

1.4 Mannose bearing glycomimetics targeting Langerin

Selective targeting of lectins is necessary to learn more about their biological role, especially Inhibiting their functions to prevent certain diseases plays an important role. Therefore, much attention is focused on developing ligands with higher affinity for their target lectin. C-type lectins such as Langerin and DC-SIGN are important pathogen recognition receptors of the immune system that contribute to immune regulation by activating the adaptive immune response. Therefore, it is important to use such lectins as targets, for example, to develop immunotherapeutic. In the following chapter, current strategies are presented, with a focus on mannose bearing glycomimetics targeting Langerin. Although Langerin has gained popularity in recent years, there are few publications on mannose-bearing multivalent glycomimetics. The use of Mannose bearing conjugates targeting Langerin has been minimally investigated. A challenge is the selective control of langerin, as it is always in competition with other mannose-recognising lectins, especially the other C-type lectins such as DC-SIGN. Another important aspect is the availability of the lectin. While a certain amount of protein is commercially available, Langerin has to be expressed. Langerin expressed from both mice and humans were studied. The comparison showed that Langerin expression from mice was not sufficient to cause BG formation. Therefore, human langerin is used in these studies. [71] The following chapter gives a selection of studied multivalent mannose conjugates that have been tested for their binding to Langerin.

Terminal Man as minimal binding motif for Langerin was identified by Stambach and Taylor. [68] They investigated the carbohydrate-binding properties of monosaccharide

Mannose and oligosaccharides $Man_9GlcNAc_2$ by using a solid phase assay resulting in 10-fold increase of binding towards Langerin. Andrea Holla and Arne Skerra investigated the effect of increasing the number of mannose from one to dimannose Man(α1-2)Man and tested the interaction on Langerin using isothermal titration calorimetry (ITC) and observed a 1.5-fold increase in the interaction. A glycan microarray was then used to print carbohydrate components onto NHS-activated glass. In this way, 28 monosaccharides, 62 disaccharides, and 185 larger oligosaccharides with mannose, sulfated and sialic acid containing structures were obtained. The finding showed that Langerin bound to compounds with terminal mannose structures, preferring small linear structures with three and four mannose groups. [72] This has then led to the development of different types of Man-functionalized glycomimetics and glycoconjugates that were tested for binding to Langerin.

A recent example that is also the starting point for the study presented in this thesis is work by Neuhaus et al, where multivalent Langerin inhibitors were developed in a rational design. Based on the structure of trimeric Langerin, they used solid-phase polymer synthesis (SPPoS) to construct trivalent Langerin inhibitors with asymmetrically branched 3-armed glycomacromolecules containing a mannose ligand on each arm. The distance between the mannose ligands was adjusted by varying the arm length of the glycomacromolecules, with distances between arms ranging from 11-15 Å for the smallest structure to 29-37 Å for the largest structure. (see Figure 5) To investigate the influence of valence as well, a 1-arm structure carrying one mannose ligand was prepared. The ^{19}F-NMR competition assay showed that the trivalent mannose ligand with the shortest arms (IC_{50} = 0.044 ± 0.006 mM) most strongly inhibited the interaction towards Langerin compared to the largest structure (IC_{50} = 0.8 ± 0.1 mM). The comparison of monovalent 1-arm structure with smallest 3-arm structure also resulted in a 200-fold increase of binding affinity. According to these findings and modeling studies, they come to the conclusion that the smallest structure in the three CRDs of the Langerin is kinetically trapped. This leads to rapid exchange between the CRDs and the individual mannose ligands, resulting in an increase in avidity due to statistical rebinding effects rather than chelation. [73]
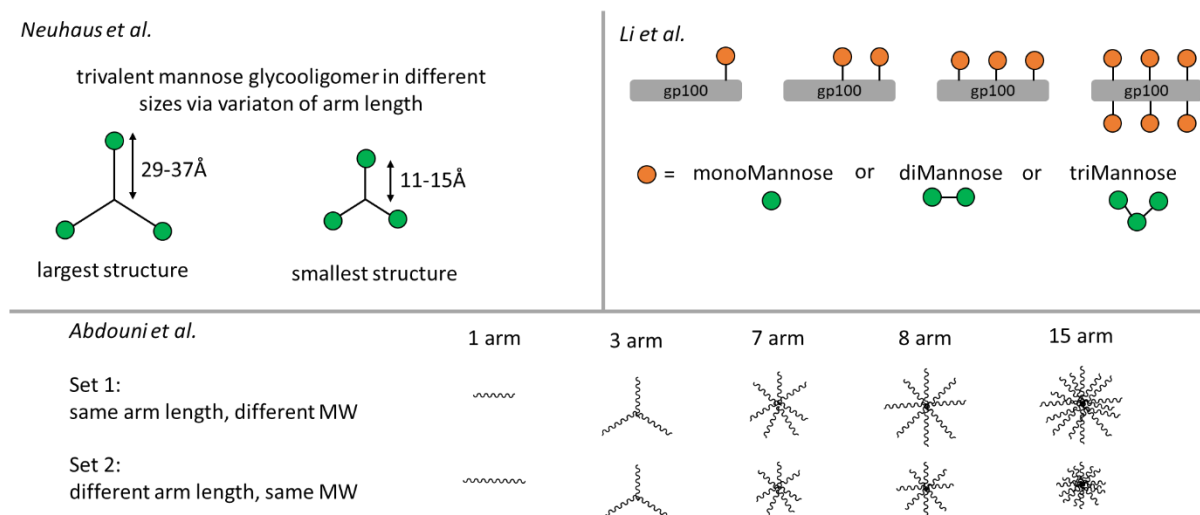
Figure 5: Selected examples of Langerin targeting glycomimetic ligands of different sizes: Neuhaus et al. showed the 3 armed glycomimetic with variation in arm length, Abdouni et al. showed the synthesis of star shaped glyocpolymers with differences in arm length and molecular weight (MW), Li et al. showed the conjugation of mono-, di- and triMannose on a peptide backbone.

Additional mannose-containing ligands to study the binding affinity towards Langerin were prepared by the group of Becer and coworkers. [74] First, they prepared mannose-containing linear glycopolymers and star-shaped glycooligomers to study the binding potential to Langerin and DC-SIGN using surface plasmon resonance (SPR). (see Figure 5) Mannose-containing star-shaped glycopolymers with different numbers and lengths of arms were synthesized using copper-mediated reversible deactivation radical polymerization. In this process, two different sets of star polymers were prepared. The first set (set S1) consists of 5 glycopolymers with an average of 1, 3, 7, 8 and 15 arms synthesized. In the second set were 5 glycopolymers (set S2) the number of carbohydrates per macromolecule was kept constant to obtain glycopolymers with similar number of mannose but different arm length. Both groups of glycopolymers were then evaluated for their lectin-binding affinity toward a number of novel and previously studied C-type mannose-specific lectins, including Langerin and DC-SIGN. In this regard, the proteins were immobilized onto an SPR chip and the direct binding of the glycopolymers was investigated. For glycopolymer S1, showing a different number of arms per molecule but the same arm length, an enhancement of the binding affinity to Langerin was observed with an increase in the number of arms compared to DC-SIGN. The glycopolymers of set S2 with different arm lengths but the same molecular weight showed very similar binding abilities towards Langerin and DC-SIGN. (see Figure 5)

To determine the optimal oligomannoside structure for binding to Langerin, Li et al. studied a set of 20 mannose ligands composed of clusters of mannosides from one, two, or three of six monomannosides, dimannosides, or trimannosides bound to a peptide scaffold (gp100). (see Figure 5) The direct binding of the ligands towards Langerin was investigated using SPR. For this purpose, Langerin was functionalized on an SPR sensor chip to imitate the natural presentation of lectin on the cell surface. The results showed that the correlation between the increase in mannose units and affinity for Langerin increased up to the µM range, which was also supported by the binding study using flow cytometry. [75]

To investigate the binding and internalization of these ligands, cell experiments were flow cytometry were performed. For this purpose, Langerin-expressing human Epstein-Barr virus-transformed B lymphoblast cell lines (BLC) were used and the ligands were labelled with biotin. After incubation with the cells, a streptavidin labelled dye was added and then assayed by flow cytometry. The assay showed increased langerin binding for the ligands with three or six copies of mono-, di- and trimannose, which is consistent with the SPR assay. To confirm the binding, the cells were blocked with a Langerin-specific antibody, which verifies the Langerin-binding specificity of the Man carrying ligands. In summary, the results of the binding assays suggest that Langerin affinity is dependent on the type of oligomannoside and can be improved by multivalence.

Overall, the hexavalent presentation of the Man units yielded ligands with a high affinity towards Langerin. Subsequently, this ligand was used to study its uptake into the cell. For this purpose, the Langerin-expressing cells were incubated at 4 °C with a biotin-functionalised hexavalent ligand. After 60 min, the cells were washed and then incubated at 37 °C. After specific time points, samples were taken, washed, mixed with streptavidin-labelled dye and then analysed by flow cytometry. After about 1 hour, 35-55 % of the ligands were internalised. This indicates that the ligands with higher mannose content remain on the surface longer before they are internalized.

2. Synthesis of Glycomimetics

Glycomimetics form a new class of materials that can be utilized to improve the understanding of carbohydrate-lectin interactions. [76] Carbohydrates in living organisms play a critical role in information storage and release, signal transduction, cell adhesion, cell-cell communication, and recognition of bacteria and viruses. [58] [77] [78] [79] [80] However, the complex structural diversity of natural carbohydrates makes it difficult to establish a direct structure-property relationship between carbohydrate ligand and receptor. To gain a better understanding of this structure-property relationship, research is utilizing artificial glycomimetics with precise control over the number, position, and spacing of carbohydrate ligands present within each molecule, which can be used to specifically address a question about the mechanism of carbohydrate-lectin interactions. Glycomimetics is used to design carbohydrate-containing macromolecules that mimic their natural counterparts by simplifying the carbohydrate ligands by excluding unnecessary carbohydrate components that potentially do not show binding to receptors. The architecture of glycocomimetics can vary depending on how they are simplified, from linear to dendrimers to star-shaped or even glycopolymers and glyconanoparticles. [81] [82] [83] [84] In view of the relevance of this work, the three systems of glycomacromolecules, glycopolymers and glyconanoparticles will be highlighted in the following chapters. (see Figure 6)
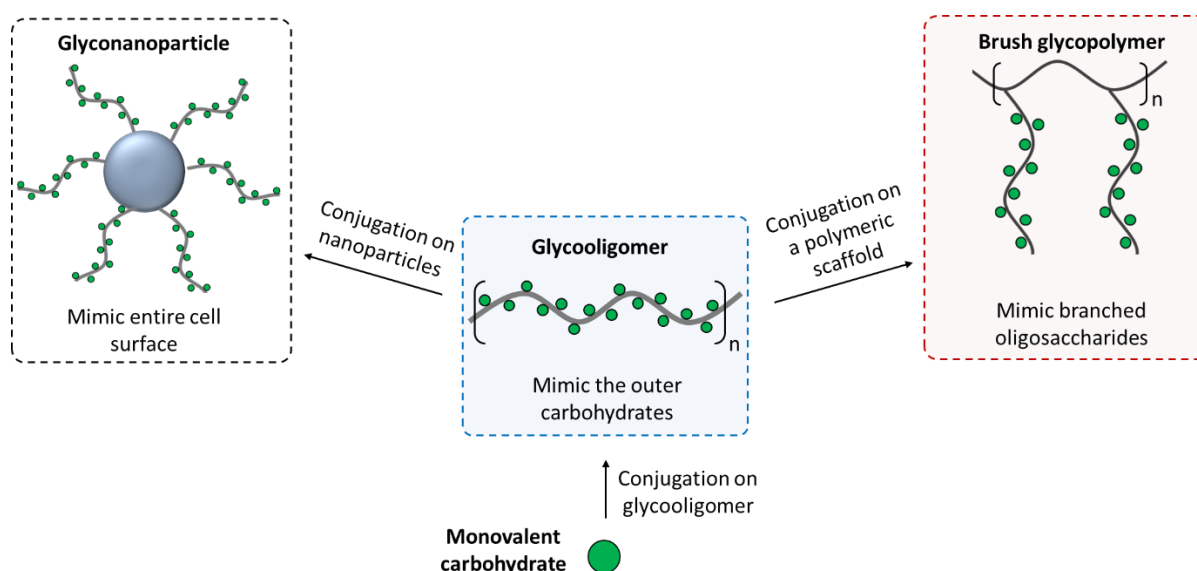
Figure 6: A monovalent carbohydrate is first presented on a glycooligomer to mimic the outermost carbohydrate of the glycocalyx. To increase multivalence, the glycooligomer is either attached to a polymer scaffold resulting in brush glycopolymer to mimic the branched oligosaccharides on the cell surface or to a nanoparticle to mimic the entire cell surface.

An important tool for obtaining a variety of glycomimetics is the solid-phase synthesis of so-called precision glycomacromolecules. [85] [86] These glycomacromolecules have an oligo(amidoamine) backbone with pendant carbohydrate side chains. A monodisperse, sequence-defined oligo(amidoamine) backbone with different functional groups in the main and side chains can be prepared by stepwise assembly of these building blocks on a solid support via SPPoS, which is based on the Merrifield peptide synthesis technique using artificial building blocks instead of natural amino acids. These glycomimetics can be used as ligands and inhibitors in the study of bacterial and viral lectins or the interaction with tumor cells. [87] [88] [89] [90] [91] Conjugation of these glycomacromolecules to polymeric scaffolds or to particles not only enhances the multivalent presentation of carbohydrate moieties, but also allows them to be studied in addition to lectins on cells or even bacteria. Thus, conjugation to polymeric scaffolds has been used to produce brush glycopolymers to study interactions with lectins such as DC-SIGN, ConA, and MBL. [92] [93] Conjugation to particular systems such as the gold nanoparticles, microgels or liposomes allowed the study on lectins such as ConA or Galectin-3. [94] [95] [96]

2.1 Solid phase polymer synthesis of precision glycomacromolecules

Solid phase synthesis was first described by E. Fischer in 1903 and used for the preparation of peptide chains. [97] More than 50 years later, R.B. Merrifield simplified and accelerated peptide synthesis and invented the stepwise coupling of amino acids to the solid phase. [98] In each cycle, the peptide chains are extended by one amino acid on the solid support, allowing rapid, efficient, and controlled assembly of different amino acids and yield in high purity by simple filtration and washing processes instead of the time-consuming and difficult purification steps after prior isolation. [99] Solid phase synthesis is not limited to amino acids, but can also be carried out with all bifunctional compounds functionalized with a carboxyl group on one side and an amide group on the other. [100]

One of the key components of solid phase synthesis is the solid support. This requires stable binding between the support and the peptide chain and specific cleavage of the substrate. Merrifield prepared a copolymer of styrene with divinylbenzene (DVB) as a crosslinking agent and used a chloromethyl group as a linker. [101] This classic so-called Merrifield resin is extremely hydrophobic and swells very strongly in organic solvents such as dichloromethane or dimethylformamide. The expansion of the surface allows diffusion of the reactants to the linker or terminal amine group of the building block and thus chain growth. [102] However, for longer chains, the synthesis of long peptide chains leads to aggregation at the resin surface and thus to termination sequences. To circumvent this problem, more hydrophilic resins, such as the Tentagel resin, can be used. The Tentagel resin is a graft polymer of polystyrene crosslinked with divinylbenzene, to which the polyethylene glycol (PEG) chain is anchored. [103] [104] The PEG chain provides greater spacing from the polystyrene backbone, resulting in greater chain flexibility and allowing easier access of reactants to the resin. The amine end groups of the bbs are provided with temporary protecting groups that can be cleaved off under various conditions. The Fmoc group is used for temporary protection of the amine end groups according to the so-called standard Fmoc coupling protocol. [105] The advantage of this method is the ease of deprotection under basic conditions from a 25 Vol % piperidine solution in DMF. The success and completeness of Fmoc cleavage can be monitored by UV absorption spectroscopy. The cleavage produces the dibenzofulvene (DBF)-piperidine adduct, which adsorbs strongly in the UV region. Functional side chains such as additional amine groups (e.g., in lysine) can for example be protected by a *tert*-butyloxycarbonyl (Boc)

protecting group or an alloxycarbonyl (Alloc) protecting group. The Boc protecting group is cleaved under acidic conditions, usually dilute hydrochloric acid, and the use of TFA simultaneously allows the final cleavage of the peptide chain from the resin. The Alloc protecting group is removed by a palladium (0) catalyst. [106] [107] To prevent the formation of undesirable by-products, known as spurious sequences, during the stepwise assembly of the peptide chain, the reactants are used in excess. The bbs are coupled by the addition of a tertiary amine (e.g. DIPEA) is used to produce a carboxylate of the N-protected amino acid, which then reacts with the activating reagent PyBOP. This produces a phosphonium oxide species, which is the driving force of the coupling reaction, and a hydroxylbenzotriazole (OBt) anion, which further reacts with the N-protected amino acid in its corresponding OBt esters. After successful coupling of the first building block, the Fmoc protecting group of the end group is removed using 25 vol% piperidine solution. The coupling and deprotection steps are repeated until the desired chain length or number of bbs is achieved. (see Figure 8)

Hartmann et al. developed solid-phase polymer synthesis (SPPoS) for the effective preparation of monodisperse sequence-defined, or so-called precision glycomacromolecules. [108] In general, precision glycomacromolecules have an oligo(amidoamine) backbone and side chains with incorporated carbohydrate residues. The backbone is constructed by SPPoS using the Fluorenylmethoxycarbonyl (Fmoc) protecting group strategy. This allows not only the construction of linear macromolecules, but also the introduction of branching when using building blocks (bbs) that have a functional side chain in addition to the acid and amino groups. [86] [109] A variety of tailormade bbs have been developed and can be divided into so-called spacer and functional bbs as shown in Figure 7. [85] [87] [110] Spacer BBs can be used to adjust the distances between the functional BBs. On the other hand, they can be utilized to regulate the hydrophobicity [111] (see Figure 7) Functional bbs carry a functionality in their side chain, e.g. alkyne for TDS or azide for BADS. These bbs can be used to prepare monodisperse biomimetic glycooligomers with different polarities, lengths, valences and carbohydrate functions.
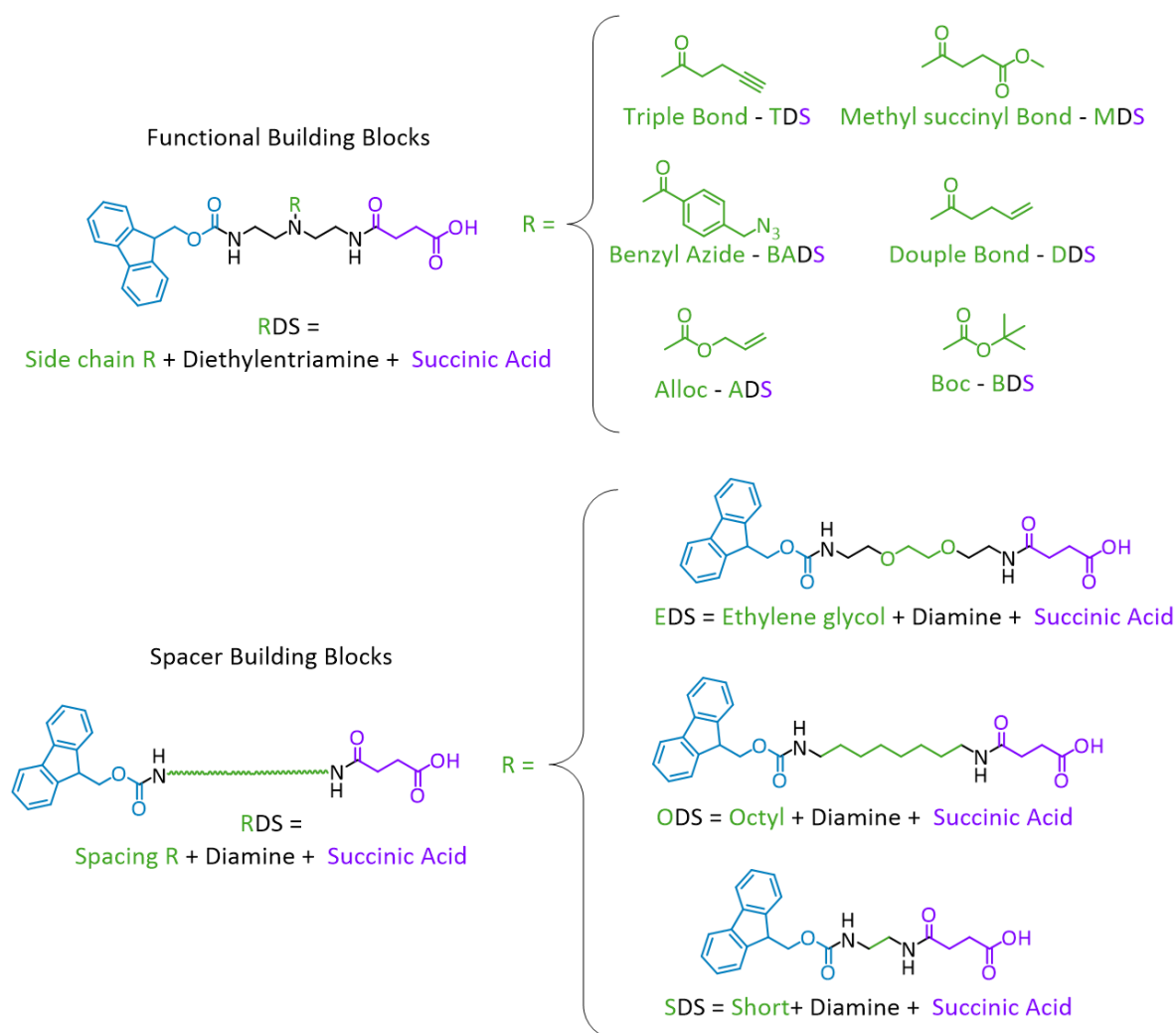
Figure 7: Examples of functional bbs with different functionalities in the side chain and spacer bbs with different spacings for application to the SPPoS. [87]

To prepare precision glycomacromolecules, an alkyne-functionalized building block and a carbohydrate-azide derivative are used for Cu(I)-catalyzed azide-alkyne cycloaddition (CuAAC). [85] [112] The beginnings of click chemistry date back to 2001 and were developed by Sharpless et al. [113] The advantages of the click reaction are the mild reaction conditions and the simple and rapid purification steps. The copper(I)-catalyzed azide-alkyne cycloaddition (CuAAC) allows the formation 1,2,3-triazol. [114] [115]

At the last step the peptide chain is isolated by cleavage from the support. Cleavage of the polymer chain from the resin requires different cleavage conditions depending on the composition of the resin. The cleavage of the resin occurs under acidic conditions and requires

trifluoroacetic acid (TFA) in concentrations ranging from 1 to 95%, depending on the linker type. [116]
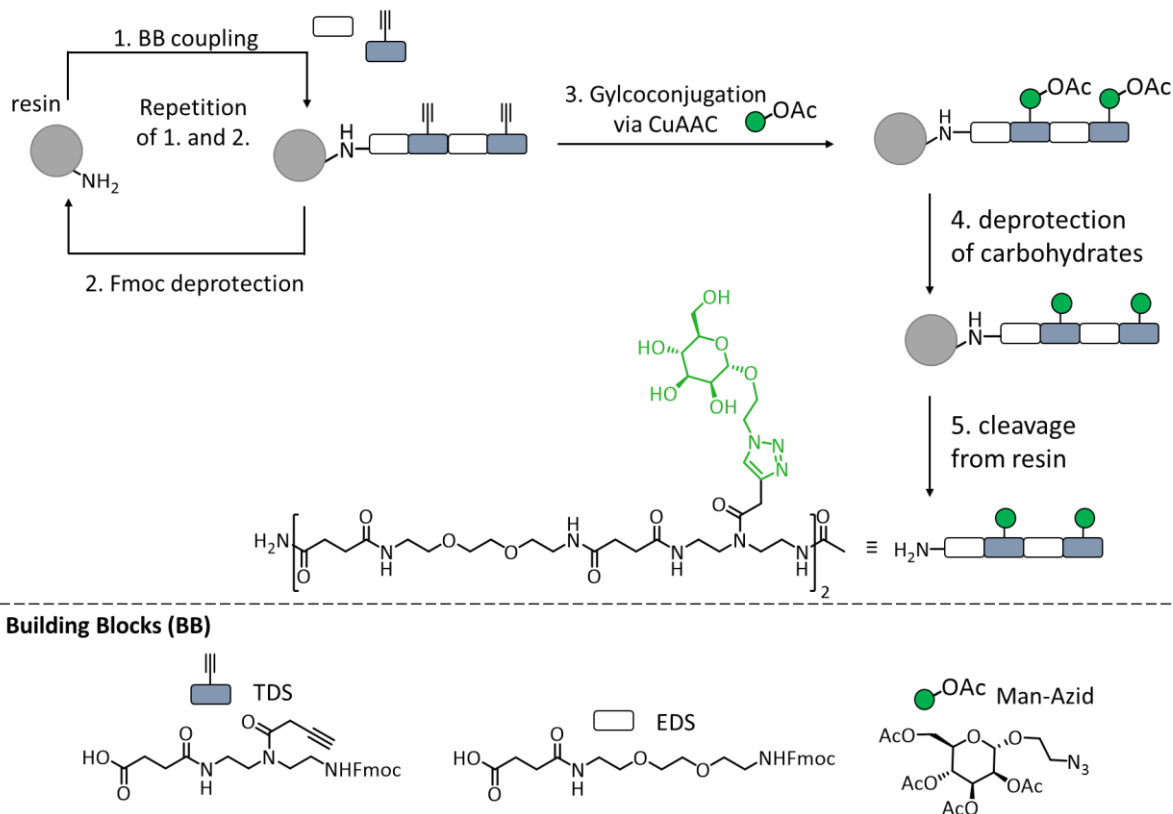

Figure 8: General mechanism of solid phase polymer synthesis (SPPoS) consisting of repetitive coupling and repetition steps followed by Cu-click reaction for functionalization with carbohydrate azides and cleavage from the resin.

Overall, solid phase synthesis allows for straightforward variation of different parameters such as number and spacing of carbohydrate ligands, hydrophilic or hydrophobic units within the scaffold, the overall length as well as architecture (e.g., linear, branched or cyclic) of the scaffold. [73] [111] [117] [118] Another advantage is the possible automation of the method e.g., by a standard peptide synthesizer. [119] The preparation of high molecular weight glycomacromolecules, however, is limited – similar to the synthesis of long chain peptides in solid phase, e.g., due to aggregation phenomena and limited diffusion of bbs to the reactive chain end. [87] [120] Therefore, strategies were developed to combine classic polymer synthesis approaches with SPPoS and derive sequence-controlled glycopolymers. [92] [121] The following sub-chapter will introduce the synthesis of brush glycopolymers.

2.2 Synthesis of brush glycopolymers

Glycopolymers are typically composed of a synthetic backbone with pendant carbohydrate side chains. They can be derived by a variety of synthetic methods, e.g. from glycomonomers or through conjugation of carbohydrates onto a polymeric scaffold. [17] [122] [123] A special subclass of glycopolymers are branched or brush-like glycopolymers and refers to polymers with a high density of side chains. The architecture of glycopolymers has been shown to affect their binding to carbohydrate receptors such as lectins. For example, Shamout et al. synthesised a series of brush-like glycooligomers by varying the degree of branching and the number of carbohydrate ligands per branch and studied their binding towards the C-type lectins Concanavalin A (ConA) , DC-SIGN and MBL. [92] Zheng et al. prepared highly branched glycopolymers and showed that most remarkable bacterial binding and inhibition abilities compared to the two linear analogues. [124] Li et al. proposed the synthesis of brush glycopolymers with an anti-adhesive interface of proteins on a gold substrate which can be used to study the adhesion and anti-adhesion effects of proteins ConA and bovine serum albumin (BSA). [125] The synthesis of brush glycopolymers can be differentiated by using "grafting through" [126], "grafting from" [127] and "grafting onto". [128]. (see Figure 9)
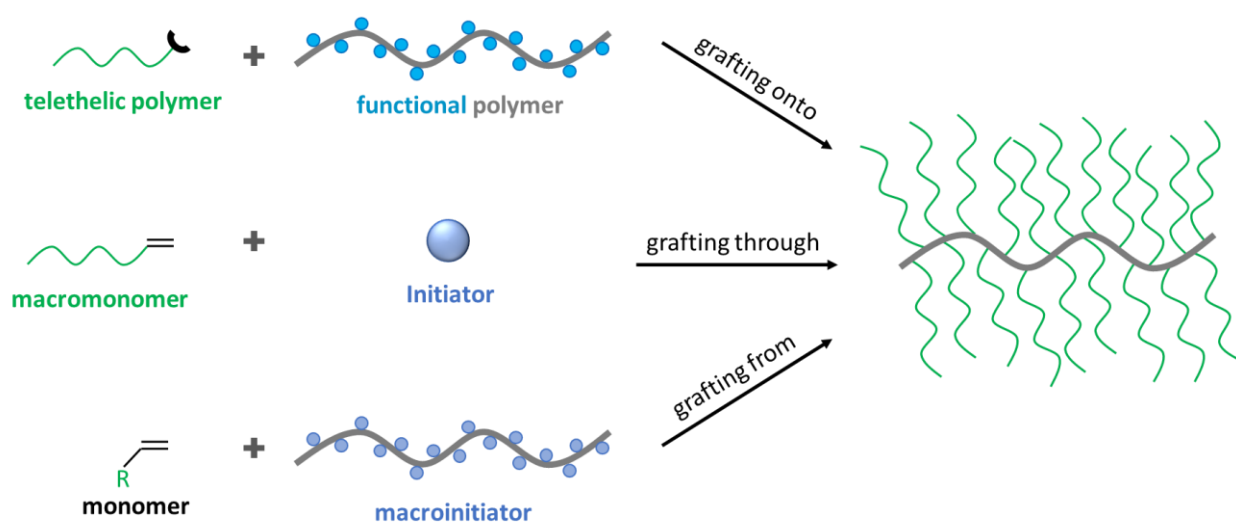

Figure 9: General synthetic methos for the preparation of brush glyocpolymers: "Grafting-onto" reactions require the coupling of a tele-functional polymer to a backbone polymer with functional side groups. "Grafting-through" is achieved by polymerization of macromonomers. In the "grafting-from" process, the precursor of the backbone polymer is prepared by using

monomer units that include functionalities that can initiate the polymerization of a second monomer. Adapted from [129]

The "grafting-onto" method allows the incorporation of side chains which are first synthesized e.g., by polymerization and carry one specific end group. This can then be used to attach these side chains to another polymer scaffold carrying (ideally in each repeating unit) functional groups that allow for covalent attachment via the end group of the side chain polymers. functional groups by chemical modification of the polymer backbone. [130] [131] [132] This leads to well-defined brush polymers as the branching sides are prepared separately and subsequently conjugated to the backbone by exchanging the functional groups for side chains. The reaction is usually very rapid, but full incorporation of the side groups into the backbone is often not possible because of steric hindrance. In addition, the polymer backbone has to go from an entangled to an elongated conformation when the side chains are incorporated, which makes the reaction entropically less favourable. [133] The molecular weight of the final brush polymer can be determined using the known molecular weights of the backbone and branches to calculate the mean number of branches. [134]

The "grafting-through" approach, which calls for an initiator and a macromonomer with a polymerizable end group, is the most straightforward method for producing a brush polymer. [135] Controlled polymerization methods make it simple to create well-defined macromonomers, but the resulting brush polymer is frequently short and has a wide molecular weight range. [136] To avoid this, the macromonomer can be readily copolymerized with another comonomer that is not sterically difficult, which reduces the amount of branching and dispersity while allowing for longer chain lengths. [137]

The "grafting-from" method is based on post-polymerization between a monomer carrying a functional end group and a macroinitiator, i.e. a polymer scaffold previously functionalized with several initiators. [138] [139] The monomers are then attached to the polymer scaffold by further polymerisation, resulting in repeating side chains, whereby the number of initiators determines the number of side chains attached. Compared to the amount of initiators on the backbone, this approach has the advantage that the length of the polymer grafting can be well controlled and the grafting density of the polymer ethers is high. [140]

2.3 Synthesis of glyconanoparticles

Carbohydrate decorated nanoparticles, also called glyconanoparticles (GNP) already find successful application in biomedicine, [141] [142] biosensing [143] and in detection and early diagnosis of cancer. [144] [145] GNPs combine two features: first, they provide distinctive qualities as a result of the core material, such as gold, silver or magnetic. On the other hand due to their high surface-to-volume ratio GNPs allow the multivalent presentation of carbohydrates and overcome the weak interaction of one carbohydrate to a protein. [146] Furthermore, the carbohydrate-lectin interaction is significantly influenced by the size and shape of the GNPs and the density of the carbohydrates conjugated on the surface of the particle. Whereas, larger-sized GNPs have flatter surfaces [147] which can be useful when examining the interactions between carbohydrates and the target organism, also the shape (rods or spheres) can affect the these interactions. [148] Furthermore, if the density of the carbohydrates on the surface of the particles is too high, the accessibility of the particles will be impaired. However, this can be remedied by using long and flexible tethers. [149] [150] In general, GNPs are divided into three different classes depending on their nature and composition: gold and silver GNPs, semiconductor glyco-quantum dots (glyco-QD) and magnetic GNPs (see Figure 10). Due to their relevance to this thesis, glyco-quantum dots and Janus particles are discussed in this chapter in more detail.
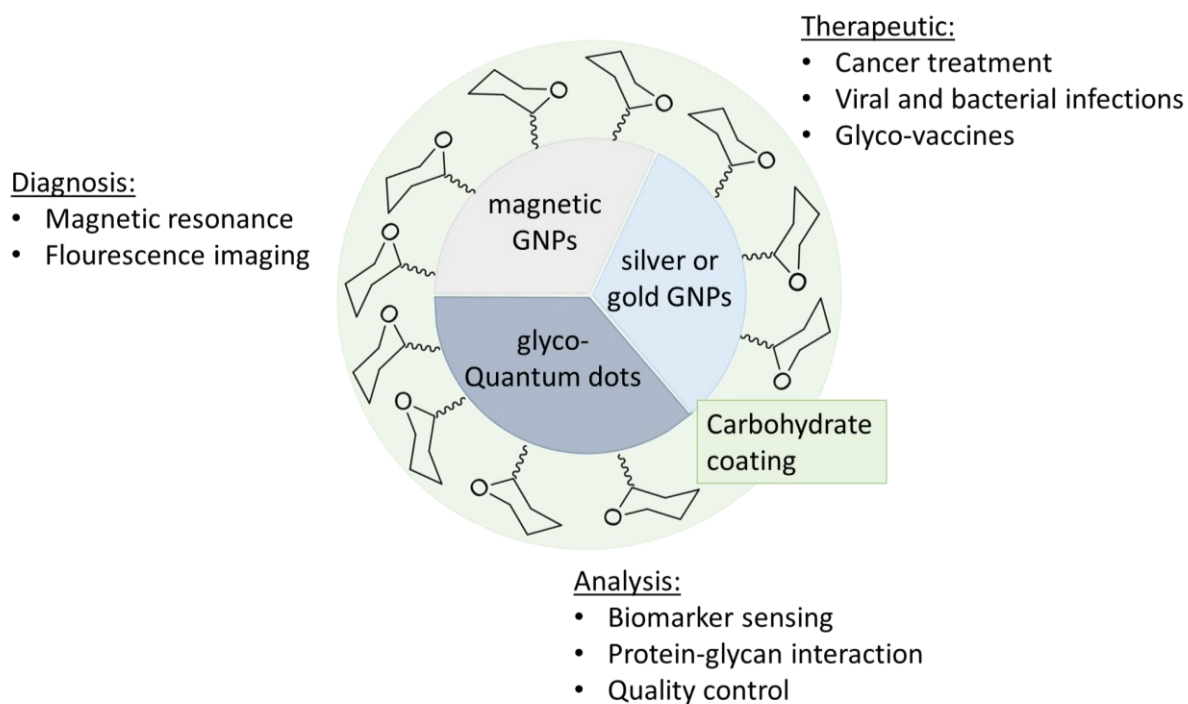
Figure 10: Three categories of glyconanoparticles divided in gold or silver GNPs, magnetic GNPs and glyco-quantum dots and their main application fields: diagnosis, therapeutic and analysis. Adapted from [151]

Quantum dots (QDs) are fluorescent semiconductor nanocrystals with unique size-dependent optical properties and can be used as fluorescent probes in biological systems due to their low cytotoxicity. [152] Their size can vary widely depending on the synthesis process and is in the range of 2 – 50 nm. [153] QDs are characterized by very high quantum yield and a high chemical stability at acidic conditions, so they can be used as biomarker for labeling cells or monitoring cells for optical imaging in in vivo studies. [154] [155] [156]

A variety of glyco-QDs has been synthesized e.g. presenting different carbohydrate motifs such as mannose and lactose. [157] [158] One area of application for such materials is their use in targeting and staining selected cell types, as will also be explored in this thesis. Especially tumor cells are known to overexpress specific carbohydrate receptors such as galectins or mannan-binding lectins. [159] [160] For example, in a recent study, Guo et al. produced mannose functionalized CdSe/ZnS-QDs and investigated the interaction to mannose recognizing lectin DC-SIGN. Therefore, mono- and divalent mannose ligands carrying thiol end groups were synthesized and conjugated onto the particle surface by using cap-exchange method. [157] This method allows the exchange of zinc-composed QDs with thiol functional ligands, resulting in compact QDs, which are better suited to Förster resonance energy transfer (FRET)-based applications. [161] [162] [163] This study showed an increase of affinity by multivalent presentation of the mannose units was detected by FRET. In another study, QDs decorated with carboxylic acid were functionalized with glucose after activation by carbodiimide chemistry. Glucose decorated QDs were successfully used for *in vivo* detection of breast cancer cells (MCF-7). [164] In a further example, glyco-QDs were prepared by coupling QD-streptavidin with biotin-functionalized lactose carrying glycopolymers. A through fluorescence staining performed by confocal microscopy the interaction between lactose glycopolymers and Ricinus communis agglutinin immobilized agarose beads was conformed. [165]

Janus particles (JPs) are particles that carry two distinct surfaces on each half of the particle. The name derives from the Roman god with two faces looking in opposite directions, symbolizing beginning and end, past and future. [166] JPs were first proposed by Pierre-Gielles

de Gennes in his Nobel Prize lecture in 1991. [167] Later, de Gennes and his collaborators introduced amphiphilic glass spheres with two hemispheres with polar and nonpolar properties. Janus particles have since gained increasing interest due to their unique architecture and the capability to combine different functions and properties in one system. [168] [169] [170]

JPs can be prepared from different materials and can be grouzped into hard (inorganic) [171], soft (organic or polymeric) [172], and hybrid (organic/inorganic) [173] JPs. Depending on the preparation process, their architecture and size can vary significantly in the nm and μm range. For example, spherical, hamburger, or dumbbell-shaped JPs can be prepared by phase separation [174] [175] [176] while snowman-shaped but also spherical JPs can be prepared by immobilization. [177] Raspberry-shaped JPs can be prepared by self-assembly or even emulsion polymerization. [178] [179]

JPs have been extensively studied for their use in biomedicine e.g., for drug delivery, cancer therapy, bio-imaging, and bio-sensing. One use for such materials is to target and stain particular cell types and bacteria, which will also be addressed in this thesis. In a recent study, Feng et al. fabricated magnetic JPs loaded with poly(lactic-co-glycolic acid) (PLGA) and Rhodamine B. While PLGA was used to destroy cancer cells, the magnetic core (Fe_3O_4) was used for targeting and Rhodamine B for fluorescence tracking. These particles showed high specificity and toxicity against breast cancer cells MDA-MB-231 compared with non-cancer cells, mouse embryonic fibroblasts (NIH-3 T3). [180] More recently, silica-based JPs with a hydrophobic polydopamine side and a hydrophilic perfluorodecanthiol side were prepared by Mo et al. Due to the hydrophilic modification, the particles were shown to possess photothermal antibacterial activity in addition to enhanced water retention, which could enable potential applications in the biomedical field. [181] However, to the best of my knowledge, there currently exist no examples for glyco-functionalized JPs.

3. Aims and Outlines

This thesis establishes a bottom-up approach towards different types of glycomimetics with a special focus on branched and brush glycomimetics so that they share structural features but also allow for their controlled yet flexible variation. As main tool, solid phase polymer synthesis as previously established by the Hartmann et al. will be used.

First, glycomacromolecules will be prepared using a new building block, the so-called TT building block, that allows for the attachment of three carbohydrate motifs in close proximity resembling the natural presentation e.g., in branched oligosaccharides. This motif also resembles an umbrella-like structure. The umbrella motif is the common denominator of the glycomimetics of this thesis and umbrella glycomacromolecules will next be conjugated to different scaffolds such as polymers yielding brush glycopolymers and particles resulting glycofunctionalized carbon-based-nanoparticles (glyco-CNPs) as well as glycofunctionalized Janus particles (glyco-Janus Particles). (see Figure 11)

In the second part, the different glycomimetics will be investigated for their binding properties and potential applications in biomedicine. Special focus is devoted to testing the umbrella glycomacromolecules and their conjugates for their binding to Langerin and DC-SIGN. Based on previous studies from the Hartmann lab, it is expected that the close presentation of three mannose ligands as is realized through the TT building block should be particularly beneficial for binding and thus potentially targeting Langerin as receptor. In order to test for the binding strength as well as potential selectivity, different binding assays e.g., by SPR or ^{19}F- NMR will be performed. In addition, glycomacromolecules will be formulated into liposomes and their binding to Langerin and DC-SIGN expressed cells will be investigated. Similarly, umbrella glycopolymers will be investigated for their binding to Langerin as isolated receptor as well as on cell surfaces. Umbrella glyconanoparticles will be explored in more applied tests, with the Janus type particles being used as inhibitors of bacterial adhesion and the carbon dots being studied for their cell uptake by different types of tumor cells. (see Figure 11)
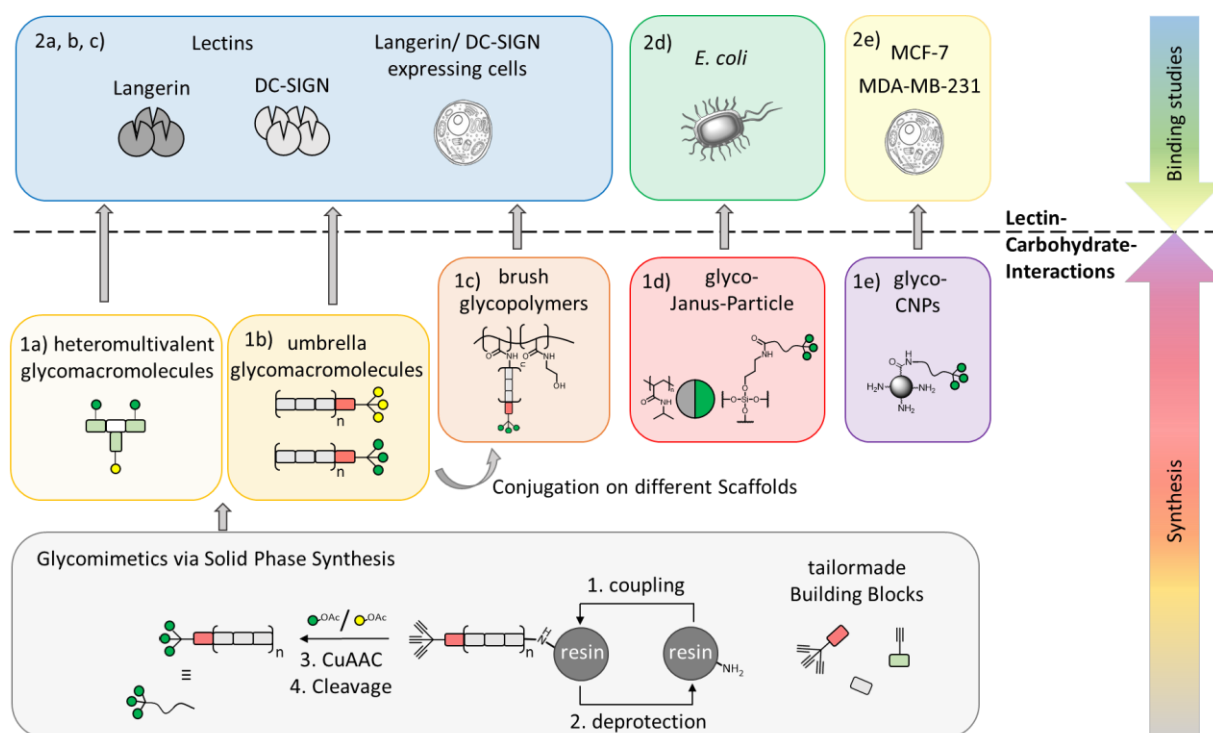
Figure 1: Overview of the topics discussed in this dissertation. Starting from the solid phase synthesis (grey) of umbrella-like and heteromultivalent glycooligomers (dark yellow) followed by the conjugation on different scaffolds to gain brush-glycopolymers (orange), glyco-Janus particles (red) and glyco-CNPs (purple) to increase the multivalency. These gylcomimetics were studied towards the lectins Langerin and DC-SIGN and lectin expressing cells (blue), *E. coli* (green) and different breast cancer cells (yellow).

Overall, the work is divided into two broad areas, synthesis and binding studies, to investigate the interactions between lectins and carbohydrates (see Figure 11):

1. a) synthesis of heteromultivalent glycomacromolecules

   b) synthesis of umbrella glycomacromolecules

   c) conjugation of umbrella glycomacromolecules onto polymer scaffolds yielding in brush glycopolymers

   d) conjugation of umbrella glycomacromolecules onto particle scaffolds yielding in glyco-Janus Particles (in collaboration with Dr. Synytska, University Bayreuth)

   e) conjugation of umbrella glycomacromolecules onto particle scaffolds yielding in glyco-CNPs (in collaboration with Prof. Heinzel, HHU)

2. investigation of the binding properties of umbrella glycomacromolecules and their conjugates, specifically:

a) heteromultivalent glycomacromolecules towards Langerin and DC-SIGN via SPR and ^{19}F- NMR Assay and Langerin and DC-SIGN expressing cells by using flow cytometry (in collaboration with Prof. Rademacher, University Vienna)

b) umbrella glycomacromolecules towards Langerin and DC-SIGN via SPR and ^{19}F- NMR Assay and Langerin and DC-SIGN expressing cells by using flow cytometry (in collaboration with Prof. Rademacher, University Vienna)

c) brush glycopolymers towards Langerin using ^{19}F- NMR Assay and their cellular uptake towards Langerin expressed HEK-291 cells (in collaboration with Prof. Rademacher, University Vienna and Prof. Thiel, Aarhus University)

d) glyco-Janus particles investigation towards adhesion behavior of *E. coli* (in collaboration with Dr. Schmidt, HHU)

e) glyco-CNPs cell uptake experiments towards MCF-7 and MDA-MB-231 breast cancer cells (in collaboration with Prof. Heinzel, HHU)

4. Results

4.1 One, two, three – heteromultivalent ligands with controlled variation of Mannose ligands targeting Langerin

Serap Üclü, Yunzhan Ning, Iris Bermejo, Nowras Rahhal, Janis Langer, Christoph Rademacher and Laura Hartmann*

Publication Draft

Own Contribution:

Collaborative project design. Synthesis and purification of building blocks for solid phase polymer synthesis and of heteromultivalent and galactose-containing glycooligomers. Measurement and evaluation of all LC-MS experiments and evaluation of all NMR and UHR spectra. Design and performance of Inhibition-Competition Assay via SPR as well as evaluation and interpretation of the IC50 values. Writing of the first publication draft.

One, two, three – heteromultivalent ligands with controlled valency targeting Langerin and DC-SIGN

Serap Üclü[a], Yunzhan Ning[b], Iris Bermejo[b], Nowras Rahhal[b], Hengxi Zhang[b], Christoph Rademacher[b] and Laura Hartmann[a,c]*

[a] Department of Macromolecular Chemistry, Heinrich-Heine University, Universitätsstr. 1, 40225 Düsseldorf, Germany

[b] Department of Pharmaceutical Sciences, University of Vienna, Josef-Holaubek-Platz 2, 1090 Wien, Austria, e-mail: christoph.rademacher@univie.ac.at

[c] Institute for Macromolecular Chemistry, University Freiburg, Stefan-Meier-Str. 31, 79104 Freiburg i.Br., Germany

* Corresponding author: laura.hartmann@makro.uni-freiburg.de

Keywords: Langerin, DC-SIGN, glycomimetic, heteromultivalency, solid phase polymer synthesis

Abstract:

Langerin and DC-SIGN are important receptors of the immune system. They are important for immune regulation and the specific targeting of these c-type lectins plays a key role, e.g., in the development of vaccines against cancer. Since both receptors recognize terminal Mannose (Man) units, Langerin with three and DC-SIGN with four Man-recognizing domains, they cannot be selectively targeted based on the carbohydrate unit alone. Rather, in the design of Man-conjugates as glycomimetics, the effect of the scaffold, e.g., its valency or size, has been explored to derive ligands that can potentially target either DC-SIGN or Langerin. Previously, a series of trimeric ligands was developed based on a receptor guided design presenting three Man ligands on trivalent oligomeric scaffolds of different sizes. The smallest ligand showed the highest avidity toward Langerin and it was hypothesized that this ligand is kinetically trapped between the Man-binding sites of the receptor.

Here now, this glycomimetic is derived as a series of heteromultivalent structures systematically exchanging Man towards non-binding galactose (Gal) ligands. These ligands are then studied by SPR and ^{19}F-R$_2$-NMR quantifying their avidity towards both, Langerin and DC-SIGN. The binding studies shows a linear decrease in IC$_{50}$ values with a decrease in the number of Man units from 3 to 0, indicating that statistical rebinding is preferred as a binding mode. The comparison of binding between the lectins shows higher binding to DC-SIGN, which is rationalized by the additional CRD and thus higher statistical probability for DC-SIGN binding. In addition, ligands are conjugated to liposomes and tested for cellular uptake on Langerin- and DC-SIGN overexpressing cells. The comparison between the cells shows an increased uptake for the liposome conjugated with the trivalent ligand on DC-SIGN-expressing cells.

Introduction

Langerin and DC-SIGN (Dendritic Cell-Specific Intercellular adhesion molecule-3-Grabbing Non-integrin) are C-type lectin receptors (CLRs) of the immune system known to bind Man glycans.[1-5] Both receptors are known to play a role in the immune response where they act as target receptors e.g., for eliciting antiviral and antitumor responses.[6-10] Activation of the receptors can lead to uptake of the pathogen, followed by digestion and presentation of antigens inducing innate immunity.[11,12] Based on this mechanism, both, Langerin and DC-SIGN

have been studied as targets for cell uptake e.g. in the development of drug delivery platforms.[13-17] Besides these commonalities, there are also key differences for these two CLRs[18]: Firstly, they are expressed on different dendritic cell (DC) subgroups, while DC-SIGN is highly expressed on the surface of DC[19], Langerin is expressed by the DC subgroup Langerhans cells (LCs)[20]. Moreover, they have different molecular orientations, with Langerin forming a trimer in the extracellular neck region through a coiled-coil structure, leading to a rigid position in the membrane. In contrast, DC-SIGN forms oligomers through its stem region, giving a higher degree of flexibility to the carbohydrate recognition domains (CRDs) that facilitate interaction with its ligands[21], forming a tetramer[22]. Both receptors target different intracellular processing and organelles. An interesting feature of Langerin is its association with Birbeck granules (BGs), which are rod-like structures and subdomains of the endosomal recycling compartment found only in LCs.[23,24] Whereas the presence of Langerin is crucial for the formation of BG.[25] Indeed, all these characteristics of these proteins indicate that these CLRs mediate different biological responses.

In order to achieve targeting of Langerin and DC-SIGN, so-called glycomimetic ligands have been designed using different approaches.[26-29] Rademacher et al. have used fragment-based screening by NMR to develop selective Langerin ligands addressing CRDs.[30] Both, Langerin and DC-SIGN are multivalent receptors presenting three and four CRDs, respectively (Figure 1). Another approach to develop glycomimetic ligands therefore makes use of combining multiple Man motifs on a synthetic scaffold deriving multivalent ligands.[31-33] Such multivalent presentation can enable increased avidity e.g., through increased statistical probability of ligand-receptor binding as well as selectivity e.g., based on the appropriate spatial presentation of the binding motifs matching the CRDs of the target receptor.

In a previous study we showed that by designing a trivalent branched scaffold a glycomimetic ligand with high affinity for Langerin was obtained (Figure 1).[34] Here, the spacing of the three Man units was varied in a controlled manner and it was observed that the structure with the shortest spacing between the Man units showed the highest binding affinity. This was surprising because this structure should not be able to occupy multiple binding pockets simultaneously. Our model proposes that the ligand sits between the binding pockets and leads to an apparent increase in affinity through statistical rebinding processes.

To investigate this model in more detail, in this study we successively exchange binding Man motifs in the trivalent ligand for non-binding galactose (Gal) motifs stepwise decreasing the ligand valency from three to zero (Figure 1). Based on our model of statistical rebinding, we would expect a decrease in binding when replacing binding through non-binding motifs. Furthermore, we study the effect of the valency on potential receptor selectivity by studying both DC-SIGN with four and Langerin with three CRDs, respectively. Binding to Langerin as well as DC SIGN is quantified by surface plasmon resonance (SPR) inhibition/competition assay and ^{19}F-NMR displacement assay. Furthermore, ligands are conjugated to liposomes and studied for Langerin and DC-SIGN targeting on cells demonstrating the potential of glycomimetic ligands for cell targeting and drug delivery.
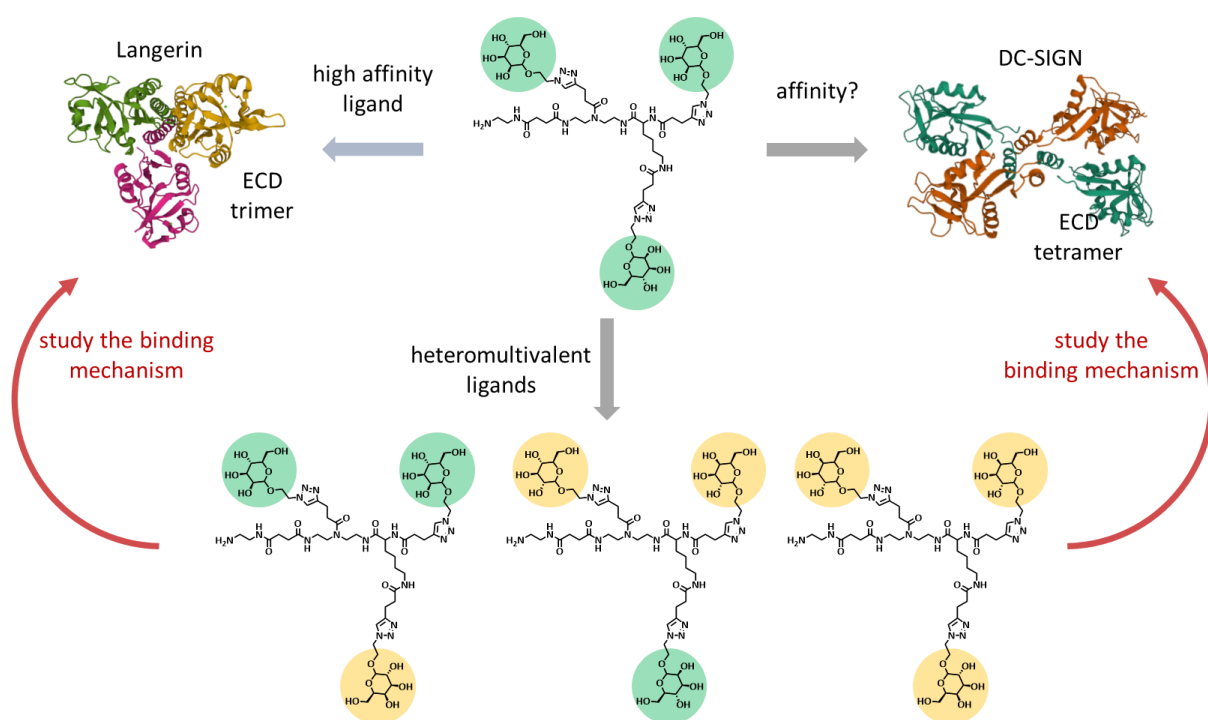
Figure 1: The trivalent mannose-containing glycooligomer exhibited high affinity for Langerin on the basis of statistical rebinding.[34] To investigate the binding mechanism heteromultivalent ligands were synthesized by reducing the number of binding Man units (green) towards non-binding Gal units (yellow) and tested towards trimeric Langerin and tetrameric DC-SIGN.

Methods

Materials: Aceton (≥ 99.8%), triethylamine (analytical grade), toluol (for HPLC) was purchased from Fischer Scientific. Succinic anhydride (≥ 99.0%) was purchased from Carbolution Chemicals. Diethyl ether (with BHT as inhibitor, ≥ 99.8%), triisopropylsilane (TIPS) (98%), (+)-sodium-L-ascorbate (≥99.0%), chloroform-*d* (99,8 atom % D), deuteriumoxid-*d₂* (99,8 atom % D), dimethylsulfoxid-*d₆* (99,8 atom % D), were purchased from Sigma-Aldrich. *N,N*-Diisopropylethylamine (DIPEA) (≥ 99%), kaliumhydroxide (≥ 85%) was purchased from Carl Roth. Methanol (100%), ethylacetate (>99.9%), n-hexan (≥99.8%) and acetic anhydride (99.7%) were purchased from VWR BDH Prolabo Chemicals. Dimethylformamide (DMF) (99.8%, for peptide synthesis), *tert*-butanol (≥ 99.0%), piperidine (99%), sodium methoxide (97%), sodium diethyldithiocarbamate (99%), tritylchloride and copper (II)sulfate (98%) were purchased from Acros Organics. Dichloromethane (DCM) (99.99%), Triethylsilan (≥ 98,0 %), trifluoroacetic acid (≥ 99,0 %), 9-fluorenylmethyl chloroformate (Fmoc-Cl) were purchased from Fluorochem UK. Benzotriazole-1-yl-oxy-tris-pyrrolidino-phosphonium hexafluorophosphat (PyBOP) were purchased from Iris Biotech GmbH. The anion resin (AG1-X8, quarternary ammonium, 100-200 mesh, acetate form) was purchased from BioRad. TentaGel® resin were purchased from Rapp Polymere. Methyl-α-D-mannopyranoside (>99%), 1-ethyl-3-(3-dimethylaminopropyl)carbodiimide hydrochloride (EDC), N-hydroxysuccinimide (NHS), 10 mM sodium acetate pH 4.0, 1.0 M ethanolamine-HCl pH 8.5, HBS-P⁺ buffer was purchased from Cytiva. Calcium chloride, Glycin, Sodium hydroxide TritonX100 was purchased from Sigma Aldrich. Diethylenetriamine was purchased from Merk (>98%), di-tert-butyldicarbonat (≥99,0 %) was purchased from Novabiochem. Ethanol (>99.9%). was purchased from Chemsolute. 2,2-(ethylenedioxy)bis(ethylamine) was obtained from TCI Europe. Citric acid, anhydrous; 4-pentynoic acid were purchased from Alfa Aesar (>99.5%).

Synthesis: The synthesis of following building blocks TDS[43], Man-N₃[44] and Gal-N₃[45] were proceeded according to literature.

Solid phase polymer synthesis of the glycooligomer: Glycooligomers were generated by repeatedly coupling and deprotecting the building units on solid support to examine the binding toward Langerin and DC-SIGN. Each time, the reactions were conducted in Multisynthech GmbH polypropylene syringe reactors with a polyethylene frit and a Luer stopper. TentaGel® SRAM resin was employed as the solid support and pre-functionalized with

ethylenediamine. The batch size for each glycooligomer was 0.1 mmol, and the loading was 0.20 mmol/g.In order to produce a branched glycooligomer, the functional building blocks PA and TDS were combined with Fmoc-Lys(Boc)-OH, which was chosen as the branching point due to its orthogonal protective groups.

Coupling and Fmoc-deprotection of the building blocks: First the resin was first swollen twice for 15 min in DCM and then washed three times with DMF. The coupling steps of TDS, Fmoc-Lys(Boc)-OH and PA were performed by shaking for 1 h with a mixture of 5 equivalents of the building block, 5 equivalents of PyBOP and 10 equivalents of DIPEA in DMF followed by washing steps ten times with DMF. After each coupling, the resin was shaken with a solution of 25 Vol% piperidine in DMF for 15 min and then washed three times with DMF. This washing step was repeated two times and then washed ten times with DMF.

Boc-deprotection of Fmoc-Lys(Boc)-OH: The resin was shaken for 5 min in a solution of 4 M HCl in dioxane. Afterwards the syringe was emptied and shaken in Boc-deprotection solution for an additional 25 minutes. The resin was then washed three times with dioxane, three times alternating with DCM and iso-propyl alcohol and remaining HCl was neutralized twice for 10 minutes with a solution of 10 % DIPEA in DCM and finally ten times with DMF.

Copper(I)-catalyzed alkyne-azide cycloaddition (CuAAC): The glycoconjugation to the glycooligomer backbone was carried out via CuAAC. For this, 2,5 equivalents of (2-azidoethyl)-2,3,4,6-tetra-O-acetyl-α-D-mannopyranoside (Man-N$_3$ or Gal-N$_3$) per alkyne was dissolved in 2 ml DMF, of 30 mol% of sodium ascorbate and of 30 mol% of copper sulfate per alkyne was dissolved in 0,5 ml water. The copper sulfate solution was drawn up first, then the sugar solution, and finally the sodium ascorbate solution. The syringe was covered with aluminum foil and shaken overnight. The resin was then washed three times with a 23 mM solution of sodium diethyldithiocarbamate in DMF/H$_2$O (1:1, v/v), three times with DMF, and three times with DCM. The washing steps were repeated with the three solutions until no coloration of the wash solution was observed.

Deprotection of sugar-pyranoside and cleavage from the resin: After successful conjugation of sugar-pyranoside, the deprotection of hydroxyl groups was performed in 0.1 M NaOMe in methanol and shaken for 60 minutes. Then the syringe was washed ten times with methanol, ten times with DMF and ten times with DCM. The glycooligomer was cleaved from the resin by shaking with a solution of 35 vol % TFA, 60 vol % DCM, and 5 vol % TIPS. The solution was

precipitation in cold diethyl ether and the white precipitate was centrifuged off. The white solid was then dissolved in water and the product isolated by lyophilization.

Inhibition-Competition Experiments via SPR: The inhibition competition assay was performed by using SPR by using the binding wizard. First, a C1 chip was immobilized via EDC/NHS with BSA mannose by using the immobilization wizard. This resulted in an immobilization level of 1125 RU and the reference cell immobilized with ethanolamine resulted in an immobilization level of 17 RU. For the inhibition competition measurements, a fixed concentration of Langerin (4 µM) or DC-SIGN (0.5 µM) was tested with each glycooligomer in a concentration range of 3.125 - 800 µM. For this purpose, a 92 µM stock solution of Langerin (20 µM for DC-SIGN) and a solution of each glycooligomer were diluted in running buffer (HBS-P$^+$ buffer with 5 mM CaCl$_2$) to a final concentration of 4 µM of Langerin (0,5 µM for DC-SIGN). The incubation time was set at 5 min before measurement. As a reference, a solution of protein without glycooligomer was measured and denoted as 0 µM. The multi-cycle run with a flow rate of 15 µl/min, an association time of 240 s and a dissociations time of 120 s was used. The regeneration was carried out by using a 0.2 M methyl-α-D-mannopyranoside in water was injected for 60 s with a flow rate of 5 µl/min. The SPR studies were performed on two different C1-Chips. The first C1-Chip had and immobilization level of 1125 RU on the measuring cell and 17 RU on the reference cell. The second C1 chip had an immobilization level of 998 RU on the measuring cell and 25 RU on the reference cell. Glycooligomers were measured 2 times on the first chip and once on the second chip.

Inhibition-Competition Experiments via ^{19}F-R2 NMR studies: ^{19}F-NMR and ^{19}F-R2-filtered NMR experiments were perfomred on a Brucker AV 500 MHz spectrometer at 298 K. Spectra were analyzed in MestReNova and data analysis was carried out with OriginPro. For each spectrum 128 scans were acquired in 5 mm sample tubes at sample volumes of 500 µl. Relaxation rates $R_{2,obs}$ were estimated with the CPMG pulse sequence, (see equation below). T represents the relaxation time and I_0 is the integral at a T value of 0 s. The relaxation delay d_1 was fixed to 2.0 s, the acquisition time t_{acq} to 0.8 s and the frequency of 180° pulses u_{CPMG} at 500 Hz.

$$I = I_0 e^{-R_{2,obs}T}$$

Because of the complex equilibrium and cooperativity effects that occur in competitive binding experiments with multivalent glycomimetics, IC_{50} values rather than K_I values were used to quantify affinities. IC_{50} values were obtained in competitive experiments with the reporter molecule at five competitor concentrations $[I]_T$.[3] Samples were made by serial dilution. The equation below was used to derive IC_{50} values and Hills factors p from $R_{2,obs}$ values in a two parameter fit. The standard errors were derived from the fitting procedures directly. $R_{2,max}$ denotes the relaxation rate of 100 mM reporter in presence of 25 µM receptor and in absence of competitor.

$$R_{2,obs} = R_{2,f} + \left(\frac{R_{2,max} - R_{2,f}}{1 + \left(\frac{IC_{50}}{[I]_T} \right)^p} \right)$$

Titration experiments with glycomimetics were carried out in presence of 10% DMSO, 10% D_2O, 5 mM $CaCl_2$, 25 mM Tris, 150 mM NaCl, at pH 7.8. TFA was used as an internal reference at a concentration of 100 µM. For ^{19}F R2-filtered NMR experiments, a 10 mM stock solution of the compound was heated in DMSO and sonicated to be completely dissolved.

Cell Binding Experiment: The human Raji cell line from hematopoietic origin was used for the binding assay of the formulated particles. DC-SIGN and human Langerin (hL) receptors were previously transfected with a lentiviral vector to the cells.[7]

Cells were cultured and incubated in round flat-bottom plastic culture dishes (Corning) at 37 °C and 5 % CO_2 (Cooling incubator KB series, Binder GmbH, Germany). For Raji suspension cells, Roswell Park Memorial Institute Medium (RPMI) 1640 medium supplemented with 10 % V/V fetal calf serum (FCS) and 100 U/ml Penicillin-Streptomycin antibiotic mixtures (Thermofisher Scientific, Germany) were used. Cells were split and maintained between 0.5-3 Mio cells/ml. In addition cells were monitored with a light microscope.

To analyse receptor specificity of targeted liposomes, binding to Raji cells transfected with human Langerin and WT cells were analysed in flow cytometric via the coformulated liposomal dye Alexa647 (Invitrogen, ThermoFisher Scientific, USA) conjugated to DSPC-PEG. Experiments were conducted in duplicates in round bottom 96 well plates. Cells were seeded at a $4*10^5$ Raji cells per well and 10 µM of the liposomes were added in a total volume of 100 µl. Naked liposomes served as a negative control and hL liposomes as a positive control.

The plate was covered with a seal sheet, kept protected from light and incubated for 1h at 4 °C on ice. Afterward, the plate was centrifuged for 3 mins at 500 g, the supernatant was aspirated, and the cell pellets were resuspended in 150 μL Dulbecco's phosphate-buffered saline (DPBS) (Gibco TM, Thermo Fisher Scientific, USA). Subsequently, Alexa647 fluorescence intensity was measured using CytoFLEX S, Research Flow Cytometery (Beckman Coulter). Alexa674 Mean Fluorescence intensity (MFIs) were detected via the red laser (RL) 1-A. The obtained data was processed using the FlowJo and Origin software.

Results and Discussion

Synthesis of heteromultivalent glycooligomers

Synthesis of glycomimetic ligands is based on the so-called solid phase polymer synthesis giving access to monodisperse, sequence-defined oligo(amidoamines).[35-37] In short, stepwise assembly of tailor-made building blocks on a solid support making use of well-established Fmoc-coupling chemistry gives access to oligomeric scaffolds presenting functional handles at defined positions within the scaffold.[38,39] Commonly alkyne groups are introduced and can then be used for Cu-mediated conjugation of azide-functionalized carbohydrate motifs to derive oligomeric glycomimetics.[40] Different strategies are available to also achieve sequence-defined heteromultivalent glycomimetics presenting different carbohydrate motifs at selected positions within one glycooligomers ligand: A) Orthogonal conjugation chemistry can be applied e.g., combining azide-alkyne conjugation for one carbohydrate motif and Staudinger ligation for the second motif.[41] B) Carbohydrate conjugation can be performed on the building blocks deriving glycofunctionalized building blocks that can then be applied in the stepwise assembly of the glycooligomers.[42] C) Iterative elongation of the scaffold and carbohydrate conjugation can be performed where the immediately after introducing the functional handle in the scaffold, the carbohydrate motif is attached and only then further elongation of the scaffold is performed.[36]

In order to replace Man motifs by Gal in the previously established trivalent Langerin ligand, here we applied the iterative elongation and coupling strategy (C). This synthesis strategy is briefly described using the heteromultivalent glycooligomer Man2 with two Man and one Gal motif as an example (see Figure 2). In the first step, the building blocks TDS with one alkyne

side chain and Fmoc-Lys(Boc)-OH are successively conjugated to the resin, whereas the lysine building block is used as the branching point in the oligo(amidoamine) backbone through their orthogonal protecting groups Fmoc and Boc. After Fmoc cleavage, the scaffold was extended using the building block 4-pentynoic acid (PA). In the next step, the alkyne groups, presented by TDS and PA, were simultaneously functionalized with Man-azide via copper-catalyzed azide-alkyne cycloaddition (CuAAC). Then, after Boc deprotection of the lysine side chain and conjugation of PA, the non-binding sugar Gal-azide was conjugated. After the deprotection of the sugar units, the heteromultivalent glycooligomer is cleaved from the resin. By the solid phase synthesis, a series of homo- and heteromultivalent trivalent glycooligomers Man3, Man2, Man1 and Man0 were produced, whereas the number at the end of the name indicates the number of Man-residues. (See Figure 2 and SI for analytical details) Thus, the glycooligomer Man3 carries three Man residues, Man2 carries two Man and one Gal residue, Man1 carries one Man and two Gal, and Man0 carries three Gal residues and no Man.
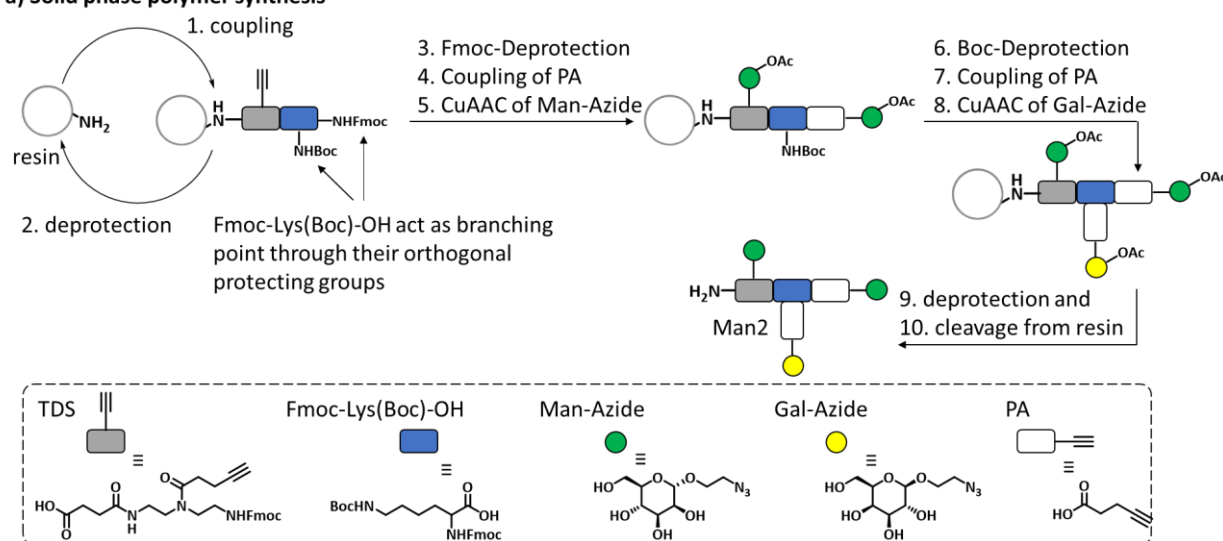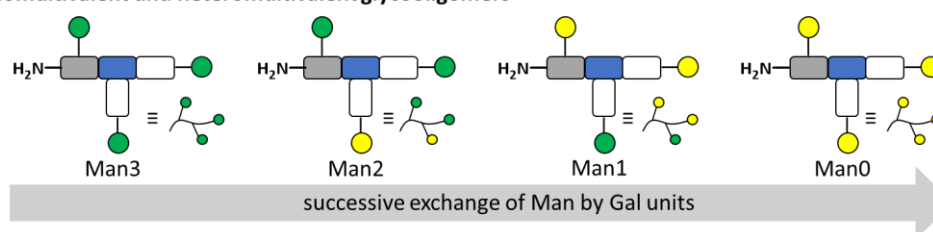
Figure 2: a) Example of solid phase polymer synthesis of heteromultivalent glycooligomer Man2, b)Series of synthesized homo- and heteromultivalent glycooligomers: Man3, Man2 Man1 and Man0.

Heteromultivalent glycooligomer binding to Langerin and DC-SIGN

To investigate the binding affinity of the heteromultivalent glycooligomers, an inhibition-competition assay allowing for direct comparison of binding towards Langerin and DC-SIGN was performed using surface plasmon resonance spectroscopy (SPR). The chip surface was functionalized with Man-conjugated bovine serum albumin (Man-BSA) to achieve high degrees of Man functionalization and thus high affinity surface for both, Langerin and DC-SIGN. Glycooligomers were then incubated in increasing concentrations with either of the proteins and binding towards the chip surface was measured. Glycooligomers bind to the proteins blocking CRDs therefore not available for interaction with the chip surface anymore and leading to a reduced binding in comparison to the free protein. This reduction in binding is proportional to the affinity of the ligand and can be expressed as the half maximum inhibitory concentration (IC_{50}) that is required to block 50% of the protein-chip binding (see SI for further details on SPR assay and Hill plots for IC_{50} evaluation) (see Figure 3).
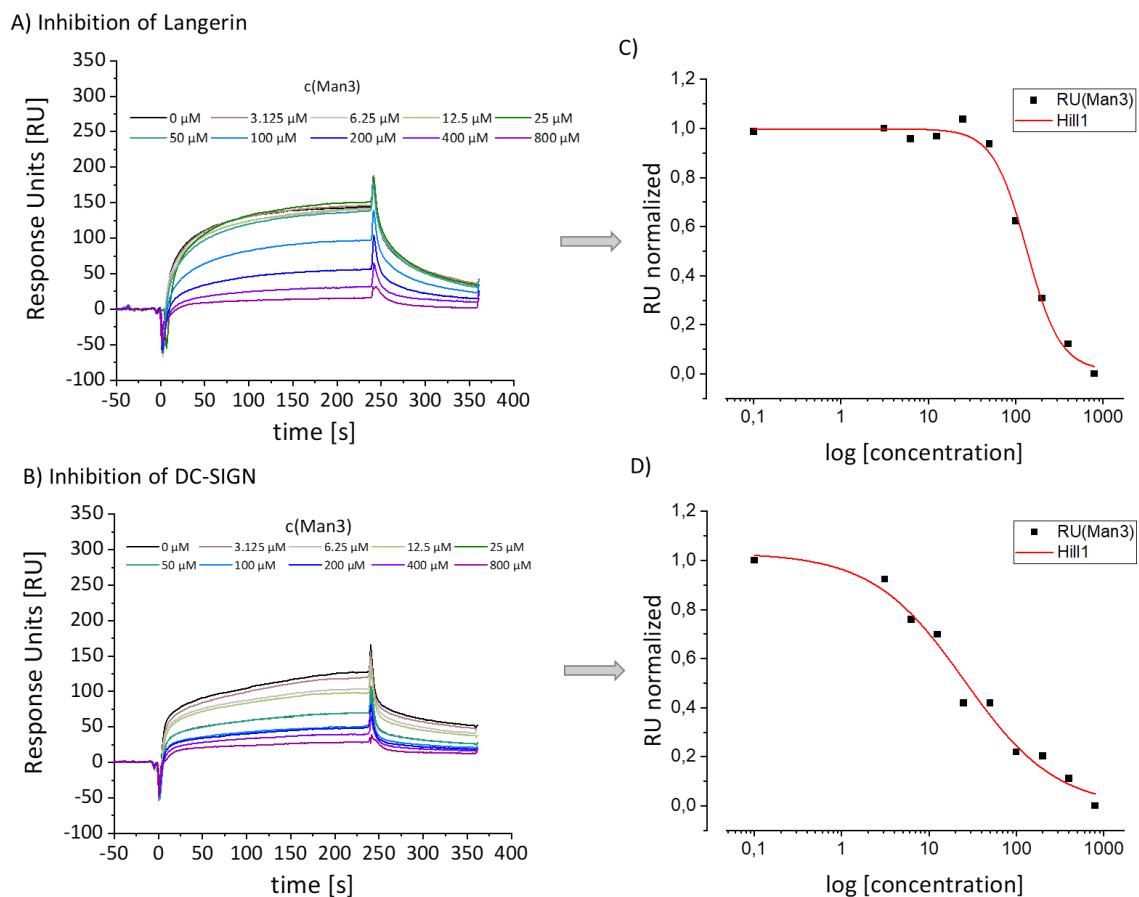
Figure 3: Exemplary binding curves for ligand Man3 and inhibition of Langerin (A) and DC-SIGN (B) as well as Hill plot evaluation to derive IC_{50} values (C, D).

First, the SPR study was performed on Langerin and shows that with increasing number of non-binding galactose units, the IC$_{50}$ value increases as the non-bound Langerin binds to the mannose functionalized chip surface and does not interact with the glycooligomer and indicates lower affinities (see Table 1). While no binding is seen for compounds Man0 with three non-binding galactose units, as expected, no binding is seen for Man1 with two galactose and one mannose unit either. Which is more expected to be due to the weak interaction of one mannose unit with the CRDs of the Langerin. A clear increase in binding affinity is seen starting at 2 mannose units for Man2 and Man3 with three binding mannose units shows the highest binding affinity to Langerin, which would indeed suggest a statistical effect of binding. Comparison to the previous study, also done with Man3 on Langerin, shows a much lower IC$_{50}$ value in the ^{19}F NMR assay with 44 µM and resulting in a higher affinity.[34] This is probably due to the assay setup, as the NMR assay is performed at lower temperature (4°C) and longer incubation time.

The comparison with DC-SIGN generally shows lower IC$_{50}$ values and hence higher affinities. (see Table 1) Since DC-SIGN is a lectin with four symmetrically located CRDs, the trivalent mannose-bearing Man3 has more opportunities to enter into a statistical rebinding effect, which would explain the higher affinities. Interestingly, it appears to be a linear trend, which further supports a statistical binding effect. Similar to Langerin, Man1 and Man0 show no binding to DC-SIGN.

Table 1: IC$_{50}$ values derived by SPR[a] towards Langerin and DC-SIGN and ^{19}F-NMR[b] assay towards Langerin. The standard deviation for IC$_{50}$ values determined by SPR is given by two independent experiments. The standard deviation for IC$_{50}$ values determined by SPR is given by three independent experiments

	Langerin IC$_{50}$ [µM][a]	DC-SIGN IC$_{50}$ [µM][a]	Langerin IC$_{50}$ [µM][b]
Man3	169 ± 32	18 ± 9	80 ± 13
Man2	256 ± 70	46 ± 3	295 ± 38
Man1	no binding	no binding	no binding
Man0	no binding	no binding	no binding

Heteromultivalent glycooligomers targeting Langerin and DC-SIGN on cells

To study cellular binding, the glycooligomers were first conjugated to a lipid and then formulated into glycoliposomes (see Figure 4 and method section for more details). Commercially available DSPE-PEG-NHS ester was used as the lipid, and reaction with the glycooligomer produced the lipid conjugate. For the conjugation the glycooligomers were dissolved in DMSO and a mixture of DIPEA and DSPE-PEG-NHS ester were added and was shaken overnight at 40 °C. After removal of the solvents, the lipid conjugates were purified by dialysis against water. After lyophilization, the products were analysed by ^{1}H-NMR to determine the coupling yield. The results are summarized in Supporting Information. For the formulation of the glycoliposomes, two solutions were mixed in a microfluidic device to produce liposomes. The organic phase contained the lipids in ethanol and an aqueous phase consisting of PBS. A syringe pump was loaded with two syringes, one containing the lipids dissolved in ethanol and the other containing the PBS. The pump was used to inject the two solutions into the inlets of the microfluidic chip via short tubes. The product solution collected at the outlet of the chip was collected. Finally, the collected samples were dialyzed overnight with x1000 volume of buffer, ensuring buffer exchange (PBS, pH 7.4) at least twice. Thus, the glycoliposomes were composed of molar ratios of 58 mol% DSPC, 37 mol% cholesterol, DSPE-PEG 4.75 mol% or DSPE-PEG-Ligand, and 0.25 mol% DSPE-PEG-Alexa647. The gylcoliposomes were characterized by DLS. The results are summarized in Supporting Information. The nomenclature for the glycooligomer functionalized liposomes is as followed: GL represents gylcoliposome followed by the name for the glycooligomer, e.g. GL-Man3 represents gylcoliposome functionalized with structure Man3.

Flow cytometry was performed to investigate cellular binding. (See Figure 4) For this purpose, Langerin (Langerin+ cells) and DC-SIGN expressing Raji cells (DC-SIGN+ cells) were used. Raji wild-type (Raji-WT) cells served as a control cell line. Human Langerin (hL) was used as a positive control for Langerin-expressing Raji cells, reflecting maximal binding of Langerin-expressing cells. The Man3-conjugated liposome GL-Man3 shows higher uptake for DC-SIGN+ cells. This is consistent with the higher apparent affinity determined by the inhibition competition assay. A comparison of the binding of GL-Man3 to Langerin+ cells shows lower uptake. However, positive control hL clearly shows maximal binding of GL-Man3 to Langerin+ cells. This could also explain the lower affinity of Man3 for Langerin measured by the inhibition

competition assay. However, it should be noted that GL-Man3 binds to both Langerin+ cells and the positive control hL. Surprisingly, comparison of WT cells with the trivalent ligand shows only slightly increased binding to Langerin+ cells. According to the findings of the inhibition competition experiment, binding of the divalent ligand is also anticipated, even though it will be decreased. Surprisingly, binding for the divalent ligand GL-Man2 is not observed for either Langerin+ or DC-SIGN+ cells. The glycoliposomes GL-Man1 and GL-Man0 also show no binding to cells, whereby GL-Man0 with three galactose units per ligand should not show binding as expected and therefore serves as a negative control. However, it should be noted that total cellular uptake is low and uptake of the trivalent ligand targeting Langerin is comparable to the positive control hL and that cellular uptake of WT cells also appears to be increased. Overall, cellular targeting of the receptors is possible. Differences in avidity may result in differential cellular uptake by ligand design and protein binding studies.
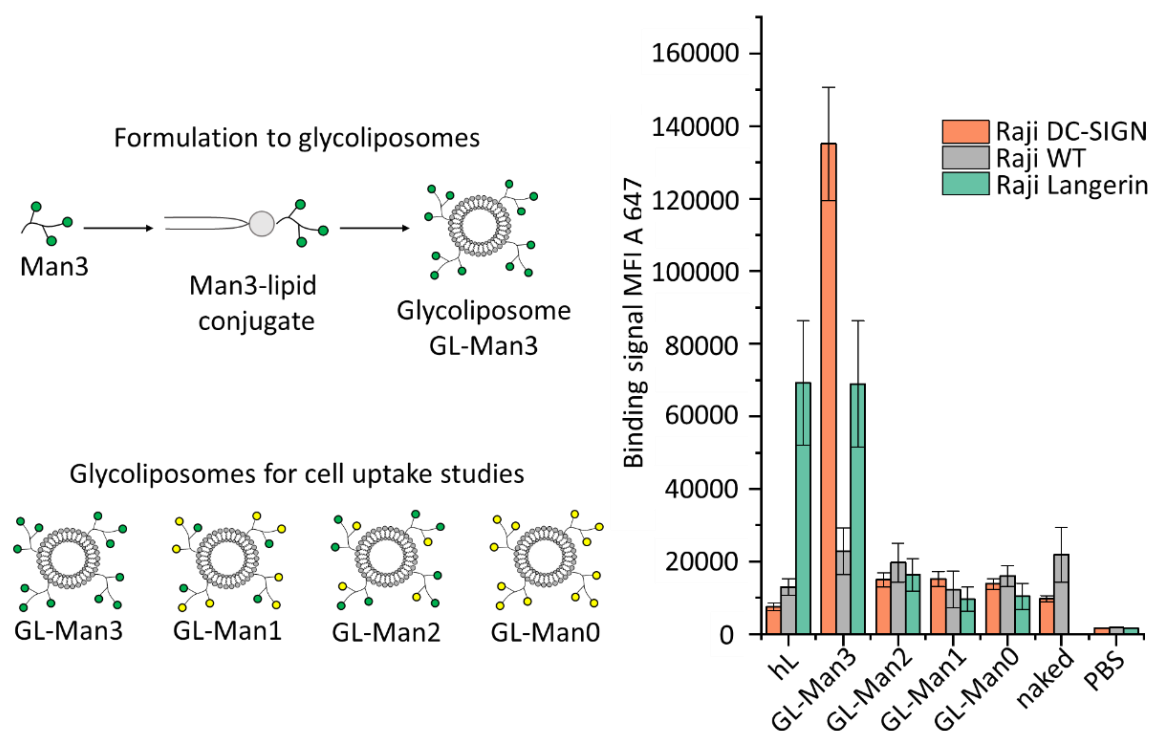
Figure 4: Formulation of the glycooligomers to glycoliposomes and their cellular interaction/uptake towards DC-SIGN and Langerin expressing Raji cells. Raji WT cells were used as control cell lines. hL was used as positive control. The standard deviation is obtained from three independent experiments. The cellular binding of the glycoliposomes to human Raji cells expressing different CLRs was measured by flow cytometry in three independent experiments at 4 °C.

Conclusion

Langerin and DC-SIGN are important surface receptors expressed on dendritic cells and Langerhans cells, respectively. Based on previous studies, a trivalent mannose-containing ligand was shown to increase binding to Langerin. To investigate the uptake mechanism, the trivalent ligand was taken as a template and a Man units were systematically exchanged for the non-binding Gal, resulting in heteromultivalent ligands. These heteromultivalent glycooligomers were studied by SPR and ^{19}F-NMR study on Langerin. Binding studies support a statistical rebinding as predominant multivalent binding mode based on a linear decrease in IC_{50} when decreasing the Man valency from 3 to 0. Similarly, the higher binding to DC-SIGN with four rather than three CRDs supports statistical binding effects as major factors responsible for the increased avidity of the trivalent glycomimetic ligands. Formulation of these glycooligomers into glycoliposomes allowed flow cytometric analysis of Langerin+ and DC-SIGN+ cells. In line with the protein binding studies, this showed highest cell binding of the trivalent Man ligand with DC-SIGN+ cells. In the future, such ligand functionalized liposomes will be explored for Langerin specific liposomal drug delivery systems.

References

(1) Feinberg, H.; Taylor, M.E.; Razi, N.; McBride, R.; Knirel, Y.A.; Graham, S. A.; Drickamer, K.; Weis, W.I. Structural basis for langerin recognition of diverse pathogen and mammalian glycans through a single binding site. *J. Mol. Biol.*, **2011**, *405*, 1027–1039.

(2) Drickamer, K. Engineering galactose-binding activity into a C-type mannose-binding protein. *Nature,* **1992**, *360*, 183–186.

(3) Stambach, N.S;Taylor, M.E. Characterization of carbohydrate recognition by langerin, a C-type lectin of Langerhans cells. *Glycobiology*, **2003**, *13*, 401–410.

(4) Geurtsen, J.; Driessen, N.N.; Appelmelk, B.J. Mannose–fucose recognition by DC-SIGN. *Microbial Glycobiology*, **2010**, 673–695

(5) Obermajer, N.; Sattin, S.; Colombo, C. Design, synthesis and activity evaluation of mannose-based DC-SIGN antagonists. *Mol Divers*; **2011**, *15*, 347–360.

(6) Flacher, V.; Tripp, C. H.; Mairhofer, D. G.; Steinman, R. M.; Stoitzner, P.; Idoyaga, J.; Romani, N. Murine Langerin+ dermal dendritic cells prime CD8+ T cells while Langerhans cells induce cross-tolerance. *EMBO Mol. Med.,* **2014**, *6*, 1191–1204.

(7) Valladeau, J.; Ravel, O.; Dezutter-Dambuyant, C.; Moore, K.; Kleijmeer, M.; Liu, Y.; Duvert-Frances, V.; Vincent, C.; Schmitt, D.; Davoust, J.; Caux, C.; Lebecque, S.; Saeland, S. Langerin, a novel C-type lectin specific to Langerhans cells, is an endocytic receptor that induces the formation of Birbeck granules. *Immunity*, **2000**, *12*, 71–81.

(8) Fehres, C.M.; Kalay, H.; Bruijns, S. C.; Musaafir, S.A.; Ambrosini,M.; Van Bloois, L.; Van Vliet, S.J.; Storm, G.; Garcia-Vallejo, J.J.; Van Kooyk, Y. Cross-presentation through langerin and DC-SIGN targeting requires different formulations of glycan-modified antigens. *J. Controlled Release*; **2015**, *203*, 67–76.

(9) Fehres, C.M.; Duinkerken, S.; Bruijns, S.C.; Kalay, H.; Van Vliet, S.J.; Ambrosini, M.; De Gruijl, T.D.; Unger, W.W.; Garcia-Vallejo, J.J.; Van Kooyk, Y. Langerin-mediated internalization of a modified peptide routes antigens to early endosomes and enhances cross-presentation by human Langerhans cells, *Cellular &. Cell. Mol. Immunol.*, **2017**, *14*, 360–370.

(10) Idoyaga, J.; Lubkin, A.; Fiorese, C.; Lahoud, M.H.; Caminschi, I.; Huang, Y.; Rodriguez, A.; Clausen, B.E.; Park, C.G.; Trumpfheller, C.; Steinman, R. M. Comparable T helper 1 (Th1) and CD8 Tcell immunity by targeting HIV gag p24 to CD8 dendritic cells within antibodies to Langerin, DEC205, and Clec9A. *Proc. Natl. Acad. Sci. U.S.A.,* **2011**, *108*, 2384–2389.

(11) Stoitzner, P.; Romani, N. Langerin, the "Catcher in the Rye": an important receptor for pathogens on Langerhans cells. *Eur. J. Immunol.*, **2011**, *41*, 2526–2529.

(12) Cambi, A.; Gijzen, K.; de Vries, lJ.; Torensma, R.; Joosten, B.; Adema, G.J.; Netea, M.G.; Kullberg, B.J.; Romani, L.; Figdor, C.G. The C-type lectin DC-SIGN (CD209) is an antigen-uptake receptor for Candida albicans on dendritic cells. *Eur. J. Immunol.*, **2003**, *33*, 532–538.

(13)   Schulze, J.; Rentzsch, M.; Kim, D.; Bellmann, L.; Stoitzner, P.; Rademacher, C.; A Liposomal Platform for Delivery of a Protein Antigen to Langerin-Expressing Cells. *Biochemistry*, **2019**, *58*, 2576–2580.

(14)   Rentzsch, M.; Wawrzinek, R.; Zelle-Rieser, C.; Strandt, H.; Bellmann, L.; Fuchsberger, F.F.; Schulze, J.; Busmann, J.; Rademacher, J.; Sigl, S.; Del Frari, B.; Stoitzner, P.; Rademacher, C. Specific Protein Antigen Delivery to Human Langerhans Cells in Intact Skin. *Front. Immunol.,* **2021**, *12*, 732298.

(15)   Wamhoff, E.C.; Schulze, J.; Bellmann, L.; Rentzsch, M.; Bachem, G.; Fuchsberger, F.F.; Rademacher, J.; Hermann, M.; Del Frari, B.; van Dalen, R.; Hartmann, D.; van Sorge, N.M.; Seitz, O.; Stoitzner, P.; Rademacher, C. A Specific, Glycomimetic Langerin Ligand for Human Langerhans Cell Targeting. *ACS Central Science*, **2019**, *5*, 808-820.

(16)   Wawrzinek, R.; Wamhoff, E.C.; Lefebre, J.; Rentzsch, M.;r Bachem, G.; Domeniconi, G.; Schulze, J.; Fuchsberger, F.F.; Zhang, H.; Modenutti, C.; Schnirch, L.; Marti, M.A.; Schwardt, O.; Bräutigam, M.; Guberman, M.; Hauck, D.; Seeberger, P.H.; Seitz, O.; Titz, A.; Ernst, B.; Rademacher C. A Remote Secondary Binding Pocket Promotes Heteromultivalent Targeting of DC-SIGN. *J. Am. Chem. Soc.* **2021**, *143*, 18977–18988.

(17)   Zhang, Y.; Luo, Y.; Li, W.; Liu, J.; Chen, M.; Gu, H.; Wang, B.; Yao, X. DC-SIGN promotes allergen uptake and activation of dendritic cells in patients with atopic dermatitis. *J. Dermatol. Sci.,* **2012**, *84*, 128-136.

(18)   Fehres, C.M.; Kalay, H.; Bruijns, S.C.M; Musaafir, S.A.M.; Ambrosini, M.; van Bloois, L.; van Vliet, S.J.;Storm, G.; Garcia-Vallejo, J.J.; van Kooyk, Y. Cross-presentation through langerin and DC-SIGN targeting requires different formulation of glycan-modified antigens, *J.Controlled Release,* **2015**, *203*, 67-76.

(19)   Soilleux, E.J.; Morris, L.S.; Leslie, G.; Chehimi, J.; Luo, Q.; Levroney, E.; Trowsdale, J.; Montaner, L.J.; Doms, R.W.; Weissman, D.; Coleman, N.; Lee, B. Constitutive and induced expression of DC-SIGN on dendritic cell and macrophage subpopulations in situ and in vitro. *J. Leukoc. Biol.,* **2002**, *71*, 445–457.

(20)   Romani, N.; Clausen, B.E.; Stoitzner, P. Langerhans cells and more: langerin-expressing dendritic cell subsets in the skin. *Immunol. Rev*., **2010**, *234*, 120–141.

(21)   Figdor, G.; van Kooyk, Y.; Adema, G.J. C-type lectin receptors on dendritic cells and Langerhans cells, *Nat. Rev. Immunol.*, **2002**, *2*, 77-84.

(22)   Feinberg, H.; Powlesland, A.S.; Taylor, M.E.; Weis, W.I. Trimeric structure of langerin, *J. Biol. Chem.,* **2012**, *285*, 13285-13293.

(23)   Valladeau, J.; Ravel, O.; zutter-Dambuyant, C.; Moore, K.; Kleijmeer, M.; Liu, Y.; Duvert-Frances, V.; Vincent, C.; Schmitt, D.; Davoust, J.; Caux, C.; Lebecque, S.; Saeland, S. Langerin, a novel C-type lectin specific to Langerhans cells, is an endocytic receptor that induces the formation of Birbeck granules. *Immunity*, **2000**, *12*, 71-81.

(24)   Mc Dermott, R.; Ziylan, U.; Spehner, D.; Bausinger, H.; Lipsker, D.; Mommaas, M.; Cazenave, J.P.; Raposo, G.; Goud, B.; de la, S.H.;n Salamero, J.; Hanau, D. Birbeck granules are subdomains of endosomal recycling compartment in human epidermal Langerhans cells, which form where Langerin accumulates. *Mol. Biol. Cell*, **2002**, *13*, 317-335.

(25)   Thepaut, M.; Valladeau, J.; Nurisso, A.; Kahn, R.; Arnou, B.; Vives, C.; Saeland, S.; Ebel, C.; Monnier, C.; zutter-Dambuyant, C.;Imberty, A.; Fieschi, F. Structural studies of langerin and Birbeck granule: a macromolecular organization model, *Biochemistry*, **2009**, *48*, 2684-2698.

(26)   Porkolab, V.; Chabrol, E.; Varga, N.; Ordanini, S.; Sutkevičiūtė, I.; Thépaut, M.; García-Jiménez, M.J.; Girard, E.; Nieto, P.M.; Bernardi, A.; Fieschi, F. Rational-Differential Design of Highly Specific Glycomimetic Ligands: Targeting DC-SIGN and Excluding Langerin Recognition. *ACS Chem. Biol.* **2018**, *13*, 600–608.

(27)   Tacken, P.J.; Ginter, W.; Berod, L.; Cruz, L.J.; Joosten, B.; Sparwasser, T.; Figdor, C.G.; Cambi, A. Targeting DC-SIGN via its neck region leads to prolonged antigen residence in early endosomes, delayed lysosomal degradation, and cross-presentation. *Blood*, **2011**, *118*, 4111-4119.

(28)   Cramer, J.; Lakkaichi, A.; Aliu, B.; Jakob, R.P.; Klein, S.; Cattaneo, I.; Jiang, X.; Rabbani, S.; Schwardt, O.; Zimmer, G.; Ciancaglini, M.; Mota, T.A.; Maier, T.; Ernst B.

Sweet Drugs for Bad Bugs: A Glycomimetic Strategy against the DC-SIGN-Mediated Dissemination of SARS-CoV-2. *J. Am. Chem. Soc.;* **2021**; *143*, 17465-17478.

(29)   Medve, L.; Achilli, S.; Serna, S.; Zuccotto, F.; Varga, N,; Thépaut, M.; Civera, M.; Vivès, C.; Fieschi, F.; Reichardt, N.; Bernardi, A. On-Chip Screening of a Glycomimetic Library with C-Type Lectins Reveals Structural Features Responsible for Preferential Binding of Dectin-2 over DC-SIGN/R and Langerin. *Chem. Eur. J.,* **2018**, *24*, 14448.

(30)   Wamhoff, E.C.; Hanske, J.; Schnirch, L.; Aretz, J., Grube, M.; Varón Silva, D.; Rademacher C. ^{19}F NMR-Guided Design of Glycomimetic Langerin Ligands. *ACS Chem. Biol.,* **2016**, *11*, 2407–2413.

(31)   Shamout, F.; Monaco, A.; Yilmaz, G.; Becer, C.R.; Hartmann, L.Synthesis of Brush-Like Glycopolymers with Monodisperse, Sequence-Defined Side Chains and Their Interactions with Plant and Animal Lectins. *Macromol. Rapid Commun.*, **2019**, *41*, 1900459.

(32)   Camaleño de la Calle, A.; Gerke, C.; Chang, X. J.; Grafmüller, A.; Hartmann, L.; Schmidt, S., Multivalent Interactions of Polyamide Based Sequence-Controlled Glycomacromolecules with Concanavalin A. *Macromol. Biosci*., **2019**, 19*,* 1900033.

(33)   Jacobi, F.; Wilms, D.; Seiler, T.; Queckbörner, T.; Tabatabai, M.; Hartmann, L.; Schmidt, S. The effect of PEGylation on receptor anchoring and steric shielding at interfaces: an adhesion and surface plasmon resonance study with precision polymers. *Biomacromolecules* **2020**, *21*, 4850–4856.

(34)   Neuhaus, K.; Wamhoff, E.C.; Freichel, T.; Grafmüller, A.; Rademacher, C.; Hartmann, L. Asymmetrically Branched Precision Glycooligomers Targeting Langerin. *Biomacromolecules*. **2019**, *20*, 4088-4095.

(35)   Hill, S.A.; Gerke, C.; Hartmann, L. Recent Developments in Solid-Phase Strategies towards Synthetic, Sequence-Defined Macromolecules. *Chem. Asian J.*, **2018**, *13*, 3611-3622.

(36)   Ponader, D.; Maffre, P.; Aretz, J.; Pussak, D.; Ninnemann, N.M.; Schmidt, S.; Seeberger, P.H.; Rademacher, C.; Nienhaus, G.U.; Hartmann, L: Carbohydrate-Lectin

Recognition of Sequence-Defined Heteromultivalent Glycooligomers. *J.Am.Chem.Soc.,* **2014**, *136*, 2008–2016.

(37)   Pussak, D.; Ponader, D.; Mosca, S.; Pompe, T.; Hartmann, L; Schmidt, S. Specific adhesion of carbohydrate hydrogel particles in competition with multivalent inhibitors evaluated by AFM, *Langmuir*, **2014**, *30*, 6142-6150.

(38)   Igde, S.; Röblitz, S.; Müller, A.; Kolbe, K.; Boden, S.; Fessele, C.; Lindhorst, T.K.; Weber, M.; Hartmann, L. Linear Precision Glycomacromolecules with Varying Interligand Spacing and Linker Functionalities Binding to Concanavalin A and the Bacterial Lectin FimH. *Macromol Biosci.* **2017**, *17*, 1700198.

(39)   Boden, S.; Reise, F.; Kania, J.; Lindhorst, T.K.; Hartmann, L. Sequence-Defined Introduction of Hydrophobic Motifs and Effects in Lectin Binding of Precision Glycomacromolecules. *Macromol. Biosci*., **2019**, *19*, 1800425.

(40)   Wojcik, F.; O'Brien, A.G.; Götze, S.; Seeberger, P.H.; Hartmann, L. Synthesis of Carbohydrate-Functionalised Sequence-Defined Oligo(amidoamine)s by Photochemical Thiol-Ene Coupling in a Continuous Flow Reactor. *Eur. J. Chem.* **2013**, *19*, 3090-3098.

(41)   Freichel T.; Eierhoff, S.; Snyder, N.L.; Hartmann, L. Toward Orthogonal Preparation of Sequence-Defined Monodisperse Heteromultivalent Glycomacromolecules on Solid Support Using Staudinger Ligation and Copper-Catalyzed Click Reactions, J. Org. Chem., 2017, 82, 9400–9409.

(42)   Wojcik,F.; Lel,S.; O'Brien, A.G.; Seeberger, P.H.; Hartmann, L.; Synthesis of Homo- and Heteromultivalent Carbohydrate-Functionalized Oligo(amidoamines) Using Novel Glyco-Building Blocks, Beilstein J. Org. Chem., 2013, 9, 2395–2403.

(43)   Ponader, D.; Wojcik, F.; Beceren-Braun, F.; Dernedde, J.; Hartmann, L.; *Biomacromolecules*, **2012**, *13*, 1845-1852.

(44)   Hayes, W.; Osborn, H.M.I.; Osborne, S.D.; Rastall, R.A.; Romagnoli, B. One-pot synthesis of multivalent arrays of mannose mono- and disaccharides. *Tetrahedron*, **2003**, *59*, 7983-7996.

(45)   Wu, L.; Sampson, N.S. Fucose, Mannose, and β-N-Acetylglucosamine Glycopolymers Initiate the Mouse Sperm Acrosome Reaction through Convergent Signaling Pathways. *ACS Chem. Biol.,* **2014**, *9*, 468-475.

Supporting Information

One, two, three – heteromultivalent ligands with controlled valency targeting Langerin and DC-SIGN

Serap Üclü[a], , Yunzhan Ning[b], Iris Bermej[b] , Nowras Rahhal[b], Janis Langer[a], Christoph Rademacher[b]* and Laura Hartmann[a]*

[a] Department of Macromolecular Chemistry, Heinrich-Heine University, Universitätsstr. 1, 40225 Düsseldorf Germany, e-mail: laura.hartmann@hhu.de

[b] Department of Pharmaceutical Sciences, University of Vienna, Josef-Holaubek-Platz 2, 1090 Wien, Austria, e-mail: christoph.rademacher@univie.ac.at

* corresponding authors

1. Instrumentation:

Nuclear Magnetic Resonance spectroscopy (NMR): ^{1}H-NMR (600 and 300 MHz) spectra were mesured on a Bruker AVANCE III – 600. Chemical shifts of all NMR spectra were expressed in parts per million (ppm). For ^{1}H NMR, the residual non-deuterated solvent was used as an internal standard (δ 4.79 ppm for HDO). The resulting multiplications were given as s for singlet, d for doublet, t for triplet, and m for multiplet.

Reversed Phase - High Pressure Liquid Chromatography - Mass Spectrometry (RP-HPLC-MS): Analysis were performed using an Agilent 1260 Infinity instrument equipped with a variable wavelength detector (VWD) (set at 214 nm) and a 6120 quadrupole LC/MS with an electrospray ionization (ESI) source (operated in positive ionization mode in an m/z range of 200 to 2000). A Poroshell 120 EC-C18 (3.0×50 mm, 2.5 µm) RP column from Agilent was used as the HPLC column. Mobile phases A and B were H_2O/ACN (95 Vol %/5 Vol %) and H_2O/ACN (5 Vol %/95 Vol %), respectively. Both mobile phases contained 0.1 % formic acid. The temperature of the column chamber was set at 25 °C. UV and MS spectral analysis was done using Agilent Technologies OpenLab ChemStation software for LC/MS.

Ultra-High Resolution - Mass Spectrometry (UHR-MS): The MS measurements were conducted with a Bruker UHR-QTOF maXis 4G instriument using a direct inlet vial syringe pump and an ESI source.

Freeze dryer: The glycooligomers were freeze dried by using Alpha 1-4 LD plus instrument from Martin Christ Freeze Dryers GmbH. The drying method was fixed to -55 °C and 0.1 mbar.

Surface Plasmon Resonance (SPR): Inhibition-Competition Experiments were performed with a Biacore X100 instrument from GE Healthcare Life Sciences. The sonograms were evaluated by using Biacore X100 Evaluation Software.

^{19}F R_2-filtered NMR: ^{19}F R_2-filtered NMR experiments were performed on a Brucker AV 500 MHz spectrometer at 298 K600 MHz spectrometer from Agilent. Spectra were processed in MestReNova and data analysis was performed with OriginPro[1]. Apparent relaxation rates $R_{2,obs}$ for the reporter ligand were determined using the CPMG pulse sequence as previously published.[1-3]

Compound Man3
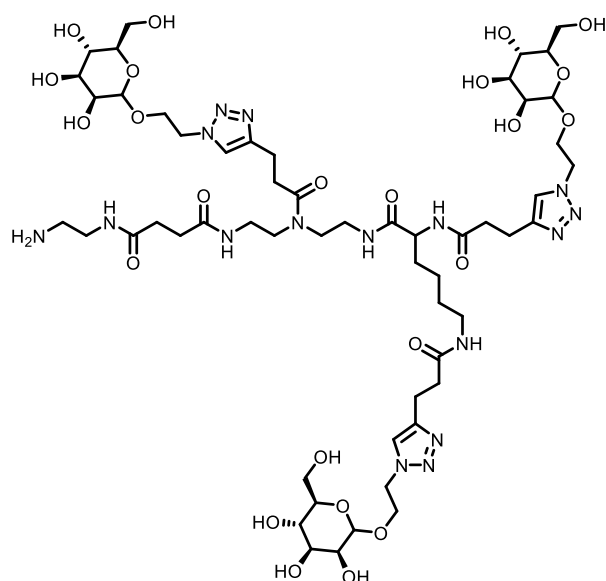
^{1}H-NMR (300 MHz, D$_2$O) δ 7.87 (dd, J = 7.0, 2.8 Hz, 3H), 4.63 (s, 6H), 4.22 − 4.04 (m, 5H), 3.96 − 3.83 (m, 7H), 3.79 − 3.31 (m, 48H), 3.20 − 2.95 (m, 15H), 2.85 − 2.46 (m, 12H), 1.39 (d, J = 7.1 Hz, 2H).

ESI-MS calculated [M+H]$^+$ 1361.2, found 1361.2; [M+2H]$^{2+}$ 681.2, found 681.2; [M+3H]$^{3+}$ 454.6, found 454.6.

RP-HPLC: (5%/95% ACN/H$_2$O→ 5%/50% ACN/H$_2$O in 30 min at 25°C, 214 nm): t$_R$ = 17.3 min.
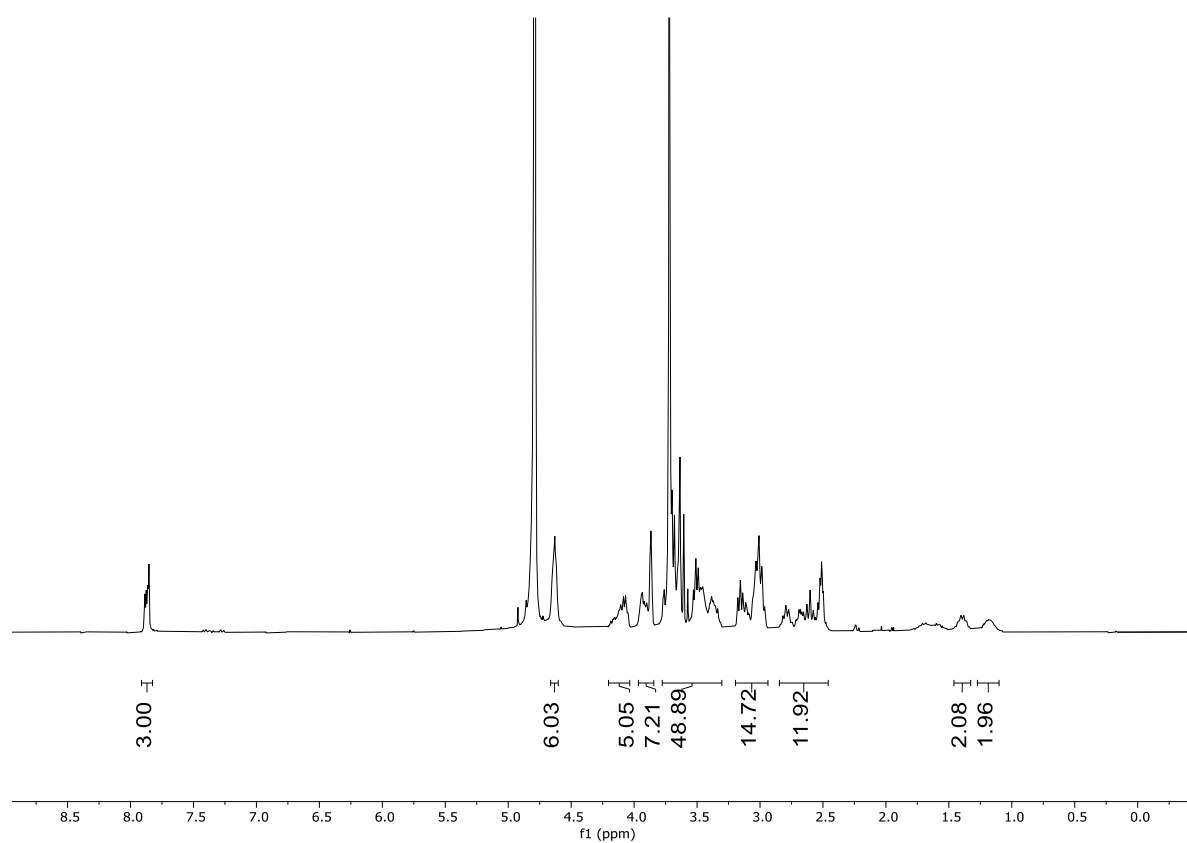
*Figure S1:^{1}H-NMR (600 MHz) spectra of **compound Man3** in HDO.*
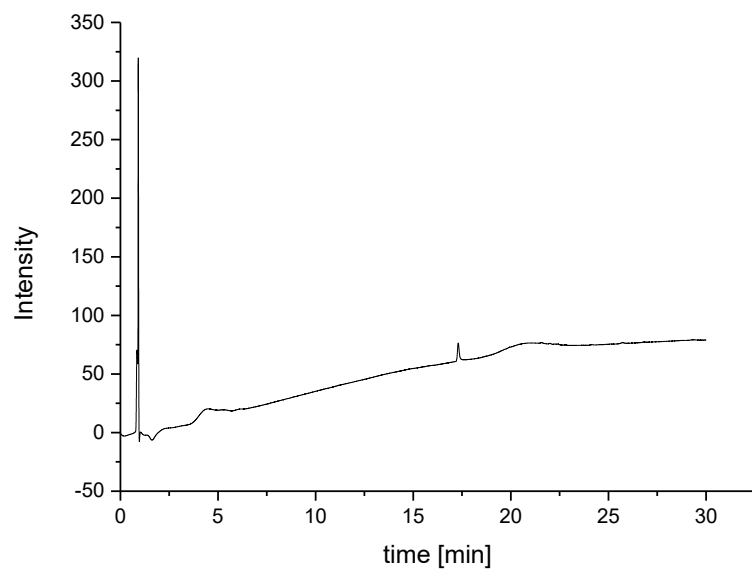

*Figure S2: RP-HPLC of **compound Man2**.*
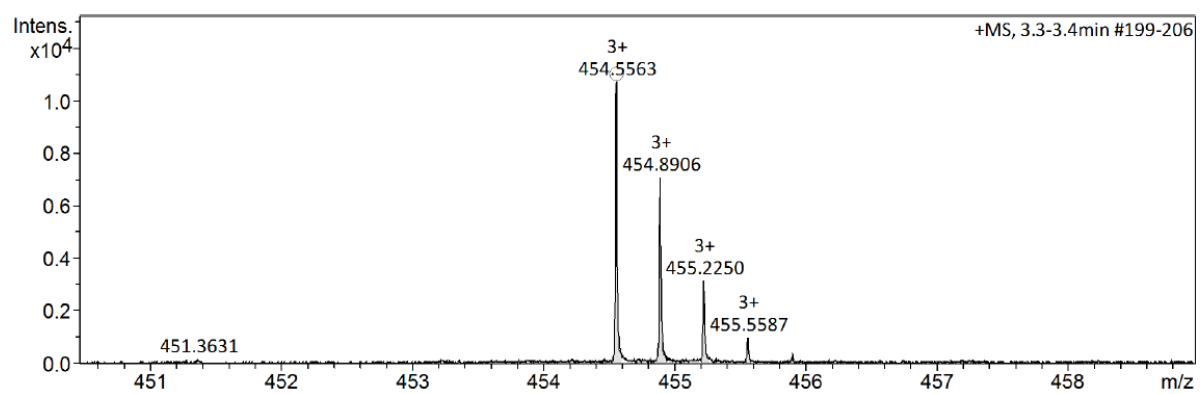
*Figure S3: HR-MS of **Man2**.*

Compound Man2
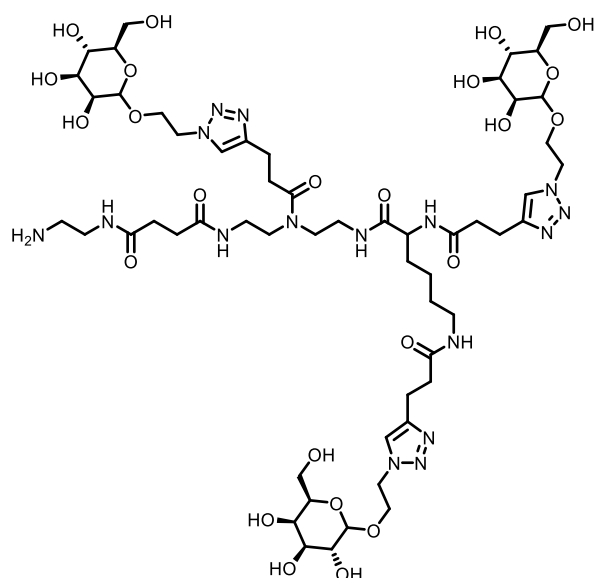
^{1}H-NMR (600 MHz, D$_2$O) δ 8.08 (s, 1H), 8.01 (d, J = 9.8 Hz, 1H), 7.97 (d, J = 3.9 Hz, 1H), 4.73 – 4.64 (m, 6H), 4.36 (dd, J = 7.9, 1.0 Hz, 1H), 4.30 (dt, J = 11.7, 4.8 Hz, 1H), 4.10 (ddt, J = 15.2, 7.2, 4.2 Hz, 5H), 3.94 – 3.86 (m, 3H), 3.85 (dt, J = 3.2, 1.4 Hz, 2H), 3.76 – 3.55 (m, 16H), 3.55 – 3.28 (m, 13H), 3.16 – 2.93 (m, 15H), 2.86 – 2.76 (m, 4H), 2.73 – 2.56 (m, 10H), 2.55 – 2.43 (m, 4H), 1.74 – 1.63 (m, 1H), 1.57 (q, J = 9.1, 7.1 Hz, 1H), 1.44 – 1.33 (m, 2H), 1.24 – 1.05 (m, 2H).

ESI-MS calculated [M+H]$^+$ 1361.2, found 1361.2; [M+2H]$^{2+}$ 681.2, found 681.2; [M+3H]$^{3+}$ 454.6, found 454.6

RP-HPLC: (5%/95% ACN/H$_2$O→ 5%/50% ACN/H$_2$O in 30 min at 25°C, 214 nm): t$_R$ = 17.3 min.

Ueclue.1360.fid
HO1
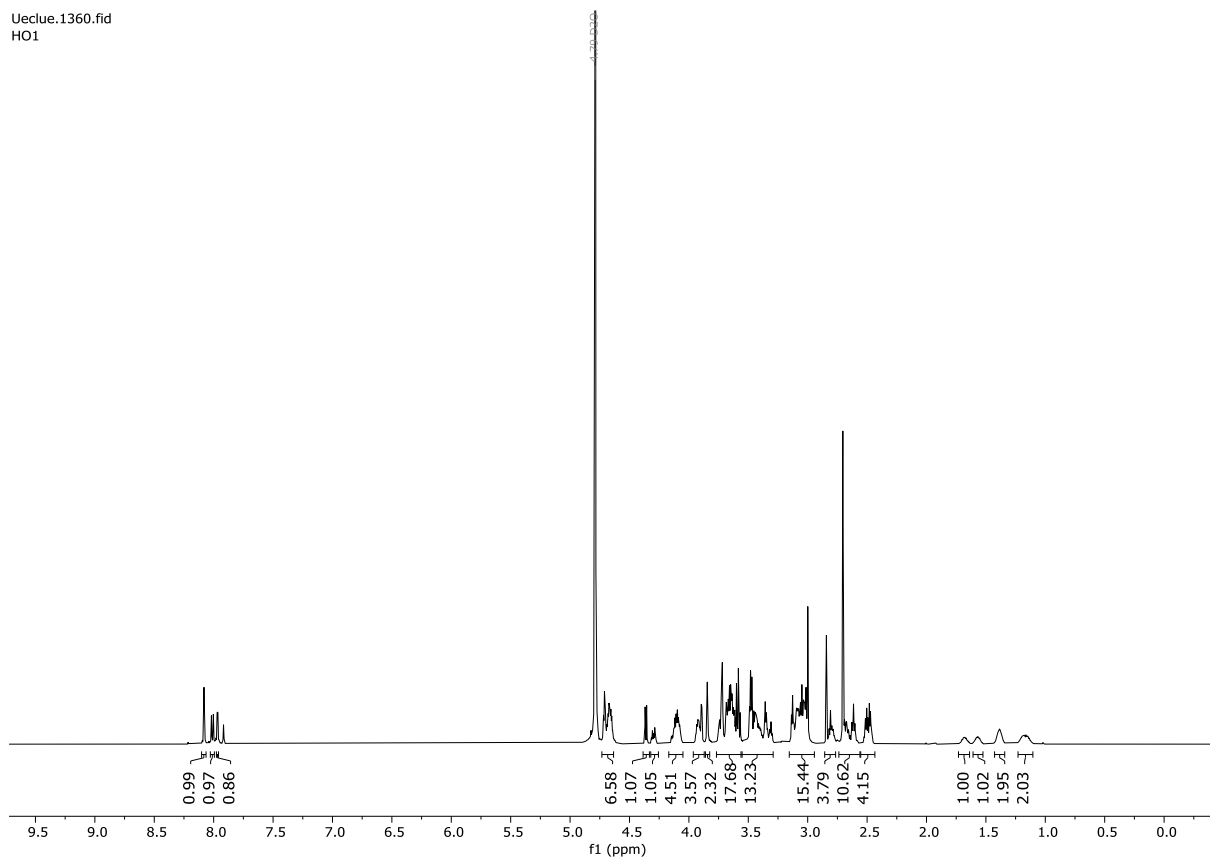
Figure S4: ^{1}*H-NMR (600 MHz) spectra of* **compound Man2** *in HDO.*
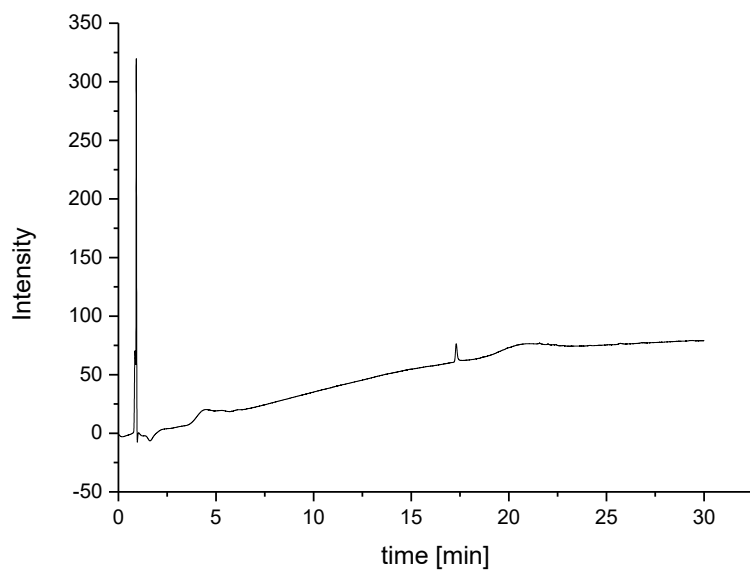
Figure S5: RP-HPLC of **compound Man2***.*

54
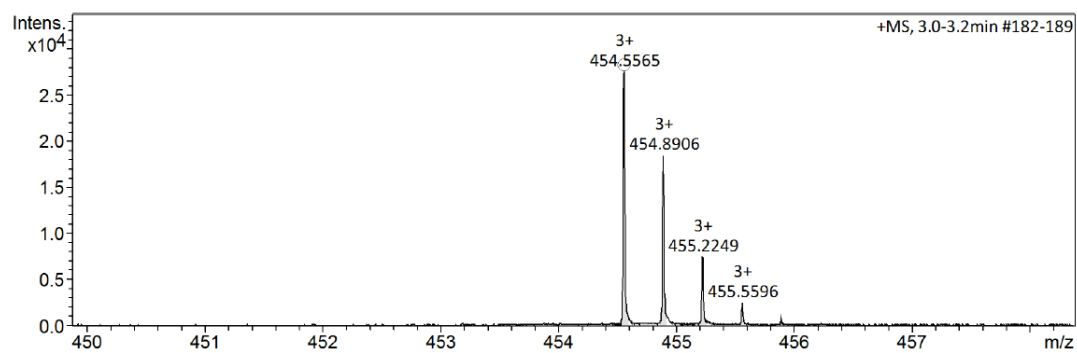
*Figure S6: HR-MS of **Man2**.*

Compound Man1
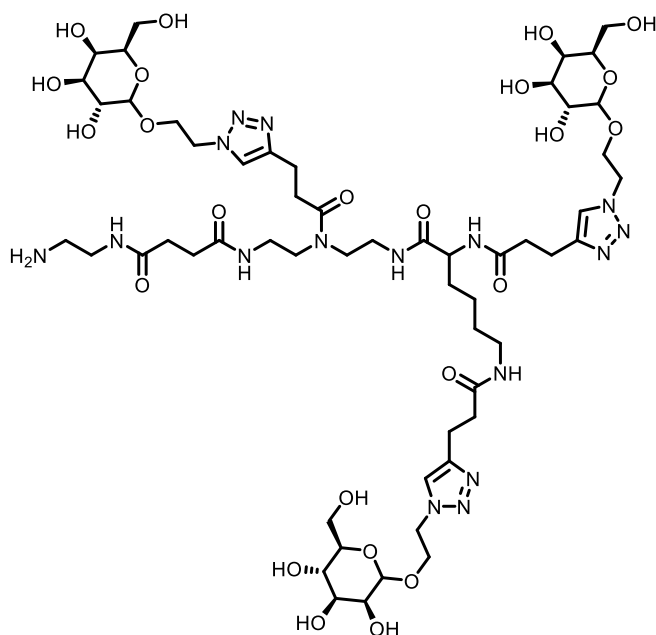
^{1}H NMR (600 MHz, D$_2$O) δ 8.02 – 7.97 (m, 2H), 7.91 (s, 1H), 4.70 – 4.60 (m, 6H), 4.37 (dd, J = 7.9, 3.7 Hz, 2H), 4.29 (ddd, J = 9.2, 6.3, 4.6 Hz, 2H), 4.17 – 4.03 (m, 5H), 3.91 (dd, J = 3.5, 1.0 Hz, 3H), 3.85 (dd, J = 3.3, 1.8 Hz, 1H), 3.76 – 3.55 (m, 17H), 3.51 – 3.40 (m, 10H), 3.39 – 3.28 (m, 4H), 3.16 – 2.97 (m, 12H), 2.80 (s, 1H), 2.68 (s, 2H), 2.63 – 2.57 (m, 2H), 2.55 – 2.43 (m, 2H), 1.75 – 1.63 (m, 1H), 1.57 (d, J = 4.9 Hz, 1H), 1.44 – 1.33 (m, 2H), 1.20 – 1.10 (m, 2H).

ESI-MS calculated [M+H]$^+$ 1361.2, found 1361.2; [M+2H]$^{2+}$ 681.2, found 681.2; [M+3H]$^{3+}$ 454.6, found 454.6

RP-HPLC: (5%/95% ACN/H$_2$O→ 5%/50% ACN/H$_2$O in 30 min at 25°C, 214 nm): t$_R$ = 17.3 min.

Ueclue.1350.fid
HO2
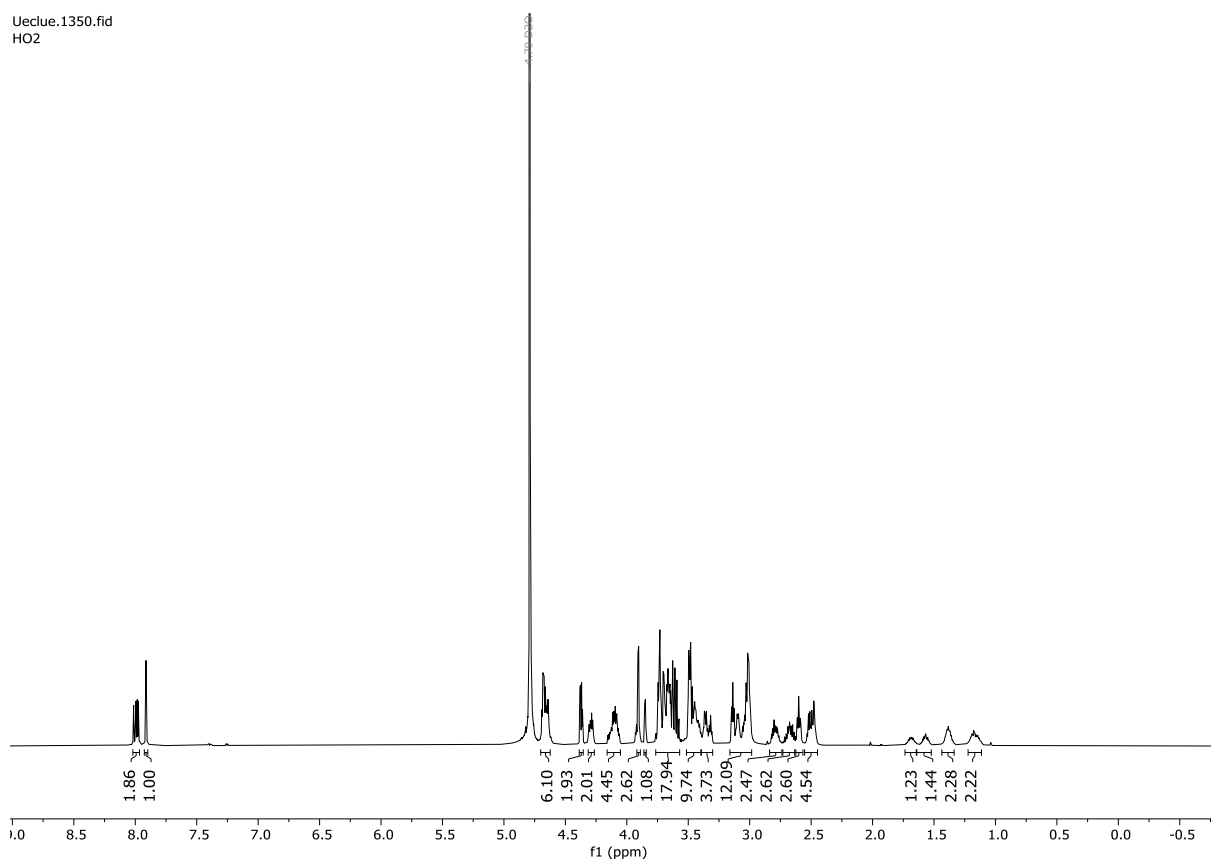
Figure S7:^{1}H-NMR (600 MHz) spectra of **compound Man1** in HDO.
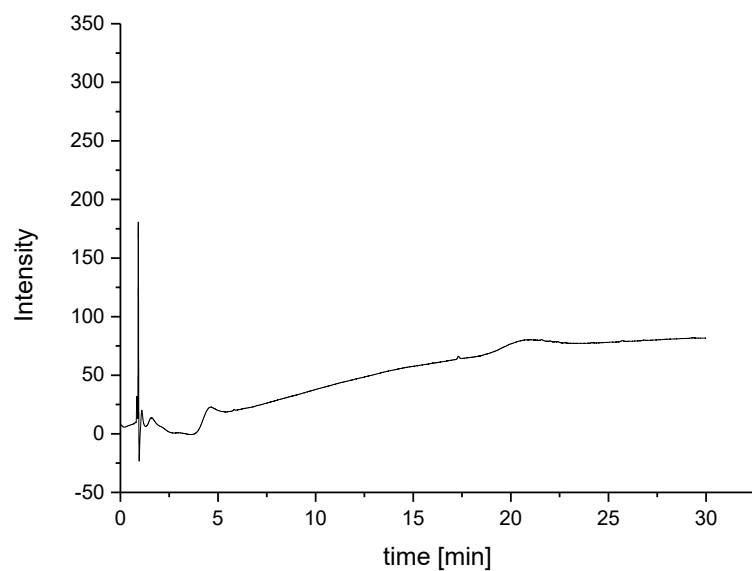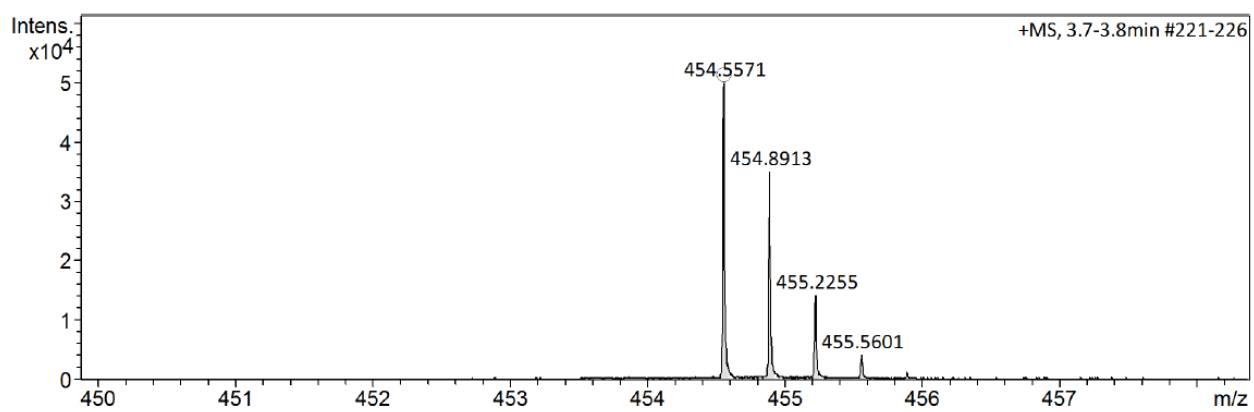

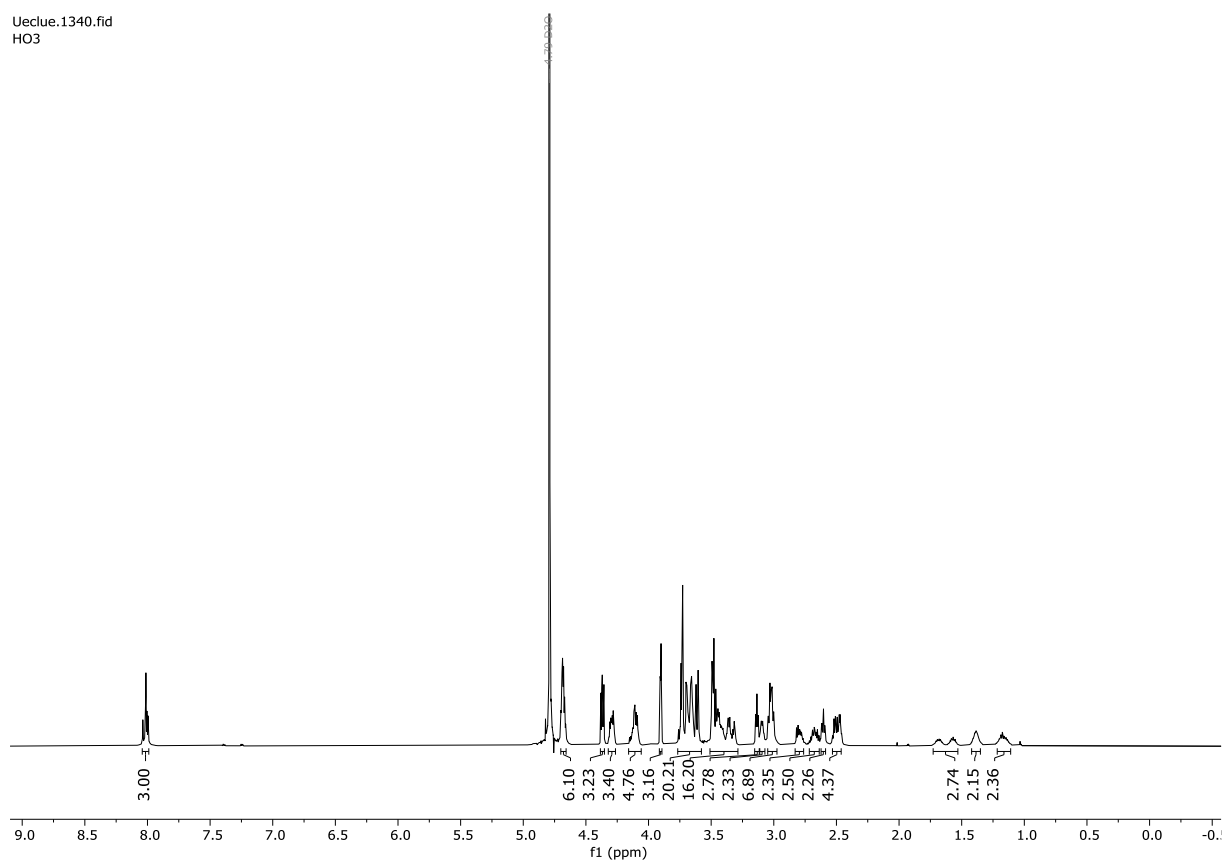Figure S8: RP-HPLC of **compound Man1**.

*Figure S9: HR-MS of **Man1**.*

Compound Man0 (old name HO3)

^{1}H NMR (600 MHz, D2O) δ 8.05 − 7.98 (m, 3H), 4.70 − 4.64 (m, 6H), 4.39 − 4.34 (m, 3H), 4.32 − 4.27 (m, 3H), 4.16 − 4.05 (m, 5H), 3.92 − 3.88 (m, 3H), 3.76 − 3.58 (m, 21H), 3.50 − 3.28 (m, 16H), 3.13 (t, J = 5.9 Hz, 3H), 3.10 − 3.07 (m, 2H), 3.05 − 2.97 (m, 7H), 2.82 − 2.76 (m, 2H), 2.71 − 2.64 (m, 2H), 2.60 (td, J = 7.5, 2.2 Hz, 2H), 2.55 − 2.44 (m, 4H), 1.73 − 1.52 (m, 3H), 1.42 − 1.34 (m, 2H), 1.23 − 1.08 (m, 2H).

ESI-MS calculated [M+H]$^+$ 1361.2, found 1361.2; [M+2H]$^{2+}$ 681.2, found 681.2; [M+3H]$^{3+}$ 454.6, found 454.6

RP-HPLC: (5%/95% ACN/H$_2$O→ 5%/50% ACN/H$_2$O in 30 min at 25°C, 214 nm): t$_R$ = 17.3 min.

Ueclue.1340.fid
HO3

*Figure S 10:^{1}H-NMR (600 MHz) spectra of **compound Man0** in HDO.*
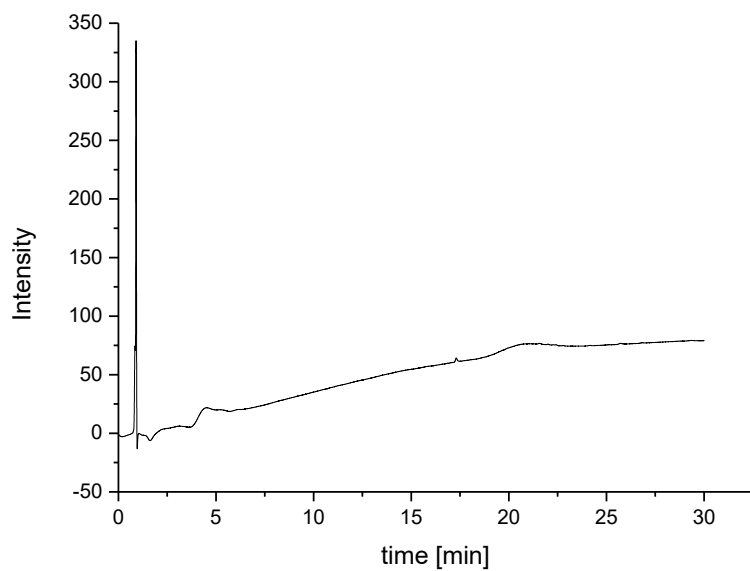
*Figure S11: RP-HPLC of **compound Man0**.*
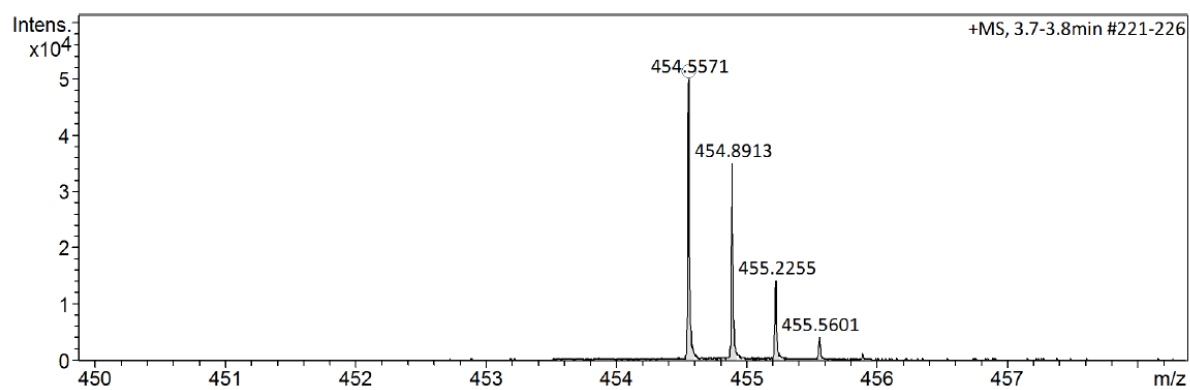
*Figure S12: HR-MS of **Man0**.*

2. Binding studies:

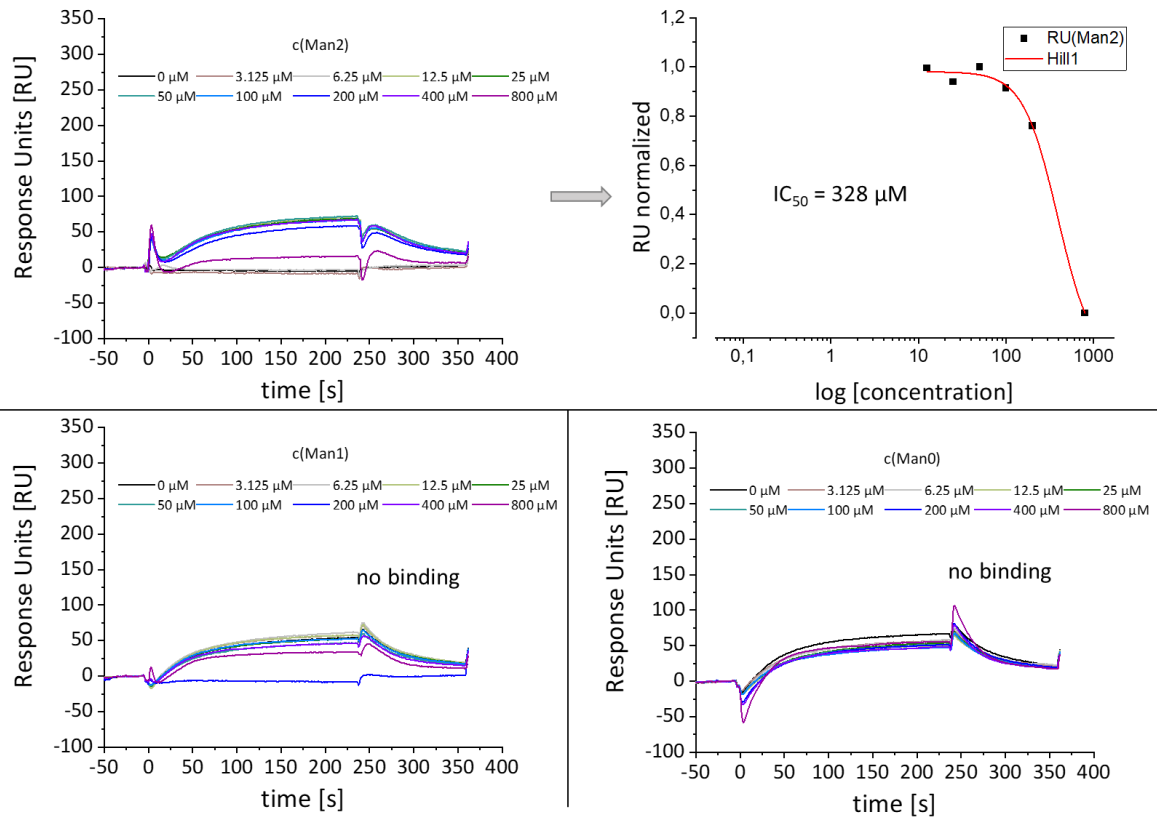### a) Inhibition-Competition Experiments via SPR:

Inhibition of Langerin on 1st Chip

Figure S13: Binding curves on 1st C1-Chip determined by SPR and inhibition of Langerin as well as Hill plot evaluation to derive IC50 values.
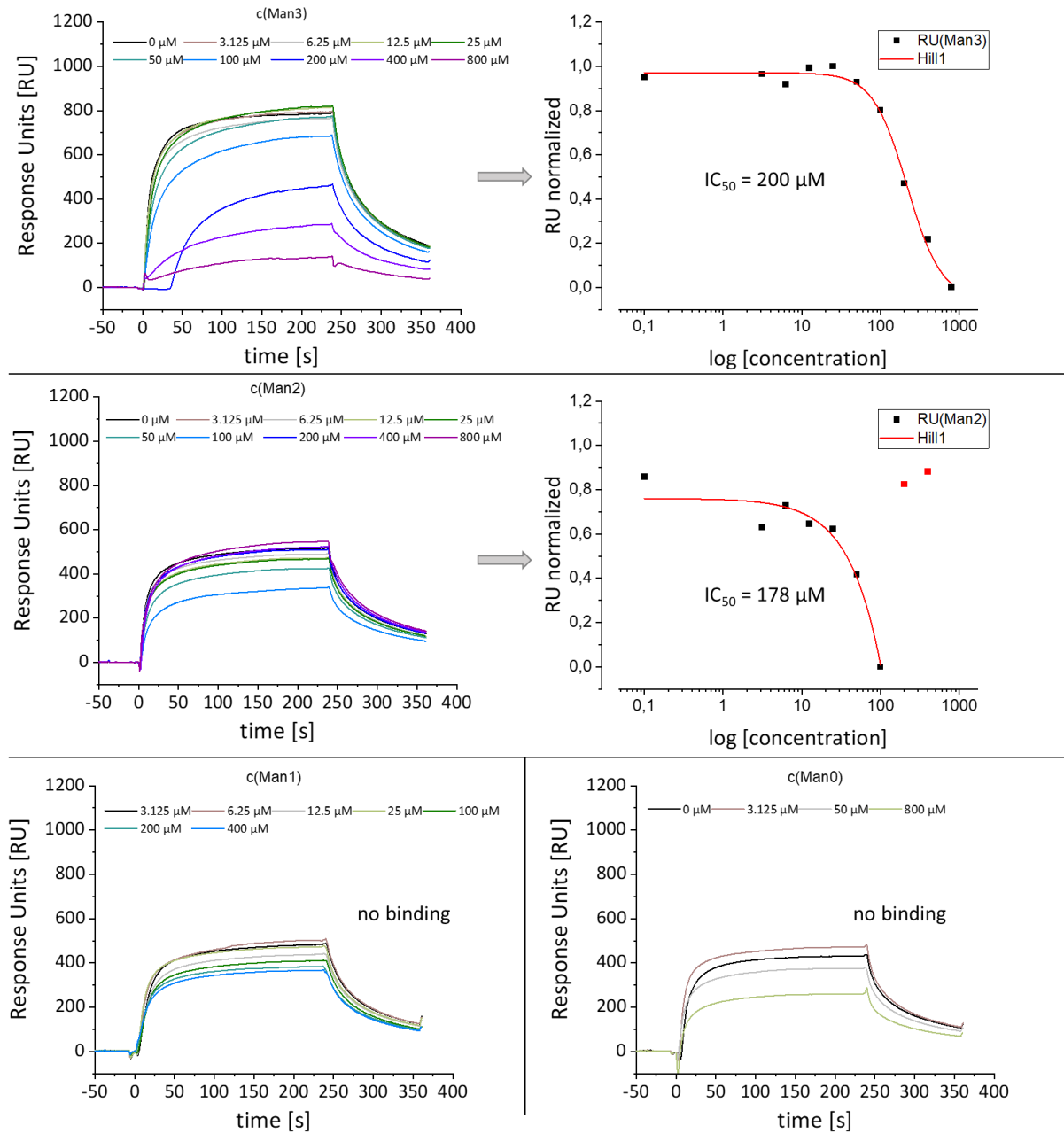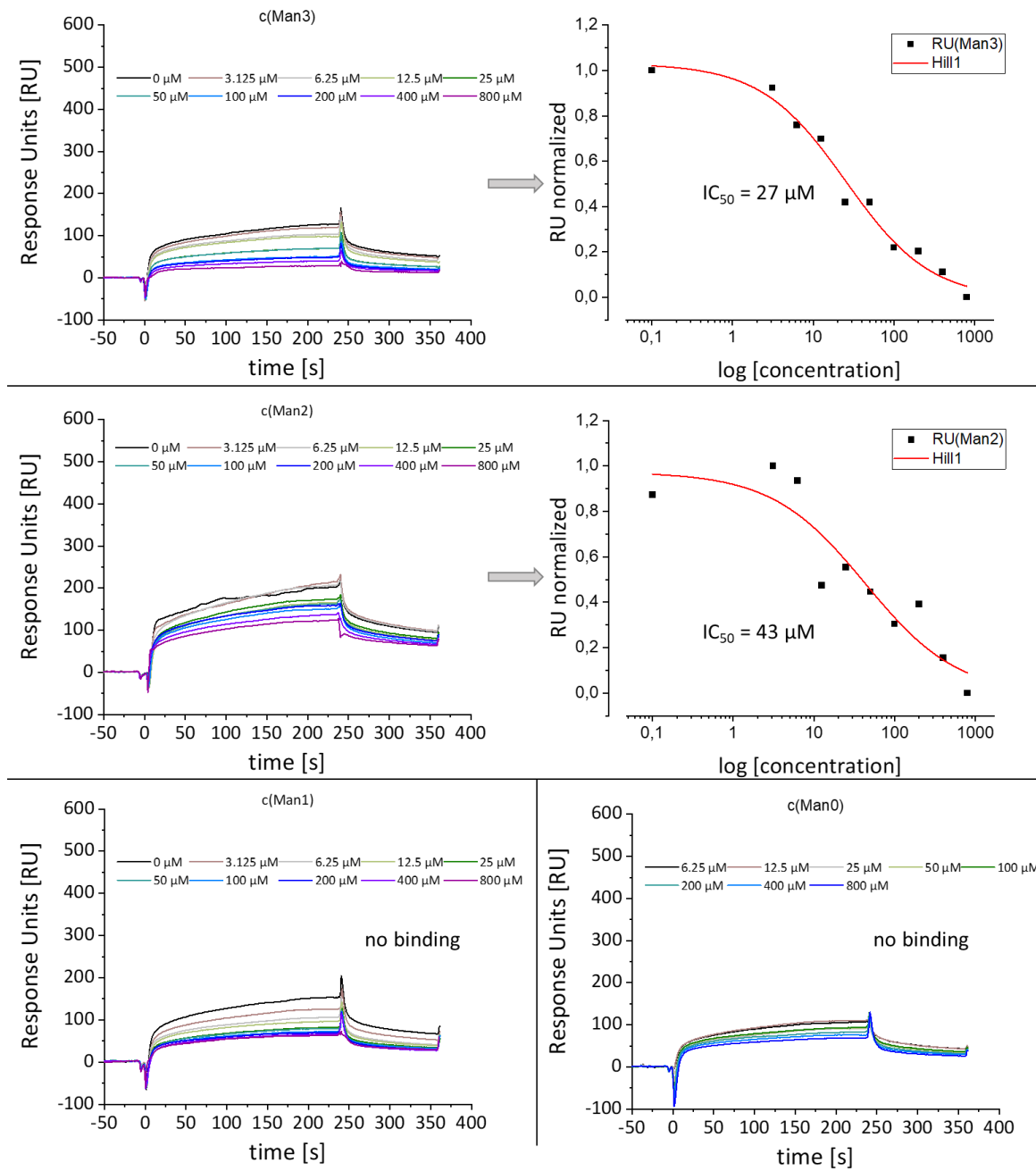
Inhibition of Langerin on 2nd Chip

Figure S14: Binding curves on 2nd C1-Chip determined by SPR and inhibition of Langerin as well as Hill plot evaluation to derive IC50 values.

Figure S15: Binding curves on 1st C1-Chip determined by SPR and inhibition of DC-SIGN as well as Hill plot evaluation to derive IC50 values.
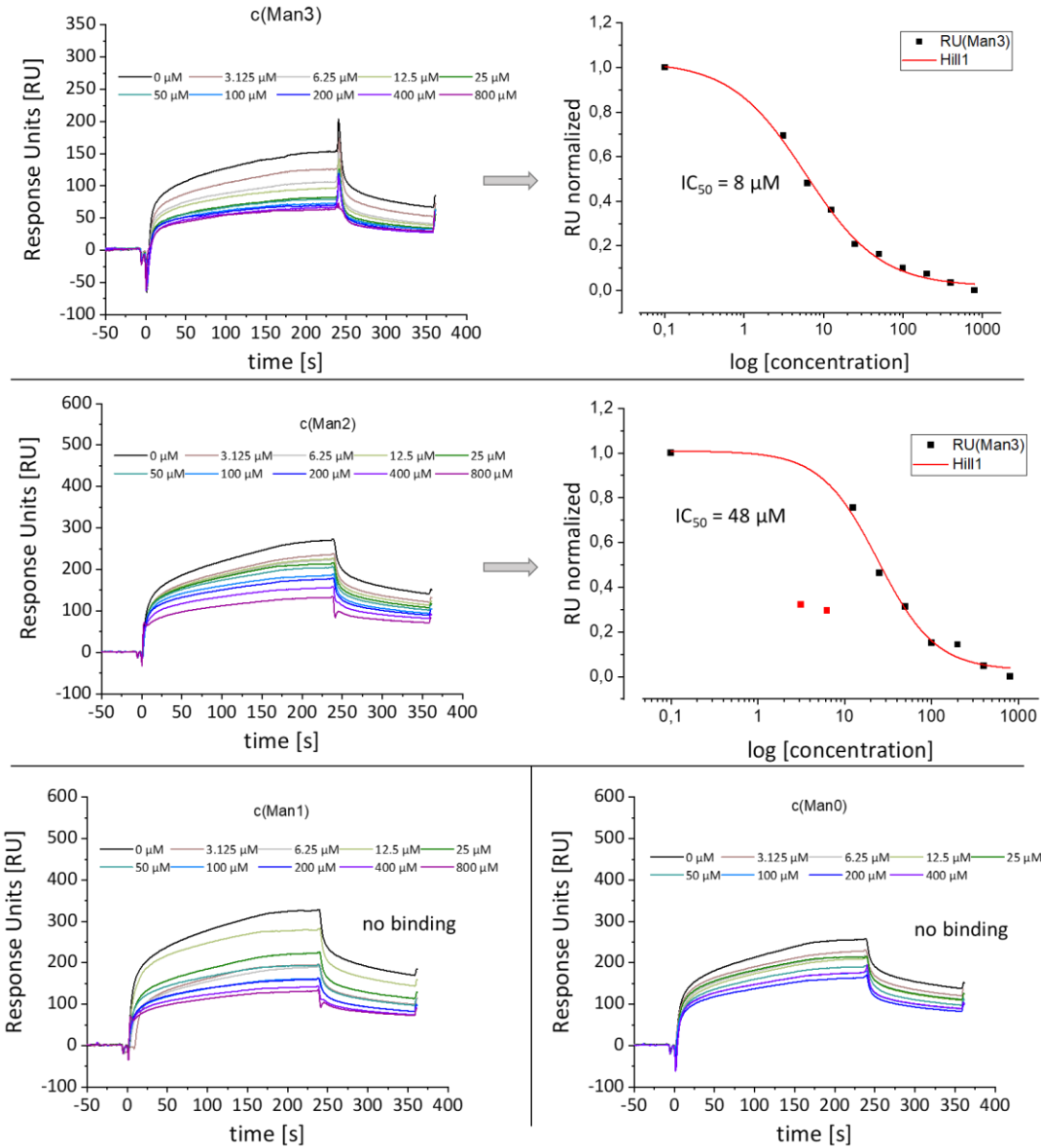
Figure S16: Binding curves on 2ⁿᵈ C1-Chip determined by SPR and inhibition of DC-SIGN as well as Hill plot evaluation to derive IC50 values.
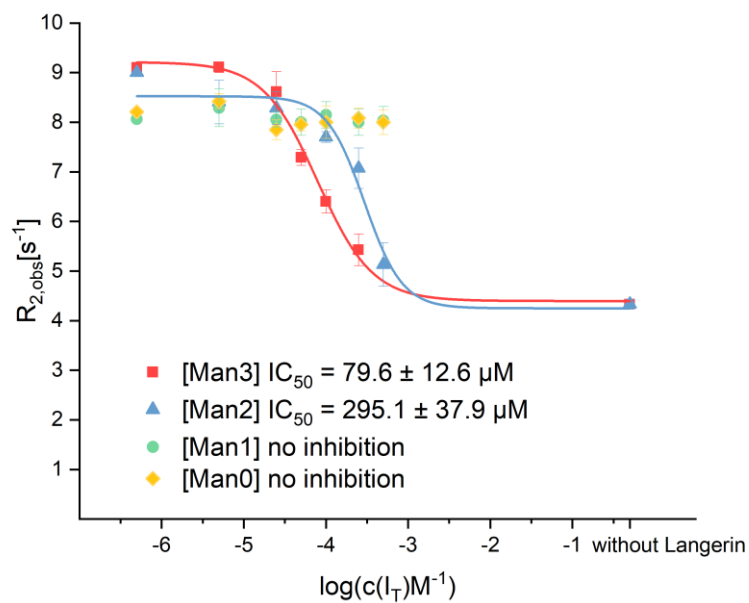
b)   Inhibition-Competition Experiments via ^{19}F-NMR

Figure S17: ^{19}F-NMR Inhibition curves towards Langerin. *While the samples Man0 (yellow) and Man1 (green) showed no inhibition, Man3 (red) showed the highest IC$_{50}$ value.*

3. Gylcooligomer conjugated Liposomes

Lipid-Glycooligomer-Coupling reaction conditions:

Glycooligomers (2 or 3 mg, 2 eq) were dissolved in 0.5 mL of DMSO and DIPEA (5 eq) and DSPE-PEG-NHS (1 eq) were added. Reaction vessels were vortex-shaken overnight at 40 °C. Samples were then dialyzed to water for 6 h x 3, using a membrane cut-off of 2 KDa. Afterwards, they were lyophilized and redissolved in DMSO-d_6. Glycooligomer-lipid coupling yields were calculated by ^{1}H-NMR (400 MHz, Bruker) comparing the DSPE methyl groups integration (6.00 protons, 0.8 ppm) to the integration of one of the methylene groups connecting the triazol and the sugar moiety for each glycooligomer (6.00 protons, 4.50 ppm).

Table 2: Coupling yields of lipid and glycooligomer conjugates obtained by comparing the integration of the DSPE methyl group and the methyl group linking the sugar residue via triazole by ^{1}H-NMR.

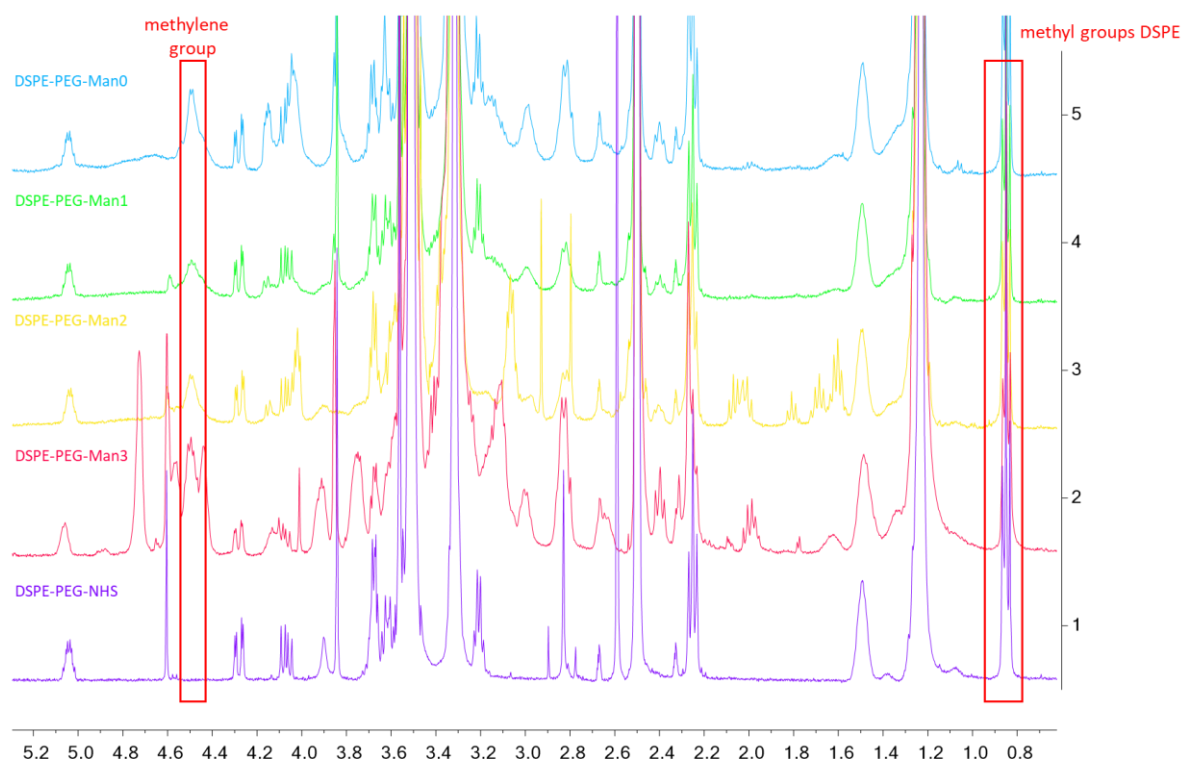| Compound	DSPE-PEG-Man0	DSPE-PEG-Man1	DSPE-PEG-Man2	DSPE-PEG-Man3
Coupling yield (%)	73	68	56	83

Figure S18: Comparison of the ^{1}H-NMR of the glycooligomers coupled to DSPE-PEG lipid and the starting material, DSPE-PEG-NHS. Highlighted into red frames the two signals used to determine the coupling yield are shown.
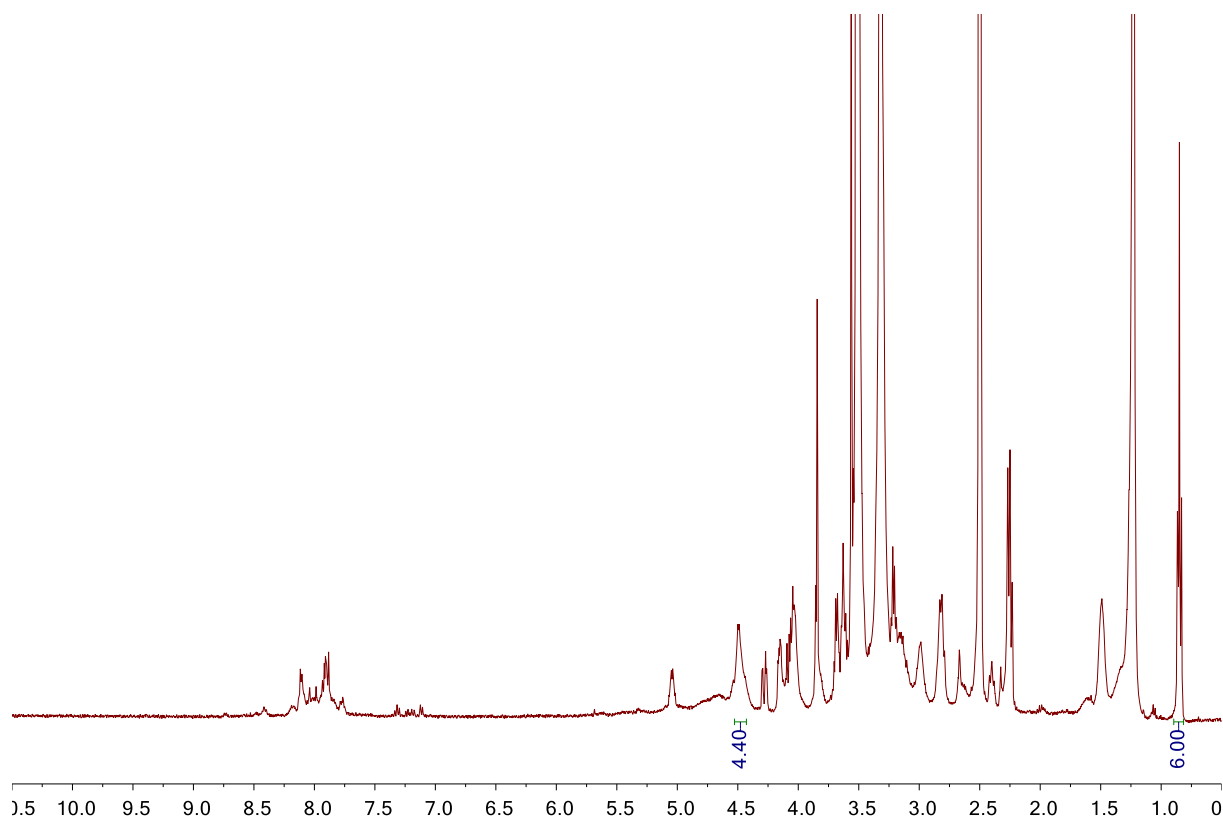

*Figure S19: ^{1}H-NMR (400 MHz) spectra of **DSPE-PEG-Man0 conjugate** in DMSO-d$_6$.*
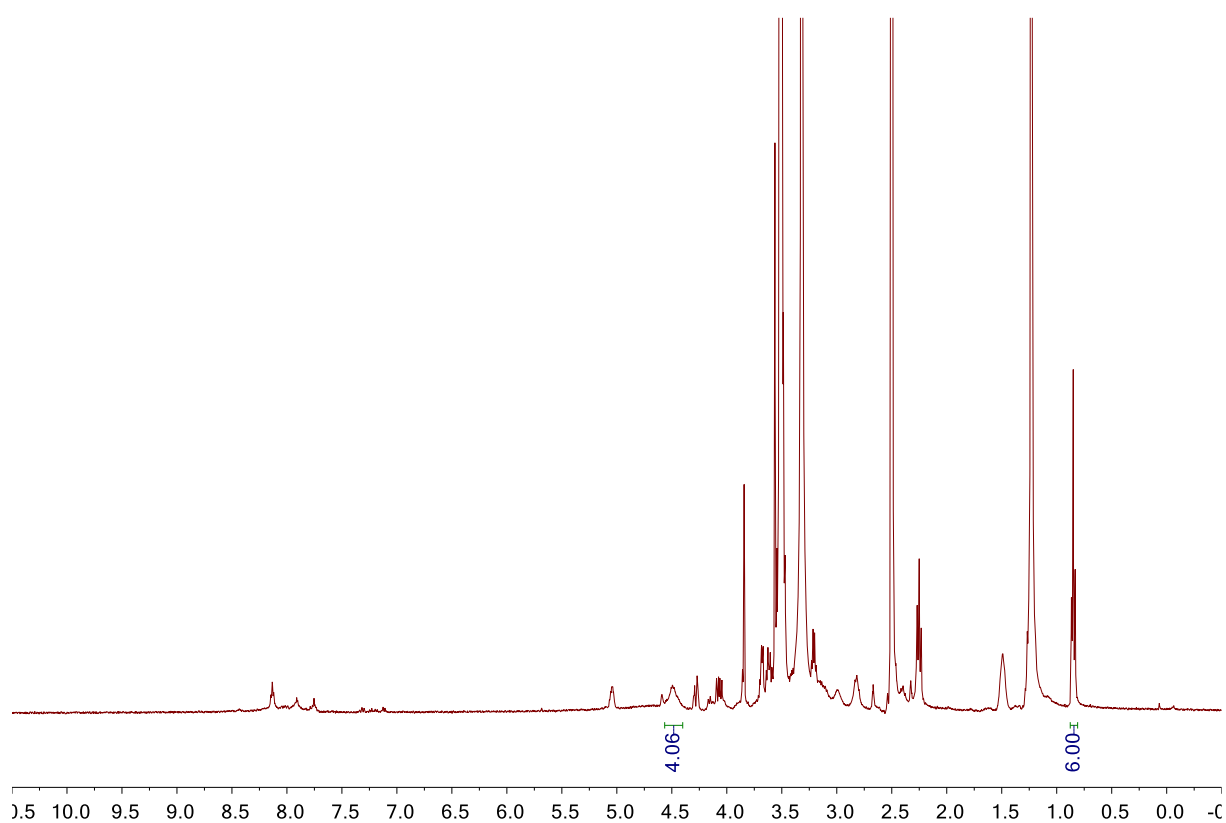
*Figure S20: ^{1}H-NMR (400 MHz) spectra of **DSPE-PEG-Man1 conjugate** in DMSO-d$_6$.*
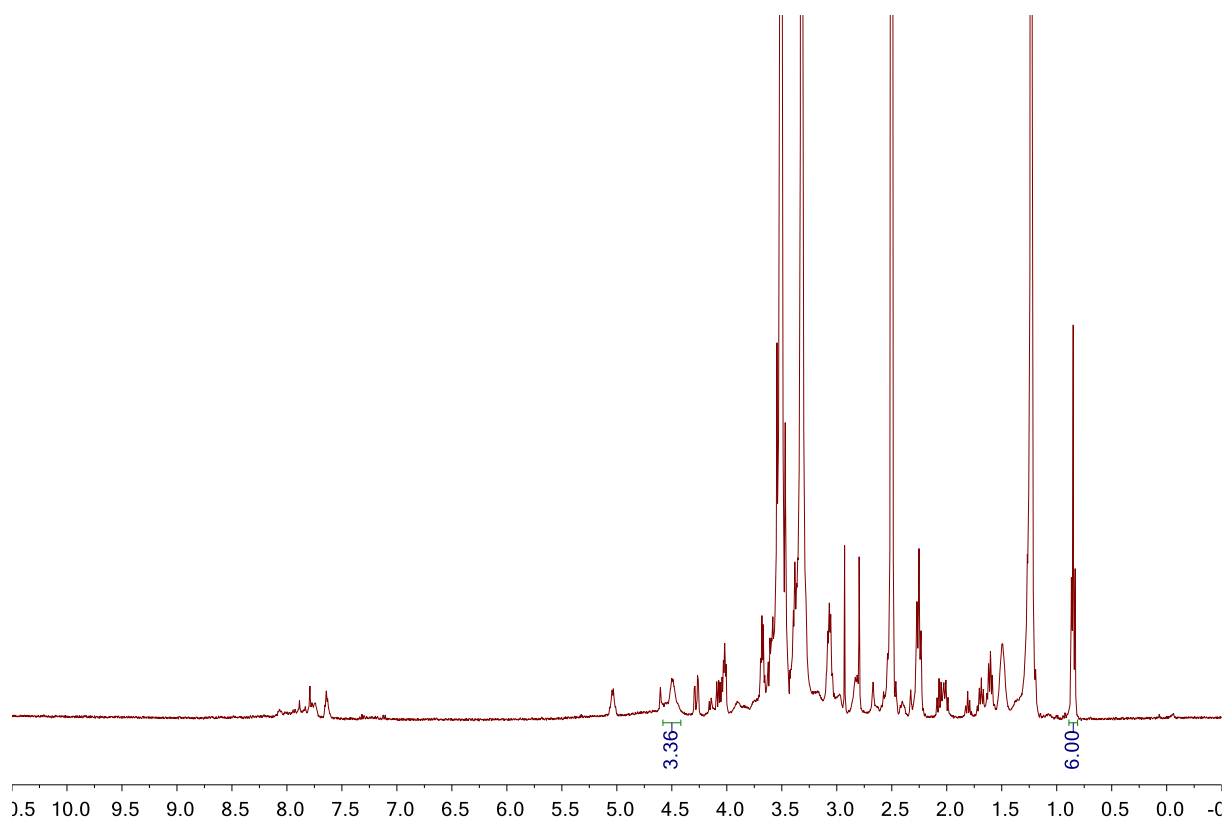

*Figure S 21: ^{1}H-NMR (400 MHz) spectra of **DSPE-PEG-Man2 conjugate** in DMSO-d$_6$.*
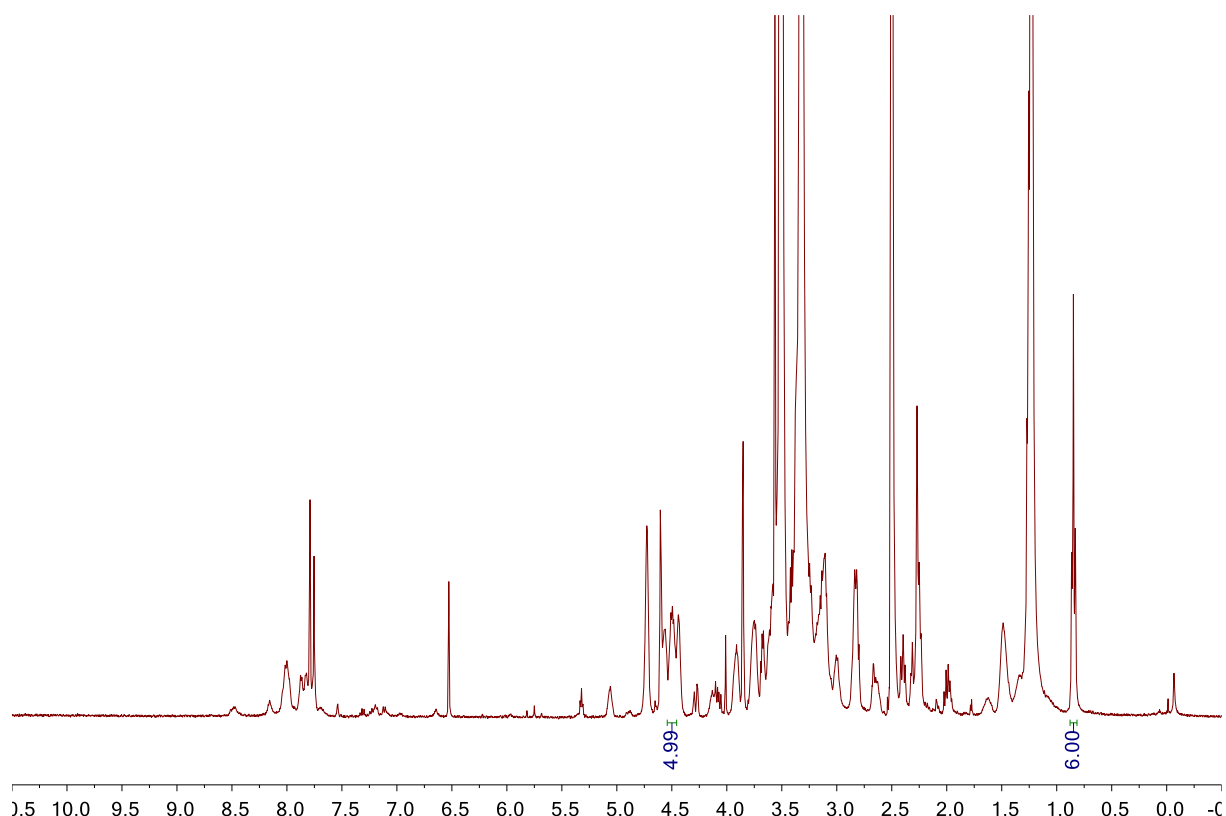
*Figure S22: ^{1}H-NMR (400 MHz) spectra of **DSPE-PEG-Man3 conjugate** in DMSO-d_6.*

Dye coupling:

Alexa Fluor 647 (A647) NHS Ester (Succinimidyl Ester) (Life Technologies, Invitrogen™, ThermoFisher, USA) was conjugated to the primary amine of NH_2-PEG-DSPE (PEG MW 2000, Sunbright, NOF EU) via amide coupling.[7]

Lipid-based nanoparticles formulation:

Briefly, liposomes were prepared by mixing two solutions in a microfluidic device. The organic phase contained the lipids in Ethanol 100 % (Ethyl alcohol, Pure, Sigma Aldrich) and an aqueous phase which was PBS buffer (50 mM) (Invitrogen, ThermoFisher Scientific, USA). A syringe pump (Pump 33 Dual Drive System Syringe Pump, Harvard Apparatus) was loaded with two syringes (Braun Injekt®, Germany) containing the dissolved lipids in ethanol in one and the PBS buffer in the other. The pump is used to inject the two solutions via short tubes (TUBE ID 0.8MM OD 1.6MM WALLTHK 0.4MM) attached to PEEK Capillary LUER lock adapters (Flangeless Fitting Delrin, Black 1/4-28 Flat-Bottom, for 1/16" OD, Luer Adapter 1/4-28 F-to-F,

IDEX-HS Corporation) to ensure pressure control into the inlets of the microfluidic chip at a flow rate ratio (FRR) organic:aquase 1:4 and a total flow rate of 500 μL/min. The product solution which was obtained from the outlet of the chip, was then collected in an Eppendorf tube. Finally, the collected samples were dialysed (Slide-A-Lyzer Dialysis cassette, 10 k MWCO, Thermo Scientific) overnight with x1000 volume of buffer ensuring at least 2 times buffer exchange (PBS, pH 7.4). Formulated particles were kept at 4 °C.

Liposomes were composed of molar ratios of 58 mol% DSPC (NOF corporation, Europe), 37 mol% cholesterol (Sigma-Aldrich), DSPE-PEG 4.75 mol% (NOF corporation, Europe) or DSPE-PEG-Ligand, and 0.25 mol% DSPE-PEG-Alexa647.

Nanoparticle characterization:

The average sizes of the formulated particles as well as the polydispersity were determined to assess liposome quality. Measurements were done using dynamic light scattering techniques (DLS, Zetasizer Pro, Malvern Panalytical GmbH). Low volume UV transparent disposable cuvettes (Sarstedt, Inc). A back scatter measurement was performed with applying a fluorescent optical filter, a material refractive index (R_I) of 1.45, 25 °C temperature and an absorption of 0.001. All liposomes were in the size range of 74-86 nm. (see Table 2)

Table 3: Average size as well as the PDI of the glycooligomer conjugated liposomes show a size range of 83-86 nm. The controls naked and hL conjugated liposome showa size range of 74-77 nm.

Sample Name	Avg. Size (nm)	PDI
GL-MAN1	83.64	0.18
GL-MAN2	83.31	0.18
GL-MAN3	82.23	0.23
GL-MAN0	86.12	0.21
hL	77.60	0.18
Naked	74.48	0.24

4. References

(1) Carr, H.Y.;Purcell, E.M. Effects of Diffusion on Free Precession in Nuclear Magnetic Resonance Experiments. *Phys. Rev*. **1954**, *94*, 630-638.

(2) Meiboom, S.; Gill, D. Modified Spin-Echo Method for Measuring Nuclear Relaxation Times. *Rev. Sci. Instrum.* **1958**, *29*, 688-691.

(3) Wamhoff, E.C.; Hanske, J.; Schnirch, L.; Aretz, J., Grube, M.; Varón Silva, D.; Rademacher C. ^{19}F NMR-Guided Design of Glycomimetic Langerin Ligands. *ACS Chem. Biol.,* **2016**, *11*, 2407–2413.

(4) Ponader, D.; Wojcik, F.; Beceren-Braun, F.; Dernedde, J.; Hartmann, L.; *Biomacromolecules*, **2012**, *13*, 1845-1852.

(5) Hayes, W.; Osborn, H.M.I.; Osborne, S.D.; Rastall, R.A.; Romagnoli, B. One-pot synthesis of multivalent arrays of mannose mono- and disaccharides. *Tetrahedron*, **2003**, *59*, 7983-7996.

(6) Wu, L.; Sampson, N.S. Fucose, Mannose, and β-N-Acetylglucosamine Glycopolymers Initiate the Mouse Sperm Acrosome Reaction through Convergent Signaling Pathways. *ACS Chem. Biol.,* **2014**, *9*, 468-475.

(7) Schulze J.; Rentzsch M.; Kim D.; Bellmann L.; Stoitzner P.; Rademacher C. A Liposomal Platform for Delivery of a Protein Antigen to Langerin-Expressing Cells. *Biochem.,* **2019**, *58*, 2576–2580.

4.2 Homo- and heteromultivalent umbrella glycooligomers targeting Langerin and DC-SIGN

Serap Üclü, Iris Bermejo, Nowras Rahhal, Felicitas Drees, Christoph Rademacher, Laura Hartmann*

Publication Draft

Own Contribution:

Collaborative project design. Synthesis and purification of building blocks for solid phase polymer synthesis and synthesis of umbrella glycooligomers. Measurement and evaluation of all LC-MS experiments of the glycooligomers and evaluation of all NMR and UHR spectra of glycooligomers. Design and performance of Inhibition-Competition Assay via SPR as well as evaluation and interpretation of the IC_{50} values. Writing of the first publication draft.

Homo- and heteromultivalent umbrella glycooligomers targeting Langerin and DC-SIGN

Serap Üclü[a], Iris Bermejo[b], Nowras Rahhal[b], Felicitas Drees[a], Christoph Rademacher[b], Laura Hartmann[a,c]*

a. Department for Organic Chemistry and Macromolecular Chemistry, Heinrich Heine University Düsseldorf, Universitätsstraße 1, Düsseldorf 40225, Germany. E-mail: laura.hartmann@hhu.de

b. Department of Pharmaceutical Sciences, University of Vienna, Josef-Holaubeck-Platz 2, 1090 Vienna, Austria. E-mail: christoph.rademacher@univie.ac.at

c. [c] Institute for Macromolecular Chemistry, University Freiburg, Stefan-Meier-Str. 31, 79104 Freiburg i.Br., Germany

* Corresponding author: laura.hartmann@makro.uni-freiburg.de

Abstract

Langerin and DC-SIGN are considered key receptors of the immune system that are selectively used in drug development e.g., for receptor-mediated delivery of antivirals or vaccines against cancer. To obtain high avidity and potentially selective ligands targetings these receptors, we created homo- and heteromultivalent glycomacromolecules with a trivalent umbrella head group. This head groups is modelled after the trimeric arrangement of carbohydrate recognition domains (CRDs) of Langerin in order to achieve high avidity binding through statistical rebinding. By further variation of the handle attached to the umbrella head group, additional effects on the binding to Langerin and DC-SIGN by potential multivalent binding and sterical shielding are explored.

Binding to both receptors is investigated using surface plasmon resonance inhibition-competition assay. The comparison between Langerin and DC-SIGN shows that distinct features of our umbrella design lead to favoured binding to either one of the receptors: While Langerin shows increased binding to the smallest umbrella glycooligomer consisting of Man umbrella head, DC-SIGN prefers the umbrella glycooligomers carrying Man umbrella head and a hydrophobic handle. Conjugating of the umbrella-like glycomacromolecules to glycoliposomes then enables the investigation of cellular binding on Langerin- and DC-SIGN-overexpressing cells. In accordance with the receptor binding study, glycoliposome decorated with an umbrella oligomer presenting three Man ligands in the head and a hydrophilic handle show highest cellular binding to DC-SIGN-expressing Raji cells.

Introduction

The dendritic cells (DC) located in the skin are our body's first line of defence.[1] In case of infection by invasion through the skin, pathogens are recognized by the dendritic cells in the epidermis and transported and presented to the B and T cells in the lymphatic system to trigger an immune response.[2-4] The B cells recognize the pathogenic antigens, produce the corresponding antibodies and release them. These antibodies are then able to selectively inhibit the pathogens and protect the healthy cells from infection. The T cells, on the other hand, recognize cells that are already infected and eliminate them before the infection can spread.[5-7] The interaction between the DCs and the pathogen occurs through the pathogen

recognition receptors (PRRs) on the cell surface.[8,9] Type C lectin receptors (CLRs) are a subfamily of PRRs that recognize glycans in response to calcium ions.[10] CLRs perform diverse immunological functions such as mediating cell-cell adhesion, migration, and endocytosis of antigens and are central sensory systems for the regulation of the immune response by DC.[11] A key function at the interface of adaptive and innate immunity is played by Langerin and DC-specific ICAM-3-grabbing nonintegrin (DC-SIGN), which are members of PRRs and CLR.[12,13] While Langerin is expressed uniquely by Langerhans cells (LCs), a subset of DCs, DC-SIGN is expressed on DCs.[14] The trimeric arranged binding sides of Langerin consist of calcium-dependent carbohydrate recognition domain (CRD) and a short cytoplasmic tail containing a proline-rich motive that is involved in pathogen recognition and signal transduction, respectively.[15] Langerin has high affinity for mannose[16], (a- 1,2-linked) fucose[16], GlcNAc[16], b-glucans[17] and sulphated glycans[18,19] in millimolar range and allows the recognition of viruses, e.g. HIV-1[20,21] and HSV[22], mycobacteria, e.g. M. tuberculosis[23] and S. cerevisiae[24], and fungi[19] e.g. C. albicans[25] and Mal. Furfur[26]. These features of Langerin overlap with the specificity and pathogen recognition of DC-SIGN.

DC-SIGN (DC-specific ICAM-grabbing non-integrin) is involved in adhesion, antigen presentation, immunomodulation and dissemination of pathogens.[27] Langerin is involved in attachment and uptake of invading pathogens during the initial stages of the immune response.[28] Interestingly, Langerin is involved in host defence and pathogen dissemination.[29] In the case of HIV infection, the virus is internalized into the LC and subsequently degraded in the Birbeck granula, protecting the LC from infection.[15, 30] However, Langerin also functions as an anchoring and internalization factor in many infectious processes involving bacteria, viruses, and fungi. In the case of influenza a virus (IAV), Langerin acts as a major mediator in IAV infections.[31] Due to its dual nature, Langerin is a challenging target for the development of novel therapeutics, as it often promotes infection, but also acts as a defensive agent, potentially triggering the production of Birbeck granules. Therefore, Langerin is a prime candidate for the development of novel ligands that can be used to modulate the immune response in favour of activation or inhibition. Such ligands are useful for both drug delivery and receptor inhibition. A particular problem is posed by the fact that the DC-SIGN and Langerin lectins both recognize the same carbohydrate components , which makes it challenging to target only one lectin.

In this study, we explore the potential of rational design of glycomimetics based on the structure of the receptor and the spatial arrangement of carbohydrate recognition domains (CRDs) to specifically target Langerin or DC-SIGN and to yield high specificity for one of the lectins. Primary carbohydrate binding sites in the symmetric trimer of Langerin are located 24 Å from the point of symmetry. In a previous study, we have already used the carbohydrate recognition domain (CRD) arrangement of Langerin as a template and produced three-fold branched mannose-containing glycooligomers in different sizes by elongating and shortening the arm lengths. We found that the smallest 3-armed branched structure with a contour length of 15-21 Å had the highest avidity towards Langerin.[32] Based on these results, we prepared a much smaller trivalent building block with a contour length of 7 Å, creating umbrella-like glycooligomers (see Figure 1). This trivalent building block forms the head group of umbrella motifs and allows triantennary carbohydrate presentation. The high local density of carbohydrates and spatial proximity hypothetically increases the avidity towards Langerin through increasing the statistical rebinding effect. Through the installation of additional carbohydrate units in the umbrella handle could further increase the statistical binding. The umbrella-like glycooligomers were used to investigate the effects of valence on potential receptor selectivity by studying DC-SIGN and langerin. First, binding to Langerin and DC-SIGN is analysed by surface plasmon resonance (SPR) inhibition competition assay. In addition, the ligands will be conjugated to liposomes and studied on Langerin and DC-SIGN overexpressed cells to demonstrate the potential of glycaemic ligands for cell targeting and drug delivery.
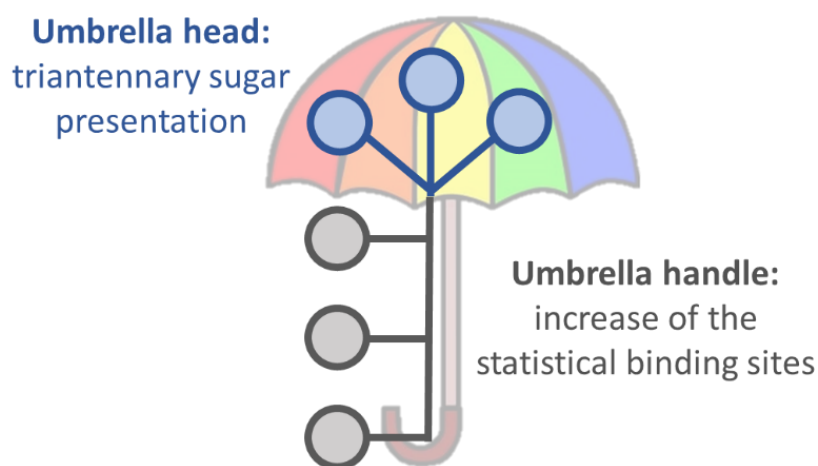

Figure 1: Schematic presentation of umbrella glycooligomer. Umbrella head allows the triantennary carbohydrate presentation in high carbohydrate density and umbrella handle allows to increase the statistical binding sites by additional carbohydrate presentation.

Methods

Materials: Aceton (≥ 99.8%), triethylamine (analytical grade), toluol (for HPLC) was purchased from Fischer Scientific. Succinic anhydride (≥ 99.0%) was purchased from Carbolution Chemicals. Diethyl ether (with BHT as inhibitor, ≥ 99.8%), triisopropylsilane (TIPS) (98%), (+)-sodium-L-ascorbate (≥99.0%), chloroform-*d* (99,8 atom % D), deuteriumoxid-*d₂* (99,8 atom % D), dimethylsulfoxid-*d₆* (99,8 atom % D), were purchased from Sigma-Aldrich. *N,N*-Diisopropylethylamine (DIPEA) (≥ 99%), potassium hydroxide (≥ 85%) was purchased from Carl Roth. Methanol (100%), ethyl acetate (>99.9%), n-hexane (≥99.8%) and acetic anhydride (99.7%) were purchased from VWR BDH Prolabo Chemicals. Dimethylformamide (DMF) (99.8%, for peptide synthesis), *tert*-butanol (≥ 99.0%), piperidine (99%), sodium methoxide (97%), sodium diethyldithiocarbamate (99%), tritylchloride and copper (II)sulfate (98%) were purchased from Acros Organics. Dichloromethane (DCM) (99.99%), Triethylsilan (≥ 98,0 %), trifluoroacetic acid (≥ 99,0 %), 9-fluorenylmethyl chloroformate (Fmoc-Cl) were purchased from Fluorochem UK. Benzotriazole-1-yl-oxy-tris-pyrrolidino-phosphonium hexafluorophosphat (PyBOP) were purchased from Iris Biotech GmbH. The anion resin (AG1-X8, quarternary ammonium, 100-200 mesh, acetate form) was purchased from BioRad. TentaGel® resin were purchased from Rapp Polymere. Methyl-α-D-mannopyranoside (>99%), 1-ethyl-3-(3-dimethylaminopropyl)carbodiimide hydrochloride (EDC), N-hydroxysuccinimide (NHS), 10 mM sodium acetate pH 4.0, 1.0 M ethanolamine-HCl pH 8.5, HBS-P⁺ buffer was purchased from Cytiva. Calcium chloride, Glycin, Sodium hydroxide TritonX100 was purchased from Sigma Aldrich. Diethylenetriamine was purchased from Merk (>98%), di-tert-butyldicarbonat (≥99,0 %) was purchased from Novabiochem. Ethanol (>99.9%). was purchased from Chemsolute. 2,2-(ethylenedioxy)bis(ethylamine) was obtained from TCI Europe. Citric acid, anhydrous; 4-pentynoic acid were purchased from Alfa Aesar (>99.5%).

Synthesis: The building blocks EDS[36], TDS[37], Man-N₃[38] and Gal-N₃[39] were synthesized according to literature.

Solid phase polymer synthesis of umbrella-like glycooligomer: Glycooligomers were generated by repeatedly coupling and deprotecting the building units on solid support to examine the binding toward Langerin and DC-SIGN. The reactions were conducted in Multisynthech GmbH polypropylene syringe reactors with a polyethylene frit and a Luer stopper. TentaGel® SRAM resin was employed as the solid support and pre-functionalized with ethylenediamine. The

batch size for each glycooligomer was 0.1 mmol, and the loading was 0.20 mmol/g. In order to produce a umbrella like glycooligomer, the functional TT linker was used as umbrella head group. The building blocks EDS and TDS were chosen to build the umbrella handle.

Coupling and Fmoc-deprotection of the building blocks: First the resin was first swollen twice for 15 min in DCM and then washed three times with DMF. The coupling steps of TDS, Fmoc-Lys(Boc)-OH and PA were performed by shaking for 1 h with a mixture of 5 equivalents of the building block (TDS, EDS or TT linker), 5 equivalents of PyBOP and 10 equivalents of DIPEA in DMF followed by washing steps ten times with DMF. After each coupling, the resin was shaken with a solution of 25 Vol% piperidine in DMF for 15 min and then washed three times with DMF. This washing step was repeated two times and then washed ten times with DMF.

Copper(I)-catalyzed alkyne-azide cycloaddition (CuAAC): The glycoconjugation to the glycooligomer backbone was carried out via CuAAC. For this, 2,5 equivalents of (2-azidoethyl)-2,3,4,6-tetra-O-acetyl-α-D-mannopyranoside (Man-N_3 or Gal-N_3) per alkyne was dissolved in 2 ml DMF, of 30 mol% of sodium ascorbate and of 30 mol% of copper sulfate per alkyne was dissolved in 0,5 ml water. The copper sulfate solution was drawn up first, then the carbohydrate solution, and finally the sodium ascorbate solution. The syringe was covered with aluminum foil and shaken overnight. The resin was then washed three times with a 23 mM solution of sodium diethyldithiocarbamate in DMF/H_2O (1:1, v/v), three times with DMF, and three times with DCM. The washing steps were repeated with the three solutions until no coloration of the wash solution was observed.

Deprotection of carbohydrate-pyranoside and cleavage from the resin: After successful conjugation of carbohydrate-pyranoside, the deprotection of hydroxyl groups was performed in 0.1 M NaOMe in methanol and shaken for 1 h. Then the syringe was washed ten times with methanol, ten times with DMF and ten times with DCM. The glycooligomer was cleaved from the resin by shaking with a solution of 35 Vol % TFA, 60 Vol % DCM, and 5 Vol % TIPS. The solution was precipitation in cold diethyl ether and the white precipitate was centrifuged off. The white solid was then dissolved in water and the product isolated by lyophilization.

Inhibition-Competition Experiments via SPR: The inhibition competition assay was performed by using SPR by using the binding wizard. First, a C1 chip was immobilized via EDC/NHS with BSA mannose by using the immobilization wizard. This resulted in an immobilization level of

1125 RU and the reference cell immobilized with ethanolamine resulted in an immobilization level of 17 RU. For the inhibition competition measurements, a fixed concentration of Langerin (4 µM) or DC-SIGN (0.5 µM) was tested with each glycooligomer in a concentration range of 3.125 - 800 µM. For this purpose, a 92 µM stock solution of Langerin (20 µM for DC-SIGN) and a solution of each glycooligomer were diluted in running buffer (HBS-P$^+$ buffer with 5 mM CaCl$_2$) to a final concentration of 4 µM of Langerin (0,5 µM for DC-SIGN). The incubation time was set at 5 min before measurement. As a reference, a solution of protein without glycooligomer was measured and denoted as 0 µM. The multi-cycle run with a flow rate of 15 µl/min, an association time of 240 s and a dissociations time of 120 s was used. The regeneration was carried out by using a 0.2 M methyl-α-D-mannopyranoside in water was injected for 60 s with a flow rate of 5 µl/min. The SPR studies were performed on two different C1-Chips. The first C1-Chip had and immobilization level of 1125 RU on the measuring cell and 17 RU on the reference cell. The second C1 chip had an immobilization level of 998 RU on the measuring cell and 25 RU on the reference cell. Glycooligomers were measured 2 times on the first chip and once on the second chip.

Cell Binding Experiment: The human Raji cell line from hematopoietic origin was used for the binding assay of the formulated particles. DC-SIGN and human Langerin (hL) receptors were previously transfected with a lentiviral vector to the cells.[40]

Cells were cultured and incubated in round flat-bottom plastic culture dishes (Corning) at 37 °C and 5 % CO$_2$ (Cooling incubator KB series, Binder GmbH, Germany). For Raji suspension cells, Roswell Park Memorial Institute Medium (RPMI) 1640 medium supplemented with 10 % V/V fetal calf serum (FCS) and 100 U/ml Penicillin-Streptomycin antibiotic mixtures (Thermofisher Scientific, Germany) were used. Cells were split and maintained between 0.5-3 Mio cells/ml. In addition cells were monitored with a light microscope.

To analyse receptor specificity of targeted liposomes, binding to Raji cells transfected with human Langerin and WT cells were analysed in flow cytometric via the coformulated liposomal dye Alexa647 (Invitrogen, ThermoFisher Scientific, USA) conjugated to DSPC-PEG. Experiments were conducted in duplicates in round bottom 96 well plates. Cells were seeded at a 4*10^5 Raji cells per well and 10 µM of the liposomes were added in a total volume of 100 µl. Naked liposomes served as a negative control and hL liposomes as a positive control.

The plate was covered with a seal sheet, kept protected from light and incubated for 1h at 4 °C on ice. Afterward, the plate was centrifuged for 3 mins at 500 g, the supernatant was aspirated, and the cell pellets were resuspended in 150 µL Dulbecco's phosphate-buffered saline (DPBS) (Gibco TM, Thermo Fisher Scientific, USA). Subsequently, Alexa647 fluorescence intensity was measured using CytoFLEX S, Research Flow Cytometery (Beckman Coulter). Alexa674 Mean Fluorescence intensity (MFIs) were detected via the red laser (RL) 1-A. The obtained data was processed using the FlowJo and Origin software.

Results and Discussion

Synthesis of umbrella like glycooligomers

The umbrella-like sequence-defined glycooligomers were synthesized according to the previously established solid-phase polymer synthesis (SPPoS).[41-44] SPPoS allows the stepwise assembly of tailor-made building blocks (bbs), well-defined scaffolds with functional side chains for specific conjugation of carbohydrate units can be produced. This synthetic approach provides easy access to glycomacromolecules that differ in several structural parameters that have been shown to influence the resulting binding properties, such as the number, position and type of carbohydrate ligands, composition, and overall architecture from linear to branched scaffolds. Briefly, by employing standard Fmoc-peptide coupling protocols to sequentially conjugate tailormade bbs instead of amino acids, sequence-defined oligo(amidoamines) with alkyne side groups added by 4-pentenoic acid can be prepared. (see Figure 2) The alkyne side chains can then be further functionalized by conjugation via copper-catalyzed azide-alkyne cycloadditions (CuAAC) with carbohydrate-azide derivatives, in this case Man-azide or Gal-azide were used.[37,45] Here we present a new building block TT-Linker that carries three alkyne groups in close proximity, and forms here the umbrella head group. (see Figure 2A) The TT linker is prepared starting from tris(hydroxymethyl)aminomethane (TRIS) by first protecting the primary amino group with di-tert-butyl dicarbonate. The three hydroxyl groups are functionalized with propargyl bromide, resulting in three terminal alkyne. In the final step, the Boc-protected amino group is first deprotected with trifluoroacetic acid (TFA) and functionalized with succinic anhydride. (see SI for more details) By introducing the free carboxy group, the TT linker is directly compatible with solid-phase polymer synthesis and can be used with standard Fmoc-peptide coupling chemistry. The three alkyne groups allow

for straightforward introduction of three carbohydrate ligands by CuAAC with well-established reaction conditions and available azido-functionalized carbohydrate building blocks.[44] (see SI for details of synthesis and analytical data). This TT linker enables a high density of carbohydrate units in close proximity after glycoconjugation, a feature often related to increases in binding avidity by statistical rebinding and chelating effects.

In order to provide stability to the umbrella head formed by TT-linker or to enable the incorporation of further carbohydrates, an umbrella handle is attached to the umbrella head. The umbrella handle were constructed using the previously established EDS[36] (ethylene glycol diamine succinic acid) building block as a spacer building block that introduces hydrophilic ethylene glycol units into the oligomeric backbone and TDS[37] bb (triple bond diethylenetriamine succinic acid) to introduce single alkyne side chains (see Figure 2B, Figure 3) Glycoconjugation and deprotection of the carbohydrate-azide derivatives on the resin followed predetermined protocols.[41] Using an ethylenediamine preloaded resin, a C-terminal amine group is released after cleavage under acidic conditions. After cleavage, high relative purity of over 95% was detected for all structures by RP-HPLC and HR-MS, and the structure was finally confirmed by ^{1}H NMR as shown in Figure 3 (see SI for further details on the synthesis procedures and analytical data) A summary of the synthesized umbrella like glycooligomers is shown in Figure 4.
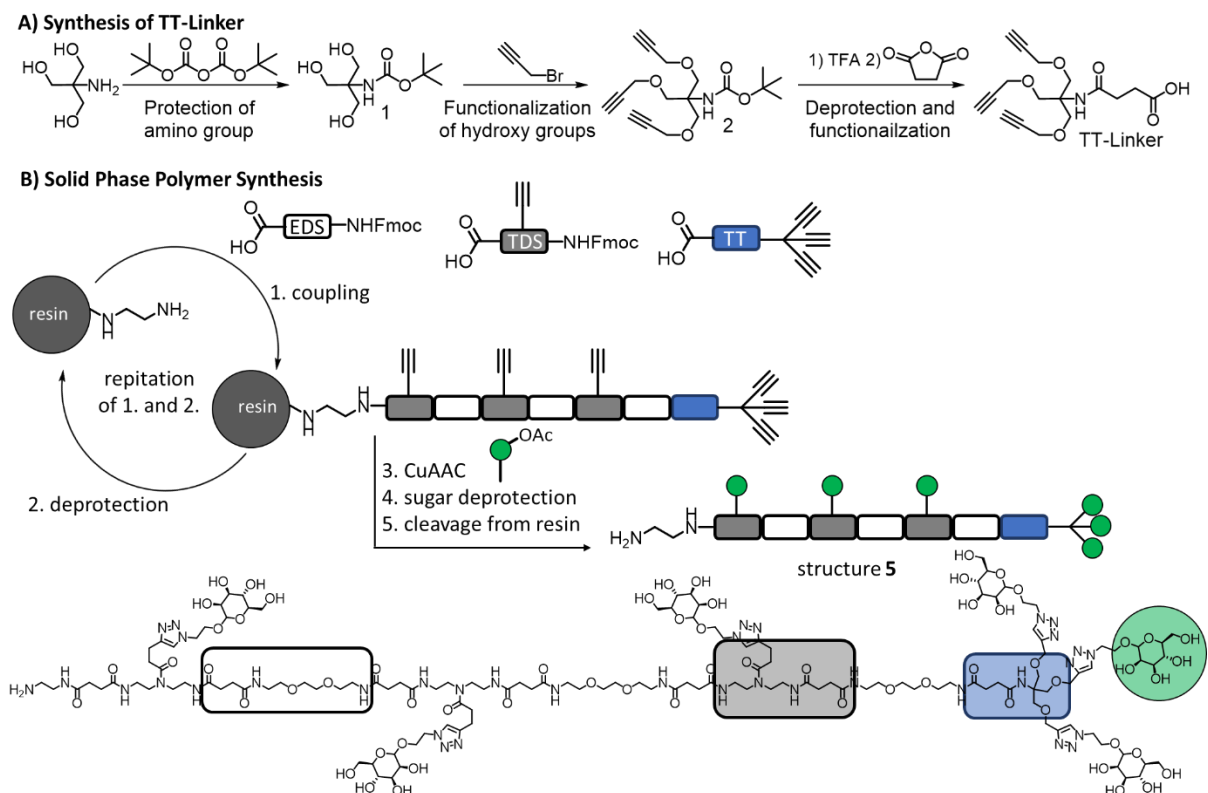
Figure 2: A) Synthesis of TT linker. B) Schematic representation of solid-phase polymer synthesis: stepwise assembly of umbrella structures with tailor-made building blocks using the example of the structure **5**. The umbrella handle consists of an alternating sequence of EDS and TDS and the TT linker forms the umbrella head. The alkyne groups are functionalized with a mannose azide derivative. BB and the carbohydrate derivatives were shown as symbols and chemical structure.
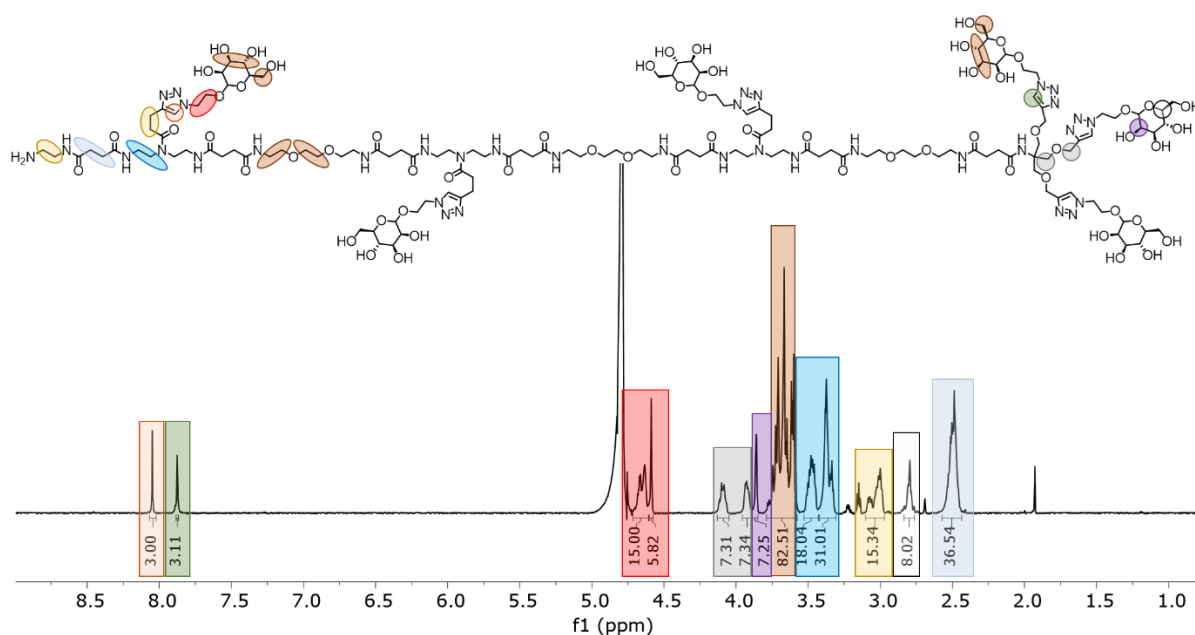
Figure 3: 600 MHz ^{1}H-NMR spectra of structure 5 measured in HDO at 25 °C.

The nomenclature of the umbrella structures is as follows: U for the umbrella head group, followed by the carbohydrate (Man or Gal), followed by the positions of EDS building blocks and the position of the carbohydrate (Man or Gal) forming the umbrella handle, e.g., U(Man)-EDS(2,4,6)-Man(1,3,5). For comparison, U(Man)-EDS(1-3) was also synthesized as a linear monovalent, non-umbrella structure by using PA (4-pentynoic acid) building block introducing only one alkyne group and named as L(Man)-EDS(1-3). However, for ease of reference, the glycooligomers were numbered (**1-7**) as shown in Figure 4.

A series of umbrella-like glycooligomers was prepared as shown in Figure 4. The structures can be divided into two sections: the trivalent umbrella head group allowing to study the influence of the geometrically arranged carbohydrate units on the binding affinity towards the trivalent Langerin and towards the tetravalent DC-SIGN and umbrella handle to investigate the impact of composition on binding. The structures 1, 2, and 4 consisting of Man bearing umbrella head and containing of increasing length of hydrophilic umbrella handle. While the structures 2 contains a handle consisting of three EDS, the glycooligomer 4 carries seven EDS units and provides steric stabilization. To study this effect, structure 1 does not contain a handle and is composed only of the umbrella head. For comparison, a monovalent mannose-containing oligomer 3 was prepared, which has a hydrophilic tail consisting of three EDS and the head group consists of the PA building block (see Figure 2).

85

The umbrella handle of the structure 5 is decorated with additional mannose units, which is expected to further increase statistical binding due to the higher valency. In parallel, heteromultivalent structures were obtained by systematically exchanging the binding Man units for the non-binding Gal units. While 6 carries trivalent Gal units in the umbrella head and the handle consists of three mannose units, it is the opposite for 7. Here, the influence of steric shielding effects is investigated in comparison to the first-generation structures carrying a handle without carbohydrate units. All glycooligomers were isolated and characterized by ^{1}H-NMR, RP-HPLC-ESI-MS and HR-MS (see SI for details on the synthesis, characterization and accompanying spectra).
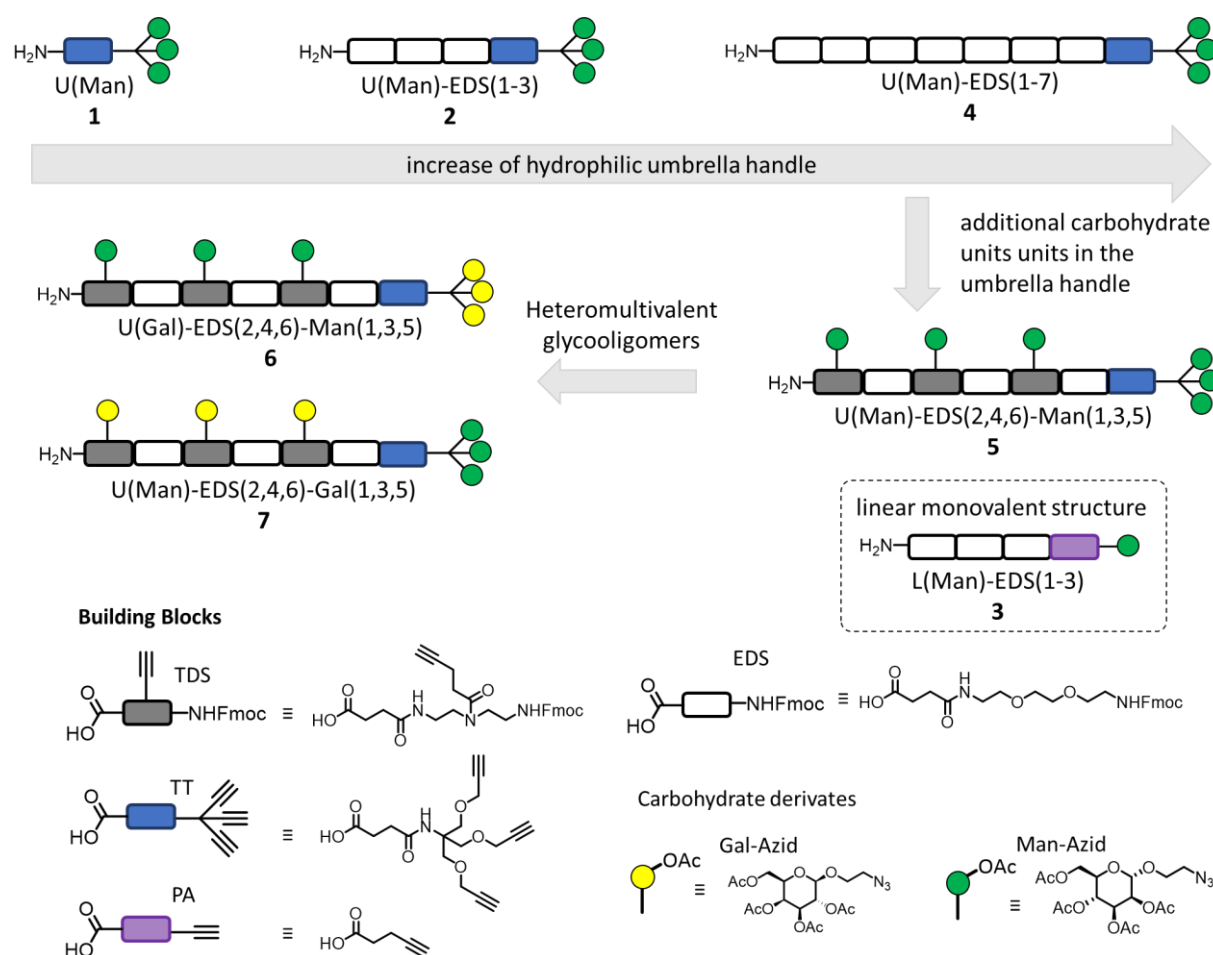

Figure 4: Overview of synthesized umbrella like precision glycomacromolecules divided in first and second generation. While the glycooligomers in the first generation introduces the trivalent umbrella head group and a hydrophilic tail in different length, the second generation displays further binding and non-binding carbohydrate units in the tail and built the umbrella handle.

Umbrella glycooligomers binding to Langerin and DC-SIGN

The binding affinities of the umbrella glycooligomers towards trimeric Langerin EDC and tetrameric DC-SIGN was determined via inhibition-competition-assay by using surface plasmon resonance spectroscopy (SPR) (see Figure 4 and SI for more details).

To obtain a high-affinity surface for both Langerin and DC-SIGN, the SPR chip surface was functionalized with Man-conjugated bovine serum albumin (Man-BSA) to reach a high level of Man functionalization. Then, the glycooligomers were mixed with either of the proteins at increasingly higher concentrations (0 – 800 µM) and binding to the SPR chip surface was measured. Glycooligomers bind to the proteins and inhibit the CRDs from interacting with the chip surface. As a result, binding is less than if the protein was free. This decrease in binding is proportional to the affinity of the ligand and can be represented as the 50 % inhibitory concentration (IC_{50}) required to completely prevent binding between protein and chip (see method section and SI for more details on the SPR assay and Hill plots for IC_{50} evaluation). The results for Langerin and DC-SIGN are summarized in Figure 5.
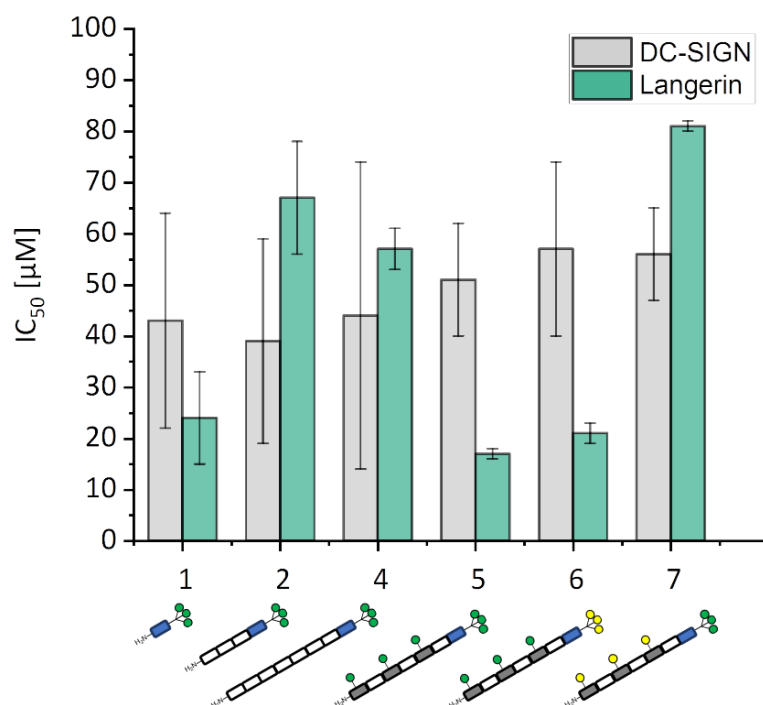

Figure 5: Inhibition-competition studies towards Langerin (green) and DC-SIGN (grey) measured via SPR show the highest bindings of **5** and **6** towards Langerin and for DC-SIGN the glycooligomers with a hydrophilic handle showed the highest binding affinity.

The comparison of the IC_{50} values between Langerin and DC-SIGN show clear differences between the structures with carbohydrate functionalized umbrella handle and with a hydrophilic handle. While for Langerin the structure **5** with three mannose units in the head group and three mannose units in the handle show the highest binding affinity. Interestingly, the structure **6** with three galactose units at the umbrella head and three mannose units at the umbrella handle shows an equally high binding affinity as **5**, while in contrast, the structure **7** with mannose as the umbrella head and galactose in the handle shows a significant decrease in binding affinity. To investigate the influence of umbrella head on binding affinities, structure **1** was measured separately against Langerin. The umbrella head with three mannose units shows a decrease in binding affinity compared to **5** and **6**, suggesting that the carbohydrate functionalized handle (whether binding Man or non-binding Gal) has a stabilizing effect on binding whereas Man functionalized handle offers further binding sites and yielding in more opportunities to achieve a statistical rebinding effect. The umbrella structures with hydrophilic handles **2** and **4** showed a decrease in binding affinities by a factor of 2 for Langerin. Interestingly, structure **7** with mannose head and galactose handle showed a decrease in binding strength by a factor of 4 compared to structure **5** and **6**, which is potentially attributed to the steric shielding effects of the handle.

In contrast, the inhibition study performed on DC-SIGN shows for all structures similar binding with only small differences for the different ligands. Thus when comparing Langerin and DC SIGN, structures **2**, **4** and **7** show higher binding to DC SIGN, while structures **1**, **5** and **6** show higher binding to Langerin. The umbrella glycooligomer **3** shows no binding for either Langerin or DC-SIGN (see SI Figure S25 and Figure S29). The comparison to a previous study in which trivalent, asymmetrically branched glycooligomers were prepared in different arm lengths and tested on Langerin.[32] The ^{19}F-NMR competition assay showed the highest binding to the smallest trivalent structure and yielded an IC_{50} value of 44 ± 6 µM.[32] The umbrella glycooligomers investigated in this study have similar IC_{50} values towards Langeirn.

Receptor specific cell targeting with umbrella glycooligomers

Ligand binding to receptors expressed on cell surfaces was studied by conjugating the umbrella glycooligomers with a lipid and then formulating them into glycoliposomes (see Figure 5 and the Method section for further details). For this purpose, commercial DSPE-PEG-

NHS ester was used as the lipid and conjugated to the glycooligomer, resulting in the lipid conjugate. For the reaction, the glycooligomers were dissolved in DMSO, a mixture of DIPEA and DSPE-PEG-NHS ester was added, and shaken overnight at 40 °C. Subsequent purification and removal of solvents was performed by dialysis against water for multiple times. After lyophilization, the products were analysed by ^{1}H-NMR, which was used to determine the coupling yield. The results are summarized in the attached information.

For formulation into glycoliposomes, two solutions were mixed in a microfluidic device. Here, lipids in ethanol formed the contained organic phase and the aqueous phase was composed of PBS buffer. A syringe pump was equipped with two syringes, one containing the lipids dissolved in ethanol and the other containing the PBS buffer. The pump was used to inject the two solutions into the inlets of the microfluidic chip via tubing, and the product solution was collected at the outlet of the chip. Finally, the collected samples were dialyzed overnight with PBS buffer. In this procedure, glycoliposomes were prepared with molar ratios of 58 mol% DSPC, 37 mol% cholesterol, 4.75 mol% DSPE-PEG or DSPE-PEG ligand, and 0.25 mol% DSPE-PEG-Alexa647. The glycoliposomes were characterized by DLS. The results are summarized in the supporting information. The nomenclature for the umbrella glycooligomer functionalized liposomes is as followed: GL represents gylcoliposome followed by the number for the glycooligomer, e.g. GL-1 represents gylcoliposome functionalized with structure **1**.

Flow cytometry was performed to investigate cellular binding. (see Figure 6) For this purpose, Langerin (Langerin+ cells) and DC-SIGN expressing Raji cells (DC-SIGN+ cells) were used. Raji wild-type (Raji-WT) cells served as a control cell line. Human Langerin (hL) was used as a positive control for Langerin+ cells, reflecting maximal binding to the Langerin+ cells.

Interestingly, the comparison of glycoliposome functionalized with glycooligomers with different hydrophilic handle lengths and the trivalent umbrella head group **1**, **2**, and **4** shows increased cellular uptake for **2** for both cell lines and highest uptake for DC-SIGN expressed cells. The interaction with receptors on cells would be expected to decrease with increasing tail length. However, it is clearly shown here that an excessively long GL-**4** or absent handle group decreases the uptake into cells. A possible explanation for GL-**4** could be that the long tail group leads to coiling and the head group with three mannose units is no longer available for interaction with surface receptors.[46] In contrast, **1** has no handle group, so it is directly conjugated to liposomes, making accessibility of the carbohydrate units more difficult. Sample

2 appears to have the correct handle length with three EDS, which is also confirmed by **3** with only one mannose unit.
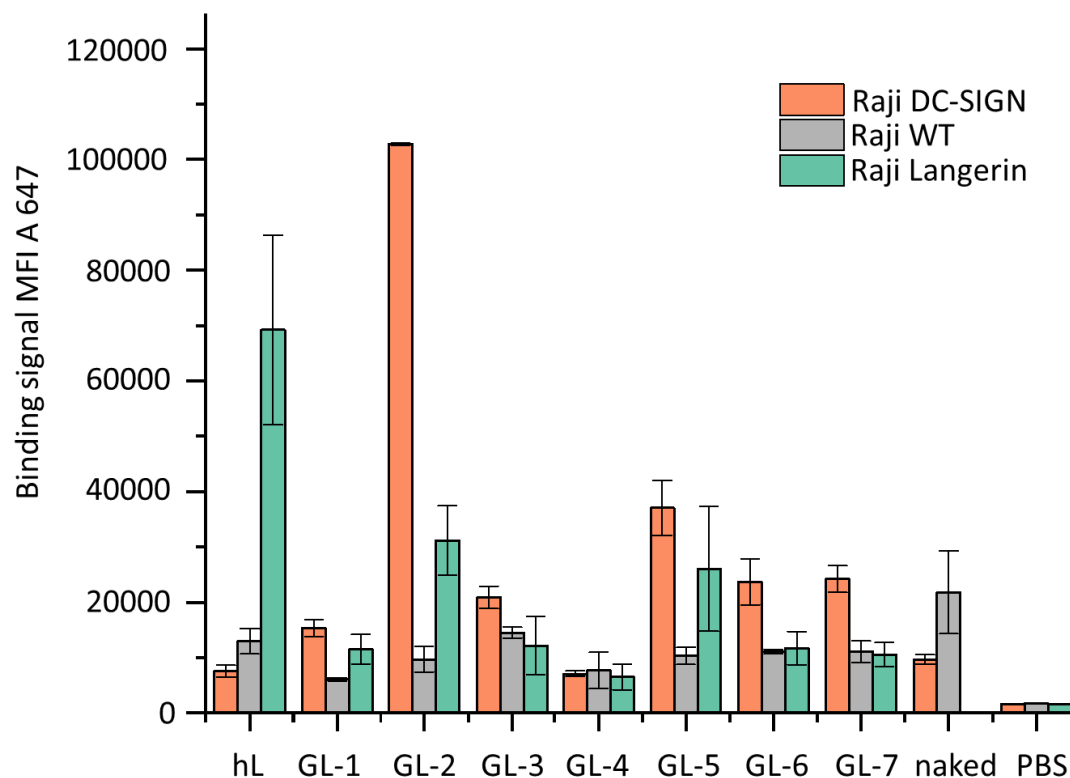

Figure 6: Glycoliposomes were incubated with Langerin (green) and DC-SIGN (orange) expressing Raji cells for 1 h on ice and the mean fluorescence intensity of A647 (MFI A627) was measured by flow cytometry. Raji WT (grey) was used as control cell line. Error bars represent the standard deviation of three independent measurements.

The glycooligomers with additional carbohydrate units positioned in the umbrella handle (see Figure 3) generally show an increase in cellular uptake for Langerin and DC-SIGN positive cells. A significantly higher uptake of **GL-5** with overall 6 Man units would be expected here. However, it shows similar uptake to **GL-7** with mannose head and galactose handle. This suggests that possibly the accessibility of the mannose units in the handle is hampered because the mannose head group can interact with the surface receptors beforehand. This is evident for **GL-6** with galactose head and mannose handle.

Conclusions

In this study, umbrella-like glycooligomers consisting of a trivalent umbrella head group to enable a high density of carbohydrate units and an umbrella handle were prepared using SPPoS. Additional binding carbohydrates to increase binding ability, non-binding carbohydrates for steric shielding, or a hydrophilic handle were inserted into the umbrella handle to examine the influence of a handle in presence of a trivalent Mannose bearing umbrella head. These umbrella-like glycooligomers were evaluated against Langerin and DC-SIGN by Inhibition-competition study conducted via SPR. According to this study, DC-SIGN binds to all structures in a similar manner with just small differences for the various ligands; however, langerin exhibits notable differences. The heteromultivalent structures made up of the mannose umbrella handle and the galactose umbrella head as well as the smallest structure composed of the umbrella head and the hexavalent mannose-bearing structure had the maximum binding to Langerin. Comparing Dc-SIGN with Langerin, however, showed that DC-SIGN favored the structures carrying a hydrophobic handle. Similar to this, stronger binding was seen between DC-SIGN and the heteromultivalent glycooligomer consisting of a mannose head and a galactose handle.

By formulating these glycoliposomes into liposomes, cellular binding to langerin- and DC-SIGN-expressing Raji cells was determined by flow cytometric analysis. While the cellular interaction of the glycoliposomes to Langerin-expressing Raji cells showed no differences, the cellular binding to DC-SIGN-expressing Raji cells was best for the glycoliposome with the hydrophobic handle composed of three EDS units and a mannose head. To investigate this mechanism in more detail, the trivalent umbrella scaffold can be combined with a higher affinity binding motif, e.g. with the positive control hL.

References

(1) Nouwen, L.V.; Everts, B. Pathogens MenTORing Macrophages and Dendritic Cells: Manipulation of mTOR and Cellular Metabolism to Promote Immune Escape. *Cells*, **2020**, *9*, 161.

(2) Banchereau, J.; Steinman, R. Dendritic cells and the control of immunity. *Nature,* **1998**, *392*, 245–252.

(3) Pollara, G.; Kwan, A.; Newton, P. J.; Handley, M. E.; Chain, B. M.; Katz, D. R. Dendritic cells in viral pathogenesis: protective or defective? *Int. J. Exp. Pathol.*, **2005**, *86*, 187-204.

(4) Chaplin D.D. Overview of the immune response. *J. Allergy Clin. Immunol.,* **2010**, *125*, 3–23.

(5) Cruz, F. M.; Colbert, J. D.; Merino, E.; Kriegsman, B. A.; Rock, K. L. The Biology and Underlying Mechanisms of Cross-Presentation of Exogenous Antigens on MHC-I Molecules. *Annu. Rev. Immunol.,* **2017**, *35*, 149–176.

(6) Gutiérrez-Martínez, E.; Planès, R.; Anselmi, G.; Reynolds, M.; Menezes, S.; Adiko, A. C.; Saveanu, L.; Guermonprez, P. Cross-Presentation of Cell-Associated Antigens by MHC Class I in Dendritic Cell Subsets. *Front. Immunol.,* **2015**, *6*, 363.

(7) Fehres, C.M.; Unger, W.W.J.; Garcia-Vallejo, J.J.; van Kooyk, Y. Understanding the Biology of Antigen Cross-Presentation for the Design of Vaccines against Cancer. *Front. Immunol.,* **2014**, *5*, 149.

(8) Buchta, C.M.; Bishop, G.A. Toll-like receptors and B cells: functions and mechanisms. *Immunol. Res.*, **2014**, *59*, 12-22.

(9) Kumar, H.; Kawai, T.; Akira, S. Pathogen recognition in the innate immune response. *Biochem.,* **2009**, *420*, 1-16.

(10) Yan H.; Kamiya T.; Suabjakyong P.; Tsuji N.M. Targeting C-Type Lectin Receptors for Cancer Immunity. *Front Immunol.,* **2015**, *6*, 408.

(11) Lepenies, B.; Lang, R. Lectins and their ligands in shaping immune responses. *Front Immunol.,* **2019**, *10*, 2379.

(12) Fehres, C. M.; Kalay, H.; Bruijns, S. C. M.; Musaafir, S. A. M.; Ambrosini, M.; Van Bloois, L.; Van Vliet, S. J.; Storm, G.; Garcia- Vallejo, J. J.; Van Kooyk, Y. Cross-Presentation through Langerin and DC-SIGN Targeting Requires Different Formulations of Glycan- Modified Antigens. *J. Controlled Release,* **2015**, *203*, 67–76.

(13)   Tacken, P.J.; De Vries, I.J.M.; Torensma, R.; Figdor, C.G. Dendritic-Cell Immunotherapy: From Ex Vivo Loading to in Vivo Targeting. *Nat. Rev. Immunol.*, **2007**, *7*, 790–802.

(14)   Merad, M.; Ginhoux, F.; Collin, M. Origin, homeostasis and function of Langerhans cells and other langerin-expressing dendritic cells. *Nat. Rev.Immunol.*, **2008**, *8*, 935–947.

(15)   Birbeck, M.S.; Breathnach, A.S.; Everall, J.D. An Electron Microscope Study of Basal Melanocytes and High-Level Clear Cells (Langerhans Cells) in Vitiligo. *J. Invest. Dermatol.*, **1961**, *37*, 51-64.

(16)   Stambach, N.S.; Taylor, M.E. Characterization of carbohydrate recognition by langerin, a C-type lectin of Langerhans cells. *Glycobiology*, **2003**, *13*, 401–410.

(17)   de Jong, M.A.; Vriend, L.E.; Theelen, B.; Taylor, M.E.; Fluitsma, D.; Boekhout, T.; Geijtenbeek, T.B. C-type lectin Langerin is a beta-glucan receptor on human Langerhans cells that recognizes opportunistic and pathogenic fungi. *Mol. Immunol.*, **2010**, *47*, 1216–1225.

(18)   Tateno, H.; Ohnishi, K.; Yabe, R.; Hayatsu, N.; Sato, T.; Takeya, M.; Narimatsu, H.; Hirabayashi, J. Dual specificity of Langerin to sulfated and mannosylated glycans via a single C-type carbohydrate recognition domain. *J. Biol. Chem.* **2010**, *28*, 6390–6400.

(19)   Galustian, C.; Park, C.G.; Chai, W.; Kiso, M.; Bruening, S.A.; Kang, Y.S.; Steinman, R.M.; Feizi, T. High and low affinity carbohydrate ligands revealed for murine SIGN-R1 by carbohydrate array and cell binding approaches, and differing specificities for SIGN-R3 and langerin. *Int. Immunol.,* **2004**, *16*, 853–866.

(20)   Turville, S.G.; Cameron, P.U.; Handley, A.; Lin, G.; Pöhlmann, S.; Doms, R.W.; Cunningham, A.L. Diversity of receptors binding HIV on dendritic cell subsets. *Nat. Immunol.*, **2002**, *3*, 975–983.

(21)   de Witte, L.; Nabatov, A.; Pion, M.; Fluitsma, D.; de Jong, M.A.; de Gruijl, T.; Piguet, V.; van Kooyk, Y.; Geijtenbeek, T. B. Langerin is a natural barrier to HIV-1 transmission by Langerhans cells. *Nat. Med.,* **2007**, *13*, 367–371.

(22)   de Jong, M. A.; de Witte, L.; Taylor, M. E.; Geijtenbeek, T.B. Herpes simplex virus type 2 enhances HIV-1 susceptibility by affecting Langerhans cell function. *J. Immunol.*, **2010**, *185*, 1633–1648.

(23)   Mihret A. The role of dendritic cells in Mycobacterium tuberculosis infection. *Virulence*, **2012**, *3*, 654–659.

(24)   De Jesus, M.; Ostroff, G.R.; Levitz, S.M.; Bartling, T.R.; Mantis, N.J. A population of Langerin-positive dendritic cells in murine Peyer's patches involved in sampling β-glucan microparticles. *PLoS One*, **2014**, *9*, e91002.

(25)   De Jesus, M.; Rodriguez, A.E.; Yagita, H.; Ostroff, G.R.; Mantis, N.J. Sampling of Candida albicans and Candida tropicalis by Langerin-positive dendritic cells in mouse Peyer's patches. *Immunol Lett*., **2015**, *168*, 64–72.

(26)   Stoitzner, P.; Romani, N. Langerin, the "Catcher in the Rye": an important receptor for pathogens on Langerhans cells. *Eur J Immunol*., **2011**, *41*, 2526–2529.

(27)   Geijtenbeek, T., Gringhuis, S. Signalling through C-type lectin receptors: shaping immune responses. *Nat. Rev. Immunol*., **2009**, *9*, 465–479.

(28)   Fehres, C.M.; Duinkerken, S.; Bruijns, S.C.; Kalay, H.; van Vliet, S.J.; Ambrosini, M.; de Gruijl, T.D.; Unger, W.W.; Garcia-Vallejo, J.J.; van Kooyk, Y. Langerin-mediated internalization of a modified peptide routes antigens to early endosomes and enhances cross-presentation by human Langerhans cells. *Cell*. *Mol. Immunol.,* **2017**, *14*, 360–370.

(29)   Mnich, M.E.; van Dalen, R.; van Sorge, N.M. C-Type Lectin Receptors in Host Defense Against Bacterial Pathogens. *Front. Cell. Infect. Microbiol*., **2020**, *10*, 309.

(30)   Sagebiel, R. W., Reed, T.H. Serial reconstruction of the characteristic granule of the Langerhans cell. *J Cell Biol.*, **1968**, *36*, 595–602.

(31)   Ng, W.C.; Londrigan, S.L.; Nasr, N.; Cunningham, A.L.; Turville, S.; Brooks, A.G.; Reading, P.C. The C-type Lectin Langerin Functions as a Receptor for Attachment and Infectious Entry of Influenza A Virus. *J. Virol.*, **2015**, *90*, 206–221.

(32)   Neuhaus, K., Wamhoff, E. C., Freichel, T., Grafmüller, A., Rademacher, C., Hartmann, L. Asymmetrically branched precision glycooligomers targeting langerin. *Biomacromolecules*, **2019**, *20* , 4088-4095.

(33)   Hayes, W.; Osborn, H.M.I.; Osborne, S.D.; Rastall, R.A.; Romagnoli, B. One-pot synthesis of multivalent arrays of mannose mono- and disaccharides. *Tetrahedron*, **2003**, *59*, 7983-7996.

(34)   Wu,L.; Sampson, N.S. Fucose, Mannose, and β-N-Acetylglucosamine Glycopolymers Initiate the Mouse Sperm Acrosome Reaction through Convergent Signaling Pathways. *ACS Chem. Biol.*, **2014**, *9*, 468-475.

(35)   Chabre, Y.M.; Contino-Pépin, C.; Placide, V.; Shiao, T.C.; Roy, R. Expeditive Synthesis of Glycodendrimer Scaffolds Based on Versatile TRIS and Mannoside Derivatives. *J. Org. Chem.*, **2008**, *73*, 5602–5605.

(36)   Ponader, D.; Igde, S.; Wehle, M.; Märker, K.; Santer, M.; Bléger, D.; Hartmann, L. *Beilstein J. Org. Chem.*, **2014**, *10*, 1603–1612.

(37)   Ponader, D.; Wojcik, F.; Beceren-Braun, F.; Dernedde, J.; Hartmann, L.; *Biomacromolecules*, **2012**, *13*, 1845-1852.

(38)   Hayes, W.; Osborn, H.M.I.; Osborne, S.D.; Rastall, R.A.; Romagnoli, B. One-pot synthesis of multivalent arrays of mannose mono- and disaccharides. *Tetrahedron*, **2003**, *59*, 7983-7996.

(39)   Wu, L.; Sampson, N.S. Fucose, Mannose, and β-N-Acetylglucosamine Glycopolymers Initiate the Mouse Sperm Acrosome Reaction through Convergent Signaling Pathways. *ACS Chem. Biol.,* **2014**, *9*, 468-475.

(40)   Schulze J, Rentzsch M, Kim D, Bellmann L, Stoitzner P. Rademacher C. A Liposomal Platform for Delivery of a Protein Antigen to Langerin-Expressing Cells. *Biochemistry*, **2019**, *58*, 2576–80.

(41)   Wojcik, F.; Mosca, S.; Hartmann, L. Solid-Phase Synthesis of Asymmetrically Branched Sequence-Defined Poly/Oligo(amidoamines). *J. Org. Chem.,* **2012**, *77*, 4226–4234.

(42)   Hill, S. A., Gerke, C., & Hartmann, L.. Recent Developments in Solid-Phase Strategies towards Synthetic, Sequence-Defined Macromolecules. *Chem. Asian J.*, **2018**, *13*, 3611–3622.

(43)   Wojcik, F.; O'Brien, A.G.; Götze, S.; Seeberger, P.H.; Hartmann, L. Synthesis of homo- and heteromultivalent carbohydrate-functionalized oligo(amidoamines) using novel glyco-building blocks. *Beilstein J. Org. Chem.*, **2013**, *9*, 2395-2403.

(44)   Freichel, T.; Eierhoff, S.; Snyder, N.L.; Hartmann, L. Toward Orthogonal Preparation of Sequence-Defined Monodisperse Heteromultivalent Glycomacromolecules on Solid Support Using Staudinger Ligation and Copper-Catalyzed Click Reaction. *J. Org. Chem.*, **2017**, *82*, 9400-9409.

(45)   Baier, M.; Giesler, M.; Hartmann, L. Split-and-Combine Approach Towards Branched Precision Glycomacromolecules and Their Lectin Binding Behavior. *Eur. J. Chem.* **2017**, *24*, 1619-1630.

(46)   Park, H.; Rosencrantz, R. R.; Elling, L.; Böker, A. Glycopolymer Brushes for Specific Lectin Binding by Controlled Multivalent Presentation of N-Acetyllactosamine Glycan Oligomers. *Macromol. Rapid Commun.*, **2015**, *36*, 45-54.

Supporting Information

Homo- and heteromultivalent umbrella glycooligomers targeting Langerin and DC-SIGN

Serap Üclü,[‡a], Maxim Denis [b], Hengxi Zhang [b], Felicitas Drees[a], Christoph Rademacher*[b] and Laura Hartmann*[a]

a. Department for Organic Chemistry and Macromolecular Chemistry, Heinrich Heine University Düsseldorf, Universitätsstraße 1, Düsseldorf 40225, Germany. E-mail: laura.hartmann@hhu.de

b. Department of Pharmaceutical Sciences, University of Vienna, Josef-Holaubeck-Platz 2, 1090 Vienna, Austria. E-mail: christoph.rademacher@univie.ac.at

1. **Instrumentation:**

Nuclear Magnetic Resonance spectroscopy (NMR)

^{1}H-NMR (600 and 300 MHz) spectra were mesured on a Bruker AVANCE III – 600. Chemical shifts of all NMR spectra were expressed in parts per million (ppm). For ^{1}H NMR, the residual non-deuterated solvent was used as an internal standard (δ 4.79 ppm for HDO). The resulting multiplications were given as s for singlet, d for doublet, t for triplet, and m for multiplet.

Reversed Phase - High Pressure Liquid Chromatography - Mass Spectrometry (RP-HPLC-MS)

Reversed Phase - High Pressure Liquid Chromatography - Mass Spectrometry (RP-HPLC-MS): Analysis were performed using an Agilent 1260 Infinity instrument equipped with a variable wavelength detector (VWD) (set at 214 nm) and a 6120 quadrupole LC/MS with an electrospray ionization (ESI) source (operated in positive ionization mode in an m/z range of 200 to 2000). A Poroshell 120 EC-C18 (3.0×50 mm, 2.5 µm) RP column from Agilent was used as the HPLC column. Mobile phases A and B were H_2O/ACN (95 Vol %/5 Vol %) and H_2O/ACN (5 Vol %/95 Vol %), respectively. Both mobile phases contained 0.1 % formic acid. The temperature of the column chamber was set at 25 °C. UV and MS spectral analysis was done using Agilent Technologies OpenLab ChemStation software for LC/MS.

Ultra-High Resolution - Mass Spectrometry (UHR-MS)

The MS measurements were conducted with a Bruker UHR-QTOF maXis 4G instriument using a direct inlet vial syringe pump and an ESI source.

Freeze dryer

The glycooligomers were lyophilized using Alpha 1-4 LD plus instrument from Martin Christ Freeze Dryers GmbH. The Drying method was fixed to -55 °C and 0.1 mbar.

Surface Plasmon Resonance (SPR)

Inhibition-Competition Experiments were run with a Biacore X100 instrument from GE Healthcare Life Sciences. The sonograms were analyzed using the Biacore X100 Evaluation Software.

2. Characterization of the umbrella glycooligomers

Compound: U(Man) **(1)**
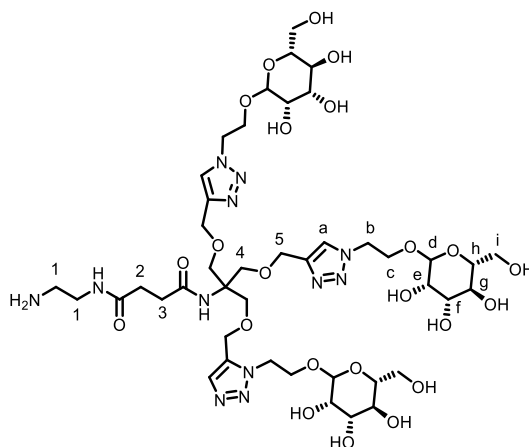
^{1}H NMR (600 MHz, D$_2$O) δ 8.06 (s, 3H), 4.78 (d, *J* = 1.5 Hz, 3H), 4.66 (td, *J* = 6.5, 5.9, 3.8 Hz, 5H), 4.58 (s, 6H), 4.09 (ddd, *J* = 11.1, 7.7, 3.7 Hz, 3H), 3.94 – 3.88 (m, 3H), 3.84 (dt, *J* = 3.3, 1.5 Hz, 3H), 3.73 – 3.62 (m, 26H), 3.58 (t, *J* = 9.7 Hz, 3H), 3.48 (t, *J* = 5.9 Hz, 2H), 3.13 (t, *J* = 6.0 Hz, 2H), 3.06 (ddd, *J* = 9.8, 5.7, 2.4 Hz, 3H), 2.49 (dt, *J* = 17.1, 4.7 Hz, 5H).

HR-MS calculated [M+2H]$^{2+}$ 563.3, found 563.2.

RP-HPLC: (5%/95% ACN/H$_2$O→ 5%/50% ACN/H$_2$O in 30 min at 25°C, 214 nm): t$_R$ = 4.91 min.
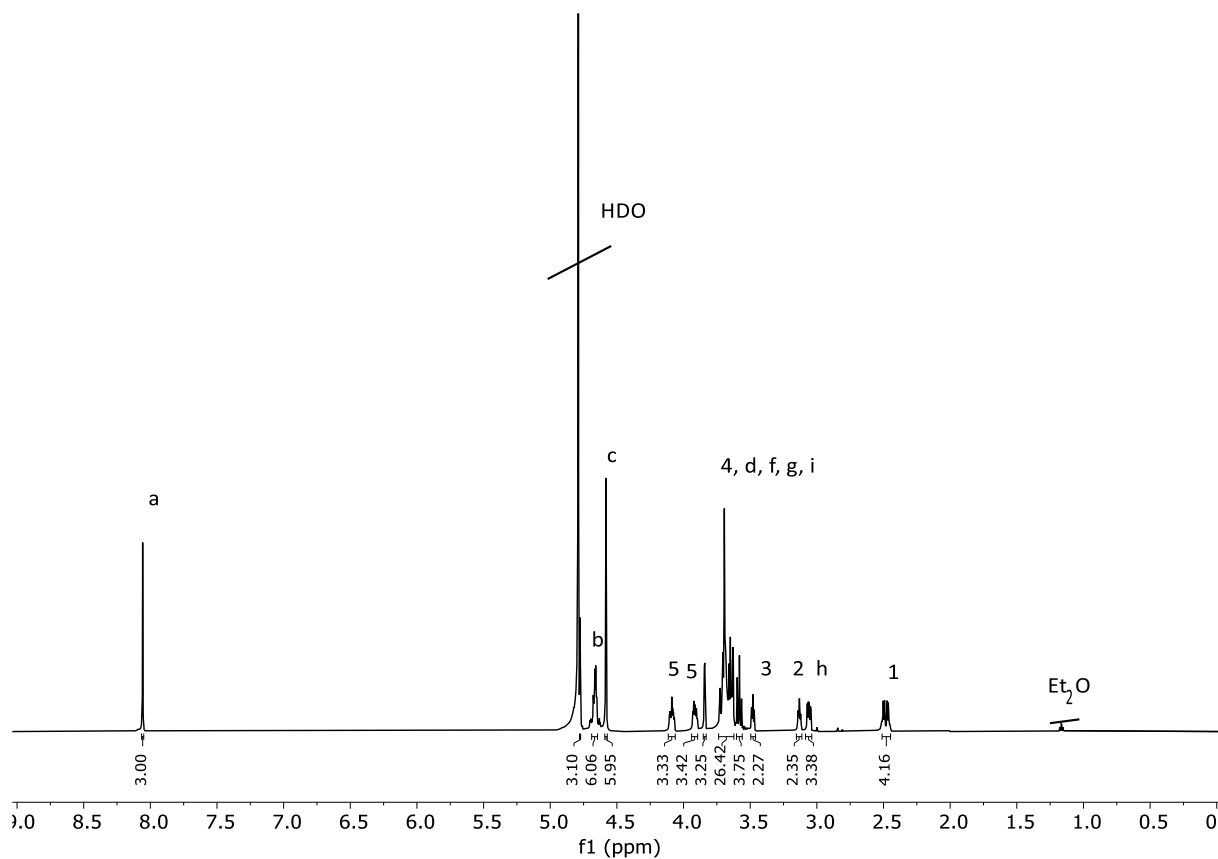
Figure S1: ^{1}H-NMR (600 MHz) spectra of U(Man) **(1)** in HDO.
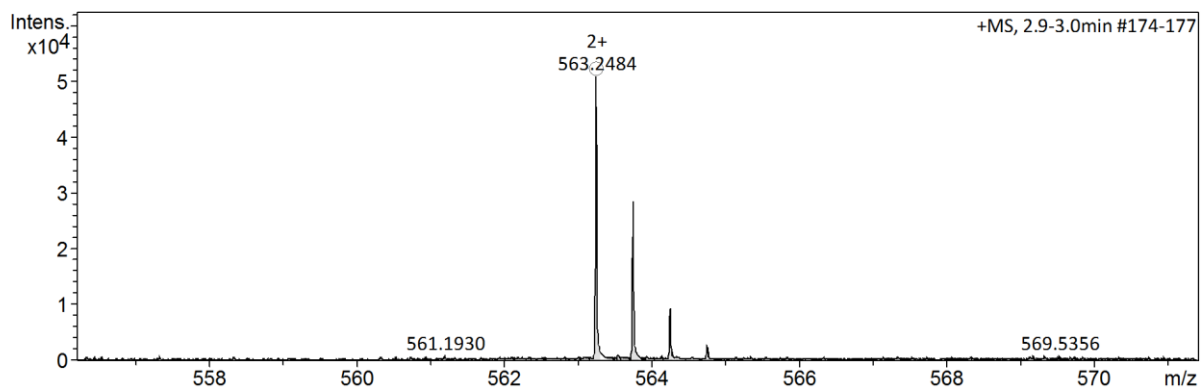
Figure S2: HR-MS of U(Man) **(1)**
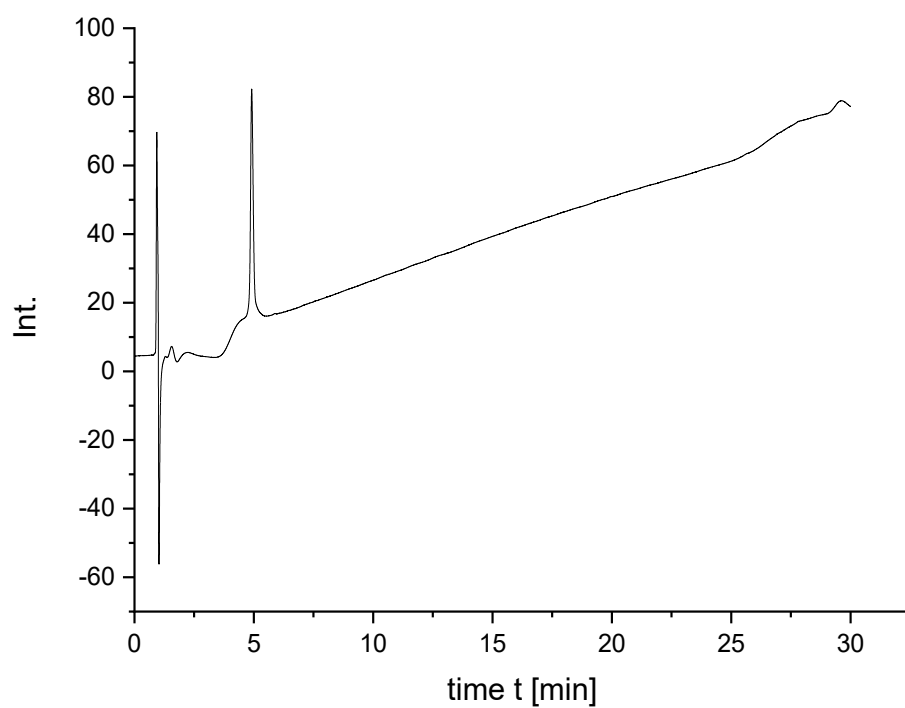
Figure S3: RP-HPLC of U(Man) **(1)**.

Compound: U(Man)-EDS(1-3) **(2)**

^{1}H NMR (600 MHz, D$_2$O) δ 8.05 (s, 3H), 4.67 (s, 2H), 4.59 (s, 6H), 4.10 (ddd, *J* = 11.0, 7.2, 3.7 Hz, 3H), 3.93 (ddd, *J* = 11.1, 5.6, 3.6 Hz, 3H), 3.86 (dd, *J* = 3.4, 1.7 Hz, 3H), 3.75 – 3.58 (m, 49H), 3.51 (t, *J* = 5.9 Hz, 3H), 3.40 – 3.36 (m, 13H), 3.15 (t, *J* = 5.9 Hz, 3H), 3.07 (ddd, *J* = 9.9, 5.8, 2.4 Hz, 3H), 2.58 – 2.53 (m, 14H), 2.48 (dd, *J* = 18.0, 6.0 Hz, 3H).

HR-MS calculated [M+3H]$^{3+}$ 606.3, found 605.9

RP-HPLC: (5%/95% ACN/H$_2$O→ 5%/50% ACN/H$_2$O in 30 min at 25°C, 214 nm): t$_R$ = 8.47 min.
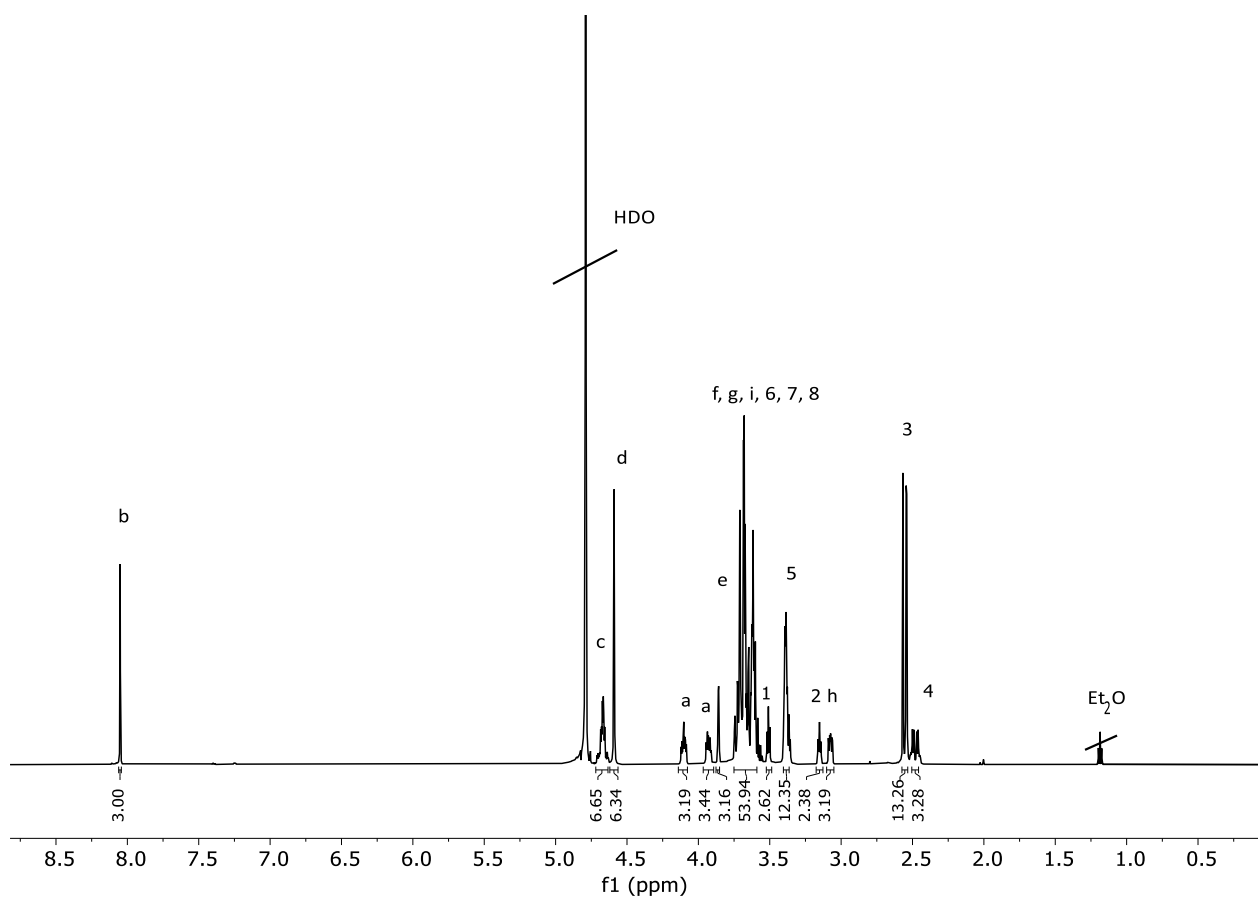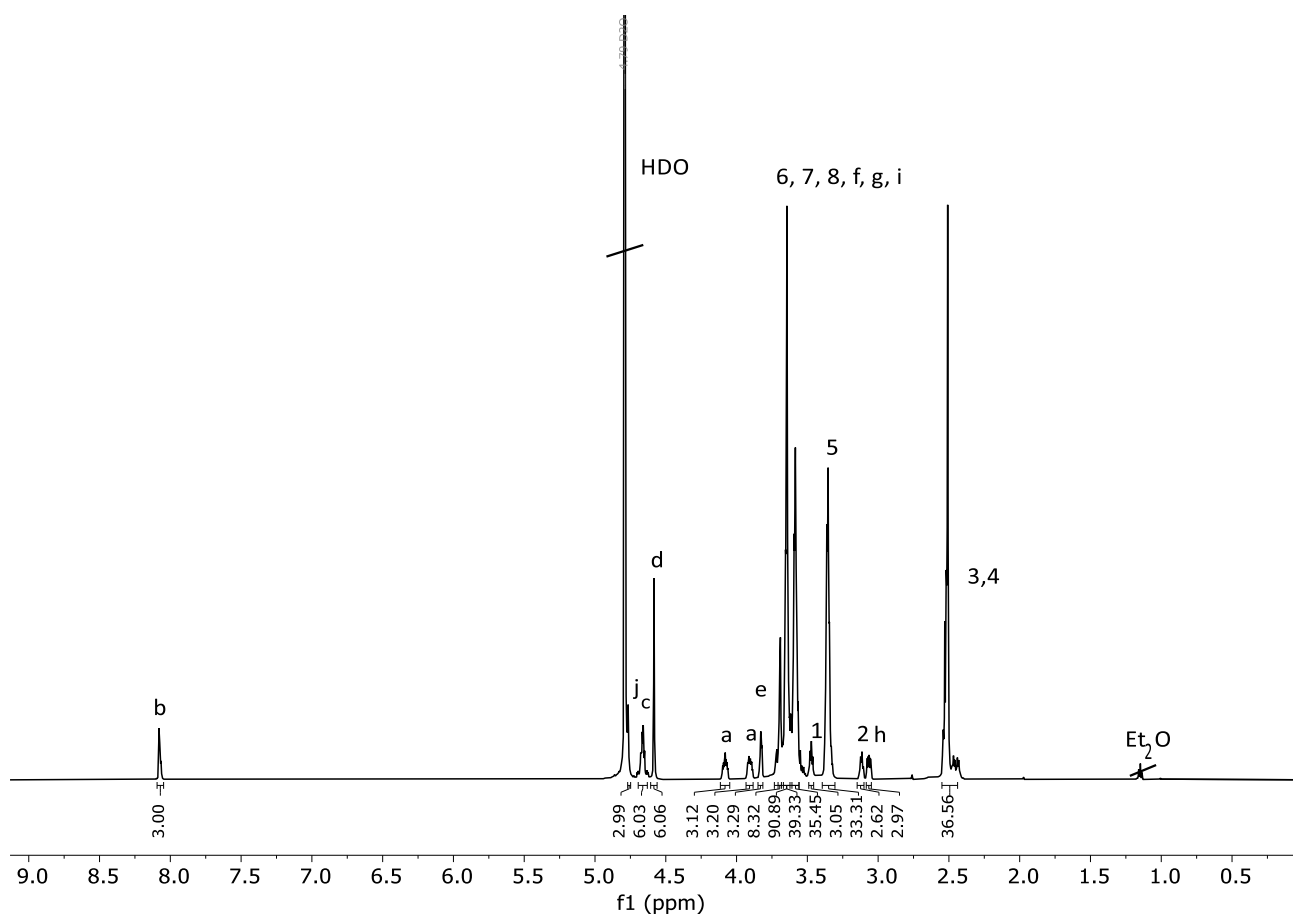
Figure S4: ^{1}H-NMR (600 MHz) spectra of U(Man)-EDS(1-3) **(2)** in HDO.
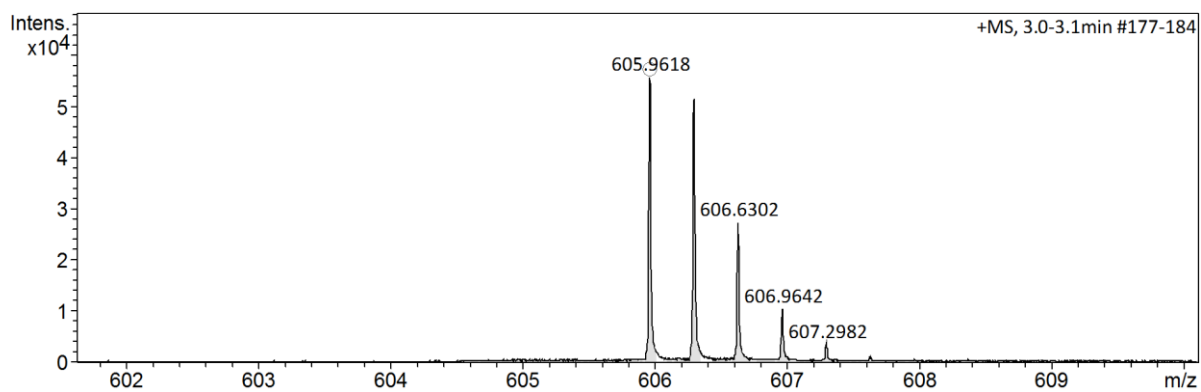
Figure S5: HR-MS of U(Man)-EDS(1-3) **(2)**.
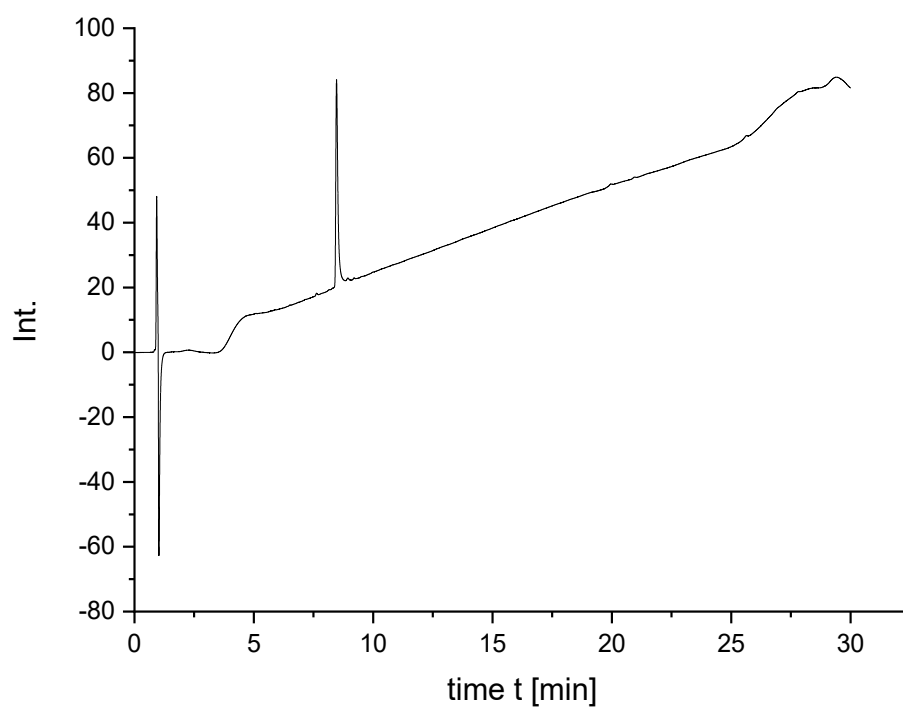
Figure S6: RP-HPLC of U(Man)-EDS(1-3) **(2)**.

Compound: L(Man)-EDS(1-3) **(3)**

^{1}H NMR (600 MHz, D$_2$O) δ 7.89 (d, J = 1.5 Hz, 1H), 4.70 – 4.58 (m, 2H), 4.09 (ddd, J = 11.0, 7.1, 4.0 Hz, 1H), 3.96 – 3.91 (m, 1H), 3.86 (dd, J = 3.3, 1.8 Hz, 1H), 3.76 – 3.54 (m, 28H), 3.51 (t, J = 5.9 Hz, 2H), 3.38 (ddd, J = 11.9, 7.2, 4.5 Hz, 12H), 3.15 (t, J = 5.9 Hz, 2H), 3.03 (t, J = 7.3 Hz, 3H), 2.64 (t, J = 7.3 Hz, 2H), 2.58 – 2.50 (m, 11H).

HR-MS calculated [M+2H]$^{2+}$ 540,8, found 540.8

RP-HPLC: (5%/95% ACN/H$_2$O→ 5%/50% ACN/H$_2$O in 30 min at 25°C, 214 nm): t_R = 7.82 min

Figure S7: ^{1}H-NMR (600 MHz) spectra of L(Man)-EDS(1-3) **(3)** in HDO.
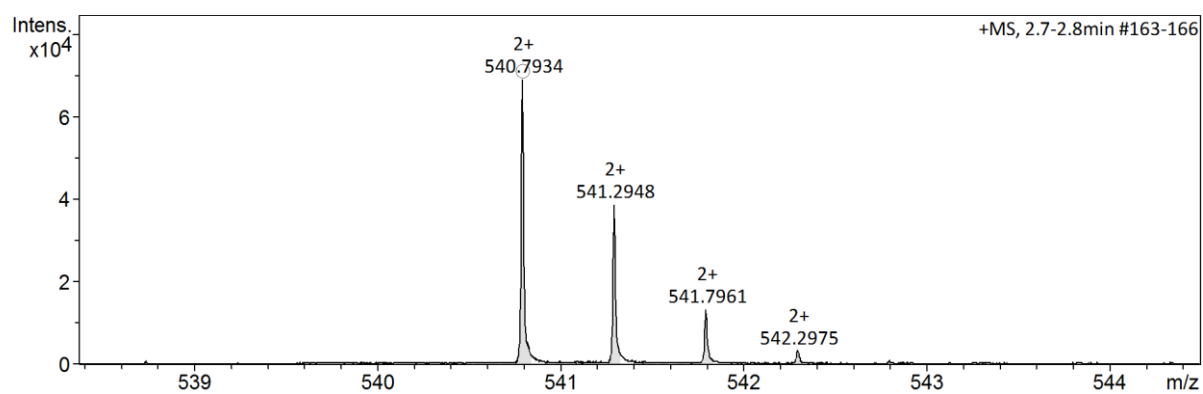
Figure S8: HR-MS of L(Man)-EDS(1-3) **(3)**.
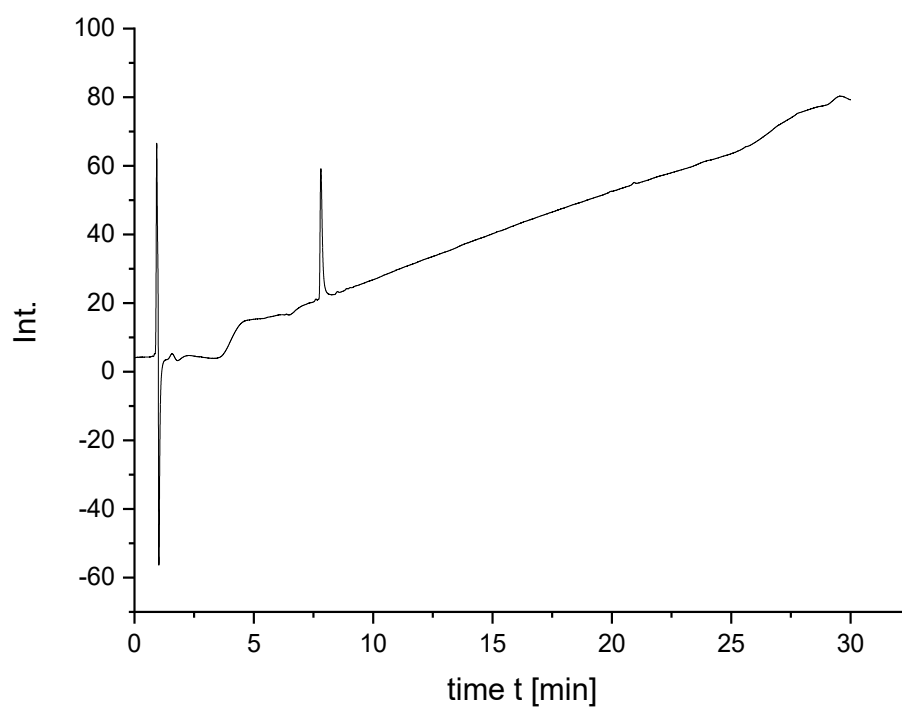
Figure S23: RP-HPLC of L(Man)-EDS(1-3) **(3)**.

Compound: U(Man)-EDS(1-7) **(4)**
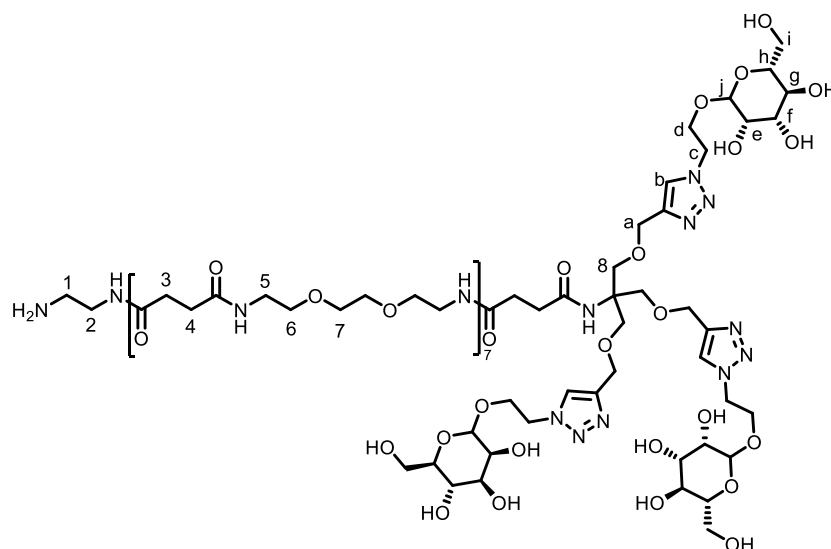
^{1}H NMR (600 MHz, D$_2$O) δ 8.08 (d, *J* = 3.2 Hz, 3H), 4.76 (d, *J* = 1.7 Hz, 3H), 4.66 (td, *J* = 6.5, 5.9, 3.6 Hz, 6H), 4.58 (s, 6H), 4.08 (ddt, *J* = 10.7, 6.9, 3.4 Hz, 3H), 3.90 (ddd, *J* = 11.1, 5.7, 3.7 Hz, 3H), 3.83 (ddd, *J* = 5.2, 3.3, 1.8 Hz, 3H), 3.74 − 3.56 (m, 91H), 3.48 (q, *J* = 6.1, 4.7 Hz, 3H), 3.36 (q, *J* = 5.4 Hz, 36H), 3.12 (q, *J* = 6.0 Hz, 3H), 3.06 (ddd, *J* = 9.7, 5.8, 2.3 Hz, 3H), 2.56 − 2.45 (m, 36H).

HR-MS calculated [M+H]$^{4+}$ 684.99, found 685.1;

RP-HPLC: (5%/95% ACN/H$_2$O→ 5%/50% ACN/H$_2$O in 30 min at 25°C, 214 nm): t$_R$ = 6.72 min.

Figure S10: 1H-NMR (600 MHz) spectra of U(Man)-EDS(1-7) **(4)** in HDO.
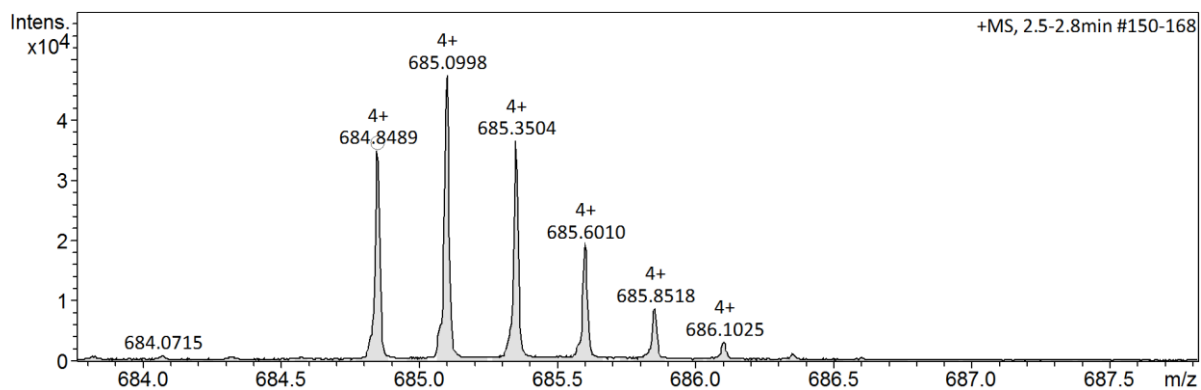
Figure S11: HR-MS of U(Man)-EDS(1-7) **(4)**.
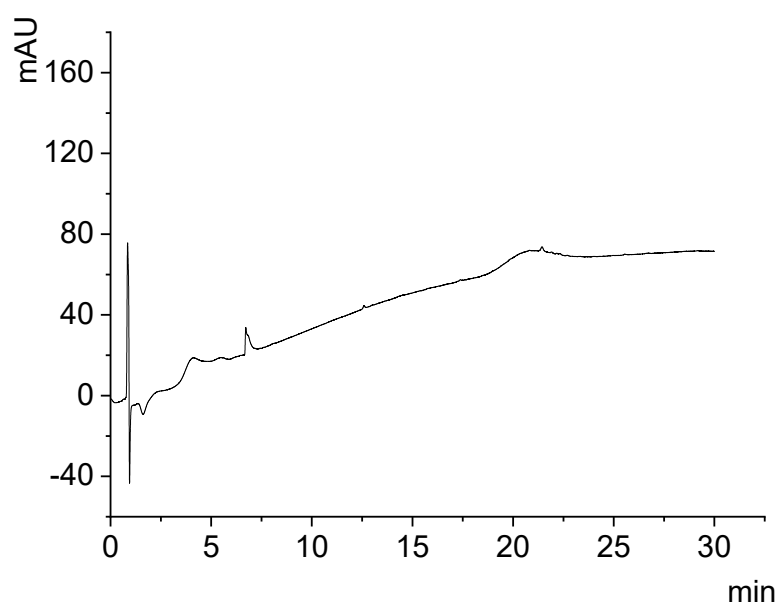
Figure S12: RP-HPLC of U(Man)-EDS(1-7) **(4)**.

Compound U(Man)-EDS(2,4,6)-Man(1,3,5) **(5)**
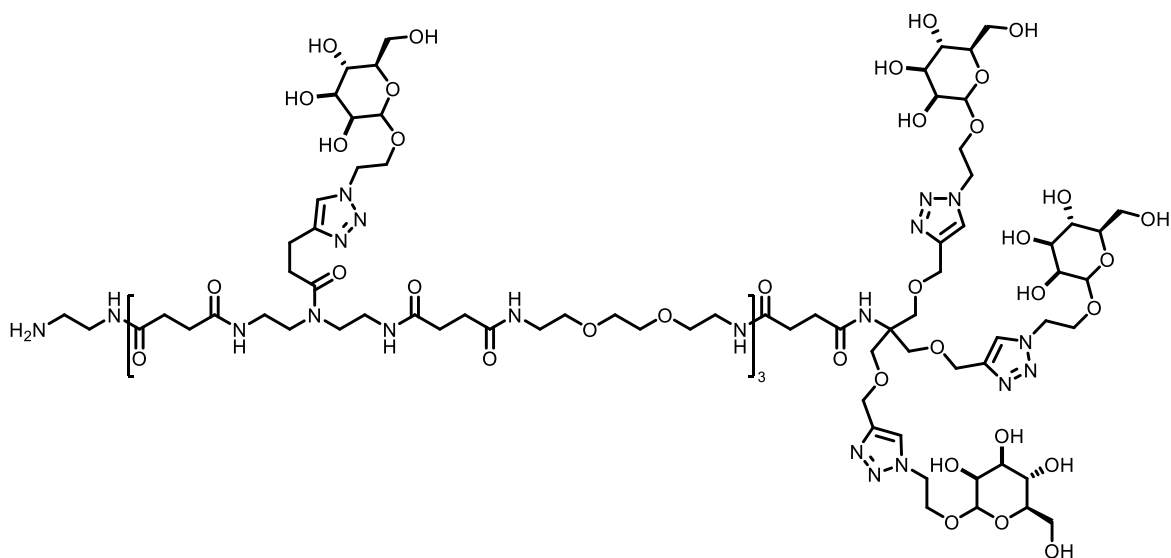
^{1}H NMR (600 MHz, D$_2$O) δ 8.05 (s, 3H), 7.88 (s, 5H), 4.71 − 4.61 (m, 17H), 4.59 (s, 7H), 4.13 − 4.05 (m, 4H), 3.97 − 3.89 (m, 9H), 3.86 (s, 7H), 3.79 − 3.58 (m, 97H), 3.53 − 3.43 (m, 16H), 3.36 (dd, J = 22.3, 6.2 Hz, 37H), 3.24 − 3.19 (m, 1H), 3.15 (t, J = 5.9 Hz, 3H), 3.04 (dt, J = 45.4, 7.9 Hz, 16H), 2.80 (d, J = 7.3 Hz, 9H), 2.58 − 2.43 (m, 12H).

HR-MS calculated [M+H]$^{4+}$ 844.87, found 844,39

RP-HPLC: (5%/95% ACN/H$_2$O→ 5%/50% ACN/H$_2$O in 30 min at 25°C, 214 nm): t$_R$ = 6.43 min.
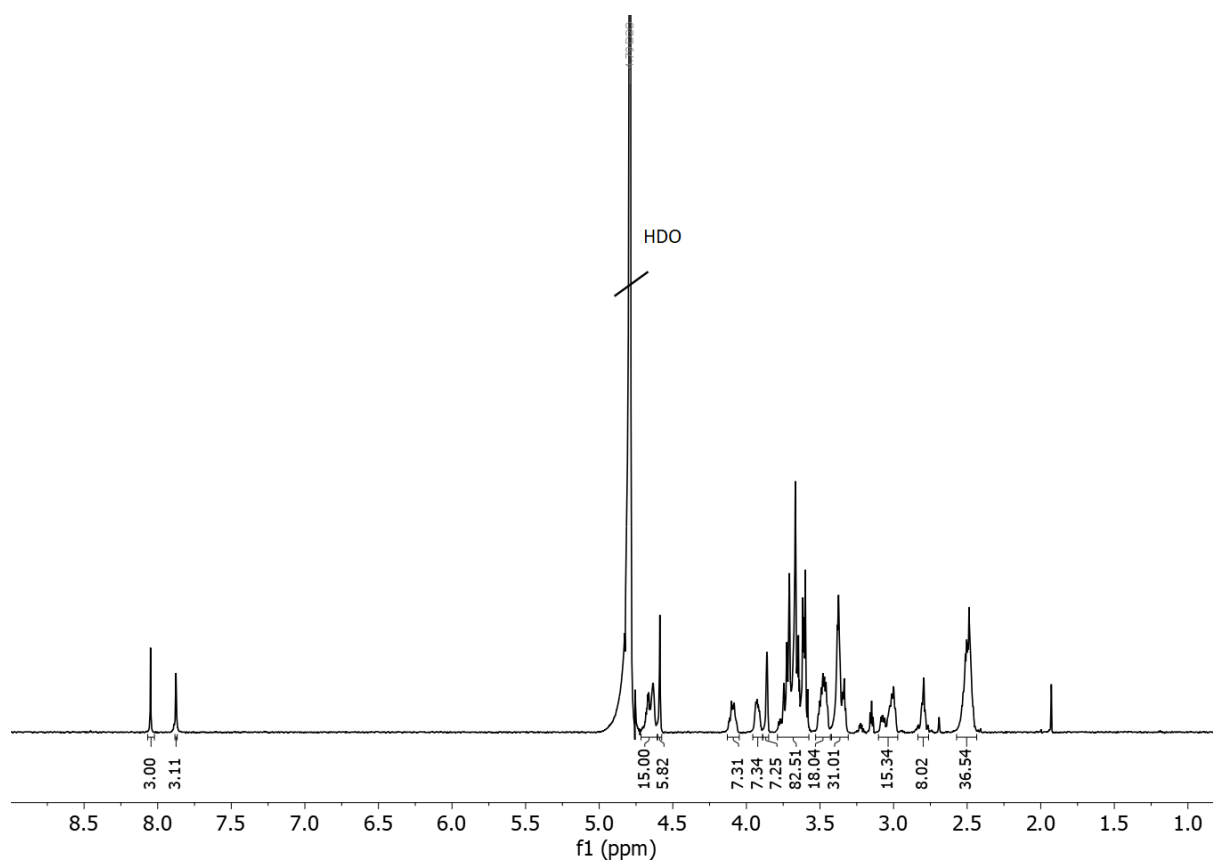
Figure S24: ¹H-NMR (600 MHz) spectra of U(Man)-EDS(2,4,6)-Man(1,3,5) **(5)** in HDO.
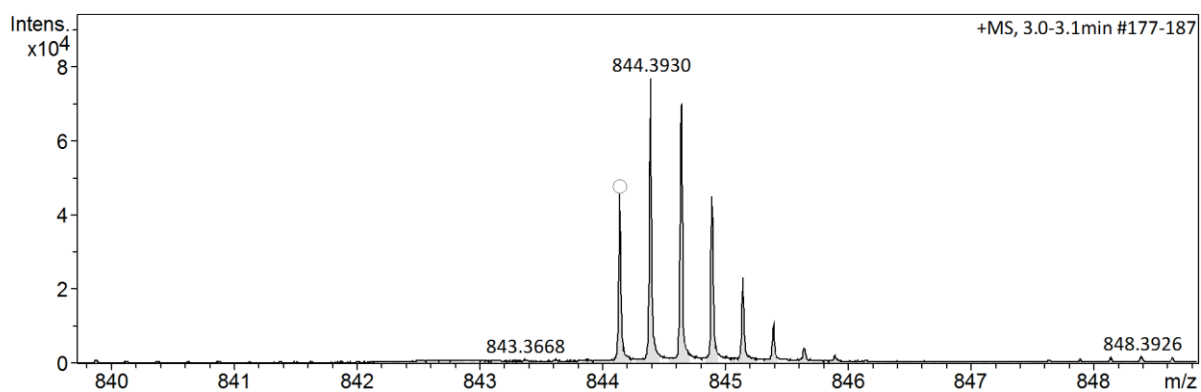
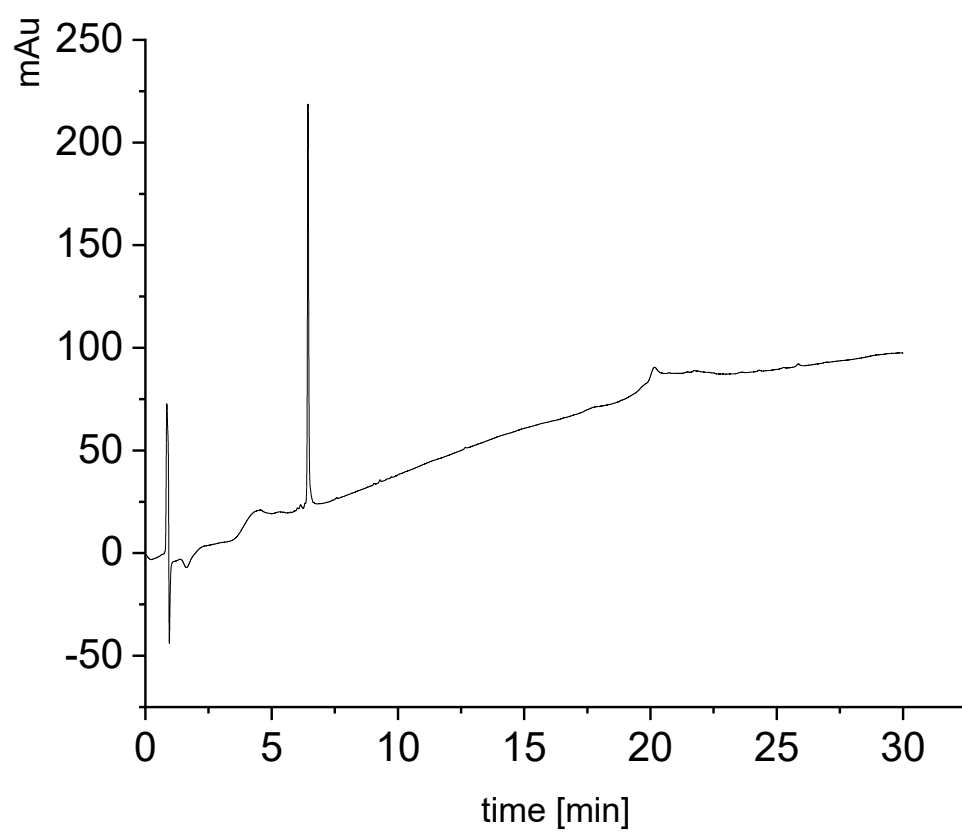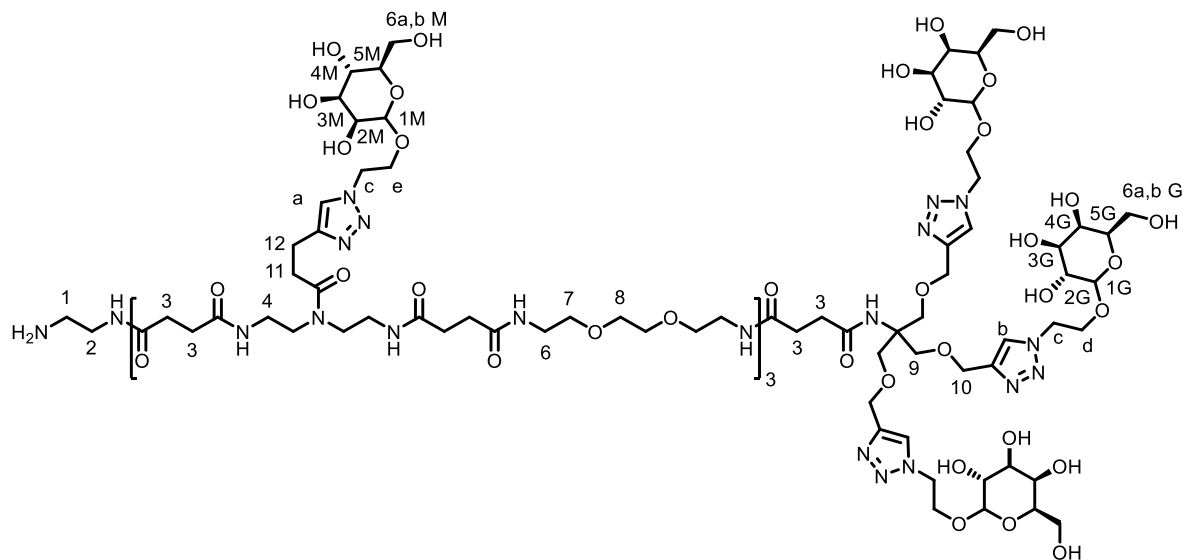*Figure S15*: HR-MS of U(Man)-EDS(2,4,6)-Man(1,3,5) **(5)**.

Figure S16: RP-HPLC of U(Man)-EDS(2,4,6)-Man(1,3,5) **(5)**.

Compound U(Gal)-EDS(2,4,6)-Man(1,3,5) **(6)**.

^{1}H NMR (300 MHz, D$_2$O) δ 8.10 (s, 3H), 8.04 – 8.00 (m, 4H), 4.72 – 4.64 (m, 18H), 4.58 (s, 6H), 4.36 (d, *J* = 7.8 Hz, 3H), 4.33 – 4.25 (m, 2H), 4.10 (dt, *J* = 9.0, 4.2 Hz, 5H), 3.98 – 3.91 (m, 2H), 3.89 (dd, *J* = 3.4, 0.9 Hz, 3H), 3.85 (dd, *J* = 3.1, 1.8 Hz, 5H), 3.79 – 3.54 (m, 69H), 3.53 – 3.41 (m, 18H), 3.35 (q, *J* = 5.5 Hz, 29H), 3.09 (dt, *J* = 29.4, 6.5 Hz, 12H), 2.82 (t, *J* = 7.1 Hz, 9H), 2.49 (dt, *J* = 10.6, 3.9 Hz, 38H).

HR-MS calculated [M+H]$^{4+}$ 840.4, found 840.7

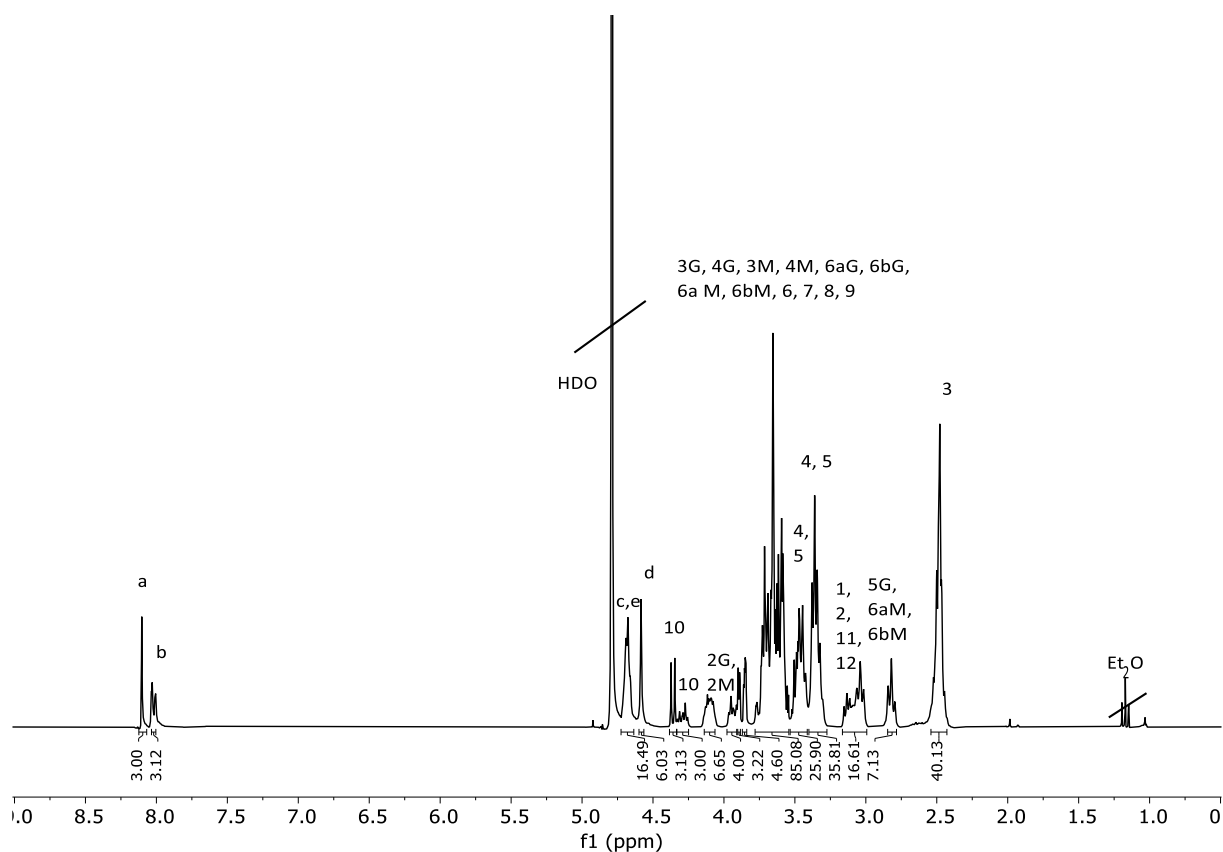RP-HPLC: (5%/95% ACN/H$_2$O→ 5%/50% ACN/H$_2$O in 30 min at 25°C, 214 nm): t$_R$ = 6,40 min.

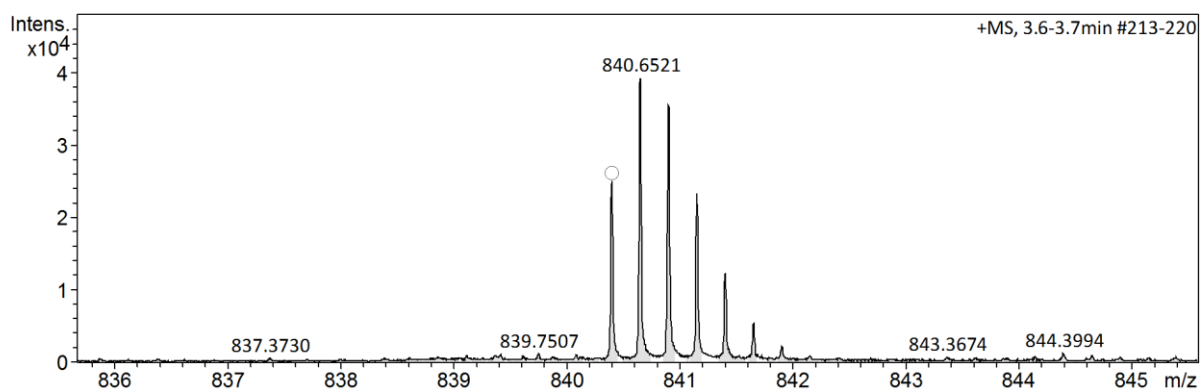*Figure S25*. ¹H-NMR (300 MHz) spectra of U(Gal)-EDS(2,4,6)-Man(1,3,5) **(6)** in HDO.

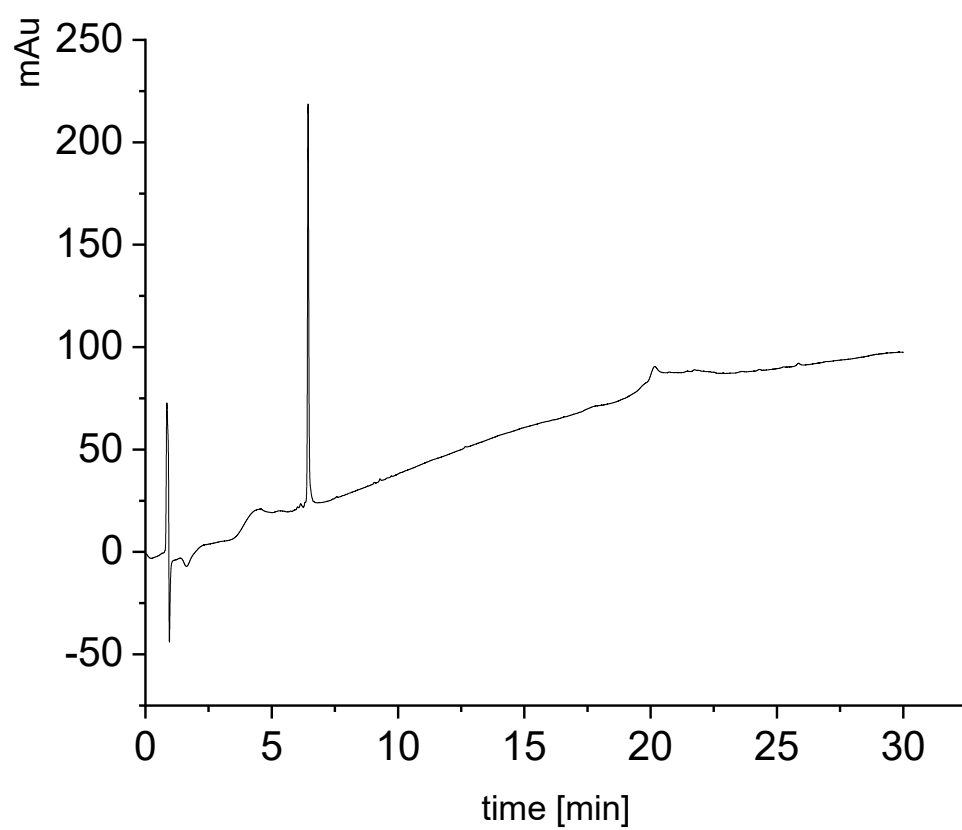*Figure S18*: HR-MS of U(Gal)-EDS(2,4,6)-Man(1,3,5) **(6)**.

Figure S19: RP-HPLC of U(Gal)-EDS(2,4,6)-Man(1,3,5) **(6)**.

Compound U(Man)-EDS(2,4,6)-Gal(1,3,5) **(7)**

^{1}H NMR (300 MHz, D$_2$O) δ 8.10 (dd, *J* = 9.0, 2.2 Hz, 4H), 8.06 (s, 3H), 4.76 – 4.63 (m, 9H), 4.58 (s, 6H), 4.37 (d, *J* = 7.8 Hz, 3H), 4.34 – 4.27 (m, 2H), 4.11 (dq, *J* = 11.1, 5.4 Hz, 7H), 3.94 (d, *J* = 4.7 Hz, 1H), 3.90 (d, *J* = 3.4 Hz, 5H), 3.84 (dd, *J* = 3.1, 1.7 Hz, 3H), 3.76 – 3.53 (m, 73H), 3.52 – 3.40 (m, 17H), 3.35 (q, *J* = 5.5 Hz, 26H), 3.09 (dt, *J* = 24.0, 6.5 Hz, 15H), 2.83 (t, *J* = 7.1 Hz, 7H), 2.48 (h, *J* = 6.2, 5.3 Hz, 35H).

HR-MS calculated [M+H]$^{4+}$ 840.4, found 840.7

RP-HPLC: (5%/95% ACN/H$_2$O→ 5%/50% ACN/H$_2$O in 30 min at 25°C, 214 nm): t$_R$ = 6.4 min.
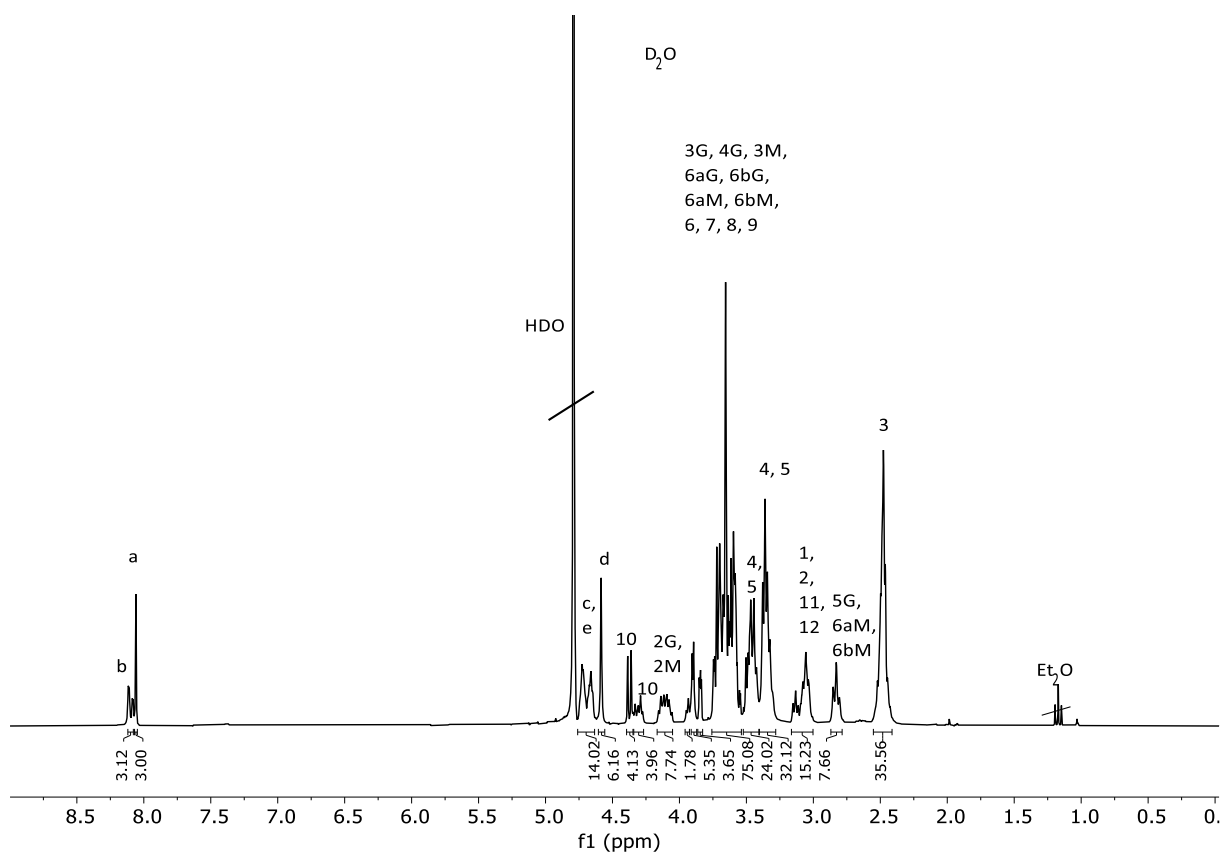
Figure S20: ¹H-NMR (300 MHz) spectra of U(Man)-EDS(2,4,6)-Gal(1,3,5) **(7)** in HDO.
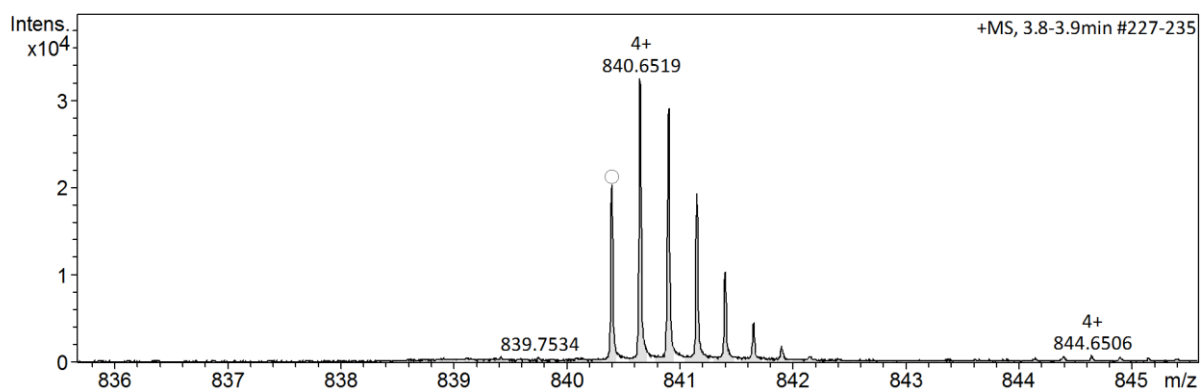

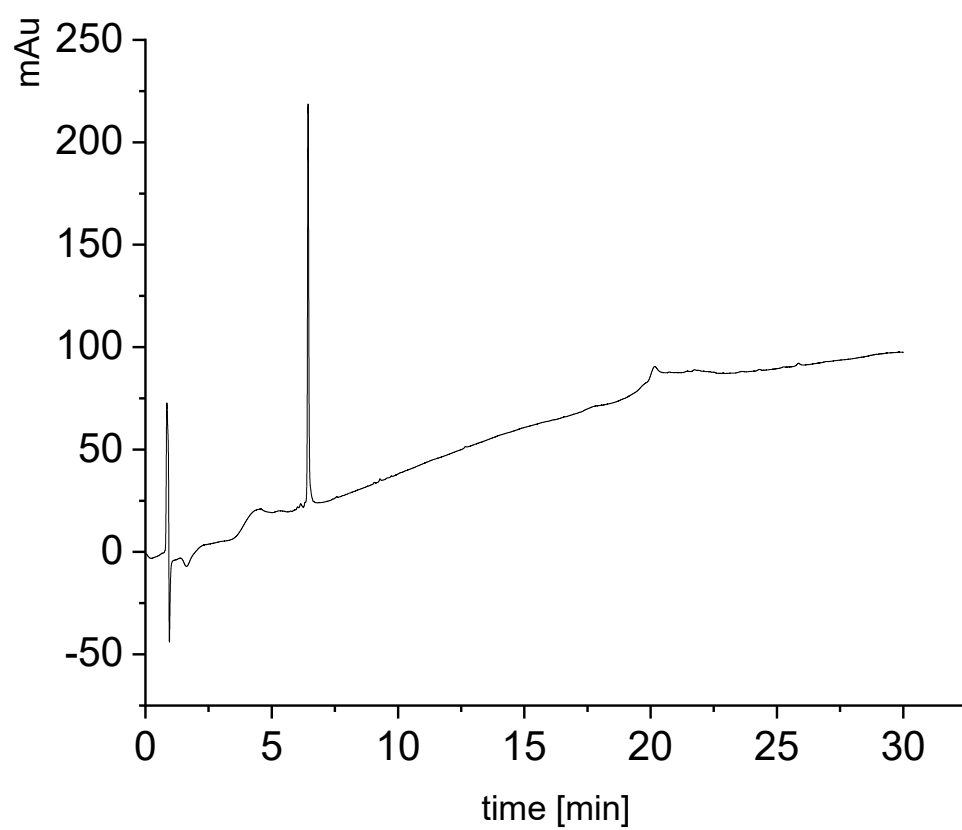*Figure S21:* HR-MS of U(Man)-EDS(2,4,6)-Gal(1,3,5) **(7)**.

Figure S22: RP-HPLC of U(Man)-EDS(2,4,6)-Gal(1,3,5) **(7)**.
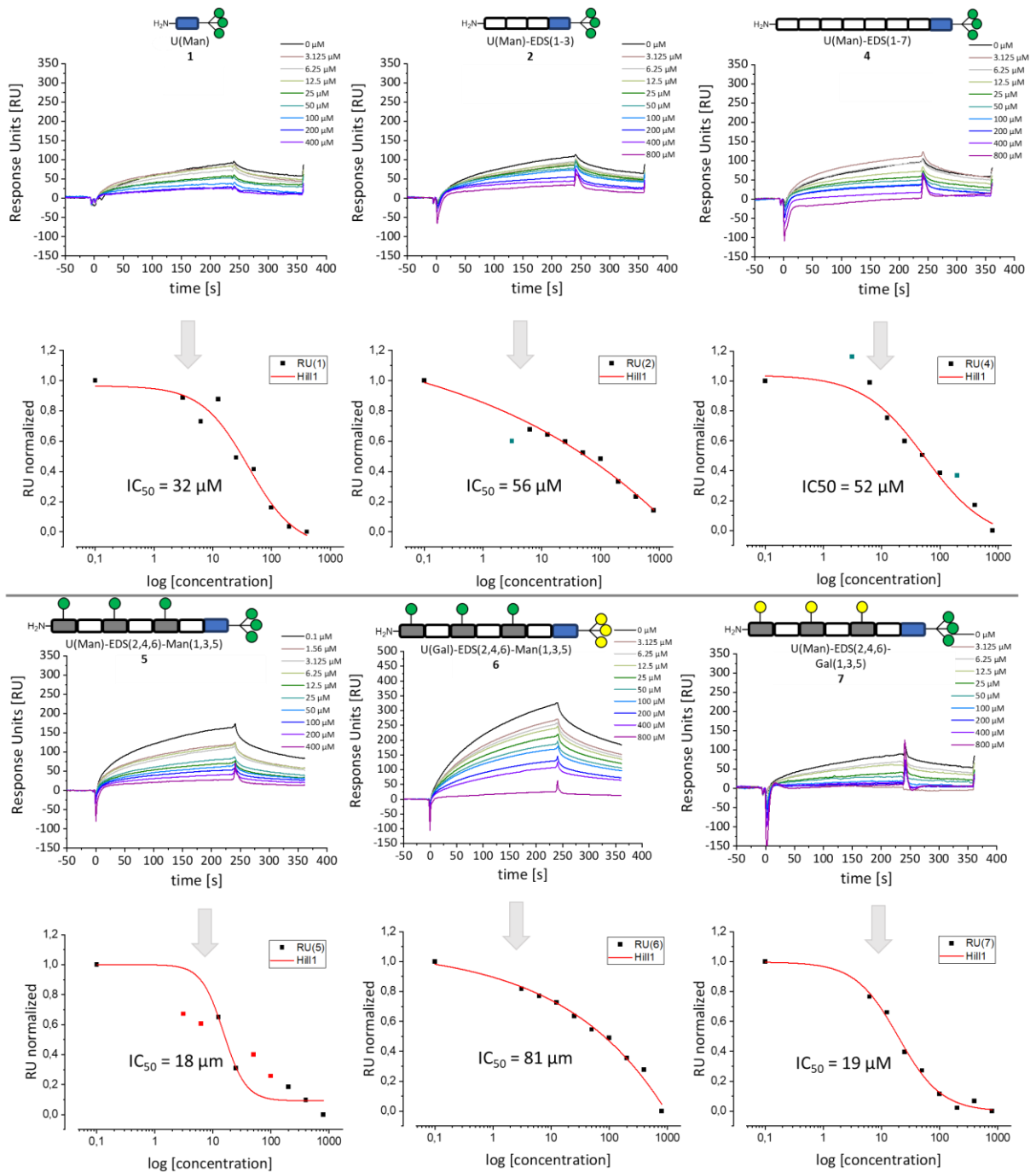
3. Inhibition-Competition Experiments via SPR:

Figure S23: Binding curves and corresponding inhibition competitions curves towards Langerin shown for 1st measurements on 1st C1-Chip.
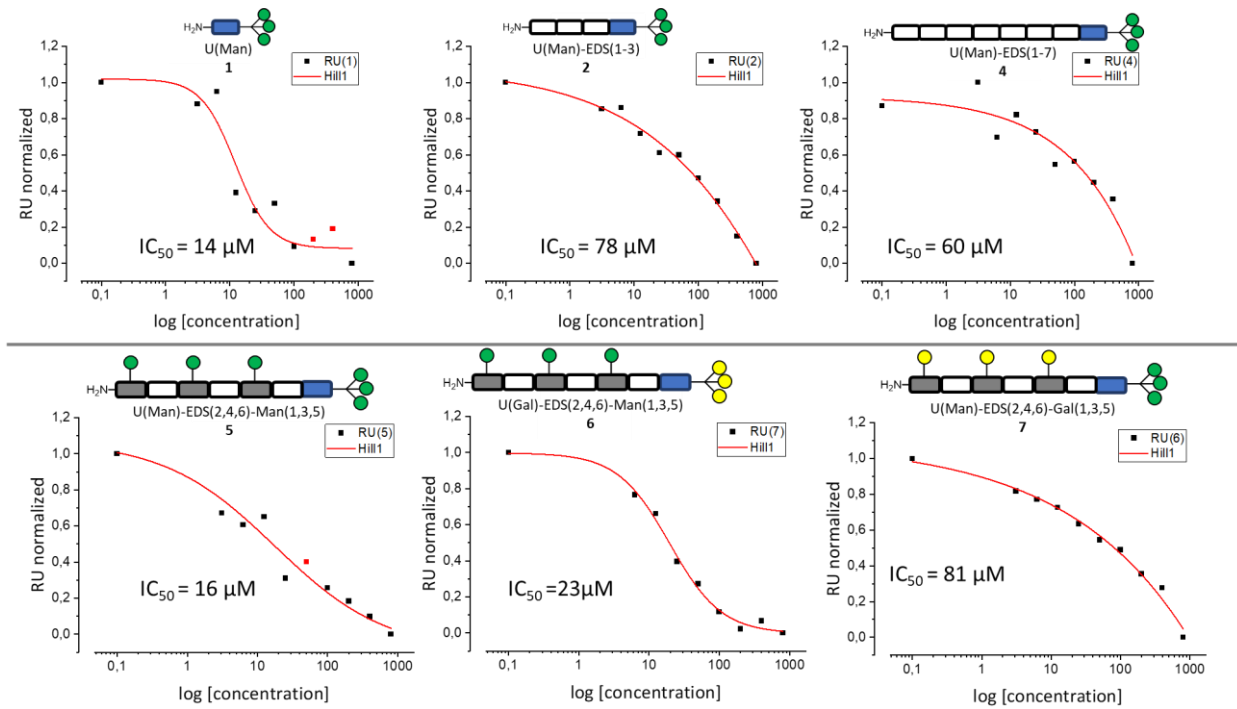
Figure S24: 2nd measurements on 1st C1-Chip: Inhibition competitions curves towards Langerin.
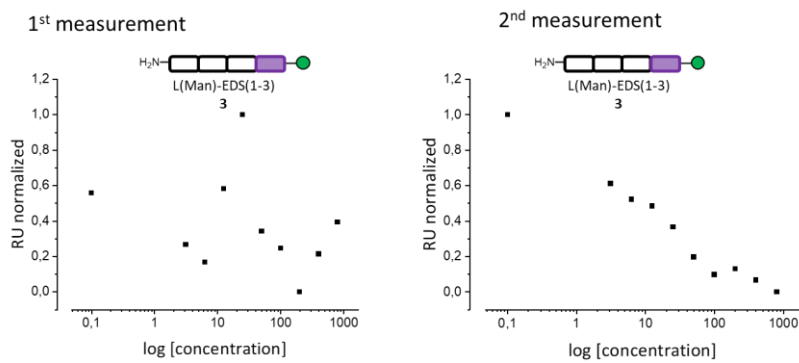

Figure S25: Inhibition competitions assay showed no inhibition of structure **3** towards Langerin shown for 1st and 2nd measurement on 1st C1-Chip.

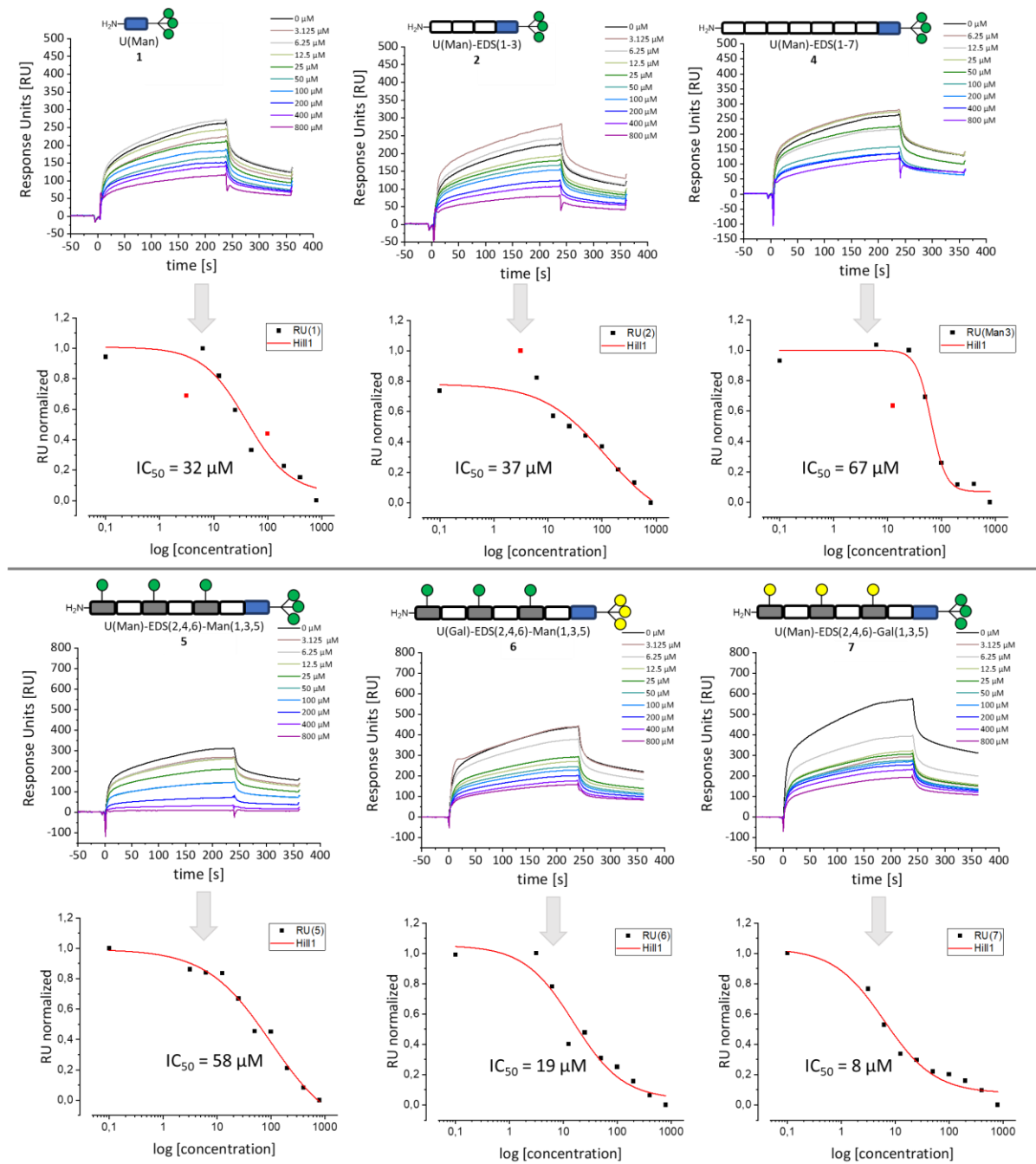*Figure S26*: Binding curves and corresponding inhibition competitions curves towards DC-SIGN shown for 1st measurement on 1st C1-Chip.
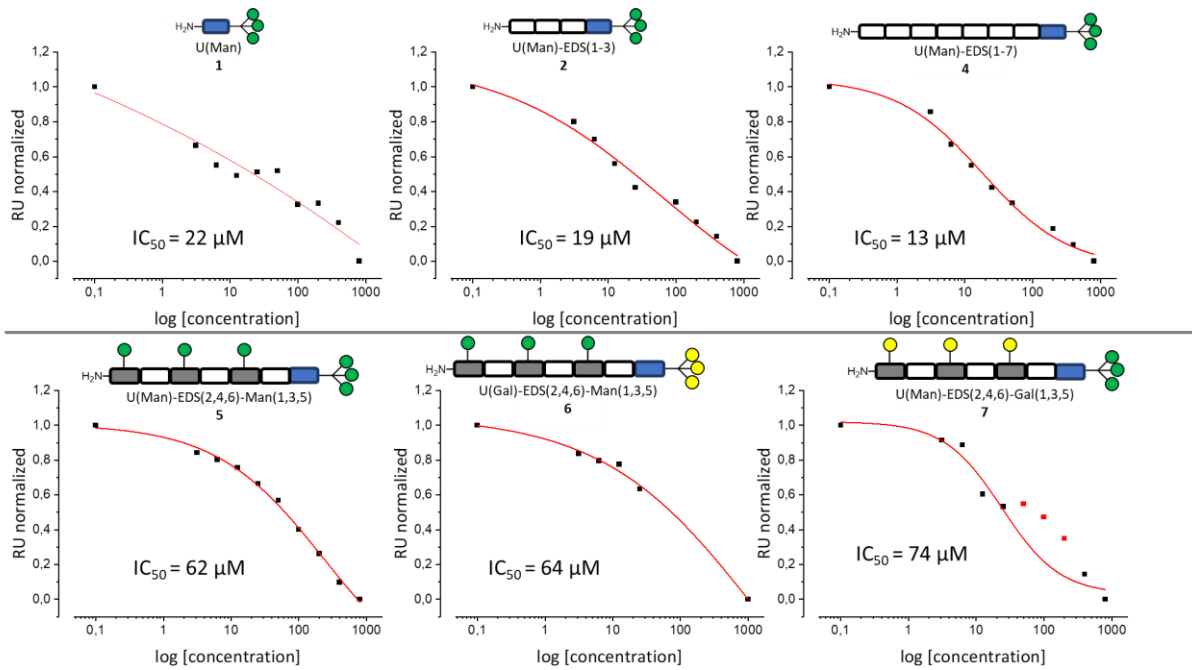
Figure S27: 2nd measurements on 1st C1-Chip: Inhibition competitions curves towards DC-SIGN.
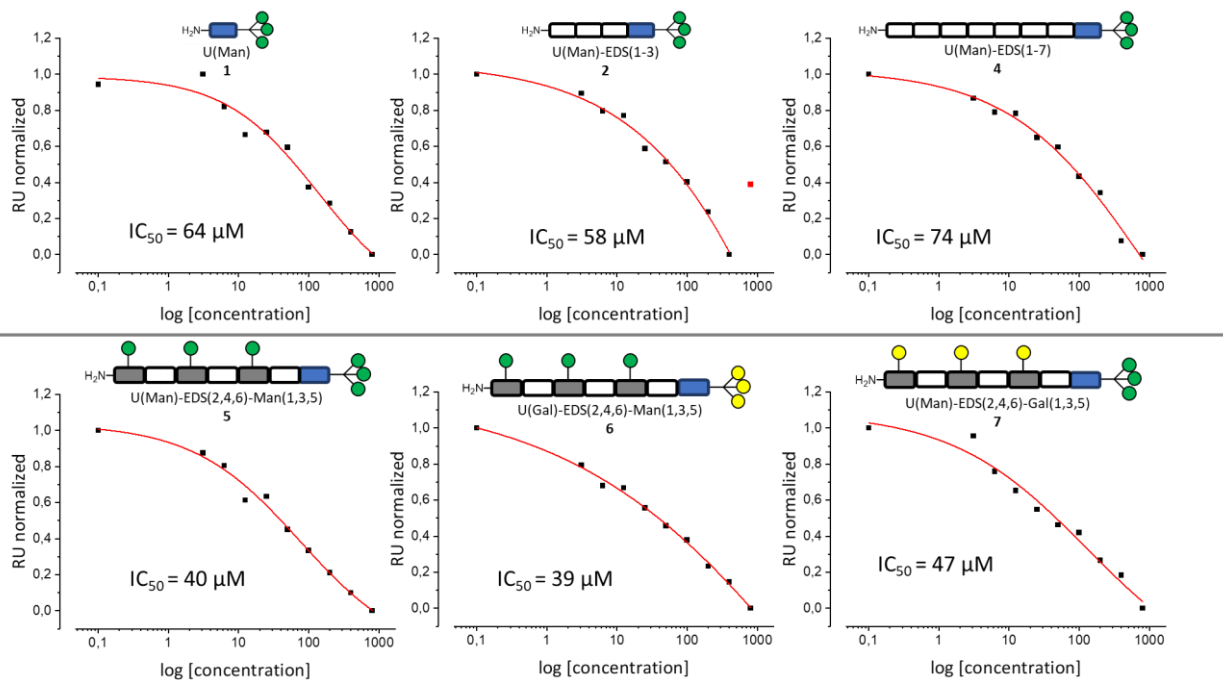

Figure S28: 1st Inhibition competition measurements towards DC-SIGN on 2nd C1-Chip.
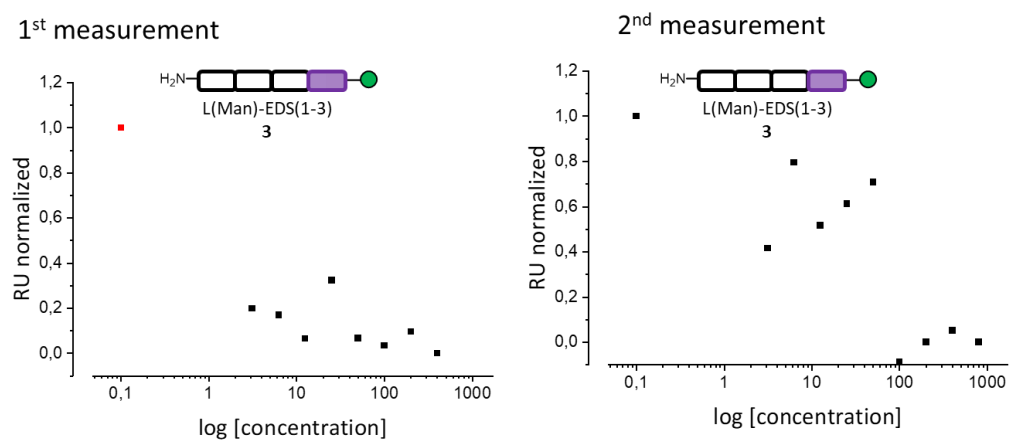
Figure S29: Inhibition competitions assay showed no inhibition of structure **3** towards DC-SIGN shown for 1st and 2nd measurement on 1st C1-Chip.

4   Umbrella glycooligomer conjugated liposomes

Lipid-umbrella glycooligomer-coupling reaction conditions:

Umbrella glycooligomers (2 or 3 mg, 2 eq) were dissolved in 0.5 mL of DMSO and DIPEA (5 eq) and DSPE-PEG-NHS (1 eq) were added. Reaction vessels were vortex-shaken overnight at 40 °C. Samples were then dialyzed to water for 6 h x 3, using a membrane cut-off of 2 KDa. Afterwards, they were lyophilized and redissolved in DMSO-d_6. Umbrella glycooligomer - lipid coupling yields were calculated by ^{1}H-NMR (400 MHz, Bruker) comparing the DSPE methyl groups integration (6.00, 0.8 ppm) to the integration of the triazole proton (3.00, ~8.00 ppm).

Table 1: Coupling yields of lipid - umbrella glycooligomer conjugates obtained by comparing the integration of the DSPE methyl group and the methyl group linking the carbohydrate residue via triazole by ^{1}H-NMR.

Compound	DSPE-PEG-U(Man)-EDS(1-7)	DSPE-PEG-L(Man)-EDS(1-3)	DSPE-PEG-U(Man)	DSPE-PEG-U(Man)-EDS(1-3)
Coupling yield (%)	59	51	65	83
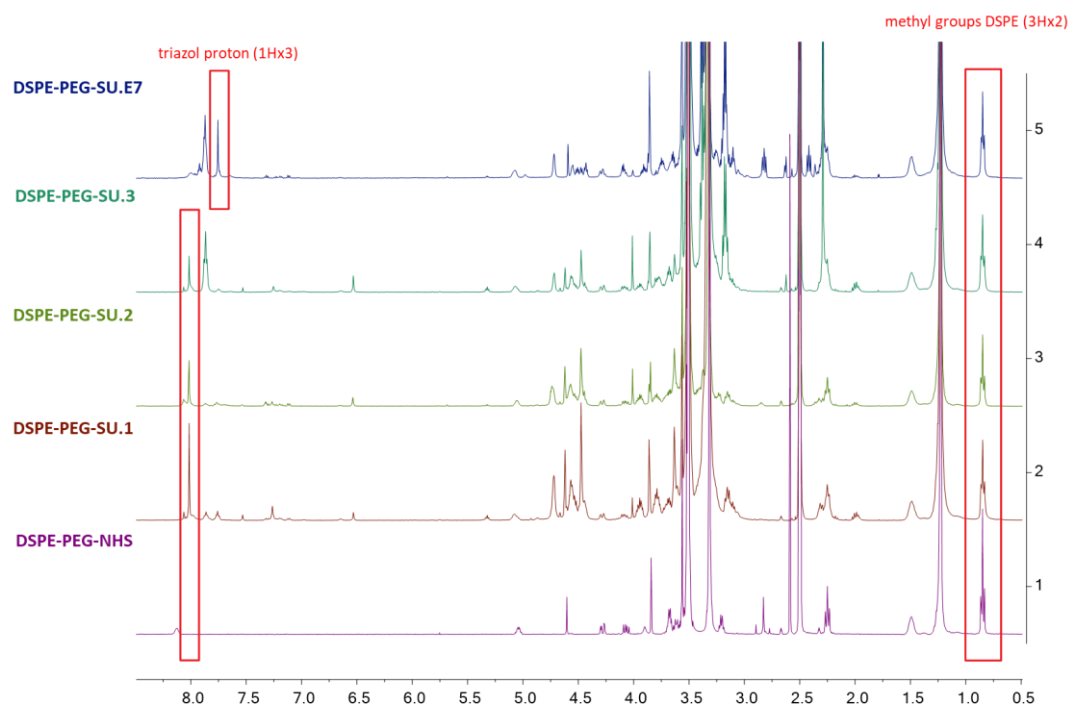
Figure S30: Comparison of the ¹H-NMR of the glycooligomers coupled to DSPE-PEG lipid and the starting material, DSPE-PEG-NHS. Highlighted into red frames the two signals used to determine the coupling yield are shown.
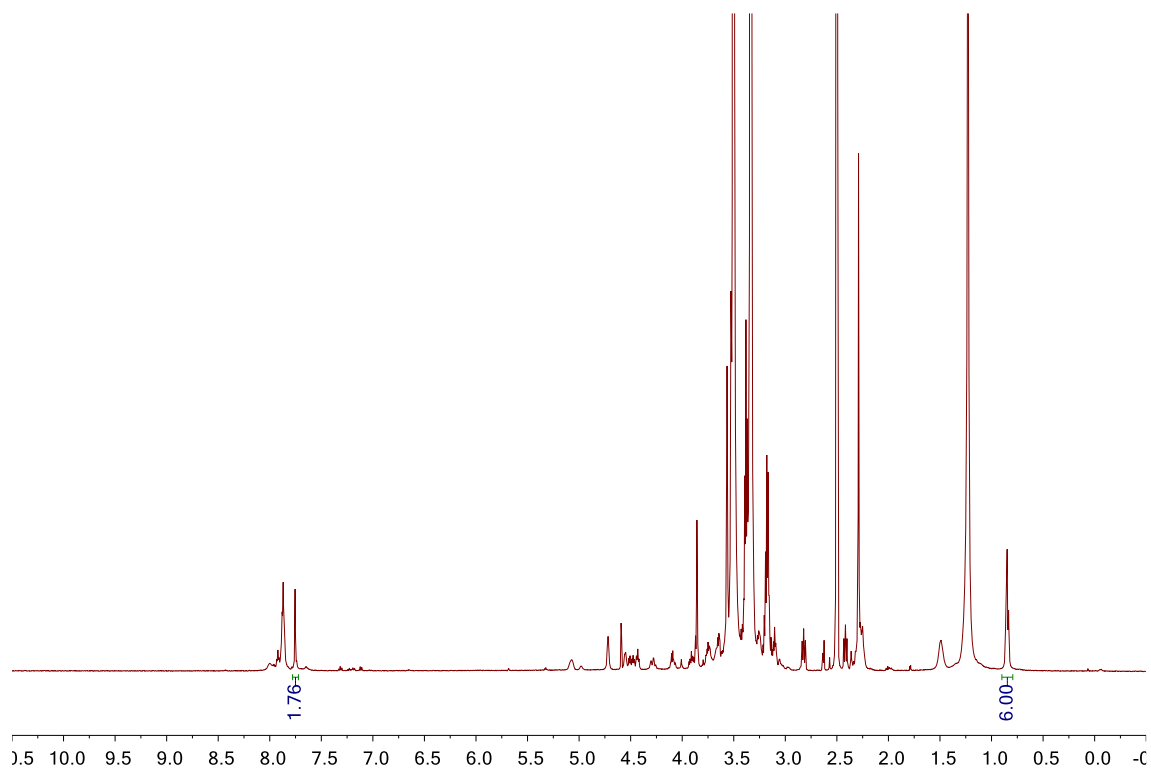
*Figure S31: ¹H-NMR (400 MHz) spectra of **DSPE-PEG-U(Man)-EDS(1-7) conjugate** in DMSO-d₆.*
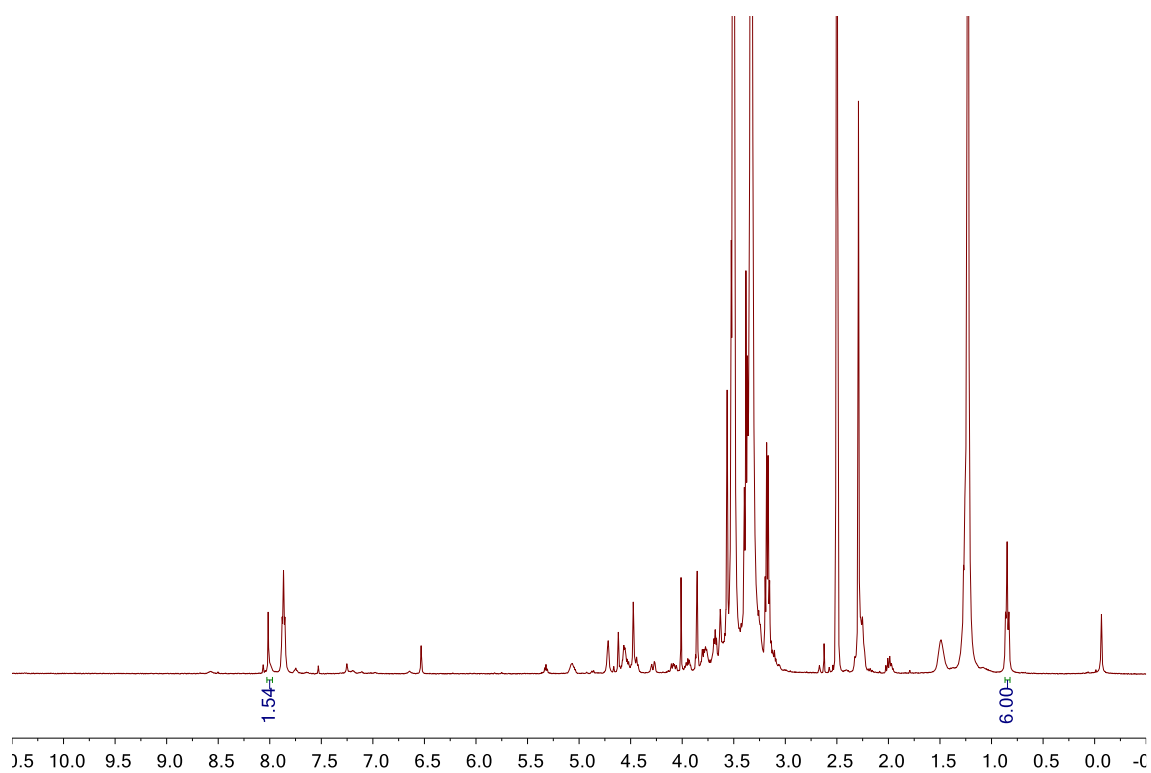
*Figure S32: ^{1}H-NMR (400 MHz) spectra of **DSPE-PEG-L(Man)-EDS(1-3) conjugate** in DMSO-d$_6$.*
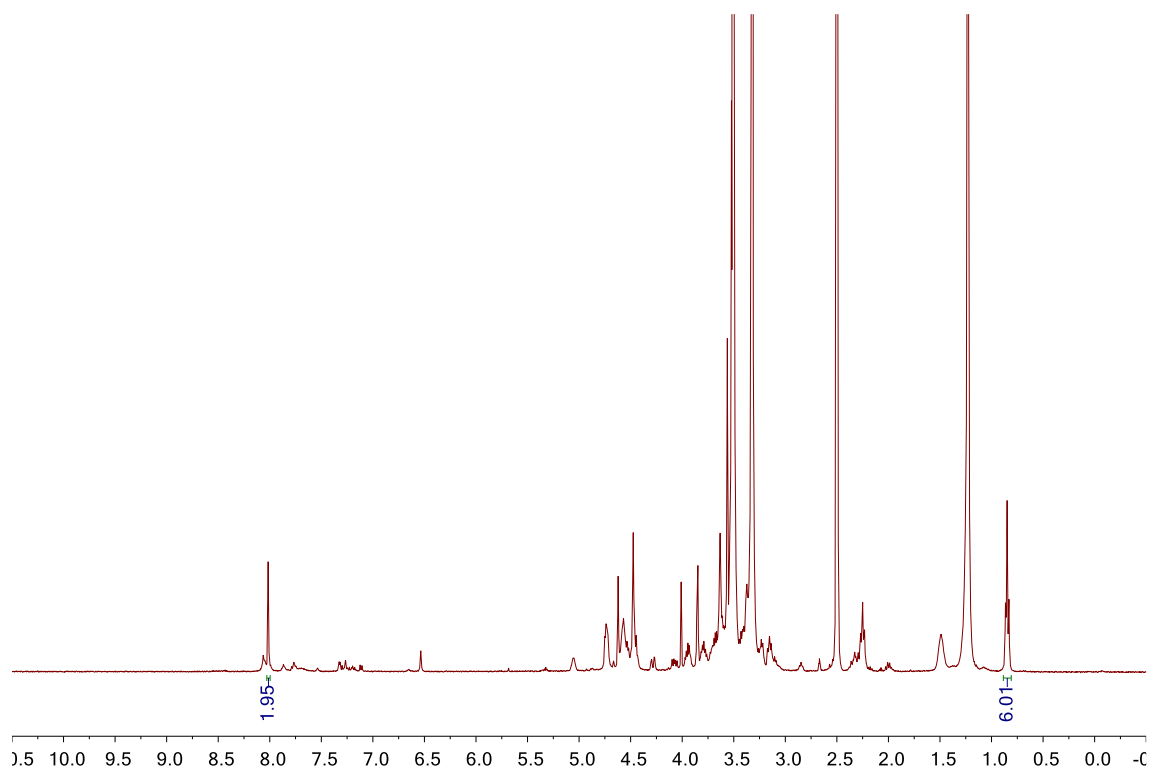
*Figure S33: ^{1}H-NMR (400 MHz) spectra of **DSPE-PEG-U(Man) conjugate** in DMSO-d$_6$.*
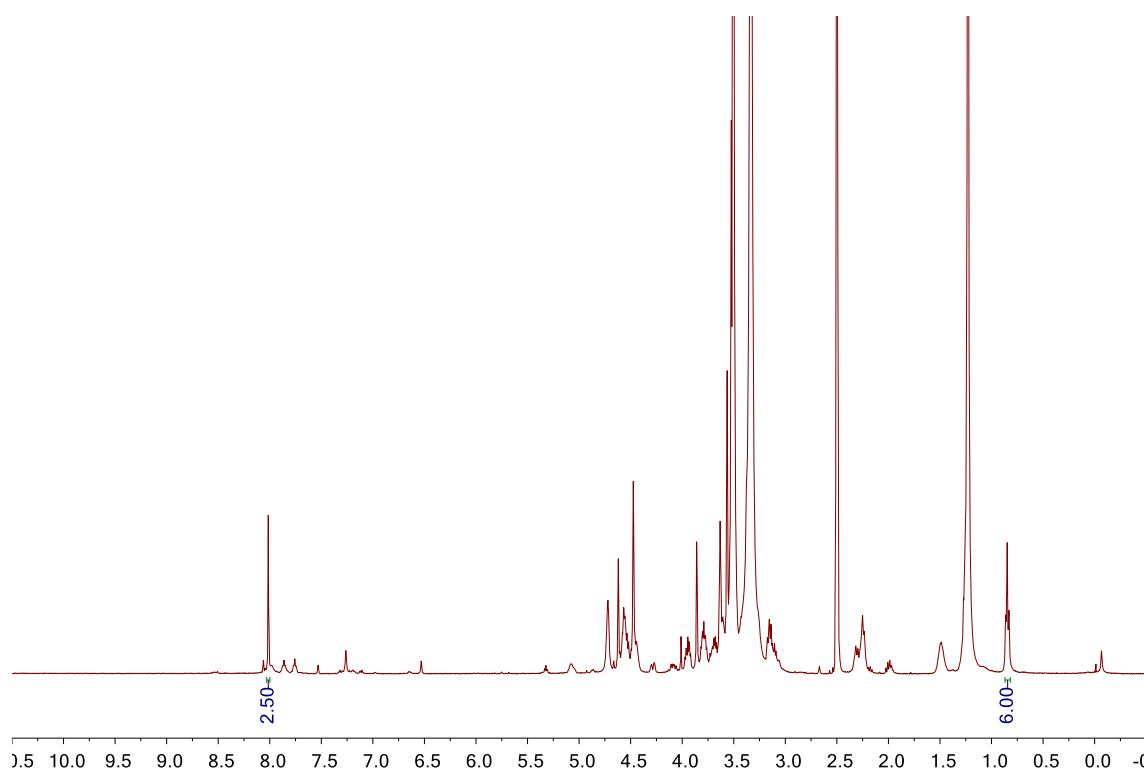
*Figure S34: ^{1}H-NMR (400 MHz) spectra of **DSPE-PEG-U(Man)-EDS(1-3) conjugate** in DMSO-d$_6$.*

Umbrella glycooligomers with carbohydrate decorated handle (2 or 3 mg, 2 eq) were dissolved in 0.5 mL of DMSO and DIPEA (5 eq) and DSPE-PEG-NHS (1 eq) were added. Reaction vessels were vortex-shaken overnight at 40 °C. Samples were then dialyzed to water for 6 h x 3, using a membrane cut-off of 2 KDa. Afterwards, they were lyophilized and redissolved in DMSO-d$_6$. Umbrella glycooligomer -lipid coupling yields were calculated by ^{1}H-NMR (400 MHz, Bruker) comparing the DSPE methyl groups integration (6.00, 0.8 ppm) to the integration of the methylene groups connecting the triazole and the sugar moiety for each glycooligomer (6.00, 4.05 ppm). Since the later signal overlaps with that from one of the protons of the phosphoglycerol linker (1.00, 4.05 ppm), to calculate the coupling yield of the binding the total integration of the signal should be taken as 7.00.

Table 2: Coupling yields of lipid and glycooligomer conjugates obtained by comparing the integration of the DSPE methyl group and the methyl group linking the sugar residue via triazole by ^{1}H-NMR.

| Compound	DSPE-PEG-U(Man)-EDS(2,4,6)-Gal(1,3,5)	DSPE-PEG-U(Gal)-EDS(2,4,6)-Man(1,3,5)	DSPE-PEG-U(Man)-EDS(2,4,6)-Man(1,3,5)
Coupling yield (%)	69	73	49
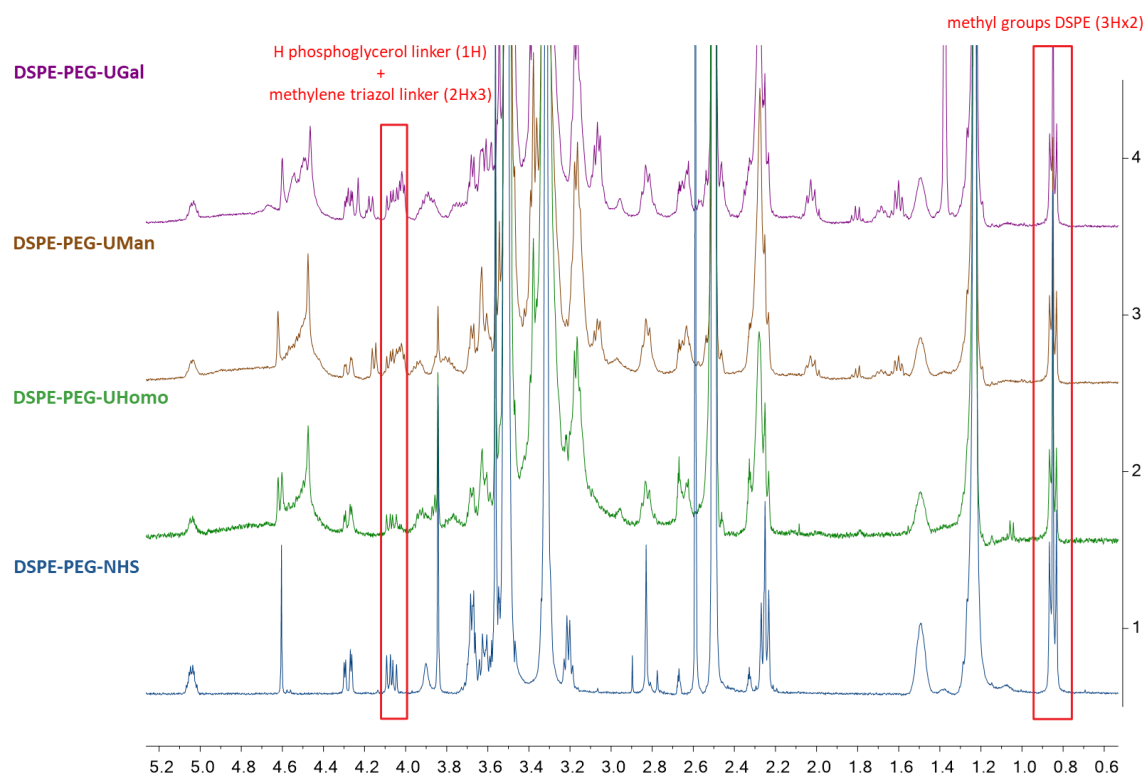
Figure S35: Comparison of the ^{1}H-NMR of the glycooligomers coupled to DSPE-PEG lipid and the starting material, DSPE-PEG-NHS. Highlighted into red frames the two signals used to determine the coupling yield are shown.
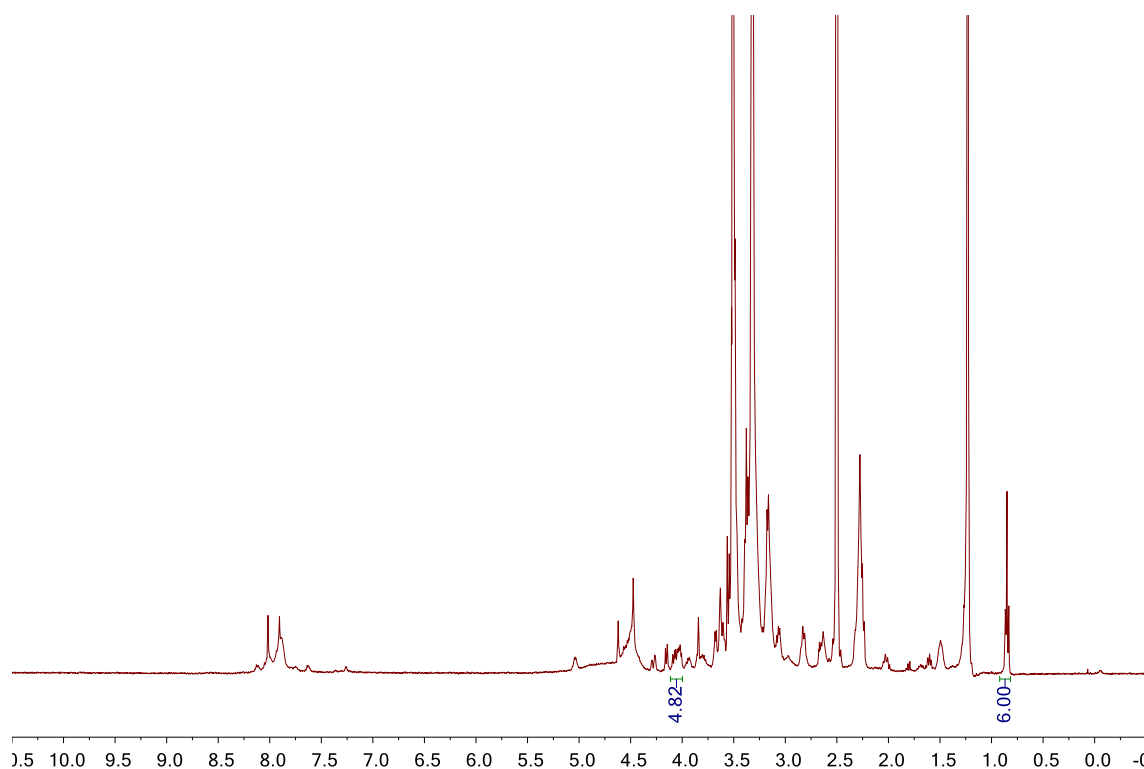
Figure S36: ^{1}H-NMR (400 MHz) spectra of **DSPE-PEG-U(Man)-EDS(2,4,6)-Gal(1,3,5) conjugate** in DMSO-d$_6$.
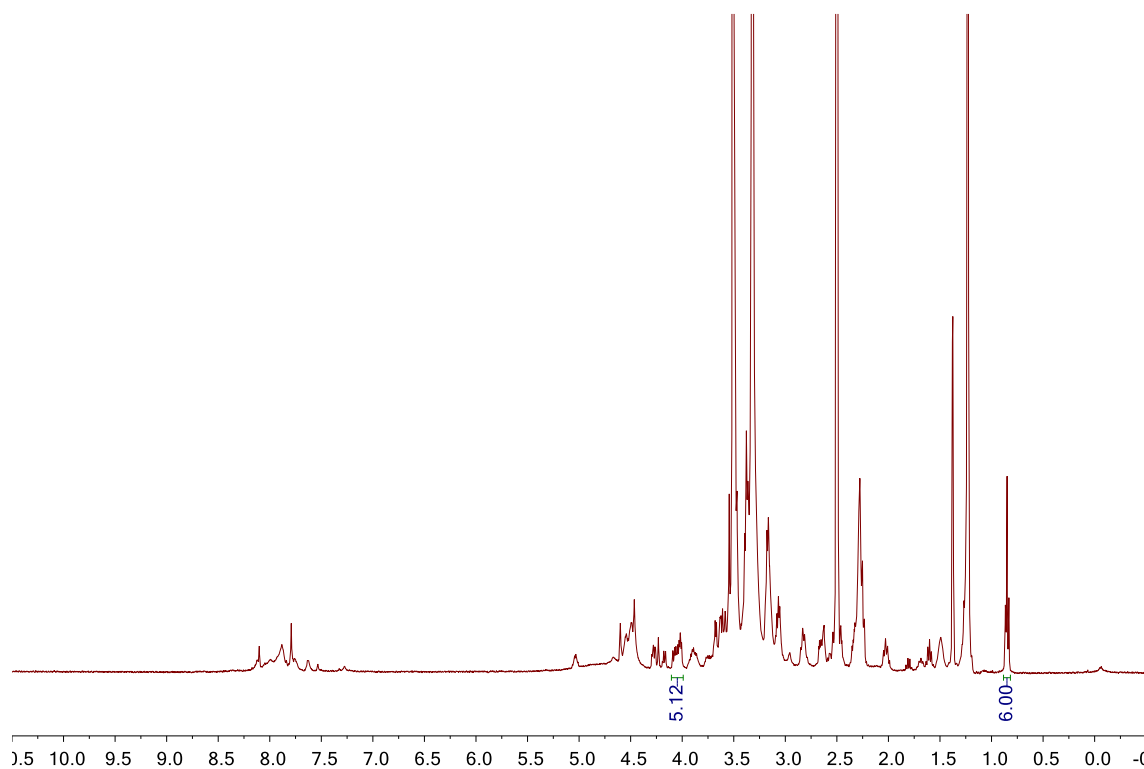
Figure S37: ^{1}H-NMR (400 MHz) spectra of **DSPE-PEG-U(Gal)-EDS(2,4,6)-Man(1,3,5) conjugate** in DMSO-d$_6$.
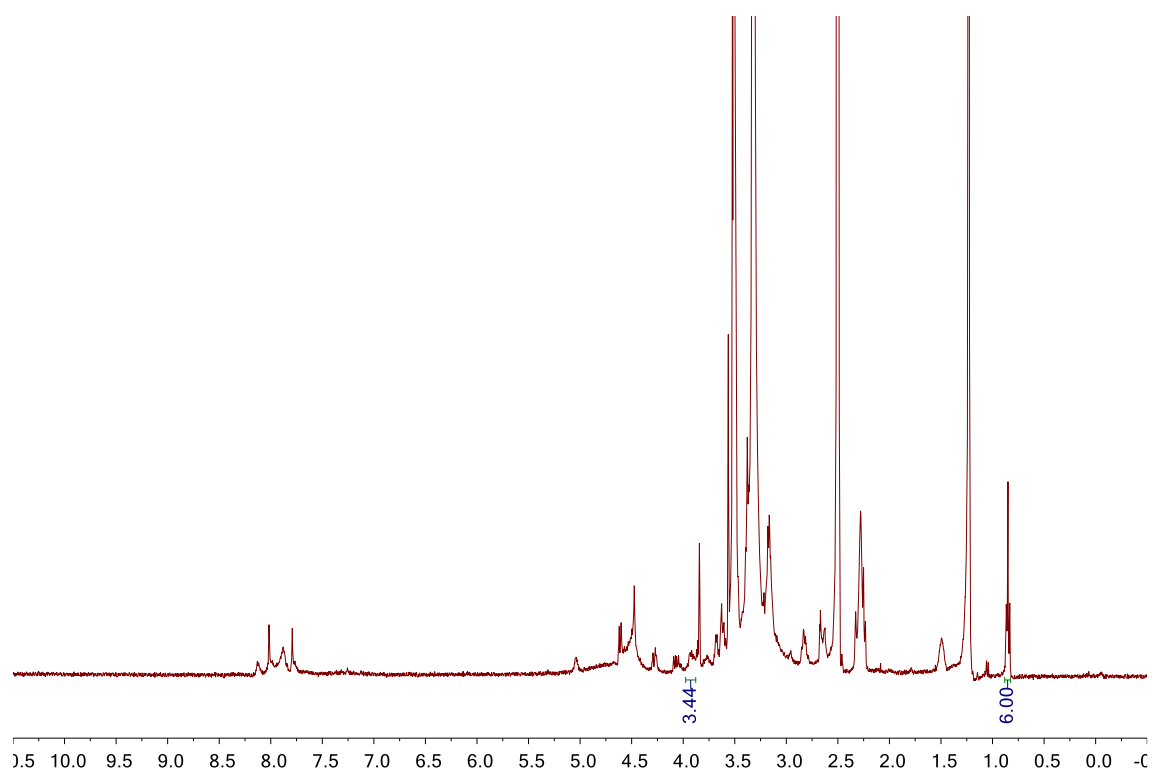
Figure S38: ^{1}H-NMR (400 MHz) spectra of **DSPE-PEG-U(Man)-EDS(2,4,6)-Man(1,3,5) conjugate** in DMSO-d[6].

4.3 Brush glycopolymer targeting Langerin on cells

Serap Üclü, Stig Hill Christiansen, Maxime Denis, Christoph Rademacher, Steffen Thiel, Laura Hartmann*

Publication Draft

Own Contribution:

Collaborative project design. Synthesis and purification of building blocks for solid phase polymer synthesis, glycooligomers and brush glycopolymers. Measurement and evaluation of all LC-MS experiments of the glycooligomers and evaluation of all NMR and UHR spectra of glycooligomers and brush glycopolymers. Collaborative planning and performance of the cell uptake experiments using Flow Cytometry. Collaborative writing of the first publication draft.

Brush glycopolymers targeting Langerin on cells

Serap Üclü[a‡], Stig Hill Christiansen[b‡], Maxime Denis[c], Christoph Rademacher[c], Steffen Thiel[b], Laura Hartmann[a,d]*

      a. Department for Organic Chemistry and Macromolecular Chemistry, Heinrich Heine University Düsseldorf, Universitätsstraße 1, Düsseldorf 40225, Germany. E-mail: laura.hartmann@hhu.de

      b. Department of Biomedicine, Aarhus University, The Skou-Building 1115, Hoegh-Guldbergs Gade 10, 8000 Aarhus C, Denmark. E-mail: st@biomed.au.dk

      c. Department of Pharmaceutical Sciences, University of Vienna, Josef-Holaubeck-Platz 2, 1090 Vienna, Austria. E-mail: christoph.rademacher@univie.ac.at

      d. Institute for Macromolecular Chemistry, University Freiburg, Stefan-Meier-Str. 31, 79104 Freiburg i.Br., Germany

‡ These authors contributed equally

* Corresponding author: laura.hartmann@makro.uni-freiburg.de

Abstract

Langerin expressed on the surface of Langerhans cells in the skin and mucosa is the key mediator in the recognition of carbohydrate-based pathogen- or danger-associated molecular patterns- and promotes the regulation of the immune response. Taking the trivalent arrangement of the CRD of Langerin as blueprint, we present a variety of umbrella-like glycooligomers with a trivalent mannose-containing head group and a hydrophilic tail group in different lengths, accessible by solid phase polymer synthesis. Binding studies by ^{19}F-NMR competition assay of umbrella-like glycooligomers towards Langerin show that the binding to Langerin decreases with increasing tail length, which can be attributed to sterical shielding effects.

The presentation of these glycooligomers on a polymeric scaffold resulting in brush glycopolymers enables the increase of the overall multivalence and the addressing of the Langerin receptor on cell surfaces. The umbrella-like glycooligomers were used as side chains of different lengths thus varying the accessibility of the trivalent mannose head groups. Flow cytometric studies on Langerin-expressed HEK293 cells show that the brush gylcopolymer with the longest tail group as side chains exhibite the highest cell binding. To investigate the effects of carbohydrate density on binding to the Langerin receptor on the cell surface, the glycopolymer with the longest side chain is used and the degree of functionalization is increased. The study on cells showed that lower carbohydrate density allows enhanced binding, and thus lower mannose concentrations are sufficient to achieve high receptor binding at the cell surface.

Introduction:

Carbohydrate-lectin interactions are key mediators of many biological processes, such as cell-cell interactions, signalling pathways and innate immune responses.[1-4] The binding of a carbohydrate ligand to a single carbohydrate recognition domain (CRD) is typically weak. Nature uses multivalency and the simultaneous interaction of multiple carbohydrate ligands and/or CRDs to achieve increased binding avidity.[5-8] In turn, mimicking the multivalent presentation of natural carbohydrate ligands or fragments thereof on a synthetic scaffold allows for the development of high affinity, possibly non-natural, ligands that can be used as

model compounds in fundamental studies as well as in the development of therapeutic approaches.[9-11] An important class of such multivalent glycomimetics are the glycopolymers, as they offer straightforward access to a variety of highly valent carbohydrate conjugates.[12-14] However, their increase in binding avidity is mostly related to a statistically increased binding probability due to the high number of binding units in close proximity to the CRDs.[15,16] A potential selectivity is typically achieved through the choice of a carbohydrate motif known as a specific binder of the targeted receptor.[17] Interestingly, recent studies suggest that also structural parameters of the polymer scaffold itself, such as the architecture, can affect both binding avidity and selectivity, likely mimicking the natural presentation of carbohydrates on protein scaffolds.[18-21] Selectivity through the choice of scaffold is more established for lower molecular weight glycomimetics, e.g., based on peptide or oligomeric scaffolds. It has been demonstrated that, e.g., by matching the spatial distribution of the CRDs of a multivalent receptor while employing multivalent ligand, higher avidity and selectivity can be achieved.[22] In many biological processes, the interaction between the glycomimetics and the receptors involves the clustering of multiple receptors, especially in binding processes on cell surface. To achieve this clustering, larger glycomimetics are required, since the small glycomimetics are dimensioned to bind only one receptor. [23, 24]

In this study, we present the combination of both approaches, an oligomeric glycomimetic ligand designed for a specific receptor and its multivalent presentation on a polymeric scaffold with a special focus on using the resulting glycopolymer to target the receptor on cell surfaces. (Figure 1) Our target receptor for this study is Langerin, a C-type lectin of the immune system known to recognize, e.g., mannose (Man) via its CRDs.[25-27] At the surface of Langerhans cells located in the skin and mucosa, this lectin mediate the recognition of carbohydrate-based pathogen- or danger-associated molecular patterns and promote immune response regulation.[28-30] Three Langerin polypeptide chains form a trimer stabilized by a coiled-coil of α-helices in the neck region.[31] This enables Langerin to gain a higher binding strength if ligands are presented to the molecule in a pattern fitting such trimer CRD structure. Previously we have developed a trivalent oligomeric Man ligand that showed higher affinity to Langerin in comparison to other C-type lectin receptors, specifically the model plant lectin Concanvalin A (ConA), recognizing Man with four CRDs.[22] We hypothesized that the higher binding to Langerin results from a rapid (re-)binding: the small ligand binds with only one Man at a time but is trapped between the other CRDs leading to a fast exchange between bound and

non- bound states efficiently occupying the receptor binding sites. In this study we use a further simplify of the branched trivalent ligand by introducing an even smaller trivalent ligand Here we use this trivalent ligand and present it on a polymeric scaffold to increase the overall multivalency and allow for receptor-specific cell interactions. The choice of polymeric scaffold and multivalent presentation is based on a previous study that demonstrated the relevance of polymer scaffold architecture going from linear to branched in addressing different receptors.[32] We found that branched glycopolymers showed higher binding to C-type lectin DC-SIGN, another Man recognizing receptor of the immune system, while linear glycopolymers showed preferred binding by ConA. Based on the structural similarities between Langerin and DC-SIGN, with Langerin having three symmetrically arranged CRDs and DC-SIGN having four CRDs with a spacing of about 4 nm, here we therefore also choose a brush-type polymer scaffold and specifically investigate the effects of brush length and number of brushes on the receptor binding. [27,33]
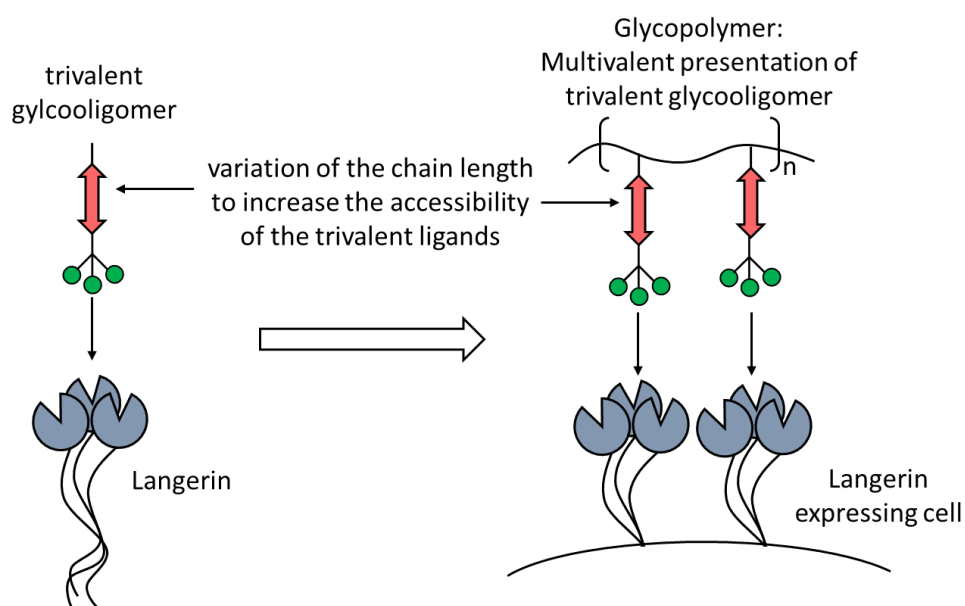

Figure 1: Schematic presentation of developing a trivalent glycomimetic ligand for binding to Langerin and its multivalent presentation on brush glycopolymers to enable effective binding to Langerin expressing cells.

Materials and Methods

Materials: Acetone (≥ 99.8%), triethylamine (analytical grade) and toluol (for HPLC) were purchased from Fischer Scientific. Succinic anhydride (≥ 99.0%) was purchased from Carbolution Chemicals. Diethyl ether (with BHT as inhibitor, ≥ 99.8%), triisopropylsilane (TIPS) (98%), (+)-sodium-L-ascorbate (≥99.0%), chloroform-d (99,8 atom % D), deuteriumoxid-d2 (99,8 atom % D), dimethylsulfoxid-d6 (99,8 atom % D), were purchased from Sigma-Aldrich. N,N-Diisopropylethylamine (DIPEA) (≥ 99%), kaliumhydroxide (≥ 85%) were purchased from Carl Roth. Methanol (100%), ethylacetate (>99.9%), n-hexan (≥99.8%) and acetic anhydride (99.7%) were purchased from VWR BDH Prolabo Chemicals. Dimethylformamide (DMF) (99.8%, for peptide synthesis), tert-butanol (≥ 99.0%), piperidine (99%), sodium methoxide (97%), sodium diethyldithiocarbamate (99%), tritylchloride and copper (II)sulfate (98%) were purchased from Acros Organics. Dichloromethane (DCM) (99.99%), Triethylsilan (≥ 98,0 %), trifluoroacetic acid (≥ 99,0 %), 9-fluorenylmethyl chloroformate (Fmoc-Cl) were purchased from Fluorochem UK. Benzotriazole-1-yl-oxy-tris-pyrrolidino-phosphonium 137lycofunctionalizat (PyBOP) was purchased from Iris Biotech GmbH. The anion resin (AG1-X8, quarternary ammonium, 100-200 mesh, acetate form) was purchased from BioRad. TentaGel® resin was purchased from Rapp Polymere. Methyl-α-D-mannopyranoside (>99%), 1-ethyl-3-(3-dimethylaminopropyl)carbodiimide hydrochloride (EDC), N-hydroxysuccinimide (NHS), 10 mM sodium acetate pH 4.0, was purchased from Cytiva. Diethylenetriamine was purchased from Merk (>98%). Di-tert-butyldicarbonat (≥99,0 %) was purchased from Novabiochem. Ethanol (>99.9%) was purchased from Chemsolute. 2,2'-(ethylenedioxy)bis(ethylamine) was obtained from TCI Europe. Citric acid, anhydrous; 4-pentynoic acid were purchased from Alfa Aesar (>99.5%).

Synthesis of Building Blocks for Solid Phase Polymer Synthesis: The synthesis of the building blocks EDS, TT, Man-N_3 and Gal-N_3 followed the detailed description in the literature. [34-37]

Solid Phase Synthesis of umbrella-like glycooligomers: The umbrella-like glycooligomers were prepared by repeated stepwise coupling and deprotection steps of the building blocks on solid support. The reactions were conducted in polypropylene syringe reactors, including a polyethylene frit and a Luer stopper from Multisynthech GmbH. As solid support, TentaGel® SRAM resin pre-functionalized with ethylenediamine with a loading of 0.20 mmol/g was used. The batch size of 0.1 mmol was employed for each glycooligomer. The triple alkyne

functionalized linker TT was used as functional building block and indicates the umbrella head and EDS was used as a spacer building block to build up the umbrella handle of the glycooligomer.

Coupling and deprotection steps: First, the resin was first swollen twice for 15 min in DCM and then washed three times with DMF. The coupling steps of EDS and TT linker were performed by shaking for 1 h with a mixture of 5 equivalents of the building block, 5 equivalents of PyBOP and 10 equivalents of DIPEA in DMF followed by washing steps ten times with DMF. After each coupling, the resin was shaken with a solution of 25 Vol% piperidine in DMF for 15 min and then washed three times with DMF. This was repeated two times and then washed ten times with DMF.

Copper(I)-catalyzed alkyne-azide cycloaddition (CuAAC): The glycoconjugation to the glycooligomer backbone was carried out by using the CuAAC. For this, 2,5 equivalents of (2-azidoethyl)-2,3,4,6-tetra-O-acetyl-α-D-mannopyranoside (Man-N$_3$ or Gal-N$_3$) per alkyne was dissolved in 2 ml DMF, of 30 mol% of sodium ascorbate and of 30 mol% of copper sulfate per alkyne was dissolved in 0,5 ml water. The copper sulfate solution was drawn up first, then the sugar solution, and finally the sodium ascorbate solution. The reactor syringe was covered with aluminum foil and shaken overnight. The resin was then washed three times with a 23 mM solution of sodium diethyldithiocarbamate in DMF/H$_2$O (1:1, v/v), three times with DMF, and three times with DCM. The washing steps were repeated with the three solutions until no coloration of the wash solution was observed.

Deprotection of sugar-pyranoside and cleavage from the resin: After successful conjugation of sugar-pyranosides, the deprotection of hydroxyl groups was performed in 0.1 M NaOMe in methanol and shaken for 60 minutes. Then the syringe was washed ten times with methanol, ten times with DMF and ten times with DCM. The glycooligomer was cleaved from the resin by shaking with a solution of 35 vol% TFA, 60 vol% DCM, and 5 vol% TIPS. The solution was precipitation in cold diethyl ether and the white precipitate was centrifuged off. The white solid was then dissolved in water and the product isolated by lyophilization.

Polymer analogues synthesis of brush glycopolymers: The conjugation of umbrella-like glycooligomers was performed following the previous description in the literature. [32]

AlexaFlour647 labelling of the brush glycopolymers: To a stock solution of brush glycopolymer (20 mg/ml) 100 µL of the AlexaFlour647 stock solution (1 mg/ml) in water was added. Subsequently, 10 eq. of NHS and 10 eq. of EDC were added and stirred overnight. The excess dye was removed by dialysis.

^{19}F-NMR experiment : ^{19}F NMR and ^{19}F R_2-filtered NMR experiments were conducted on a Brucker AV 500 MHz spectrometer under 298 K. Spectra were processed in MestReNova and data analysis was performed with OriginPro. For each spectrum 128 scans were recorded in 5 mm sample tubes at sample volumes of 500 µl. Relaxation rates $R_{2,obs}$ were determined with the CPMG pulse sequence, equation below. T represents the relaxation time and I_0 is the integral at a T value of 0 s. The relaxation delay d_1 was set to 2.0 s, the acquisition time t_{acq} was set to 0.8 s and the frequency of 180° pulses u_{CPMG} was set to 500 Hz.

$$I = I_0 e^{-R_{2,obs}T}$$

Langerin-expressing cell line: We produced cells that express the C-type lectin Langerin. The Freestyle 293-F cell line (Thermo Fisher Scientific, Waltham, MA) was cultured in 6-well plates to a final density of ~10^6 cells/ml per well (70-90% confluent at transfection) in Gibco Freestyle 293-F Expression Medium (Cat.no.: 12338026, Thermo Fisher Scientific) with 10% fetal bovine serum (FBS, Merck, Munich, Germany), 100 units/ml penicillin, and 100 µg/ml streptomycin (Thermo Fischer Scientific). The cells were replenished with new Freestyle 293-F expression medium with 10% fetal bovine serum (FBS) on the day of transfection.

The target gene encoding Langerin (accession number NM_015717.5) was synthesized and cloned into the mammalian expression vector pcDNA3.1/Zeo+ (a service provided by Genscript, NJ), a plasmid conferring resistance to the phleomycin family of antibiotics, e.g., to zeocin.

The Langerin-encoding vector or a control vector (mock, i.e., the pcDNA3.1/Zeo+ vector without any protein cassette) was introduced into the adherent Freestyle 293-F cell line by transfection. DNA and Lipofectamine 3000 (Thermo Fisher Scientific) were mixed in two steps following the instructor's manual. First, the lipofectamine 3000 reagent was diluted in OptiPRO SFM SFM (Thermo Fisher Scientific). Second, a master mix of 5 µg plasmid DNA was

diluted in OptiPRO SFM, and 10 µl P3000 reagent was added. The two mixtures were combined, incubated for 10-15 min, and DNA-lipid complexes were added to the cells by gently swirling the 6-well plate to ensure a homogenous distribution. After 24 hours of incubation at 37 °C and 8% CO_2, the cells were replenished with fresh expression medium with penicillin, streptomycin, and 10% FBS. Forty-eight hours after transfection, cells were supplemented with 500 µg/mL zeocin to select stably transfected cells. Cells were fed a new medium every three days and analyzed for clonal outgrowth after 10-14 days of culture. Resistant clones were trypsinized and cloned by limiting dilution into 96-well microtiter plates. Individual clones were screened for lectin expression by flow cytometry using APC-labelled anti-Langerin antibody (cat.no.: 352206, BioLegend, San Diego, US). Clones expressing Langerin and mock control clones not expressing Langerin were expanded for cryopreservation. Cells were cryopreserved at -150° 140lycofu in Freestyle 293F Expression Medium with 20% FCS and 10% DMSO.

Flow cytometry: The Langerin-expressing and mock cell lines were thawed by gently resuspending and diluting ten times in Freestyle 293F Expression Medium. Cells were sedimented by centrifugation at 200 x g and replenished in Freestyle 293F Expression Medium with 10% FBS, 100 units/ml penicillin, and 100 µg/ml streptomycin (culture medium). Cells were incubated in standard T75 culture flasks (Sarstedt, Newton, NC) at 37 °C and 8% CO_2. The next day, the culture medium was discarded and replaced with a culture medium containing 500 µg/ml zeocin to ensure the growth of Langerin-expressing cells. The culture medium was changed every third day until the cells reached 80-90% confluence; then, the cells were harvested by incubating in PBS with 5 mM EDTA and immediately transferred into a buffer of 20 mM HEPES, 150 mM NaCl, 5 mM $CaCl_2$, 5 mM $MgCl_2$, and 0.5% bovine serum albumin (BSA), pH 7.4 (HBS/Ca/Mg) by centrifugation at 200 x g for 5 minutes and adding the HBS/Ca/Mg.

Binding experiments of glycopolymers towards cells: For the binding assay, cells were replenished in HBS/Ca/Mg and adjusted to 500,000 cells/mL. Glycopolymers conjugated with Alexa Fluor 647 were aliquoted to a volume of 50 µl at 100 or 50 µM in HBS/Ca/Mg in V-bottom 96-well wells, and immediately mixed with the freshly reconstituted cells to a final volume of 100 µL per well. The cells were incubated with glycopolymers for 30 min at RT, protected from light. After incubation, cells were pelleted by centrifugation at 200 x g for 2

min, washed twice in HBS/Ca/Mg, and subsequently reconstituted in 200 µl HBS/Ca/Mg for flow cytometry analysis.

Competitions experiments: We tested whether mannose-BSA competes with glycopolymer for binding to Langerin-expressing cells. For this, mannose-BSA (cat.no.: NGP1108, Dextra, Reading, UK) was two-fold serially diluted from 200 to 6.25 µg/ml in HBS/Ca/Mg in a V-bottom 141lycofunct plate and mixed with 50 µl Langerin-expressing or mock cell lines at 500,000 cells/mL, to a final volume of 100 µl per well. The cells pre-incubated with mannose-BSA for 15 min at RT, and, subsequently, 25 µM Alexa Fluor 647-conjugated P3 was added to the cells for 30 min at RT, protected from light. After incubation, cells were pelleted by centrifugation at 200 x g for 2 min and washed twice in HBS/Ca/Mg. The cells were reconstituted with 200 µl HBS/Ca/Mg for flow cytometry analysis.

Flow cytometry data were collected on an ACEA Novocyte flow cytometer (ACEA Biosciences Inc., San Diego, CA) and analyzed using FlowJo v10.8 (FlowJo LLC, Ashland, OR).

Results and discussion

Synthesis of trivalent Man containing umbrella-like glycooligomers

Our previous study used the stepwise assembly of tailor-made building blocks on a solid support to synthesize a series of trivalent Man ligands with different lengths of the arms connecting the three carbohydrate motifs. We found that the smallest ligand showed the highest affinity to Langerin.[22] Based on this finding, we previously developed a new building block – the so-called TT (three triple bonds) linker – allowing for the straightforward presentation of three Man units in close proximity. In short, the TT linker (4-((1,3-bis(prop-2-yn-1-yloxy)-2-((prop-2-yn-1-yloxy)methal)propan-2-yl)amino)-4-oxobutanoic acid) is derived starting from tris(hydroxymethyl)aminomethane (TRIS). First, the primary amine group is protected by di-*tert*-butyldicarbonat, followed by functionalization of the hydroxyl groups with propargyl bromide introducing three terminal alkyne groups. In the final step, the amine group is deprotected by trifluoroacetic acid (TFA) and functionalized with succinic anhydride to give a free carboxy group. Through its carboxylic functionality on one end, the TT linker is directly compatible with our solid phase polymer platform making use of standard Fmoc-peptide coupling chemistry employing natural and non-natural amino acids and tailor-made

building blocks. The three alkyne groups allow for the straightforward introduction of three Man ligands by Cu-mediated azido alkyne conjugation (CuAAC) with well-established reaction conditions and available azido-Man building blocks. [38-41] In order to allow for control over the length of the brush in the brush-type polymer, EDS building blocks introducing an ethylene glycol unit in the oligomeric backbone were then used in the solid phase assembly of a series of glycooligomers that resemble an umbrella and are thus called umbrella structures (see Figure 2). Three different lengths of the umbrella handle were synthesized with either no, three or seven EDS building blocks. In all cases, the TT linker was used to introduce three alkynes and, after glycoconjugation, three Man ligands at the N-terminus of the oligomer and as umbrella head. For later use as a negative control, the umbrella structure with the longest handle was also synthesized as galactose (Gal) derivative by conjugation of azido-Gal building block instead of azido-Man. All glycooligomers were synthesized on a trityl resin that was preloaded with ethylenediamine thereby releasing a primary amine at the C-terminus after cleavage from the resin. This will later be relevant for conjugation onto the polymeric scaffolds. The nomenclature of the umbrella structures is as follows: U for the umbrella motif, followed by the carbohydrate (Man or Gal), followed by the number of EDS building blocks forming the handle, e.g., U(Man)-3. For comparison, U(Man)-3 was also synthesized as a monovalent, non-umbrella structure by using PA (4-pentynoic acid) building block introducing only one alkyne group. All glycooligomers (see Figure 2C) were isolated and characterized by ^{1}H-NMR, RP-HPLC-ESI-MS and HR-MS (see SI for details on the synthesis, characterization and accompanying spectra).

Figure 2: A) Synthesis of umbrella-like glycooligomers with an exemplary chemical structure for compound U(Man)-3. B) Schematic structure of all glycooligomers of this study. The building block TT was labelled as blue squares, EDS as white squares, and PA as grey squares. The mannose units were marked as green dots and galactose as yellow dots.

Umbrella structures binding to Langerin

To determine the binding of umbrella structures to Langerin, and for comparison with our previous Langerin ligand, ^{19}F-NMR displacement assay was performed. In short, this homogeneous assay monitors the displacement of a [19]F 143lycofun, monovalent N-acetylmannosamine analogue from the primary binding site of Langerin using R2-relaxation in NMR yielding inhibitory constants (K_I) and half maximum inhibitory concentrations. Table 1 summarizes the results of the displacement assay. Overall, umbrella structure U(Man)-7 shows a higher K_I, indicative of a lower affinity, in comparison to a previously described trivalent ligand by a factor of 10.[22] Nevertheless, K_I is still lower by a factor of ~10 in comparison to monovalent Man with $K_I = 4.5 \pm 0.5$ mM.[42] Increasing the handle by adding EDS building blocks leads to an increase in K_I values, which can potentially be attributed to steric effects. Overall, all umbrella structures show binding to Langerin and thus will be further used in the glycopolymer design.

Table 1: ^{19}F-NMR displacement assay quantifying glycooligomer binding to Langerin resulting in inhibitory constants, K_I, and showing that with increase of length the K_I values increases.

The names refer to the structures given in Figure 1. The numbers are given as mean with the chain length by number of EDS. The data represent replicates from three independent experiments.

#	K_I [mM]
U(Man)-0	0.712 ± 0.169
U(Man)-3	0.230 ± 0.044
U(Man)-7	1.410 ± 0.622
L(Man)-3	0.754 ± 0.319

Brush glycopolymers synthesized from umbrella-like glycooligomers

For the synthesis of the brush glycopolymers, a poly(pentafluorophenyl acrylate) (pPFP) scaffold with a Pn of 50 was synthesized following previously presented protocols.[32] This polyactive ester derivative allows for a straightforward polymer-analogue reaction with primary amines and displacement of the pentafluorophenyl side chains. Using our previously derived umbrella structures presenting a terminal amine group enables the introduction of glycooligomer side chains giving brush-like glycopolymers (Figure 3).
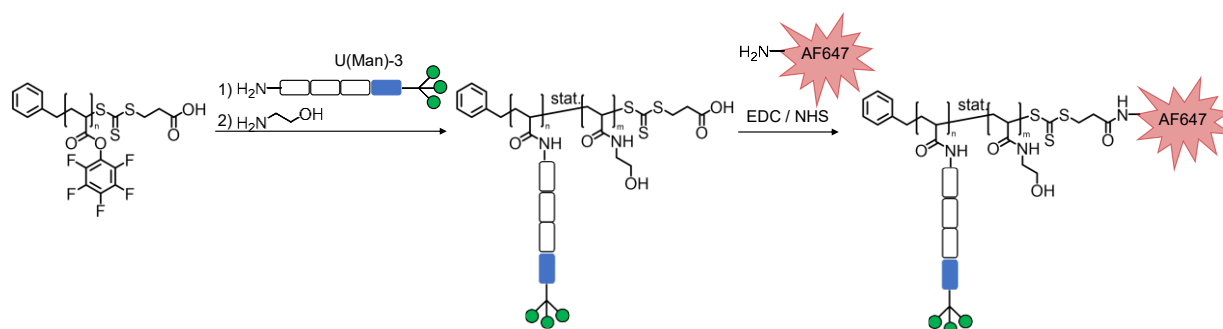
Figure 3: Schematic presentation of the glycopolymer synthesis starting from a pPFP scaffold and polymer-analogue reaction with glycooligomers and conjugation of AlexaFluor647 (AF647).

By using umbrella structures with different lengths of the handle (number of EDS building blocks) (0-7), different brush lengths are realized (P1 – P4 in Figure 4). Furthermore, by adding different amounts of glycooligomers during the polymer-analogue reaction, the number of side chains/brushes can be varied (P3 and P4). In all cases, the remaining pentafluorophenyl

side chains are quenched by reaction with ethanolamine. Complete conversion is confirmed by ^{19}F-NMR showing no remaining pentafluorophenyl groups (see SI for details on the synthesis and polymer characterization). We used non-umbrella brush (P6) as well as linear glycopolymer (P(Man)) as one kind of controls. P6 was synthesized using the monovalent glycooligomers (L-(Man)-3) and P(Man) using amino-functionalized Man. As negative controls brush (P5) as well as linear glycopolymers (P(Gal)), presenting Gal instead of Man were produced. As a further negative control a non-carbohydrate containing polymer derived by complete quenching with ethanolamine giving poly(hydroxyethylacrylamide) (pHEAA) (P(EtOH)). Figure 4 summarizes all glycopolymers synthesized in this study. All polymers were characterized by ^{1}H and ^{19}F-NMR (see SI for details of the polymer synthesis and characterization). For later cell studies, glycopolymers were labelled with the fluorophore Alexa Fluor 647 (AF647). Therefore, the glycopolymers were dissolved in water and (AF647) was added for conjugation to the terminal carboxy group available from the employed RAFT agent after activation by carbodiimide chemistry (see SI for details of the labelling reaction and analytical results).
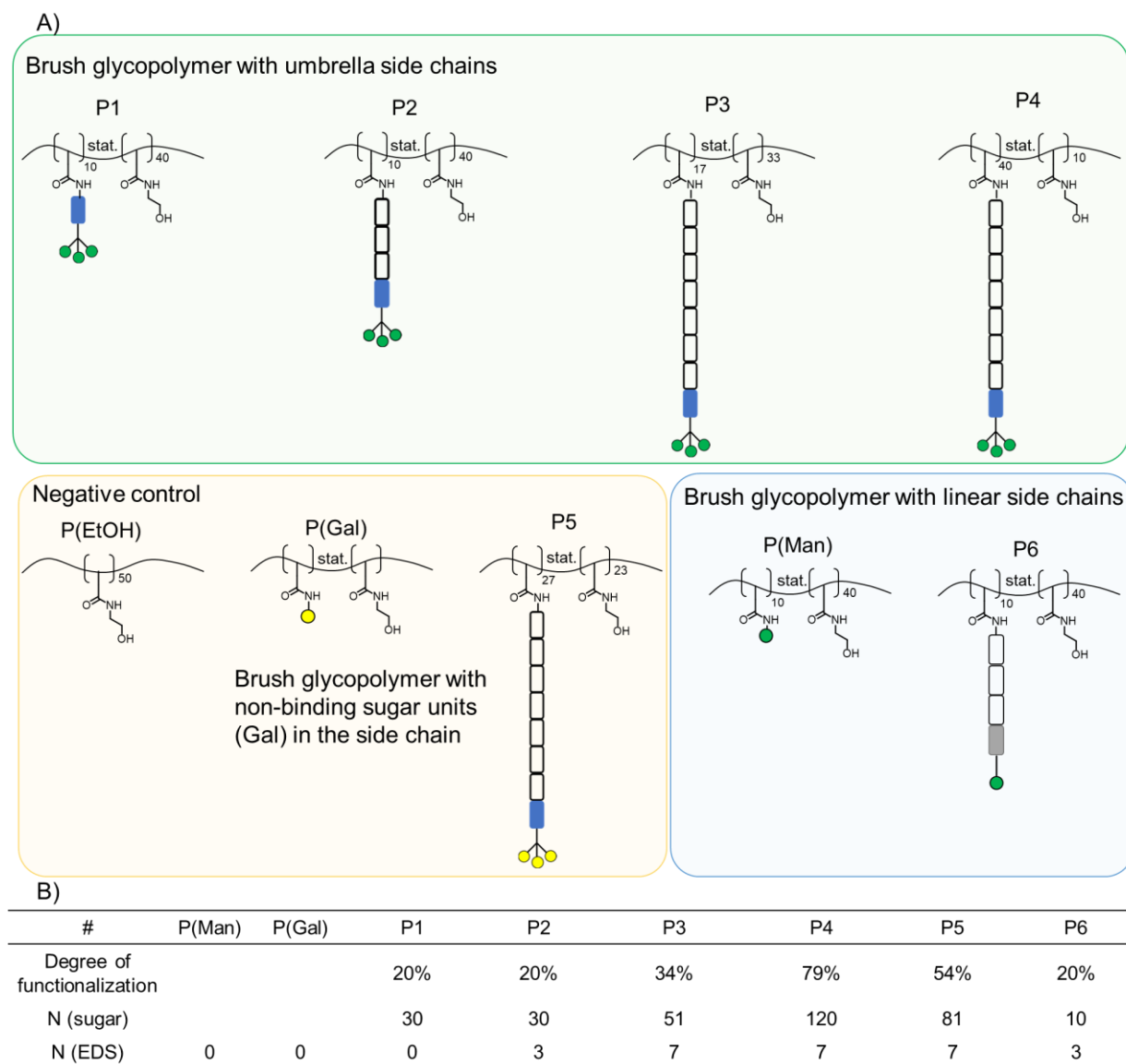
A)

Figure 4: A) Schematic presentation of glycopolymers derived from reacting umbrella glycooligomers with polyactive ester scaffold with corresponding linear control polymers. B) The degree of functionalization was determined by ^{1}H-NMR (see SI for spectra and details of the calculation).

#	P(Man)	P(Gal)	P1	P2	P3	P4	P5	P6
Degree of functionalization			20%	20%	34%	79%	54%	20%
N (sugar)			30	30	51	120	81	10
N (EDS)	0	0	0	3	7	7	7	3

Interaction of glycopolymers with cells expressing lectin

Langerin expressing HEK293F cells as well as a control cell line only carrying the zeocin resistance used for the selection of the cells were produced.

Prior to studying receptor-mediated interactions of the glycopolymers, we tested whether the glycopolymers had a direct effect on cell viability. For this purpose, cells were first mixed with the polymers and then incubated with propidium iodide (PI). Flow cytometric measurements

revealed PI uptake of less than 20% for the cell lines tested, indicating that the glycopolymers are not cytotoxic and can be further used for studying binding to the cells (see SI for details and results of the cytotoxicity study).

We then investigated whether the glycopolymers could specifically target Langerin-expressing cells; Langerin-expressing cells (Langerin-HEK293) were compared to cells not expressing Langerin (EV-HEK293). For these experiments, the glycopolymers were offered to the cells in a buffer containing the calcium needed for the C-type lectin domain to be active. To study the concentration-dependent interaction with the cells, the experiments were initially performed with polymer concentrations of 25 µM and 50 µM. After an incubation period of 30 minutes, the cells were washed, and the amount of bound polymer is given as the mean fluorescence intensity of the cells, as quantified via flow cytometry. Figure 5 shows the results for all tested glycopolymers. At both of the tested concentrations, the highest binding was observed for P3 and P4, i.e., the glycopolymers derived from the umbrella structure with the longest handle and, thus, the longer brushes. P1, as well as P2 with shorter brushes, show significantly lower binding. It was previously demonstrated for other glycopolymers that introducing longer linkers between the carbohydrate motif and polymer backbone can affect the overall affinity, likely due to a higher accessibility of the carbohydrate motifs and increased flexibility enabling the contact with the CRD.[13,43,44] This finding is also in agreement with our previous study showing a higher affinity of brush-like glycopolymers for other, structurally similar C-type lectin receptors of the immune system.[32] Similarly, going from the umbrella glycooligomer P2 to the derivative with the linear, monovalent side chain P6, we also see a decrease in binding. Changing the valency of the side chain also changes the overall valency of the glycopolymer in this case, thus, this could also be an effect of a reduced statistical probability of binding at a lower overall concentration of Man ligands. This is also in agreement with the lower binding of the monovalent Man ligand in comparison to the trivalent umbrella motif, as observed from the previous ^{19}F-NMR binding study. (see Table 1) Interestingly, when comparing the two best binding systems, P3 and P4, both derived from the same umbrella glycooligomers but differing in the number of side chains per polymer, the glycopolymers with the lower number of side chains and thus also a lower concentration of Man ligands shows the higher binding. Indeed, we and others have previously observed that for glycopolymers, more is not always better and that there seems to be a critical density of binding carbohydrate motifs that gives maximum receptor binding.[45-47] Increasing the density above this critical value either does not further

increase or even, as seems to be the case also in this study, decreases the binding. These results thus further highlight that polymer architecture can affect the overall binding avidity and potentially also selectivity. Importantly, negative controls of Gal-presenting glycopolymers and p(EtOH) showed no significant interaction with either Langerin-HEK293 or EV-HEK293. Thus, these results indicate the successful targeting of cells expressing Langerin with our glycopolymers, with higher binding being achieved for the brush-type glycopolymers derived from the umbrella structure.
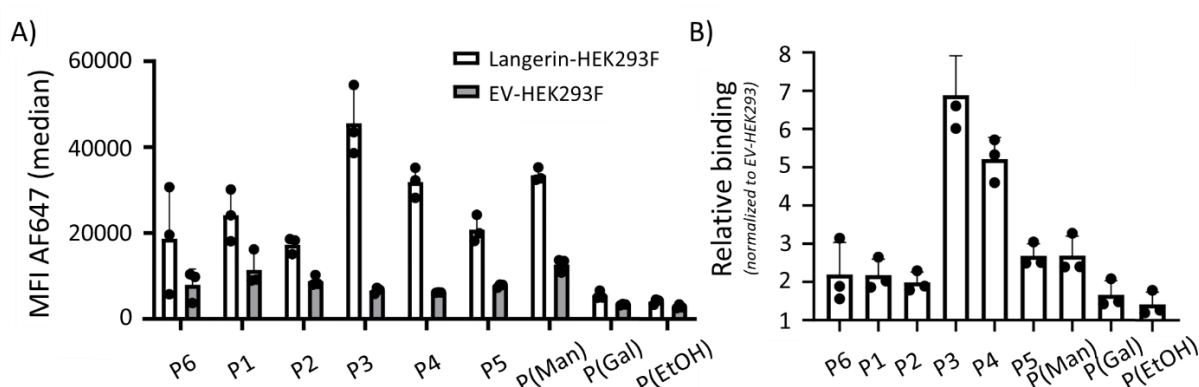
Figure 5: Assessment of the binding of glycopolymers to lectin-expressing cells. (A) Glycopolymers labeled with AF647 were incubated with Langerin-expressing HEK293F cells (Langerin-293F) or non-Langerin-expressing cells (EV-HEK293F), and binding was subsequently quantified by flow cytometry. Glycopolymers were tested at 25 µM. The bars show the median fluorescence intensity (MFI). The symbols in each bar are the data points, and the line in each bar gives the standard deviation. (B) The same data as in (A), but here the bars show the relative binding of glycopolymers to Langerin-HEK293 when normalized to MFI of EV-HEK293. The names below the x-axis refer to the glycopolymers used in the main text. The data represent biological replicates from three independent experiments.

To further investigate the selectivity of glycopolymers in binding to the cells expressing Langerin we compared the best binder, P3, to Man-functionalized BSA, i.e. an alternative multivalent Man ligand we have used before in other studies of interactions with C-type lectins.[48-50] Langerin-positive cells and EV-HEK293 cells as negative control were incubated with Man-BSA at different concentrations, and then P3 was added. In this setup, Man-BSA competes with the binding of other carbohydrate ligands to Langerin, and we test whether this hinders the binding of the glycopolymer to Langerin (Figure 6A). We used a buffer

containing BSA to decrease non-specific binding of Man-BSA to the cells. We found that as the concentration of Man-BSA increased, the fluorescence readout decreased, i.e., the binding of P3 to the Langerin-positive cells was outcompeted. The Langerin-negative EV-HEK293 cells showed no binding of the glycopolymer at all tested concentrations (Figure 6B).
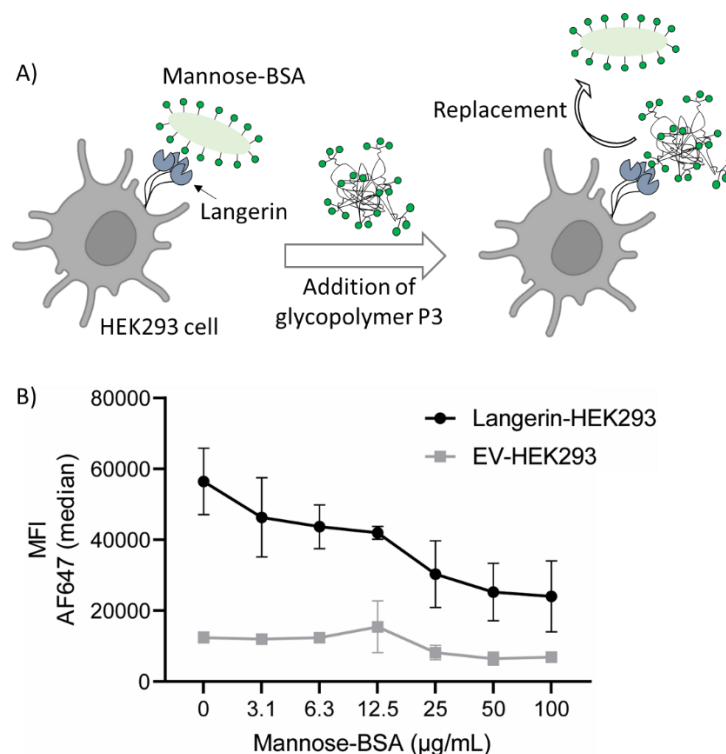

Figure 6: A) Procedure of the competition experiment. B) Competition of the binding of glycopolymer P3 to Langerin-HEK293F cells with mannose-BSA. Different concentrations of mannose-BSA were incubated with Langerin-HEK293F cells, followed by 25 µM AF647-labeled glycopolymer P3. The mannose-BSA and the glycopolymer P3 were allowed to compete for binding to the Langerin-expressing cells for 30 min, and subsequently, binding was quantified by flow cytometry. The symbols show the median fluorescence intensity (MFI), and the lines give the standard deviation. The data represent biological replicates from two independent experiments.

Conclusion

Langerin, localized to Langerhans cells, plays a critical role in regulating the immune response by recognizing carbohydrate-based pathogen-associated molecular patterns. To study the

binding and inhibition of Langerin, umbrella-like glycooligomers with a trivalent head group and a umbrella handle were prepared whereas the length of the umbrella handle was varied. These umbrella-like glycooligomers were tested by ^{19}F NMR competition assay to Langerin and showed that an increase in handle length resulted in inhibition of the binding by 50 % to Langerin, which is potentially attributed to steric effects of the umbrella handle. We propose that the glycooligomer with the trivalent umbrella head U(Man)-0 is highly accessible to the binding pockets of Langerin and leads to high inhibition constant due to rapid rebinding effects.

For investigation at the cellular level, the glycooligomers were conjugated to a polymer backbone to form brush glycopolymers whereas the umbrella-like glycooligomers forming the side chains. In this manner, brush glycopolymers with different length of the side chains were prepared. Additionally, the longest glycooligomer U(Man)-7 was used to prepare brush glycooligomers in two different incorporation ratios of 34% (P3) and 79% (P4). Examination of Langerin-expressed HEK293 cells using flow cytometry showed that the brush glycopolymer P3 the highest binding to the Langerin receptors, although fewer mannose units were present compared to P4. This suggests that the critical density of binding mannose motifs was reached here to achieve maximum receptor binding. To confirm the specific binding the competition experiment with BSA-mannose to Langerin was conducted on non-Langerin-expressing EV-HEK293 cells, confirms the specific binding to Langerin.

References

(1) Lepenies B.; Lang R. Editorial: Lectins and Their Ligands in Shaping Immune Responses. *Front. Immunol*. **2019**, *10*, 2379.

(2) Brandley, B.K.; Schnaar, R.L. Cell-surface carbohydrates in cell recognition and response. *J. Leukoc. Biol.*, **1986**, *40*, 97–111.

(3) Geijtenbeek, T.; Gringhuis, S. Signalling through C-type lectin receptors: shaping immune responses. *Nat Rev Immunol*, **2009**, *9*, 465–479.

(4) Fujita, T.; Matsushita, M.; Endo, Y. The lectin-complement pathway–its role in innate immunity and evolution. *Immunol. Rev.*, **2004**, *198*, 185–202.

(5) McCormack, F.X; Pattanajitvilai, S.; Stewart, J.; Possmayer, F.; Inchley, K.; Voelker, D.R. The Cys6 intermolecular disulfide bond and the collagen-like region of rat SP-A play critical roles in interactions with alveolar type II cells and surfactant lipids. *J Biol Chem*., **1997**, *272*, 27971– 27979.

(6) Seaton, B.A.; Crouch, E.C. ,McCormack, F.X.; Head, J.F.; Hartshorn, K.L.; Mendelsohn, R. Review: structural determinants of pattern recognition by lung collectins. *Innate Immun*, **2010**, *16*, 143– 150.

(7) Lu, W.; Pieters, R.J. Carbohydrate-protein interactions and multivalency: implications for the inhibition of influenza A virus infections. *Expert Opin Drug Discov*., **2019**, *14*, 387-395.

(8) Taylor, M.E.; Bezouska, K.; Drickamer, K. Contribution to ligand binding by multiple carbohydrate-recognition domains in the macrophage mannose receptor. *J. Biol. Chem.*, **1992**, *267*, 1719–1726.

(9) Lindhorst, T.K. Artificial Multivalent Sugar Ligands to Understand and Manipulate Carbohydrate-Protein Interactions. Host-Guest Chemistry **2001**, 201-235.

(10) Sakai, S.; Tomikazu S.Multivalent Carbohydrate Ligands Assembled on a Metal Template. *J. Am. Chem. Soc*. **1994**, *116*, 1587–1588.

(11) Müller, C.; Depras, G.; Lindhorst, T.K. Organizing multivalency in carbohydrate recognition. *Chem. Soc. Rev*., **2016**, *45*, 3275—3302.

(12) Stenzel, M.H. Gylcopolymers for Drug Delivery: Opportunities and Challenges. *Macromolecules,* 2022, *55*, 12, 4867–4890.

(13)   Becer, C.R. The Glycopolymer Code: Synthesis of Glycopolymers and Multivalent Carbohydrate-Lectin Interactions. *Macromol. Rapid Commun*. **2012**, *33*, 742– 752.

(14)   Mammen, M.; Choi, S.K.; Whitesides, G.M. Polyvalent interactions in biological systems: implications for design and use of multivalent ligands and inhibitors. *Angew. Chem., Int. Ed.* **1998**, *37*, 2754– 2794.

(15)   Weber, M.; Bujotzek, A.; Haag, R. Quantifying the rebinding effect in multivalent chemical ligand-receptor systems. *J. Chem. Phys.*, **2012**, 137, 054111.

(16)   Rao, J.; Lahiri, J.; Weis, R.M; Whitesides,, G.M. Design, synthesis, and characterization of a high-affinity trivalent system derived from Vancomycin and L-Lys-D-Ala-D-Ala. *J. Am. Chem. Soc.,* **2000**, *122*, 2698–2710.

(17)   Ward, E.M.; Kizer, M.E.; Imperiali, B. Strategies and Tactics for the Development of Selective Glycan-Binding Proteins. *ACS Chem. Biol.,* **2021**, *16*, 1795–1813.

(18)   Richards, S. J.; Jones, M. W.; Hunaban, M.; Haddleton, D. M.; Gibson, M. I. Probing bacterial-toxin inhibition with synthetic glycopolymers prepared by tandem post-polymerization modification: role of linker length and carbohydrate density. *Angew. Chem., Int. Ed.*, **2012**, *51*, 7812–7816.

(19)   Polizzotti, B.D.; Kiick, K.L. Effects of Polymer Structure on the Inhibition of Cholera Toxin by Linear Polypeptide-Based Glycopolymers. *Biomacromolecules* **2006**, *7*, 483 – 490.

(20)   Mitchell, D.A.; Zhang, Q.; Voorhaar, L.; Haddleton, D. M.; Herath, S.; Gleinich, A. S.; Randeva, H. S.; Crispin, M.; Lehnert, H.; Wallis, R.; Patterson, S.; Becer, C. R. Manipulation of Cytokine Secretion in Human Dendritic Cells Using Glycopolymers with Picomolar Affinity for DC-SIGN. *Chem. Sci*. **2017**, *8*, 6974 – 6980.

(21)   Yilmaz, G.; Uzunova, V.; Napier, R.; Becer, C. R. Single-Chain Glycopolymer Folding via Host- Guest Interactions and Its Unprecedented Effect on DC-SIGN Binding. *Biomacromolecules* **2018**, *19*, 3040 – 3047.

(22)   Neuhaus, K.; Wamhoff, E.C.; Freichel, T.; Grafmüller, A.; Rademacher, C.; Hartmann, L. Assymetrically Branched Precision Glycooligomers Targeting Langerin. *Biomacromolecules* **2019**, *20*, 4088 – 4095.

(23)   Caré, B.R.; Soula, H.A. Impact of receptor clustering on ligand binding. *BMC Syst Biol.* **2011**, *5*.

(24)   Erickson, J.; Goldstein, B.; Holowka, D.; Baird, B. The effect of receptor density on the forward rate constant for binding of ligands to cell surface receptors. *Biophys. J.*, **1987**, *52*, 657-662.

(25)   Feinberg, H.; Taylor, M. E.; Razi, N.; McBride, R.; Knirel, Y. A.; Graham, S. A.; Drickamer, K.; Weis, W. I. Structural basis for langerin recognition of diverse pathogen and mammalian glycans through a single binding site. *J. Mol. Biol.* **2011**, *405*, 1027–1039.

(26)   Stoitzner, P.; Romani, N. Langerin, the "Catcher in the Rye": An important receptor for pathogens on Langerhans cells. *Eur. J. Immunol.,* **2011**, *41*, 2526–2529.

(27)   Feinberg, H.; Powlesland, A.S.; Taylor, M.E.; Weis, W.I. Trimeric Structure of Langerin. *The J. Biol. Chem* **2010**, *285*; 13285–13293.

(28)   Singh, S.K.; Stephani, J.; Schaefer, M.; Kalay, H.; García-Vallejo, J.J.; den Haan, J.; Sealand, E.; Sparwasser, T.; van Kooyk, Y. Targeting glycan modified OVA to murine DC-SIGN transgenic dendritic cells enhances MHC class I and II presentation. *Mol. Immunol.,* **2009**, *47*, 164-174.

(29)   Demento, S.L.; Siefert, A.L.; Bandyopadhyay, A.; Sharp, F.A.; Fahmy, T.M.; Pathogen-associated molecular patterns on biomaterials: a paradigm for engineering new vaccines. *Trends Biotechnol.,* **2011**, *29*, 294–306.

(30)   Gauglitz, G.G.; Callenberg, H.; Weindl, G.; Korting, H.C. Host Defence Against Candida albicans and the Role of Patternrecognition Receptors. *Acta Derm Venereol.* **2012**; *92*, 291–298.

(31)   Stambach, N.S.; Taylor, M.E. Characterization of carbohydrate recognition by langerin, a C-type lectin of Langerhans cells. *Glycobiology*, **2003**, *13*, 401–410.

(32)   Shamout, F.; Monaco, A.; Yilmaz, G.; Becer, C. R.; Hartmann, L. Synthesis of Brush-Like Glycopolymers with Monodisperse, Sequence-Defined Side Chains and Their Interactions with Plant and Animal Lectins. *Macromo. Rapid Commun.* **2019**, *41*, 1900459.

(33)   Feinberg, H.; Guo, Y.; Mitchell, D. A.; Drickamer, K.; Weis, W. I. Extended neck regions stabilize tetramers of the receptors DC-SIGN and DC-SIGNR. *J. Biol. Chem.* **2005**, *280*, 1327–1335.

(34)   Boden, S.; Reise, F.; Kania, J.; Lindhorst, T.K.; Hartmann, L. Sequence-Defined Introduction of Hydrophobic Motifs and Effects in Lectin Binding of Precision Glycomacromolecules. *Macromol. Biosci.,* **2019**, *19*, 1800425.

(35)   Hayes, W.; Osborn, H.M.I.; Osborne, S.D.; Rastall, R.A.; Romagnoli, B. One-pot synthesis of multivalent arrays of mannose mono- and disaccharides. *Tetrahedron*, **2003**, *59*, 7983-7996.

(36)   Wu,L.; Sampson, N.S. Fucose, Mannose, and β-N-Acetylglucosamine Glycopolymers Initiate the Mouse Sperm Acrosome Reaction through Convergent Signaling Pathways. *ACS Chem. Biol.*, **2014**, *9*, 468-475.

(37)   Chabre, Y.M.; Contino-Pépin, C.; Placide, V.; Shiao, T.C.; Roy, R. Expeditive Synthesis of Glycodendrimer Scaffolds Based on Versatile TRIS and Mannoside Derivatives. *J. Org. Chem.*, **2008**, *73*, 5602–5605.

(38)   Boden, S.; Reise, F.; Kania, J.; Lindhorst, T.K.; Hartmann, L. Sequence-Defined Introduction of Hydrophobic Motifs and Effects in Lectin Binding of Precision Glycomacromolecules. *Macromol. Biosci.,* **2019**, *19*, 1800425.

(39)   Wojcik, F.; O'Brien, A.G.; Götze, S.; Seeberger, P.H.; Hartmann, L. Synthesis of Carbohydrate-Functionalised Sequence-Defined Oligo(amidoamine)s by Photochemical Thiol-Ene Coupling in a Continuous Flow Reactor. *Eur. J. Chem.* **2013**, *19*, 3090-3098.

(40)   Ponader, D.; Maffre, P.; Aretz, J.; Pussak, D.; Ninnemann, N.M.; Schmidt, S.; Seeberger, P.H.; Rademacher, C.; Nienhaus, G.U.; Hartmann, L. Carbohydrate-Lectin

Recognition of Sequence-Defined Heteromultivalent Glycooligomers. *J. Am. Chem. Soc.* **2014**, *136*, 2008–2016.

(41)   Hill, S.; Galan, M.C. Fluorescent carbon dots from mono- and polysaccharides: synthesis, properties and applications. *Beilstein J. Org. Chem.* **2017**, *13*, 675–693.

(42)   Handlogten, M.W.; Kiziltepe, T.; Bilgicer, B. Design of a heterotetravalent synthetic allergen that reflects epitope heterogeneity and IgE antibody variability to study mast cell degranulation. *Biochem. J.* **2013**, *449*, 91–99.

(43)   Nagao, M.; Kichize, M.; Hoshino, Y.; Miura, Y. Influence of Monomer Structures for Polymeric Multivalent Ligands: Consideration of the Molecular Mobility of Glycopolymers. *Biomacromolecules* **2021**, *22*, 3119-3127.

(44)   Martyn, B.; Biggs C.I.; Gibson M.I. Comparison of systematically functionalized heterogeneous and homogenous glycopolymers as toxin inhibitors, *Polymer Chemistry* **2018**, *57*, 40-47.

(45)   Cairo, C.W.; Gestwicki, J.E.; Kanai, M.; Kiessling, L.L. Control of Multivalent Interactions by Binding Epitope Density. *J. Am. Chem. Soc.* **2002**, *124*, 1615–1619.

(46)   Chittasupho C. Multivalent ligand: design principle for targeted therapeutic delivery approach. *Ther Deliv.*, **2012**, *3*, 1171–1187.

(47)   Bakshi, A.K.; Haider, T.; Tiwari, R.; Soni, V. Critical parameters for design and development of multivalent nanoconstructs: recent trends. *Drug Deliv. And Transl. Res.*, 2022, **12**, 2335–2358.

(48)   Zacho, R.M.; Jensen, L.; Terp, R.; Jensenius, J.C.; Thiel, S. Studies of the pattern recognition molecule H-ficolin: specificity and purification. *J. Biol. Chem.*, **2012**, *287*, 8071–8081.

(49)   Vázquez-Mendoza, A.; Carrero, J. C.; Rodriguez-Sosa, M. Parasitic infections: a role for C-type lectins receptors. *BioMed research international*, **2013**, *2013*, 456352.

(50)   Hespanhol R.C.; Soeiro M de N.C.; Meuser M.B.; Meirelles M de N.S.L.; Côrte-Real S. The Expression of Mannose Receptors in Skin Fibroblast and Their Involvement in Leishmania (L.) amazonensis Invasion. *J. Histochem. Cytochem.,* **2005**, *53*, 35-44.

(51)   Wamhoff E.C.; Hanske, J.; Schnirich, L.; Aretz, J.; Grube, M.; Varón Silva, D.; Rademacher, C. ^{19}F NMR-Guided Design of Glycomimetic Langerin Ligands. *ACS Chem. Biol.,* **2016**, *11*, 2407-2413.

Supporting Information

Gylcopolymer targeting Langerin expressing cells

Serap Üclü[a‡], Stig Hill Christiansen[‡], Maxime Denis[c], Hengxi Zhang[c], Christoph Rademacher[c], Steffen Thiel[b], Laura Hartmann[a]*

‡ These authors contributed equally

a. Department for Organic Chemistry and Macromolecular Chemistry, Heinrich Heine University Düsseldorf, Universitätsstraße 1, Düsseldorf 40225, Germany. E-mail: laura.hartmann@hhu.de

b. Department of Biomedicine, Aarhus University, The Skou-Building 1115, Hoegh-Guldbergs Gade 10, 8000 Aarhus C, Denmark. E-mail: st@biomed.au.dk

c. Department of Pharmaceutical Sciences, University of Vienna, Josef-Holaubeck-Platz 2, 1090 Vienna, Austria. E-mail: christoph.rademacher@univie.ac.at

1. Instrumentation:

Nuclear Magnetic Resonance spectroscopy (NMR)

^{1}H-NMR (600 and 300 MHz) spectra were mesured on a Bruker AVANCE III – 600. Chemical shifts of all NMR spectra were expressed in parts per million (ppm). For ^{1}H NMR, the residual non-deuterated solvent was used as an internal standard (δ 4.79 ppm for HDO). The resulting multiplications were given as s for singlet, d for doublet, t for triplet, and m for multiplet.

Reversed Phase - High Pressure Liquid Chromatography - Mass Spectrometry (RP-HPLC-MS)

Reversed Phase - High Pressure Liquid Chromatography - Mass Spectrometry (RP-HPLC-MS): Analysis were performed using an Agilent 1260 Infinity instrument equipped with a variable wavelength detector (VWD) (set at 214 nm) and a 6120 quadrupole LC/MS with an electrospray ionization (ESI) source (operated in positive ionization mode in an m/z range of 200 to 2000). A Poroshell 120 EC-C18 (3.0×50 mm, 2.5 μm) RP column from Agilent was used as the HPLC column. Mobile phases A and B were H_2O/ACN (95 Vol %/5 Vol %) and H_2O/ACN (5 Vol %/95 Vol %), respectively. Both mobile phases contained 0.1 % formic acid. The temperature of the column chamber was set at 25 °C. UV and MS spectral analysis was done using Agilent Technologies OpenLab ChemStation software for LC/MS.

Ultra-High Reso–ution - Mass Spectrometry (UHR-MS)

The MS measurements were run with a Bruker UHR-QTOF maXis 4G instriument using a direct inlet vial syringe pump and an ESI source.

Freeze dryer

The glycooligomers were freeze dried by using Alpha 1-4 LD plus instrument from Martin Christ Freeze Dryers GmbH. The Drying method was fixed to -55 °C and 0.1 mbar.

2. Synthesis and characterization

Compound U(Man)-3
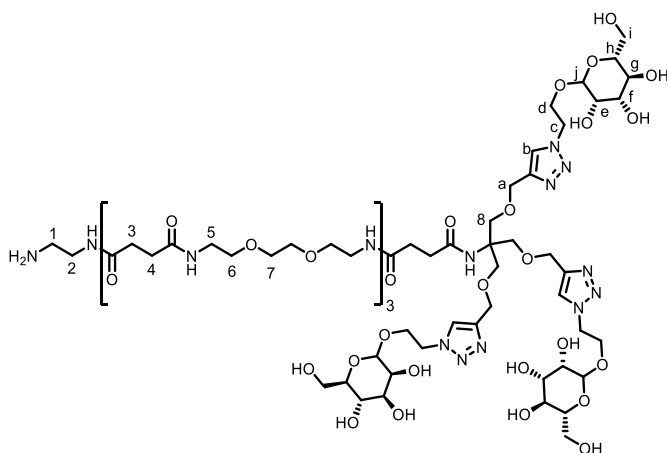
^{1}H NMR (600 MHz, D$_2$O) δ 8.05 (s, 3H), 4.67 (s, 2H), 4.59 (s, 6H), 4.10 (ddd, *J* = 11.0, 7.2, 3.7 Hz, 3H), 3.93 (ddd, *J* = 11.1, 5.6, 3.6 Hz, 3H), 3.86 (dd, *J* = 3.4, 1.7 Hz, 3H), 3.75 – 3.58 (m, 49H), 3.51 (t, *J* = 5.9 Hz, 3H), 3.40 – 3.36 (m, 13H), 3.15 (t, *J* = 5.9 Hz, 3H), 3.07 (ddd, *J* = 9.9, 5.8, 2.4 Hz, 3H), 2.58 – 2.53 (m, 14H), 2.48 (dd, *J* = 18.0, 6.0 Hz, 3H).

HR-MS calculated [M+3H]$^{3+}$ 606.3, found 606.6

RP-HPLC: (5%/95% ACN/H$_2$O→ 5%/50% ACN/H$_2$O in 30 min at 25°C, 214 nm): t$_R$ = 8.47 min.
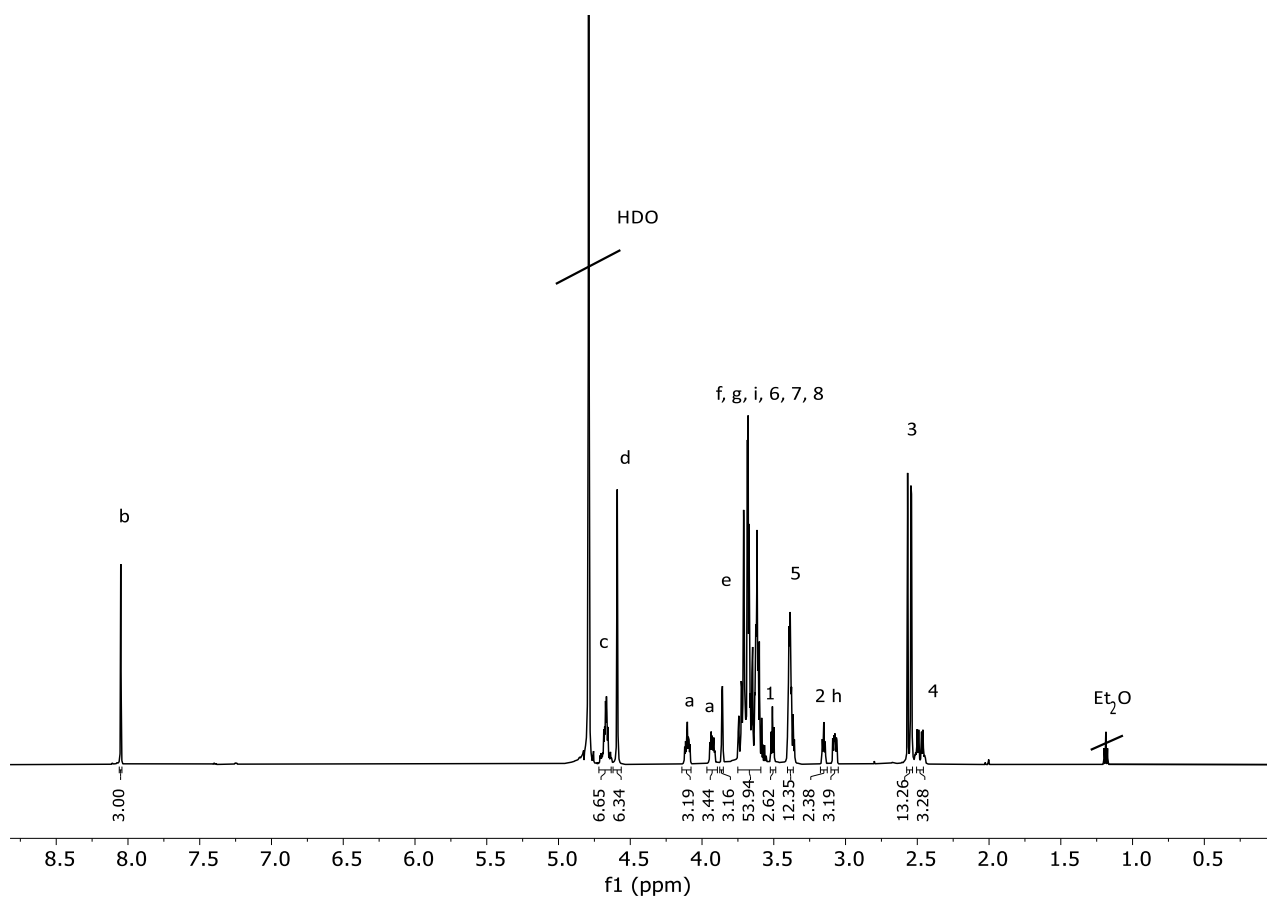
*Figure S26: ¹H-NMR (600 MHz) spectra of **compound U(Man)-3** in HDO.*
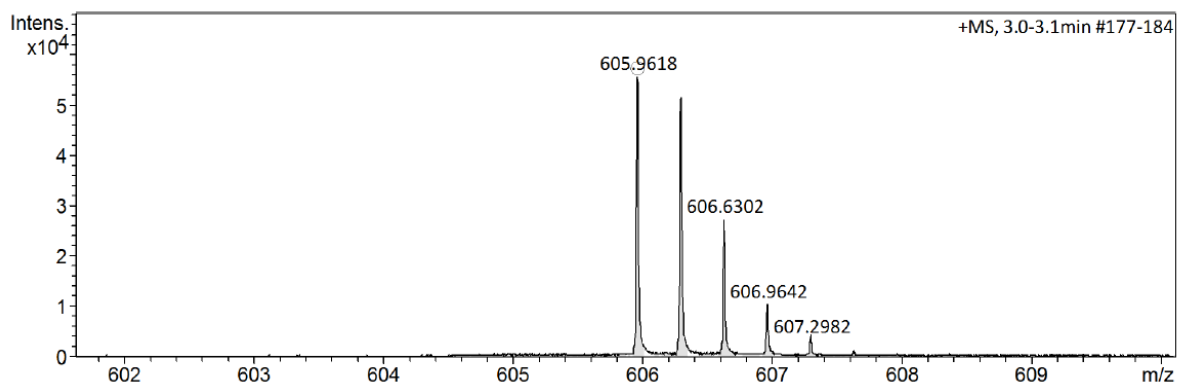
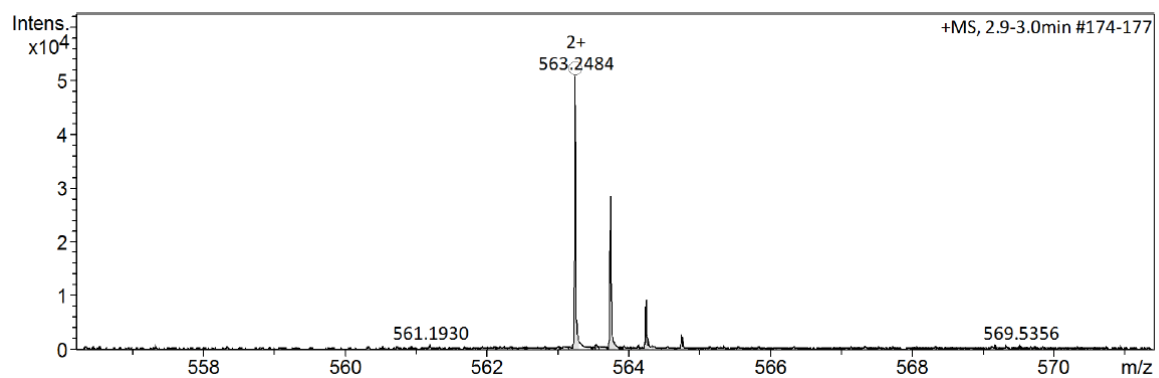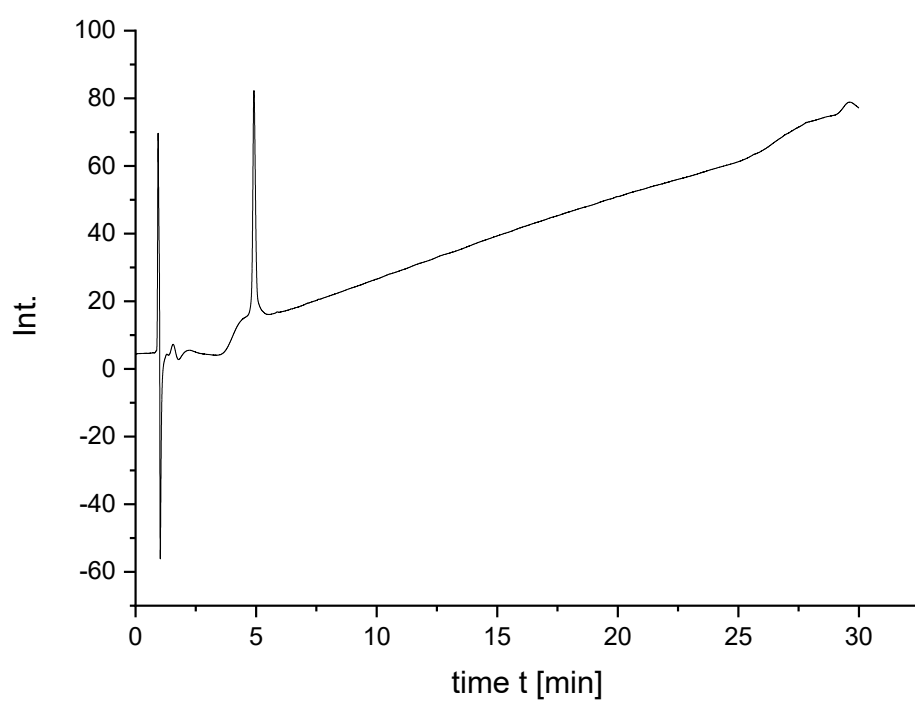*Figure S27: HR-MS of **compound U(Man)-3**.*
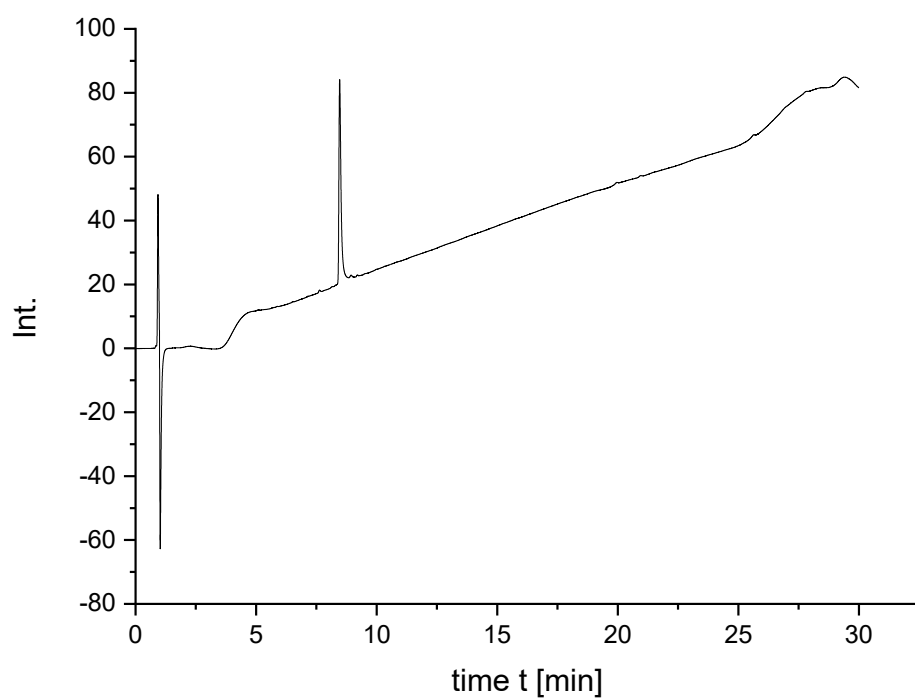
*Figure S28: RP-HPLC of **compound E3TT**.*

Compound U(Man)-0
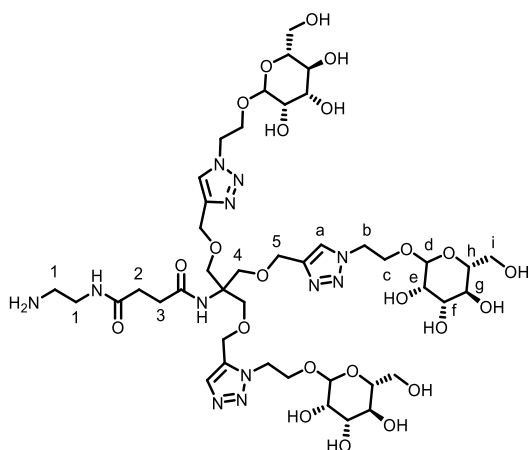
^{1}H NMR (600 MHz, D$_2$O) δ 8.06 (s, 3H), 4.78 (d, J = 1.5 Hz, 3H), 4.66 (td, J = 6.5, 5.9, 3.8 Hz, 5H), 4.58 (s, 6H), 4.09 (ddd, J = 11.1, 7.7, 3.7 Hz, 3H), 3.94 − 3.88 (m, 3H), 3.84 (dt, J = 3.3, 1.5 Hz, 3H), 3.73 − 3.62 (m, 26H), 3.58 (t, J = 9.7 Hz, 3H), 3.48 (t, J = 5.9 Hz, 2H), 3.13 (t, J = 6.0 Hz, 2H), 3.06 (ddd, J = 9.8, 5.7, 2.4 Hz, 3H), 2.49 (dt, J = 17.1, 4.7 Hz, 5H).

HR-MS calculated [M+2H]$^{2+}$ 563.3, found 563.5.

RP-HPLC: (5%/95% ACN/H$_2$O→ 5%/50% ACN/H$_2$O in 30 min at 25°C, 214 nm): t_R = 4.91 min.
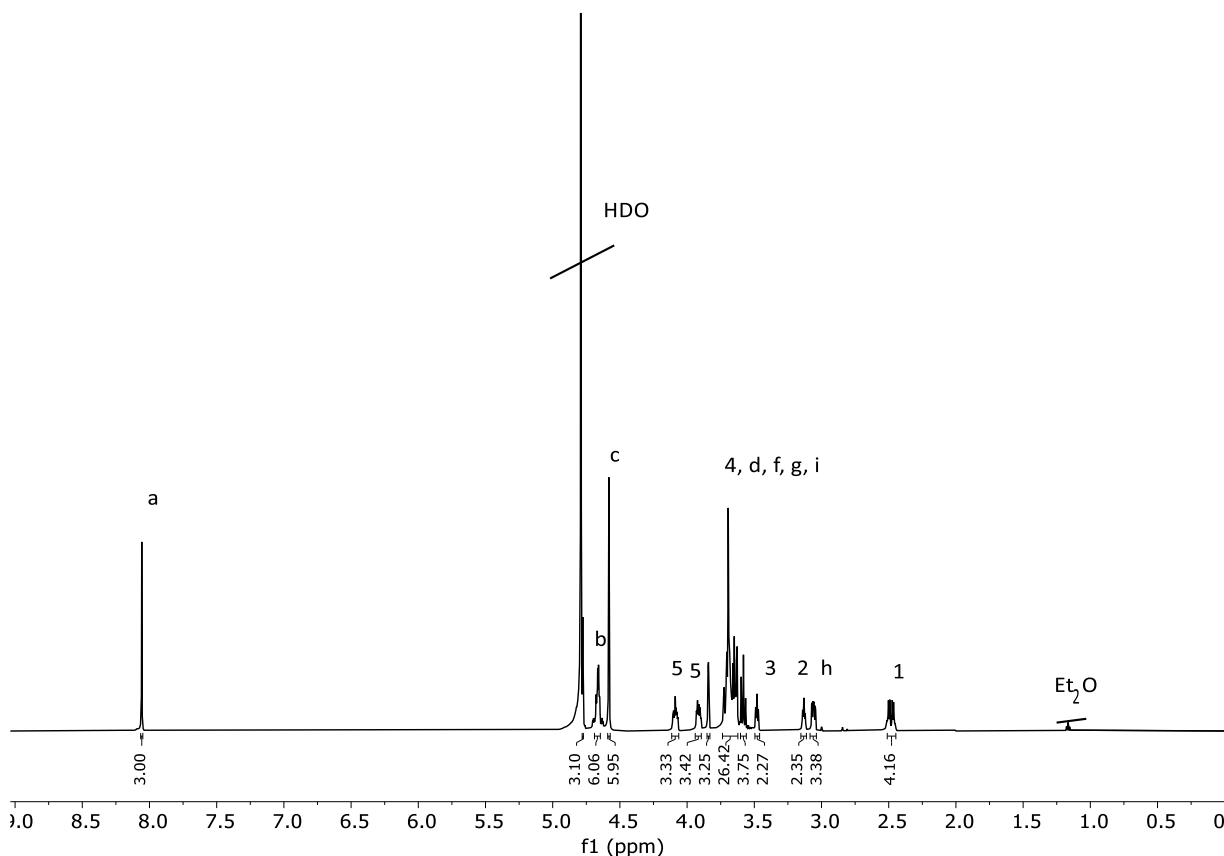
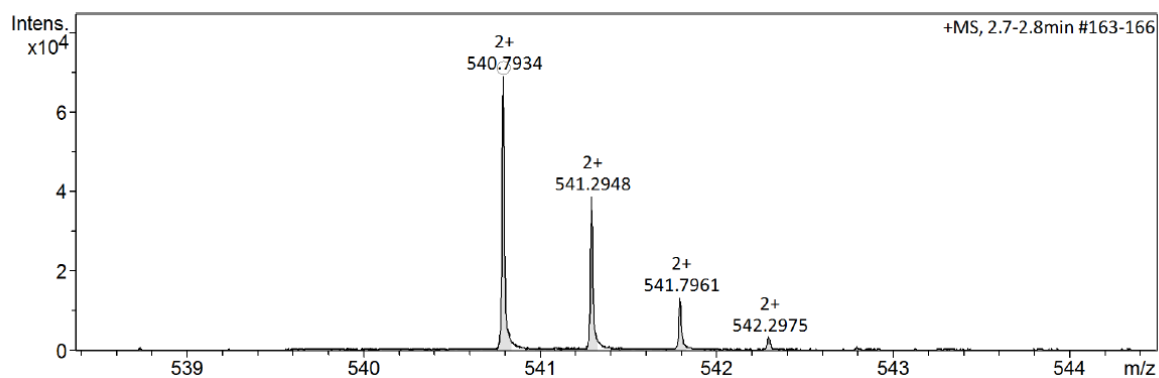*Figure S29: ^{1}H-NMR (600 MHz) spectra of **compound U(Man)-0** in HDO.*

*Figure S30: HR-MS of **compound U(Man)-0**.*

*Figure S31: RP-HPLC of **compound U(Man)-0**.*

Compound L(Man)-3
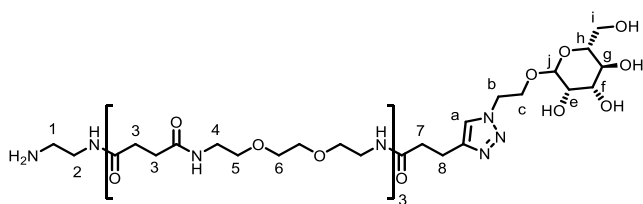
^{1}H NMR (600 MHz, D$_2$O) δ 7.89 (d, *J* = 1.5 Hz, 1H), 4.70 − 4.58 (m, 2H), 4.09 (ddd, *J* = 11.0, 7.1, 4.0 Hz, 1H), 3.96 − 3.91 (m, 1H), 3.86 (dd, *J* = 3.3, 1.8 Hz, 1H), 3.76 − 3.54 (m, 28H), 3.51 (t, *J* = 5.9 Hz, 2H), 3.38 (ddd, *J* = 11.9, 7.2, 4.5 Hz, 12H), 3.15 (t, *J* = 5.9 Hz, 2H), 3.03 (t, *J* = 7.3 Hz, 3H), 2.64 (t, *J* = 7.3 Hz, 2H), 2.58 − 2.50 (m, 11H).

HR-MS calculated [M+H]$^+$ 1080.6, found 1080,6; [M+2H]$^{2+}$ 540,8, found 540.8; [M+3H]$^{3+}$ 360,9, found 361.0.

RP-HPLC: (5%/95% ACN/H$_2$O→ 5%/50% ACN/H$_2$O in 30 min at 25°C, 214 nm): t$_R$ = 7.82 min
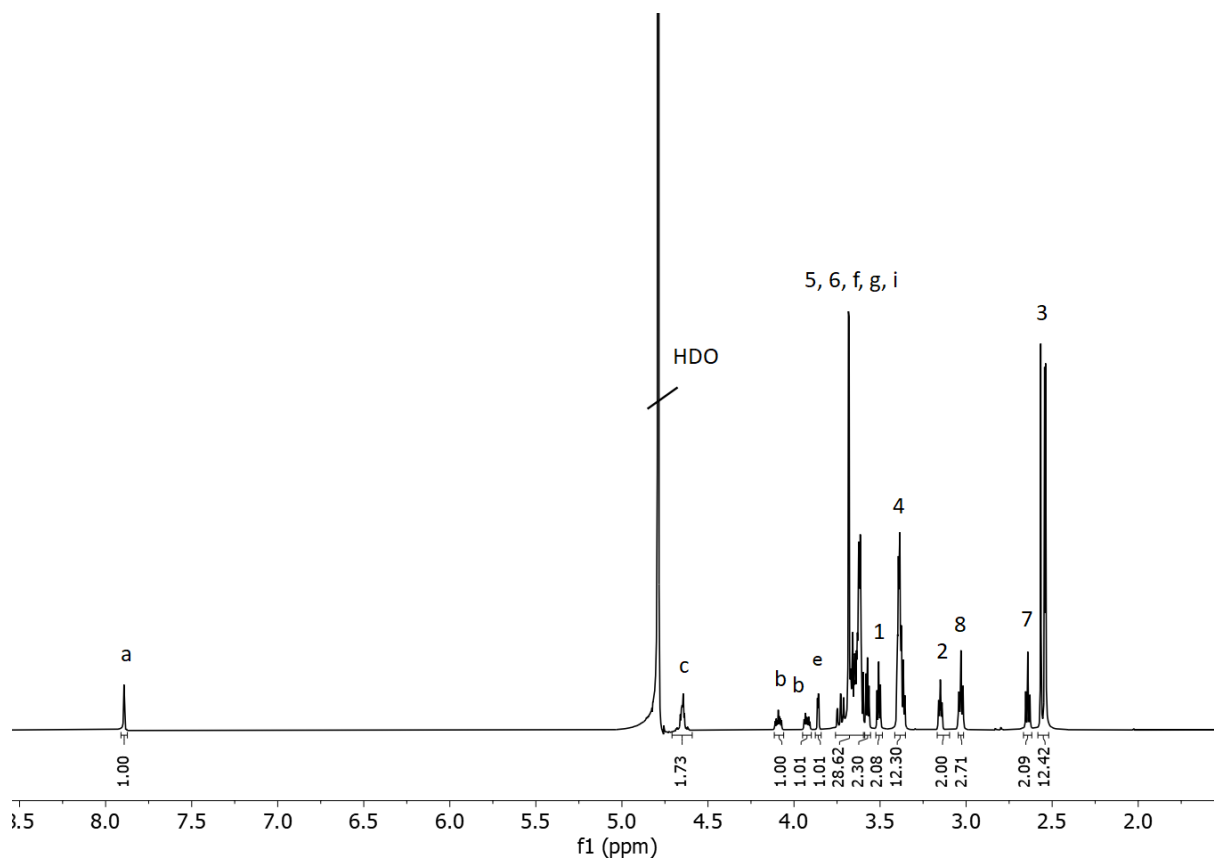
*Figure S32: ^{1}H-NMR (600 MHz) spectra of **compound L(Man)-3** in HDO.*
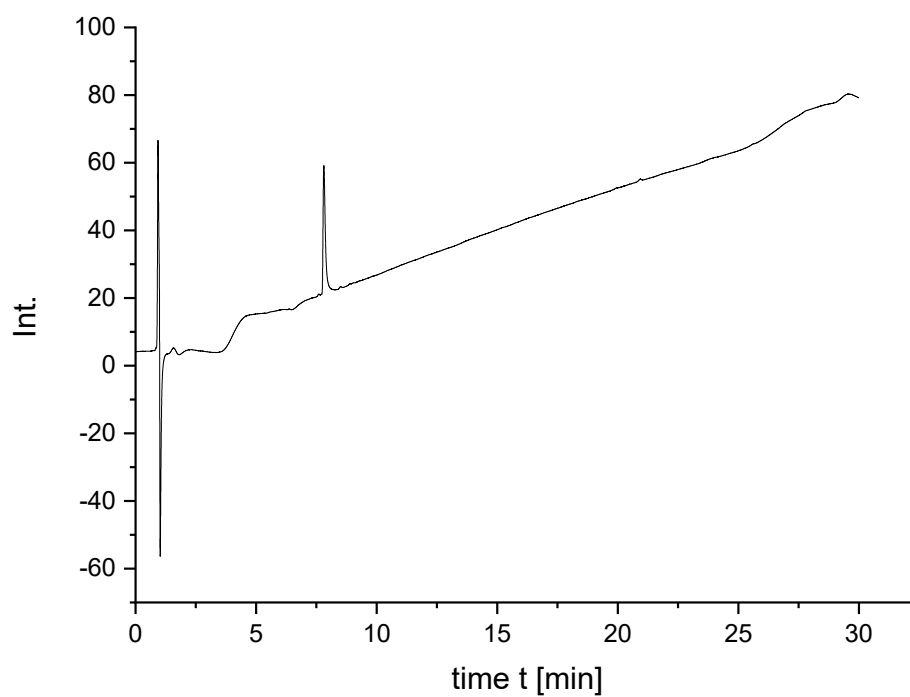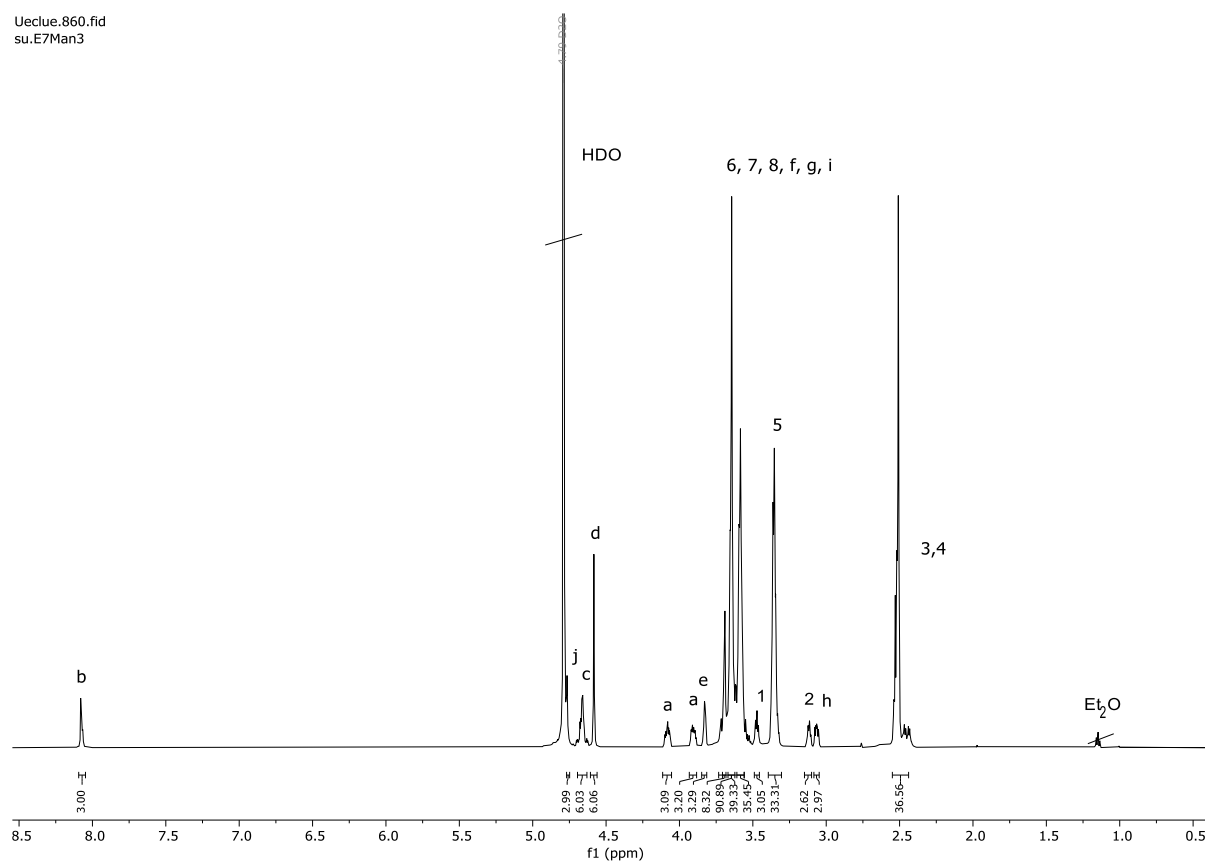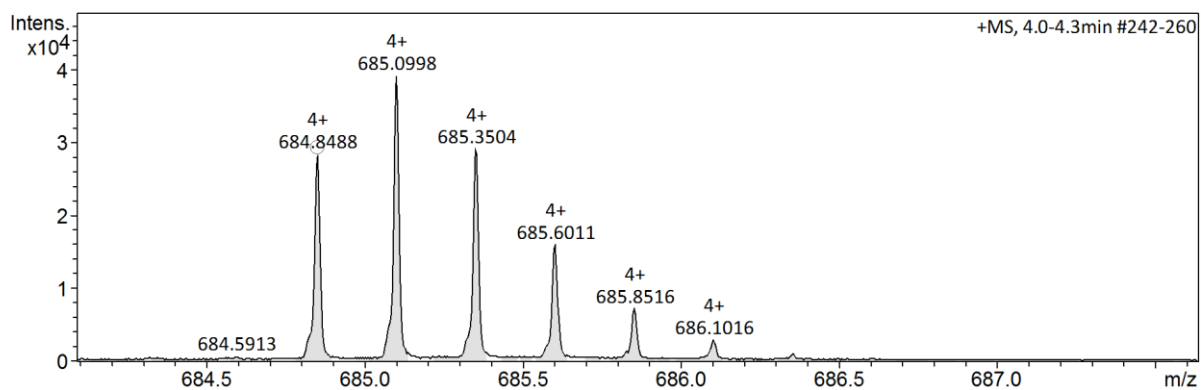
*Figure S33: HR-MS of **compound L(Man)-3**.*

*Figure S34: RP-HPLC of **compound L(Man)-0**.*

Compound U(Man)-7

^{1}H NMR (600 MHz, D$_2$O) δ 8.08 (d, J = 3.2 Hz, 3H), 4.76 (d, J = 1.7 Hz, 3H), 4.66 (td, J = 6.5, 5.9, 3.6 Hz, 6H), 4.58 (s, 6H), 4.08 (ddt, J = 10.7, 6.9, 3.4 Hz, 3H), 3.90 (ddd, J = 11.1, 5.7, 3.7 Hz, 3H), 3.83 (ddd, J = 5.2, 3.3, 1.8 Hz, 3H), 3.74 − 3.56 (m, 91H), 3.48 (q, J = 6.1, 4.7 Hz, 3H), 3.36 (q, J = 5.4 Hz, 36H), 3.12 (q, J = 6.0 Hz, 3H), 3.06 (ddd, J = 9.7, 5.8, 2.3 Hz, 3H), 2.56 − 2.45 (m, 36H).

HR-MS calculated [M+4H]$^{4+}$ 684,99, found 685,1.

RP-HPLC: (5%/95% ACN/H$_2$O→ 5%/50% ACN/H$_2$O in 30 min at 25°C, 214 nm): t_R = 6.75 min.

*Figure S35: ¹H-NMR (600 MHz) spectra of **compound U(Man)-7** in HDO.*

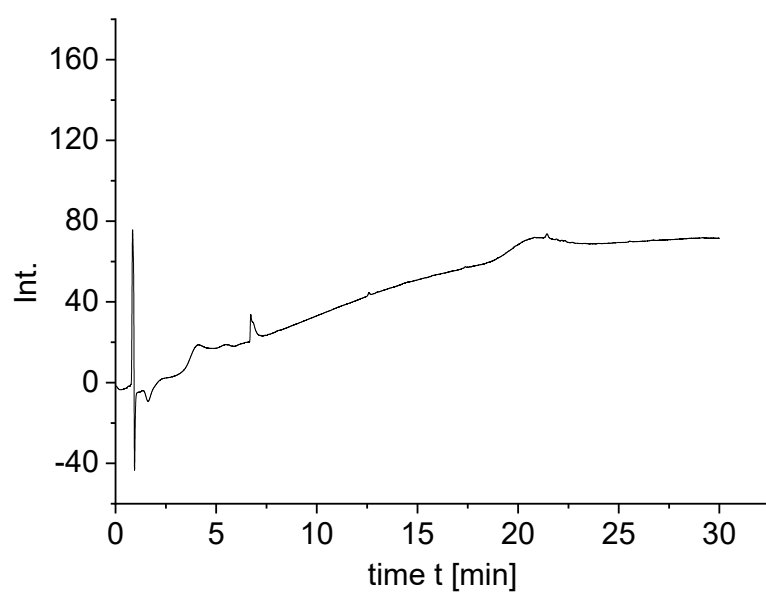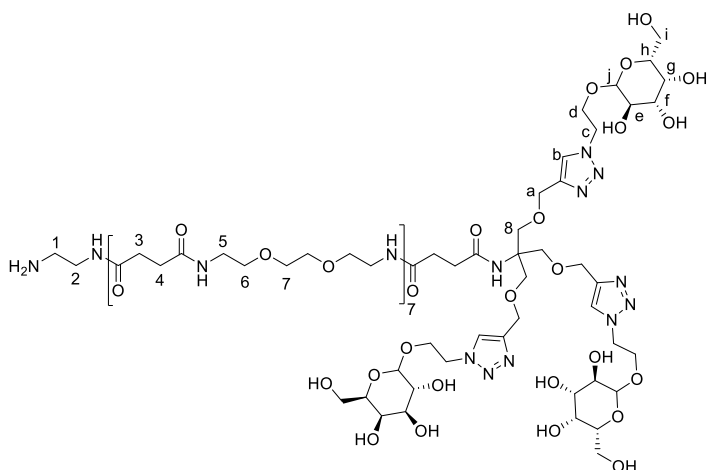

*Figure S36: HR -MS of **compound U(Man)-7**.*

*Figure S37: RP-HPLC of **compound U(Man)-7.***

Compound U(Gal)-7

^{1}H NMR (600 MHz, D$_2$O) δ 8.09 (d, J = 1.4 Hz, 3H), 4.68 (t, J = 5.2 Hz, 6H), 4.59 (s, 6H), 4.37 (d, J = 7.9 Hz, 3H), 4.30 (dt, J = 11.6, 4.6 Hz, 3H), 4.14 – 4.08 (m, 3H), 3.90 (dd, J = 3.5, 1.0 Hz, 3H), 3.53 – 3.47 (m, 6H), 3.42 – 3.31 (m, 33H), 3.15 (t, J = 6.0 Hz, 2H), 2.59 – 2.41 (m, 37H).

HR-MS calculated [M+4H]$^{4+}$ 684,99, found 685,1.

RP-HPLC: (5%/95% ACN/H$_2$O→ 5%/50% ACN/H$_2$O in 30 min at 25°C, 214 nm): t_R = 6.75 min.
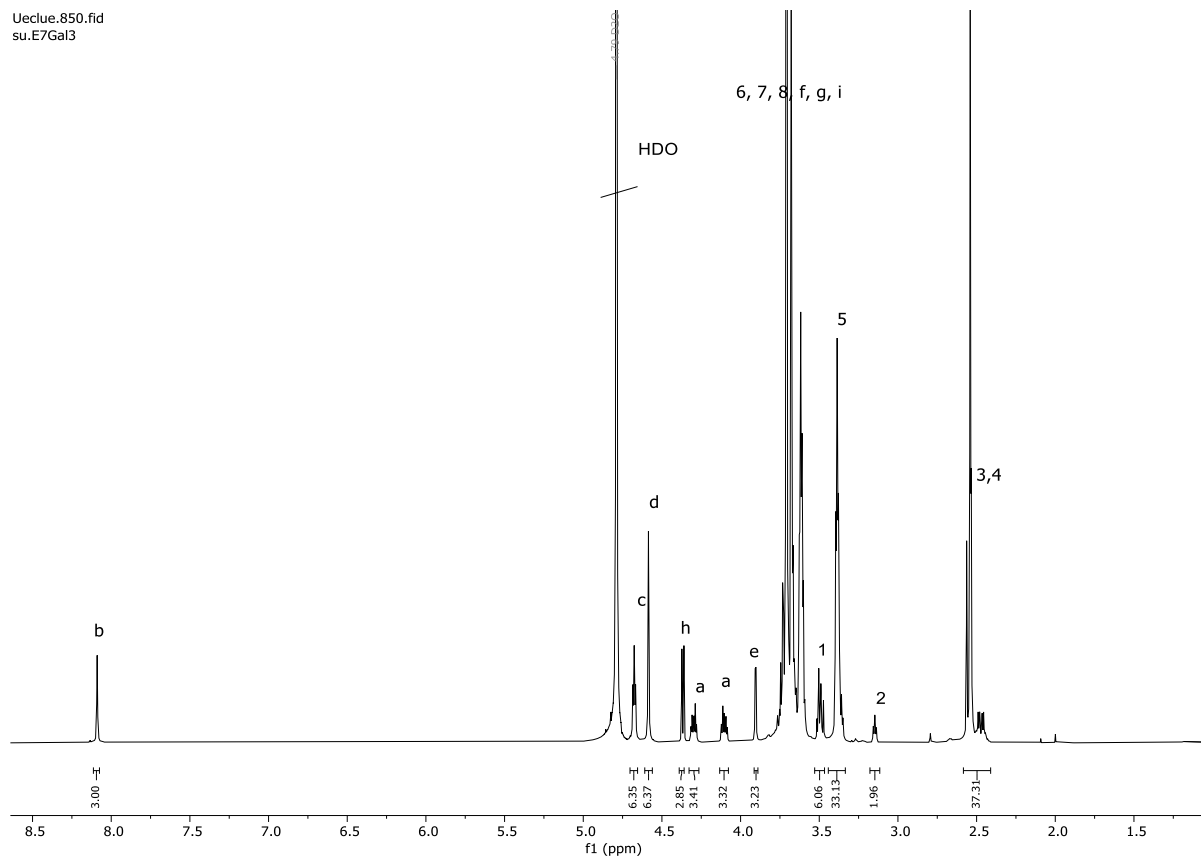
*Figure S38: 600 MHz ^{1}H-NMR spectrum of **compound U(Gal)-7** in D$_2$O at 25°C.*
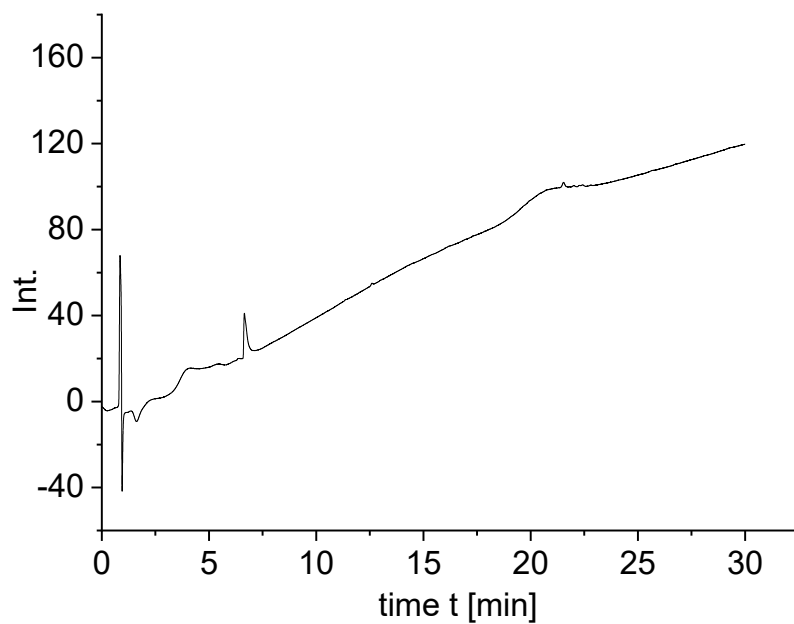

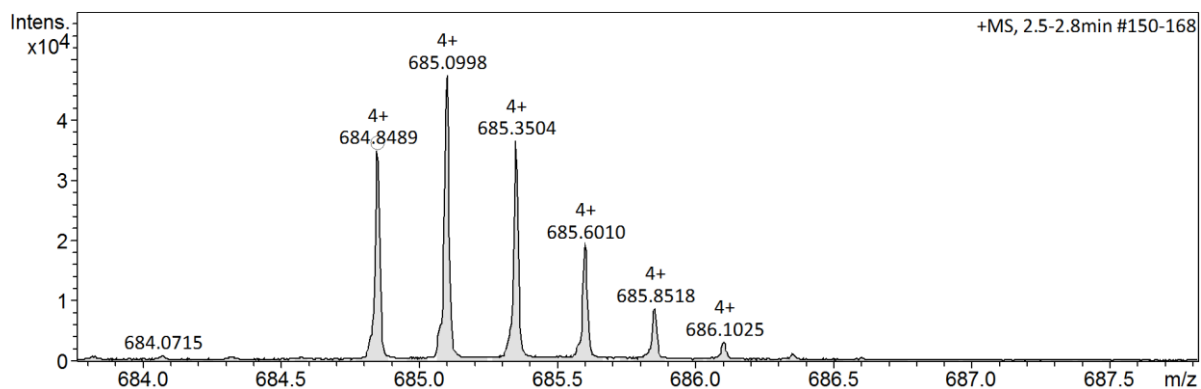*Figure S39: RP-HPLC of **compound U(Gal)-7.***

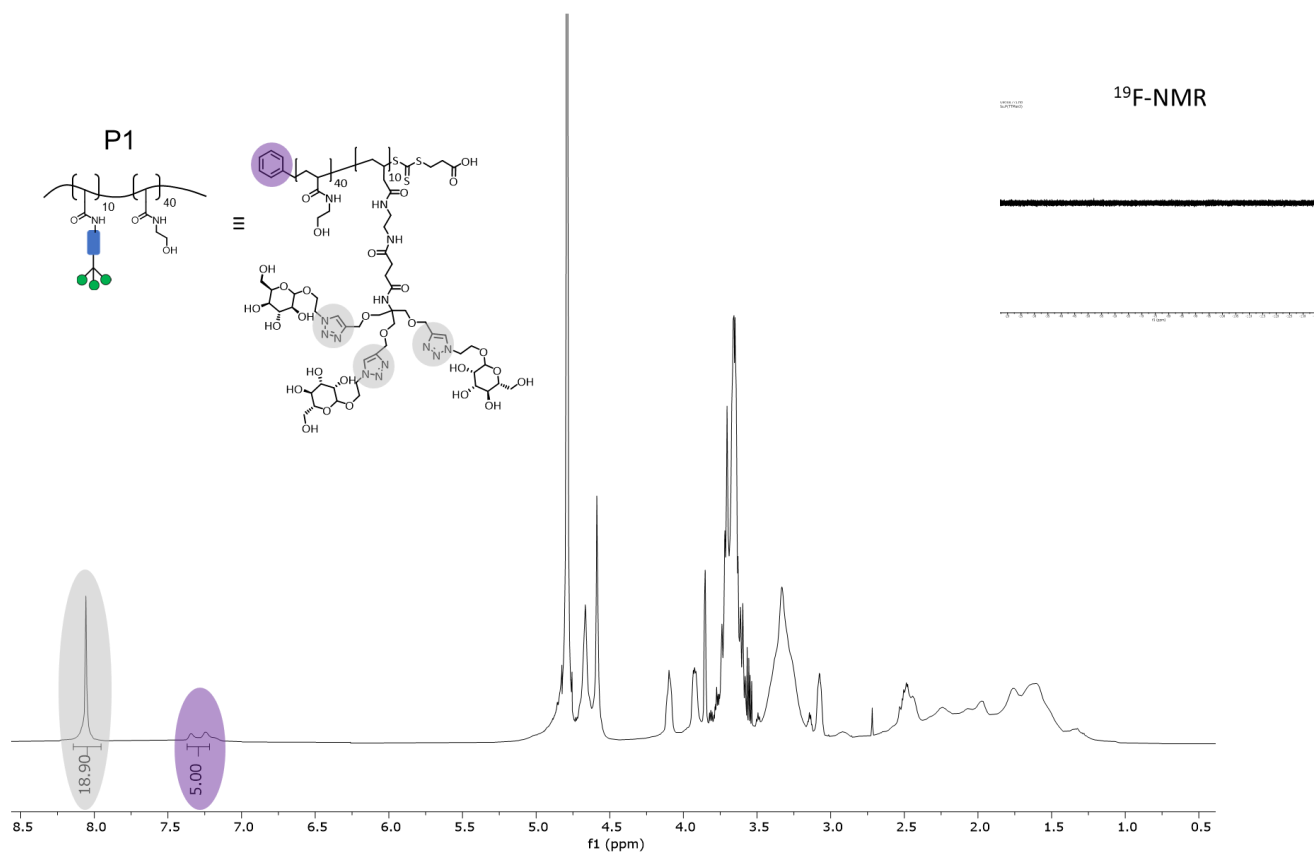*Figure S40: HR-ESI-MS of **compound U(Gal)-7.***

*Figure S 41: 600 MHz ^{1}H-NMR spectrum of **compound P1** in D$_2$O at 25°C. The ratio of the protons of the triazole (grey) to the protons of the benzene (purple) shows a degree of functionalization of 20%. The ^{19}F-NMR spectrum confirms the complete conversion of the pentafluoro groups by the glycooligomer and ethanolamine.*

*Figure S42: 600 MHz ^{1}H-NMR spectrum of **compound P2** in D$_2$O at 25°C. The ratio of the protons of the triazole (grey) to the protons of the benzene (purple) shows a degree of functionalization of 20%. The ^{19}F-NMR spectrum confirms the complete conversion of the pentafluoro groups by the glycooligomer and ethanolamine.*
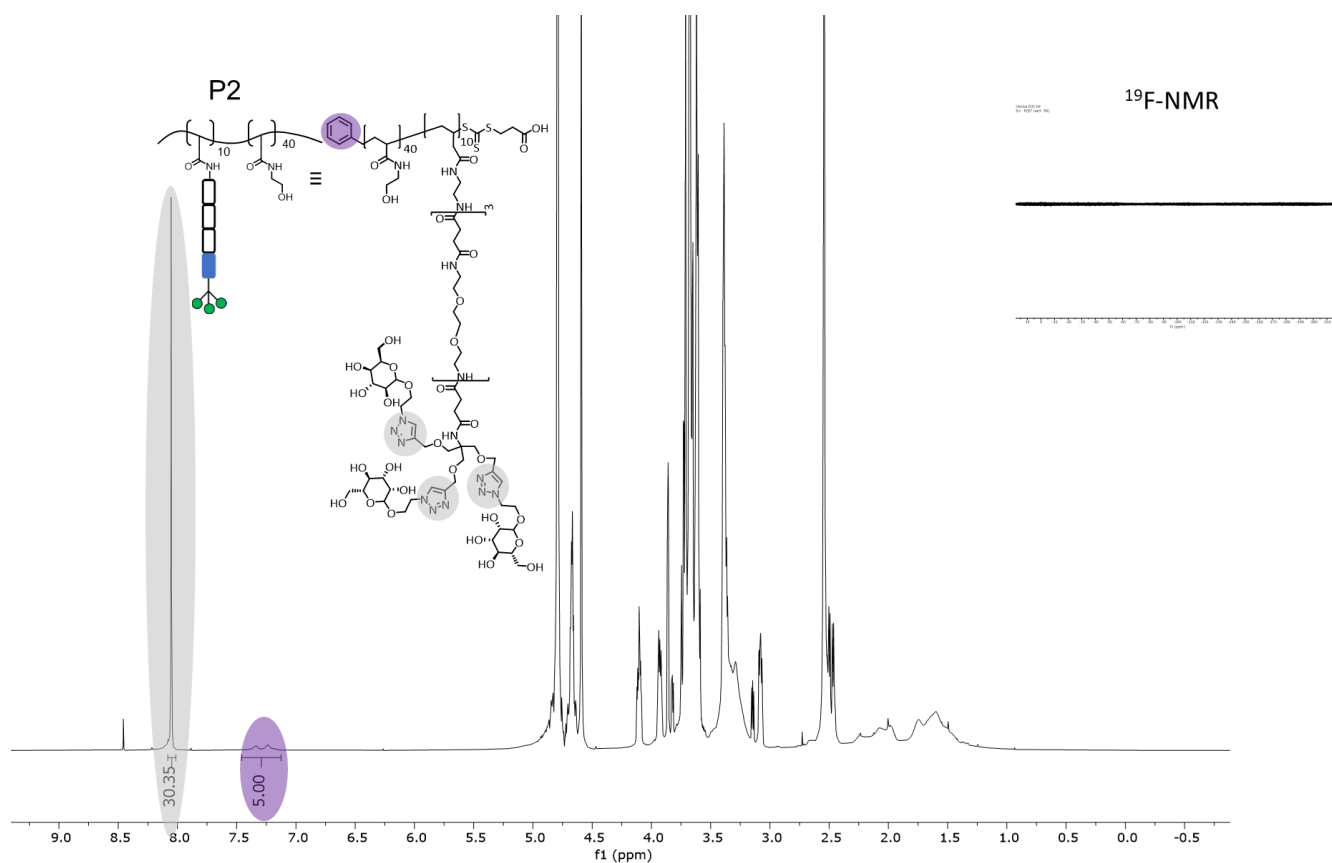
*Figure S43: 600 MHz ^{1}H-NMR spectrum of **compound P3** in D$_2$O at 25°C. The ratio of the protons of the triazole (grey) to the protons of the benzene (purple) shows a degree of functionalization of 34%. The ^{19}F-NMR spectrum confirms the complete conversion of the pentafluoro groups by the glycooligomer and ethanolamine.*
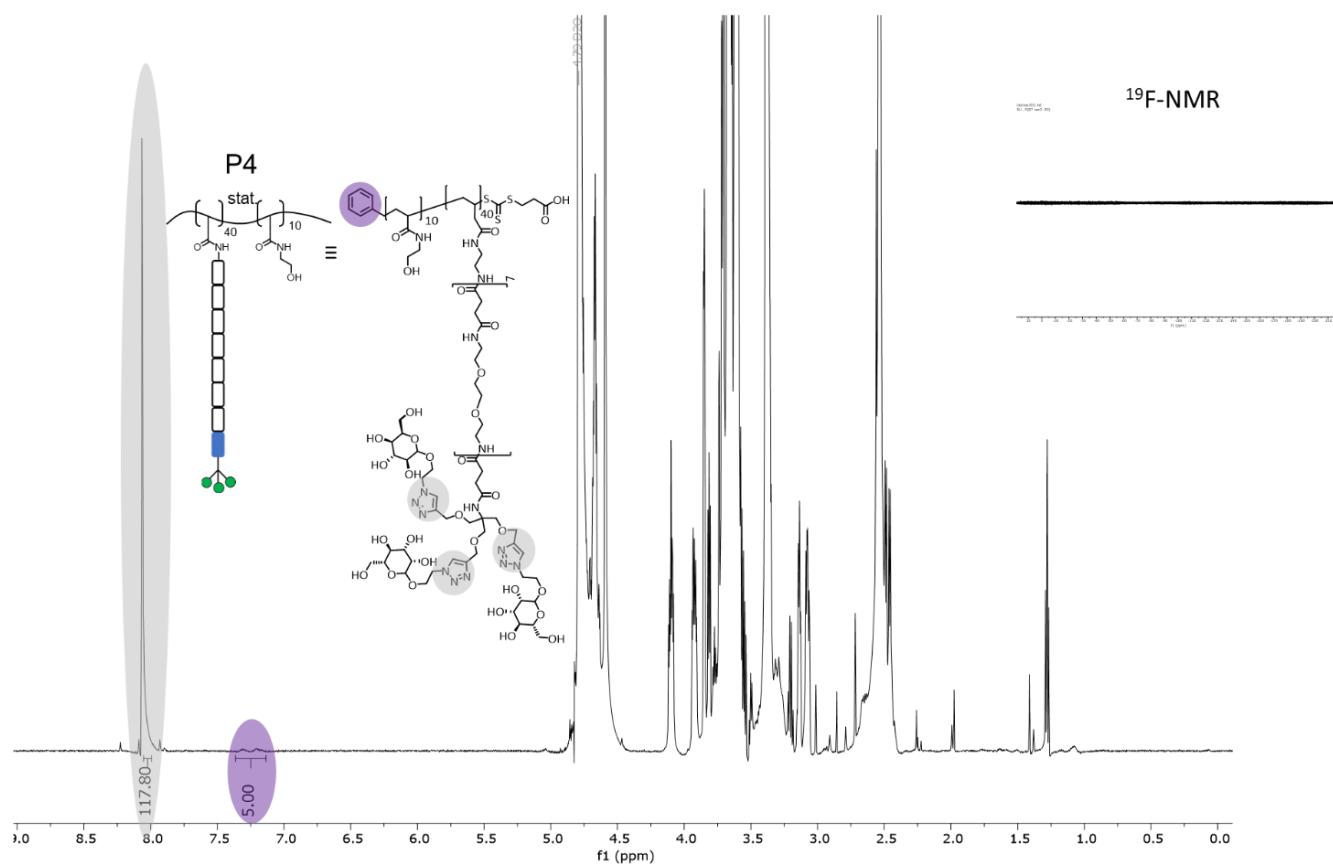
*Figure S 44: 600 MHz ^{1}H-NMR spectrum of **compound P4** in D$_2$O at 25°C. The ratio of the protons of the triazole (grey) to the protons of the benzene (purple) shows a degree of functionalization of 80%. The ^{19}F-NMR spectrum confirms the complete conversion of the pentafluoro groups by the glycooligomer and ethanolamine.*
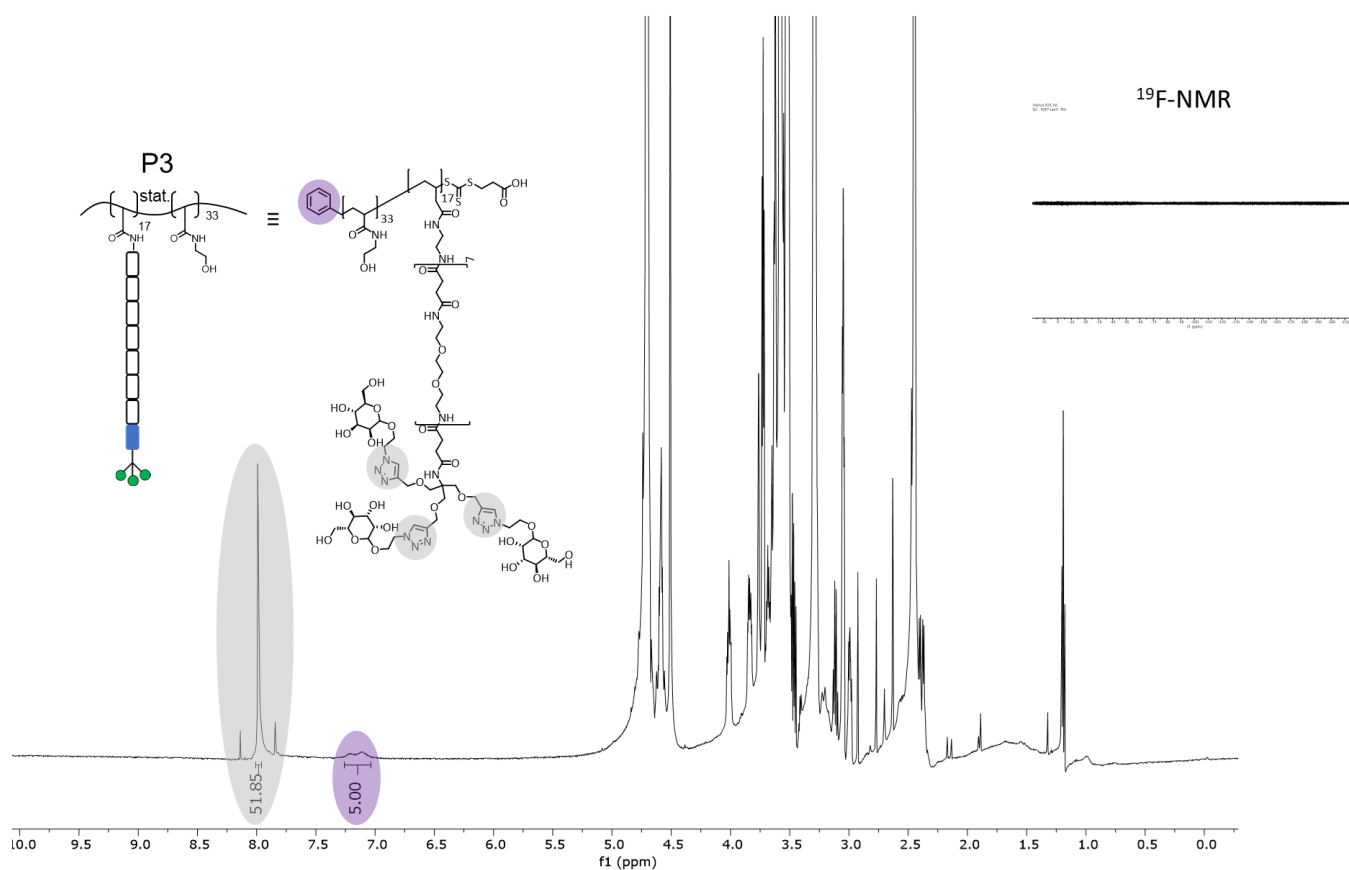
*Figure S 45: 600 MHz ^{1}H-NMR spectrum of **compound P6** in D$_2$O at 25°C. The ratio of the protons of the triazole (grey) to the protons of the benzene (purple) shows a degree of functionalization of 17%. The ^{19}F-NMR spectrum confirms the complete conversion of the pentafluoro groups by the glycooligomer and ethanolamine.*
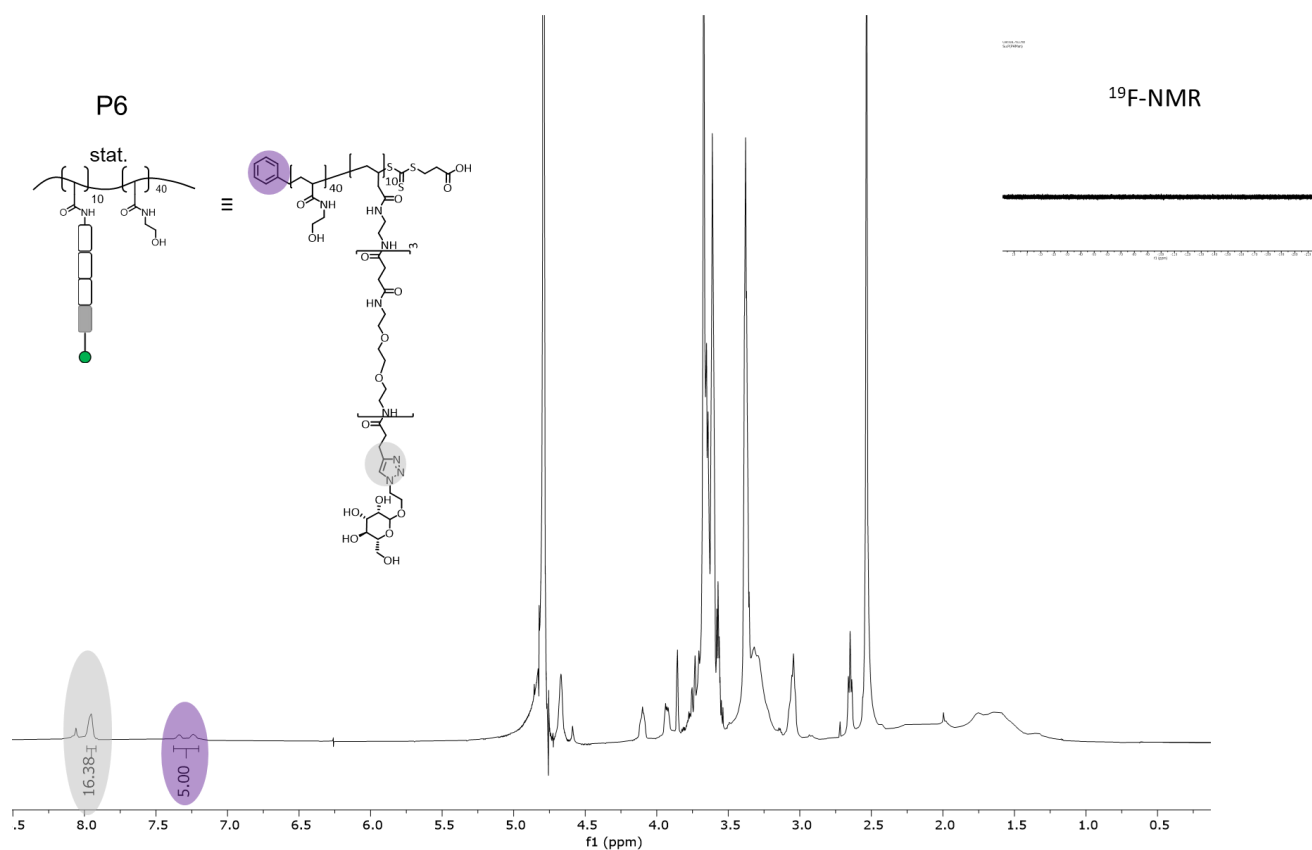
4.4 Sweet Janus Particles: glyco-functionalized janus particles for the binding and inhibition of *E. coli*

Serap Üclü, Claudia Marschelke, Markus Geisler, Dimitri Wilms, Thorben Koehler, Miriam Bäumers, Stephan Schmidt, Alla Synytska and Laura Hartmann

Publication Draft

Own Contribution:

Collaborative project design. Synthesis and purification of building block for solid phase polymer synthesis. Measurement and evaluation of all LC-MS experiments of the glycooligomer and evaluation of all NMR and UHR spectra of glycooligomer. Conjugation of the glycooligomer to the particles and performance and evaluation of the phenol-sulfuric acid assay as well as the DLS assay regarding the carbohydrate loading. Design and performance of Inhibition-Competition Assay of the glycooligomer towards ConA via SPR as well as evaluation and interpretation of the K_D value. Collaborative performance of binding and inhibition studies of glycofunctionalized particles towards ConA and *E. coli*. Collaborative writing of the first publication draft.

Sweet Janus Particles: glyco-functionalized janus particles for the binding and inhibition of *E. coli*

Serap Üclü[a], Claudia Marschelke[b,#], Markus Geisler[a,#], Dimitri Wilms[a], Thorben Koehler[a], Miriam Bäumers[c], Stephan Schmidt[a], Alla Synytska[b*] and Laura Hartmann[a,d,*]

a. Department for Organic Chemistry and Macromolecular Chemistry, Heinrich Heine University Düsseldorf, Universitätsstraße 1, Düsseldorf 40225, Germany. E-mail: laura.hartmann@hhu.de

b. Leibniz Institute of Polymer Research Dresden, University of Bayreuth, Research Group Functional Polymer Interfaces, Ludwig-Thoma Str. 36a, 95447 Bayreuth, Germany

c. Center of Advanced Imaging, Heinrich-Heine-Universität Düsseldorf, Universitätstr. 1, 40225 Düsseldorf, Germany

d. Institute for Macromolecular Chemistry, University Freiburg, Stefan-Meier-Str. 31, 79104 Freiburg i.Br., Germany

[#] These authors contributed equally

[*] Corresponding author: laura.hartmann@makro.uni-freiburg.de

Abstract

E. coli and other bacteria use adhesion receptors such as FimH to attach to carbohydrates on the cell surface as a first step of colonization and infection. Efficient inhibitors blocking these interactions for infection treatment are multivalent carbohydrate-functionalized scaffolds. However, these multivalent systems often lead to the formation of large clusters of bacteria, which may pose problems for clearing the bacteria from the infected site. Here we present Man-containing Janus particles (JPs) decorated on one side with glycomacromolecules to address Man-specific adhesion receptors of *E. coli.* On the other side, PNIPAM is attached to the particle hemisphere, providing temperature dependent sterical shielding against binding and cluster formation. While homogeneously functionalized particles cluster with multiple bacteria to form large aggregates, glycofunctionalized JPs are able to form aggregates only with individual bacteria. The formation of large aggregates from the JP decorated single bacteria can still be induced in a second step by raising the temperature and making use of the collapse of the PNIPAM hemisphere. This is the first time that carbohydrate-functionalized JPs are derived and used as inhibitors of bacterial adhesion. Furthermore, the developed JPs offer well-controlled single bacteria inhibition in combination with cluster formation upon an external stimulus, which is not achievable with conventional carbohydrate-functionalized particles.

Introduction

Bacterial infections are a major cause of mortality and morbidity worldwide.[1] The excessive and incorrect use of antibiotics leads to microbial resistance, making medical treatment more difficult.[2] Thus, it is becoming increasingly important to develop new antimicrobial agents that can withstand the range of bacterial resistance mechanisms.[3-5] So-called anti-adhesion therapy as a potential alternative to antibiotic therapy addresses one of the first steps of the infection process, where bacteria and other pathogens make use of carbohydrate-mediated adhesion onto the cell surface or tissue.[6] Inhibiting this adhesion by competitive binders blocking the bacterial adhesion receptors can thus prevent the infection.[7] A well-studied example of bacterial attachment to glycosylated cell surfaces is Escherichia coli (*E. coli*). *E. coli* make use of the mannose (Man)-specific adhesion receptor FimH at the tip of their fimbriae.[8]

It has been shown for a variety of Man based natural as well as synthetic carbohydrates, glycoconjugates and glycofunctionalized materials that they can be used as inhibitors of the FimH receptor, reduce the adhesion of the pathogen and thus the infection.[9-15] Furthermore, glycofunctionalized materials such as glycoparticles can capture bacteria, e.g., in water purification or to detect biological contaminants.[16] The ability to actively release the bacteria from the glycoparticles further enables material recovery and reuse.[16,23] Glycoparticle-bacteria interaction typically lead to the formation of large aggregates formed by multiple bacteria and particles, which in a filtration set-up supports an easier separation. However, in anti-adhesion therapy, large bacteria clusters are more likely to withstand clearance by the immune system from the infected site. Alternatively, glycoparticles that would allow the formation of individual bacteria-particle aggregates could be developed. Here, we will explore so-called Janus particles (JPs) to interact only at one hemisphere with the bacteria, leaving the other side for steric stabilization and specifically form single bacteria-particle aggregates and prevent formation of larger clusters (Figure 1).

In general, JPs have been successfully used in various applications where they provide important advantages over conventional particles with homogenous surfaces.[17] Their characteristics include, for example, a high surface-to-volume ratio or high interfacial activity. Combinations with reactive polymers also lead to the control of interfacial activity by external influences such as temperature, light, pH or ionic strength and to the achievement of an alternation between stable emulsions and macrophase separation.[18] Furthermore, they can be used as carrier materials for immobilized catalytically active substances, leading to improved charge separation and transfer properties and tunable multiple functionalities in one particle, which can be used for recovery or recycling. Alternatively, JPs can retain their site-selective binding to substrates, leaving another functionality active for further reactions.[19] These advantages make JPs also highly relevant for biotechnological applications such as (bio-)sensing,[17,18] (bio-)catalysis[19], coatings with controlled bio-fouling[20] and icing/de-icing[21] or optoelectronic applications.[22] However, to the best of our knowledge, so far no glycofunctionalized JPs (glyco-JPs) for specific binding to carbohydrate receptors, here bacterial adhesins, have been developed.

In this study, JPs are developed that allow for the combination of Man-containing glycomacromolecules on one hemisphere and a poly(N-isopropylacrylamide) (PNIPAM) layer

on the opposite side to obtain so-called glyco-JPs. We expect the carbohydrate layer to provide bacterial adhesion through the interaction with surface lectins and the thermoresponsive PNIPAM hemisphere to provide steric shielding and prevent adhesion of multiple bacteria and bridging with other particles (Figure 1). Interestingly, choosing PNIPAM as sterical shield will allow us to investigate the formation of larger aggregates as induced by heating above the lower critical solution temperature (LCST) where PNIPAM chains will collapse and should lead to particle-particle aggregation [23-25].

Experimental section

Man-glycooligomer synthesis: The Man-glycooligomer was synthesized by stepwise coupling of tailor-made building blocks and amino acids on a solid support following general solid phase polymer protocols as presented previously.[28-30] The reactions were carried out in 10 ml polypropylene syringe reactors with a polyethylene frit and a Luer stopper from Multisynthech GmbH. A Fmoc Gly TentaGel® R Trt resin (pre-functionalized) with a loading of 0.21 mmol g^{-1} was used as a solid phase and the batch size was 0,1 mmol. As functional building blocks, a triple alkyne functionalized linker (TT linker),a single alkyne functionalized building block TDS (1-(Fluorenyl)-3,11-dioxo-7-(pent-4-ynoyl)-2-oxa-4,7,10-triazatetradecan-14-oic acid) for coupling and (1-(9H-Fluoren-9-yl)-3,14-dioxo-2,7,10-trioxa-4,13-diazaheptadecan-17-oic acid) EDS as spacer building block were used to build up the backbone of the glycooligomer.

The synthesis was started by swelling the resin twice for 15 min in DCM followed by washing with DMF. For Fmoc deprotection after each building block coupling, the resin was shaken with a solution of 25 vol% piperidine in DMF for 15 min and then washed three times with DMF. This was followed by shaking again with the piperidine solution for 15 min and washing ten times with DMF. Coupling of TDS, EDS and TT-Linker was performed by shaking for 60 min with a solution of 5 eq of building block, 5 eq of PyBOP, and 10 eq of DIPEA in DMF, followed by washing ten times with DMF.

For Man-coupling via copper(I)-catalyzed alkyne-azide cycloaddition (CuAAC), 2.5 eq of (2-azidoethyl)-2,3,4,6-*tetra*-O-acetyl-α-D-mannopyranoside 36 per alkyne was dissolved in DMF, 30 mol% of sodium ascorbate and 30 mol% of copper sulfate per alkyne was dissolved in

water. The copper sulfate solution was drawn up first, then the Man-solution, and finally the sodium ascorbate solution. The reactor syringe was covered with aluminum foil and shaken overnight. The resin was then repeatedly washed until the wash solution was colorless: three times with a 23 mM solution of sodium diethyldithiocarbamate in DMF/H2O (1:1, v/v), three times with DMF, and three times with DCM. Next, the mannopyranoside was deprotected and the glycooligomer was cleaved from the resin in a solution of 0.05 mol NaOH in MeOH for 60 min. Afterwards the solution was added to cold diethyl ether and the white precipitate was centrifuged off. The solid was then dissolved in water and the product was isolated by freeze-drying. The chemical characterization (NMR, RP-HPLC, MS) is shown in the supporting information (Figures S10 and S12).

Surface Plasmon Resonance (SPR): ConA was immobilized on the CM5 sensor chip surface on flow cell 1 and 2 via carbodiimide chemistry by the wizard template for immobilization. Therefore, a 3.88 mg ml^{-1} solution of ConA in 10 mM acetate buffer (pH 4.5, GE Healthcare) was diluted in acetat buffer to get a final protein concentration of 50 µg ml^{-1}. For flow cell 2 an immobilization level of 2742.1 RU was reached. The flow cell 1 was blocked by a solution of ethanolamine (1M, pH 8.5, GE Healthcare) and an immobilization level of 132.2 RU was obtained. As running buffer lectin binding buffer (LBB) (10 mM HEPES ((4-(2-hydroxyethyl)-1-piperazineethanesulfonic acid), 1 mM calcium chloride, 1 mM manganese chloride and 50 mM sodium chloride). The pH of 7.4 was adjusted with 1 M NaOH. After immobilization the system was primed with the running buffer and two startup cycles were performed. The glycooligomer was injected in concentrations of 0– 400 µM in HBS-P$^+$ buffer with a dilution factor of 2. At a flow rate at 10 µL min^{-1}, the contact time were 180 s and dissociation time were 120 s were used. After each measurement, the sensor chip was regenerated by injection of 200 mM aMeMan in HBS-P$^+$ buffer at a flow rate of 10 µL min -1 with a contact time of 30 s to ensure that all sample was washed out and to achieve a stable baseline for the following measurements. For each sample the measurements were repeated three times. These measurements were repeated three times.

Synthesis and modification of monodisperse SiO2 particles: 200 nm silica particles were synthesized using a multistep hydrolysis-condensation procedure of Tetraethylorthosilicate (TEOS, 99%, Fluka) in ammonium hydroxide (NH4OH, 28–30% solution, Acros)-ethanol ethanol abs. (EtOH, 99.9%, VWR), solution based on the Stöber approach.[24] In short, TEOS was mixed

with a solution of ethanol and ammonia. The resulting particles were used as nuclei in the next step. Each reaction was run under successive stirring at 500 rpm overnight at room temperature. Afterwards, the particles of the targeted size were removed from the solvent by centrifugation, resulting in monodisperse silica particles. The prepared particles were dried in a vacuum oven under reduced pressure at 60 °C.

Synthesis of PNIPAM-APTES- JPs: In the next step colloidosomes were prepared with the 200 nm large APTES-modified silica particles using a Pickering emulsion approach as described elsewhere. [17-19, 25] The exposed particle hemisphere was then modified with the ATRP-initiator α-bromoisobutyric acid (BiBA, 98%, Aldrich). Subsequently, the paraffin wax (mp. 53–57 °C, Aldrich) was dissolved in hot hexane (95%, Aldrich) and the partly initiator-covered were used for surface-initiated ARGET-ATRP of NIPAAm as described elsewhere.[39,40]. Afterwards, particles partly covered with poly(N-isopropylacrylamide) PNIPAAm and partly covered with APTES were obtained.

Particle surface modification: For glycofunctionalization, the particles were suspended in deionized water to give a concentration of 1 mg ml^{-1} followed by adding N-(3-(dimethylamino)propyl)-N'-ethylcarbo-diimide hydrochloride (EDC, Aldrich) (10 eq) and N-hydroxysuccinimide (NHS, Aldrich) (10 eq) and stirring for 10 minutes. Glycooligomers were dissolved in water and were added to the particle suspension and stirred overnight. The excess glycooligomer, EDC and NHS were removed by washing with deionized water 5 times by centrifugation.

RhodaminB-labelling of particles: The particle were suspended in deionized water to give a concentratin of 1 mg ml^{-1}. N-(3-(dimethylamino)propyl)-N'-ethylcarbo-diimide hydrochloride (EDC, Aldrich) (10 eq) and N-hydroxysuccinimide (NHS, Aldrich) (10 eq) was added and stirred for 10 minutes. Afterwards RhodaminB with carboxylic acid as functional group (Sigma Aldrich, ≥95%) was added to the particle suspension and stirred overnight. The excess RhodaminB, EDC and NHS was removed by washing with deionized water until no more coloration was visible.

FITC-ConA Adhesion Inhibition Assay: A stock solution of ConA (concanavalin A) in lectin binding buffer (LBB, 10 mM HEPES (4-(2-hydroxyethyl)-1-piperazineethanesulfonic acid), 1 mM calcium chloride, 1 mM manganese chloride and 50 mM sodium chloride, pH 7.4) and a

stock solution of particles in 10mM phosphate buffered saline (PBS, pH 7.4) buffer were prepared. The two stock solutions were mixed to obtain a ConA concentration of 1 mg ml^{-1} and particle concentration of 0.1 mg ml^{-1} in each sample. The particle/ConA mixture was incubated overnight at room temperature, then examined by microscopy. To study the temperature responsivity, the samples were heated to 40 °C for 3 hours in a water bath. For inhibition with methyl-α-D-mannose (aMeMan, Acros Organics, 99%) a stock solution was prepared, then added to particle/ConA mixtures to achieve a concentration of 200 mM and incubated overnight at room temperature.

Bacteria experiments: For bacterial adhesion and aggregation studies, particles decorated with the Man containing glycooligomer were prepared in 10 mM PBS buffer (pH 7.4) at a concentration of 0.1 mg·mL^{-1}. This solution was combined with a green fluorescent protein (GFP) tagged type 1-fimbriated *E. coli* strain (PPKL1162)[14] in PBS containing the bacteria at a concentration of 2 mg·mL^{-1} and incubated at 37 °C under constant shaking for 2 h. Afterward, 30 µL of the solution was transferred to an ibidi 18 well slide (ibidi GmbH, Germany). Images were acquired on an IX 73 microscope (Olympus, Japan) equipped with a halogen lamp, a FITC filter set, and a UPlanFL N 60x/1.35 oil objective (Olympus, Japan). Similarly, an aggregation study was conducted using the mannose binding protein ConA (2 mg·mL-1) labeled with FITC in LBB and incubated as described before.

ConA capture study: To quantify ConA binding to the glycofunctionalized and non-functionalized particles, a stock solution of ConA at a concentration of 2 mg ml^{-1} and a stock solution of particles at a concentration of 0.2 mg ml^{-1} were prepared in LBB. The pH of 7.4 was adjusted with 1 M NaOH.) First, the protein solution was filtered and the absorbance was measured at 280 nm. Next, 500 µL of ConA solution and 500 µL of particle solution were mixed to achieve a final protein concentration of 1 mg ml^{-1} and a final particle concentration of 0.1 mg ml^{-1}. The mixture was incubated at 20 °C for 3 h and centrifuged at 13500 rpm for 5 min. The supernatant was removed, transferred to a PMMA microcuvette and measured at 280 nm. A mixture of 500 µL ConA and 500 µL LBB was used as a blank. The pellet was dissolved in 1 ml of a 200 µM solution of aMeMan in LBB, incubated overnight, centrifuged at 13500 rpm for 5 min, and the protein concentration was measured at 280nm using an extinction coefficient of 28500 M^{-1}·cm^{-1}.

Results and Discussion

Synthesis of glyco-particles

In order to gain access to glyco-JPs, previously established protocols were used to obtain silica microparticles bearing pendant PNIPAM chains on one side and free amine groups (via 3-aminopropyltriethoxysilane, APTES) on the other side of the particle surface. These amine groups can then be used for the covalent attachment of carboxyl-functionalized Man glycooligomers via amide bond formation (Figure 2). Overall, four types of particles were synthesized and studied for bacterial binding: APTES and APTES-Man as non-Janus type particles, as well as PNIPAM-APTES-JP and PNIPAM-Man-JP, where one side is coated with PNIPAM and the other side is either APTES or carries Man glycooligomers.
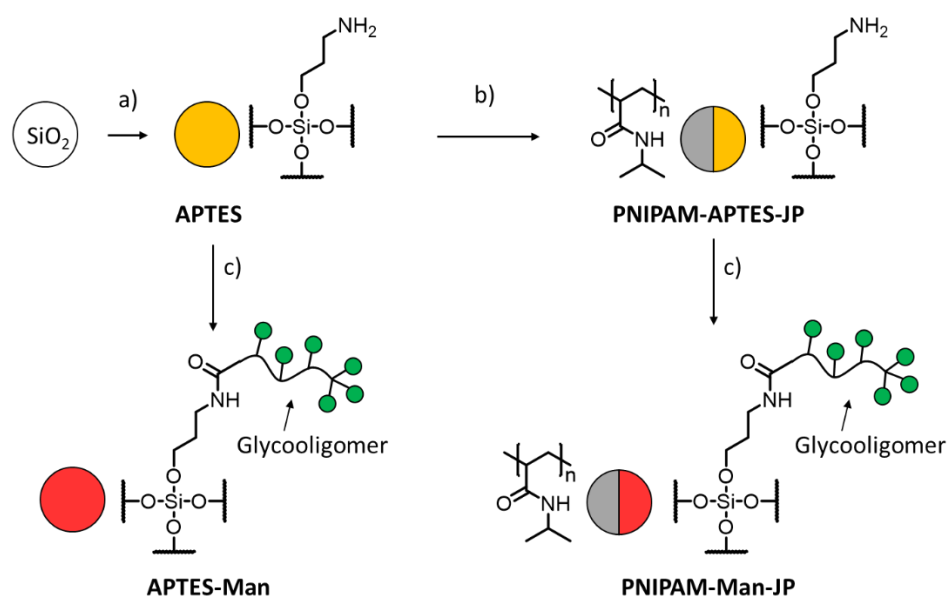

Figure 2. Schematic presentation of the synthesis of glycofunctionalized particles: a) APTES functionalization of silica particles, b) formation of JPs by functionalization of one hemisphere with PNIPAM, c) glycoconjugation by amide coupling of carboxy-terminated glycooligomers (see experimental section for details on the synthetic procedures and particle analysis). The particles were labelled with RhodaminB (not shown in the figure, see experimental section for synthetic details)

The APTES coating on silica particles was obtained through a Stöber synthesis[24] to introduce amino groups to the surface of the particles. The JPs functionalization was carried out by using a Pickering emulsion approach and side-by-side grafting of polymers.[25] Briefly, to mask one

hemisphere of the APTES-modified silica particles, they were mechanically stirred with molten wax and hot water to form so-called colloidosomes in a Pickering emulsion.[16,17,25] After cooling down the colloidosomes, the particles were entrapped at the wax/water interface covering roughly half of the particle by wax. The non-masked hemispheres of the particles were modified with ⍺-bromoisobutyric acid via carbodiimide chemistry to introduce bromine to the particle surface. The colloidosome structure is well-preserved during this modification step. In order to remove the wax, the colloidosomes containing the particles were repeatedly washed with hot hexane and dichloromethane. The resulting APTES and PNIPAM-APTES-JP were analyzed by DLS, Zeta potential, and TEM (see Table1 and SI). The comparison of the hydrodynamic radii between the APTES particles and the PNIPAM functionalized JPs showed an increase of about 330 nm from 128 ± 3 nm for APTES to 455 ± 29 nm for PNIPAM-APTES-JP verifying the successful polymer conjugation (see Table 1 and SI for further details on synthetic procedures and analytical data).

For glycofunctionalization, we employed previously established solid-phase polymer synthesis (SPPoS) to first produce a monodisperse, sequence-defined glycooligomers (Figure 3). In short, SPPoS is based on the stepwise coupling of tailor-made building blocks on a solid support using standard Fmoc-peptide chemistry giving sequence-defined oligo(amidoamines).[28,29] By using building blocks with pending functional groups such as alkyne side groups, the oligomers can then further be functionalized with carbohydrate-azide derivatives, here Man-azide by Cu-mediated azide-alkyne conjugation (CuAAC).[30] The Man carrying glycooligomer for particle functionalization was assembled using previously introduced building blocks TT-linker (three triple linker), EDS (ethylene glycol diamine succinic acid) and TDS (triple bond diethylenetriamine succinic acid) [31] giving a hexavalent ligand. Three Man ligands are positioned in close proximity at one chain end in an umbrella-like fashion, while the other three Man ligands are positioned along the linear scaffold (Figure 3). By using a preloaded resin carrying a glycine, a C-terminal carboxyl group is introduced at the other chain end that will next be used for conjugation to the amine-functionalized particle surface. The relative purity and structure of the final glycooligomer was confirmed by RP-HPLC-ESI-MS and ^{1}H NMR (see SI).
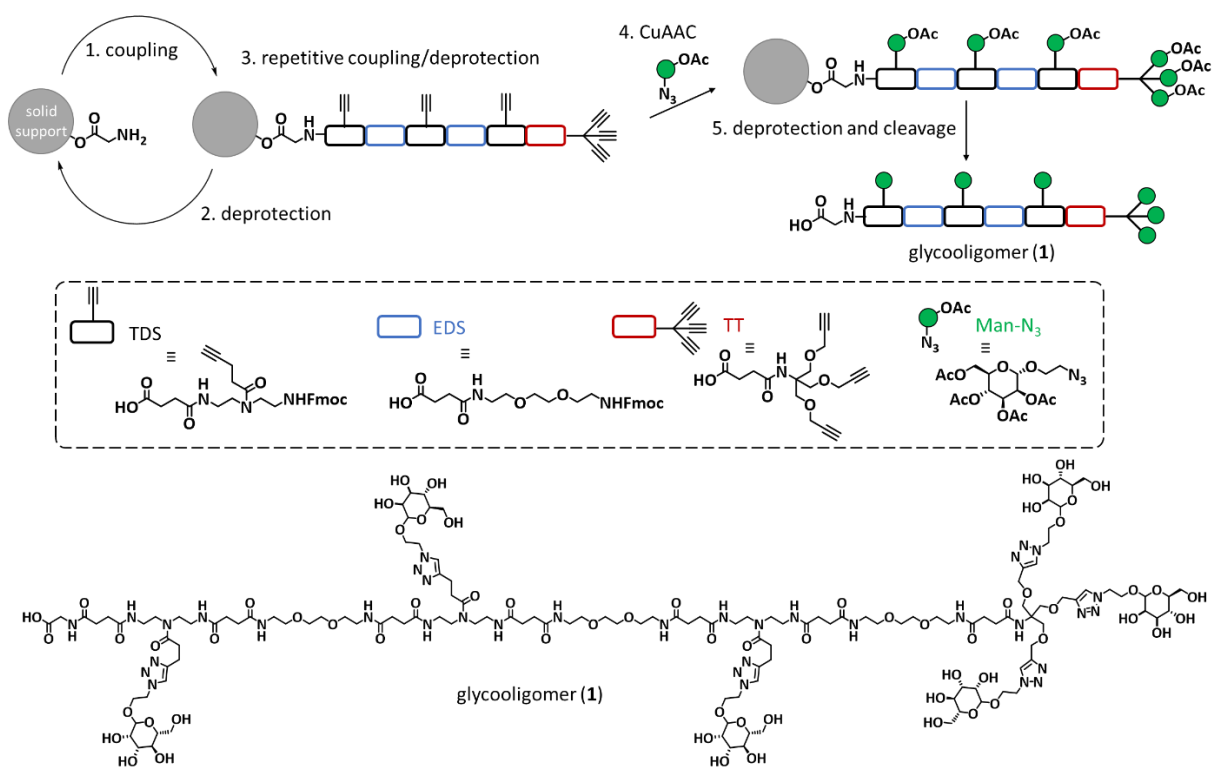
Figure 3: Solid phase polymer synthesis of the glycooligomer for particle functionalization.

While similar glycooligomers have been previously been studied as inhibitors of *E. coli* [16,28], here we adapted the structure to potentially maximize both accessibility and binding affinity of glycooligomers on the particle surface. On the one hand, we introduce a linear scaffold between the anchoring group on the particle surface and the carbohydrate motifs to give better accessibility. On the other hand, we maximize number of Man ligands in the overall structure with higher density Man umbrella-like motif at the outer chain end to enhance statistical binding effects. To gain insights into the overall affinity of the glycooligomer based on this design, a binding study with the well-established model lectin Concanavalin A (ConA) was performed (Figure 4). ConA contains four carbohydrate-recognizing domains (CRD) that specifically bind D-mannosyl and D-glucosyl residues in response to calcium(II) and manganese(II) ions and is often used as standard for comparing binding properties of Man containing glycoconjugates such as the glycooligomer of this study.[32] Direct binding experiment was performed by surface plasmon resonance (SPR) using immobilized ConA on an SPR chip and addition of the glycooligomer at increasing concentrcantions in flow. Analysis of the resulting binding curves reveals binding of the glycooligomer in the µM range which

agrees with studies of similar glycooligomers from previous studies[29] (Figure 4, see experimental section for details).
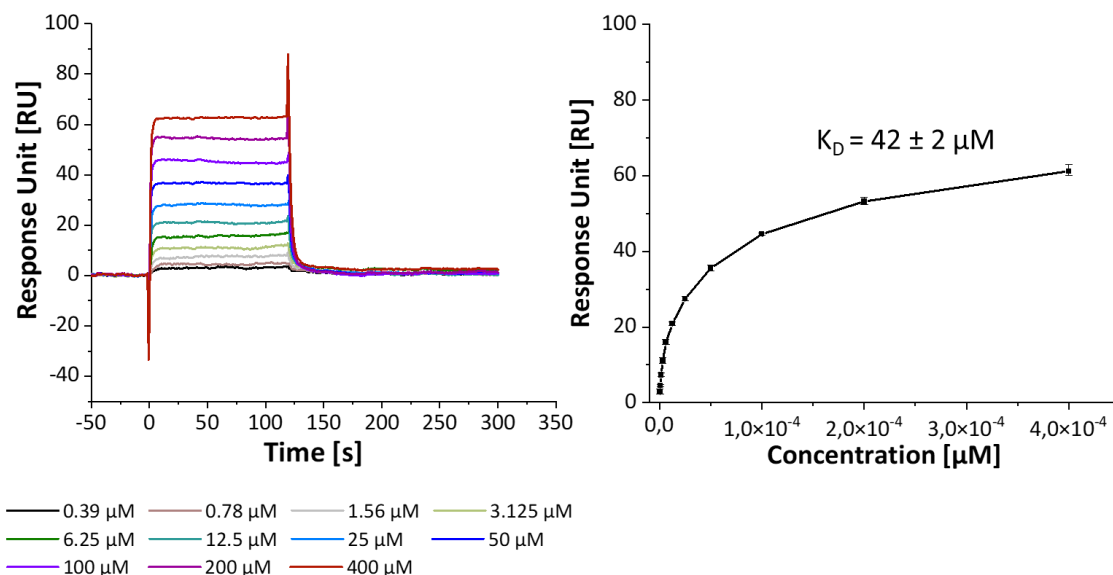

Figure 4: Direct binding assay on a ConA surface via SPR. The error bars show the standard deviation for three different runs.

Next, the conjugation of the glycooligomer onto APTES and the APTES-PNIPAM-JP was achieved by activation of the terminal carboxy group with EDC/NHS (1-ethyl-3-(3-dimethylaminopropyl)carbodiimide/N-hydroxysuccinimid) in water and addition of preactivated glycooligomers to the according particles in solution. After the reaction, excess of glycooligomer was removed by washing with water and glycofunctionalized particles (APTES-Man and PNIPAM-Man-JP) were isolated by centrifugation. All particles were analyzed by DLS and Zeta potential measurements and the degree of Man functionalization was determined by phenol sulfuric acid colorimetric test (see Table 1 and SI for details on the synthetic procedure and analytical data).

Table 1: Hydrodynamic radii (R$_h$), PDI, degree of Man functionalization and Zeta potential of all particle samples.

#	R$_h$[a]	PDI[a]	Man functionalization degree [μmol/g][b]	Zeta potential [mV]		
				pH = 4	pH = 7	pH = 19
APTES-PNIPAM-JP	455 ± 29	0.358 ± 0.044	0	34 ± 1	19 ± 0.4	-20 ± 0.5
PNIPAM-Man-JP	380 ± 16	0.510 ± 0.048	36 ± 12	28 ± 1	7 ± 0.1	-28 ± 0.5
APTES	128 ± 3	0.045 ± 0.019	0	40 ± 1	69 ± 2	-26 ± 1
APTES-Man	154 ± 4	0.188 ± 0.053	48 ± 9	49 ± 0.5	33 ± 0.5	-44.5

(0) (a) R$_h$ and PDI were determined by DLS at 20 °C, (b) degree of Man functionalization was determined by using the phenol sulfuric method (see SI for details). The error bars show the standard deviation for three independent runs.

The APTES-Man particles show an increase of hydrodynamic radii in comparison to the non-functionalized APTES particles from 128 nm to 154 nm, a first indication for the successful conjugation of the glycooligomers. Interestingly, the comparison between JP and JP-Man shows a decrease from 455 nm to 380 nm. It is possible that this decrease in hydrodynamic radius after glycooligomer coupling is due to a smaller ion and hydration layer at these particles.

Phenol sulfuric acid colorimetric test gives the concentration of Man per particle in μmol/g. Both glycofunctionalized particles (APTES-Man and PNIPAM-Man-JP) show similar loading of Man with 48 ± 9 μmol g^{-1} and 36 ± 12 μmol g^{-1}, respectively. We attribute this to the same concentration of glycooligomer in the functionalization step which will later enable direct comparison of both particle systems independent of the amount of Man ligands per particle. As theoretically APTES particles should be able to accommodate twice the number of ligands on their surface based in comparison to the JPs, this also indicates that potentially for APTES particles, higher Man loading could be achieved e.g., when using higher amounts of glycooligomers in the functionalization step. However, this has not been attempted here.

Further characterization of the particles was performed by Zeta potential measurements at pH values 4, 7 and 10 in water, respectively. Due to the cationic free primary amines on the surface, the non-functionalized APTES particles have a positive Zeta potential at pH 7.

Significant differences are seen after functionalization of the particles, as the amines are converted to amides, resulting in a decrease in the positive surface charge of the particles and decrease of the Zeta potential roughly by a factor of two. At pH 4, due to protonation an increase in Zeta potential was observed. As expected, at pH 10, the Zeta potential decreased. Comparison of non-functionalized and glycofunctionalized particles shows a significant difference in Zeta potential values, which can be attributed to the change in surface chemistry, thus demonstrating successful glycofunctionalization. To visualize the glycofunctionalized and non-functionalized particles, transmission electron microscopy (TEM) images were taken. No changes in shape were observed, with JPs showing a more homogeneous size distribution than the APTES particles, both before and after glycofunctionalization (see SI, Figure S12).

Glycofunctionalized particles binding to ConA

First, to study carbohydrate-mediated binding of glycofunctionalized particles vs. potential non-specific interactions e.g., from the particle surface, an interaction study with ConA was performed. Therefore, particle dispersions and ConA solutions at defined concentrations were mixed and turbidity increase was measured. Especially for glycofunctionalized particles (APTES-Man and PNIPAM-Man-JP) pronounced turbidity was observed.[34] As expected, multivalent receptor ConA can bind to Man ligands also on different particles leading to cluster formation and precipitation. To quantify the amount of ConA within the clusters as a means of the binding affinity of the particles, clusters and supernatant containing non-bound ConA were separated by centrifugation. Non-bound ConA was quantified by UV-vis spectroscopy at 280 nm (see Figure 5B). In parallel, alpha-methylmannose (αMeMan) was added to the clusters in large excess, competing with particle-ConA binding and dissolving the clusters. Concentration of ConA dissolved from the clusters was quantified by UV-vis spectroscopy. Figure 5 shows the results for both, ConA quantified from the supernatant as well as from the particle clusters. Both Man functionalized particle systems are able to bind similar amounts of ConA, as was expected based on the similar levels of Man functionalization. The non-carbohydrate functionalized systems, however, also show ConA binding. This can be attributed to non-specific interactions likely from the APTES surfaces. This is supported by the PNIPAM-JPs showing reduced non-specific lectin binding. Likely, PNIPAM chains act as sterical shield against non-specific protein adsorption below the LCST.[42,48,49] Indeed, APTES particles

show twice as much ConA binding as PNIPAM-APTES-JPs, which correlates with twice as much APTES-surface available for protein interactions. Thus, PNIPAM-Man-JPs show lower non-specific interaction while maintaining a similar level of Man-mediated interactions. In general, ConA binding is low for both glycofunctionalized particles compared to similar systems that were previously reported[41]. This could indicate that not all Man units are accessible for ConA binding. Due to the umbrella-like glycooligomer structure, the accessibility of the Man units in the main chain could be hindered, thereby decreasing the overall number of Man ligands that is available for ConA binding.
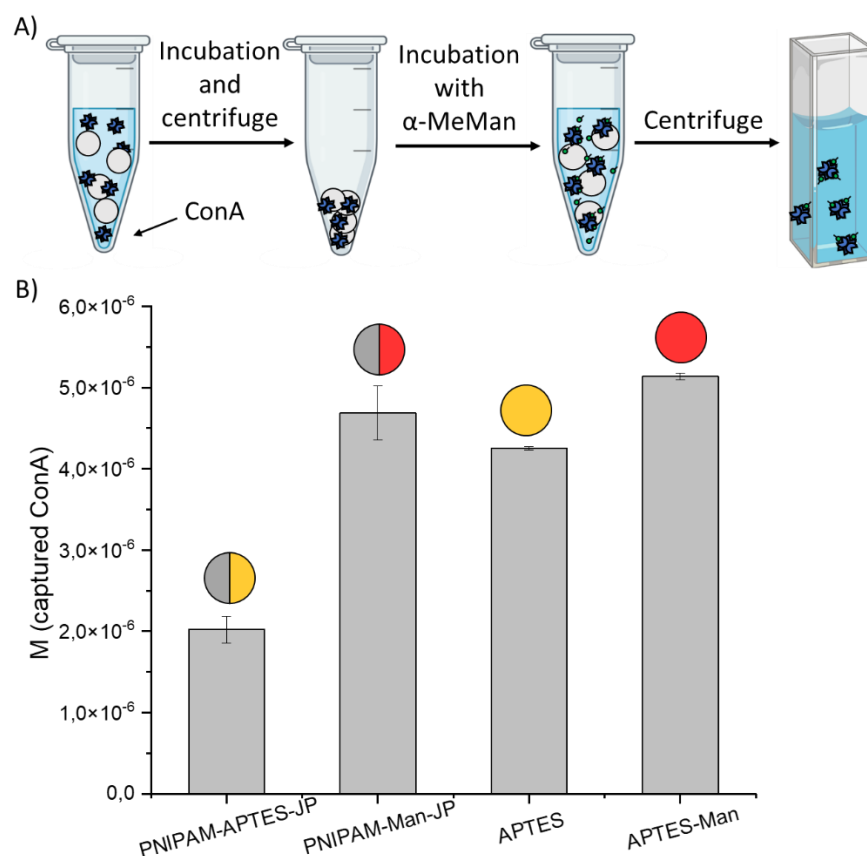
Figure 5. A) Schematic presentation of interaction study of particles with ConA. B) Absolute quantities of bound and non boud ConA binding for 100 µg particle and 1 mg ConA. The error bars show the standard deviation for three different runs.

Further studies on the interaction of the different particle systems with ConA were performed by fluorescence microscopy. Therefore, particles were statistically labeled with Rhodamine B and incubated with FITC labeled ConA (see experimental section for labeling conditions). Here

again, cluster formation between particles and ConA is observed. In comparison to APTES-Man, PNIPAM-Man-JP showed smaller aggregates, which can be attributed to the shielding effect of PNIPAM. The aggregates could subsequently be inhibited by addition of aMeMan, which confirmed the specific binding between mannose and CRDs of ConA. Examination of non-functionalized APTES particles and JPs with ConA showed no interaction based on the fluorescence of particles and ConA. However, particle-particle aggregation was observed for both, non-functionalized APTES and JPs (see SI).

Glycofunctionalized particles binding to *E. coli*

After showing the successful glycofunctionalization of the particles and the binding towards ConA, binding to *E. coli* was investigated by fluorescence microscopy. *E. coli* are covered with so-called pili that present Man-recognizing FimH receptors.[43] These receptors can bind to Man ligands on cell surfaces and thereby act as cell attachment factors and important mediators of bacterial infection processes.[44,45] By blocking these receptors with competing ligands in so-called anti-adhesion therapy, inhibition of the cell attachment can be achieved and thereby reduce or stop the infection.[7]

The inhibitory potential of the particles was quantified using an adhesion inhibition assay on *E. coli*-binding mannan-coated microplate surfaces. The microplates were incubated fluorescent *E. coli* in presence or absence of the different particles and the fluorescence signal was determined using a microplate reader (Figure 5). Upon addition of methyl α-D-mannose (MeMan), a well-known FimH binding molecule, the Man-binding sites are blocked, *E. coli* cannot bind to mannosylated surfaces anymore, and the fluorescence signal is decreased.[24] At a particle concentration of 0.1 mg ml^{-1}, fully non-Man functionalized APTES particles showed no inhibition and PNIPAM-APTES-JP showed weak inhibition signifying weak non-specific interactions. In comparison to aMeMan, APTES-Man and PNIPAM-Man-JP showed a high inhibitory potency, as was expected for such particle-based systems from previous studies e.g., using Man-functionalized gold nanoparticles to inhibit *E. coli*.[35] As expected, the inhibition was somewhat weaker for APTES-Man-JP since it was not fully coated with Man. Furthermore, the fully mannosylated APTES-Man particles may inhibit more bacteria since it could form large clusters with *E. coli*, whereas APTES-Man-JP likely does not lead to further clustering since the side of the particles facing away from the bacteria does not bind. Thus,

PNIPAM-Man-JPs bind fewer *E. coli* than APTES-Man at the same concentration and thus are expected to also show a lower inhibition potency.
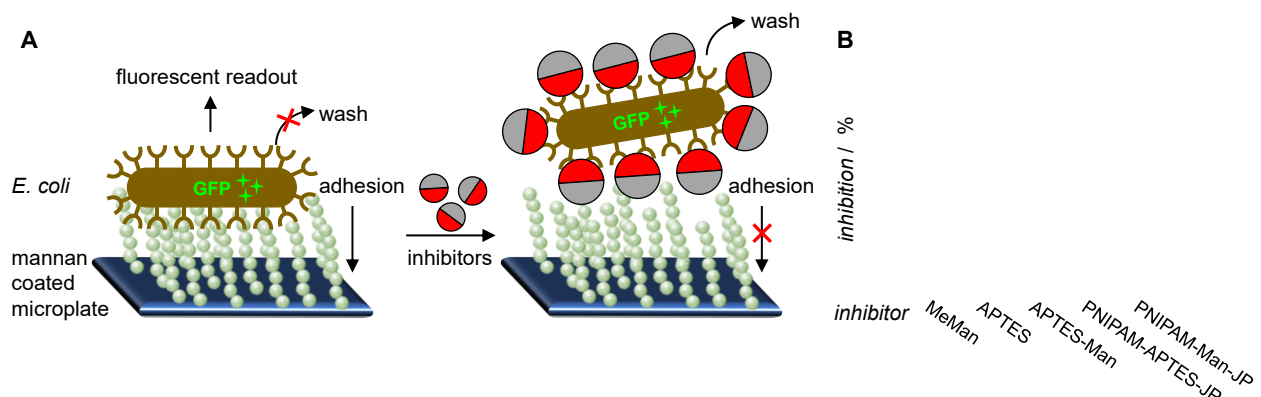

Figure 5: Adhesion inhibition assay: A) *E. coli* attaches to mannan coated microplates via the FimH receptor, which can be read out by GFP-fluorescence. In presence of inhibitors blocking the receptor, the bacterial adhesion is reduced signifying the inhibitory potential. B) The relative inhibition (normalized to aMeMan) for the different particles. The error bars show the standard deviation for three independent experiments.

To directly observe the binding of *E. coli* with the particles and the potential formation of large clusters, fluorescence microscopy was employed. Rhodamine B-labeled APTES-Man or PNIPAM-Man-JP, as well as the non-functionalized APTES and PNIPAM-APTES-JP as negative controls were added to the bacteria suspension. As suspected, APTES-Man particles form large clusters of particles and bacteria (Figure 6) as has also been described for other glyco-functionalized particle systems before.[46,47] In contrast, PNIPAM-Man-JPs show the formation of predominantly discrete aggregates where single bacteria are covered by several PNIPAM-Man-JPs forming a particle corona or shell around the bacterium (Figure 6). Importantly, non-mannosylated APTES and PNIPAM-APTES-JPs show no bacterial binding. To further demonstrate the specificity of binding between *E. coli* and glycofunctionalized particles, binding was inhibited by the addition of aMeMan (see SI). Cluster formation for both glyco-functionalized particle systems can be fully inhibited further demonstrating that binding is mediated by specific carbohydrate interactions (see SI for further details). This confirms the results obtained from the adhesion inhibition assay on microplates and shows that indeed the Janus particle approach is useful when inhibition without further glycoclustering is desired.
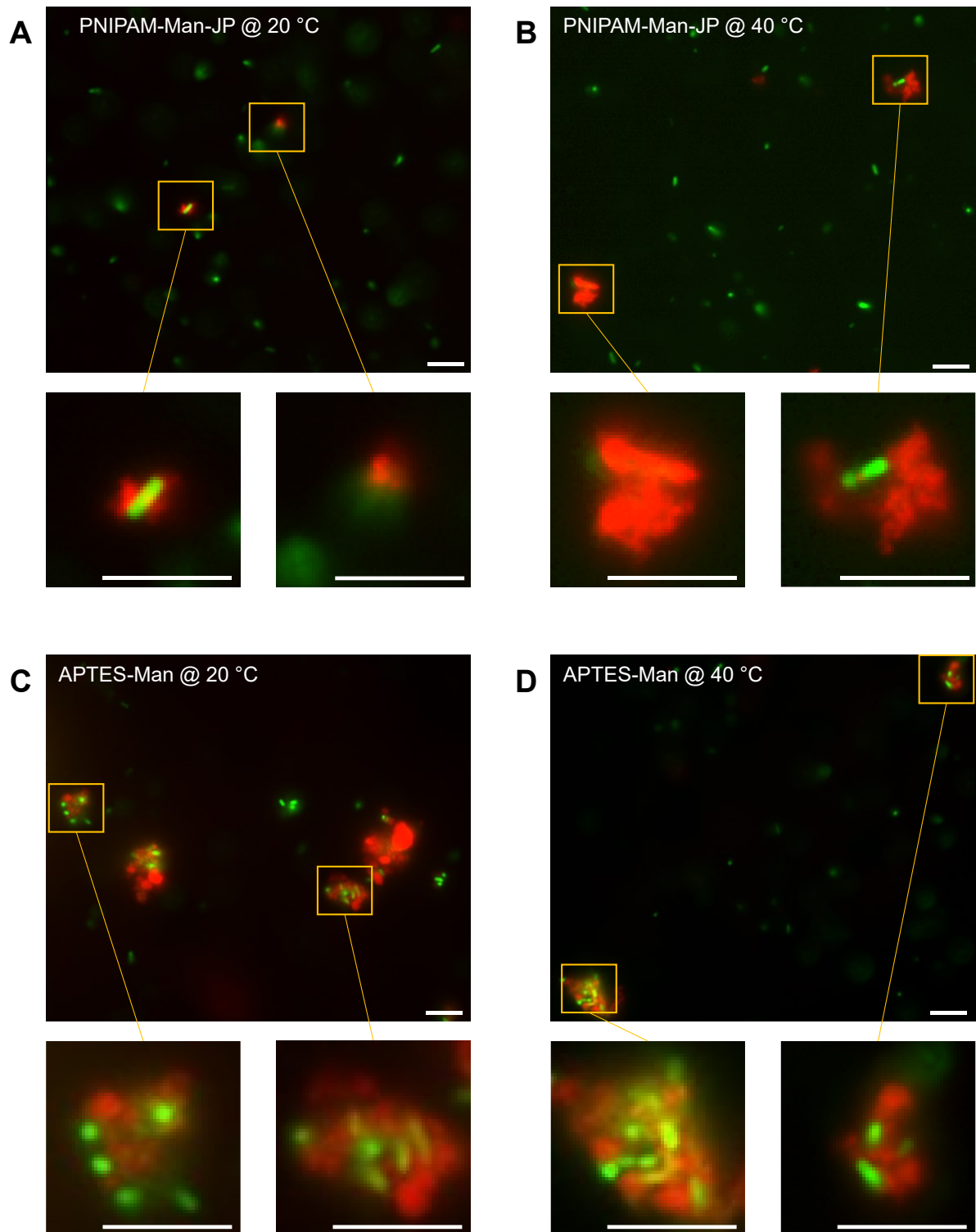
Figure 6: Particle attachment to *E. coli*: A) The bacteria (green) bind only few PNIPAM-APTES-JPs (red) at 20 °C and show a low tendency of cluster formation. B) Above the phase transition temperature large clusters of particles and-*E. coli* are present. C), D) For APTES-Man clusters of particles and bacteria form regardless of the temperature. Scale bars: 10 µm.

Based on the temperature-switchable PNIPAM hemisphere of JPs, bacterial binding studies were also carried out above and below 32 °C, the LCST of PNIPAM. When looking at PNIPAM-Man-JPs as well as full PNIPAM-APTES-JPs at 40°C, as expected, clustering of the particles due to collapse and aggregation of PNIPAM is observed (Figure 6). For the PNIPAM-Man-JPs formation of both, particle clusters as well as clusters containing bacteria and particles is observed (see Figure 6 and SI). At the same temperature, we observe no significant differences for the APTES-Man particles as they do not carry any PNIPAM chains (see SI). This demonstrated that by the design of glyco-JPs, additional functions beyond pure carbohydrate mediated binding, such as thermoresponsivity, could be implemented.

Conclusion

Glycofunctionalized particles that are uniformly coated with carbohydrate ligands are well-known to result in the formation of large bacteria-particle aggregates. To demonstrate the ability of glyco-JPs to form single bacteria-particle aggregates here we successfully synthesized JPs with presenting Man glycooligomers in one hemisphere and PNIPAM in the other hemisphere. Glycofunctionalization of the particles was verified by Zeta potential and a colorimetric test. Binding studies with ConA and E*. coli* were conducted via precipitation, inhibition competition experiments and fluorescence microscopy. While PNIPAM-Man-JP showed a halo-like arrangement on the surface of *E. coli* and resulted in isolation of single bacteria, the APTES-Man particles formed large clusters with *E. coli* due to their uniform glycofunctionalization. Furthermore, temperature-dependent experiments with PNIPAM-Man-JP and non-functionalized PNIPAM-APTES-JP showed particle aggregation above the LCST of PNIPAM. Thus, the Janus-type glycofunctionalization lead to a well-controlled aggregation behavior of single bacteria-particle clusters and the ability to trigger formation of larger clusters upon external stimuli. Future studies will further explore the glyco-JPs in more complex bacterial inhibition studies including disruption of biofilms as well as for the delivery of antibacterial e.g. through release from the PNIPAM hemisphere.

References

(1) Baker, R.E.; Mahmud, A.S.; Miller, I.F.; Rajeev, M.; Rasambainarivo, F.; Rice B.L.; Takahashi, S.; Tatem, A.J.; Wagner C.E.; Wang L.-F. Wesolowski A.; Metcalf C.J.E. Infectious disease in an era of global change. *Nat Rev Microbiol* **2022**, *20*, 193–205.

(2) Larsson, D.G.J.; Flach C.-F. Antibiotic resistance in the environment. *Nat Rev Microbiol* **2022**, *20*, 257-269.

(3) Zhao, L.; Xie, S.; Liu, Y.; Liu, Q.; Song, X.; Li, X. Janus micromotors for motion-capture-lighting of bacteria. *Nanoscale* **2019**, *11*, 17831-17840.

(4) Campuzano, S.; Orozco, J.; Kagan, D.; Guix, M.; Gao, W.; Sattayasamitsathit, S.; Claussen, J.C.; Merkoçi, A.; Wang, J. Bacterial isolation by lectin-modified microengines. *Nano Lett.* **2012**, *12*, 396-401.

(5) Pacheco, M.; Jurado-Sánchez, B.; Escarpa, A. Sensitive Monitoring of Enterobacterial Contamination of Food Using Self-Propelled Janus Microsensors. *Anal Chem.* **2018**, 90, 2912-2917.

(6) Krachler, A.M.; Orth, K. Targeting the bacteria-host interface: strategies in anti-adhesion therapy. *Virulence*. **2013**, *4*, 284-294.

(7) Ofek, I.; Hasty, D.L.; Sharon, N. Anti-adhesion therapy of bacterial diseases: prospects and problems. *FEMS Immunol Med Microbiol.* **2003**, *38*, 181-191.

(8) Knight, S.D.; Bouckaert, J. Structure, function, and assembly of type 1 fimbriae. *Top Curr Chem.* **2009**, *288*, 67-107.

(9) Fasting, C.; Schalley, C.A.; Weber, M.; Seitz, O.; Hecht, S.; Koksch, B.; Dernedde, J.; Graf, C.; Knapp, E.W.; Haag, R. Multivalency as a chemical organization and action principle. *Angew Chem Int Ed Engl.* **2012**, *51*, 10472-10498.

(10) Bernardi, A.; Jiménez-Barbero, J.; Casnati, A.; De Castro, C.; Darbre, T.; Fieschi, F.; Finne, J.; Funken, H.; Jaeger, K.E.; Lahmann, M.; Lindhorst, T.K.; Marradi, M.; Messner, P.; Molinaro, A.; Murphy, P. V.; Nativi, C.; Oscarson, S.; Penadés, S.; Peri, F.; Pieters, R.J.; Renaudet, O.; Reymond, J.L.; Richichi, B.; Rojo, J.; Sansone, F.; Schäffer, C.; Turnbull, W.B.; Velasco-Torrijos, T.; Vidal, S.; Vincent, S.; Wennekes, T.; Zuilhof, H.; Imberty, A.

Multivalent glycoconjugates as anti-pathogenic agents. *Chem Soc Rev.* **2013**, *42*, 4709-4727.

(11) Bhatia, S.; Camacho, L.C.; Haag, R. Pathogen Inhibition by Multivalent Ligand Architectures. *J. Am. Chem. Soc.* **2016**, *138*, 8654–8666.

(12) Müller, C.; Despras, G.; Lindhorst, T.K. Organizing multivalency in carbohydrate recognition. *Chem. Soc. Rev.*, **2016**, *45*, 3275-3302.

(13) Hudak, J.E.; Bertozzi, C.R. Glycotherapy: new advances inspire a reemergence of glycans in medicine. *Chem Biol.*, **2014**, *21*, 16-37.

(14) Jacobi, F.; Camaleño de la Calle, A.; Boden, S.; Grafmüller, A.; Hartmann, L.; Schmidt, S. Multivalent Binding of Precision Glycooligomers on Soft Glycocalyx Mimicking Hydrogels. *Biomacromolecules*, **2018**, *19*, 3479–3488.

(15) Soria-Martinez, L.; Bauer, S.; Giesler, M.; Schelhaas, S.; Materlik, J.; Janus, K.; Pierzyna, P.; Becker, M.; Snyder, N.L.; Hartmann, L.; Schelhaas, M. Prophylactic Antiviral Activity of Sulfated Glycomimetic Oligomers and Polymers. *J. Am. Chem. Soc.* **2020**, *142*, 5252–5265.

(16) Paul, T.J.; Rubel, S.; Hildebrandt, M.; Strzelczyk, A.K.; Spormann, S.; Lindhorst, T.K. Thermosensitive Display of Carbohydrate Ligands on Microgels for Switchable Binding of Proteins and Bacteria. *ACS Appl Mater Interfaces* **2019**, *11*, 26674-26683.

(17) Marschelke, C.; Fery, A.; Synytska, A. Janus particles: from concepts to environmentally friendly materials and sustainable applications. *Colloid Polym Sci*. **2020**, *298*, 841–865.

(18) Kirillova, A.; Marschelke, C.; Synytska, A. Hybrid Janus Particles: Challenges and Opportunities for the Design of Active Functional Interfaces and Surfaces. *ACS Appl. Mater. Interfaces* **2019**, *11*, 9643–9671.

(19) Kirillova, A.; Schliebe, C.; Stoychev, G.; Jakob, A.; Lang, H.; Synytska, A. Hybrid Hairy Janus Particles Decorated with Metallic Nanoparticles for Catalytic Applications. *ACS Appl. Mater. Interfaces* **2015**, *7*, 21218–21225.

(20) Kirillova, A.; Marschelke, C.; Friedrichs, J.; Werner, C.; Synytska, A. Hybrid Hairy Janus Particles as Building Blocks for Antibiofouling Surfaces. *ACS Appl. Mater. Interfaces* **2016**, *8*, 32591–32603.

(21) Kirillova, A.; Ionov, L.; Roismann, I.; Synytska, A. Hybrid Hairy Janus Particles for Anti-Icing and De-Icing Surfaces: Synergism of Properties and Effects. *Chem. Mater.* **2016**, *28*, 6995–7005.

(22) Du, Y.; Li, Y.; Aftenieva, O.; Tsuda, T.; Formanek, P.; König, T.A.F.; Synytska, A. High Yield Synthesis of Water-Processable Donor: Acceptor Janus Nanoparticles with Tuned Internal Morphology and Highly Efficient Charge Separation/Transfer. Adv. Opt. Mater. **2022**, *10*, 2101922.

(23) Schmidt, S.; Paul, T.J.; Strzelczyk, A.K. Interactive Polymer Gels as Biomimetic Sensors for Carbohydrate Interactions and Capture–Release Devices for Pathogens. *Macromol. Chem. Phys.* **2019**, *220*, 1900323.

(24) Paul, T.J.; Strzelczyk, A.K.; Feldhof, M.I.; Schmidt, S. Temperature-Switchable Glycopolymers and Their Conformation-Dependent Binding to Receptor Targets. *Biomacromolecules* **2020**, *21*, 2913-2921.

(25) Strzelczyk, A.K.; Paul, T.J.; Schmidt, S. Quantifying Thermoswitchable Carbohydrate-Mediated Interactions via Soft Colloidal Probe Adhesion Studies. *Macromol. Biosci.* **2020**, *20*, 2000186.

(26) Stöber, W.; Fink, A.; Bohn, E. Controlled Growth of Monodisperse Silica Spheres in the Micron Size Range. *Colloid Interface Sci.* **1968**, *26*, 62−69.

(27) Synytska, A.; Kirillova, A.; Isa, L. Synthesis and Contact Angle Measurements of Janus Particles*. ChemPlusChem*, **2014**, *79*, 656-661.

(28) Igde, S.; Röblitz, S.; Müller, A.; Kolbe, K.; Boden, S.; Fessele, C.; Lindhorst, T.K.; Weber, M.; Hartmann, L. Linear Precision Glycomacromolecules with Varying Interligand Spacing and Linker Functionalities Binding to Concanavalin A and the Bacterial Lectin FimH. *Macromol Biosci.* **2017**, *17*, 1700198.

(29) Boden, S.; Reise, F.; Kania, J.; Lindhorst, T.K.; Hartmann, L. Sequence-Defined Introduction of Hydrophobic Motifs and Effects in Lectin Binding of Precision Glycomacromolecules. *Macromol. Biosci.,* **2019**, *19*, 1800425.

(30) Wojci', F.; O'Brien, A.G.; Götze, S.; Seeberger, P.H.; Hartmann, L. Synthesis of Carbohydrate-Functionalised Sequence-Defined Oligo(amidoamine)s by Photochemical Thiol-Ene Coupling in a Continuous Flow Reactor. *Eur. J. Chem.* **2013**, *19*, 3090-3098.

(31) Ponader, D.; Maffre, P.; Aretz, J.; Pussak, D.; Ninnemann, N.M.; Schmidt, S.; Seeberger, P.H.; Rademacher, C.; Nienhaus, G.U.; Hartmann, L. Carbohydrate-Lectin Recognition of Sequence-Defined Heteromultivalent Glycooligomers. *J. Am. Chem. Soc.* **2014**, *136*, 2008−2016.

(32) Hill, S.; Galan, M.C. Fluorescent carbon dots from mono- and polysaccharides: synthesis, properties and applications. *Beilstein J. Org. Chem.* **2017**, *13*, 675−693.

(33) Camaleño de la Calle, A.; Gerke, C.; Chang, X.J.; Grafmüller, A.; Hartmann, L.; Schmidt, S. Multivalent Interactions of Polyamide Based Sequence-Controlled Glycomacromolecules with Concanavalin A. Macromol Biosci., **2019**, *19*, e1900033.

(34) Wittmann, V.; Pieters, R.J. Bridging lectin binding sites by multivalent carbohydrates. *Chem. Soc. Rev.* **2013**, *42*, 4492-4503.

(35) Gestwicki, J.E.; Cairo, C.W.; Strong, L.E.; Oetjen, K.A.; Kiessling, L.L. Influencing Receptor−Ligand Binding Mechanisms with Multivalent Ligand Architecture. *Am. Chem. Soc* **2002**, *124*, 14922−14933.

(36) Locke, A. K.; Cummins, B. M.; Abraham, A. A.; Coté, G. L. PEGylation of concanavalin A to improve its stability for an in vivo glucose sensing assay. *Anal. Chem.* **2014**, *86*, 9091−9097.

(37) Boden, S.; Wagner, K.G.; Karg, M.; Hartmann, L. Presenting Precision Glycomacromolecules on Gold Nanoparticles for Increased Lectin Binding. *Polymers* **2017**, *9*, 716.

(38)   Hayes, W.; Osborn, H.M.I.; Osborne, S.D.; Rastall, R.A.; Romagnoli, B. One-pot synthesis of multivalent arrays of mannose mono- and disaccharides. *Tetrohedron* **2003**, *59*, 7983–7996.

(39)   Kirillova, A; Stoychev, G.; Eichhorn, K.-J.; Malanin M.; Synytska A. Platelet Janus Particles with Hairy Polymer Shells for Multifunctional Materials. *ACS Appl. Mater. Interfaces* **2014**, *6*, 13106-13114.

(40)   E. Svetushkina, E.; Ionov, L.; Puretskiy, N.; Stamm, M.; Synytska, A. A Comparative Study on Switchable Adhesion Between Thermoresponsive Polymer Brushes on Flat and Rough Surfaces. *Soft Matter*, **2011**, *7*, 5691–5696.

(41)   Kohri, M.; Sato, M.; Abo, F.; Inada, T.; Kasuya, M.; Taniguchi, T.; Nakahira, T. Preparation and lectin binding specificity of polystyrene particles grafted with glycopolymers bearing S-linked carbohydrates. *Eur. Polym. J.* **2011**, *47*, 2351-2360.

(42)   Sun, Y.; Li, Z.; Wu, J.; Wang, Z.; Dong, Y.; Wang, H.; Brash, J.L.; Yuan, L.; Chen, H. Gold nanoparticle–protein conjugate dually-responsive to pH and temperature for modulation of enzyme activity. *J. Mater. Chem. B.* **2019**, *7*, 3260-3267.

(43)   Sauer M.M; Jakob, R.P.; Luber T.; Canonica, F.; Navarra G.; Ernst B.; Unverzagt, C.; Maier, T.; Glockshuber R. *J. Am. Chem. Soc.* **2019**, *141*, 936-944.

(44)   Schembri, M.A.; Hasman, H.; Klemm, P. Expression and purification of the mannose recognition domain of the FimH adhesin. *FEMS Microbio. Lett.* **2000**, *188*, 147–151.

(45)   Jones, C.H.; Pinkner, J.S.; Roth, R.; Heuser, J.; Nicholes, A.V.; Abraham, S.N.; Hultgren, S.J. FimH adhesin of type 1 pili is assembled into a fibrillar tip structure in the Enterobacteriaceae. *Proc Natl Acad Sci USA.* **1995**, *92*, 2081–2085.

(46)   Gutiérrez-Ramos, S.; Hoyos, M.; Ruiz-Suárez, J.C. Induced clustering of Escherichia coli by acoustic fields. *Scientific reports* **2018**, *8*, 4668.

(47)   Yan, X.; Sivignon, A.; Alcouffe, P.; Burdin, B.; Favre-Bonte, S.; Bilyy, R.; Barnich, N.; Fleury, E.; François Ganachaud, F.; Bernard, J. Brilliant glyconanocapsules for trapping of Bacteria. *Chem. Commun.* **2015**, *51*, 13193—13196.

(48) Agrawal, G.; Agrawal, R. Stimuli-Responsive Microgels and Microgel-Based Systems: Advances in the Exploitation of Microgel Colloidal Properties and Their Interfacial Activity. *Polymers* **2018**, *10*, 418.

(49) Cross, M.C.; Toomey, R.G.; Gallant, N.D. Protein-surface interactions on stimuli-responsive polymeric biomaterials. *Biomed. Mat*. **2016**, *11*, 022002.

Supporting Information

Sweet Janus Particles: glycofunctionalized Janus particles for the binding and inhibition of *E. coli*

1. Materials:

Acetone (≥ 99.8%), trimethylamine (analytical grade), Toluene (for HPLC) was purchased from Fischer Scientific. Succinic anhydride (≥ 99.0%) was purchased from Carbolution Chemicals. Diethyl ether (with BHT as inhibitor, ≥ 99.8%), triisopropylsilane (TIPS) (98%), (+)-sodium-L-ascorbate (≥99.0%), chloroform-d (99,8 atom % D), deuteriumoxid-d_2 (99,8 atom % D), dimethylsulfoxid-d_6 (99,8 atom % D), were purchased from Sigma-Aldrich. N,N-Diisopropylethylamine (DIPEA) (≥ 99%), potassium hydroxide (≥ 85%) was purchased from Carl Roth. Methanol (100%), ethylacetate (>99.9%), n-hexan (≥99.8%) and acetic anhydride (99.7%) were purchased from VWR BDH Prolabo Chemicals. Dimethylformamide (DMF) (99.8%, for peptide synthesis), tert-butanol (≥ 99.0%), piperidine (99%), sodium methoxide (97%), sodium diethyldithiocarbamate (99%) and copper (II) sulfate (98%) were purchased from Acros Organics. Dichloromethane (DCM) (99.99%), Triethylsilane (≥ 98,0 %), trifluoroacetic acid (≥ 99,0 %) were purchased from Fluorochem. Benzotriazole-1-yl-oxy-tris-pyrrolidino-phos202lycofunctionalizatphosphat (PyBOP) were purchased from Iris Biotech GmbH. The anion resin (AG1-X8, quarternary ammonium, 100-200 mesh, acetate form) was purchased from BioRad. TentaGel® resin were purchased from Rapp Polymere. Methyl-α-D-mannopyranoside (>99%), 1-ethyl-3-(3-dimethylaminopropyl)carbodiimide (EDC), N-hydroxysuccinimide (NHS), Citric acid, anhydrous, was purchased from Alfa Aesar (>99.5%). Diethylenetriamine was purchased from Merk (>98%), di-tert-butyldicarbonate (≥99,0 %) was purchased from Novabiochem. Ethanol (>99.9%). was purchased from Chemsolute. 3-aminopropyltriethoxysilane (APS, 97%, ABCR), , dichloromethane (>99%, Acros), copper(II) bromide (99.999%, Aldrich), tin(II) 2-ethylhexanoate (95%, Aldrich), N,N,N',N'',N''-pentamethyldiethylenetriamine (PMDTA, 99%, Aldrich), ethyl α-bromoisobutyrate (EBiB, 98%; Aldrich), toluene (99.8%, Aldrich), chloroform (99.8%, Aldrich), tetrahydrofuran (>99%, Acros), methanesulfonic acid (99.5%, Aldrich), diethyl ether (99.7%, Aldrich), tert-butyl acrylate (tBA,

98%, Aldrich; was passed prior to polymerization through basic, neutral, and acidic aluminum oxides). N-Isopropylacrylamide (Aldrich, 99%) was recrystallized from hexane.

2. Instrumentation:

Nuclear Magnetic Resonance spectroscopy (NMR): ^{1}H-NMR (600 MHz) spectra were recorded on a Bruker AVA–CE III - 600. Chemical shifts of all NMR spectra were reported in delta (δ) expressed in parts per million (ppm). For 1H-NMR the residual, non-deuterated solvent was used as internal standard (δ 4.79 ppm for D2O). The following abbreviations are used to indicate the multiplicities: s, singlet, d, doublet; t, triplet; m multiplet.

Reverse– Phase - High Pressure Liquid Chromat–graphy - Mass Spectrometry (RP-HPLC-MS): Measurements were performed on an Agilent 1260 Infinity instrument coupled to a variable wavelength detector (VWD) (set to 214 nm) and a 6120 Quadrupole LC/MS containing an Electrospray Ionization (ESI) source (operated in positive ionization mode in a m/z range of 200 to 2000). As HPLC column a Poroshell 120 EC-C18 (3.0×50 mm, 2.5 µm) RP column from Agilent was used. The mobile phases A and B wcan H2O/ACN (95/5) and H2O/ACN (5/95), respectively. Both mobile phases contained 0.1% of formic acid. Samples were analyzed at a flow rate of 0.4 mL/min using a linear gradient starting with 100% mobile phase A reaching 50% mobile phase B within 30 min. The temperature of the column compartment was set to 25 °C. UV and MS spectral analysis was performed within the OpenLab ChemStation software for LC/MS from Agilent Technologies.

Ultra-High –esolution - Mass Spectrometry (UHR-MS): UHR-MS measurements were performed with a Bruker UHR-QTOF matrix 4G instrument with a direct inlet via syringe pump, an ESI source and a quadrupole followed by a Time of Flight (QTOF) mass analyzer.

UV-VIS photometer: UV-VIS spectroscopic measurements were performed using a dual-trace spectrometer Specord® 210 Plus from Analytik Jena AG . The instrument was operated using Win Aspect Plus software. For ConA concentration determination, a Spectral Scan from 270-290 nm was used. The concentration of ConA expressed in terms of the monomer (M= 26 500

g/mol) was then determined at 280 nm applying the Beer-Lambert law with $\varepsilon_{280}= 26380$ M^{-1} cm^{-1} for divalent ConA. The Fmoc deprotection efficiency was surveyed at 301 nm in a spectral scan from 280-320 nm. The Coupling Efficiency was determined at 290 nm in a spectral scan from 280-320 nm. All solutions were placed in a 3.5 mL precision quartz glass cuvette (d = 1 cm) from Hellma Analytics.

Freeze dryer: The final oligomers were freeze dried with an Alpha 1-4 LD plus instrument from Martin Christ Freeze Dryers GmbH. The Main Drying method was set to -55 °C and 0.1 mbar.

DLS and Zeta potential: The hydrodynamic radius of the microgels was determined by dynamic light scattering using Malvern Zetasizer nano ZS. The zeta potential was determined with the same instrument.

Fluorescence Microscopy: An inverted microscope (Olympus IX73, Japan) equipped with an Olympus 60× NA 1.35 oilimmersion objective (Olympus, Japan), and a CMOS camera (DMK 33UX174L, the Imaging Source, Germany) was used for the fluorescence microscopy.

Microplate reader: The fluorescence measurements were conducted using the FLS980 Fluorometer from Edinburgh Instruments and with a CLARIOstar plate reader from BMG Labtech.

Surface Plasmon Resonance Spectroscopy: The measurements were performed on a Biacore X100 from GE Healthcare Life Sciences, Uppsala, Sweden. The sensograms were recorded with the Biacore X100 Control Software and evaluated with the Biacore X100 Evaluation Software. For the measurements a CM5 sensor chip from GE Healthcare Life Science was used

3. Synthesis:

Building Block Synthesis:

1-(Fluorenyl)-3,11-dioxo-7-(pent-4-ynoyl)-2-oxa-4,7,10-triazatetradecan-14-oic acid, TDS [3]

The overall yield of the synthesis was 23%.

^{1}H-NMR (600 MHz, DMSO-d6): δ = 11.84 (br s, O-H), 8.03 (t, $3J$HH = 5.75 Hz, N-H), 7.87 (d, $3J$HH= 7.55 Hz, 2H, Ar-H), 7.67 (dd, $3J$HH= 7.36, $4J$HH = 2.47 Hz, 2H, Ar-H), 7.43 (t, $3J$HH= 7.44 Hz, 3H, Ar-H),7.39 (t, $3J$HH= 5.93 Hz, N-H), 7.37 – 7.30 (m, 2H, ar-H), 4.30 (d , $3J$HH= 6.82 Hz, 1H, C(O)OC**H**2CH), 4.27 (d, $3J$HH= 6.94 Hz, 1H, C(O)OC**H**2CH), 4.21 (t, $3J$HH = 6.79 Hz, 1H, C(O)OCH2C**H**), 3.34 – 3.22 (m, 4H, NC**H**2CH2NH), 3.21 – 3.06 (m, 4H, NCH2C**H**2NH), 2.78 – 2.70 (m, 1H, C(O)CH2CH2CC**H**), 2.54 – 2.47 (m, 2H, C(O)C**H**2CH2CCH, overlapped by DMSO-d5), 2.46 – 2.38 (m, 2H, C(O)CH2C**H**2CCH), 2.37 – 2.25 (m, 4H, C(O)C**H**2C**H**2COOH).

ESI-MS**:** M/z calcd. for C28H31N3O6 [M+H]+ 506.2; found 506.2.

1-(9H-Fluoren-9-yl)-3,14-dioxo-2,7,10-trioxa-4,13-diazaheptadecan-17-oic acid, EDS [4]

The overall yield of the synthesis was 59%.

^{1}H-NMR (600 MHz, DMSO-d6): δ = 11.86 (br s, O-H), 7.94 – 7.85 (m, 3H, N-H, Ar-H), 7.69 (d, $3J$HH= 7.46 Hz, 2H, Ar-H), 7.41 (t, $3J$HH = 7.46 Hz, 2H, Ar-H), 7.33 (t, $3J$HH= 7.50 Hz, 2H, Ar-H), 4.30 (d, $3J$HH= 6.97 Hz, 2H, C(O)OC**H**2CH), 4.21 (t, $3J$HH = 6.92 Hz, 1H, C(O)OCH2C**H**), 3.50 (s, 4H, OC**H**2C**H**2O), 3.44 – 3.35 (m, 4H, NHCH2C**H**2O), 3.19 (q, $3J$HH = 5.82 Hz, 2H, NHC**H**2CH2O), 3.14 (q, $3J$HH = 5.87 Hz, 2H, NHC**H**2CH2O), 2.42 (t, $3J$HH = 6.72 Hz, 2H, C(O)CH2C**H**2COOH), 2.32 (t, $3J$HH = 7.22 Hz, 2H, C(O)C**H**2CH2COOH).

ESI-MS: M/z calcd. for C25H30N2O7 [M+H]+ 471.2; found 471.2, [M+Na]+ 493.2, found 493.2.

Synthesis of (2-azidoethyl)-2,3,4,6-tetra-O-acetyl-α-D-mannopyranoside[5]

The overall yield of the synthesis was 17%.

1H-NMR (300 MHz, CDCl3): δ = 5.34 (dd, 3*J*HH= 10.01, 3.44 Hz, 1H, H3), 5.29 (d, 3*J*HH= 9.99 Hz, 1H, H4), 5.26 (dd, 3*J*HH= 3.33, 1.72 Hz, 1H, H2), 4.86 (d, 3*J*HH= 1.45 Hz, 1H, H1), 4.27 (dd, 3*J*HH= 5.32 Hz, 2*J*HH= 12.26 Hz, 1H, H6), 4.11 (dd, 3*J*HH= 2.35 Hz, 2*J*HH= 12.27 Hz, 1H, H6), 4.06 – 4.01 (m, 1H, H5), 3.89 – 3.83 (m, 1H, OC**H**2CH2N3), 3.69 – 3.63 (m, 1H, OC**H**2CH2N3), 3.52 – 3.40 (m, 2H, OCH2C**H**2N3), 2.15 (s, 3H, OCH3), 2.09 (s, 3H, OCH3), 2.04 (s, 3H, OCH3), 1.99 (s, 3H, OCH3).

ESI-MS: M/z calcd. for C16H23N3O10 [M+NH4]+ 435.2; found 435.3.

Synthesis of TT-Linker: The new trivalent building block TT-linker was synthesized in a three-step procedure.
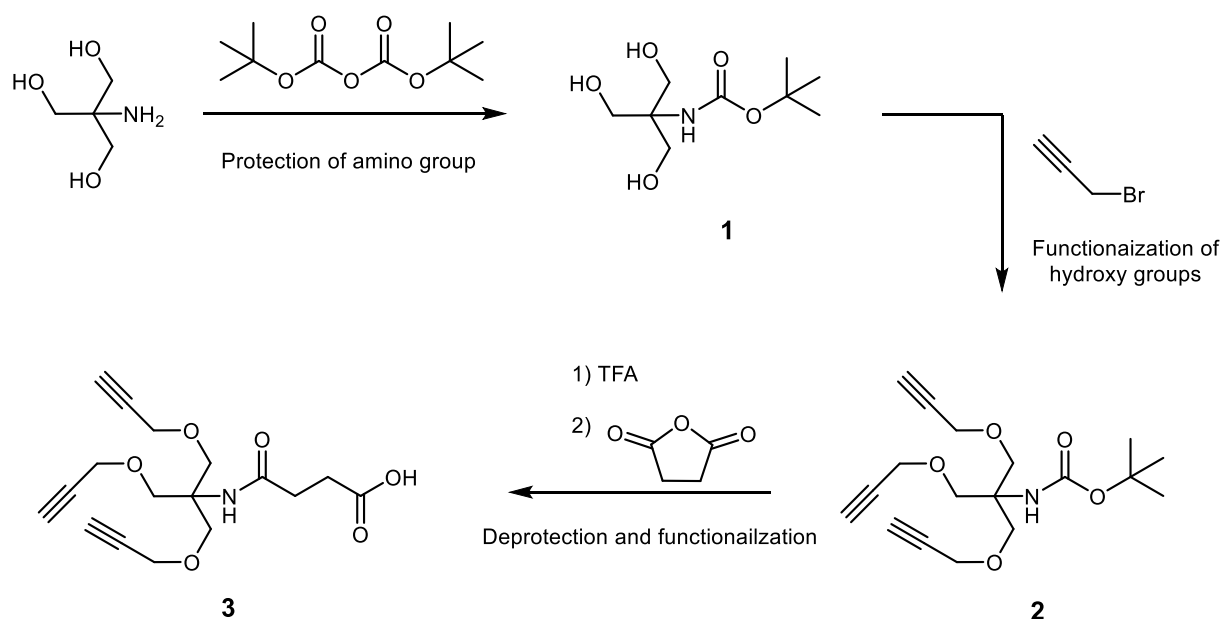
Figure S1: Schematic representation of the synthesis of TT building block.

Synthesis of tert-Butyl (1,3-diehydroxy-2-(hydroxymethyl)p207lycofuncyl)carbamat **1** [6]
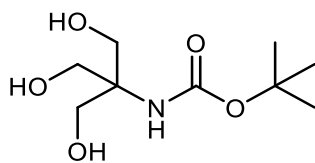
In a 500 ml round bottom flask, 10 g (83 mmol) of tris(hydroxymethyl)-aminomethane was dissolved in a mixture of 50 ml methanol and 50 ml tert-butanol. A solution of 23.42 g (23 ml, 107 mmol) di-207lycofunctidicarbonate in 100 ml tert-butanol was added via a dropping funnel. The reaction solution was stirred at room temperature for 18 hours. The reaction was monitored by thin layer chromatography using an ethyl acetate/ethanol mobile phase (5:1 vol%), followed by staining with anisaldehyde/sulfuric acid. After complete conversion of the starting material, the solvent was concentrated on the rotary evaporator and the product 1 precipitate as a solid. The product was filtered, washed with ice-cold ethyl acetate and dried in vacuo. Product 1 was obtained in the form of a crystalline white solid and dried on the vacuum line.

Yield: 98%

^{1}H NMR (300 MHz, DMSO-d$_6$,): δ (ppm) = 5.73 (s, 1H, NH), 4.47 (t, 3J = 5.7 Hz, 3H, OH), 3.49 (d, 3J = 5.8 Hz, 6H, CH$_2$-OH), 1.37 (s, 9H, CH$_3$).

LC-MS: m/z calculated for C$_9$H$_{19}$NO$_5$ [M+Na]$^+$ 244.2; found 244.2.

*Figure S2: 300 MHz ^{1}H-NMR spectrum of **1** in D$_2$O at 25°C.*

Figure S3: MS-spectrum of **1**.

Synthesis of tert-Butyl (1,3-bis(prop-2-yn-1-yloxy)-2-((prop-2-yn-1-yloxy)methyl)p209lycofuncyl)carbamat **2** [6]

15.5 g (70 mmol) of 1 was dissolved in dry DMF in a 500 ml three-neck flask. 50 g (24.5 ml, 420 mmol) of propargyl bromide (80 wt% in toluene) was added via a dropping funnel in nitrogen atmosphere. The reaction was cooled to 0 °C and 23.5 g (420 mmol) of ground potassium hydroxide was added in portions. The reaction mixture was then heated to 35 °C and stirred under nitrogen atmosphere for 24 hours. The reaction was followed by thin layer chromatography (hexane/ethyl acetate, 7:3 vol%). After completion of the reaction, 100 ml of ethyl acetate was added to the reaction mixture and the mixture was extracted once with 400 ml of ethyl acetate and three times with 300 ml of water. The organic phases were combined and dried over magnesium sulfate. The solvent was removed via rotary evaporator and the crude yellow product was purified by column chromatography (n-hexane/ethyl acetate, 7:3% by volume). Product 2 was isolated as a yellow oil.

Yield: 29 %

^{1}H NMR (300 MHz, CDCl$_3$-d): δ (ppm) = 4.86 (s, 1H, NH), 4.09 (d, $^4J_{HH}$ = 2.4 Hz, 6H, C-CH$_2$-O), 3.72 (s, 6H, O-CH$_2$-C≡CH), 2.39 (t, $^4J_{HH}$ = 2.4 Hz, 3H, CH$_2$-C≡CH), 1.38 – 1.33 (s, 9H, CH$_3$).

LC-MS: m/z calculated for C$_{19}$H$_{25}$NO$_5$ [M+Na]$^+$ 358,4; found 358,2.

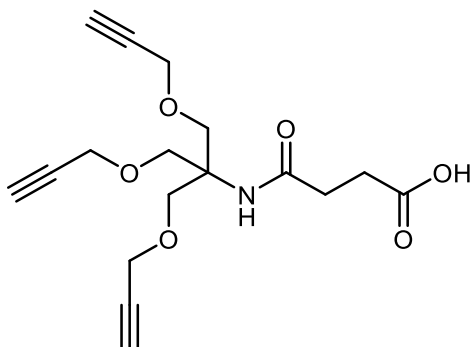Figure S4: 300 MHz ¹H-NMR spectrum of **2** in CHCl₃-d at 25°C.

Figure S5: MS-spectrum of **2**.

Synthesis of 4-((1,3-bis(prop-2-yn-1-yloxy)-2-((prop-2-yn-1-yloxy)methal)propan-2-yl)amino)-4-oxobutanoic acid 3

In a 500 ml round bottom flask, 9 g (26.8 mmol) of 2 was dissolved in 90 ml of dichloromethane. The reaction solution was cooled to 0 °C and 61 ml (536 mmol) of trifluoroacetic acid was slowly added dropwise. The reaction mixture was stirred at room temperature for four hours and the conversion was followed by thin layer chromatography (dichloromethane/methanol, 9/1 vol% + 1 drop of acetic acid). After complete conversion, the dichloromethane solvent was removed on the rotary evaporator. The trifluoroacetic acid was evaporated from the reaction solution by azeotroping with toluene. The dark red crude product was then precipitated in ice-cold diethyl ether, centrifuged, and the diethyl ether phase was rotated in on the rotary evaporator.

The crude product (13.12 g) was placed in a 500 ml round bottom flask and dissolved in 270 ml dichloromethane followed by 2.69 g (26.8 mmol) of succinic anhydride. The pH of the reaction solution was adjusted to pH = 10 by addition of 11.14 ml (80.4 mmol) of triethylamine and stirred at room temperature for three hours. Reaction conversion was followed by thin layer chromatography (dichloromethane/methanol, 10:1 vol % + 1 drop of acetic acid). After complete conversion, the reaction solution was extracted three times with 250 ml of 10% citric acid. The organic phase was dried over magnesium sulfate, and the solvent was removed on the rotary evaporator. The crude product was recrystallized in dichloromethane.

Yield: 67%

^{1}H NMR (300 MHz, CDCl$_3$-d): δ (ppm) = 10.26 (s, 1H, COOH), 5.96 (s, 1H, NH), 4.11 (d, 4J = 2.4 Hz, 6H, C-CH$_2$-O), 3. 79 (s, 6H, O-CH$_2$-C≡CH), 2.63 (t, 4J = 6.9 Hz, 2H, NH-C=O-–H$_2$), 2.51 - 2.42 (m, 5H, H$_2$, CH$_2$-C≡CH, CH$_2$-COOH).

^{13}C NMR (600 MHz, CDCl$_3$-d): δ (ppm) = 177.18 (s, COOH), 172.21 (s, C(=O)NH), 79.57 (s, C-C≡H), 74. 93 (s, C≡H), 68.47 (s, CH$_2$-O), 59.96 (s, tert-C), 58.75 (s, O-CH$_2$), 31.38 (s, CH$_2$COOH), 29.70 (s, CH$_2$(C=O)).

LC-MS: m/z calculated for C$_{17}$H$_{21}$NO$_6$ [M+H]$^+$ 335.4; found 336.2 t$_R$ = 19.56 min. (MeCN/H$_2$O 1:1 vol %).
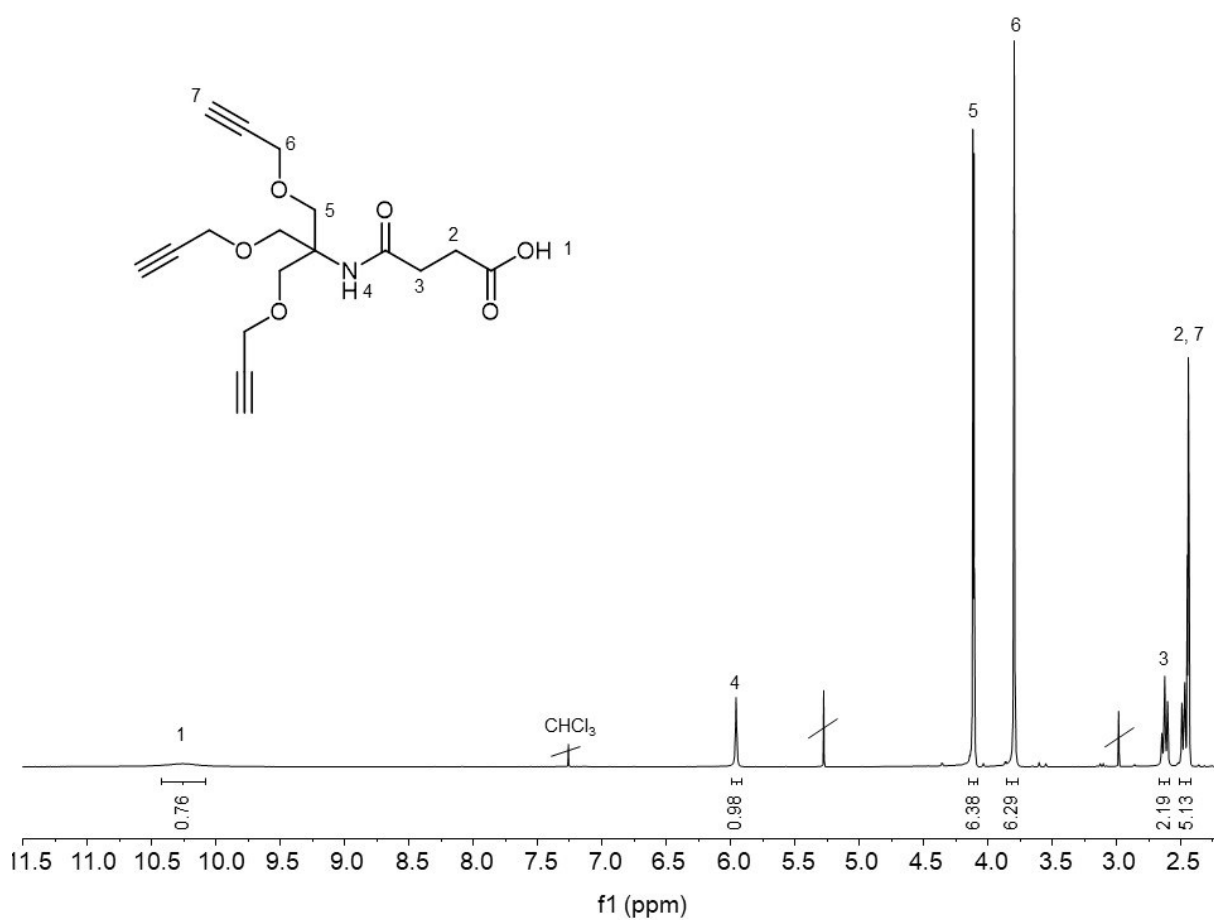
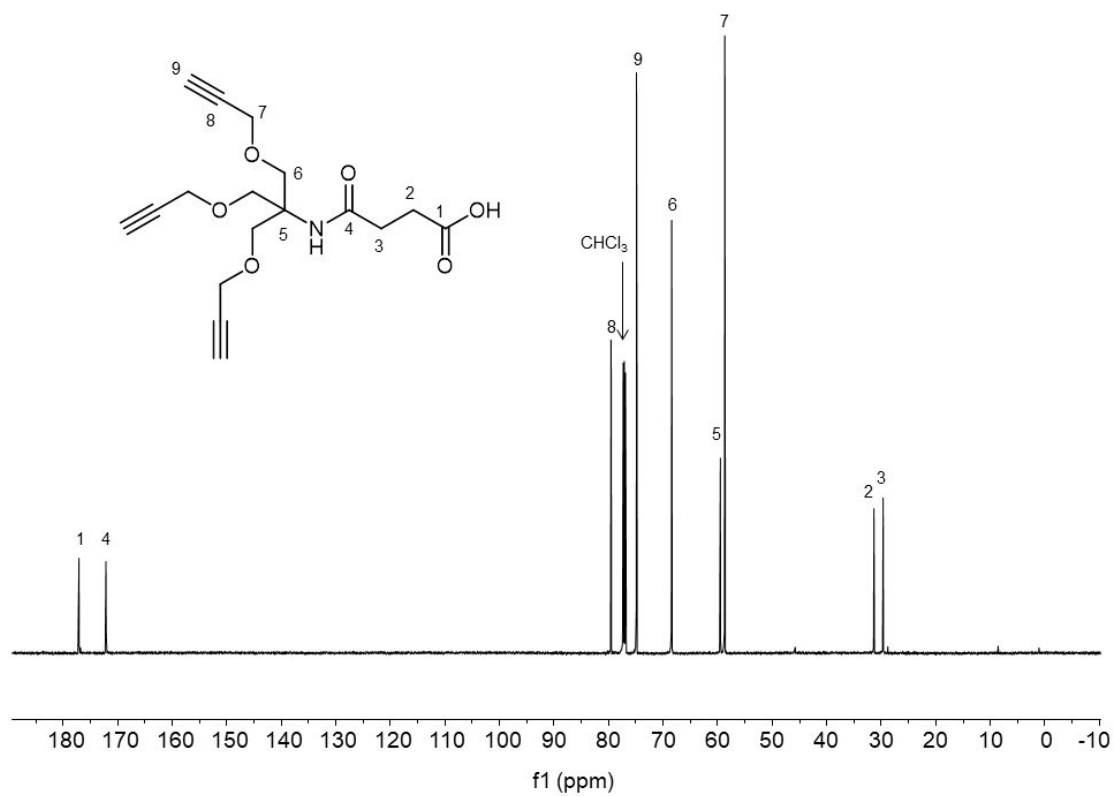Figure S6: 300 MHz ^{1}H-NMR spectrum of **3** in CHCl$_3$-d at 25°C.
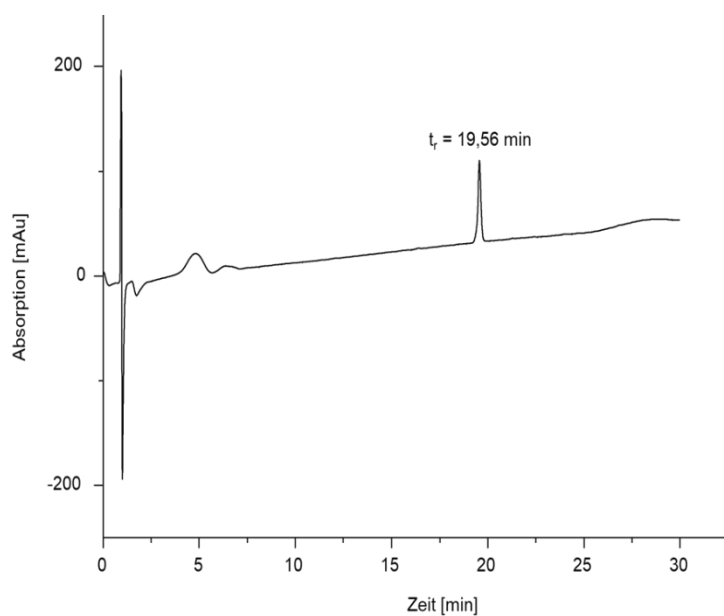
Figure S7: 300 MHz ^{13}C-NMR spectrum of **3** in CHCl$_3$-d at 25°C.

*Figure S8: **3** detected with relative purities >95% by RP-HPLC analysis.*

*Figure S9: HR-ESI-MS of **3**.*

The synthesis of glycooligomer was performed according to the description in section Methods via solid phase polymer synthesis.
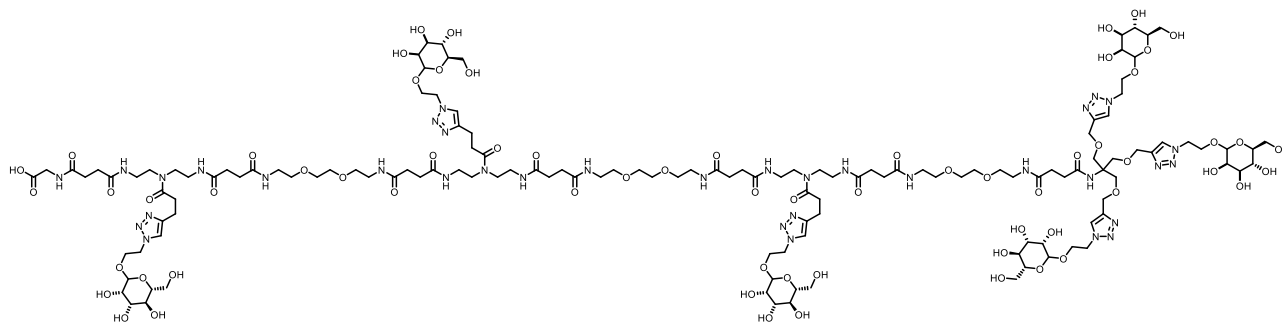
^{1}*H-NMR (600 MHz, D$_2$O): δ (ppm) = 8.04 and 7.87 (2s, 6H, H-9), 4.68-4.91 (m, 12H, H-10), 4.58 (s, 6H, H-13), 4.11- 4.06 (m, 6H, H-11), 3.94-3.89 (m, 6H, H-11'), 3.85 (s, 6H, H-12), 3.75-3.57 (m, 48H, H-3/H4/H-c/H-d/H-f/H-f'), 3.50-3.43 (m, 14H, H-1), 3.38-3.31 (m, 30H, H-5/H-6/H-a) 3.09-2.96 (m, 9H, H-a/H-8) 2.81-2.76 /m, 3H, H-8') 2.58-2.44 (m, 34H, H-2/H-7).*

ESI-MS: exact mass: 3372,5428: [M+2H]$^{2+}$ calculated 1687,3, found 1686,9; [M+3H]$^{3+}$ calculated 1125,2, found 1125,3; [M+4H]$^{4+}$ calculated 844,1, found 844,2; [M+5H]$^{5+}$ calculated 675,5, found 675,6.

RP-HPLC (Linear gradient of 5-95% acetonitrile in water over 30 min at 25∘C): t$_R$ = 5,44 min. Determined relative purity ≥ 95%.
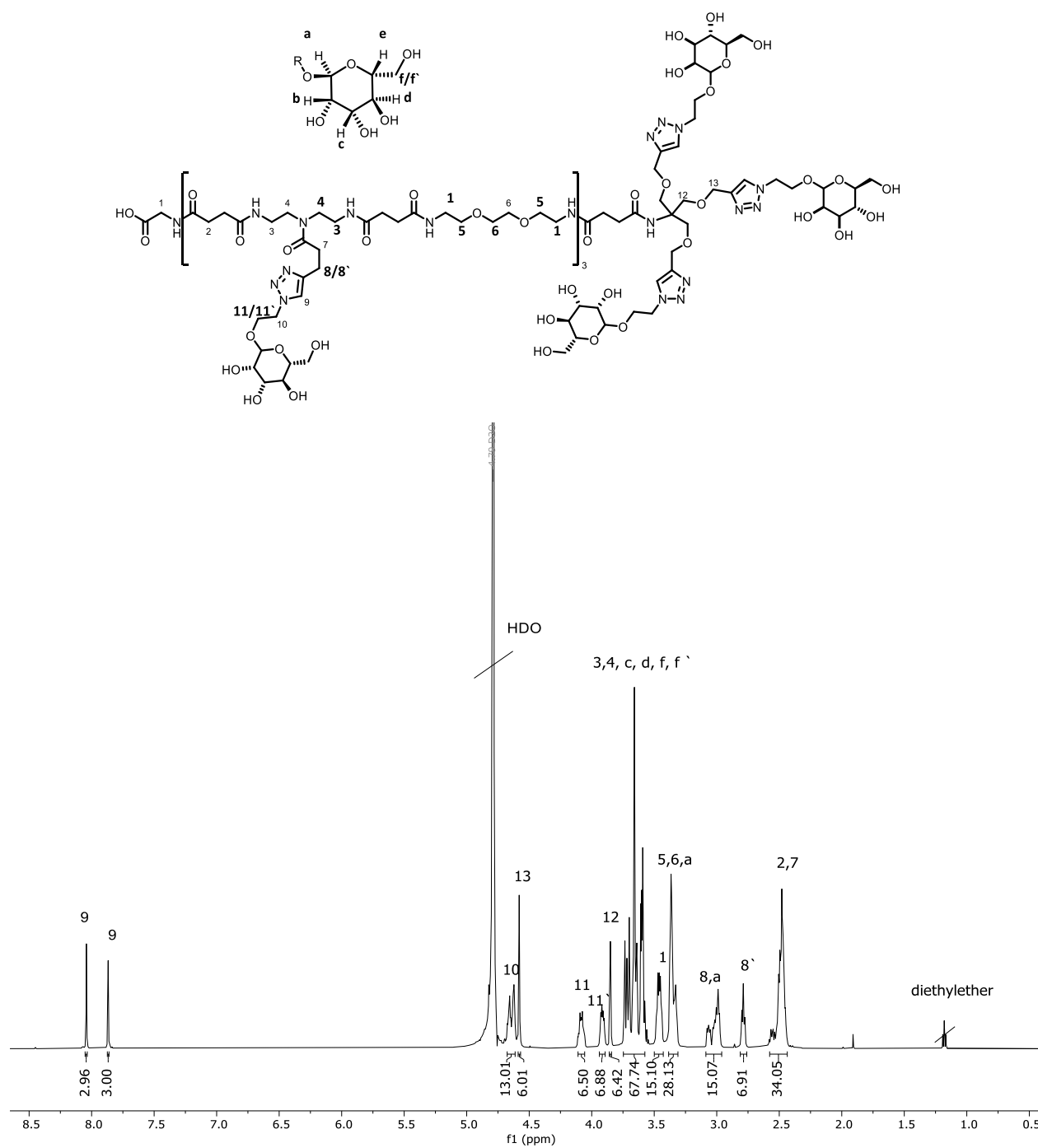
Figure S10: 600 MHz ^{1}H-NMR spectrum of 215lycofunctionalizatcromolecule in HDO at 25°C.
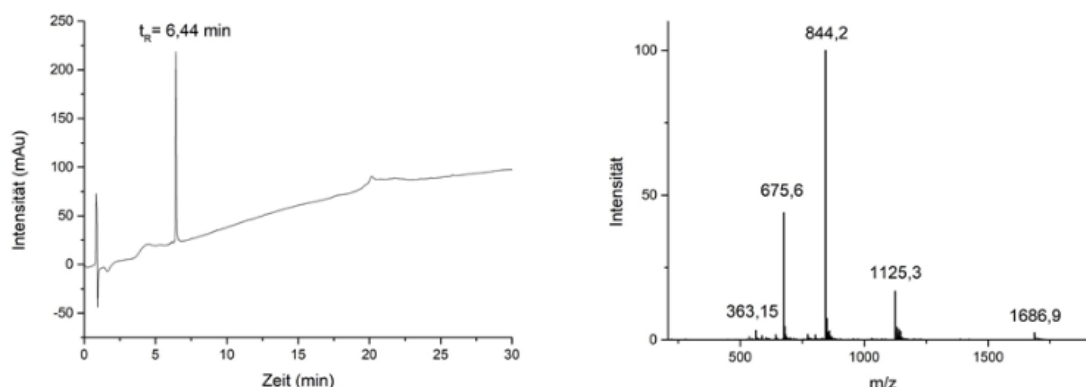
Figure S11: Left: 216lycofunctionalizatcromolecule detected with relative purities >95% by RP-HPLC analysis. Ri216lycofunctionalizatcromolecule

Phenol-Sulphuric Acid Method:

This method was reported by Dubois et al. and was used to estimate the degree of mannose functionalization on the particles. [1] First, to a 250μL particle solution were added 250 μL of a 5 weight percent aqueous phenol solution and 1250 μL of concentrated sulfuric acid. The mixture was then stirred for 30 minutes at room temperature. The concentration of Mannose was determined at 490 nm in a spectral scan of 450-550 nm at 25 °C using the Specord® 210 Plus dual-trace spectrometer from Analytik Jena AG. As a reference, Milli-Q water was used and the absorbance at 490 nm of control series B, C and the zero sample (250 μL water, 250 μL 5 wt% aqueous phenol solution, 1250 μL concentrated sulfuric acid) was subtracted from the absorbance at 490 nm. Measurements were performed in triplicate.

ConA and Mannan experiments:

Glass surfaces were coated with mannan by drop casting. For this purpose, a solution of mannan with a concentration of 1.2 mg·mL-1 in carbonate buffer is prepared. The solution is transferred to an ibidi 8 well slide and left to dry overnight under constant agitation. After washing with PBS buffer for 3 times the wells are filled with the sample solution.

TEM-Microscopy:

The TEM images were performed on a Zeiss TEM 902. A suspension with a concentration of 1 mg/ml in water was used for the images.
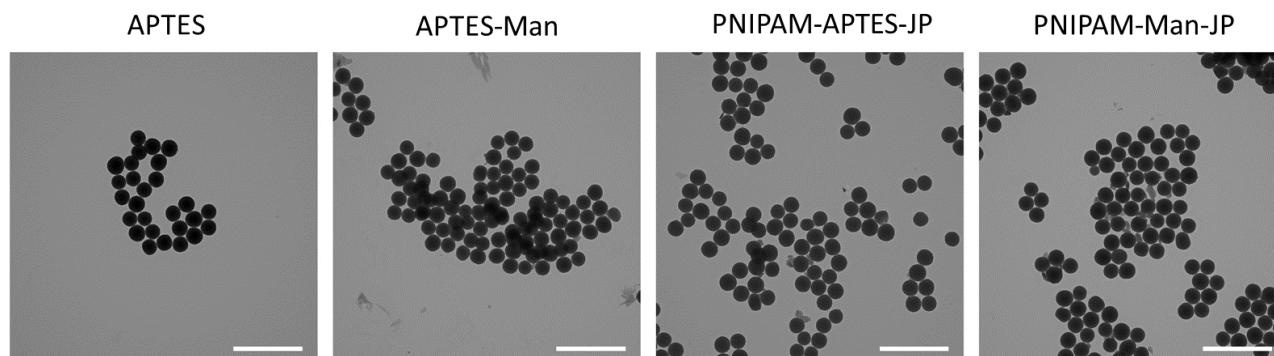
| APTES | APTES-Man | PNIPAM-APTES-JP | PNIPAM-Man-JP |

Figure S12: Overview of functionalized and naked particles measured via TEM. The scale bar represents 1 µm.

Fluorescence microscopy experiment:

RhodamineB-labeled particles were suspended in 10mM PBS buffer (1 mg/ml). A 96-well plate was coated with ConA-FITC in LB buffer (LBB). To do this, 30 µL of ConA solution (200 µg/ml in LBB) was added to the wells (Ibidi slides) and shaken for 2 hours. The wells were then rinsed three times. Stock solution of the particles was then added to the plate and made up with LB buffer to achieve concentrations of 0.5 mg/mL in the plate. The plate was incubated at RT for 1 h and then examined under a fluorescence microscope. Then, αMeMan (200 mM in LBB) was added and incubated overnight at RT. Before taking fluorescence images, the solutions in the well plate were washed three times with LBB. Measurements were performed in two different channels, one with GFP filter for ConA (green) and one with Rhodamine filter for the particles (red). The images were then merged.
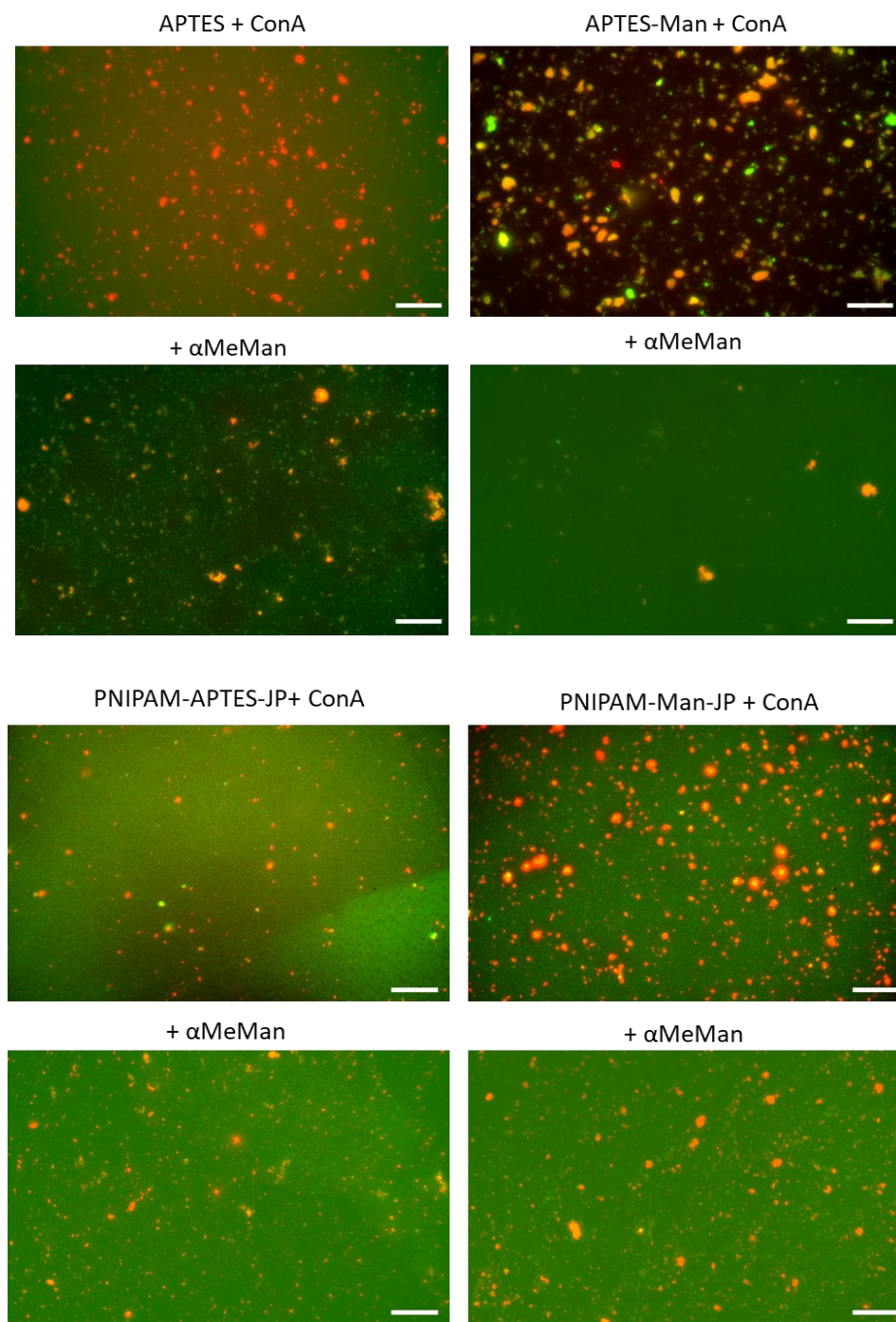
APTES + ConA

APTES-Man + ConA

+ αMeMan

+ αMeMan

PNIPAM-APTES-JP+ ConA

PNIPAM-Man-JP + ConA

+ αMeMan

+ αMeMan

Figure S13: Fluorescence microscopy to investigate the binding of Rhodamin B labeled glyco-particle (red) on FITC-labeled ConA (green) immobilized surface. For APTES-Man big cluster formation is observed and for Janus-Man smaller clusters were observed. After treatment with αMeMan the clusters were washed off the ConA surface. The images were recorded in red and green channels and then merged. The scale bar represents 20 µm.

References:

[1] Dubois, M., Gilles, K. A., Hamilton, J. K., Rebers, P. A. & Smith, Anal. Chem. 1956, 28, 3, 350–356.

[2] M. Hartmann, A. K. Horst, P. Klemm and T. K. Lindhorst, Chem.Commun., 2010, 46, 330-332.

[3] D. Ponader, F. Wojcik, F. Beceren-Braun, J. Dernedde, L. Hartmann, Biomacromolecules, 2012, 13, 1845-1852

[4] Sophia Boden, Franziska Reise, Jessica Kania, Thisbe K. Lindhorst and Laura Hartmann, Macromol. Biosci., 2019, 19, 1800425.

[5] W. Hayes, H. M. I. Osborn, S. D. Osborne, R. A. Rastall, B. Romagnoli, Tetrahedron, 2003, 59, 7983.

[6] Y. M. Chabre, C. Contino-Pépin, V. Placide, T. C. Shiao, and R. Roy, J. Org. Chem., 2008, 73, 14, pp. 5602–5605.

[7] Kirillova, A.; Schliebe, C.; Stoychev, G.; Jakob, A.; Lang, H.; Synytska, ACS Appl Mater Interfaces, 2015, 7 (38), 21218-25.

[8] Berger, S.; Synytska, A.; Ionov, L.; Eichhorn, K.-J.; Stamm, Macromolecules 2008, 41 (24), 9669-9676.

[9] Synytska, A.; Kirillova, A.; Isa, L., ChemPlusChem 2014, 79 (5), 656-661.

[10] Kirillova, A.; Marschelke, C.; Friedrichs, J.; Werner, C.; Synytska, A., ACS Appl Mater Interfaces 2016, 8 (47), 32591-32603.

[11] Kirillova, A.; Ionov, L.; Roisman, I. V.; Synytska, Chemistry of Materials, 2016, 28 (19), 6995-7005.

[12] Kirillova, A.; Stoychev, G.; Synytska, A., Faraday Discussion, 2016, 191, 89-104.

4.5 Sweet carbon dots: synthesis of carbohydrate-functionalized carbon nanoparticles and their cellular uptake

Serap Üclü, Christian Wimmenauer, Cathrin Nollmann, Andrea Liu, Stephen A. Hill, Nicole L. Snyder, Thomas Heinzel and Laura Hartmann

Publication Draft

Own Contribution:

Collaborative project design. Synthesis and purification of building blocks for solid phase polymer synthesis and glycooligomers. Measurement and evaluation of all LC-MS experiments and evaluation of all NMR and UHR spectra. Conjugation of the glycooligomer to the carbon nanoparticles and evaluation of the NMR analysis regarding the carbohydrate loading. Collaborative writing of the publication draft.

Sweet carbon dots: synthesis of carbohydrate-functionalized carbon nanoparticles and their cellular uptake

Serap Üclü[‡a], Christian Wimmenauer[‡b], Cathrin Nollmann[b], Andrea Liu[c], Stephen A. Hill[a], Nicole L. Snyder[c], Thomas Heinzel*[b] and Laura Hartmann*[a,d]

a.   Department for Organic Chemistry and Macromolecular Chemistry, Heinrich Heine University Düsseldorf, Universitätsstraße 1, Düsseldorf 40225, E-mail: laura.hartmann@hhu.de

b.   Institute for Experimental Condensed Matter Physics, Heinrich Heine University Düsseldorf, Universitätsstraße 1, Düsseldorf 40225, E-Mail: thomas.heinzel@hhu.de

c.   Department of Chemistry Davidson College 102 North Main Street, Davidson, NC 28035 USA, E-mail: nisnyder@davidson.edu

d.   Institute for Macromolecular Chemistry, University Freiburg, Stefan-Meier-Str. 31, 79104 Freiburg i.Br., Germany, E.mail: laura.hartmann@makro.uni-freiburg.de

[‡] These authors are contributed equally.

* Corresponding authors

Abstract

Carbon nanoparticles (CNPs) are coupled covalently to various monosaccharides as well as glycooligomers and studied for their interaction with different tumor cell lines overexpressing carbohydrate-recognizing lectin receptors. Glyco-functionalized CNPs (glyco-CNPs) show reduced cell cytotoxicity. Differently monosaccharide-conjugated CNPs show an enhanced uptake rate as compared to both pristine as well as glycooligomer-coated particles. However, coating with mannose, galactose, N-acetylglucosamine or glycooligomers derived thereof does not influence uptake into different cancer cell lines overexpressing mannose-recognizing lectin receptors. The intracellular distribution of the glyco-CNPs shows that – similar –o pristine CNPs - they are preferably stored in the endolysosomal pathway. Overall, this study supports the potential use of glyco-CNPs in biomedical applications but also highlights ongoing challenges when trying to achieve their receptor-mediated uptake via carbohydrate-recognizing cell surface receptors.

1. Introduction

Functionalized nanoparticles and their application in biomedical research have developed into a mature scientific field over the last two decades.[1-3] Multicolor fluorescence spectroscopy based on quantum dots is used routinely within various diagnostic medical protocols.[4-6] Carbon nanoparticles (CNPs)[7,8] are a promising complement to conventional semiconducting quantum dots in these respects, due to their low mass, intrinsic water solubility, easy functionalization and low toxicity.[9,10] They have been used as intracellular pH meter,[11] selectivity enhancers during cisplatin[12] or doxorubicin[13] uptake, or in confocal fluorescence microscopy[14-16], to name just a few examples. Surface functionalization has been employed to further tailor the properties of CNPs for specific applications such as their passivation with polyethyleneglycol (PEG) and use in bacteria[17] and cancer cell[18] uptake and imaging or the improvement of their overall biocompatibility by functionalization with ionic liquid moieties.[19] However, so far there are only a few studies on functionalizing CNPs with carbohydrates.[20] Carbohydrate-functionalization of nanoparticles is a well-established strategy to obtain improved biological properties such as improved biocompatibility or even achieve selective targeting of cell surface receptors.[21] First studies by the Galan group on lactose-functionalized

CNPs has demonstrated the potential to achieve increased bioavailability and obtain diffuse cell internalization into human cancer cells.[22,23] Recently, Cooper et al. showed that lactose-functionalized CNPs localize in the lysosome after cell uptake.[24] While the potential to employ the carbohydrate-functionalization of CNPs to target specific carbohydrate-recognizing receptors such as lectins has been successfully demonstrated with protein arrays[25] and in targeting the adhesins of bacteria[26], it is still unclear if the improved cancer cell internalization is related to a receptor mediated or rather a passive uptake mechanism.[20] A potential specific uptake was shown in a recent study by Ortega-Munoz et al where they observed enhanced uptake of mannose or lactose-functionalized CNPs with cells expressing surface receptors specific either for mannose or lactose, respectively.[27] From the carbohydrate-functionalization of other nanoparticles it is well understood that not only the type but also the linkage or presentation of the carbohydrates can affect receptor interactions.[28,29] Since single carbohydrate-receptor interactions are typically weak, nature as well as chemists employ multivalency – the presentation of multiple carbohydrates on a natural or synthetic scaffold – to increase the overall binding strength.[30] To the best of our knowledge, so far carbohydrate functionalization of CNPs has relied on the conjugation of single carbohydrates (mono- and disaccharides). In this study, we employ our previously established solid phase polymer platform to derive multivalent carbohydrate-functionalized oligomers and attach these to CNPs to now derive carbohydrate-functionalized CNPs (glyco-CNPs) with increased degrees of carbohydrate functionalization in comparison to direct attachment of the according monosaccharides (Figure 1). The glyco-CNPs are then studied for both, their fluorescent properties as well as cell uptake in dependence of the type of carbohydrate f–nctionalization - the type of monosaccharide as well as mono- *vs*. multivalent attachment. Special focus is devoted to human cancer cell lines overexpressing mannose recognizing receptors (MCF-7 and MDA-MB-231) in comparison to a control cell line (HEK-293).
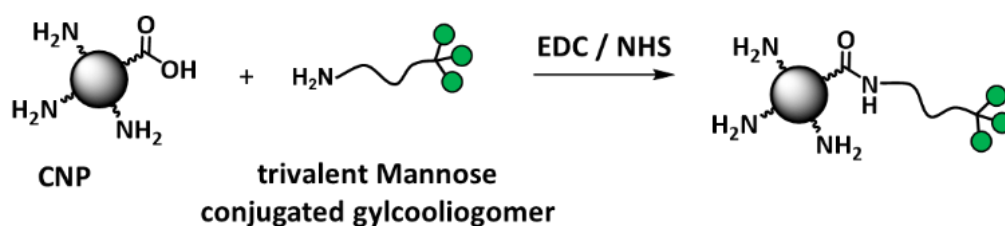

Figure 1: Schematic presentation of the carbohydrate-functionalization of CNPs through attachment of glycooligomers.

2. Experimental details

2.1 Materials for the synthesis

Acetone (≥ 99.8 %), trimethylamine (analytical grade), Toluene (for HPLC) was purchased from Fischer Scientific. Succinic anhydride (≥ 99.0 %) was purchased from Carbolution Chemicals. Diethyl ether (with BHT as inhibitor, ≥ 99.8 %), triisopropylsilane (TIPS) (98 %), (+)-sodium-L-ascorbate (≥99.0 %), chloroform-d (99,8 atom % D), deuteriumoxid-d_2 (99,8 atom % D), dimethylsulfoxid-d_6 (99,8 atom % D), were purchased from Sigma-Aldrich. N,N-Diisopropylethylamine (DIPEA) (≥99 %), potassium hydroxide (≥ 85 %) was purchased from Carl Roth. Methanol (100 %), ethylacetate (>99.9 %), n-hexan (≥99.8 %) and acetic anhydride (99.7 %) were purchased from VWR BDH Prolabo Chemicals. Dimethylformamide (DMF) (99.8 %, for peptide synthesis), $tert$-butanol (≥ 99.0 %), piperidine (99 %), sodium methoxide (97 %), sodium diethyldithiocarbamate (99 %) and copper (II) sulfate (98 %) were purchased from Acros Organics. Dichloromethane (DCM) (99.99 %), Triethylsilane (≥98,0 %), trifluoroacetic acid (≥ 99,0 %) were purchased from Fluorochem. Benzotriazole-1-yl-oxy-tris-pyrroli225lycofunctionalizatexafluorophosphat (PyBOP) were purchased from Iris Biotech GmbH. The anion resin (AG1-X8, quarternary ammonium, 100-200 mesh, acetate form) was purchased from BioRad. TentaGel® resin were purchased from Rapp Polymere. Methyl-α-D-mannopyranoside (>99 %), 1-ethyl-3-(3-dimethylaminopropyl)carbodiimide (EDC), N-hydroxysuccinimide (NHS), Citric acid, anhydrous, was purchased from Alfa Aesar (>99.5 %). Diethylenetriamine was purchased from Merk (>98 %), di-tert-butyldicarbonate (≥99,0 %) was purchased from Novabiochem. Ethanol (>99.9 %). was purchased from Chemsolute.

2.2 Materials for cell culture and uptake experiments

Fetal Bovine Serum purchased from Sigma. RPMI 1640 purchased from Biowest Penicillin/Streptomycin Solution was purchased from Sigma. Dubecco's phosphine buffered saline (DPBS) without Ca^{2+} and Mg^{2+} was purchased from Gibco. Trypsin/EDTA Solution was purchased from Sigma. Ethylenediaminetetraacetic acid di-sodium salt (>99 %) was purchased from Grüssing GmbH. Dublecco's minimal essential medium (DMEM) high glucose with sodium pyruvate was purchased from Biowest. Formaldehyde (4 %) in PBS was purchased from Alfa Aesar. Celllight Lysosomes RFP, BacMam 2.0 and the CyQuant XTT viability assay were purchased from Invitrogen.

See SI for information on methods employed in this study.

2.3 Solid Phase Synthesis of Glycooligomers

Glycooligomers for functionalization of CNPs were synthesized by stepwise coupling and deprotection of tailor-made building blocks (bb) on the solid support – the so-called solid phase polymer synthesis as presented previously.[31-33] The reactions were each carried out in 10 ml polypropylene syringe reactors with a polyethylene frit and a Luer stopper from Multisynthech GmbH. A TentaGel® R Trt resin prefunctionalised with ethylenediamine and a loading of 0.20 mmol/g was used as solid phase and the batch size was 0.1 mmol. Functionalizable triple tribond linker (TT-linker) and an ethylene glycol containing spacer bb EDS were used to build up the backbone of the glycooligomer.

a) Coupling and deprotection of the building blocks: First, the resin was swollen two times for 15 min in DCM and then washed three times with DMF. Coupling of EDS and TT-Linker was performed by shaking for 90 min with a solution of 5 eq of bb, 5 eq of PyBOP, and 10 eq of DIPEA in DMF, followed by washing ten times with DMF. After each bb coupling the resin was shaken with a solution of 25 vol% piperidine in DMF for 15 min to remove the Fmoc protecting group, and then washed three times with DMF. This was followed by shaking again with the piperidine solution for 15 min and washing ten times with DMF.

b) Copper(I)-catalyzed alkyne-azide cycloaddition (CuAAC): Three α-D-mannopyranosides were simultaneously conjugated to theoligomeric backbone via CuAAC. For this, 2.5 eq of (2-azidoethyl)-2,3,4,6-tetra-O-acetyl-α-D-mannopyranoside per alkyne was dissolved in DMF, 30 mol% of sodium ascorbate and 30 mol% of copper sulfate per alkyne was dissolved in water. The copper sulfate solution was drawn up first, followed by the carbohydrate solution, and finally the sodium ascorbate solution. The reactor syringe was covered with aluminum foil and shaken overnight. The resin was then washed three times with a 23 mM solution of sodium diethyldithiocarbamate in DMF/H_2O (1:1, v/v), three times with DMF, and three times with DCM. The washing steps were repeated with the three solutions until no further coloration of the wash solution was observed.

c) Deprotection of mannopyranoside/galactopyranoside side chains: For the deprotection of the acetate groups of the mannopyranoside/galactopranoside analogs attached to the

226

oligomeric backbone, the resin was shaken with a solution of 0.1 M NaOMe in MeOH for 60 min and then washed 10 times with MeOH, 10 times with DMF, and 10 times with DCM.

d) Cleavage from the resin: The resin was shaken with a solution of 65 vol% TFA, 30 vol% TIPS and 5 vol% DCM for 20 min. Afterwards the solution was added to cold diethyl ether and the product precipitated as white solid. The white precipitate was centrifuged off, and the procedure was repeated three times. The solid was then dissolved in water and the product was isolated byeze-drying.

2.4 Microwave assisted carbon nanoparticle synthesis

CNPs were prepared via microwave assisted pyrolysis of citric acid (CA) and diethylenetriamine (DETA) following a modified version of the method originally published by Qu et al.[34], as described in detail elsewhere[35]. 210 g anhydrous CA (Alfa Aesar) and 340 mg DETA (Merk) were added to a 10 ml sealed pressure vessel (CEM), which was subsequently placed in a microwave reaction chamber (CEM Discover). The mixture was treated in the microwave reaction chamber at 180 °C for a hold time of 150 s under continuous stirring. The reaction was quenched with pressurised air cooling after the hold time was reached. Temperature, pressure, and power were recorded during the process. The product was dissolved in DI water and dialyzed in a 100-500 Da dialysis tube (10 ml, Float-A-Lyser) against 2 L of deionized water. The water was exchanged three times within 48 h. The dialysed product was lyophilized and redissolved in phosphate buffered saline (pH 7.4). The as prepared particles have previously been characterized regarding their size and shape with transmission electron microscopy (TEM) and atomic force microscopy (AFM) as well as regarding their chemical composition with X-ray photoelectron microscopy (XPS), CHN elemental analysis and Raman spectroscopy, as described by our group elsewere[35]. To summarize briefly, the results indicate few layer graphitic nanoparticles with an average diameter of 3.3 nm and a mixture of sp2 and sp3 carbon domains, that also contain substantial amounts of nitrogen oxygen.

2.5 Preparation of glyco-CNPs

Prior to glycofunctionalization, one half of the CNPs were combined with succinic anhydride before glyco-functionalization so that the amine groups on their surface would react with the CNPs and change them into extra carboyl groups. These CNPs were referred to as AcCNPs in the following, whereas the untreated CNPs were referred to as CNPs. The CNPs or AcCNPs were dissolved in MilliQ-H_2O and EDC, NHS and the carbohydrates or glycooligomers were added to the solution. The mixtures were stirred overnight at room temperature. The mixture was purified by dialysis (MWCO:500 Da) for 24 hours. Glyco-CNPs were isolated by ze-drying.

2.6 Cell culture

MCF-7 and MDA-MB-231 cells were both cultivated in medium consisting of RPMI 1640 with 10 % foetal bovine serum (FBS) and 1 % penicillin/streptomycin (PS) solution. HEK cells were cultivated in medium consisting of DMEM high glucose (Dublecco's Minimal Essential Medium) with 10 % FBS and 1 % PS solution. All cell lines were split twice per week using trypsin and EDTA as detachment agent, with an exposure tof 3-4 min.

2.7 Confocal microscopy

The cells were imaged with a Zeiss LSM 710 confocal microscope. The cells were seeded at a density of 10.000 cells per well and incubated in their respective full cell culture medium without phenol red and CNPs, in a concentration of 500 µg/ml, 24 h prior to imaging in tissue culture treated 8 well µ-slides (Ibidi). In the cases in which the lysosomes were stained, transient transfection was performed also 24 h prior to the measurement. To facilitate the expression of a fusion protein of the lysosome resident protein LAMP1 and RFP, 20 µl of the reagent Celllight Lysosomes-RFP, BacMam 2.0 (Invitrogen) were added to the respective wells. Right before imaging the medium with CNPs was aspirated out of the well, the cells were washed with PBS and replaced by fresh full medium without phenol red. To image the CNPs the build in 405 nm diode laser was used for excitation. A 543 nm HeNe-laser was used for excitation to image the RFP-td lysosomes.

2.8 Flow cytometry

To determine the cell uptake of CNPs and glyco-CNPs, flow cytometry measurements with the FACSLyric (BD Biosciences) were conducted. The cells were incubated with 500 µg/ml CNPs in full medium without phenol red in a 24 well plate 24 h prior to the flow cytometry measurements. Before the measurement, the medium was aspirated out of the well plates and the cells were washed with 0.5 ml PBS and subsequently treated with 100 µl trypsin and EDTA solution per well for 4 minutes at 37 °C, to facilitate detachment. A total of 600 µl of full medium were added to inactivate the trypsin. The suspension was transferred to round bottom tubes and centrifuged at 300 g for 5 minutes. The supernatant was discarded, and the cells were redistributed in PBS with 0.75 mM EDTA. The suspension was filtered through a cell strainer with a mesh size of 40 µm, to remove remaining clusters and retain single cells in suspension. The cells were transferred to round bottom tubes, again centrifuged at 300 g for 5 minutes and the supernatant was discarded. The cells were fixed with 200 µl of 0.5 % formaldehyde and measured. Since all particles show different quantum yields Φ and extinction coefficients ϵ, the measured signals F cannot be compared to infer the uptake of nanoparticles. Thus, the signals were divided by the Brightness $B = \Phi \epsilon$, which is approximately proportional to the ratio of the number of emitted photons and incident photons per Concentration.

$$Uptake_{mass} \propto \frac{F}{\Phi \epsilon}$$

Since ϵ was determined in relation to the mass concentration in solution the resulting uptake relates to the mass of particles taken up into each cell and can be compared for particle species with differeroperties.

2.9 XTT viability assay

For the XTT Cell Viability Assay a XTT kit was used from Sigma Aldrich. Cells were seeded in 96 well plates at a density of 5000 cells/well in 100 µL full growth medium without phenol red. A total of 10 µL of the respective CNP solution (5 mg/ml) was added to a finale volume of 100 µL per well, to yield a final CNP concentration of 0.5 mg/ml. Incubation was performed for 48 h

at 37 °C and 5 % CO_2. For background subtraction wells only containing 100 µL full growth medium and 10 nM solutions of CNPs in MilliQ water were prepared.

XTT working solution was prepared immediately before use by heating XTT solution to 37 °C and gently swirling the solution until a clear solution is obtained. For one 96 well plate to be tested 5 mL of XTT solution were mixed with 25 µL activation reagent. Subsequently, 50 µL of the activated XTT solution were added to each well to obtain total volumes of 100 µL. After 3 h further incubation at 37 °C and 5 % CO_2 absorbance at 475 nm and background absorbance at 660 nm was recorded ll wells.

2.10 Fluorescence correlation spectroscopy (FCS)

FCS was performed on the Olympus Fluoview 1000 confocal microscope available via the CAi@HHU in Claus Seidel's lab. The setup is modified with a 6-channel detection unit with single photon sensitivity (HydraHarp 400, PicoQuant). Measurements were performed with a U Plan S Apo objective 60x with water immersion and a numeric aperture of 1.2. The particles were excited with a 405 nm continuous wave diode laser and the channels for vv and vh polarization were subsequently correlated using the Kristine software correlator.[54] To yield the diffusional correlation time a model for diffusion through a gaussian focal volume without blinking was fitted to the data. To determine the diffusion coefficient D and the hydrodynamic radius r_H rhodamine 110 with the known diffusion coefficient of $(4.3\pm0.3) \times 10^{-10}$ m^2/s was used as a reference. Rhodamine 110 was excited with a 488 nm pulsed diode laser.

3. Results and discussion

Synthesis of glyco-CNPs

We opted to use CNPs prepared by microwave assisted pyrolysis from citric acid and diethylenetriamine, leading to free carboxy and primary amine groups at the surface of the CNPs, as was previously established.[35] In addition to acceptable fluorescence properties, these CNPs are extremely stable known to have only a marginal toxicity, even on the gene expression level.[36] CNPs have been characterized regarding their size and shape with transmission electron microscopy (TEM) and atomic force microscopy (AFM) as well as regarding their

230

chemical composition with X-ray photoelectron microscopy (XPS), CHN elemental analysis and Raman spectroscopy described previously.[35] In summary, few layer graphitic nanoparticles with an average diameter of 3.3 nm and a mixture of sp2 and sp3 carbon domains, that also contain substantial amounts of nitrogen and oxygen, were obtained. Glycoconjugation on these CNPs was performed by using amide coupling attaching amine-functionalized monosaccharides as well as glycooligomers to carboxy groups present on the CNP surface. To increase the number of carboxy groups and thereby potentially increase the degree of glycoconjugation, one half of the particles was first coupled to succinic anhydride in order to react with the amine groups present on the CNP surface and turn them into additional carboxylic groups (AcCNPs) (see Figure 2).
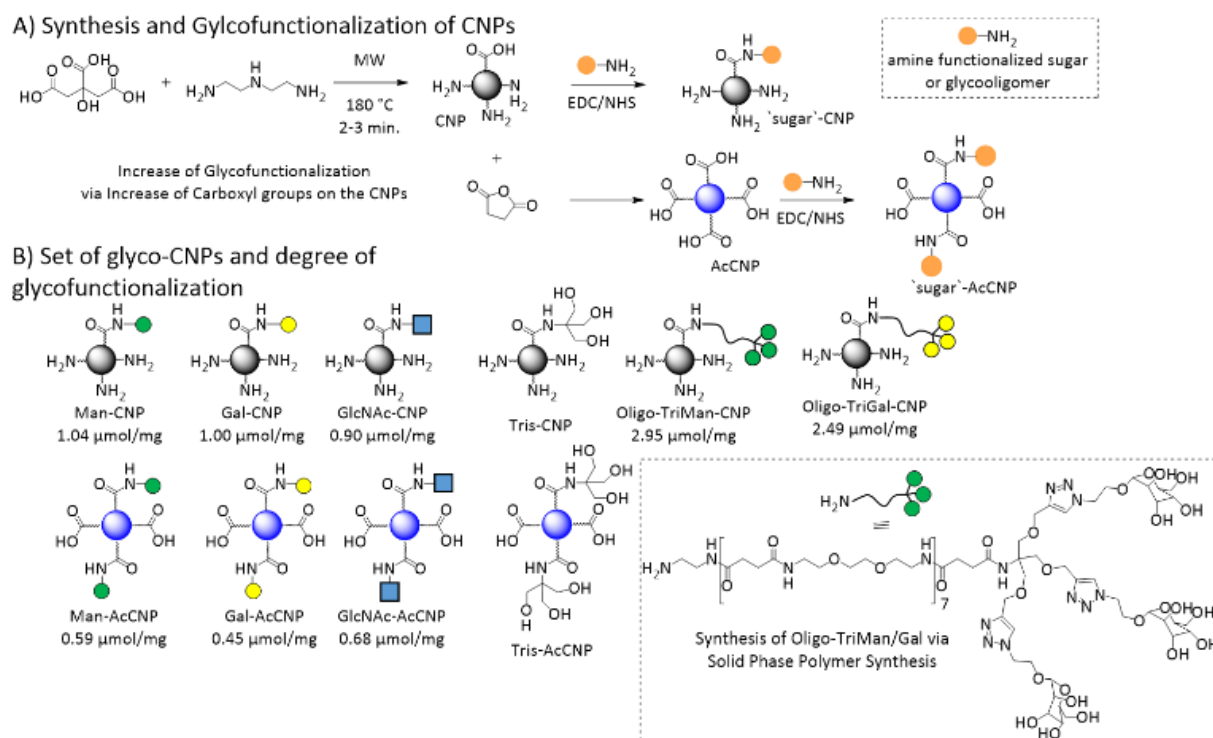
Figure 2: A) Synthesis and glycofunctionalization of CNPs: The CNPs were prepared using microwave assisted pyrolysis from citric acid and diethylenetriamine, leading to free carboxy and primary amine groups at the surface. One part of the CNPs were further functionalized by succinic anhydride (AcCNPs) to increase the carboxyl groups and therefore increase the level of glycofunctionization. The glycofunctionalization was occurred by activation of the carboxyl groups on the surface of the paticles by EDC/NHS. B) Set of synthesized glyco-CNPs and their degree of functionalization degrees determined by ^{1}H-NMR and by using an internal standard. For more details see SI.

For glycofunctionalization, three different monosaccharides were employed: Mannose (Man), *N*-Acetylglucosamine (GlcNAc) and Galactose (Gal). All three monosaccharides are known to bind to different types of cell surface lectin receptors. For example, different human cancer cell lines have been shown to overexpress Mannose receptor (MR) such as MDA-MB-231 breast cancer cells used in this study.[37,38] GlcNAc residues binds to vimentins on the cell surface which occurs in the cytoplasm of all cells.[39,40] Gal functionalized CNPs could potentially target asialoglycoprotein receptors known for their expression on endocytotic cell by hepatocytes, e.g. HepG2 cells.[41] In addition to conjugation of the monosaccharides, glycooligomers presenting multiple copies of Man or Gal were synthesized according to previously established solid phase polymer protocols[42,43] and applied for the functionalization of the CNPs. In short, stepwise conjugation of tailor-made building blocks using standard Fmoc-peptide coupling protocols on resin provided access to sequence-defined oligo(amidoamines) with alkyne side chains, which were used for further conjugation of carbohydrate-azide derivatives via a copper-mediated click reaction (CuAAc)[44] (see the SI for analytical data of the products). All glycooligomers were isolated with a free primary amine group at the C-terminus by using an ethylendiamine-preloaded resin (see Experimental Section for more details). This amine group can then be used to attach the glycooligomers via amide coupling to the carboxylic groups present on the CNP surface. Therefore, CNPs as well as AcCNPs were first activated with EDC/NHS and then conjugated with different amine-functionalized monosaccharides (Man, GlcNAc and Gal), trishydroxyamine (TRIS) as non-carbohydrate control as well the amine-functionalized glycooligomers presenting either Gal or Man (see Figure 2). After the glycofunctionalization the excess of monosaccharides and glycooligomers were removed by dialysis (see ESI, 232lycofuncti.

The multivalent presentation of carbohydrates by use of the glycooligomers is expected to increase binding and thus potentially also cell uptake, e.g. through increased statistical possibility of monosaccharide units encountering a cell surface receptor.[45] Furthermore, the hydrophilic chain installed in the glycooligomer provides flexibility of CNP presented carbohydrates and may potentially increase the accessibility of the ligands in binding to cell surface receptors.

Characterization of glyco-CNPs

First, the degree of functionalization of the glyco-CNPs was studied by ^{1}H NMR, see Figure 3. Hydroquinone was used as an internal standard and compared to either the anomeric protons of the carbohydrate (green frame) or the protons of the triazole ring of the glycooligomers (grey frame), which provided the overall carbohydrate concentration. Successful glycofunctionalization was demonstrated for both AcCNPs and CNPs, but with different degrees of functionalization. While AcCNPs are expected to have more available carboxyl groups that should in turn lead to a higher degree of glycofunctionalization, they show lower carbohydrate concentration as compared to the glycofunctionalized CNP system, see Figure 1C. This can potentially be attributed to steric effects, where – in contrast to–our expectation - the lower carboxylic group density on the CNP surface results in better accessibility for glycofunctionalization. Based on this finding, only the CNP system was used for functionalization with glycooligomers. Confirming and quantifying the degree of carbohydrate functionalization was again performed via NMR (see Figure 2). In the NMR spectra, we identified an EDC contamination (red frame in Figure 3) for the monosaccharide functionalized CNPs. Since we were unable to remove this contamination with extensive washing protocols, this is likely either covalently attached to the surface of the CNPs or strongly adsorbed through ionic interactions. Since the EDC contamination present also after dialysis against high ionic buffer (PBS), covalent binding strikes us as more plausible. This contamination is not seen in the CNPs functionalized with glycooligomers, which could be related to the flexible oligomer covering a larger surface area on the CNPs, thus preventing EDC binding to the surface.

Visualization by TEM was already a challenge for the non-functionalized CNPs, since the particles are composed mainly of carbon and a high-resolution microscope is required due to the dispersion on an ultrathin amorphous carbon lattice. Since the glyco-functionalization by the monosaccharides and glycooligomers also mainly consists of carbon atoms, it can be assumed that no difference between non- and glyco-functionalized CNPs would be observed by TEM. As alternative method, well-established for the analysis of similar small particle systems, diffusion ordered spectroscopy (DOSY) measurements were performed to evaluate the change of the hydrodynamic radii before and after glyco-functionalization for CNP, AcCNP, GlcNAc-CNP and GlcNAc-AcCNP. All derived diffusion coefficients lie in the range of $4 - 6 \times 10^{-10}$ m^2 s^{-1}, corresponding to hydrodynamic radii around 0.4 nm. These values are almost

independent of the type and degree of glyco-functionalization (see Table 1 and SI). However, it is known that CNP synthesis from citric acid and DETA produces smaller fluorophores besides larger particles, which are then likely to be detected by DOSY and fluorescence diffusion spectroscopy. According to Qu et al, larger fragments are detected by NMR after further degradation of small molecules. Also in the NMR in Figure 2, in addition to the typical CNP peaks, peaks of smaller fluorophores can be seen, which may be located at the edges of the CNPs and therefore cannot be separated by dialysis.[46-48]
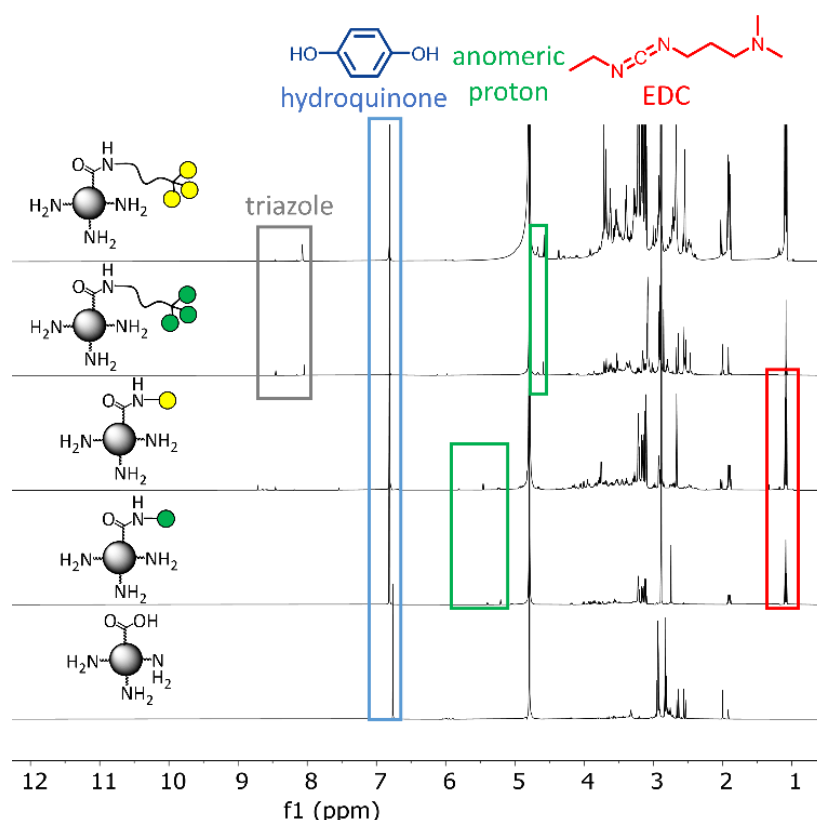
Figure 3: ^{1}H NMR spectra of pristine and functionalized CNPs. Hydroquinone was used as internal standard (blue frame). Green frame: anomeric proton signal of Man/Gal. Grey frame: signal from the protons of the triazole ring of the glycooligomers. The EDC signal is framed in red.

Fluorescence spectroscopy reveals that all functionalized CNPs show a weak but noticeable redshift of the fluorescence maximum, while the shape of the spectrum remains approximately constant (see ESI Table S2).

Table 1: Hydrodynamic radii r_H of non-functionalized CNP and AcCNP and after GlcNAc-functionalization determined by DOSY. The diffusions coefficients were all in the same range between $4\text{-}6 \times 10^{-10}$ m^2 s^{-1}, so that the resulting radii are also in the range of r_H=0.4 nm.

before glycofunctionalization		after glycofunctionalization	
CNP	0.340-0.475	GlcNAc-CNP	0.319-0.493
AcCNP	0.333-0.537	GlcNAc-AcCNP	0.265-0.480

Additionally, comparing CNPs before and after glycofunctionalization, fluorescence correlation spectroscopy (FCS) measurements were performed (see the section experimental details). A simple model was fitted for a diffusing particle species without blinking. Due to the relatively low excitation wavelength (405 nm), there is strong scattering that affects the signal-to-noise ratio compared to larger wavelengths (488 nm), so the resulting autocorrelation function is quite noisy. Assuming that the particles are spherical, the results of the measurements were obtained for hydrodynamic radii in the range of $r_H = 0.5$ nm using rhodamine as the reference molecule. Thus, the results are in agreement with the results of the DOSY measurements.

In summary, the CNPs were successfully functionalized with glycooligomers and incorporation could be determined by ^{1}H-NMR analysis. The particles functionalized with glycooligomers carry a factor of 2 to 3 greater carbohydrates compared to the monosaccharide functionalization, which can be attributed to the trivalent head group on the glycooligomer and verifies that the loading can be increased by using glycooligomers. The analysis by DOSY and FCS demonstrate consistent hydrodynamic radii of $r_H \approx 0.4\text{–}0.5$ nm, which is also compatible with previously reported results from other groups, despite the difficulty of further analyses.

Cell toxicity and cell uptake studies of glyco-CNPs

With this set of glyco-CNPs in hand, we then performed flow cytometry, confocal microscopy, and XTT assays to determine their cellular uptake rates, subcellular distribution, and cell toxicity, respectively. Two breast cancer cell lines MCF-7 and MDA-MB-231 as well as the embryonic kidney cell line HEK-293 were employed in these experiments. Whereas MCF-7

cells were chosen because of their high uptake of CNPs shown in previous studies[15], MDA-MB-231 was chosen as a further breast cancer cell line and overexpress MR on their surface[49,50], and HEK293 with low MR expression was chosen as a non-cancer cell line.[49] In all cell lines tested, glyco-CNPs showed lower cell toxicity as determined via the cell viability 24 h post incubation and quantified via XTT assay as compared to pristine CNPs (see Figure 4). This difference is particularly significant for HEK-293 cells, where pristine CNPs lead to decrease in cell viability to 29 %, whereas glycol-CNPs maintain cell viability at 47-59 %. To quantify cellular uptake, glyco-CNPs were incubated with the different cell lines for 24 h and flow cytometry was performed quantifying the fluorescence per cells as a means236lycoantify the amoung of glyco-CNPs per cell. In order to express the results as the total mass of nanoparticles per cell, the fluorescence intensity of an event detected in flow cytometry was corrected with the brightness of each particle species (see SI, Table S1). Here, the quantum yield under an excitation wavelength of 360 nm was determined using Coumarin 1 with a quantum yield of 0.5 as a reference. The excitation coefficient is obtained from a fit of Lambert-Beer's law to the concentration dependence of the absorption. We define the brightness of a particle type as the product of the quantum yield and the extinction coefficient.
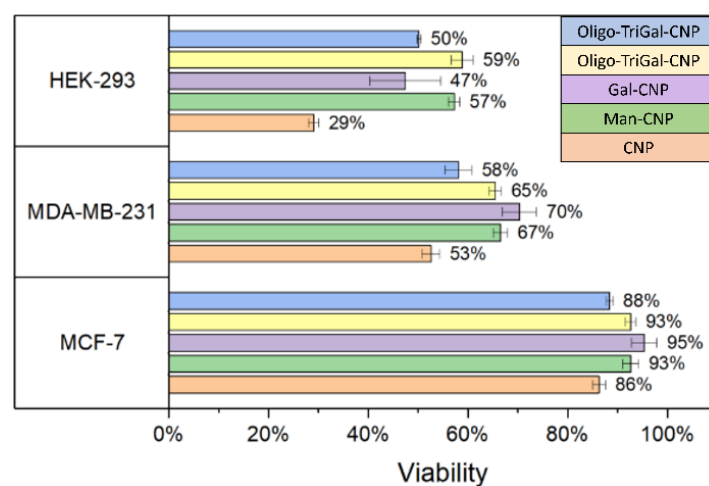
Figure 4: Cell viability after 24h incubation with glyco-CNPs for HEK-293, MDA-MB-231 and MCF-7 cells as determined by XTT assay.

We observe an approximately two- to threefold increase in uptake rate for monosaccharide functionalized CNPs compared to CNPs functionalized with glycooligomers or the pure CNPs (see Figure 5a). This is surprising as the glycooligomer functionalized CNPs have higher number

of carbohydrates per particle (see Figure 1C). However, we also observe almost no difference for the uptake of one type of glycofunctionalization for the different cell lines. Only the Man-functionalized CNPs show a slightly elevated uptake in the HEK-293 cells. This is counterintuitive to the expectation that rather the MR overexpressing cancer cell lines (MDA-MB-231 and MCF-7) should show increased uptake here.

Overall, our results rather indicate a non-specific uptake and seem to show no involvement of carbohydrate recognizing cell surface receptors in the uptake of glyco-CNPs from this study. We tentatively explain this uptake behaviour using the following, qualitative picture: During endocytosis, both pristine and glycoconjugated CNPs are taken up from the encapsulated extracellular solution; the uptake rate is proportional to the density of the CNPs in solution. In addition to this process, monosaccharide-conjugated CNPs may adhere to the outer membrane surface, likely due to non-specific, physical interactions. This picture is commensurate with a quantitative estimation (see SI).

Subcellular localization of glyco-CNPs

While we did not observe any clear influence of the type of carbohydrate on the cellular uptake of glyco-CNPs, it is still relevant to also investigate subcellular distribution. On the one hand this shows that indeed glyco-CNPs can be taken up by the cells and on the other hand this can give additional insights on how glycofunctionalization might affect subcellular distribution. Confocal microscopy revealed that all glyco-CNPs accumulate in small sub-spaces inside MDA-MB-231 cells, which most likely correspond to vesicles in the endo-lysosomal pathway (Figure 3 (b), (c).) This is in agreement with previous studies on pristine CNPs.[15] Pristine and glyco-CNPs share this characteristic subcellular distribution 24 h after their incubation.

To explore this further, MCF-7 and MDA-MB-231 cells were incubated with CNPs, Man-CNPs, Gal-CNPs, Oligo-TriMan-CNPs and Oligo-TriGal-CNPs and labelled lysosomes (see SI, Figure S40 and S41). The colocalization of the CNPs and the fusion protein LAMP-1 indicates that the CNPs are (at least to a large extent) lysosomal cargo. If particles are taken up via endocytosis, the endocytic vesicle usually merges with an early endosome, that matures into a late endosome. If no interaction with other organelles occurs, the late endosome merges with a

237

lysosome, where the particles end up.[51] It was also already previously shown that CNPs with amino groups on the surface tend to be trapped inside of lysosomes owing to the acidotropic behaviour of weakly basic amines.[52] While the lysosomes accumulate in a perinuclear region[53], they never enter the nucleus under physiological conditions. Therefore, the nuclear region is spatially strictly distinct from the lysosomes. While CNPs prepared or modified via other protocols have been shown before to enter the nucleus[52], we do not observe nuclear entry for the glyco-CNPs. The fact that glycoconjugation of the CNPs does not influence the viability of the cells supports the picture that the nanoparticles are captured in the endolysosomal pathway, where they exert only a marginal influence on cellular metabolism.
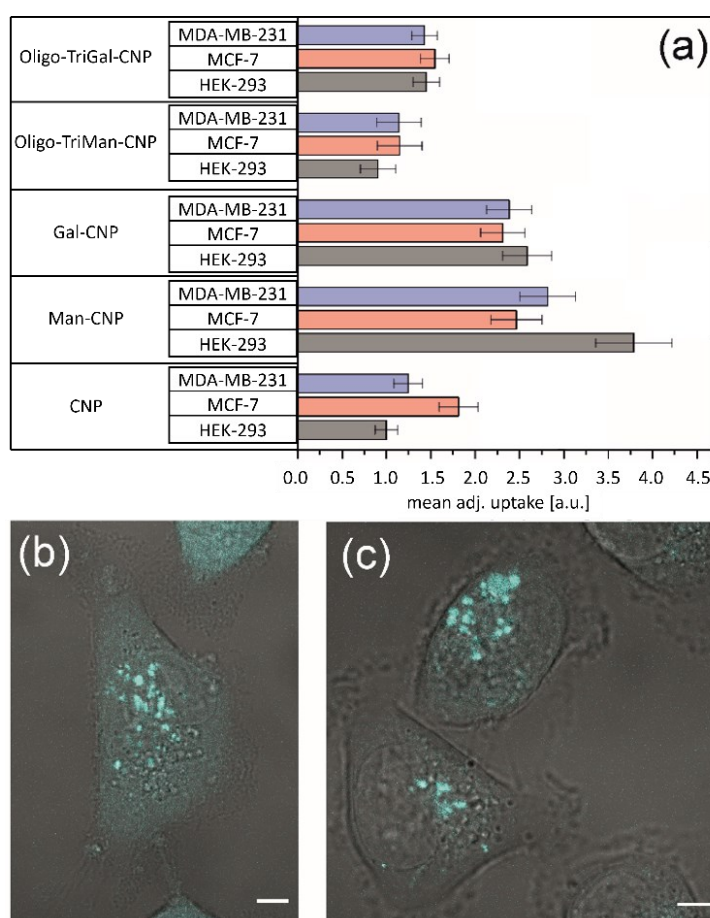
Figure 5: (a) CNP uptake as determined from flow cytometry measurements. Confocal microscopy on MDA-MB-231 cells after uptake of pristine (b) and mannose-conjugated (c), CNPs. The fluorescence signal (cyan) in (b) and (c) was linearly scaled to ensure the best utilization of the dynamic range, while displaying all acquired data. Therefore, (b) and (c) only allow for a qualitative assessment of the subcellular distribution and intensity values may not be quantitatively compared against each other between both images. Quantitative assessments of the uptake are valid based on the values derived from flow cytometry measurements (a). The size of the scale bars is 5 μm.

4. Conclusions

In conclusion, we have prepared a series of glycofunctionalized CNPs using both monosaccharides as well as multivalent glycooligomers. NMR studies were used to verify the conjugation of carbohydrates and glycooligomers to the particle surface and to determine the degree of functionalization. Indeed, CNPs functionalized with glycooligomers enable a two- to threefold increase in the overall degree of carbohydrate functionalization. In comparison to pristine CNPs, glyco-CNPs show reduced cell cytotoxicity. Uptake studies with different cell lines showed an approximately threefold increase for the monosaccharide functionalized CNPs compared to the pristine and glycooligomer-functionalized CNPs. Potentially carbohydrate motifs in the glycooligomers-CNP conjugates are less accessible for interactions with cell surface receptors. However, for CNPs functionalized with different monosaccharides we see only very little difference in their cell uptake despite using cell lines with distinctly different overexpression of carbohydrate recognizing receptors, specifically MR. This indicates that cell uptake of glyco-CNPs of this study is not or only very little cell surface receptor mediated. Nevertheless, confocal microscopy shows that glyco-functionalization does not alter the intracellular distribution in which nanoparticles are preferentially taken up into the endolysosomal pathway, making these glyco-CNPs potentially attractive for cell imaging or drug delivery applications. To further investigate the uptake mechanisms into the cell and enable receptor mediated uptake, future studies could investigate the effects of using more complex oligosaccharide ligands or non-carbohydrate ligands such as antibodies.

References

1 X. Michalet, F. F. Pinaud, L A Bentolila, J M Tsay, S Doose, J J Li, G Sundaresan, A M Wu, S S Gambhir, S Weiss, Science, 2005, **307**, 538.

2 I. L. Medintz, H. T. Uyeda, E. R. Goldman, H. Mattoussi, Nature Materials, 2005, **4**, 435.

3 W. R. Algar, M. Massey, K. Rees, R. Higgins, K. D. Krause, G. H. Darwish, W. J. Peveler, Z. Xiao, H.-Y. Tsai, R. Gupta, K. Lix, M. V. Tran, H. Kim, Chem. Rev., 2021, **121**, 9243.

4 J. Kim, Y. Piao, T. Hyeon, Chem. Soc. Rev., 20, **38**, 372-390.

0   5 L.-L. Chen, L. Zhao, Z.-G. Wang, S.-L. Liu, D.-W. Pang, Small, 20, **18**, 2104567.

0   6 R. Thangam, R. Paulmurugan, H. Kang, Nanomaterials, 2021, **12**, 18.

7 F. Arcudi, L. Đorđević, M. Prato, Acc. Chem. Res. 2019, **52**, 2070.

8 Y. Park, J. Yoo, B. Lim, W. Kwon, S.-W. Rhee, J. Mater. Chem. A, 2016, **4**, 11582.

9 J. Shen, Y. Zhu, X. Yanga, C. Li, Chem. Commun., 2012, **48**, 3686.

10 L. Cao, X. Wang, M. J. Meziani, F. Lu, H. Wang, P. G. Luo, Y. Lin, B. A. Harruff, L. M. Veca, D. Murray, S.-Y. Xie, and Y.-P. Sun, J. Am. Chem. Soc., 2007, **129**, 11318.

11 Wu, Z. L. M. X. Gao, T. T. Wang, X. Y. Wan, L. L. Zhenga, C. Z. Huang, Nanoscale, 2014, **6**, 3868.

12 Sui, X. C. Luo, C. Wang, F. Zhang, J. Zhang, S. Guo, Nanomedicine: Nanotech., Biol. Med., 2016, **12**,1997.

13 X. Gong, Q. Zhang, Y. Gao, S. Shuang, M. M. F. Choi, C. Dong, ACS Appl. Mater. Interfaces, 2016, **8**, 11288.

14 J. Du, N. Xu, J. Fan, W. Sun, X. Peng, Small, 2019, **15**, 1805087.

15 D. Kersting, S. Fasbender, R. Pilch, J. Kurth, A. Franken, M. Ludescher, J. Naskou, A. Hallenberger, C. von Gall, C. J. Mohr, R. Lukowski, K. Raba, S. Jaschinski, I. Esposito, J. C Fischer, T. Fehm, D. Nnieeracher, H. Neubauer, T. Heinzel, Nanotechnology, 2019, **30**, 39.

16 N. Panwar, A. M. Soehartono, K. K. Chan, S. Zeng, G. Xu, J. Qu, P. Coquet, K.-T. Yong, X. Chen, Chem. Rev., 2019, **119**, 9559.

17 Y.-P. Sun, B. Zhou, Y. Lin, W. Wang, K. A. S. Fernando, P. Pathak, M. J. Meziani, B. A. Harruff, X. Wang, H. Wang, P. G. Luo, H. Yang, M. E. Kose, B. Chen, L. M. Veca and S.-Y. Xie, J. Am. Chem. Soc., 2006, **128**, 7756.

18 L. Cao, X. Wang, M. J. Meziani, F. Lu, H. Wang, P. G. Luo, Y. Lin, B. a. A. Harruff, L. M. Veca, D. Murray, S.-Y. Xie and Y.-P. Sun, J. Am. Chem. Soc., 2007, **129**, 11318.

19 Q.-X. Mao, L. Han, Y. Shu, X.-W. Chen, J.-H. Wang, Talanta, 2016, **161**, 54.

20 J. Ramos-Soriano, M. Ghirardello, M. C. Galan, Chem. Soc. Rev., 2022,**51**, 9960.

21 R. Sunasee, C.K. Adokoh, J. Darkwa, R. Narain, Expert Opin Drug Deliv., 2014, **11**, 867.

22 D. Benito-Alifonso, S. Tremel, B. Hou, H. Lockyear, J. Mantell, D.J. Fermin, P. Verkade, M. Berry, M.C. Galan, Angew. Chem. Int. Ed., 2014, **53**, 810.

23 S.A. Hill, D. Benito-Alifonso, D.J. Morgan, S.A. Davis, M. Berry, M.C. Galan, Nanoscale, 2016, **8**, 18630.

24 O. Cooper, E. Eftekhari, J. Carter, B. Mallard, J. Kaur, M.J. Kiefel, T. Haselhorst, Q. Li, J. Tiralongo, ACS Appl. Nano Mater. 2020, **3**, 7804.

25 A.T. Thodikayil, S. Sharma, S. Saha, ACS Appl. Bio Mater. 2021, **4**, 2907.

26 N. Kottari, Y. M. Chabre, R. Sharma, R. Roy, Adv. Polym. Sci., 2013, **254**, 297.

27 M.Ortega-Muñoz, P. Vargas-Navarro, F. Hernandez-Mateo, A. Salinas-Castillo, L. F. Capitan-Vallvey, S. Plesselova, R. Salto-Gonzalez, M. D. Giron-Gonzalez, F. J. Lopez-Jaramillo, F. Santoyo-Gonzalez, Nanoscale, 2019,**11**, 7850.

28 M. Marradi, F. Chiodo, I. García, S. Penadés, *Chem. Soc. Rev., 2013,* **42**, 4728.

29 F. Compostella, O. Pitirollo, A. Silvestri, L. Polito, *Beilstein J. Org. Chem., 2017,* **13**, 1008.

30 C. Fasting, C.A. Schalley, M. Weber, O. Seitz, S. Hecht, B.Koksch, J. Dernedde, C. Graf,. E.-W.Knapp, R. Haag, Angew. Chem. Int. Ed., 2012, **51**, 2.

31 F. Wojcik, S. Mosca, L. Hartmann, J. Org. Chem. 2012, **77**, 4226.

32 F. Jacobi, A. Camaleño de la Calle, S. Boden, A. Grafmüller, L. Hartmann, S. Schmidt, Biomacromolecules, 2018, **19**, 3479.

33 F. Shamout, A. Monaco, G. Yilmaz, C. R. Becer, L. Hartmann, Macromol Rapid Commun., 2020, **41**, 1900459.

34 Qu, D., Zheng, M., Li, J., Xie, Z., & Sun, Z., *Light Sci Appl*., 2015, **4**, e364.

35 D. Rosenblum, N. Joshi, W. Tao, J. M. Karp, D. Peer, Nat. Commun., 2018, **9**, 1410.

36 S. Fasbender, L. Zimmermann, R.P. Cadeddu, M. Luysberg, B. Moll, C. Janiak, T. Heinzel, R. Haas, Sci. Rep., 2019, **9**, 12018.

37 D. Brevet, M. Gary-Bobo, L. Raehm, S. Richeter, O. Hocine, K. Amro, B. Loock, P. Couleaud, C. Frochot, A. Morère, P. Maillard, M. Garcia, J.-O. Durand, Chem. Commun., 2009, **12**, 1475.

38 Y.-H. Tang H.-C. Lin, C.-L. Lai, P.-Y. Chen, C.-H. Lai , Biosens. Bioelectron., 2018, **116**, 100.

39 B. Singh, S. Maharjan, Y.-K. Kim, T. Jiang, M. A. Islam, S.-K. Kang, M.-H. Cho, Y.-J. Choi, C.-Su Cho, J Nanosci Nanotechnol., 2014, **11**, 8356.

40 H. Ise, S. Kobayashi, M. Goto, T. Sato, M. Kawakubo, M. Takahashi, U. Ikeda, T. Akaike, Glycobiology, 2010, **20**, 843.

41 Y. Li, G. Huang, J. Diakur, L.I. Wiebe, Curr. Drug Deliv., 2008, **5**, 299.

42 F' Wojcik, A. G. O'Brien, S. Götze, P. H. Seeberger, L. Har–mann, *Chemistry - A European Journal* **2013**, *19*, 3090-3098.

43 D. Ponader, P. Maffre, J. Aretz, D. Pussak, N. M. Ninnemann, S. Schmidt, P. H. Seeberger, C. Rademacher, G. U. Nienhaus, L. Hartmann, J. *Am. Chem. Soc.,* **2014**, *136,* 2008–2016.

44 S. Hill and M. C. Galan, Beilstein J. Org. Chem., 2017, **13**, 1136.

45 L. Raviv, M. Jaron-Mendelson, A. David, Mol. Pharmaceutics, 2015, **12**, 453.

46 Qu, D., Sun, Z., Mater. Chem. Front., 2020, **4**, 400.

47 Kasperzyk, W., Swiergosz, T., Bednarz, S., Walas, K., Bashmakova N.V., Bogdal, D. Nanosclae, 2018, **10**, 13889.

48 Schneider, J., Rackmeier, C.J., Xiong, Y., von Seckendorff, M., Susha, A.S., Kasak, P., Rogach A.L., J. Phys. Chem. C. 2017, **121**, 2014.

49 Z. Ye, Q. Zhang, S. Wang, P. Bharate, S. Varela-Aramburu, M. Lu, P. H. Seeberger, J. Yin, Chem. Eur. J., 2016, **22**, 15216.

50 D. Brevet, M. Gary-Bobo, L. Raehm, S. Richeter, O. Hocine, K. Amro, B. Loock, P. Couleaud, C. Frochot, A. Morere, P. Maillard, M. Garcia, J. O. Durand, Chem. Commun., 2009, **12**, 1475.

51 L.M. Bareford, P.W. Swaan, Adv. Drug. Deliv. Rev. 2007, 58, 748-758.

52 H. Liu, J. Guo, A.A. Aryee, L. Hua, Y. Sun, Z. Li, J. Liu J, W. Tang, Front. Chem. 2021, **9**, 784851.

53 B. Cabukusta, J. Neefjes J., Traffic, 2018, **19**, 761.

54 S. Felekyan, R. Kühnemuth, V. Kudryavtsev, C. Sandhagen, W. Becker, C.A.M Seidel, C. A. M. Rev. Sci. Instrume., 2005, **76**, 083104.

Supporting Information

Sweet carbon dots: interaction of carbohydrate-functionalized carbon nanoparticles with human cells

Serap Üclü, [‡a] Christian Wimmenauer, [‡b] Cathrin Nollmann,[b] Andrea Liu,[c] Stephen A. Hill,[a] Nicole L. Snyder,[c] Thomas Heinzel*[b] and Laura Hartmann*[a,d]

a. Department for Organic Chemistry and Macromolecular Chemistry, Heinrich Heine University Düsseldorf, Universitätsstraße 1, Düsseldorf 40225, Germany. E-mail: laura.hartmann@hhu.de

b. Institute of Experimental Condensed Matter Physics, Heinrich Heine University Düsseldorf, Universitätsstraße 1, Düsseldorf 40225, E-mail: thomas.heinzel@hhu.de

c. Department of Chemistry Davidson College 102 North Main Street, Davidson, NC 28035 USA E-mail: nisnyder@davidson.edu

d. Institute for Macromolecular Chemistry, University Freiburg, Stefan-Meier-Str. 31, 79104 Freiburg i.Br., Germany, E.mail: laura.hartmann@makro.uni-freiburg.de

‡ These authors contributed equally

* Corresponding authors

1. Instrumentation:

Nuclear Magnetic Resonance Spectroscopy (¹H-NMR) and DOSY

¹H-NMR (600 MHz, 300 MHz), ¹³C-NMR and DOSY spectra were recorded on a B–uker AVANCE III - 600. Chemical shifts of all NMR spectra were reported in delta (δ) expressed in parts per million (ppm). For ¹H-NMR, the residual, non-deuterated solvent was used as internal standard (δ 4.79 ppm for D_2O, δ 7.26 ppm for $CDCl_3$). The following abbreviations are used to indicate the multiplicities: s, singlet, d, doublet; t, triplet; m multiplet.–

Reversed Phase - High Pressure Liqui– Chromatography - Mass Spectrometry (RP-HPLC-MS)

Analyses were run on an Agilent 1260 Infinity instrument equipped with a variable wavelength detector (VWD) (set to 214 nm) and a 6120 Quadrupole LC/MS with an Electrospray Ionization (ESI) source (operated in positive ionization mode in a m/z range of 200 to 2000). As HPLC column a Poroshell 120 EC-C18 (3.0×50 mm, 2.5 µm) RP column from Agilent was used. The mobile phases cannd B were H_2O/ACN (95 %/5 %) and H_2O/ACN (5 %/95 %), respectively. Both mobile phases contained 0.1 % of formic acid. Samples were analyzed at a flow rate of 0.1 mL/min using a linear gradient starting with 100 % mobile phase A reaching 50 % mobile phase B within 30 min. The temperature of the column compartment was set to 25 °C. UV and MS spectral analysis was performed within the OpenLab ChemStation software for LC/MS from Agilent Technologies.

Microplate reader

The fluorescence measurements were conducted using the FLS980 Fluorometer from Edinburgh Instruments and with a CLARIOstar plate reader from BMG Labtech

Optical spectroscopy

Excitation emission matrices (EEM) and absorption spectra of the products were measured with a Horiba Duetta Spectrometer. The fluorescence quantum yields (QY) were determined with the method of Williams et al..[1] To elaborate briefly, the absorption A_x at the wavelength of interest and the spectrally integrated emission signal $E_x = \int F_x d\lambda$, when exited at the

wavelength of interest, of the sample as well as the absorption A_{ref} and integrated emission signal E_{ref} of a reference fluorophore with a known QY Φ_{ref} are determined at different concentrations. Via linear regression to the plot of F_i against A_i, the slope $m_i = \dfrac{dF_i}{dA_i}$ was found for the sample and the reference. The QY of the sample is calculated with the expression $\Phi_x = \Phi_{\text{Ref}} \dfrac{m_x}{m_{ref}} \dfrac{n_x^2}{n_{ref}^2}$, with the refractive indices of the solvent of the sample n_x and the reference fluorophore n_{ref}. Coumarin 1 in ethanol with a QY of 0.50 was used as a reference.[2]

The extinction coefficient ϵ was determined from a linear fit to the plot of absorption against the concentration applying Lambert-Beers-law $A = \epsilon dc$, with the concentration c and the length of the optical path d. Since there is a high degree of uncertainty in the molar mass of the particles, the concentration is measured in mass per volume.

2. Synthesis and characterization:

Building Block Synthesis:

The synthesis of EDS, Man-N₃ and Gal-N₃ were proceeded according to literature. [3-5]

Synthesis of TT: The new trivalent building block TT-linker was synthesized in a three-step procedure.

Figure S1: Schematic representation of the synthesis of TT building block.

Synthesis of *tert*-Butyl (1,3-diehydroxy-2-(hydrox247lycofuncpropan-2-yl)carbamat **1** [6]

In a 500 ml round bottom flask, 10 g (83 mmol) of tris(hydroxymethyl)-aminomethane was dissolved in a mixture of 50 ml methanol and 50 ml tert-butanol. A solution of 23.42 g (23 ml, 107 247lycofunctirt-butyl dicarbonate in 100 ml tert-butanol was added via a dropping funnel. The reaction solution was stirred at room temperature for 18 hours. The reaction was monitored by thin layer chromatography using an ethyl acetate/ethanol mobile phase (5:1 vol%), followed by staining with anisaldehyde/sulfuric acid. After complete conversion of the starting material, the solvent was concentrated on the rotary evaporator and the product 1 precipitate as a solid. The product was filtered, washed with ice-cold ethyl acetate and dried in vacuo. Product 1 was obtained in the form of a crystalline white solid and dried on the vacuum line.

Yield: 98 %

1H NMR (300 MHz, DMSO-d6,): δ (ppm) = 5.73 (s, 1H, NH), 4.47 (t, 3J = 5.7 Hz, 3H, OH), 3.49 (d, 3J = 5.8 Hz, 6H, CH2-OH), 1.37 (s, 9H, CH3).

LC-MS: m/z calculated for C9H19NO5 [M+Na]+ 244.2; found 244.2.

Figure S2: 300 MHz ¹H-NMR spectrum of **1** in D₂O at 25°C.

Figure S3: MS-spectrum of **1**.

Synthesis of *tert*-Butyl (1,3-bis(prop-2-yn-1-yloxy)-2-((prop-2-yn-1-yloxy249lycofuncpropan-2-yl)carbamat **2** [6]

15.5 g (70 mmol) of 1 was dissolved in dry DMF in a 500 ml three-neck flask. 50 g (24.5 ml, 420 mmol) of propargyl bromide (80 wt% in toluene) was added via a dropping funnel in nitrogen atmosphere. The reaction was cooled to 0 °C and 23.5 g (420 mmol) of ground potassium hydroxide was added in portions. The reaction mixture was then heated to 35 °C and stirred under nitrogen atmosphere for 24 hours. The reaction was followed by thin layer chromatography (hexane/ethyl acetate, 7:3 vol%). After completion of the reaction, 100 ml of ethyl acetate was added to the reaction mixture and the mixture was extracted once with 400 ml of ethyl acetate and three times with 300 ml of water. The organic phases were combined and dried over magnesium sulfate. The solvent was removed via rotary evaporator and the crude yellow product was purified by column chromatography (n-hexane/ethyl acetate, 7:3% by volume). Product 2 was isolated as a yellow oil.

Yield: 29 %

^{1}H NMR (300 MHz, CDCl$_3$-*d*): δ (ppm) = 4.86 (s, 1H, NH), 4.09 (d, $^4J_{HH}$ = 2.4 Hz, 6H, C-CH$_2$-O), 3.72 (s, 6H, O-CH$_2$-C≡CH), 2.39 (t, $^4J_{HH}$ = 2.4 Hz, 3H, CH$_2$-C≡CH), 1.38 − 1.33 (s, 9H, CH$_3$).

LC-MS: m/z calculated for C$_{19}$H$_{25}$NO$_5$ [M+Na]$^+$ 358,4; found 358,2.

*Figure S4: 300 MHz ^{1}H-NMR spectrum of **2** in CHCl$_3$-d at 25°C.*
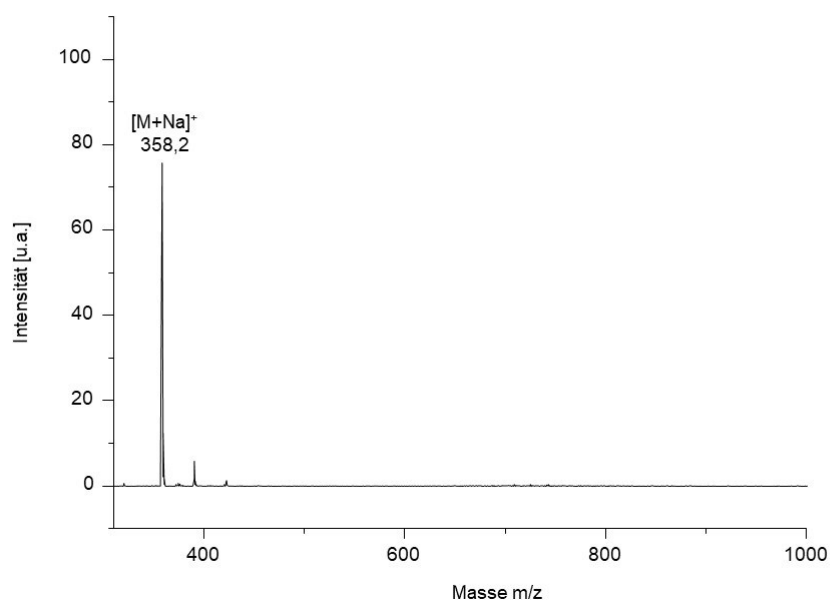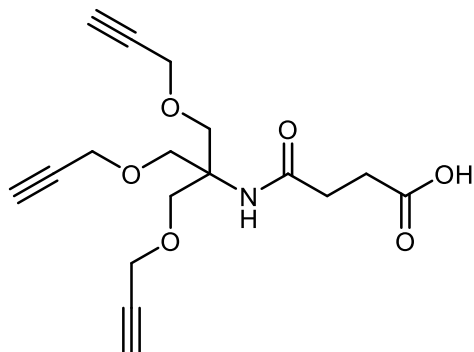

*Figure S5: MS-spectrum of **2**.*

Synthesis of 4-((1,3-bis(prop-2-yn-1-yloxy)-2-((prop-2-yn-1-yloxy)methal)propan-2-yl)amino)-4-oxobutanoic acid *3*

In a 500 ml round bottom flask, 9 g (26.8 mmol) of 2 was dissolved in 90 ml of dichloromethane. The reaction solution was cooled to 0 °C and 61 ml (536 mmol) of trifluoroacetic acid was slowly added dropwise. The reaction mixture was stirred at room temperature for four hours and the conversion was followed by thin layer chromatography (dichloromethane/methanol, 9/1 vol% + 1 drop of acetic acid). After complete conversion, the dichloromethane solvent was removed on the rotary evaporator. The trifluoroacetic acid was evaporated from the reaction solution by azeotroping with toluene. The dark red crude product was then precipitated in ice-cold diethyl ether, centrifuged, and the diethyl ether phase was rotated in on the rotary evaporator.

The crude product (13.12 g) was placed in a 500 ml round bottom flask and dissolved in 270 ml dichloromethane followed by 2.69 g (26.8 mmol) of succinic anhydride. The pH of the reaction solution was adjusted to pH = 10 by addition of 11.14 ml (80.4 mmol) of triethylamine and stirred at room temperature for three hours. Reaction conversion was followed by thin layer chromatography (dichloromethane/methanol, 10:1 vol % + 1 drop of acetic acid). After complete conversion, the reaction solution was extracted three times with 250 ml of 10% citric acid. The organic phase was dried over magnesium sulfate, and the solvent was removed on the rotary evaporator. The crude product was recrystallized in dichloromethane.

Yield: 67%

^{1}H NMR (300 MHz, CDCl3-d): δ (ppm) = 10.26 (s, 1H, COOH), 5.96 (s, 1H, NH), 4.11 (d, 4J = 2.4 Hz, 6H, C-CH2-O), 3. 79 (s, 6H, O-CH2-C≡CH), 2.63 (t, 4J = 6.9 Hz, 2H– NH-C=O-CH2), 2.51 - 2.42 (m, 5H, H2, CH2-C≡CH, CH2-COOH).

^{13}C NMR (600 MHz, CDCl3-d): δ (ppm) = 177.18 (s, COOH), 172.21 (s, C(=O)NH), 79.57 (s, C-C≡H), 74. 93 (s, C≡H), 68.47 (s, CH2-O), 59.96 (s, tert-C), 58.75 (s, O-CH2), 31.38 (s, CH2COOH), 29.70 (s, CH2(C=O)).

LC-MS: m/z calculated for $C_{17}H_{21}NO_6$ [M+H]+ 335.4; found 336.2 t_R = 19.56 min. (MeCN/H$_2$O 1:1 vol %).
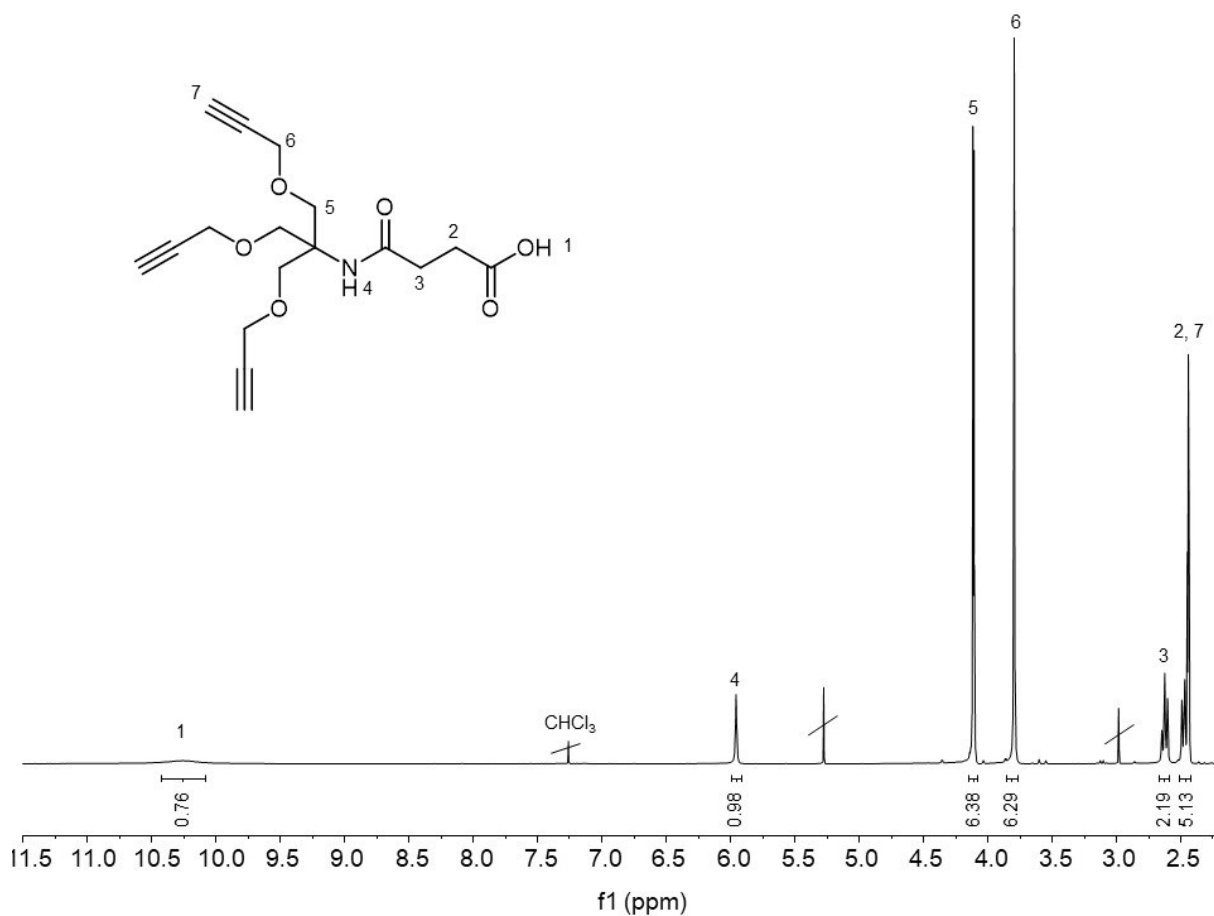
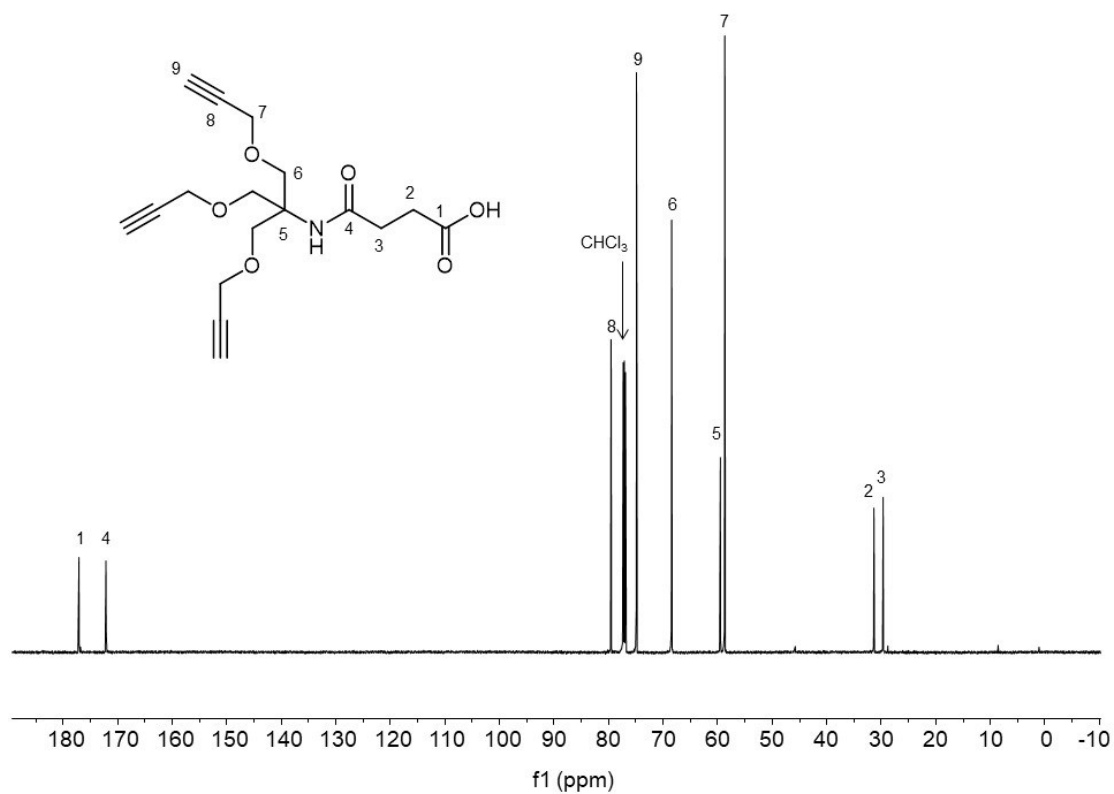*Figure S6: 300 MHz ^{1}H-NMR spectrum of **3** in CHCl$_3$-d at 25°C.*

*Figure S7: 300 MHz ^{13}C-NMR spectrum of **3** in CHCl$_3$-d at 25°C.*

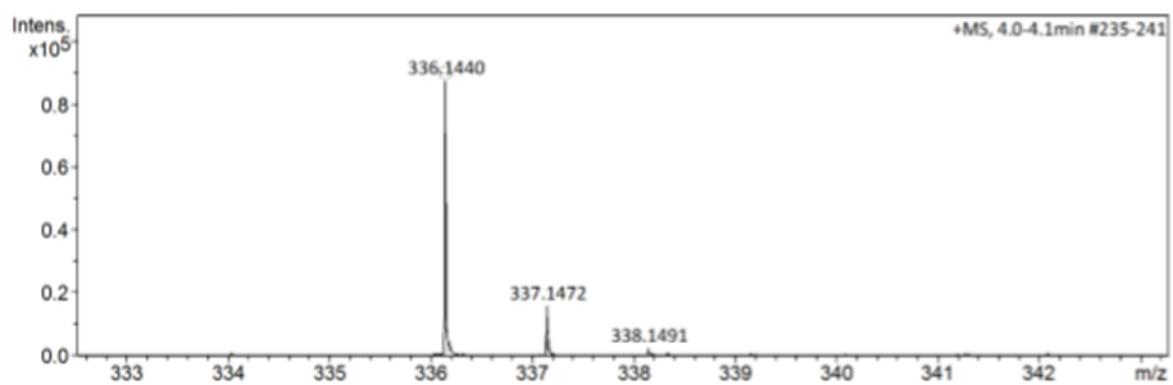*Figure S8: **3** detected with relative purities >95% by RP-HPLC analysis.*

Figure S9: HR-ESI-MS of 3.

Oligo-TriMan

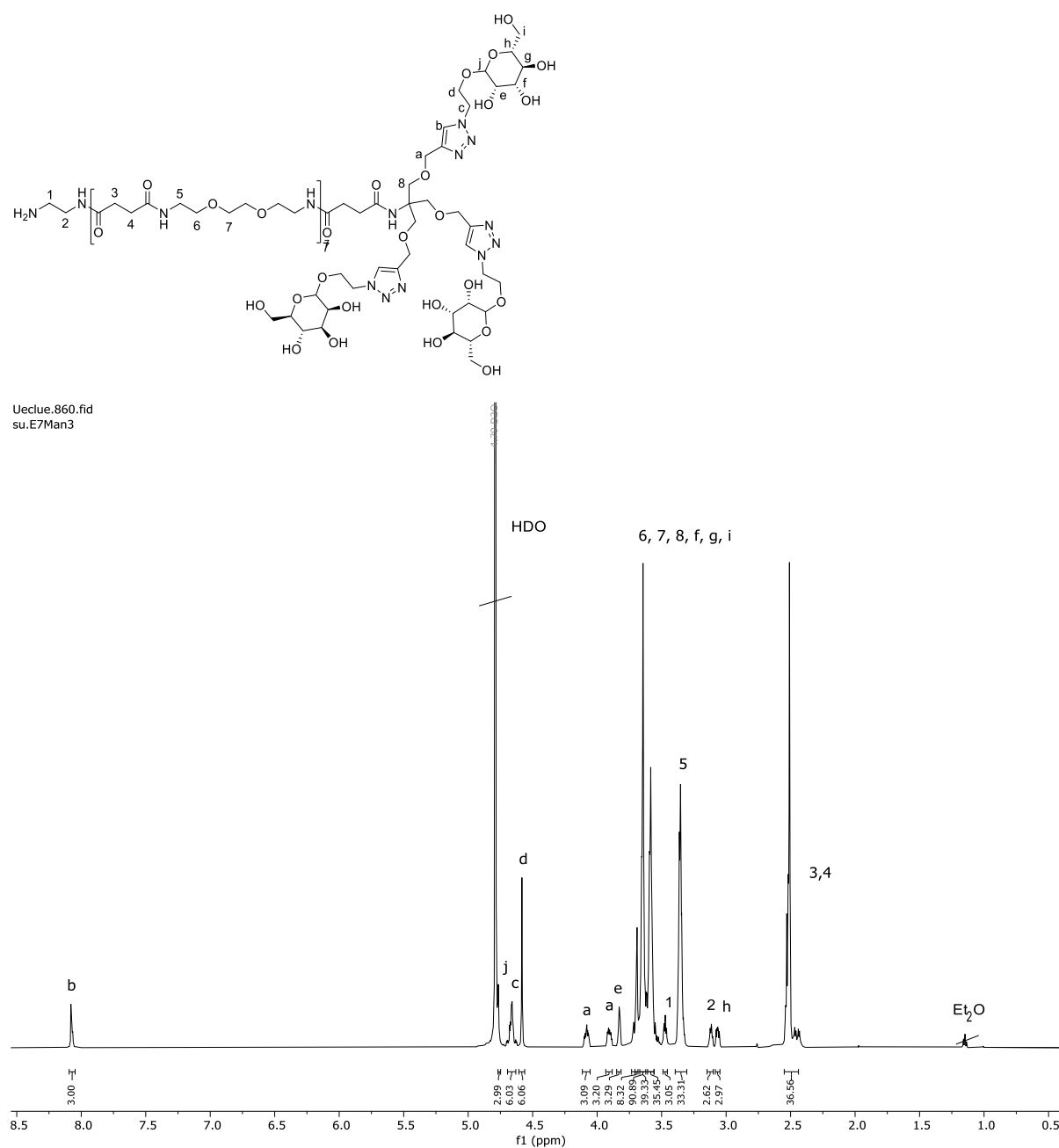*Figure S10: 600 MHz ^{1}H-NMR spectrum of Oligo-TriMan in D$_2$O at 25°C.*

^{1}H NMR (600 MHz, D$_2$O) δ 8.10 – 8.04 (m, 3H), 4.76 (d, *J* = 1.7 Hz, 3H), 4.66 (d, *J* = 3.9 Hz, 6H), 4.58 (s, 6H), 4.08 (ddt, *J* = 10.7, 6.9, 3.4 Hz, 3H), 3.90 (ddd, *J* = 11.1, 5.7, 3.7 Hz, 3H), 3.83 (ddd, *J* = 5.2, 3.3, 1.8 Hz, 3H), 3.73 – 3.56 (m, 84H), 3.48 (q, *J* = 6.1, 4.7 Hz, 3H), 3.36 (q, *J* = 5.4 Hz, 33H), 3.12 (q, *J* = 6.0 Hz, 3H), 3.06 (ddd, *J* = 9.7, 5.8, 2.3 Hz, 3H).
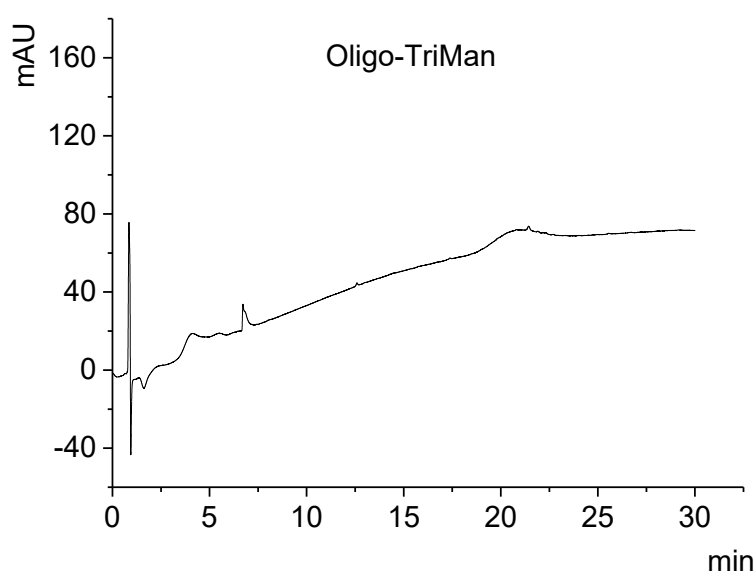
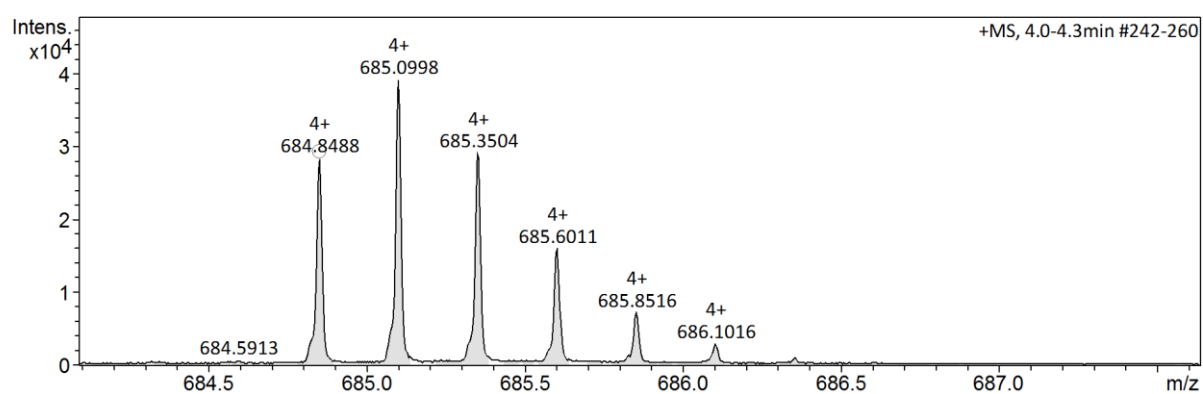*Figure S11: Oligo-TriMan detected with relative purities >95% by RP-HPLC analysis.*

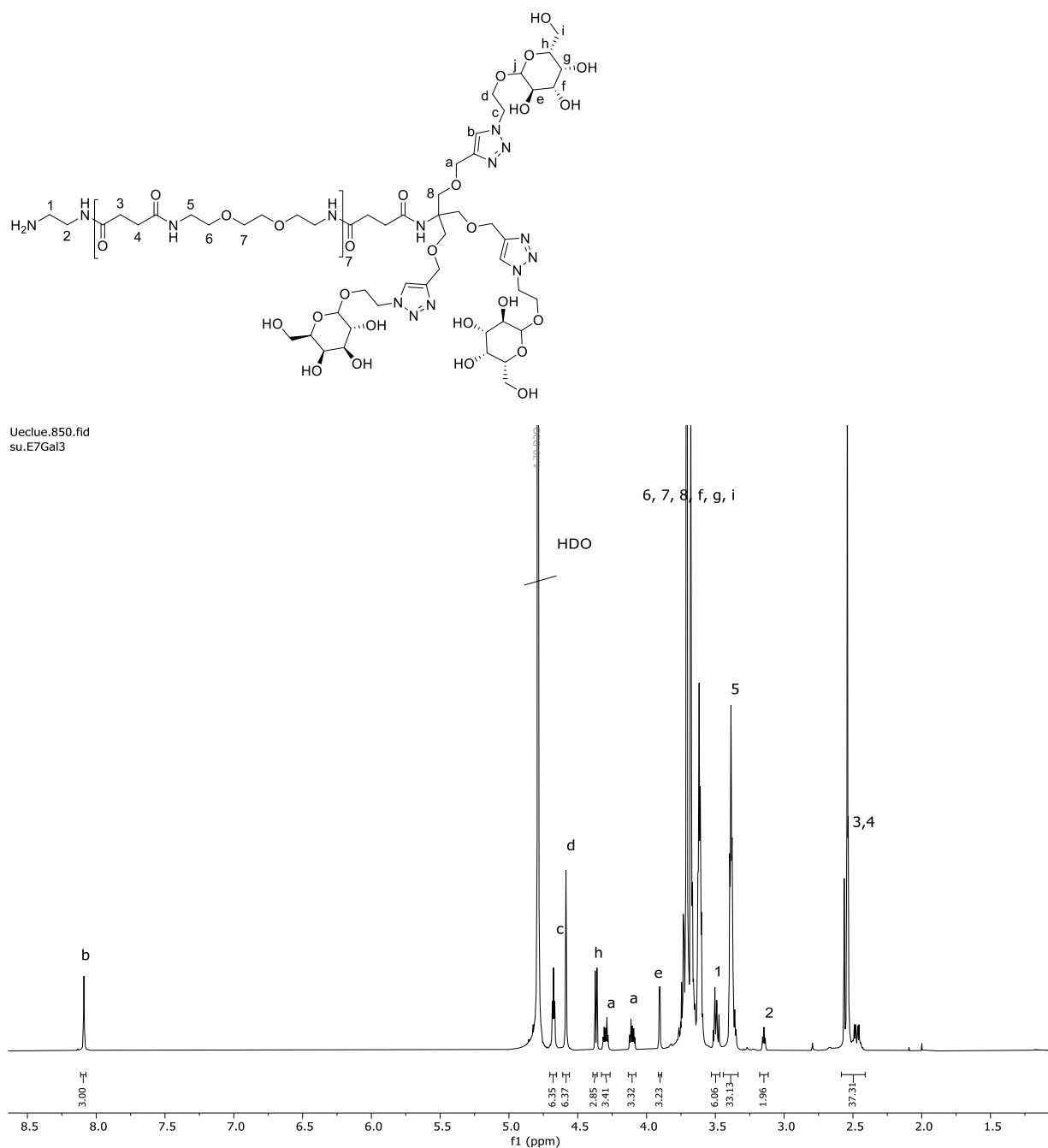*Figure S12: HR-ESI-MS of Oigo-TriMan.*

Oligo-TriGal

Figure S13: 600 MHz ¹H-NMR spectrum of Oligo-TriGal in D₂O at 25°C.

¹H NMR (600 MHz, D₂O) δ 8.09 (d, *J* = 1.4 Hz, 3H), 4.68 (t, *J* = 5.2 Hz, 6H), 4.59 (s, 6H), 4.37 (d, *J* = 7.9 Hz, 3H), 4.30 (dt, *J* = 11.6, 4.6 Hz, 3H), 4.14 – 4.08 (m, 3H), 3.90 (dd, *J* = 3.5, 1.0 Hz, 3H), 3.53 – 3.47 (m, 6H), 3.42 – 3.31 (m, 33H), 3.15 (t, *J* = 6.0 Hz, 2H), 2.59 – 2.41 (m, 37H).
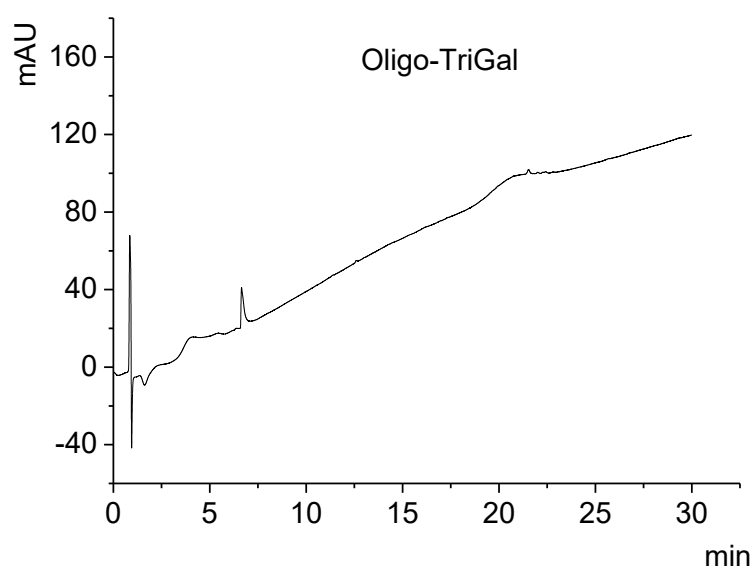
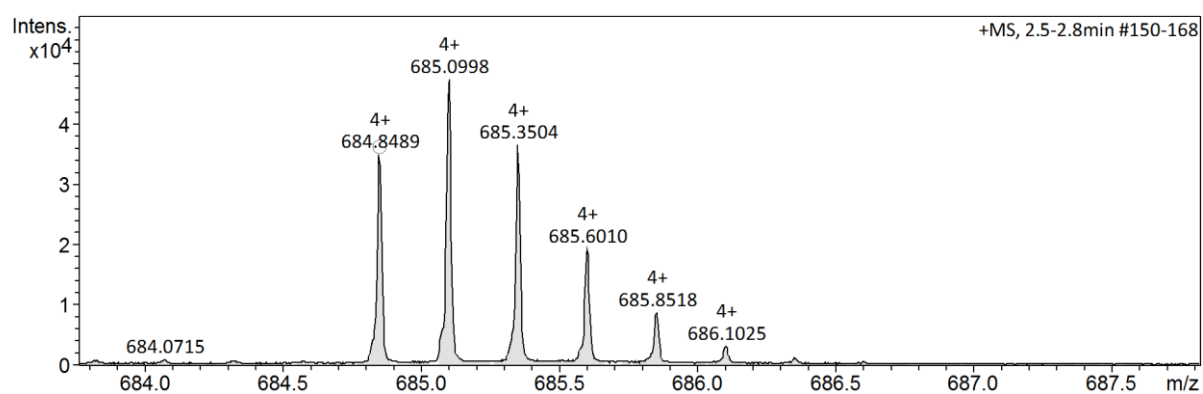*Figure S14: Oligo-TriGal detected with relative purities >95% by RP-HPLC analysis.*

Figure S15: HR-ESI-MS of OligoTriGal.

NMR Spectra of glycofunctionalized and non-functionalized CNPs:
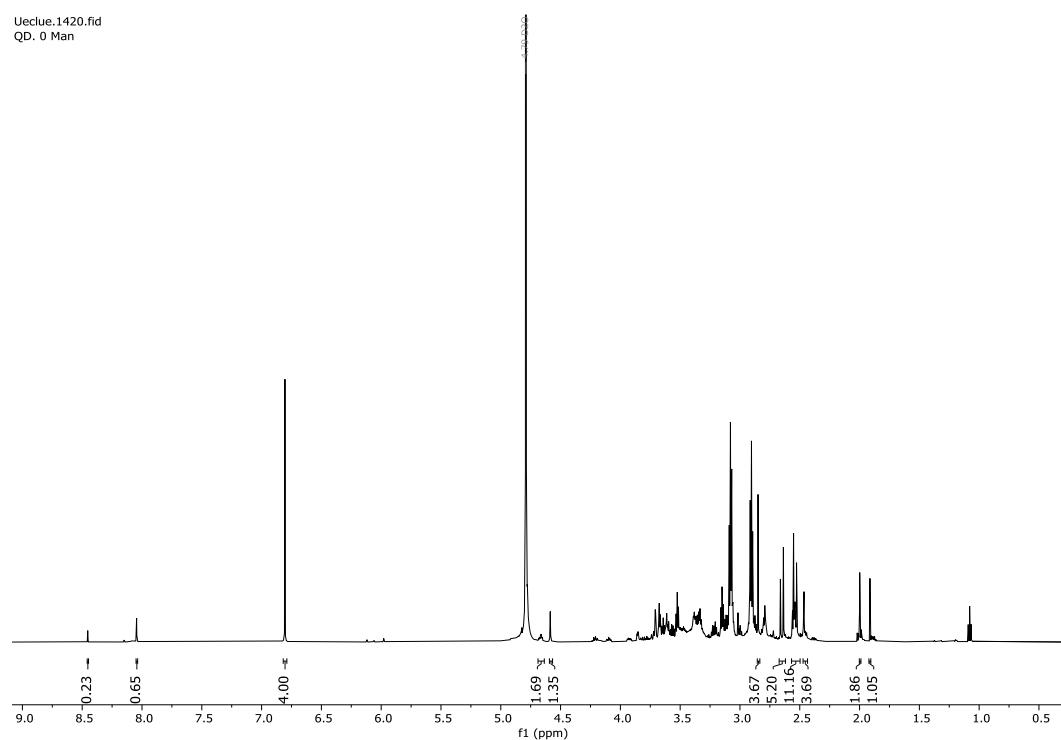
Ueclue.1420.fid
QD. 0 Man

Figure S16: 600 MHz ^{1}H-NMR spectrum of Oligo-TriMan-CNP in D$_2$O at 25°C.

Ueclue.1430.fid
QD. 0 Gal
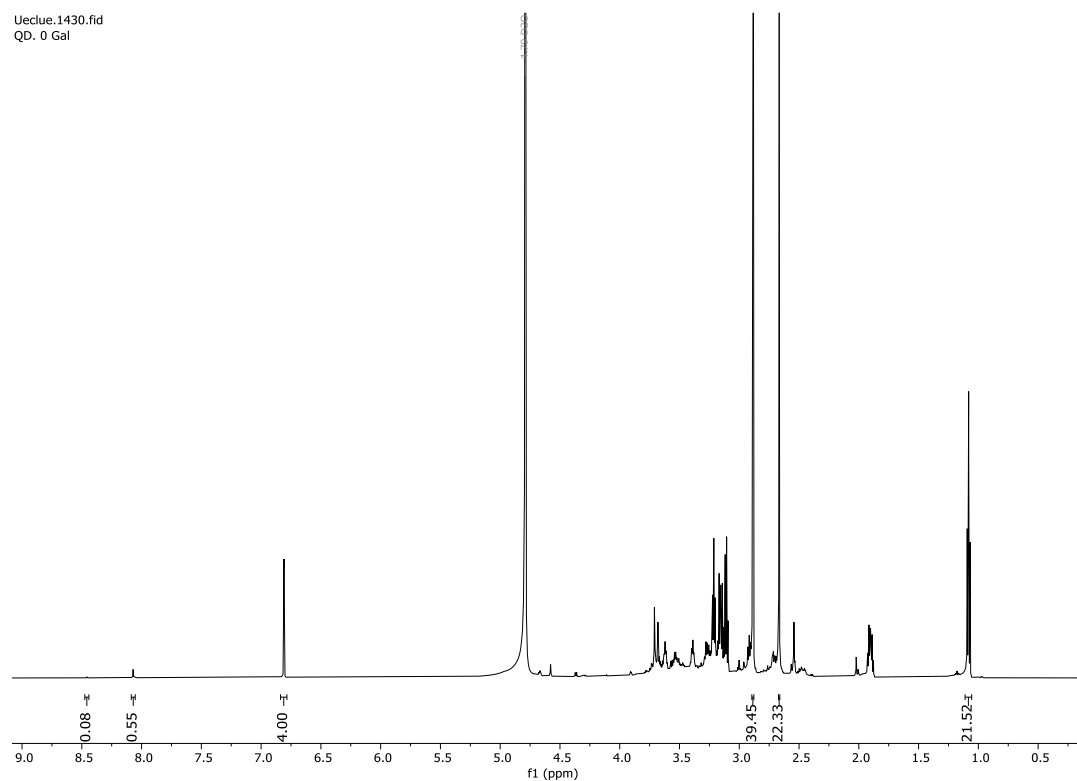
Figure S17: 600 MHz ^{1}H-NMR spectrum of Oligo-TriGal-CNP in D$_2$O at 25°C.

Ueclue.1020.fid
Acid. Tris

4.00

0.74
1.65
0.89
2.01
2.05
0.85

f1 (ppm)

Figure S18: 600 MHz ^{1}H-NMR spectrum of Acid-TRIS-CNP in D$_2$O at 25°C.

Ueclue.1110.fid
Acid

4.00

1.02
1.74
1.55
4.08
6.61

f1 (ppm)
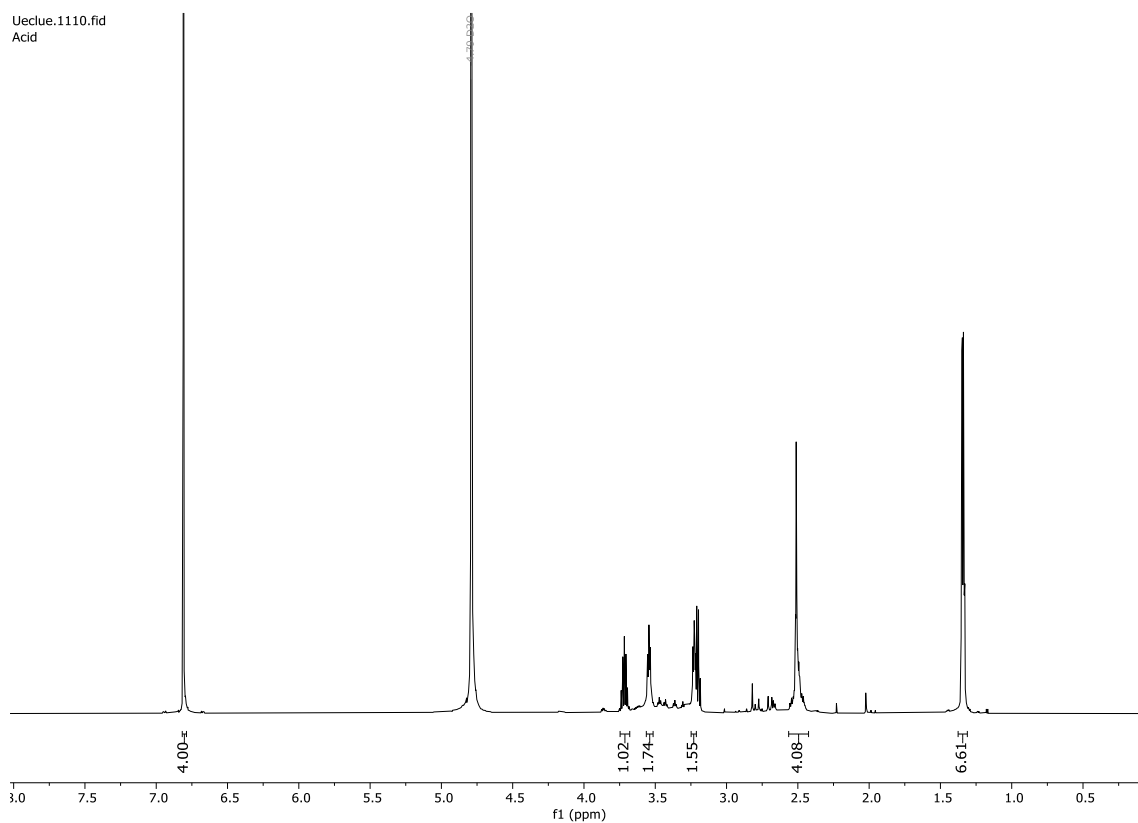
Figure S19: 600 MHz ^{1}H-NMR spectrum of Acid-CNP in D$_2$O at 25°C.

Figure S20: 600 MHz ^{1}H-NMR spectrum of Acid-Man-CNP in D$_2$O at 25°C.
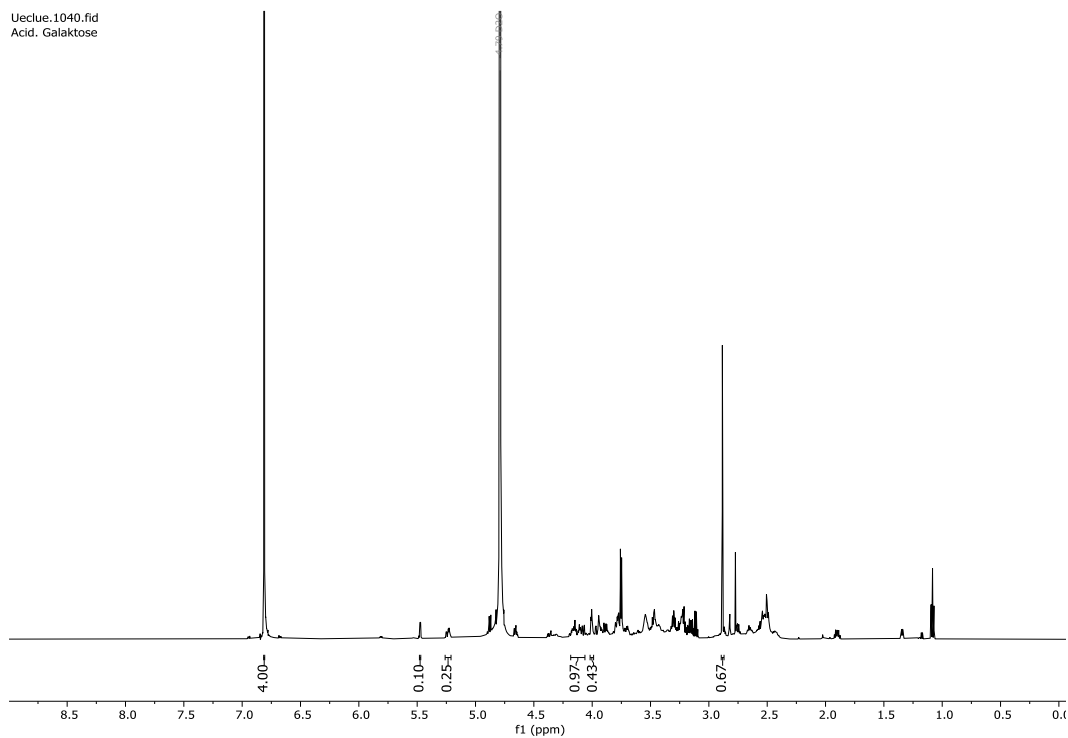
Figure S21: 600 MHz ^{1}H-NMR spectrum of Acid-Gal-CNP in D$_2$O at 25°C.

Figure S22: 600 MHz ^{1}H-NMR spectrum of Acid-GlcNAc-CNP in D$_2$O at 25°C.
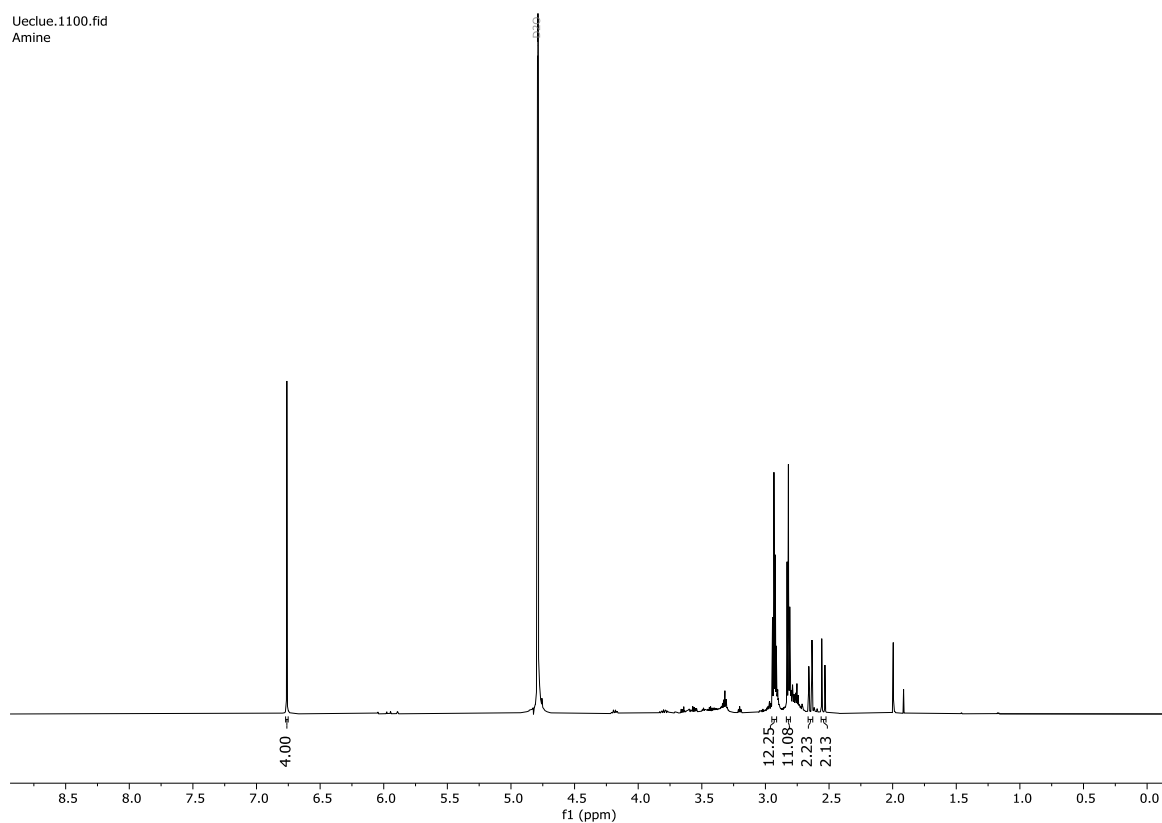
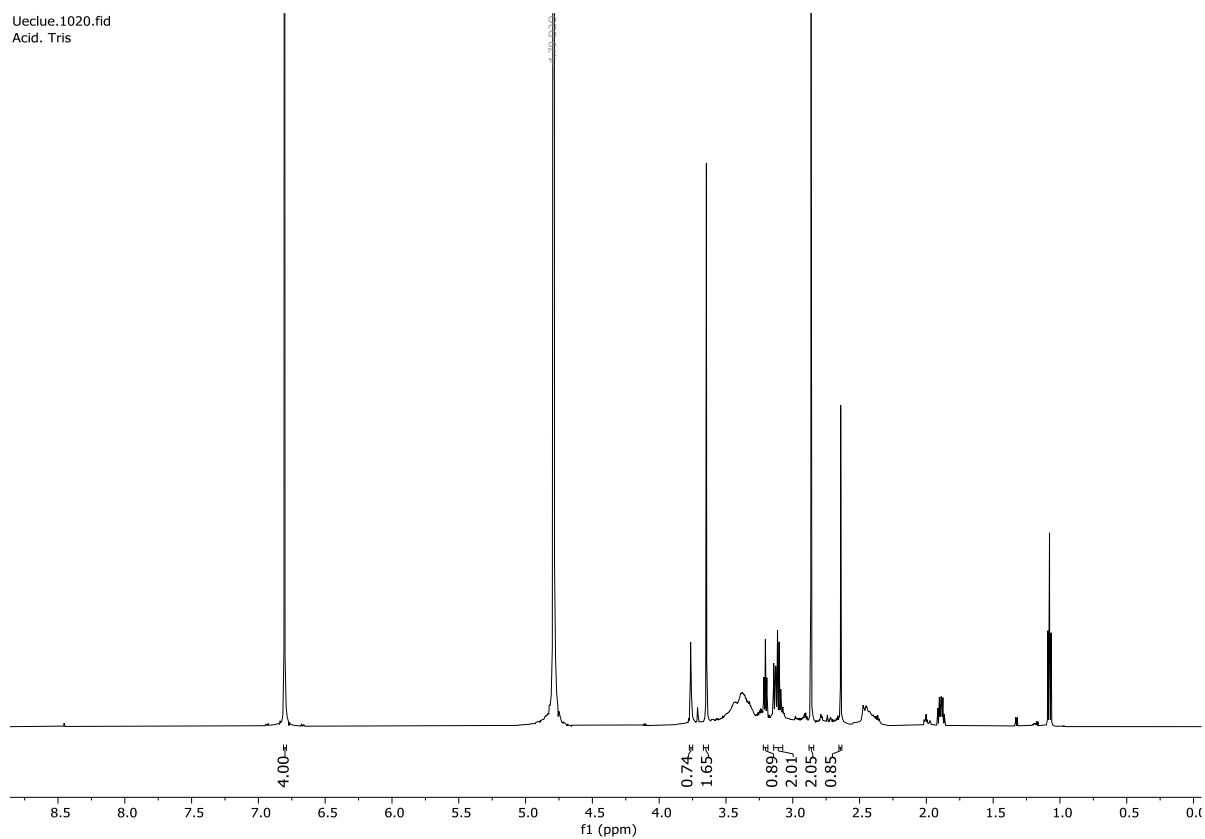Figure S23: 600 MHz ^{1}H-NMR spectrum of CNP in D$_2$O at 25°C.
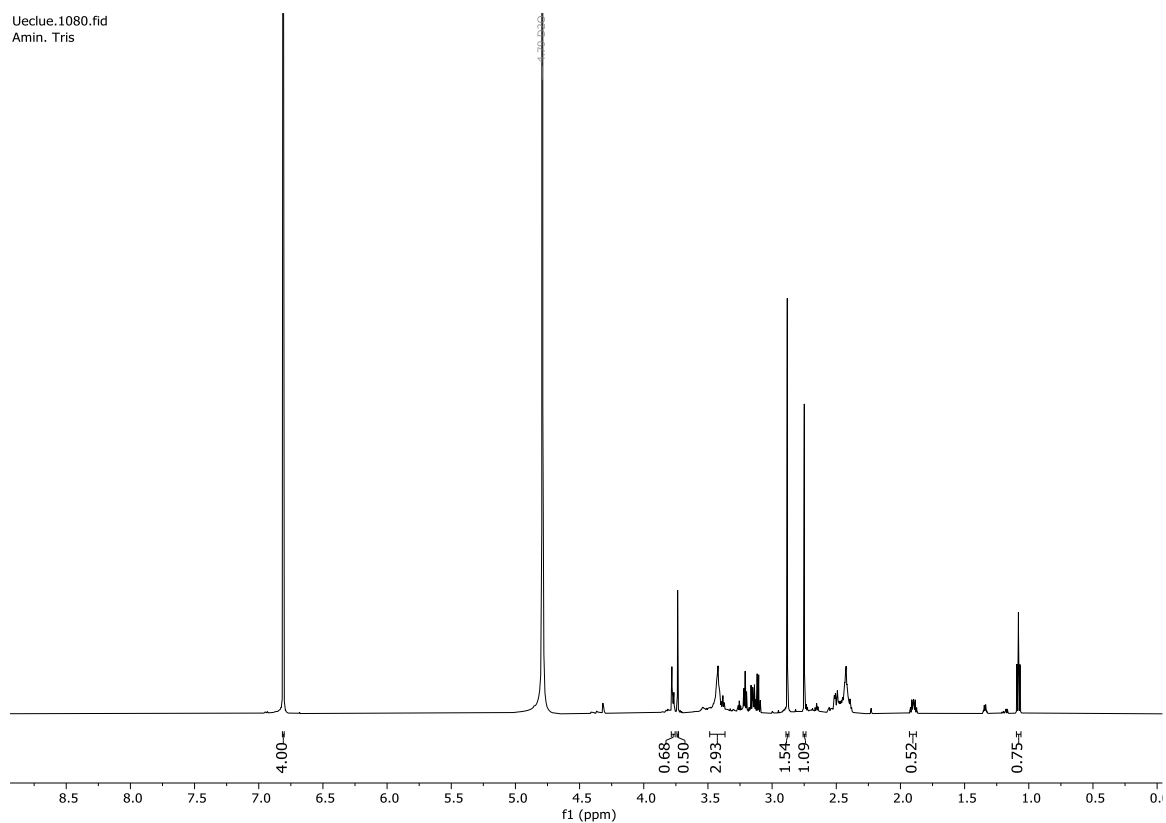
Figure S24: 600 MHz ^{1}H-NMR spectrum of Tris-CNP in D$_2$O at 25°C.
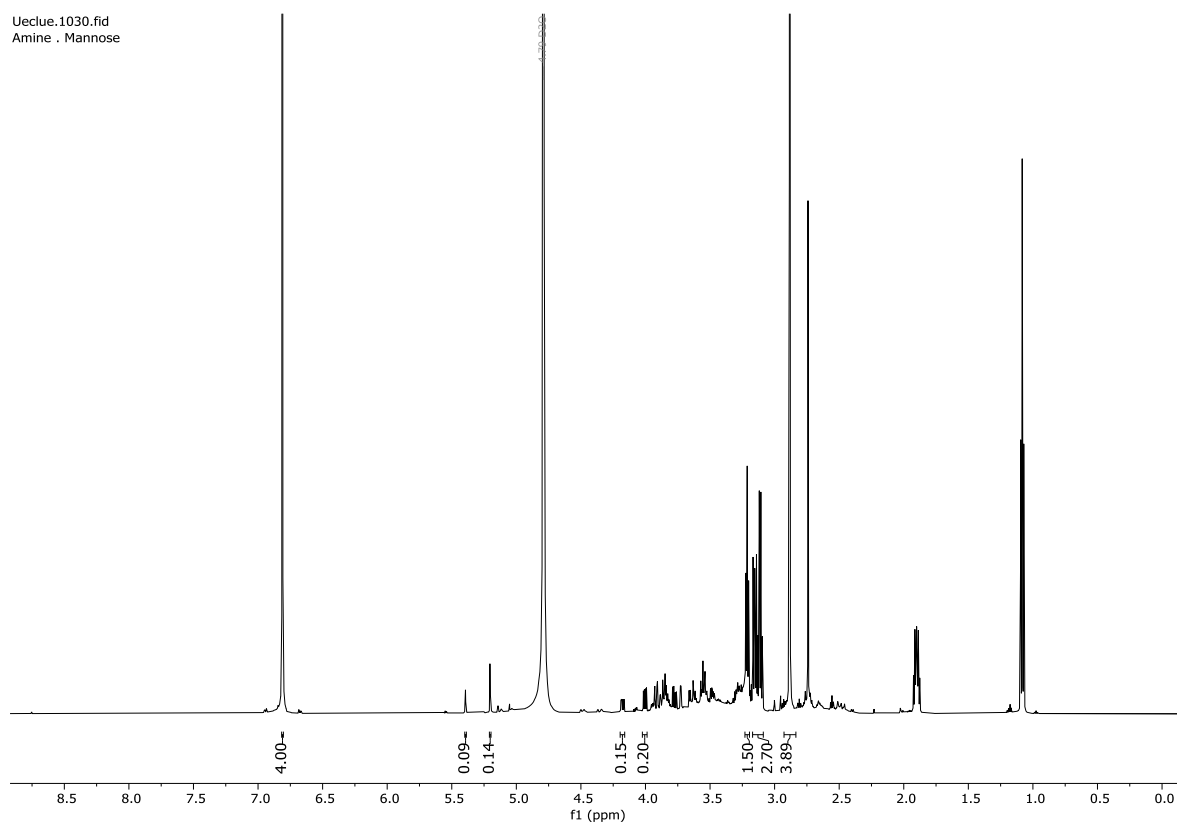
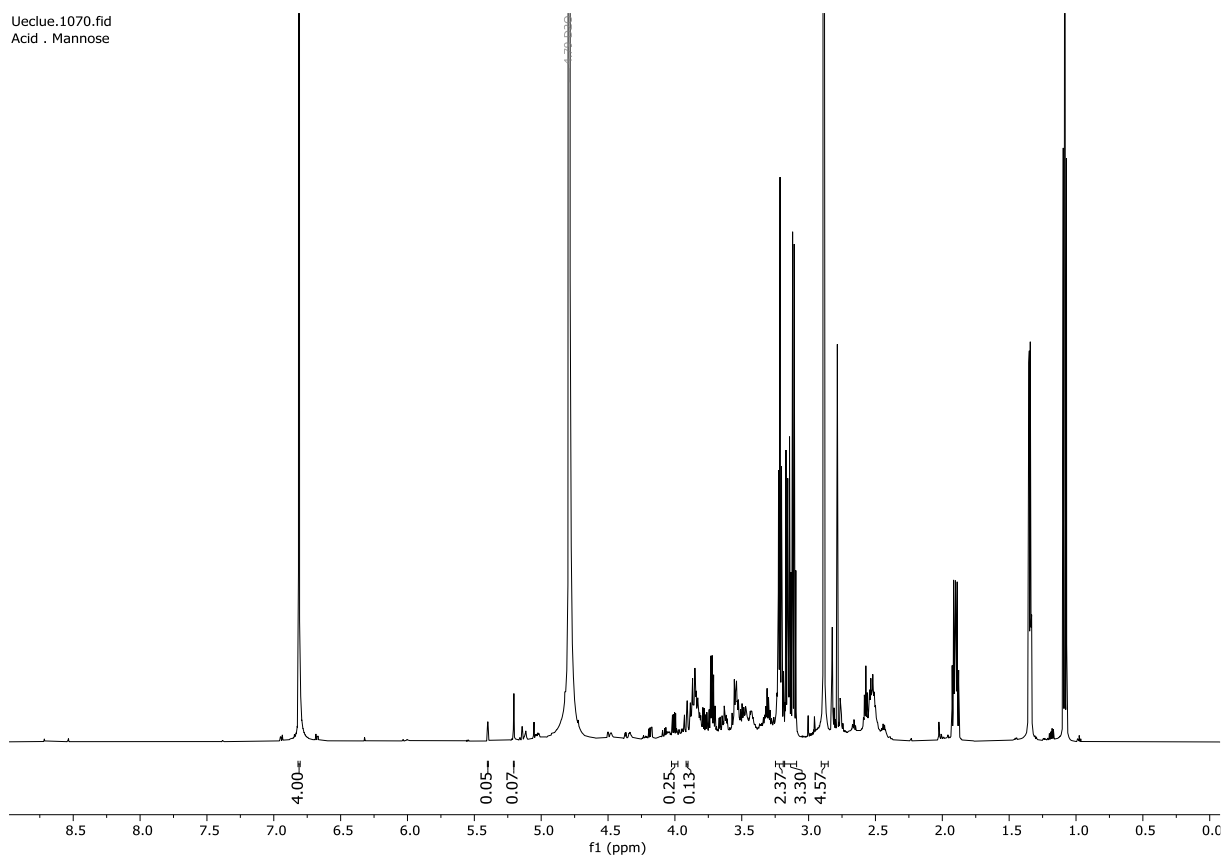Figure S25: 600 MHz ^{1}H-NMR spectrum of Man-CNP in D$_2$O at 25°C.

Ueclue.1050.fid
Amine . Galaktose

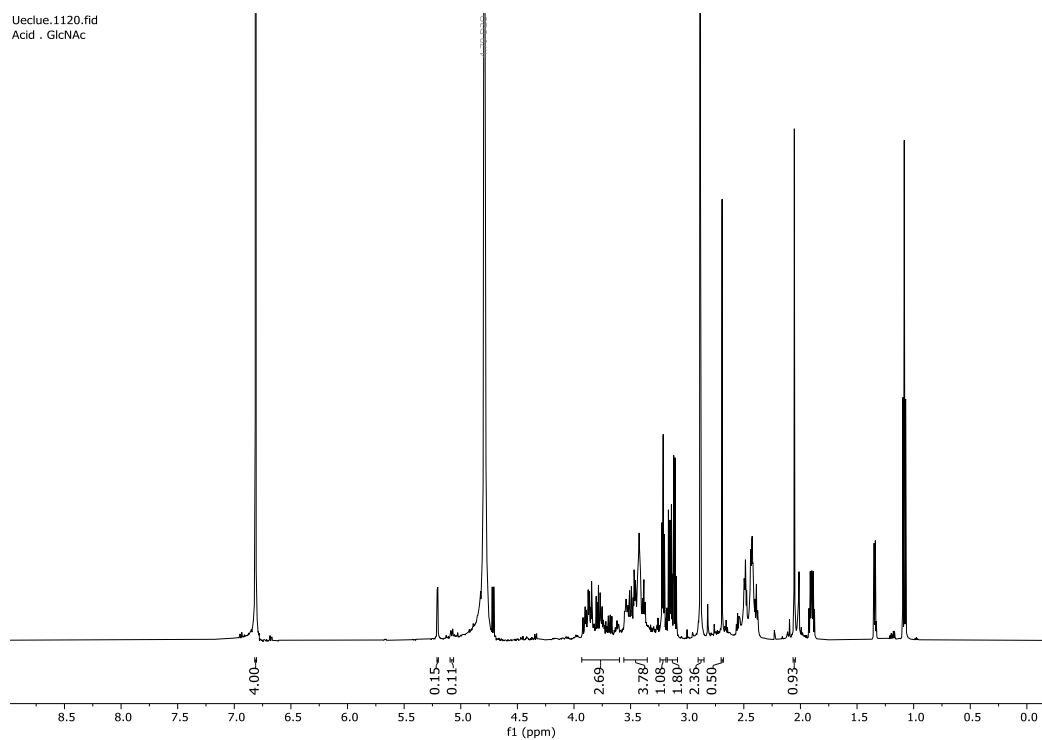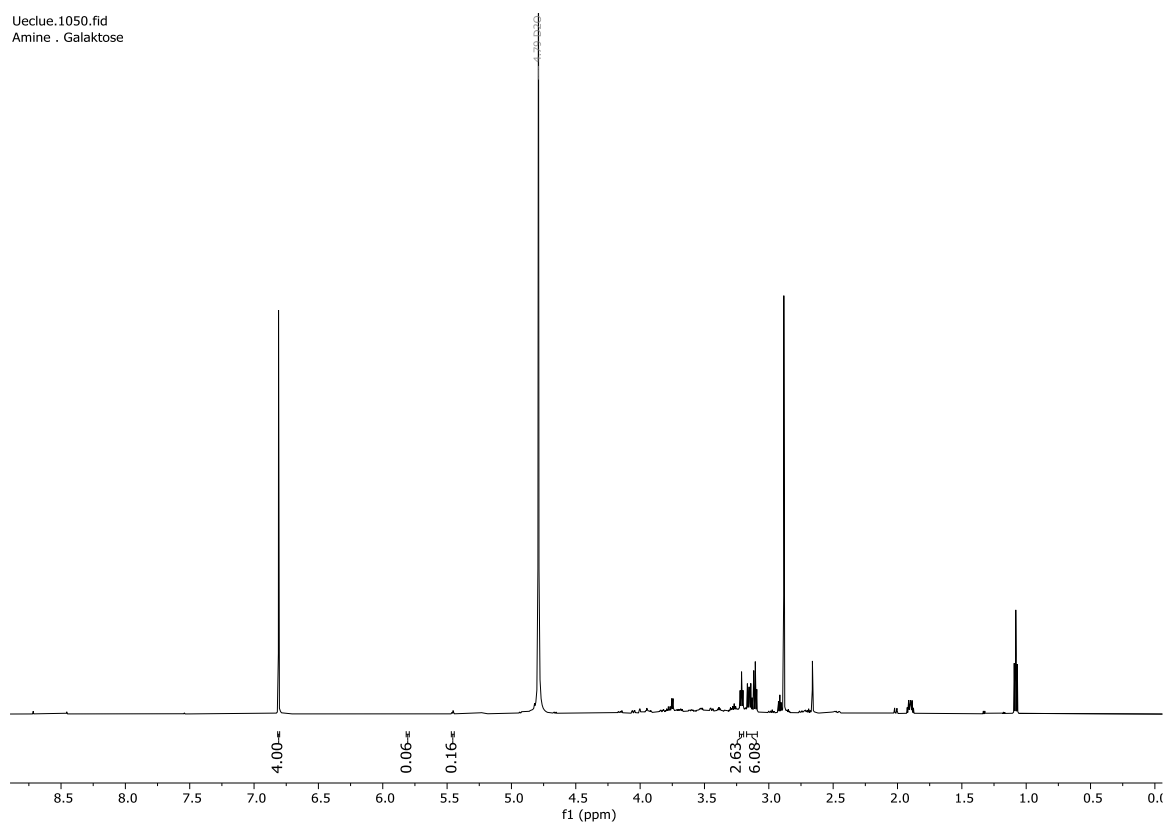Figure S26: 600 MHz ^{1}H-NMR spectrum of Gal-CNP in D$_2$O at 25°C.

Ueclue.1090.fid
Amine . GlcNAc
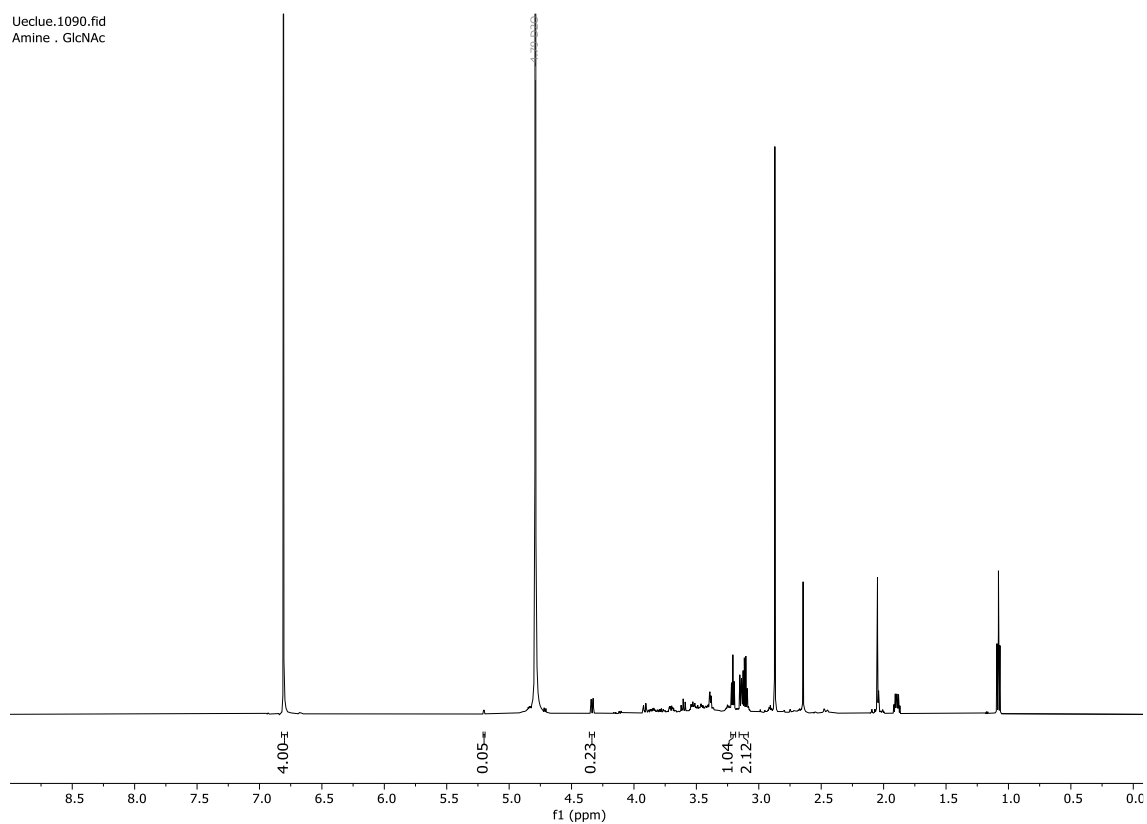
Figure S27: 600 MHz ^{1}H-NMR spectrum of GlcNAc-CNP in D$_2$O at 25°C.

Determination of hydrodynamic radii:

264

The change of the hydrodynamic radius before and after functionalization for CNP, Acid-CNP, GlcNAc-CNP and GlcNAc-Acid-CNP was determined by using diffusion-ordered spectroscopy (DOSY). The DOSY spectra were evaluated with the program GNAT from Manchester NMR Methodology Group. The diffusions coefficients were entered into the Stokes-Einstein equation and the hydrodynamic radii were calculated. The diffusions coefficients were all in the same range between 4-6 x 10^{-10} m^2 s^{-1}, so that the resulting radii are also in the same range. Red frame shows the surface related protons e.g. sugar or linker.

Stokes-Einstein equation $D = \dfrac{k_B T}{6\pi\eta r_h}$

Here

D is the diffusions coefficient

k_B is Boltzmann´s constant

T is the absolute temperature

η is the solvent viscosity

r_h is the hydrodynamic radius.
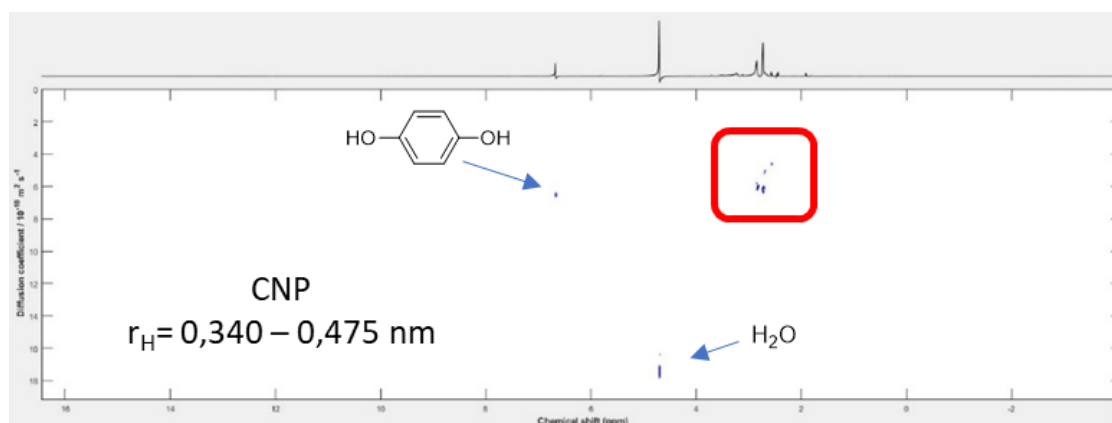
Figure S28: Diffusions coefficient of CNP showed a hydrodynamic radius of r_H =0.340 − 0.475 nm evaluated by the program GNAT.
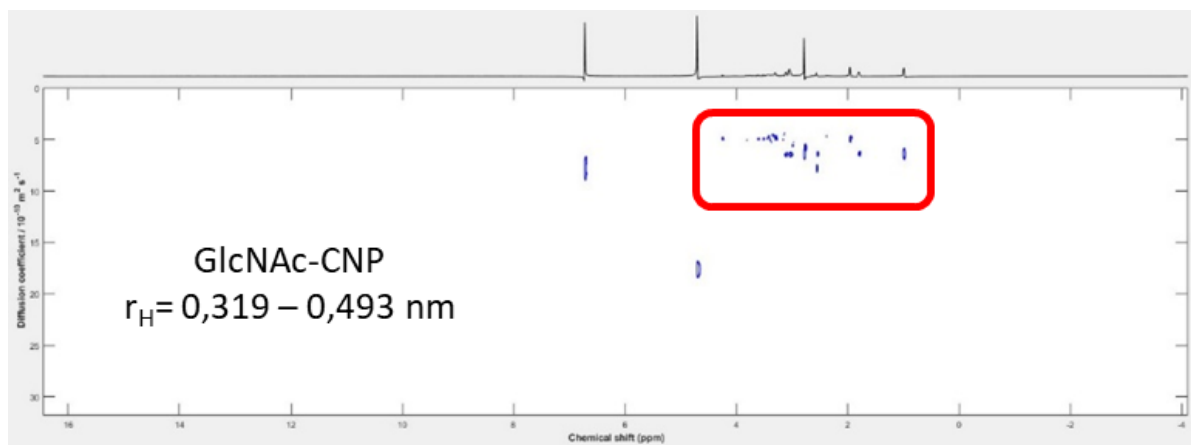
Figure S29: Diffusions coefficient of GlcNAc-CNP showed a hydrodynamic radius of r_H =0.319 – 0.493 nm evaluated by the program GNAT.
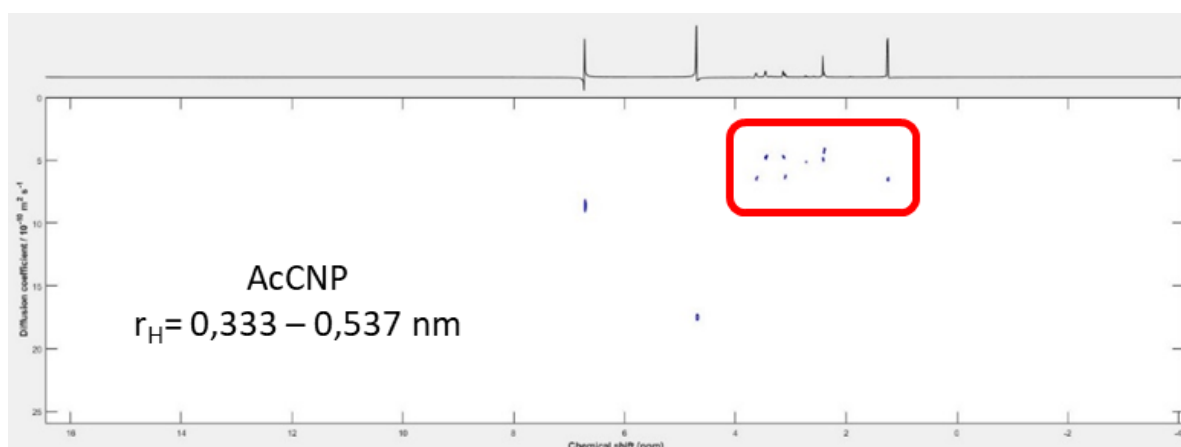
Figure S30: Diffusions coefficient of Acid-CNP showed a hydrodynamic radius of r_H =0.333 – 0.537 nm evaluated by the program GNAT.
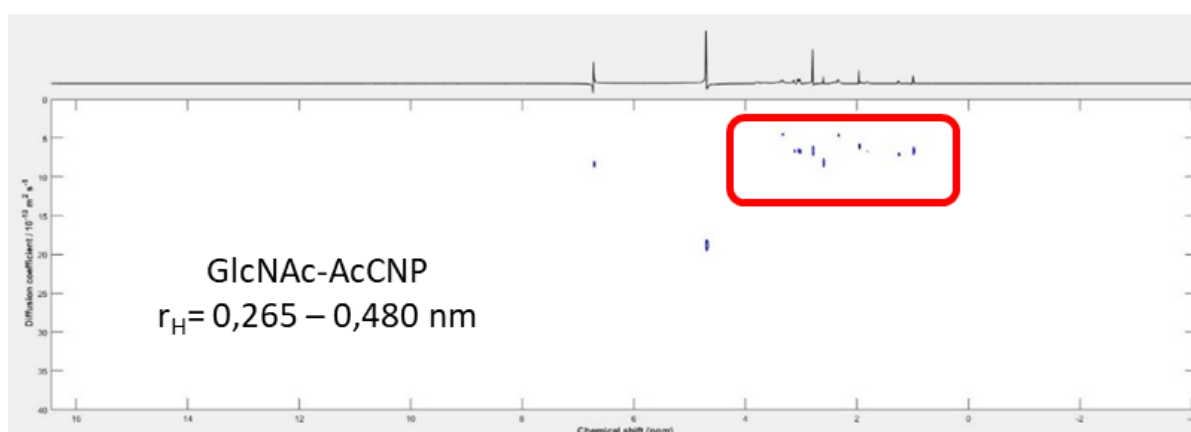
Figure S31: Diffusions coefficient of GlcNAc-AcCNP showed a hydrodynamic radius of r_H =0.265 – 0.480 nm evaluated by the program GNAT.
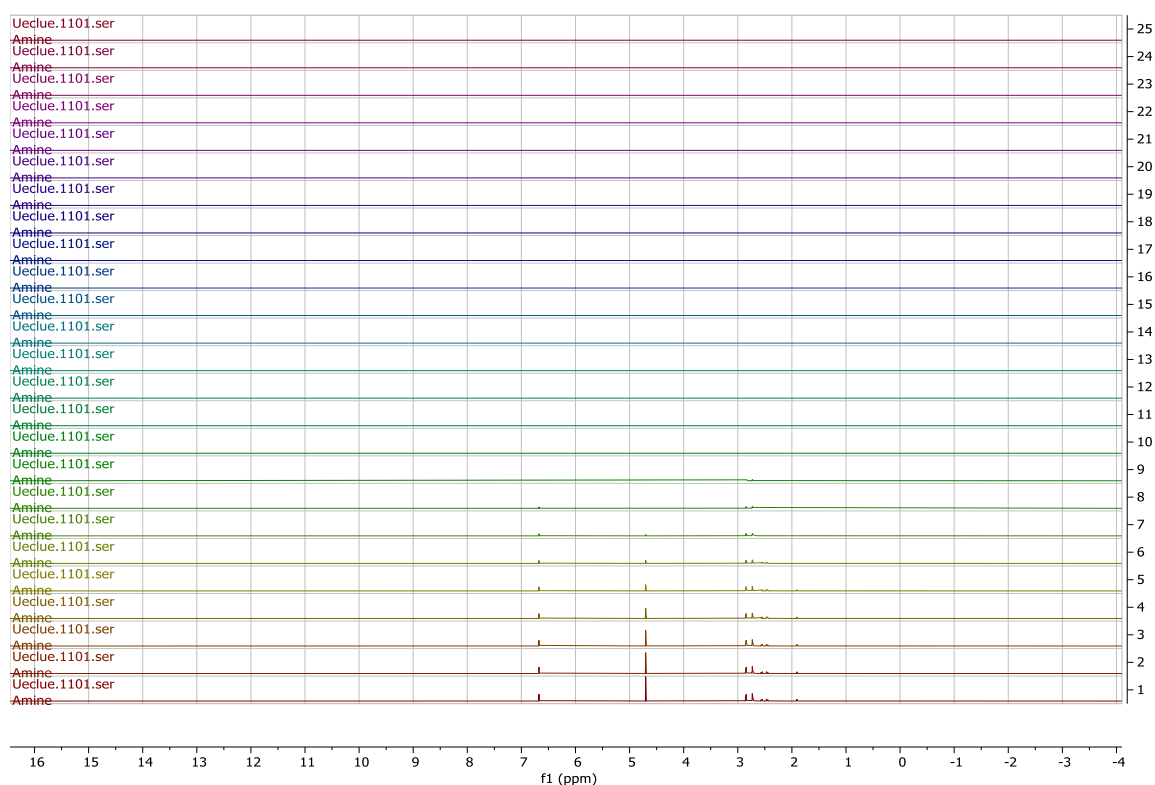
Figure S32: DOSY spectrum of CNP in D₂O at 25°C.
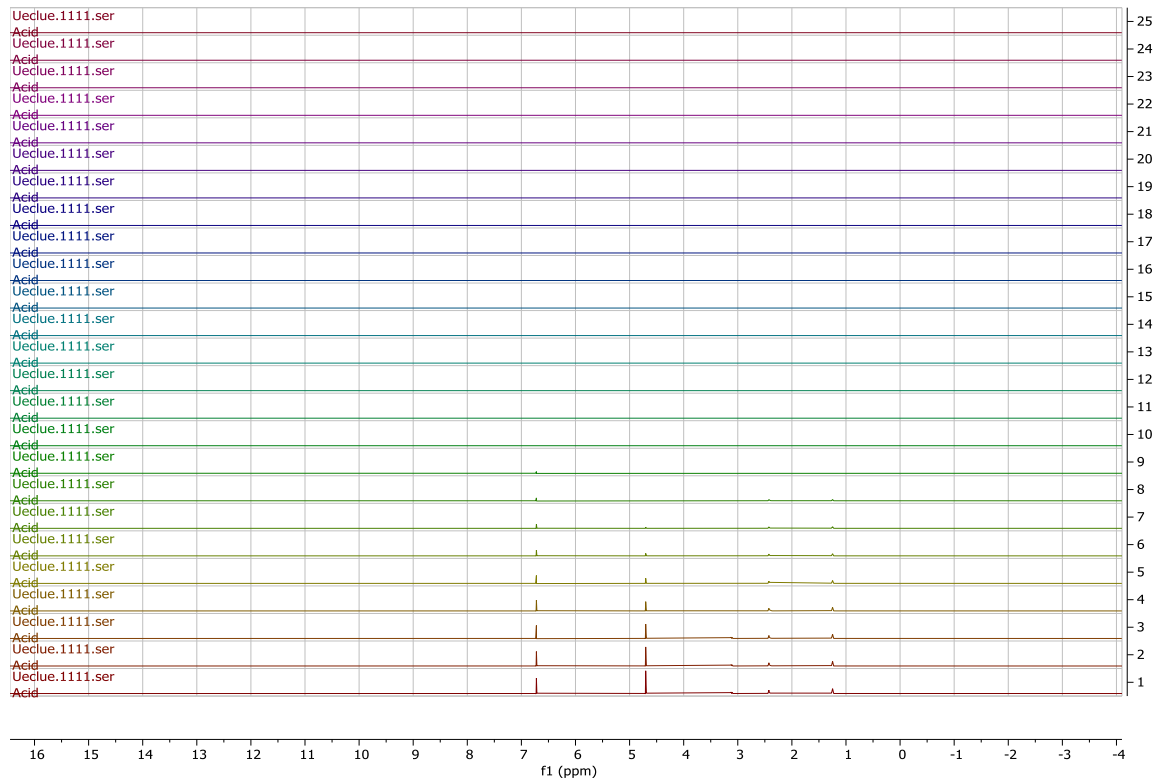
Figure S33: DOSY spectrum of AcCNP in D₂O at 25°C.
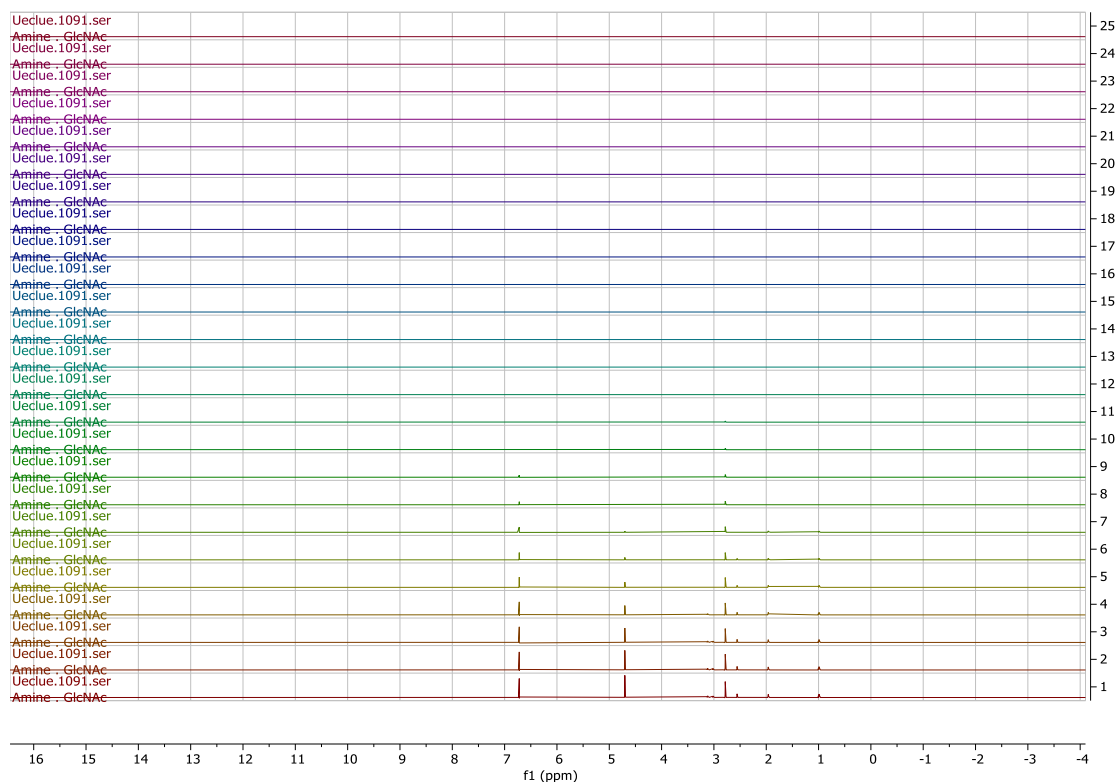
Figure S34: DOSY spectrum of GlcNAc-CNP in D$_2$O at 25°C.
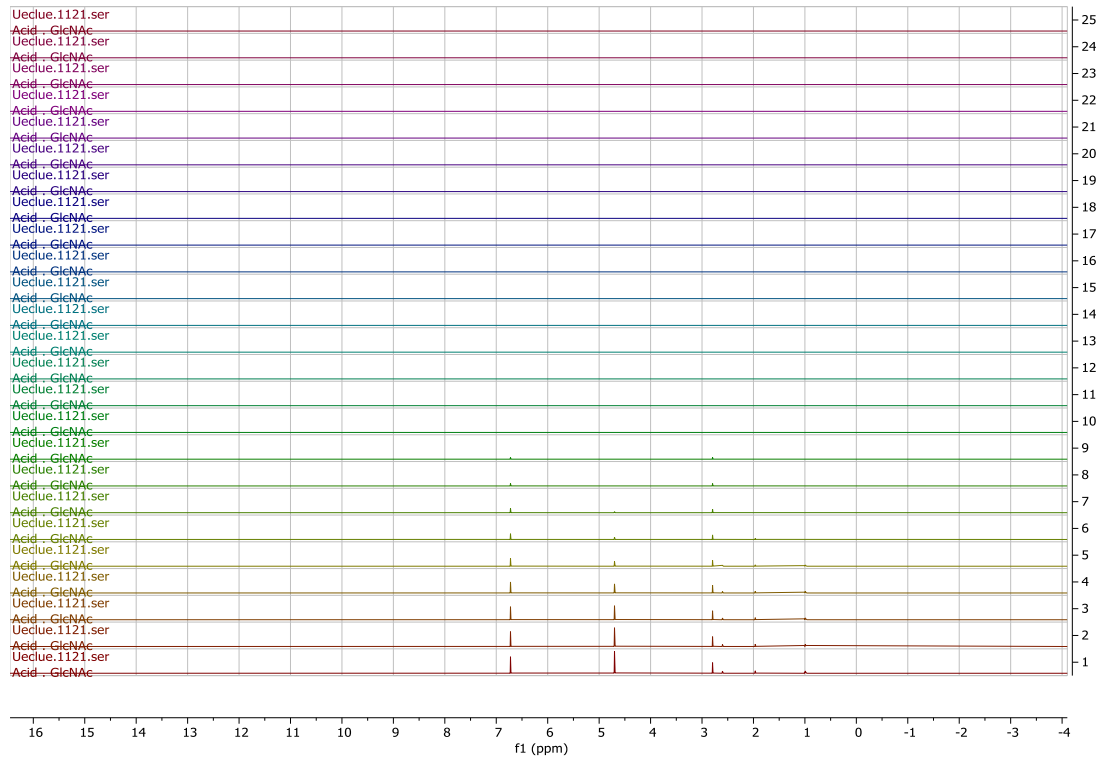
Figure S35: DOSY spectrum of GlcNAc-AcCNP in D$_2$O at 25°C.
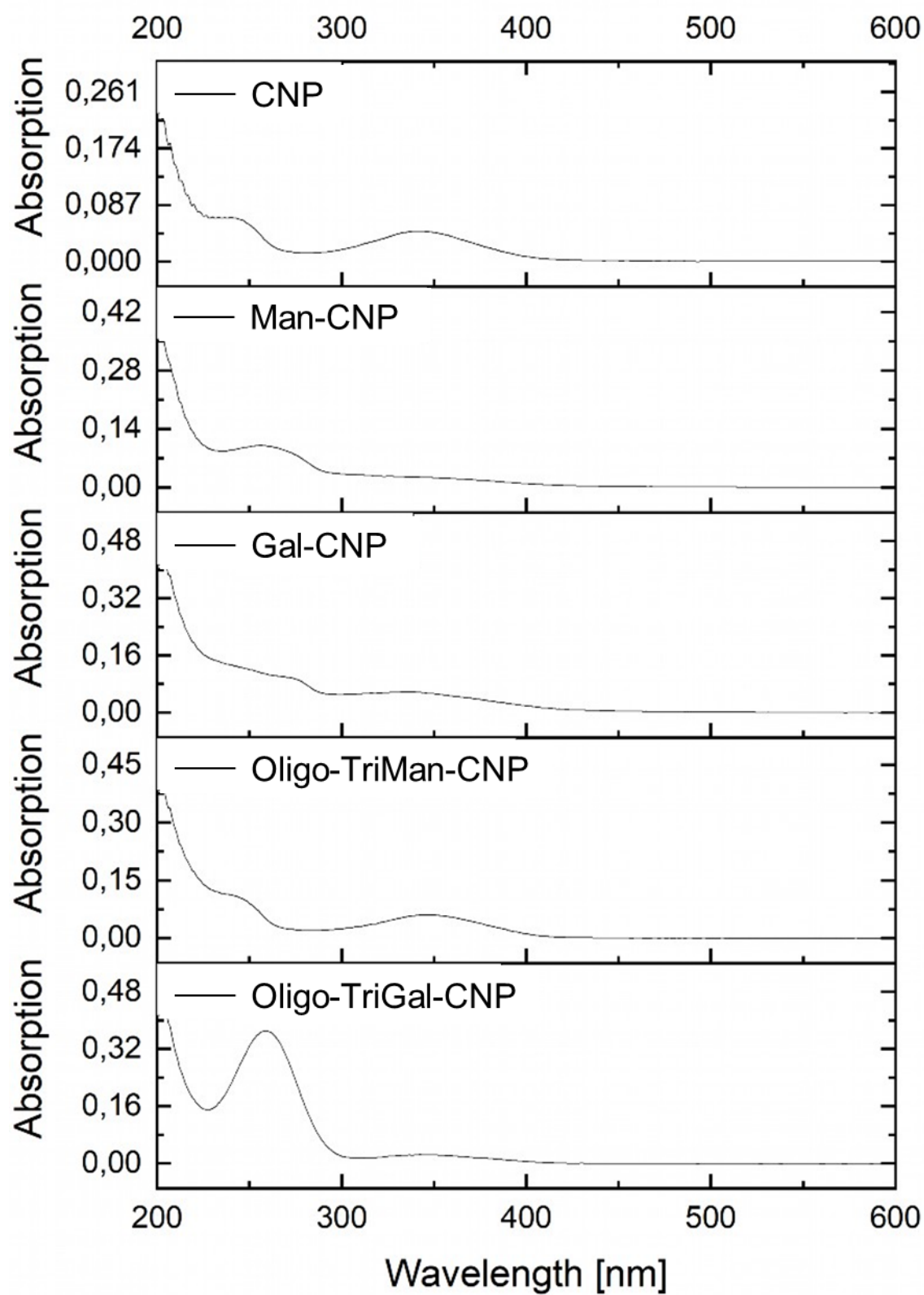
Figure S36: Absorption spectra of functionalized CNPs.
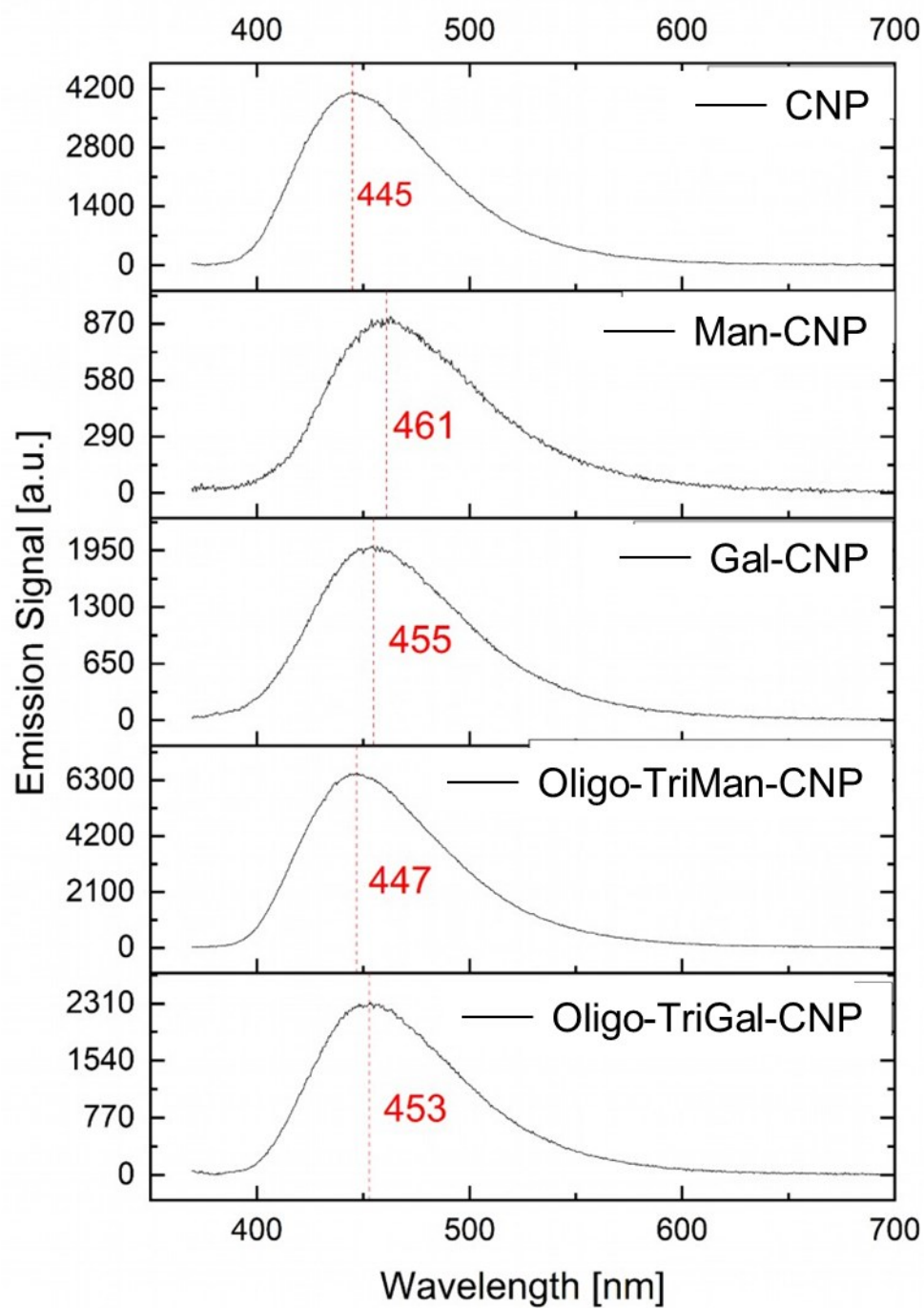
Figure S37: Emission spectra of the five CNP species. For all functionalized species a slight red shift of the emission maximum is visible after coupling.

Table 1: Op271lycofunctionalizatf glycofunctioalized carbon nanoparticles. The quantum yield at 360 nm was determined with the method of Wiliams at al. using Coumarin 1 as a reference. The extinction coefficient at 360 nm was determined by fitting Lambert-Beer's law to the absorption values at different mass concentrations. The Brightness of each particle type is the product of the quantum yield and the extinction coefficient. All functionalized particles show a redshift in their emission spectrum relative to nonfunctionalized carbon nanoparticles. For more details, please consult the subsection "optical spectroscopy" in section 2 in the manuscript.

Property	CNPs	Man-CNPs	Gal-CNPs	Oligo-TriMan-CNPs	Oligo-TriGal-CNPs
Quantum Yield	0.28 ± 0.03	0.12 ± 0.01	0.13 ± 0.01	0.31 ± 0.05	0318 ± 0.03
Extinction coefficient [$mg^{-1}cm^{-1}$]	3.05 ± 0.04	0.764 ± 0.003	1.47 ± 0.01	1.76 ± 0.09	0.657 ± 0.009
Brightness [$mg^{-1}cm^{-1}$]	0.85 ± 0.10	0.09 ± 0.03	0.19 ± 0.02	0.55 ± 0.012	0.20 ± 0.02
Position of maximum in emission [nm]	445	461	455	447	453

Fluorescence Correlation Spectroscopy
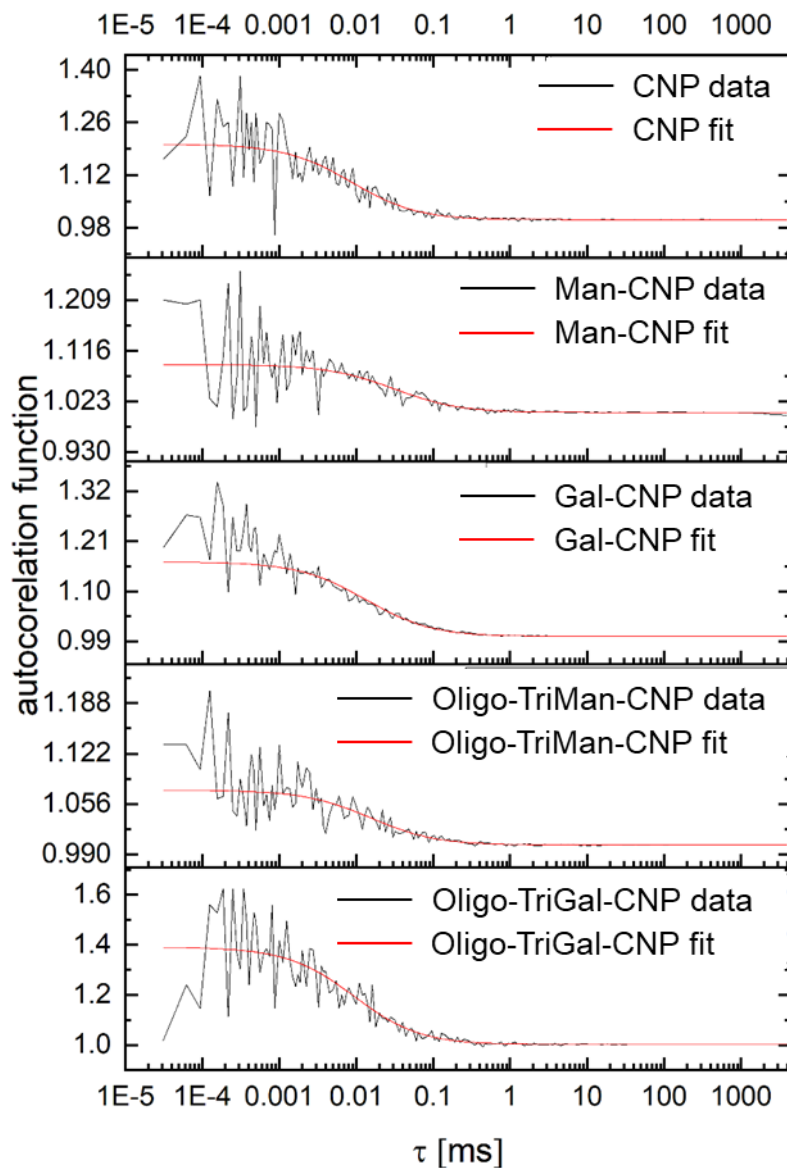
Figure S38: Fluorescence correlation spectroscopy data for the five different types of NPs. The data was recorded on a Fluoview 1000 (Olympus) confocal microscope under excitation with a 405 nm continuous wave diode laser. The fit (red) to the experimentally determined correlation curves (black) assumes one particle diffusing through a gaussian focal volume without any further bunching terms (blinking).
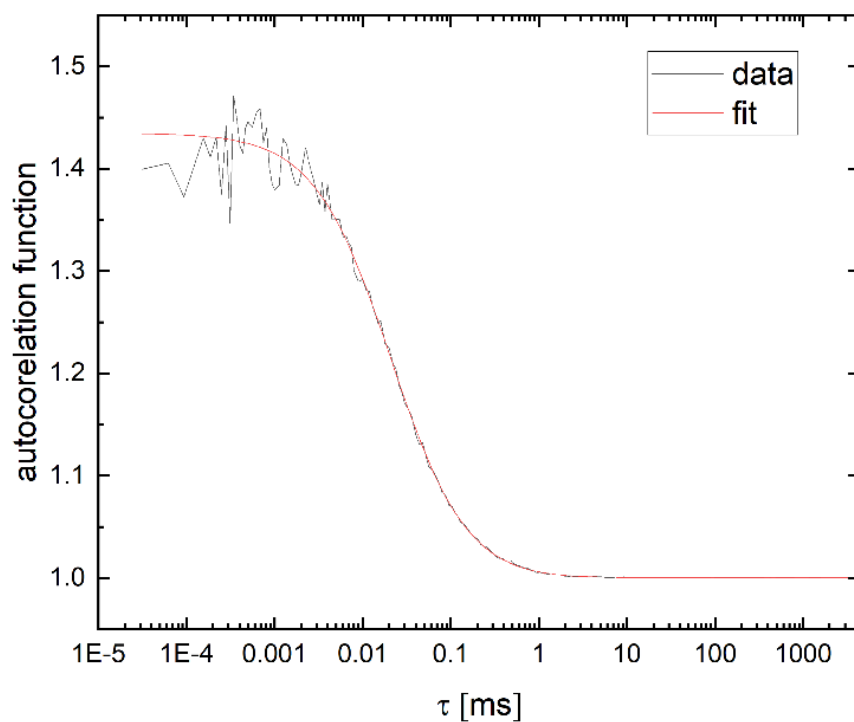
Figure S39: Fluorescence correlation curve of rhodamine 110. The data was recorded on a Fluoview 1000 (Olympus) confocal microscope under excitation with a 488 nm pulsed diode laser. Rhodamine 110 was used as a reference with known diffusional coefficient $D = (4.3 \pm 0.3) \times 10^{-10} \frac{m^2}{s}$ [8]

Table S2: Values of the diffusion coefficient D and hydrodynamic radius R_H estimated from the fits to the FCS data displayed in S38 and S39. Please note that the explanatory power of the values calculated from the fitted model is limited. The correlation curves are noisy due do large amounts of scattering at low wavelengths. Therefore, it was reasonable to only fit the simplest model to the data. If dark states or more diffusing components are present, the actual values R_H may be deviate beyond the given error estimates (which are only valid for the given model assumptions).

	$D \, [10^{-10} \frac{m^2}{s}]$	$R_H \, [nm]$
CNP	10 ± 6	0.21 ± 0.13
Man-CNP	2.8 ± 1.7	0.7 ± 0.5
Gal-CNP	6.6 ± 2.0	0.32 ± 0.10
Oligo-TriManCNP	6 ± 4	0.37 ± 0.24
Oligo-TriGal-CNP	10 ± 5	0.22 ± 0.12

3. Biological Experiments:
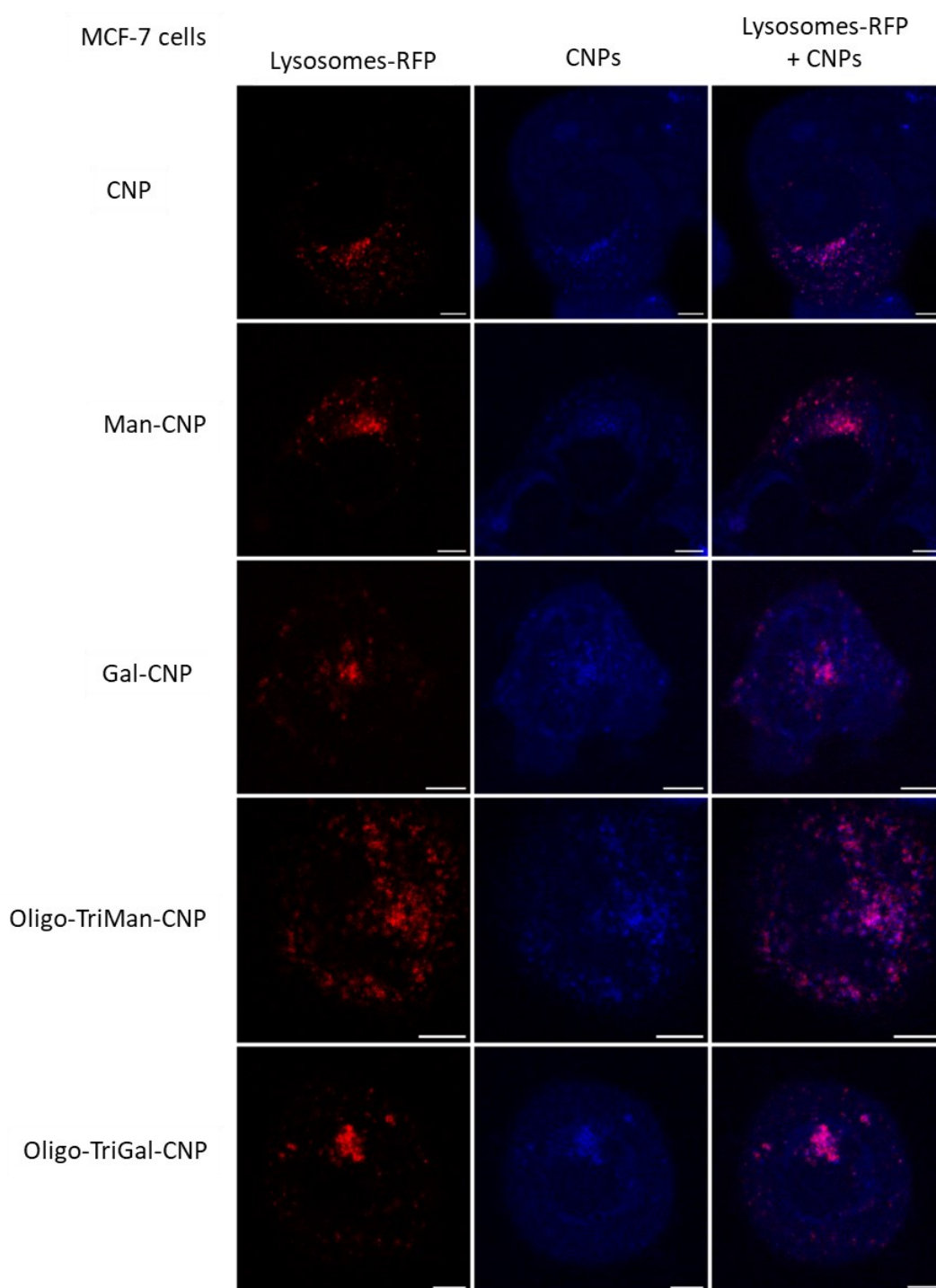
Figure S40: Confocal microscopy images of MCF-7 breast cancer cells. Lysosomes were fluorescently tagged via a transfection with BacMam 2.0, Lysosomes RFP (Invitrogen) as shown in the left column. The CNP fluorescence under 405 nm excitation is shown in the middle column. The right column shows the overlay of both channels. Both channels coincide spatially, indicating colocalization of the CNPs with the lysosomes. The length of the scale bars amount to 5 µm.
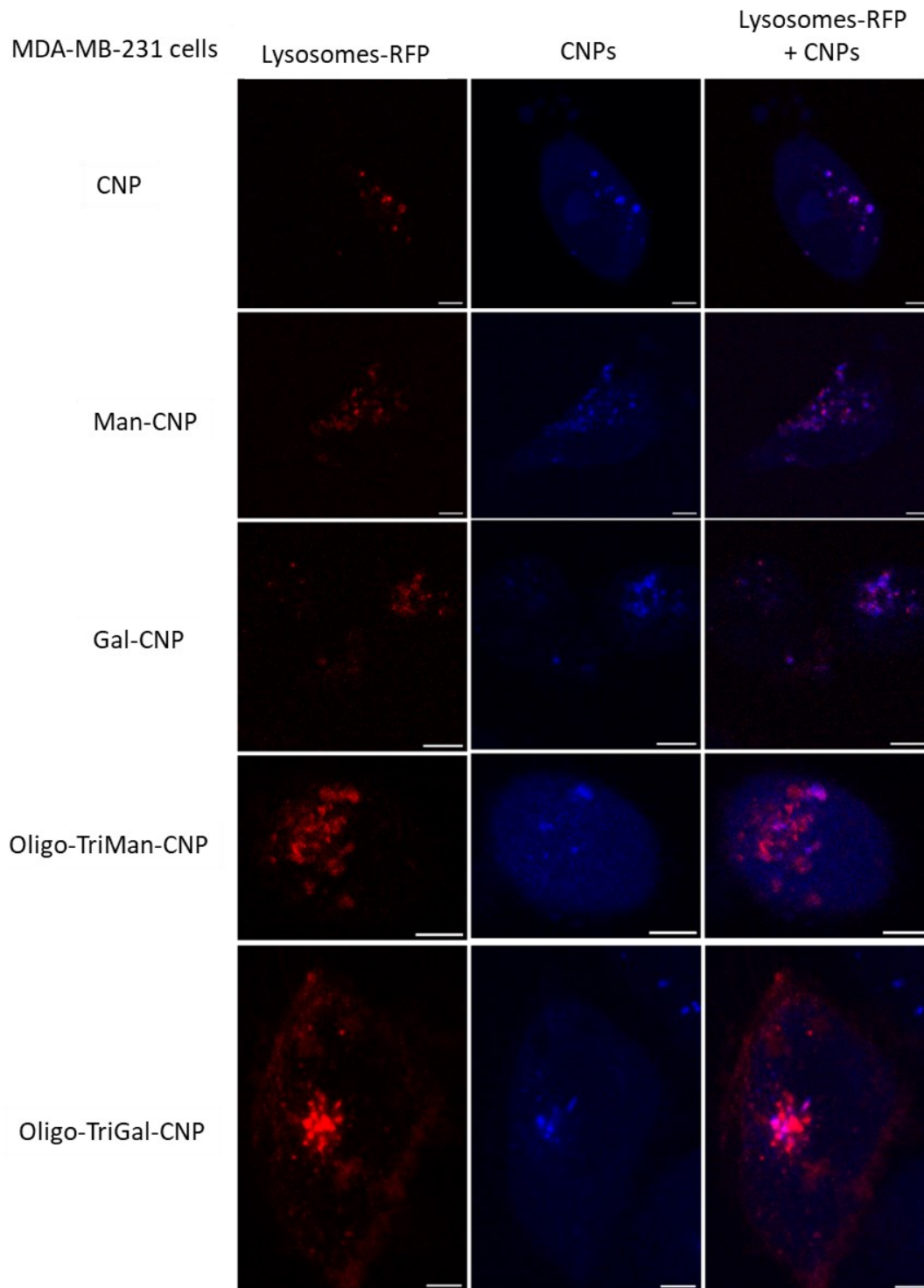
Figure S41: Confocal microscopy images of MDA-MB-231 breast cancer cells. Lysosomes were fluorescently tagged via a transfection with BacMam 2.0, Lysosomes RFP (Invitrogen) as shown in the left column. The CNP fluorescence under 405 nm excitation is shown in the middle column. The right column shows the overlay of both channels. As in the case of MCF-7 cells both channels coincide spatially, indicating colocalization of the CNPs with the lysosomes. The length of the scale bars amount to 5 μm.

4. Explanations for particle dependent uptake rates

The different uptake rates, measured via flow cytometry, depend on the particle type, but not on the cell type. The CNPs functionalized with oligomers had comparable uptake rates to the non-functionalized CNPs, while the uptake of nanoparticles functionalized with monosaccharides saw a two- to three-fold increase in uptake compared to the other CNP species.

A possible explanation might be that the interaction of the monosaccharides with the cell surface is enhanced by receptor unspecific interactions since the uptake is independent of the cell type and therefore of the receptor expression. While the uptake rate of non-functionalized CNPs and oligomer functionalized CNPs would be mainly determined by the volume incorporated by the endocytotic vesicles, in this model the uptake rates of the monosaccharide functionalized CNPs is governed by the particles in the bulk and by those adsorbed to the inner surface of the endocytic vesicle. From transmission electron microscopy (TEM) measurements the average diameter of the CNPs was determined to be 3.3 nm and from atomic force microscopy (AFM) the particle hight was 1 nm − 2 nm and therefore the number of graphene layers was estimated to be two to three. [7]

To test whether this assumption is reasonable, i.e. if sufficiently many particles fit on the surface of a vesicle, we perform an estimate of the distance of the particles on the cell surface necessary to explain that increase in uptake rate. For these geometry parameters assuming a honeycomb lattice of carbon atoms for each layer we arrive at an estimate of 5 kDa for the molar mass per CNP. The average distance at a concentration of 500 µg/ml therefore amounts to 25.5 nm in solution. Let there be a spherical endocytotic vesicle forming from a cell membrane invagination with the radius r. The number of incorporated CNPs will be $n_{incorporated} = \frac{4}{3}\pi r^3 c N_A$ with the molar concentration of particles/molecules in solution $c \left[\frac{mol}{m^3}\right]$ and the Avogadro constant N_A. If there are k-times the number of particles adsorbed to the surface, the average area per particle on the surface is therefore $A_N = \frac{4\pi r^2}{k\frac{4}{3}\pi r^3 c N_A} = \frac{3}{krcN_A}$. The average distance of the particles is then given by $a_S = \sqrt{A_N} = \sqrt{\frac{3}{krcN_A}}$. For reasonable values of the radius of an endocytotic vesicle (50 nm/100 nm) and $k = 2$ we arrive at plausible distances of $a_s(r = 50\ nm) = 22.4\ nm$ and $a_s(r = 100\ nm) = 15.8\ nm$.

Possible mechanisms that increase the interaction rate with the cell surface of monosaccharide functionalized CNPs compared to the other CNP species may be (1) electrostatic or (2,3) sugar mediated but not receptor specific:

(1) The non-functionalized CNPs present both carboxylic as well as amino groups. In the coupling reaction the carboxylic groups are targeted and transition into amide bonds. The amino groups on the particle surface on the other hand are still present and may accept protons in aqueous solution. The functionalized CNPs may therefore yield a net positive potential in solution and adsorb to the surface via electrostatic interactions. This effect may be reduced in the oligomer functionalized CNPs since the oligomers can act as spacers of the positively charged particle core to the surface.

(2) The interaction may be sugar mediated and the sugars in the periphery adsorb to interaction sites on the cell surface. A possible explanation for the oligomer functionalized CNPs not experiencing a significant increase in their uptake may be that the oligomers spread out on the surface, thereby covering many interaction sites per particle, while the monosaccharide functionalized CNPs on the other hand interact only with few interaction sites and can cover the surface at a larger number density.

(3) The interaction with the cell surface is sugar mediated, but due to the conformational flexibility of the linkers the sugars on the oligomer functionalized CNPs are only partially available for binding. For the monomer functionalized CNPs there are only few degrees of freedom, and the sugars are always available on the surface, but with increasing linker length the probability of presenting the sugars on the outside decreases.
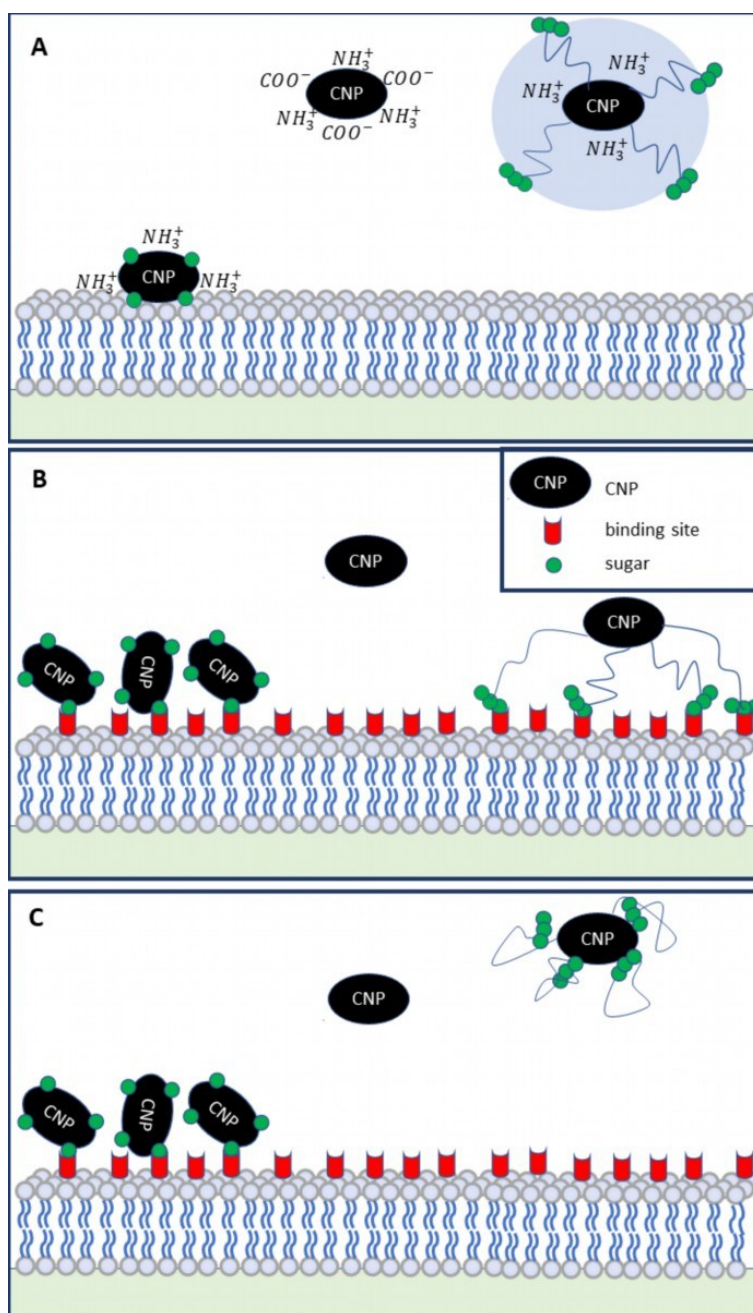
Figure S42: Illustration of possible mechanisms of membrane interaction of different CNP species and explanation of the relatively low adsorption of oligomer functionalized and pristine CNPs compared to monosaccharide functionalized CNPs. Subfigure (A) deals with the picture of electrostatic interaction with protonated amino groups. Subfigures (B) and (C) display sugar mediated explanations. The oligomer functionalized CNPs may only bind to a lesser extend to the surface due to (B) the binding to multiple binding sites at once or (C) a lower availability of the sugars due to linker flexibility.

Comment on the effect of the protein corona on the uptake of CNPs

In a preliminary experiment we tested the effect of the protein concentration in the growth medium during incubation on the uptake rate of the CNPs. MCF-7 cells were incubated with RPMI 1640 and 10% FBS with 500 µg/mL CNPs for 24 h at 37°C and 5% CO_2. In a different well MCF-7 cells were seeded in RPMI 1640 and 10% FBS without CNPs. 4 h later, the medium was aspirated out, the cells were washed with PBS and the medium was replaced by RPMI 1640 without FBS and 500 µg/mL CNPs. The cells were incubated for 20 h at 37 °C and 5% CO_2. In subsequent flow cytometry measurements, there was no difference in the signal and therefore uptake rate that could not be explained by the 4 h difference in incubation. We therefore conclude that the formation of a protein corona does not play a major role in mediating the uptake of our particles.
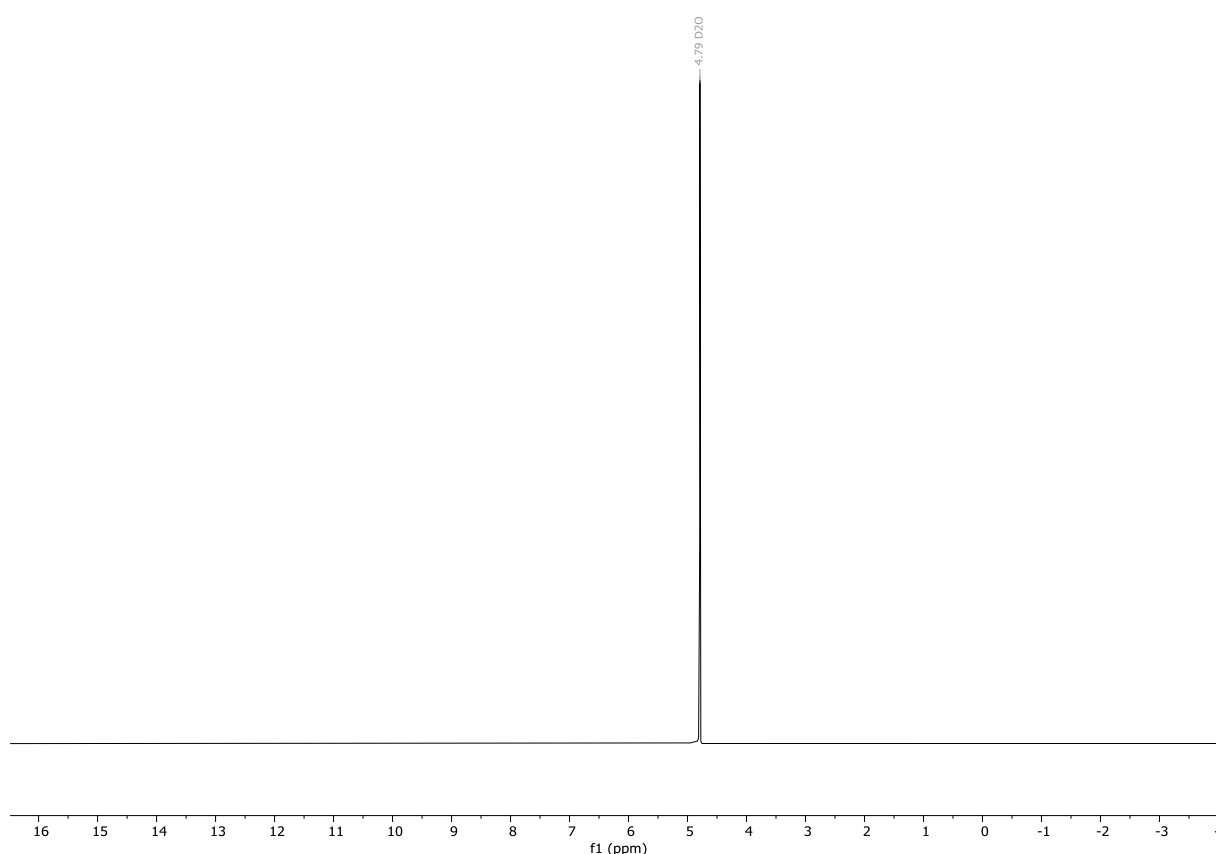
Figure S43: 300 MHz ^1H-NMR spectrum in D_2O at 25°C of the test experiment for the280lycofunctionalizationlycofunctionlization to verify the successful purification by using dialysis with a cutoff 500Da.

References:

[1] A.T.R Williams, S.A. Winfield, J.N. Miller, J. N., *Analyst*, 1983, **108**, 1067-1071.

[2] M. Taniguchi, J. S. Lindsey, *Photochem. Photobiol.*2018, **94**, 290-327.

[3] S.Boden, F.Reise, J. Kania, T. K. Lindhorst, L. Hartmann, *Macromol. Biosci*., 2019, **19**, 1800425.

[4] W. Hayes, H. M. I. Osborn, S. D. Osborne, R. A. Rastall, B. Romagnoli, *Tetrahedron*, 2003, **59**, 7983.

[5] L. Wu, N. S. Sampson, *ACS Chem. Biol*., 2014, **9**, 2, 468-475.

[6] Y. M. Chabre, C. Contino-Pépin, V. Placide, T. C. Shiao, and R. Roy, *J. Org. Chem.,* 2008, **73**, 14, 5602–5605.

[7] S. Fasbender, L. Zimmermann, R.P. Cadeddu, M. Luysberg, B. Moll, C. Janiak, T. Heinzel, R. Haas, *Sci Rep,* 2019, **9**, 12028.

[8] P.O. Gendron, F. Avaltroni, K.J., *J. Fluoresc.,*2008, **18**, 1093-1101.

5. Conclusion and Outlook

Oligo- and polysaccharides presented on cell surfaces play an important role as adhesion, recognition and signalling molecules in biological systems. They are critical for the identification of cell-cell communication, proliferation and host-pathogen interactions and further important biological signal transduction activities. Overcoming the usually weak binding of individual carbohydrate components, multivalency - the simultaneous presentation and interaction of several carbohydrate motifs and their associated receptors - is a strategy used by Nature to boost binding strength. By creating glycomimetics, which present multiple carbohydrate motifs on a synthetic scaffold such as a polymer or a nanoparticle, this concept has been effectively adapted for synthetic molecules. On the one hand, these glycomimetics are used as model systems for understanding the physiological function of carbohydrates and, on the other hand, they are used in biomedicine e.g., for bio-imaging and bio-sensing in early detection of cancer cells or as drug delivery systems to combat infectious diseases.

In this thesis, a systematic bottom-up approach was established to derive branched and brush glycomimetics of different sizes, including branched heteromultivalent and umbrella-like homo- and heteromultivalent glycooligomers using SPPoS. These glycooligomers represent the smallest structure being studied for receptor binding. To create larger and more highly multivalent ligands, these glycooligomers were conjugated to polymers yielding in brush glycopolymers, liposomes and nanoparticles such as glyco-functionalized carbon nanoparticles or Janus particles. These ligands share structural properties but also provide controlled and flexible alterations e.g., the number and type of carbohydrates or length of conjugated glycooligomers and thus can serve as model systems to systematically study the correlation between their structure and receptor binding. This was studied in this thesis by SPR and in collaboration by ^{19}F-NMR competitions assay as well as in cells studies.
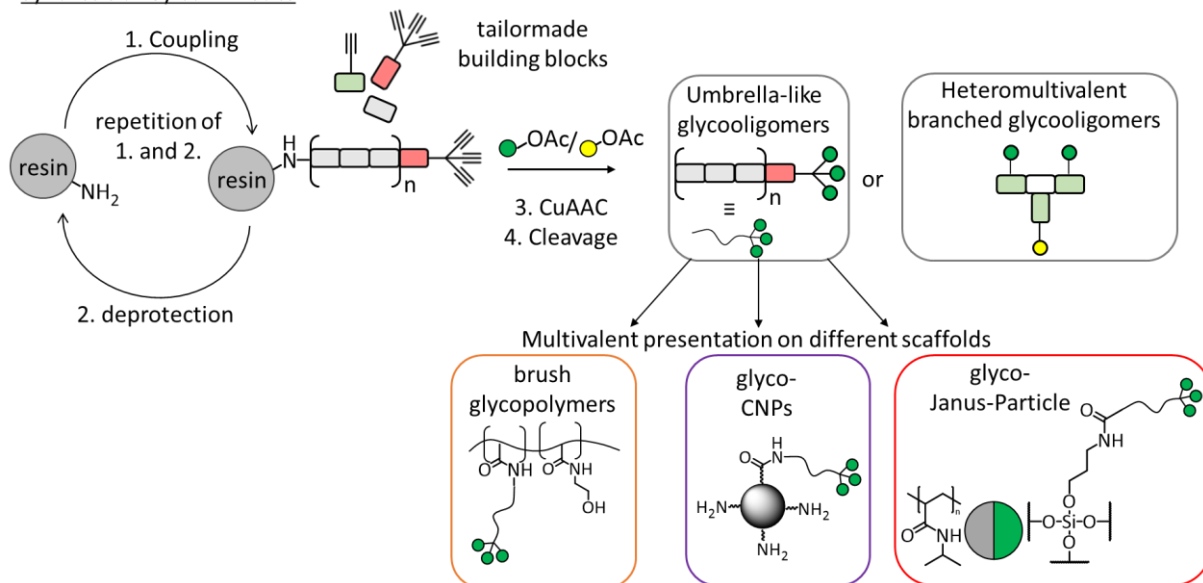
Figure 11: Synthesis of Glycomimetics. SPPoS was utilized to prepare umbrella glycooligomers and branched glycooligomers. The umbrella glycooligomers were conjugated polymer resulting in brush glycopolymers and particles yielding in glyco-carbon based nanoparticles (glyco-CNPs) and glyco-Janus Particles (glyco-JPs).

In the first part of this thesis, based on a trivalent ligand that had previously been developed as high affinity ligand for Langerin, heteromultivalent branched glycooligomers were established. (see Figure 12) The binding studies using SPR and ^{19}F-NMR inhibition competition analysis showed a linear decrease in IC_{50} when the binding is replaced by non-binding galactose and confirms a statistical rebinding of Langerin. In a similar manner, the studies were performed with DC-SIGN, another important C-type lectin of the immune system recognizing Man with four CRDs, showing even higher binding for the trivalent ligand.. The studies suggest that statistical rebinding effects are responsible for the higher binding to DC-SIGN as the main factors for the increased avidity of the trivalent glycomimetic. Conjugation of these glycooligomers to liposomes allowed flow cytometric analysis of binding to Langerin- and DC-SIGN-expressing Raji cells. Generally, as expected, the uptake of trivalent mannose-containing branched glycooligomers was observed to be higher than that of heteromultivalent glycooligomers. Comparison between cells with different C-type lectins on the cell surface revealed the highest cell interaction for DC-SIGN-expressing cells. Overall, the interaction of trivalent glycomimetic ligand on both, receptor and cell level is increased for DC-SIGN, potentially due to the additional binding site, which increases the binding avidity.
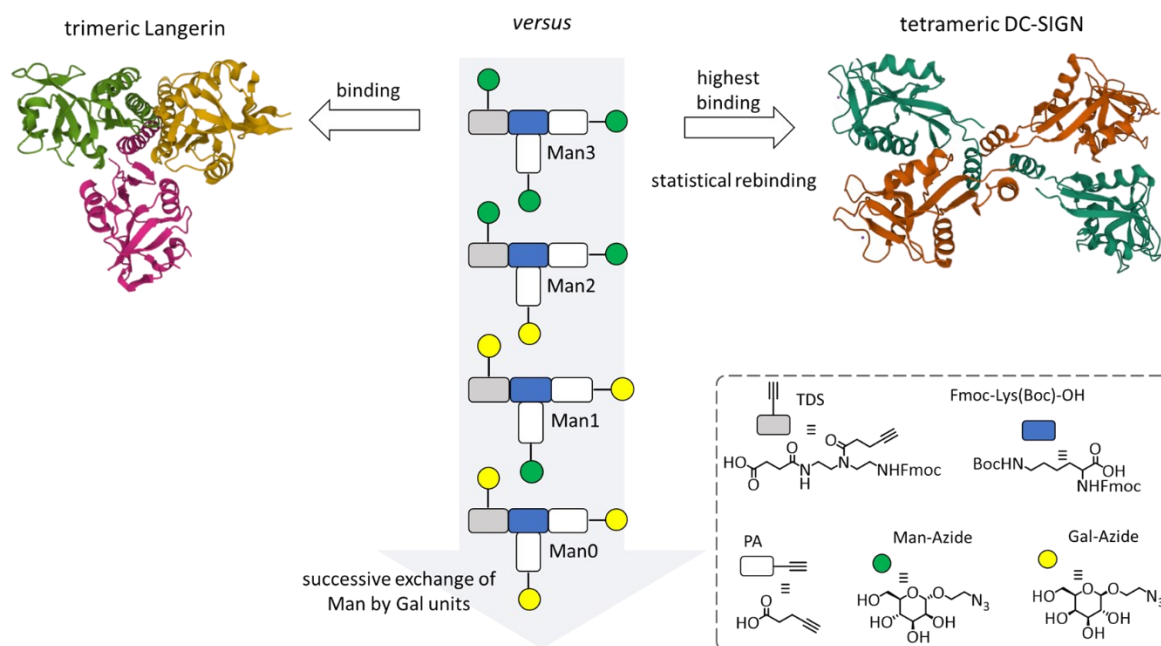
Figure 12: Branched homo- and heteromultivalent glycooligomers Man3, Man2, Man1 and Man0 synthesized using SPPoS for binding studies towards trimeric Langerin (RCSB PDB – 3KQG) and tetrameric DC-SIGN (RCSB PDB - 1XAR).

After the mechanism of statistical rebinding was supported by the synthesis of heteromultivalent branched glycooligomers and their investigation towards Langerin, in the next part of the thesis, a novel building block, the so-called TT-linker, was developed for the preparation of umbrella-like glycooligomers via SPPoS. (see Figure 11) By connecting three carbohydrate motifs in close proximity, this building block simulates natural ligands of Man-recognizing C-Typ lectins such as highly branched oligomannosides. Moreover, this structure resembles an umbrella-like design. The umbrella motif served as the unifying denominator for the further glycomimetics in this work. The umbrella-like glycooligomers consist, on the one hand, of a trivalent head group through TT linkers enabling a high carbohydrate density, and, on the other hand, of an umbrella handle. The umbrella handle allows the binding avidity to be increased by the incorporation of further binding mannose units, or in the case of non-binding galactose for potential sterical shielding e.g., to prevent non-specific interaction or clustering.

285

To enable a comparison to previous binding studies using branched glycooligomers, a ligand composed only of the umbrella head was prepared first. (see Figure 13) As expected, this ligand leads to a significant increase of the binding affinity to Langerin by a factor of 7 compared to the three-armed branched glycooligomer, which confirms the hypothesis of kinetically trapped ligand. The introduced hydrophilic handle also showed no effect regarding the binding affinity to Langerin. However, the comparison to DC-SIGN showed a significant increase in binding affinity by a factor of 2. In direct comparison to trimeric Langerin, DC-SIGN consists of four CRDs and thus potentially offers an additional binding site and an increase in binding affinity is supported by statistical rebinding effects. The investigation of the structures with additional binding mannose units also shows, as expected, high binding affinity towards Langerin. An interesting binding behaviour can be observed in the heteromultivalent umbrella-like glycooligomers. The structure with Man head group and non-binding galactose umbrella handle shows a decrease in binding by a factor of 2 compared to its counterpart with Gal head group and Man umbrella handle.
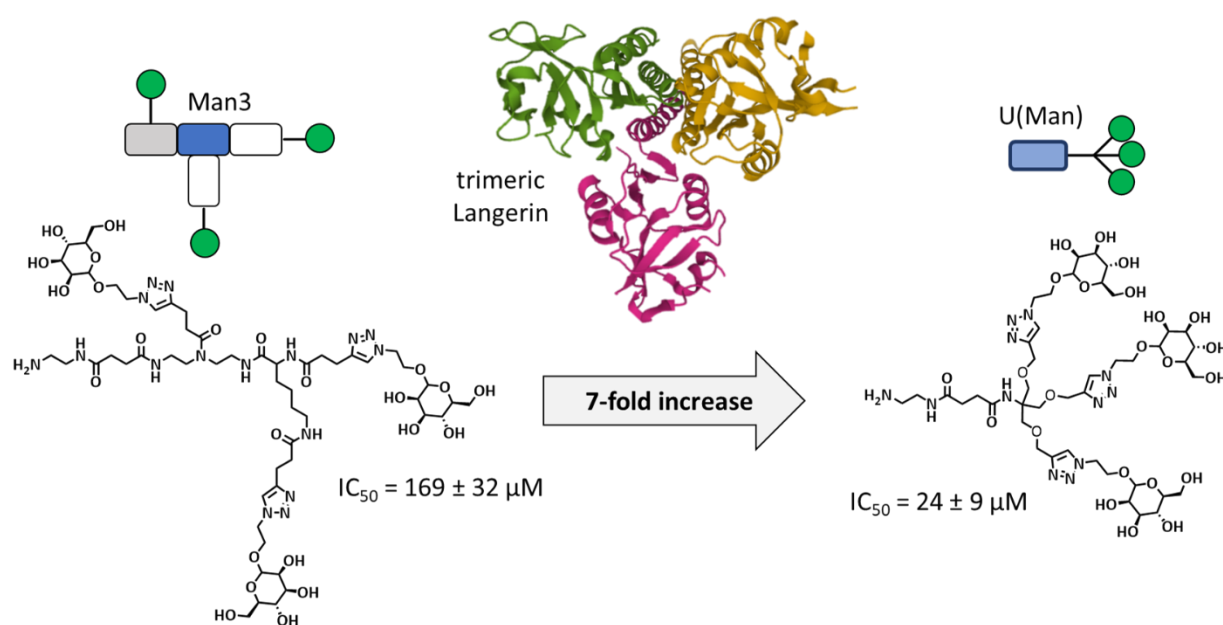
Figure13: Inhibition-competition assay using SPR showed a sevenfold increase in the binding strength of the triple-branched mannose-bearing glycooligomer Man3 to the umbrella glycooligomer consisting of the umbrella head U(Man) towards Langerin (RCSB PDB – 3KQG).

The conjugation of these umbrella-like glycooligomers onto liposomes allowed the investigation of cellular uptake towards Langerin- and DC-SIGN expressing Raji cells in collaboration with Prof. Rademacher, University Vienna. In general, the flow cytometric measurements showed no differences in uptake for Langerin-expressing cells. A clear difference was observed for the uptake analysis conducted on DC-SIGN- expressing cells. The glycoliposome decorated with an umbrella-like glycooligomer with three EDS units apparently has the correct length where the trivalent mannose umbrella head is most evident and has the highest receptor accessibility, resulting in increased cellular uptake compared to other umbrella-like glycooligomers. Future studies should investigate this mechanism in more detail for example by combining the trivalent TT-linker with a higher affinity binding motif hL which was used as positive control in flow cytometric cell uptake analysis.

In the next part of this thesis the umbrella-like glycooligomers were conjugation to a polymeric scaffold. Umbrella glycooligomers with a hydrophilic handle in different lengths were synthesized using SPPoS. As polymeric scaffold pPFP poly(active ester) was chosen. Brush glycopolymers were realized by grafting the umbrella glycooligomers onto a poly(active ester) scaffold. (see Figure 14) Additionally, brush glycopolymers were labeled with AlexaFlour647 for flow cytometric analysis to investigate the cellular binding on Langerin-expressing HEK293 cells. These analyses showed that a certain side chain length which build the brushes is required for the recognition of the trivalent mannose umbrella head and Langerin expressed on the surface of the cells.
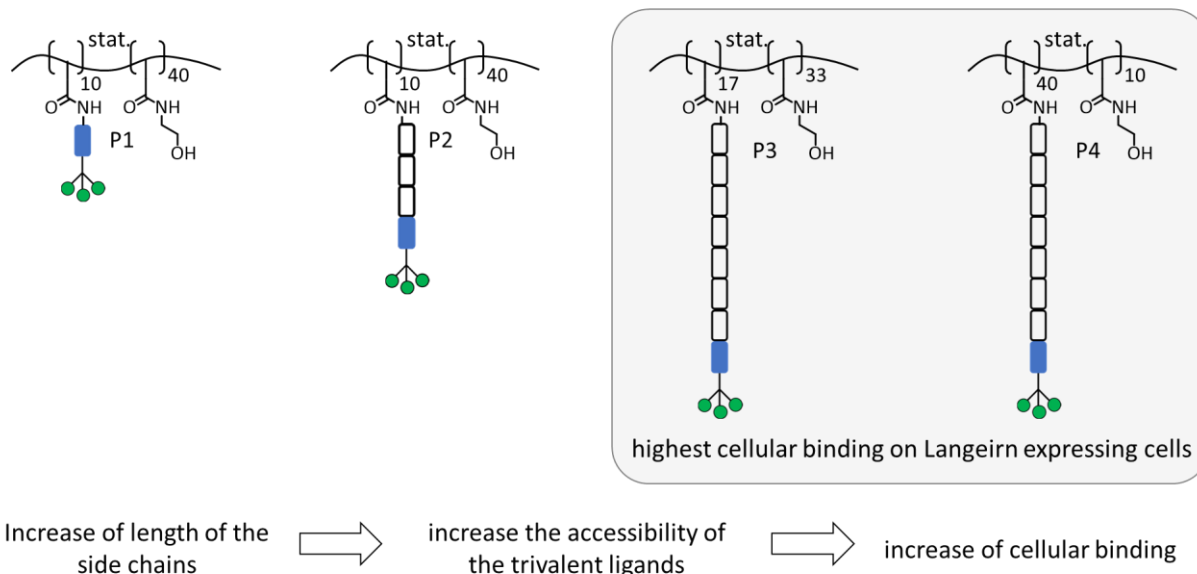
Figure 14: A set of brush glycopolymers with Man bearing umbrella-like glycooligomer as side chains were synthesized. Flow cytometric studies towards Langerin-HEK293F cells showed the highest cellular binding to brush glycopolymer with longest side chains P3 and P4. Studies towards control cell line EV-HEK293F showed no significant cellular interactions.

The highest cellular binding was observed for P3 and P4 with the longest umbrella-like glycooligomer consisting of 7 hydrophilic spacer bb EDS. Therefore, it can be assumed that the brush glycopolymers P3 and P4 have the required side chain length and thus the required distance from the polymer scaffold for the recognition of the Langerin receptors on the cell surface. The degree of functionalization applied to the polymer backbone differentiates P3 from P4. While P3 has an degree of functionalization of 34 %, P4 consists of 79 % umbrella glycooligomer side chains. Although it is expected that P4 has a higher potential to occupy multiple ligands on the cell and therefore has a high binding, the opposite is observed. In other studies it was already observed that glycopolymers with lower overall glycan density can exhibit higher avidity than their high density analogues. This can be attributed e.g., to sterical hindrance and is indeed confirmed for brush glycopolymers binding to Langerin, where a lower side chain density results in a higher apparent receptor binding. Thus, this study also shows that there is a critical density that is the limiting factor for the interaction between trivalent mannose umbrella head and Langerin in this study.

To confirm the specific binding to Langerin expressed cells, brush glycopolymers with non-binding Gal-bearing umbrella head and a chain length of 7 EDS units and a polymer without carbohydrates were also prepared. The flow cytometric study of these brush polymers on Langerin expressed cells showed no binding. In addition, all brush glycopolymers were tested on a cell line without Langerin expression (EV-HEK293F), which served as an additional control and confirmed the specific interaction between the trivalent mannose units and Langerin on the cell surface.

Future studies could investigate the effects of using other binding carbohydrates, such as sialic acids, fucose or sulphated carbohydrate components on umbrella-like scaffolds, or even more complex oligosaccharide ligands with respect to binding and possible differentiation of Langerin and DC-SIGN at the lectin and cell level. In addition, the combination of, e.g., a DNA scaffold and the mannose umbrella head is a way to test selectivity and affinity on cells or lectin. As a result of their higher selectivity, glycooligomers conjugated on liposomes could find potential applications e.g., as drug delivery systems in immune therapy.

Another important scaffold for the multivalent presentation of carbohydrates are nanoparticles. In this thesis, the combination of the umbrella motif with different nanoparticle systems was explored, leading to glyco-Janus particles (glyco-JPs) and carbon-based glyco-nanoparticles (glyco-CNPs).

The glyco-JPs were used to study bacterial adhesion towards *E. coli*. For this purpose, glyco-JPs were developed combining Man-containing umbrella glycomacromolecules on one hemisphere of the particle and a poly(N-isopropylacrylamide) (PNIPAM) layer on the opposite side and termed in as PNIPAM-Man-JP. The glyco-functionalization of the particles was verified by the zeta potential and a colorimetric test of the so-called sulphuric acid phenol method. The carbohydrate half-layer provides bacterial adhesion by interacting with lectins located on the surface of *E. coli* termed as FimH receptors that specifically recognise mannose, while the thermoresponsive PNIPAM hemisphere provides steric shielding and prevents adhesion of multiple bacteria and clustering with other particles (see Figure 15).

Using the choice of PNIPAM as a steric shield, investigate the formation of larger aggregates triggered by heating above the lower critical solution temperature (LCST), at which the PNIPAM chains would collapse and potentially result in particle-particle aggregation. To analyse the binding and clustering behaviour binding studies with ConA and *E. coli* were

performed by precipitation, inhibition competition experiments and fluorescence microscopy. While PNIPAM-Man-JP showed a halo-like arrangement on the surface of *E. coli* and led to the isolation of individual bacteria, the uniform glycofunctionalized particleswere used as control and showed a large cluster formation with *E. coli*. Furthermore, temperature-dependent experiments with PNIPAM-Man-JP and non-glycofunctionalized JP showed particle aggregation above the LCST of PNIPAM. Thus, Janus-type glyco-functionalisation resulted in controlled aggregation behaviour of individual bacterial particle clusters but retain the ability to trigger the formation of larger clusters by external stimulus, here temperature. In the future, more complex bacterial inhibition experiments such as biofilm or their use as antibacterial drug delivery can be performed to study this mechanism and the interaction of glyco-JP with FimH receptors.
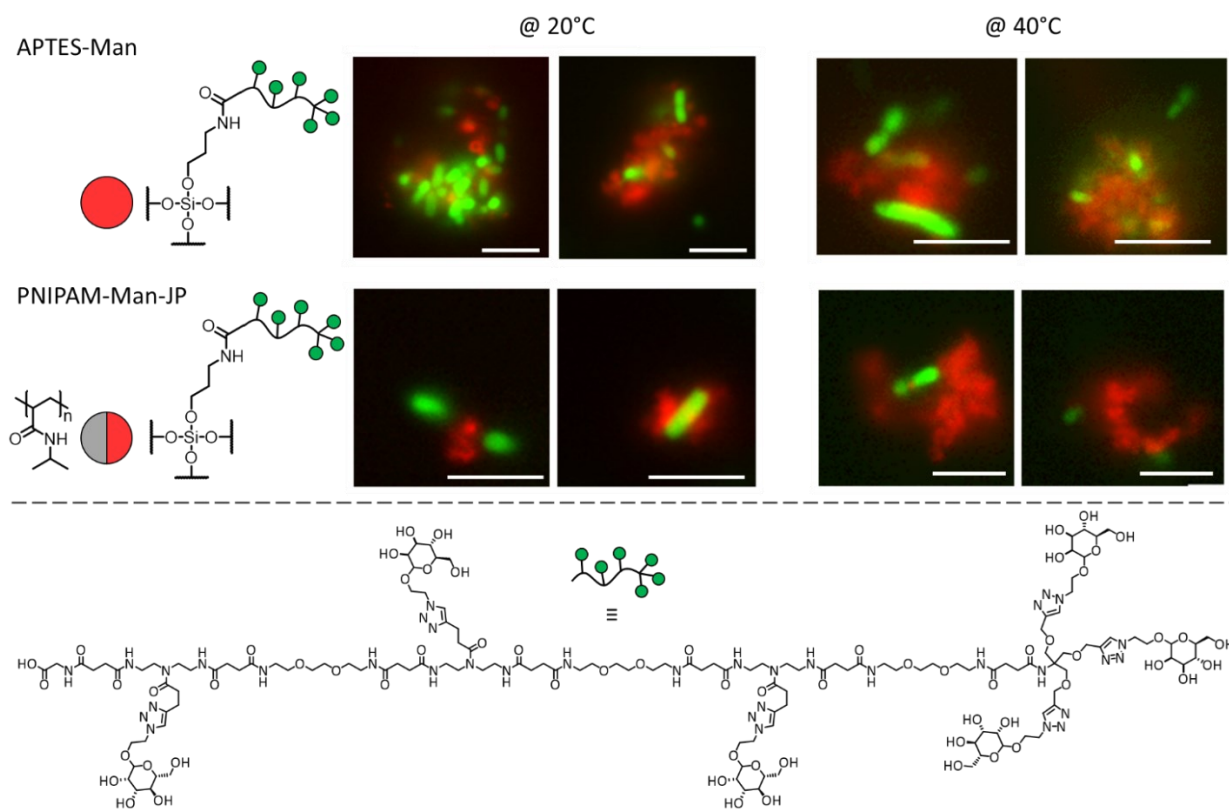
Figure 15: Uniform APTES-Man (red) functionalised with umbrella glycooligomer and PNIPAM-Man-JP (red) functionalised with umbrella glycooligomer on one side and PNIPAM on the other side were used to study adhesion behaviour towards GFP-expressed *E.coli* (green). Analysis by fluorescence microscopy showed that APTES-Man leads to accumulation of multiple *E.coli* and particles at both 20 °C and 40 °C, while PNIPAM-Man-JP significantly reduces this accumulation and adhesion of PNIPAM-Man-JP to individual E.coli is observed at 20 °C. Increasing the temperature to 40 °C leads to the collapse of the particles and thus to the aggregation of PNIPAM-Man-JP.

CNPS have attracted a lot of interest in recent years due to their advantageous properties in comparison to other nanoparticles or fluorophores, such as excellent biocompatibility, low toxicity, nanoscale size, easy modification and tuneable photoluminescence performance. Based on these special properties, CNPs are now a promising platform for bioimaging, drug delivery systems and as antibacterial agents.

In this study, different glyco-functionalised CNPs were prepared using monosaccharides and umbrella glycooligomers. The degree of functionalisation and conjugation of the carbohydrates and glycooligomers to the particle surface was evaluated by ^{1}H-NMR studies using hydroquinone as an internal standard. The ratio of triazole or anomer protons to hydroquinone protons showed that the overall degree of functionalisation is increased two- to threefold when the CNPs are functionalised with glycooligomers. (see Figure 16)
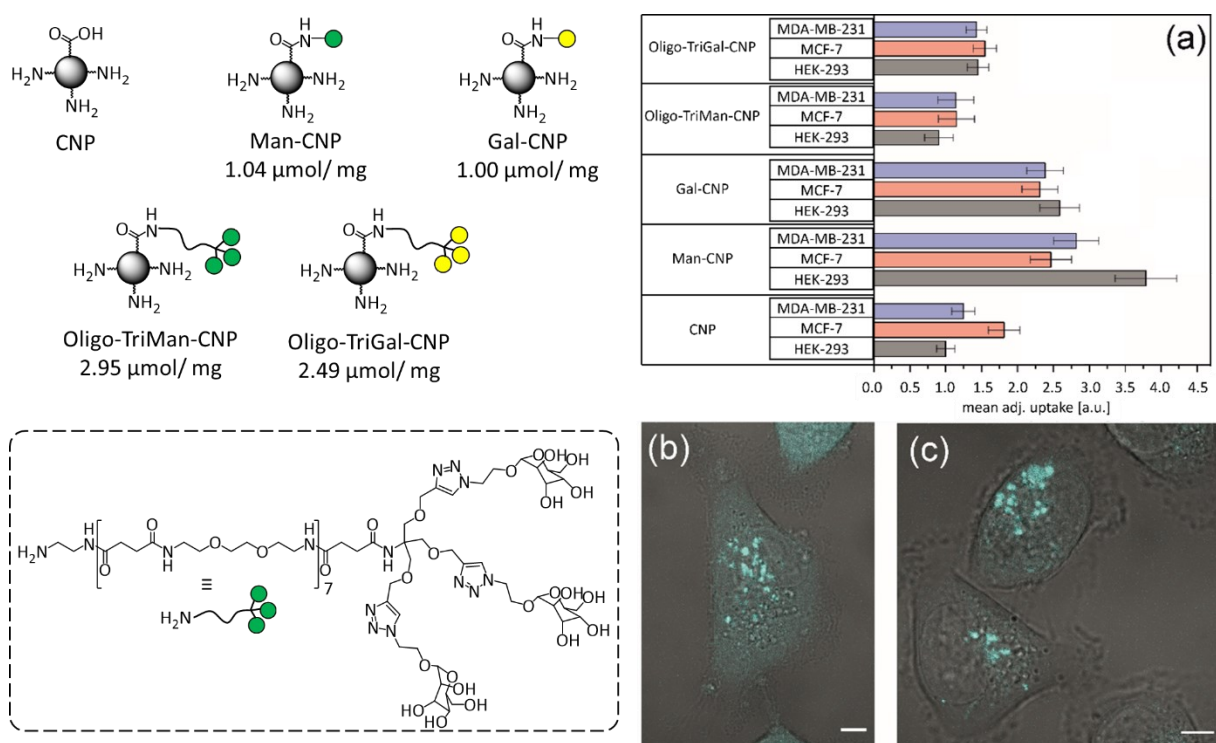
Figure 16: Series of glyco-CNPs: For the functionalization the carboyxl group of the CNPs and the amine functionality of the monosaccharide and umbrella glycooligomers Oligo-TriMan and Oligo-TriGal were conjugated using EDC and NHS coupling methods. The degree of functionalization was determined by ^{1}H-NMR analysis.

The cellular experiments towards breast cancer cell lines MDA-MB-231 and MCF-7 and non-cancer cell line HEK-293 showed that glyco-CNPs have lower cytotoxicity relative to non-glycofunctionalized CNPs. A comparison of the non-functionalised CNPs and the glycooligomer-CNPs with the monosaccharide-CNPs showed an almost threefold increase in uptake capacity. The glycooligomer-CNP conjugates may have less accessible carbohydrate motifs for interaction with cell surface receptors. However, the cellular uptake of CNPs functionalized with different monosaccharides differs only minimally. Even using cell lines with different overexpression of carbohydrate recognition receptors, especially mannose receptor (MR), very little difference in the cellular uptake of CNPs functionalised with different monosaccharides was observed. This suggests that cell absorption of the glyco-CNPs used in this study is not or only to a small extent mediated by cell surface receptors. The analysis via confocal microscopy showed that glyco-functionalisation does not alter the intracellular distribution in which the nanoparticles are preferentially taken up via the endolysosomal pathway, potentially suggesting these glyco-CNPs could have applications in cell imaging or drug delivery. In order to better understand the absorption pathways into the cell and enable receptor-mediated uptake, future study may investigate the mechanism of cellular uptake utilizing more complicated oligosaccharide ligands or non-carbohydrate ligands such as antibodies.

In summary, this thesis demonstrates the construction of glycomimetics in various shapes and sizes using a bottom-up method, starting with the simplest building block, a TT-linker made specifically for Langerin. The trivalent design this building block to be used to produce high affinity langerin glycomimetics. By specific modification of the design of the brush glycooligomers, binding to Langerin was explored. This thesis thus demonstrated the successful design of high avidity glycomimetics and their potential to achieve selectivity from a bottom-up approach starting with a small umbrella-like scaffold that was derived by a target-based rational design focusing on Langerin. This motif is not only suitable for Langerin as it enables a higher probability for statistical rebinding also for other multivalent lectins and in the future can also be explored for other multivalent receptors e.g., the adhesins of bacteria or the cell receptors of viruses. One of the key advantages of the bottom-up approach is the high flexibility in then combining the umbrella motif with a variety of other scaffolds as was successfully demonstrated for polymeric and nanoparticle-based scaffolds of different shape and size. It is one of the key findings of this thesis that indeed, binding properties of the

umbrella motif can be translated also into higher valent glycomimetics derived thereof e.g., the higher selectivity for DC-SIGN vs. Langerin. This now enables the rational design of functional materials from such glycomimetics e.g. glycofunctionalized liposomes for a targeted drug delivery, as was also already demonstrated in a proof-of-concept study in this work. Based on the importance and abundance of carbohydrates in biological interactions, it can be expected that glycoconjugates and glycomimetics as were developed in this thesis continue to play an important role in the development of next generation therapeutics.

6. Appendix

Abbreviation	Definition
ASPGR	Asialoglycoprotein receptor
BC	Birbeck Granula
BLC	B-lymphoblastic cell
CLR	C-type lectin receptor
CNP	Carbon based nanoparticles
CRD	Carbohydrate recognition domain
DC	Dendritic Cell
DC-SIGN	Dendritic Cell-Specific Intercellular adhesion molecule-3-Grabbing Non-integrin
E. coli	Escherichia coli
et al.	et alii
HCV	Hepatitis C virus
HIV-1	Human immunodeficiency virus type 1
JP	Janus particle
LC	Langerhans Cell
LCST	lower critical solution temperature
MR	Mannose receptor
TLR	Toll-like receptor

Chemicals	Trivial name
Alloc	Allyloxycarbonyl group
APTES	3-Aminopropyl)triethoxysilane

Boc	*tert*-butyloxycarbonyl
Boc$_2$O	Di-*tert*-butyl dicarbonate
CDCl$_3$-d	Deuterated chloroform
CD$_3$OD-d$_4$	Deuterated methanol
ConA	Concanavalin A
D$_2$O	Deuterium oxide
DCC	*N,N`*-Dicyclohexylcarbodiimide
DIPEA	*N,N*-Diisopropylethylamine or Hünig´s base
DMF	Dimethylformamide
DVB	Divinylbenzole
EDC	1-Ethyl-3-(3-dimethylaminopropyl)carbodiimide
EDS	Ethylene glycol spacer building block
Fuc	Fucose
Fmoc(-Cl)	9-Fluorenylmethyloxycarbonyl chloride)
Gal	β-Galactose
GlcNac	*N*-Acetylglucosamine
HOBt	1-Hydroxybenzotriazole
Man	α-Mannose
MeCN	Methyl cyanide or acetonitrile
NHS	*N*-Hydroxysuccinimid
PEG	Polyethylene glycol
PNIPAM	Poly(N-isopropylacrylamide)
pPFP	poly(pentafluorophenyl acrylate)

PyBOP	Benzotriazole-1-yl-oxy-tris-pyrrolidino-phosphonium hexafluorophosphate
TES	Triethylsilane
TDS	Triple bond-functionalized building block
TIPS	Triisopropyl silane
TFA	Trifluoroacetic acid
TRIS	Tris(hydroxymethyl)aminomethane
Trt	Trityl protecting group
TT-Linker	Three triple bond-Linker

Methods	Definition
CuAAC	Copper(I)-catalyzed azide-alkyne cycloaddition
ESI-MS	Electrospray ionization-mass spectroymetry
LC-MS	Liquid chromatography-mass spectrometry
NMR	Nuclear Magnet Resonance Spectroscopy
RP-HPLC-MS	Reverse phase high-performance liquid chromatography-mass spectrometry
SPPoS	Solid Phase polymer Synthesis
SPR	Surface Plasmon Resonance

Units and symbols	Definition
°C	degree Celcius
δ	chemical shift
g	gramm

g/mol	gramm per Mol
h	hour
IC_{50}	half maximal inhibitory concentration
K_D	equilibrium dissociation constant
K_I	inhibitory constant
MHz	megahertz
mg	milligramm
mmol	milli mol
µmol	miro mol
min	minutes
ml	milliliter
nm	nanometre
µl	microliter
m/z	Mass-to-charge ratio
pH	pondus Hydrogenii
ppm	parts per million
t_R	retention time
RT	Room temperature
RU	Response units

7. References

1. **H. S. Bennet.** Morphological aspects of extracellular polysaccharides. 1963, 11, S. 11-23.

2. **A. R. Pries, T. W. Secomb, T. W., P. Gaehtgens.** The endothelial surface layer. *Pflug. Arch. Eur. J.* 2000, 440, S. 653–666.

3. **C. R. Bertozzi, L. L. Kiessling, ,.** Chemical Gylcobiology. *Science.* 2001, 291, S. 2357-2364.

4. **K.-A. Karlsson.** Glycobiology: a growing field for drug design. *TIPS.* 12, 1991, S. 265-272.

5. **A. Varki.** Biological roles of oligosaccharides: all of the theories are correct. *Glycobiology.* 1993, 3, S. 97-130.

6. **A., Imberty, A. Varrot, A.** Microbial recognition of human cell surface glycoconjugates. *Curr. Opin. Struct. Biol.* 2008, 18, S. 567–576.

7. **J. R. Bishop, P. Gagneux.** Evolution of carbohydrate antigens–microbial forces shaping host glycomes? *Glycobiology.* 2007, 17, S. 23-34.

8. **D. B. Werz, P. H. Seeberger,.** Carbohydrates as the Next Frontier in Pharmaceutical Research. *Chem. Eur. J. .* 2005, 11, S. 3194-3206.

9. **R. A. Dwek.** Glycobiology: Toward Understanding the Function of Sugars. *Chem. Rev.* 1996, 96, S. 683-720.

10. **L. L. Kiessling, J. C. Grim,.** Glycopolymer probes of signal transduction. *Chem. Soc. Rev.* 2013, 42, S. 4476-4491.

11. **K. De Schutter, E. J. M. Van Damme.** Protein-Carbohydrate Interactions as Part of Plant Defense and Animal Immunity. *Molecules.* 2015, 20, S. 9029-9053.

12. **W. C. Boyd, E. Shapleigh,.** Specific Precipitating Activity of Plant Agglutinins (Lectins). *Science.* 1954, 119, S. 419.

13. **A. F. S. Santos, M. D. C., Da Silva, T. H. Napoleão, P. M. G. Paiva, M. T. S. Correia, L. C. B. B.Coelho.** Lectins: Function, structure, biological properties andpotential applications. *Curr. Top. Pept. Protein Res.* 2014, 15, S. 41–62.

14. **E. Kottgen, W. Reutter, R. Tauber.** Endogene Lectine des Menschen und ihre Zuckerliganden. *Med. Klin.* 2003, 98, S. 717-738.

15. **O. C. Grant, H.M, Smith, D. Firsova, E. Fadda, R. J. Woods.** Presentation, presentation, presentation! Molecular-level insight into linker effects on glycan array screening data. *Glycobiology.* 2014, 24, S. 17–25.

16. **L. L. Kiessling, J. E. Gestwicki, L. E. Strong.** Synthetic multivalent ligands in the exploration of cell-surface interactions . *Curr. Opin. Chem. Biol.* 2000, 4, S. 696–703.

17. **J. E. Gestwicki, C. W. Cairo, L. E. Strong, K. A. Oetjen, L.L. Kiessling.** Influencing Receptor–Ligand Binding Mechanisms with Multivalent Ligand Architecture. *J. Am. Chem. Soc. .* 2002, 124, S. 14922–14933.

18. **R. J. Pieters.** Maximising multivalency effects in protein-carbohydrate interactions. *Org. Biomol. Chem.* 2009, 7, S. 2013–2025.

19. **M. Weber, A. Bujotzek, R. Haag.** Quantifying the rebinding effect in multivalent chemical ligand-receptor system. *J. Chem. Phys.* 2012, 137, S. 054111.

20. **N. Jayaraman.** Multivalent ligand presentation as a central concept to study intricate carbohydrate-protein interactions. *Chem. Soc. Rev.* 2009, 38, S. 3463–3483.

21. **Y. C. Lee, R. T. Lee,.** Carbohydrate-Protein Interactions: Basis of Glycobiology. *Acc. Chem. Res.* 1995, 28, S. 321-327.

22. **J.J. Lundquist, E.J. Toone.** The Cluster Glycoside Effect. *Chem. Rev.* 2002, 102, S. 555–578.

23. **J. Vonnemann, S. Liese, C. Kuehne, K. Ludwig, J. Dernedde, C. Böttcher, R. R. Netz, R. Haag.** Size-dependence of steric shielding and multivalency effects for globular binding inhibitors. *J. Am. Chem. Soc.* 2015, 137, S. 2572-2579.

24. **A. Robinson, J. M. Fang, P. T. Chou PT, K. W. Liao, M. Chu, S.J. Lee.** Probing lectin and sperm with carbohydrate-modified quantum dots. *ChemBioChem.* 2005, 6, S. 1899–1905.

25. **Nicholson L. B. (). Essays in biochemistry, (3),.** The immune system. *Essays Biochem.* 2016, 60, S. 275–301.

26. **Y. Ni, I. Tizard.** Lectin-carbohydrate interaction in the immune system. *Vet. Immunol. Immunopathol.* 1996, 55, S. 205–223.

27. **J. S. Marshall, R. warrington, W. Watson, H. L. Kim.** An introduction to immunology and immunopathology. *Allergy. Asthma Clin. Immunol.* 2018, 14, S. 49.

28. **M. S. Diamond, T. D. Kanneganti.** Innate immunity: the first line of defense against SARS-CoV-2. *Nat. Immunol.* 2022, 23, S. 165–176.

29. **M. Riera Romo, D. Perez-Martinez, C. Castillo Ferrer.** Innate immunity in vertebrates: an overview. *Immunology.* 2016, 148, S. 125–139.

30. **P. Ferraboschi, S. Ciceri, P. Grisenti.** Applications of Lysozyme, an Innate Immune Defense Factor, as an Alternative Antibiotic. *Antibiotics (Basel).* 2021, 10, S. 1534.

31. **Marshall, J. S.** Mast-cell responses to pathogens. *Nat. Rev. Immunol.* 2004, 4, S. 787–799.

32. **M. Metz, F. Siebenhaar, M. Maurer.** Mast cell functions in the innate skin immune system. *Immunobiology.* 2008, 213, S. 251–260.

33. **E. B. Thangam, E. A. Jemima, H. Singh, M. S. Baig, M. Khan, C. B. Mathias, M. K. Church, R. Saluja.** The Role of Histamine and Histamine Receptors in Mast Cell-Mediated Allergy and Inflammation: The Hunt for New Therapeutic Targets. *Front. Immunol.* 2018, 9.

34. **M. T. Silva, M. Correia-Neves.** Neutrophils and Macrophages: the Main Partners of Phagocyte Cell Systems . *Front. Immunol.* 2012, 3, S. 174.

35. **S. Paust, B. Senman, U. H. von Andrian.** Adaptive Immune Responses Mediated by Natural Killer Cells. *Immunol. Rev.* 2010, 235, S. 286–296.

36. **Lanier, L. L.** Up on the tightrope: natural killer cell activation and inhibition. *Nat. Immunol.* 2008, 9, S. 495–502.

37. **M. Gorelik, P. A. Frischmeyer-Guerrerio.** Innate and Adaptive Dendritic Cell Responses to Immunotherapy. *Curr. Opin. Allergy Clin. Immunol. .* 2015, 15, S. 575–580.

38. **T. W. LeBien, T. F. Tedder.** B lymphocytes: how they develop and function. *Blood.* 2008, 112, S. 1570–1580.

39. **K. Pallmer, A. Oxenius.** Recognition and Regulation of T Cells by NK Cells. *Front. Immunol.* 2016, 7, S. 251.

40. **W. Hoffman, F. G. Lakkis,G. Chalasani.** B Cells, Antibodies, and More. *Clin. J. Am. Soc. Nephrol.* 2016, 11, S. 137–154.

41. **M. D. Cooper, M. N. Alder.** The evolution of adaptive immune systems. *Cells.* 2006, 124, S. 815-822.

42. **K. Shortman, Y. J. Liu.** Mouse and human dendritic cell subtypes. *Nat. Rev. Immunol.* 2002, 2, S. 151–161.

43. **D. Jarrossay, G. Napolitani, M. Colonna, F. Sallusto, A. Lanzavecchia.** Specialization and complementarity in microbial molecule recognition by human myeloid and plasmacytoid dendritic cells. *Eur. J. Immunol.* 2001, 31, S. 3388–3393.

44. **A. Szabo, E. Rajnavolgyi.** Collaboration of Toll-like and RIG-I-like receptors in human dendritic cells: tRIGgering antiviral innate immune responses. *Am. J. Clini. Exp. Immunol.* 2013, 2, S. 195–207.

45. **Unterholzner, L.** The interferon response to intracellular DNA: why so many receptors? *Immunobiology.* 2013, 218, S. 1312–1321.

46. **I. G. Zizzari, C. Napoletano, F. Battisti, H. Rahimi, S. Caponnetto, L. Pierelli, M. Nuti, A. Rughetti.** MGL Receptor and Immunity: When the Ligand Can Make the Difference. *J. Immunol. Res.* 2015, 015, S. 450695.

47. **C. G. Figdor, Y. van Kooyk, G. Adema.** C-type lectin receptors on dendritic cells and Langerhans cells. *Nat. Rev. Immunol.* 2002, 2, S. 77–84.

48. **E. J. Soilleux, R. Barten, J. Trowsdale.** DC-SIGN; a related gene, DC-SIGNR; and CD23 form a cluster on 19pl3. *J. Immunol.* 2000, 165, S. 2937–2942.

49. **M. van der Vlist, T. B. Geijtenbeek.** Langerin functions as an antiviral receptor on Langerhans cells. *Immunol Cell Biol.* 2010, 88, S. 410–415. .

50. **N. Romani, M. Thurnher, J. Idoyaga, R. M. Steinman, V. Flacher.** Targeting of antigens to skin dendritic cells: possibilities to enhance vaccine efficacy. *Immunol. Cell Biol. .* 2010, 88, S. 424-430.

51. **J. Valladeau, V. Duvert-Frances, J. J. Pin, C. Dezutter-Dambuyant, C. Vincent, C. Massacrier, J. Vincent, K. Yoneda, J. Banchereau, C. Caux, J. Davoust, S. Saeland.** The monoclonal antibody DCGM4 recognizes Langerin, a protein specific of Langerhans cells, and is rapidly internalized from the cell surface. *Eur. J. Immunol.* 1999, 29, S. 2695-2704.

52. **H. Feinberg, M.E. Taylor, N.Razi, R. McBride, Y.A. Knirel, S.A. Graham, K. Drickamer, W. I. Weis.** Structural basis for langerin recognition of diverse pathogen and mammalian glycans through a single binding site . *J. Mol. Biol.* 2011, 405, S. 1027-1039.

53. **H. Feinberg, A. S. Powlesland, M. E. Taylor, W. I. Weis.** Trimeric structure of langerin. *J. Biol. Chem. .* 2010, 285 , S. 13285–13293.

54. **H. Feinberg, Y. Guo, D. a. Mitchell, K. Dirckamer, W. I. Weis.** Extended neck regions stabilize tetramers of the receptors DC-SIGN and DC-SIGNR. *J. Biol. Chem.* 2005, S. 1327-1335.

55. **D. A. Mitchell, A. J. Fadden, K. Drickamer.** A Novel Mechanism of Carbohydrate Recognition by the C-type Lectins DC-SIGN and DC-SIGNR: SUBUNIT ORGANIZATION AND BINDING TO MULTIVALENT LIGANDS. *J. Biol. Chem.* 2001, 276, S. 28939–28945.

56. **A. Cambi, M.G. Netea, H. M. Mora-Montes, N. A.R. Gow, S. V. Hato, D. W. Lowman, B.-J. Kullberg, R. Torensma, D. L. Williams, C. G. Figdor.** Dendritic Cell Interaction with Candida albicans Critically Depends on N-Linked Mannan. *JBC.* 2008, 283, S. 20590-20599.

57. **A. Varki, Volume 27, Issue 1, 1 January , Pages 3–49,.** Biological roles of glycans. *Glycobiology,.* 2017, 27, S. 3–49.

58. **T. B. H. Geijtenbeek, D. S. Kwon, R. Torensma, S. J. van Vliet, G. C. van Duijnhoven, J. Middel, I. L. Cornelissen, H. S. Nottet, V. N. KewalRamani, D. R. Littman, C. G. Figdor, Y. van Kooyk.** DC-SIGN, a dendritic cell-specific HIV-1-binding protein that enhances trans-infection of T cells. *Cells.* 2000, 100, S. 587–597.

59. **S. Pohlmann, J. Zhang, F. Baribaud, Z. Chen, G.J. Leslie, G. Lin, A. Granelli-Piperno, R.W. Doms, C.M. Rice, J.A. McKeating.** Hepatitis C virus glycoproteins interact with DC-SIGN and DC-SIGNR. *J. Virol.* 2003, 77, S. 4070-4080.

60. **N. Maeda, J. Nigou, J.L. Herrmann, M. Jackson, A. Amara, P.H. Lagrange, G. Puzo, B. Gicquel, O. Neyrolles.** The cell surface receptor DC-SIGN discriminates between Mycobacterium species through selective recognition of the mannose caps on lipoarabinomannan. *J. Biol. Chem.* 2003, 278, S. 5513-5516.

61. **M. L. del Rio, J. I. Rodriguez-Barbosa, E. Kremmer, R. Forster.** CD103- and CD103+ bronchial lymph node dendritic cells are specialized in presenting and cross-presenting innocuous antigen to CD4+ and CD8+ T cells. *J. Immunol.* 2007, 178, S. 6861–6866.

62. **A. N. Desch, G. J. Randolph, K. Murphy, E. L. Gautier, R. M. Kedl, M. H. Lahoud, I. Caminschi, K. Shortman, P. M. Henson, C. V. Jakubzick.** CD103+ pulmonary dendritic cells preferentially acquire and present apoptotic cell-associated antigen. . *J. Exp. Med.* 2011, 208, S. 1789–1797.

63. **L. de Witte, A. Nabatov, M. Pion, D. Fluitsma, M. A. W. P. de Jong, T. de Gruijl, V. Piguet, Y. van Kooyk, T. B. H. Geijtenbeek.** Langerin is a natural barrier to HIV-1 transmission by Langerhans cells. *Nat. Med.* 2007, 13, S. 367–371.

64. **L. Burleigh, P. Y. Lozach, C. Schiffer, I. Staropoli, V. Pezo, F. Porrot, B. Canque, J. L. Virelizier, F. Arenzana-Seisdedos, A. Amara.** Infection of dendritic cells (DCs), not DC-SIGN-mediated internalization of human immunodeficiency virus, is required for long-term transfer of virus to T cells. *J. Virol.* 2006, 80, S. 2949–2957.

65. **A. L. Smith, L. Ganesh, K. Leung, J. Jongstra-Bilen, J. Jongstra, G. J. Nabel.** Leukocyte-specific protein 1 interacts with DC-SIGN and mediates transport of HIV to the proteasome in dendritic cells. *J. Exp. Med.* 2007, 204, S. 421–430.

66. **M. Thepaut, J.Valladeau, A. Nurisso, R. Kahn, B. Arnou, C. Vivès, S. Saeland, C. Ebel, C.Monnier, C. Dezutter-Dambuyant, A. Imberty, F. Fieschi.** Structural studies of langerin and Birbeck granule: a macromolecular organization model. Biochemistry. 2009, 48, S. 2684–2698.

67. **W. C. Ng, S. L. Londrigan, N. Nasr, A. L. Cunningham, S. Turville, A. G. Brooks, P. C. Reading.** The C-type Lectin Langerin Functions as a Receptor for Attachment and Infectious Entry of Influenza A Virus. *J. Virol. .* 2015, 90, S. 206–221.

68. **N. S. Stambach, M. E. Taylor.** Characterization of carbohydrate recognition by langerin, a C-type lectin of Langerhans cells. *Glycobiology.* 2003, 13, S. 401–410.

69. **M. A. de Jong, L. de Witte, S. J. Santegoets, D. Fluitsma, M. E. Taylor, T. D. de Gruijl, T. B. Geijtenbeek.** Mutz-3-derived Langerhans cells are a model to study HIV-1 transmission and potential inhibitors. *J. Leikocyte Biol.* 2010, 87, S. 637-643.

70. **M. A. Naarding, I. S. Ludwig, F. Groot, B. Berkhout, T. B. Geijtenbeek, G. Pollakis, W. A. Paxton.** Lewis X component in human milk binds DC-SIGN and inhibits HIV-1 transfer to CD4+ T lymphocytes. . *J. Clin. Invest.* 2005, 115, S. 3256-3264.

71. **C. L Bennett.** Editorial: Faux amis: Langerin-expressing DC in humans and mice. *J. Leukoc. Biol.* 2015, 97, S. 621–623.

72. **A. Holla, A. Skerra.** Comparative analysis reveals selective recognition of glycans by the dendritic cell receptors DC-SIGN and Langerin. *PEDS.* 2011, 24, S. 659–666.

73. **K. Neuhaus, E. C. Wamhoff, T. Freichel, A. Grafmüller, C. Rademacher, L. Hartmann.** Asymmetrically Branched Precision Glycooligomers Targeting Langerin. . *Biomacromolecules.* 2019, 20, S. 4088-4095.

74. **Y. Abdouni, G. Yilmaz, A. Monaco, R. Aksakal, C. R. Becer.** Effect of Arm Number and Length of Star-Shaped Glycopolymers on Binding to Dendritic and Langerhans Cell Lectins. *Biomacromolecules.* 2020, 21, S. 3756–3764.

75. **R.-J.E. Li, T.P. Hogervorst , S. Achilli, S.C.M. Bruijns, S. Spiekstra, C. Vivès, M. Thépaut, D.V. Filippov, G.A. van der Marel, S.J. van Vliet, F. Fieschi, J.D.C. Codée, Y. van Kooyk.** Targeting of the C-Type Lectin Receptor Langerin Using Bifunctional Mannosylated Antigens. *Front. Cell Dev. Biol.* 2020, 8, S. 556.

76. **B. Ernst, J. Magnani.** From carbohydrate leads to glycomimetic drugs. *Nat. Rev. Drug Discov.* 2009, 8, S. 661–677.

77. **G. B. Sigal, M. Mammen, G. Dahmann, G. M. Whitesides.** Polyacrylamides Bearing Pendant α-Sialoside Groups Strongly Inhibit Agglutination of Erythrocytes by Influenza Virus: The Strong Inhibition Reflects Enhanced Binding through Cooperative Polyvalent Interactions. *J. Am. Chem. Soc. .* 1996, 118, S. 3789–3800.

78. **T. W. Rademacher, R. B. Parekh, R. A. Dwek.** Gylcobiology. *Annu. Rev. Biochem.* 1988, 57, S. 785-838.

79. **M. Phillips, E. Nudelman, F. Gaeta, M. Perez, A. Singhal, S. Hakomori, J. Paulson.** ELAM-1 mediates cell adhesion by recognition of a carbohydrate ligand, sialyl-Lex. *Science.* 1990, 250, S. 1130-1132.

80. **H. Feinberg, D. A. Mitchell, K. Drickamer, W. I. Weis.** Structural basis for selective recognition of oligosaccharides by DC-SIGN and DC-SIGNR. *Science.* 2001, 294, S. 21632166.

81. **Y. Gou, J. Geng, S.-J. Richards, J. Burns, C. R. Becer, D. M. Haddleton.** A detailed study on understanding glycopolymer library and Con A interactions. *J. Polym. Sci. A.* 2013, 51, S. 2588-2597.

82. **S. André, R. J. Pieters, I. Vrasidas, H. Kaltner, I. Kuwabara, F. T. Liu, R. M. J. Liskamp, H. J. Gabius.** Wedgelike glycodendrimers as inhibitors of binding of mammalian galectins to glycoproteins, lactose maxiclusters, and cell surface glycoconjugates. . *Chembiochem.* 2001, 2, S. 822-830.

83. **H. Xue, L. Peng, Y. Dong, Y. Zheng, Y. Luan, X. Hu, G. Chen, H. Chen.** Synthesis of star-glycopolymers by Cu(0)-mediated radical polymerisation in the absence and presence of oxygen. *RSC Adv.* 2017, 7, S. 8484-8490.

84. **M. Nagao, Y. Fujiwara, T. Matsubara, Y. Hoshino, T. Sato, Y. Miura.** Design of Glycopolymers Carrying Sialyl Oligosaccharides for Controlling the Interaction with the Influenza Virus. *Biomacromolecules.* 2017, 18, S. 4385-4392.

85. **D. Ponader, F. Wojcik, F. Beceren-Braun, J. Dernedde, L. Hartmann.** Sequence-Defined Glycopolymer Segments Presenting Mannose: Synthesis and Lectin Binding Affinity. *Biomacromolecules.* 2012, 13, S. 1845-1852.

86. **C. Gerke, M. F. Ebbesen, D. Jansen, S. Boden, T. Freichel, L. Hartmann.** Sequence-Controlled Glycopolymers via Step-Growth Polymerization of Precision Glycomacromolecules for Lectin Receptor Clustering. . *Biomacromolecules.* 2017, 18, S. 787-796.

87. **S. A. Hill, C. Gerke, L. Hartmann.** Recent Developments in Solid-Phase Strategies towards Synthetic, Sequence-Defined Macromolecules. *Chem. Asian J.* 2018, 13, S. 3611-3622.

88. **A. Banger, J. Sindram, M. Otten, J. Kania, D. Wilms, A. Strzelczyk, A. Miletic, T. C. Marlovits, M. Karg, L. Hartmann.** Synthesis and Self-assembly of Amphiphilic Precision Glycomacromolecules. *Polym. Chem.* 2021.

89. **T. Freichel, V. Heine, D. Laaf, A. E. Mackintosh, S. Sarafova, L. Elling, N. L. Snyder, L.Hartmann.** Sequence-Defined Heteromultivalent Precision Glycomacromolecules Bearing Sulfonated/Sulfated Nonglycosidic Moieties Preferentially Bind Galectin-3 and Delay Wound Healing of a Galectin-3 Positive Tumor Cell Line in an In Vitro Wound Scratch Assay. *Macromol. Biosci. .* 2020, 20, S. 202000163.

90. **L. Fischer, R. C. Steffens, T. J. Paul, L. Hartmann.** Catechol-functionalized sequence-defined glycomacromolecules as covalent inhibitors of bacterial adhesion. *Polym. Chem.* 2020, 11, S. 6091-6096.

91. **F. Jacobi, D. Wilms, T. Seiler, T. Queckbörner, M. Tabatabai, L. Hartmann, S. Schmidt.** Effect of PEGylation on Receptor Anchoring and Steric Shielding at Interfaces: An Adhesion and Surface Plasmon Resonance Study with Precision Polymers. *Biomacromolecules.* 2020, 21, S. 4850–4856.

92. **F. Shamout, A. Monaco, G. Yilmaz, C. R. Becer, L. Hartmann.** Synthesis of Brush-Like Glycopolymers with Monodisperse, Sequence-Defined Side Chains and Their Interactions with Plant and Animal Lectins. *Macromol. Rapid Commun.* 2020, 41, S. 1900459.

93. **M. D. Illmann, L Schäfl, F. Drees, L. Hartmann, S. Schmidt.** Glycan-Presenting Coacervates Derived from Charged Poly(active esters): Preparation, Phase Behavior, and Lectin Capture. *Biomacromolecules.* 2023, XXX, S. XXX-XXX.

94. **S. Boden, K. G. Wagner, M. Karg, L. Hartmann.** Presenting Precision Glycomacromolecules on Gold Nanoparticles for Increased Lectin Binding. *Polymers (Basel).* 2017, 9, S. 716.

95. **F. Jacobi, A. Camaleño de la Calle, S. Boden, A. Grafmüller, L. Hartmann, S. Schmidt.** Multivalent Binding of Precision Glycooligomers on Soft Glycocalyx Mimicking Hydrogels. *Biomacromolecules.* 2018, 19, S. 3479-3488.

96. **T. Freichel, D. Laaf, M. Hoffmann, P. B. Konietzny, V. Heine, R. Wawrinek, C. Rademacher, N. L. Snyder, L. Elling, L. Hartmann.** Effects of linker and liposome anchoring on lactose-functionalized glycomacromolecules as multivalent ligands for binding galectin-3. *RSC Adv.* 2019, 9, S. 23484-23497.

97. **E. Fischer ()., (3),.** Synthese von Polypeptiden. *Berichte der deutschen chemischen Gesellschaft.* 1903, 36, S. 2982–2992.

98. **E. Fischer, E. Fischer, E. Fourneau.** *Ueber einige derivate des Glykocolls.* s.l. : Springer Berlin Heidelberg, 1906. S. 279-289.

99. **Merrifield, R. B.** Solid phase peptide synthesis. I. The synthesis of a tetrapeptide. . *J. Am. Chem. Soc.* 1963, 85, S. 2149-2154.

100. —. Solid phase synthesis (Nobel lecture). *Angew. Chem. Int. Ed.* 1985, 24, S. 799-810.

101. **Mitchell, A. R.** Bruce Merrifield and solid-phase peptide synthesis: a historical assessment. . *Biopolymers.* 2008, 90, S. 175-184.

102. **Merrifield, B.** Solid phase synthesis. *Science.* 1986, 232, S. 341-347.

103. **P. T. Shelton, K. J. Jensen KJ. (Clifton, N.J.). und 23943476., 1047:23-41. DOI: 10.1007/978-1-62703-544-6_2. PMID:.** Linkers, resins, and general procedures for solid-phase peptide synthesis. Methods in Molecular Biology. *Methods in molecular biology (Clifton, N.J.).* 2013, S. 23–41.

104. **S. Zalipsky, J. L. Chang, F. Albericio, G. Barany.** Preparation and applications of polyethylene glycol-polystyrene graft resin supports for solid-phase peptide synthesis. *Reactive Polymers.* 1994, 22, S. 243-258.

105. **Carpino, L.** The 9-fluorenylmethyloxycarbonyl family of base-sensitive amino-protecting groups. *Acc. Chem. Res.* 1987, 20, S. 401-407.

106. **B. M. Trost, T. J. Fullerton.** Organic syntheses by means of noble metal compounds XVII. Reaction of π-allylpalladium chloride with nucleophiles. *J. Am. Chem. Soc.* 1973, 95, S. 292-294.

107. **B. M. Trost, P. E. Strege.** Asymmetric induction in catalytic allylic alkylation. *J. Am. Chem. Soc.* 1977, 99, S. 1649–1651.

108. **L. Hartmann, E. Krause, M. Antonietti, H. G. Börner.** Solid-phase supported polymer synthesis of sequence-defined, multifunctional poly(amidoamines). *Biomacromolecules.* 2006, 4, S. 1239-1244 .

109. **F. Wojcik, S. Mosca, L. Hartmann.** Solid-Phase Synthesis of Asymmetrically Branched Sequence-Defined Poly/Oligo(amidoamines). *J. Org. Chem.* 2012, 77, S. 4226–4234.

110. **F. Wojcik, A. G. O'Brien, S. Götze, P. H. Seeberger, L. Hartmann.** Synthesis of carbohydrate-functionalised sequence-defined oligo(amidoamine)s by photochemical thiol-ene coupling in a continuous flow reactor. *Chem. Eur. J.* 2013, 19, S. 3090-3098.

111. **S. Boden, F. Reise, J. Kania, T. K. Lindhorst, L. Hartmann.** Sequence-Defined Introduction of Hydrophobic Motifs and Effects in Lectin Binding of Precision Glycomacromolecules. *Macromol Biosci.* 2019, 19, S. e1800425.

112. **T. Freichel, S. Eierhoff, N. L. Snyder, L. Hartmann.** Toward Orthogonal Preparation of Sequence-Defined Monodisperse Heteromultivalent Glycomacromolecules on Solid Support Using Staudinger Ligation and Copper-Catalyzed Click Reactions. *J. Org. Chem.* 2017, 82, S. 9400-9409.

113. **H. C. Kolb, M. G. Finn, K. B. Sharpless.** Click Chemistry: Diverse Chemical Function from a Few Good Reactions. *Angew Chem Int Ed Engl.* 2001, 40, S. 2004-2021.

114. **L. Liang, D. Astruc.** he copper(I)-catalyzed alkyne-azide cycloaddition (CuAAC) "click" reaction and its applications. An overview. *Coord. Chem. Rev.* 2011, 255, S. 2933-2945.

115. **C. W. Tornøe, C. Christensen, M. Meldal.** Peptidotriazoles on Solid Phase: [1,2,3]-Triazoles by Regiospecific Copper(I)-Catalyzed 1,3-Dipolar Cycloadditions of Terminal Alkynes to Azides. *J. Org. Chem.* 2002, 67, S. 3057–3064.

116. **M. Amblard, J.-A. Fehrentz, J. Martinez, G. Subra.** Methods and protocols of modern solid phase Peptide synthesis. *Mol. Biotechnol.* 2006, 33, S. 239-254.

117. **S. Igde, S. Röblitz, A. Müller, K. Kolbe, S. Boden, C. Fessele, T.K. Lindhorst, M. Weber, L. Hartmann, Linear Precision Glycomacromolecules withS. Igde, S. Röblitz, A. Müller, K. Kolbe, S. Boden, C. Fessele, T.K. Lindhorst, M. Weber, L. Hartmann.** Linear Precision Glycomacromolecules with Varying Interligand Spacing and Linker Functionalities Binding to Concanavalin A and the Bacterial Lectin FimH. *Macromol. Biosci.* 2017, 12, S. 1700198-n/a.

118. **S. A. Hill, R. Steinfort, S. Mücke, J. Reifenberger, T. Sengpiel, L. Hartmann.** Exploring Cyclic Sulfamidate Building Blocks for the Synthesis of Sequence-Defined Macromolecules. *Macromol. Rapid Commun.* 42, 2021, S. 2100193.

119. **F. Shamout, L. Fischer, N. L. Snyder, L. Hartmann.** Recovery, Purification, and Reusability of Building Blocks for Solid Phase Synthesis. *Macromol. Rapid Commun.* 2020, 41, S. 1900473.

120. **D. S. King, C. G. Fields, G. B. Fields.** A cleavage method which minimizes side reactions following Fmoc solid phase peptide synthesis. *Int. J. Pept. Protein Res.* 1990, 3, S. 255-266.

121. **T. Pelras, K. Loos.** Strategies for the synthesis of sequence-controlled glycopolymers and their potential for advanced applications. *Prog. Polym. Sci.* 2021, 117, S. 101393.

122. **V. Ladmiral, E. Melia, D. M. Haddleton.** Synthetic glycopolymers: an overview. *Eur. Polym. J. .* 2004, 40, S. 431-449.

123. **Becer, R. C.** The Glycopolymer Code: Synthesis of Glycopolymers and Multivalent Carbohydrate–Lectin Interactions. *Macromol. Rapid Commun.* 2012, 33, S. 742-752.

124. **L. Zheng, Y. Luo, K. Chen, Z. Zhang, G. Chen.** Highly Branched Gradient Glycopolymer: Enzyme-Assisted Synthesis and Enhanced Bacteria-Binding Ability. *Biomacromolecules.* 2020, 21, S. 5233–5240.

125. **J. Li, X.-Y. Tian, L.-P. Zong, Q. Zhang, X.-J. Zhang, R. Marks, S. Cosnier, D. Shan.** Uniform and Easy-to-prepare Glycopolymer-brush Interface for Rapid Protein (anti-)Adhesion Sensing. *ACS Appl. Mater. Interfaces.* 2019, 11, S. 32366-32372.

126. **G. Cheng, A. Boeker, M. Zhang, G. Krausch, A. H. E. Mueller ,.** Amphiphilic Cylindrical Core-Shell Brushes via a "Grafting From". *Macromolecules.* 2001, 34, S. 6883-6888.

127. **R. Fleet, E. T. van den Dungen, B. Klumperman.** Novel Glycopolymer Brushes via ATRP: 1. Synthesis and Characterization. *Macromol. Chem. Phys.* 2011, 212, S. 2191-2208.

128. **L. Nuhn, S. Hartmann, B. Palitzsch, B. Gerlitzki, E. Schmitt, R. Zentel, H. Kunz, , , 10652.** Water-Soluble Polymers Coupled with Glycopeptide Antigens and T-Cell Epitopes as Potential Antitumor Vaccines. *Angew. Chem. Int. Ed.* 2013, 52, S. 10652-10656.

129. **Y. Deng, S. Zhang, G. Lu, X. Huang.** Constructing well-defined star graft copolymers. *Polym. Chem.* 2013, 4, S. 1289-1299.

130. **J. Roovers, P. Toporowski, J. Martin.** Synthesis and characterization of multiarm star polybutadienes. *Macromolecules.* 1989, 22, S. 1897–1903.

131. **D. Rahlwes, J. E. L. Roovers, S. Bywater.** Synthesis and Characterization of Poly(styrene-g-isoprene) Copolymers. *Macromolecules.* 1977, 10, S. 604–609.

132. **F. Candau, F. Afchar-Taromi, P. Rempp.** Synthesis and characterization of polystyrene-poly(ethylene oxide) graft copolymers. *Polymer.* 1977, 18, S. 1253-1257.

133. **K. L. Beers, S. G. Gaynor, K. Matyjaszewski, S. S. Sheiko, M. Möller.** The Synthesis of Densely Grafted Copolymers by Atom Transfer Radical Polymerization. *Macromolecules.* 1998, 31, S. 9413-9415.

134. **J. H. Lettow, H. Yang, P.F. Nealey, S. J. Rowan.** Effect of Graft Molecular Weight and Density on the Mechanical Properties of Polystyrene-Grafted Cellulose Nanocrystal Films. *Macromolecules .* 2021, 54, S. 10594–10604.

135. **A. Nese, N. V. Lebedeva, G. Sherwood, S. Averick, Y.Li, H. Gao, L. Peteanu, S. S. Sheiko, K. Matyjaszewski.** pH-Responsive Fluorescent Molecular Bottlebrushes Prepared by Atom Transfer Radical Polymerization. *Macromolecules.* 2011, 44, S. 5905-5910 .

136. **C. Li, N. Gunari, K. Fischer, A. Janshoff, M. Schmidt.** New perspectives for the design of molecular actuators: thermally induced collapse of single macromolecules from cylindrical brushes to spheres. *Angew. Chem. Int. Ed. Engl.* 2004, 43, S. 1101-1104.

137. **Y. Li, E. Themistou, J. Zou, B. P. Das, M. Tsianou, C. Cheng,.** Facile Synthesis and Visualization of Janus Double-Brush Copolymers. *ACS Macro Lett.,.* 2011, 1, S. 52–56.

138. **B. Zhao, W. J. Brittain.** Polymer brushes: surface-immobilized macromolecules. *Prog. Polym. Sci.* 2000, 25, S. 677-710.

139. **R. C. Advincula.** Surface initiated polymerization from nanoparticle surfaces. *J. Dispers. Sci. Technol.* 2003, 24, S. 343-361.

140. **C. M. Hui, J. Pietrasik, M. Schmitt, C. Mahoney, J. Choi, M. R. Bockstaller,K. Matyjaszewski.** Surface-initiated polymerization as an enabling tool for multifunctional (Nano-)engineered hybrid materials. *Chem. Mater.* 2014, 26, S. 745–762.

141. **E. Dosekova, J. Filip, T. Bertok, P. Both, P. Kasak, J. Tkac.** Nanotechnology in Glycomics: Applications in Diagnostics, Therapy, Imaging, and Separation Processes. *Med. Res. Rev.* 2017, 37, S. 514–626.

142. **F. Kveton, A. Blsakova, P. Kasak, J. Tkac.** Glycan Nanobiosensors. *Nanomaterials.* 2020, 10, S. 1406–1430.

143. **R. M. Fratila, M. Moros, J. M. de la Fuente.** Recent Advances in Biosensing Using Magnetic Glyconanoparticles. *Anal. Bioanal. Chem.* 2016, 408, S. 1783–1803.

144. **P. F. Hockl, A. Wolosiuk, J. M. Pérez-Sáez, A. V. Bordoni, D. O. Croci, Y. Toum-Terrones, G. J. A. A. Soler-Illia, G. A. Rabinovich,.** Glyco-nano-oncology: Novel therapeutic opportunities by combining small and sweet. *Pharmacol. Res.* 2016, 109, S. 45–54.

145. **S. A. Torres-Pérez, C. E. Torres-Pérez, M. Pedraza-Escalona, S. M. Pérez-Tapia, E. Ramón-Gallegos.** Glycosylated Nanoparticles for Cancer-Targeted Drug Delivery. *Front. Oncol.* 2020, 10, S. 1–10.

146. **J. J.Lundquist, E. J. Toone.** The Cluster Glycoside Effect. *Chem. Rev.* 2002, 102, S. 555–578.

147. **Y.-Y. Chien, M.-D. Jan, A. K.Adak, H.-C. Tzeng, Y.-P. Lin, Y.-J. Chen, K.-T.Wang, C.Ti. Chen, C. C. Chen, C. C. Lin.** Globotriose-functionalized Gold Nanoparticles as Multivalent Probes for Shiga-like Toxin. *ChemBioChem.* 2008, 9, S. 1100–1109.

148. **P. M. Chaudhary, S. Sangabathuni, R. V. Murthy, A. Paul, H. V. Thulasiram, R. Kikkeri.** Assessing the Effect of Different Shapes of Glyco-Gold Nanoparticles on Bacterial Adhesion and Infections. . *Chem. Commun.* 2015, 51, S. 15669–15672.

149. **F. Compostella, O. Pitirollo, A. Silvestri, L. Polito.** Glyco-gold Nanoparticles: Synthesis and Applications. . *Beilstein J. Org. Chem.* 2017, 13, S. 1008–1021.

150. **M. Marradi, F. Chiodo, I. García, S. Penadés.** Glyconanoparticles as Multifunctional and Multimodal Carbohydrate Systems. *Chem. Soc. Rev.* 2013, 42, S. 4728–4745.

151. **M. Kalita, M. M. Payne, S. H. Bossmann.** Glyco-nanotechnology: A biomedical perspective. *Nanomedicine: NBM .* 2022, 42, S. 102542.

152. **D. Kim, N. Rahhal, C. Rademacher.** Elucidating Carbohydrate-Protein Interactions Using Nanoparticle-Based Approaches. *Approaches. Front. Chem.* 2021, 9, S. 669969.

153. **K. J. McHugh, L. Jing, A. M. Behrens, S. Jayawardena, W. Tang, M. Gao, R. Langer, A. Jaklenec.** Biocompatible Semiconductor Quantum Dots as Cancer Imaging Agents. *Adv. Mater.* 30:, S. 1706356.

154. **J. Chen, A. Than, N. Li, A. Ananthanarayanan, X. Zheng, F. Xi, J. Liu, J. Tian, P. Chen,.** Sweet graphene quantum dots for imaging carbohydrate receptors in live cells. *FlatChem.* 2017, 5, S. 25-32.

155. **Tan, R. S.** Glycosylated and non-glycosylated quantum dot-displayed peptides trafficked indiscriminately inside lung cancer cells but discriminately sorted in normal lung cells: an indispensable part in nanoparticle-based intracellular drug delivery. *Asian J. Pharm. Pharm. Sci.* 2018, 13, S. 197–211.

156. **Y. Fu, M.-S. Jang, T. Wu, J. H. Lee, Y. Li, D. S. Lee, H. Y. Yang,.** Multifunctional hyaluronic acid-mediated quantum dots for targeted intracellular protein delivery and real-time fluorescence imaging. *Carbohydrate Polymers.* 2019, 224, S. 115174.

157. **Y. Guo, I. Nehlmeier, E. Poole, C. Sakonsinsiri, N. Hondow, A. Brown, Q. Li, S. Li, J. Whitworth, Z. Li, A. Yu, R. Brydson, W. B. Turnbull, S. Pöhlmann, D. Zhou.** Dissecting Multivalent Lectin–Carbohydrate Recognition Using Polyvalent Multifunctional Glycan-Quantum Dots. *J. Am. Chem. Soc.* 2017, 139, S. 11833-11844 .

158. **S. A. Hill, D. Benito-Alifonso, S. A Davis, D. J. Morgan, M. Berry, M. C. Galan.** Practical Three-Minute Synthesis of Acid-Coated Fluorescent Carbon Dots with Tuneable Core Structure. . *Sci. Rep.* 2018, 8, S. 12234.

159. **C. P. Modenutti, J. I. B. Capurro, S. Di Lella, M. A. Marti.** The Structural Biology of Galectin-Ligand Recognition: Current Advances in Modeling Tools, Protein Engineering, and Inhibitor Design. *Front. Chem.* 2019, 7.

160. **J. Li, H. Li, Y. Yu, Y. Liu, Y. Liu, Q. Ma, L. Zhang, X. Lu, X. Y. Wang, Z. Chen, D. Zuo, J. Zhou.** Mannan-binding lectin suppresses growth of hepatocellular carcinoma by regulating hepatic stellate cell activation via the ERK/COX-2/PGE2 pathway. *Oncoimmunology.* 2018, 8, S. e1527650.

161. **W. Wang, Y. Guo, C. Tiede, S. Chen, M. Kopytynski, Y. Kong, A. Kulak, D. Tomlinson, R. Chen, M. McPherson, D. Zhou.** Ultraefficient Cap-Exchange Protocol To Compact Biofunctional Quantum Dots for Sensitive Ratiometric Biosensing and Cell Imaging. *ACS Appl Mater Interfaces.* 2017, 18, S. 15232-15244.

162. **D. Liu, P. T. Snee.** Water-Soluble Semiconductor Nanocrystals Cap Exchanged with Metalated Ligands. *ACS Nano.* 2011, 5, S. 546–550.

163. **Y. Guo, J. Li, Y. Yuan, L. Li, M. Zhang, C. Zhou, Z. Lin.** A Rapid Microwave-Assisted Thermolysis Route to Highly Crystalline Carbon Nitrides for Efficient Hydrogen Generation. *Angew. Chem.* 2016, 128, S. 14913 - 14917.

164. **X.-L.Ge, B. Huang, Z.-L.Zhang, X. Liu, M. He, R. Cui, X.-J. Liang, D.-W. Pang.** Glucose-functionalized near-infrared Ag2Se quantum dots with renal excretion ability for long-term in vivo tumor imaging. *J. Mater. Chem. B.* 2019, 7, S. 5782-5788.

165. **F. Vincent, T. M. Gloster, J. Macdonald, C. Morland, R. V. Stick, F. M. Dias, J. A. Prates, C. M., Fontes, H. J. Gilbert, G. J. Davies.** Common inhibition of both beta-glucosidases and beta-mannosidases by isofagomine lactam reflects different conformational itineraries for pyranoside hydrolysis. *Chembiochem.* 2004, 5, S. 1596–1599.

166. **S. Jiang, Q. Chen, M. Tripathy, E. Luijten, K. S. Schweizer, S. Granick.** Janus Particle Synthesis and Assembly. *Adv. Mater.* 2010, 22, S. 1060– 1071.

167. **Gennes, P. G. de.** Soft Matter. *Science.* 1992, 256, S. 495– 497.

168. **Z. Zhang, H. D. Li, X. Y. Huang, D. Y. Chen.** Solution-Based Thermodynamically Controlled Conversion from Diblock Copolymers to Janus Nanoparticles. *ACS Macro Lett.* 2017, 6, S. 580–585.

169. **L. Cheng, G. Z. Zhang, L. Zhu, D. Y. Chen, M. Jiang.** Nanoscale Tubular and Sheetlike Superstructures from Hierarchical Self-Assembly of Polymeric Janus Particles. *Angew. Chem., Int. Ed.* 2008, 47,, S. 10171– 10174.

170. **T. S. Skelhon, Y. Chen, S. A. Bon.** Hierarchical Self-Assembly of 'Hard-Soft' Janus Particles into Colloidal Molecules and Larger Supracolloidal Structures. *Soft Matter.* 2014, 10, S. 7730–7735.

171. **I. Schick, S. Lorenz, D. Gehrig, S. Tenzer, W. Storck, K. Fischer, D. Strand, F. Laquai, W. Tremel.** Inorganic Janus particles for biomedical applications. *Beilstein J. Nanotechnol.* 2014, 5, S. 2346–2362.

172. **Z.W. Li, Z.Y. Lu, Z.Y Sun.** Soft Janus particles: ideal building blocks for template-free fabrication of two-dimensional exotic nanostructures. *Soft Matter.* 2014, 10, S. 5472-5477.

173. **A. Kirillova, C. Marschelke, A. Synytska.** Hybrid Janus Particles: Challenges and Opportunities for the Design of Active Functional Interfaces and Surfaces. *ACS Appl. Mater. Interfaces .* 11, S. 9643–9671.

174. **K.H. Ku, Y.J. Lee, G.-R. Yi, S.G. Jang, B.V.K.J. Schmidt, K. Liao, D. Klinger, C.J. Hawker, B.J. Kim.** Shape-tunable biphasic janus particles as pH-responsive switchable surfactants. *Macromolecules.* 2017, 50, S. 9276-9285.

175. **L. Wang, M. Pan, S. Song, L. Zhu, J. Yuan, G. Liu.** Intriguing morphology evolution from noncrosslinked poly(tertbutyl acrylate) seeds with polar functional groups in soap-free emulsion polymerization of styrene. *Langmuir.* 2016, 32, S. 7829-7840.

176. **M. Urban, B. Freisinger, O. Ghazy, R. Staff, K. Landfester, D. Crespy, A. Musyanovych.** Polymer janus nanoparticles with two spatially segregated functionalizations. *Macromolecules.* 2014, 47, S. 7194-7199.

177. **C.-C. Lin, C.-W. Liao, Y.-C. Chao, C. Kuo.** Fabrication and characterization of asymmetric janus and ternary particles. *ACS Appl. Mater. Interfaces.* 2010, 2, S. 3185-3191.

178. **R. Deng, F. Liang, X. Qu, Q. Wang, J. Zhu, Z. Yang.** Diblock copolymer based janus nanoparticles. *Macromolecules.* 2015, 48, S. 750-755.

179. **J. Yuan, W. Zhao, M. Pan, L. Zhu.** Self-assembled colloidal particle clusters from in situ pickering-like emulsion polymerization via single electron transfer mechanism. *Macromol. Rapid Commun.* 2016, 37, S. 1282-1287.

180. **Z.-Q. Feng, K. Yan, J. Li, X. Xu, T. Yuan, T. Wang, J. Zheng,.** Magnetic Janus particles as a multifunctional drug delivery system for paclitaxel in efficient cancer treatment. *Mater. Sci. Eng. C.* 2019, 104, S. 110001.

181. **M. Mo, S. Du, Y. Gao, B. Peng, L. Zhang, J. Zhu.** Bioinspired Janus particles for hydrophobic modification of hydrogels with photothermal antibacterial capability. *J Colloid Interface Sci.* 2022, 616, S. 93-100.

182. **N. Wang, X. Wei, A.-Q. Zheng, T. Yang, M. L.Chen, J. H. Wang,.** Dual Functional Core-Shell Fluorescent Ag2S@Carbon Nanostructure for Selective Assay of E. coli O157:H7 and Bactericidal Treatment. *ACS Sens.* 2017, 2, S. 371–378.

183. **C. Zhang, D.-T.Shi, K.-C. Yan, A. C. Sedgwick, G.-R. Chen, X.-P. He, T. D. James, B. Ye, X.-L. Hu, D. Chen.** A glycoconjugate-based gold nanoparticle approach for the targeted treatment of Pseudomonas aeruginosa biofilms. *Nanoscale.* 2020, 12, S. 23234-23240.

184. **J. Simpson, D. Craig, K. Faulds, D. Graham.** Mixed-monolayer Glyconanoparticles for the Detection of cholera Toxin by Surface Enhanced Raman Spectroscopy. *Nanoscale Horiz.* 2016, 1, S. 60-63.

185. **K. El-Boubbou, D. C. Zhu, C. Vasileiou, B. Borhan, D. Prosperi, W. Li, X. Huang.** Magnetic Glyco-Nanoparticles: A Tool to Detect, Differentiate, and Unlock the Glyco-Codes of Cancer via Magnetic Resonance Imaging. *J. Am. Chem. Soc.* 2010, 132, S. 4490–4499.

186. **S. J. Malek, R. Khoshchehreh, N. Goodarzi, M. R. Khoshayand, M. Amini, F. Atyabi, M. Esfandyari-manesh, S. Tehrani, R. M.Jafari, M. S. Maghazei, F. Alvandifar, M. Ebrahimi, R. Din.** cis-Dichlorodiamminoplatinum (II) glyconanoparticles by drug-induced ionic gelation technique targeted to prostate cancer: Preparation, optimization and in vitro characterization. *Colloids Surf. B.* 2014, 112, S. 350-358.

187. **J. M. de la Fuente, A. G. Barrientos, T. C. Rojas, J. Rojo, J. Cañada, A. Fernández, S. Penadés.** Gold glyconanoparticles as water-soluble polyvalent models to study carbohydrate interactions. *Angew. Chem. Int. Ed.* 2001, 40, S. 2257-2261.

188. **I. Garcia, M. Marradi, S. Penades.** Glyconanoparticles: multifunctional nanomaterials for biomedical applications. *Nanomedicine.* 2010, 5, S. 777-792.

8. Acknowledgements

First and foremost, I want to thank my supervisor Prof. Dr. Laura Hartmann, who gave me the opportunity to work on different, very interesting interdisciplinary projects. This allowed me to broaden my horizon and think outside the box. I thank her for her trust, helpful and supportive advice and her patience during the entire time.

Special thanks goes to my Co-supervisor PD Klaus Schaper for taking the time to read and evaluate my dissertation.

Furthermore, I would like to thank Prof. Dr. Steffen Thiel and Dr. Stig Hill Christiansen for giving me the opportunity to spend a research visit at Aarhus University in Denmark. Thank you very much for the wonderful time.

I would also like to thank my collaboration partners PD Dr. habil. Alla Synytska, Prof. Dr. Christoph Rademacher and Prof. Dr. Thomas Heinzel for the support and the professional discussions in the very different projects.

A big thanks also goes to Dr. Monir Tabatabai for helping me with the analysis of the NMR spectra. Furthermore, I would like to thank Mr. Mohanad Aian and Dr. Peter Tommes for the measurements of the NMR samples and mass spectra. In addition, I would like to thank the technicians Sonja Coors, Birgit Ohler and Stephanie Scheelen for providing the laboratory equipment and supplies.

Additionally, I would like to thank our former PostDoc Dr. Stephen A. Hill for the hilarious discussions and crazy rides. I am very grateful that our partnership started as a PostDoc – PhD student and ended in a wonderful friendship.

Ich möchte mich bei meinen Bürokollegen Dr. Ulla Gerling-Driessen für die unterstützenden Gespräche, Patrick Konietzny für seine beruhigende Art und Lorand Bonda für seine Leichtigkeit während der Zeit bedanken. Ein besonderer Dank geht ebenfalls an Michaela Kitza für ihre liebe Art, ein immer offenes Ohr und das ganze „Organisatorische".

Bei Theresa Seiler und Michele Illmann möchte ich mich für ihre Freundschaft seit meiner Ankunft in Düsseldorf bedanken, bei Miriam Hoffmann und Luca-Cesare Blawitzki möchte ich mich für den Besuch in Dänemark bedanken. Danke, dass ihr den langen Weg auf euch

genommen habt, es war wirklich sehr schön. Ein großes Dankeschön geht ebenfalls an den Rest der Gruppe, dank euch werde ich mit einem Lächeln an meine Promotion zurückdenken.

Anschließend möchte ich mich bei meinem größten Unterstützer, meinem Fels in der Brandung, Dr. med. univ. Malimmes Grötsch bedanken. Es war sicherlich nicht einfach – für uns beide. Ohne dich wäre ich heute nicht da, wo ich bin. Ohne dich hätte ich es nicht geschafft. Danke für die bedingungslose Begleitung und Ermutigung während der gesamten Zeit.

Son olarak sevgili anneme (Zehra Üclü), sevgili babama (Mustafa Üclü) ve canim dedelerime bana inandıkları, bu süreçte bana koşulsuz destek oldukları ve beni her zaman cesaretlendirdikleri için çok teşekkür ederim.